National and Kapodistrian University of Athens
School of Health Sciences
Faculty of Pharmacy
Department of Pharmacognosy and Natural Products Chemistry

Secondary Metabolites from Fungi *Aspergillus Ochraceopetaliformis* and *Myrothecium Verrucaria* with Antimicrobial Activity

MOSTAFA ABDELMOATAMED ALHAM ASMAEY

El-Menia (Egypt)

Supervisor: Assoc. Prof. Nektarios Aligiannis

Co-supervisors: Asst. Prof. Nikolas Fokialakis

Dr. Aikaterini Termentzi

Referee committee: Prof. Nicholas H. Oberlies

Prof. Maria-Ioanna Chinou

Prof. Evangelos Gikas

Asst. Prof. Khaled A. Shaaban

Submitted in partial fulfilment of the requirements for
Doctor of Philosophy degree in Pharmacy

Division of Pharmacognosy and Natural Products Chemistry

Department of Pharmacy

School of Health Sciences

National and Kapodistrian University of Athens, Greece

[2021]

KEYWORDS

Alkaloids; amino acids; anthraquinones; antimicrobial activities; *Aspergillus*; chromatographic techniques; cyclic peptides; diketopiperazine alkaloids; endophytic fungi; indole alkaloids; lyxofuranoside; miophytocens; *Myrothecium*; natural products; NMR spectroscopic; phytochemistry; prenylated indole alkaloids; roridins; terrestrial fungi; trichothecenes; tichoverrins; trichoverroids; triterpenes; verrucarins.

ΠΕΡΙΛΗΨΗ

Η παρούσα Διδακτορική Διατριβή παρουσιάζει την απομόνωση, την φασματοσκοπική ανάλυση της μοριακής δομής και την αντιβακτηριακή αξιολόγηση δευτερογενών μεταβολιτών από τον χερσαίο μύκητα *Aspergillus ochraceopetaliformis* και τον - ενδοφυτικό του φαρμακευτικού φυτού Datura (*Datura stramonium L.*) - μήκυτα *Myrothecium verrucaria*. Και οι δύο μικροοργανισμοί συλλέχθηκαν, απομονώθηκαν και καλλιεργήθηκαν στην Αίγυπτο το 2015. Ο *Aspergillus ochraceopetaliformis* από την περιφέρεια της Γκίζας*, ενώ ο Myrothecium verrucaria* από την προστατευμένη περιοχή Wadi El Assuity στην επαρχία Assiut.

Η χημική ανάλυση του εκχυλίσματος οξικού αιθυλεστέρα της καλλιέργειας του μήκυτα *Aspergillus ochraceopetaliformis* οδήγησε στην απομόνωση και δομικό χαρακτηρισμό **24** συνολικά δευτερογενών μεταβολιτών, **5** από τους οποίους είναι νέα φυσικά προϊόντα. Οι νέοι μεταβολίτες από τον *A. Ochraceopetaliformis* – όπως ονομάστηκαν στη παρούσα εργασία – είναι οι: 8-OH-echinulin (**38**), Epoxy-echinulin (**39**), Neoechinulin F (**46**), (12*R*) Dehydro-echinulin (**49**) και Ochraceopyronide (**52**) που φέρει κι μια σπάνια απαντώμενη στα φυσικά προϊόντα λυξοφουρανική σακχαρική μονάδα. Η χημική ανάλυση του εκχυλίσματος οξικού αιθυλεστέρα της καλλιέργειας του μήκυτα *M. verrucaria* οδήγησε στην **απομόνωση** και δομικό χαρακτηρισμό **19** συνολικά δευτερογενών μεταβολιτών, **4** από τους οποίους είναι νέα φυσικά προϊόντα. Οι νέοι μεταβολίτες από τον *M. verrucaria* – όπως ονομάστηκαν στη παρούσα εργασία – είναι οι: Miophytocen E (**60**), Miophytocen F (**64**), Miophytocen G (**65**), and Roridin G (**67**). Πολλοί από τους απομονωνένους μεταβολίτες στην παρούσα διατριβή εξετάστηκαν για την αντιμικροβιακή τους δράση.

Οι δευτερογενείς μεταβολίτες που παρουσιάζονται εδώ, απομονώθηκαν μετά από μια μεγάλη σειρά χρωματογραφικών διαχωρισμών, διαφόρων τύπων και η δομή τους καθορίστηκε μέσα από την λεπτομερή ανάλυση και συνδυαστική μελέτη φασματοσκοπικών δεδομένων πυρηνικού μαγνητικού συντονισμού μιάς και δύο διαστάσεων (NMR 1D και 2D) και φασματομετρίας μάζας υψηλής ανάλυσης (HR-ESI-MS). Η στερεοχημεία (σχετική και απόλυτη) των μεταβολιτών που προτείνεται στην εργασία, βασίστηκε στην μελέτη φασμάτων 1D και 2D NOESY, στην ανάλυση Marfey's, στις μετρήσεις οπτικής στροφικής ικανότητας και σε θεωρητικούς υπολογισμούς (στην περίπτωση του Ochraceopyronide (**52**).

ABSTRACT

This thesis describes the isolation, structure elucidation and biological activity evaluation of secondary metabolites of the soil-derived fungus *Aspergillus ochraceopetaliformis* which collected at Giza province, Egypt, as well as those produced by the endophytic fungus *Myrothecium verrucaria* isolated from healthy wild medicinal plant datura (*Datura stramonium L*.) which collected from Wadi El Assuity, protective area, Assiut Governorate, Upper Egypt in 2015.

Chemical investigations of the soil-derived fungus *Aspergillus ochraceopetaliformis* led to the isolation and characterization of 24 compounds, **five** of which were identified as new; 8-OH-echinulin (**38**), 27-28-epoxyechinulin (**39**), neoechinulin F (**46**), (12*R*)dehydroechinulin (**49**) and ochraceopyronide (**52**) which had a rare lyxofuranoside. On the other hand, 19 compounds were identified from the endophytic fungus *Myrothecium verrucaria* amongst, **four** new compounds named miophytocen E (**60**), miophytocen F (**64**), miophytocen G (**65**), and roridin G (**67**). Many of the fungal metabolites encountered in this work have been tested for their antimicrobial effects.

The compounds identified in this work were isolated using multiple chromatographic techniques, and the structures were established based on detailed analysis of 1D and 2D NMR data combined with HR-ESIMS. The study of the stereochemistry of the isolated compounds was based on 1D and 2D NOESY experiments, Marfey's analysis, specific optical rotation measurements, thorough comparison with literature data along with theoretical calculations in the case of Ochraceopyronide.

PREFACE

This dissertation is submitted for the partial fulfilment of the degree of doctor of philosophy. It is based on work carried out between December 2016 and May 2021 in the Division of Pharmacognosy and Natural Products Chemistry, Department of Pharmacy, School of Health Sciences, National and Kapodistrian University of Athens, Greece, under the supervision of Assoc. Professor Aligiannis Nektarios. My scholarship from the Egyptian ministry of higher education (Cultural Affairs and Missions Sector) and the Greek ministry of foreign affairs (E1 sector) is gratefully acknowledged.

MOSTAFA ABDELMOATAMED ALHAM ASMAEY

May 2021

TABLE OF CONTENTS

Contents

LIST OF FIGURES

LIST OF TABLES

LIST OF SCHEMES

LIST OF ABBREVIATIONS

Abbreviation	Item
AC	Acetyl
ACN	Acetonitrile.
amu	Atomic mass unit
br.	Broad
^{13}C NMR	Carbon-13 Nuclear Magnetic Resonance
$CDCl_3$	Deuterated Chloroform
CoA	Coenzyme A
d	Doublet
dd	Doublet of doublet
DCM	Dichloromethane
DEPT	Destortionless Enhancement by Polarization Transfer
DMSO-d_6	Deuterated Dimethylsulphoxide
ESI-MS	Electrospray Ionization Mass Spectrometry
EtOAc	Ethyl acetate
gm	Gram
^{1}HNMR	Proton Nuclear Magnetic Resonance
H,HCOSY	^{1}H,^{1}H-Correlated Spectroscopy
HRMS	High Resolution Mass Spectra
HMBC	Heteronuclear Multiple Bond Connectivity
HPLC	High Performance Liquid Chromatography
HSQC	Heteronuclear Single Quantum Coherence

IC_{50}	Half maximal inhibitory concentration
IR	Infrared
J	Coupling constant
$[M+H]^+$	Pseudo-molecular ion (Positive ion mode)
m	Multiplet
MHz	Megahertz
MeOD-d_4	Deuterated methanol
MIC	Minimum inhibitory concentration
MTs	Macrocyclic Trichothecens
m/z	Mass over charge
N	Normality
NOESY	Nuclear Overhauser Effect Spectroscopy
ppm	Part per million
PTLC	Preparative Thin Layer Chromatography
q	Quartet
s	Singlet
sp.	Species
t	Triplet
UK	United Kingdom
UV/VIS	Ultraviolet-Visible spectroscopy
$[\alpha]^D$	Optical rotation
δ	Chemical shift value
λ	Wavelength
µM	Micromolar

STATEMENT OF ORIGINAL AUTHORSHIP

The work contained in this thesis has not been previously submitted to meet requirements for an award at this or any other higher education institution. To the best of my knowledge and belief, the thesis contains no material previously published or written by another person except where due reference is made.

Signature: _____

Date: _____

ACKNOWLEDGEMENTS

Praise is to ALLAH, the lord of the universe, who guided and aided me to bring forth to light this work and by whose grace this work has been completed.

Without direct and indirect involvement of the following persons, this dissertation would have not been made possible. I would like therefore to convey my sincere gratitude and thankfulness to Prof. Dr. Niktarios Aligiannis, Associate Professor Division of Pharmacognosy and Natural Products Chemistry, Department of Pharmacy, School of Health Sciences, National and Kapodistrian University of Athens. I wish to express my deep appreciation for his kindness, admirable supervision, direct guidance, generous considerations and valuable support during my study in his group.

I would like to express my cordial thanks and gratitude to Asst. Prof. Nikolas Fokialakis, Division of Pharmacognosy and Natural Products Chemistry, Department of Pharmacy, School of Health Sciences, National and Kapodistrian University of Athens and Dr. Aikaterini Termentzi, Researcher in Benaki Phytopathological Institute for their valuable suggestions, their fruitful discussions, their unforgettable support as well as for accepting to read and edit my thesis. My work would never be fully completed without the help from the man of wisdom Dr. Dennis Abatis, valuable and constructive discussions, guiding and fruitful advice, which enriched the quality of this work.

Many thanks for the friendly cooperation to Prof. Dr. Ioana Chinou, Division of Pharmacognosy and Natural Products Chemistry, Department of Pharmacy, School of Health Sciences, National and Kapodistrian University of Athens, for carrying out the antimicrobial tests, I also appreciate the sincere cooperation of Prof. Nikos Thomaidis and his student Sophia Drakoupolou, Department of Analytical Chemistry, Faculty of Chemistry, National and Kapodistrian University of Athens, for performing and interpretation of HR-MS analysis

A special thanks go to Prof. Mohamed Shaaban, Dr. Ahmed S. Abdel-Razek National Research Center, Cairo, Egypt and Dr. Ismael R. Abdel-Rahim, Department of Microbiology, Faculty of Science, Assuit University, for the isolation, identification of the fungi strains and some administrative help. All of my thanks goes to Dr. George Lambrinidis, Division of Pharmaceutical Chemistry, Department of Pharmacy, School

of Health Sciences, National and Kapodistrian University of Athens, for the computational work.

My sincere thank goes to Dr Evangelia D. Chrysina, Senior Researcher, ICB-NHRF Instruct-EL hub / Inspired-RIs coordinator, and her cooperators Dr Dimitris Kalofolias and Dr Marianna Charavgi for the X-Ray analysis.

My special thanks to Dr. Ahmed M. Metwaly, Faculty of Pharmacy, Al-Azhar University, Egypt, for the molecular docking work and to Dr. Demitra Benaki, Division of Pharmaceutical Chemistry, Department of Pharmacy, School of Health Sciences, National and Kapodistrian University of Athens, for her constructive advises, sharing her expertise in NMR data interpretation as well as for her help and support in good times and bad times.

During my PhD study, I received help, support, and happiness from time to time, so I would like to take this opportunity to express my profound gratitude to all of these group members:

- The postdoctors Dr. Nikolas Tsafantakis, Dr.Antigoni Cheliari and Dr. Eirini Piara for their helping me to start my study here. Not only shared their scientific knowledge but also instructed living in the new environment. Dr. Argyro Vontzalidou for sharing techniques and improvement on biology part knowledge.
- All the students associated with me; Eva Dina, Akis Amoutzias, Angelos Charalambidis and the others, have been obedient, and extremely responsive. I am deeply thankful for your friendships, the warm atmosphere, support and collaboration during my study and the good times we had together.

I also would like to thank Dr Hamdi Nasr and all the academic staff at the Chemistry Department, Faculty of Science, Al-Azhar University, Egypt, for their permanent support. My great appreciation to the Egyptian ministry of higher education (Cultural Affairs and Missions Sector) and the Greek ministry of foreign affairs (E1 sector), for the financial support during my stay in Greece.

I will not forget my parents, sisters and other family members for all their support, financially and spiritually. I am forever grateful to my mother and father. Words are inadequate to express my feelings for their financial and moral support. Providing me the opportunity to enrich my academic career was the greatest gift they could have given me. Their love, prayers and encouragement, helped me in every stage of my life.

Finally, the credit for this extensive and detailed work in such a wide topic goes to the many hours each day and night that have extended to me to do the task. For this, I am grateful to Allah for giving me the strength to endure.

I am especially grateful to my wife and sons Hamza and Mohammed for their continuous support, encouragement, love patience and understanding during this work.

To all of you, thank you very much!

1. Introduction

1.1 History of Natural Products

Since ancient times, Nature played a major role as the prime source of medicinal extracts used, as well as the source of several natural products that led to the expansion of assorted drugs currently used for the treatment of a vast range of diseases. However, the science of isolation and elucidation of their active constituents is not older than 150 years. Natural products are defined as chemical compounds, isolated/derived from living organisms (e.g. plants, animals and microorganisms). Predominantly these compounds are secondary metabolites[1]. Hence, the chemistry of natural products is especially related to the biosynthesis, isolation, and structure elucidation of products obtained from nature.

Medicinal plants were and are still in use as folk medicines, especially in developing countries, for the treatment of different diseases. Depending on the evaluation of The World Health Organization (WHO) there are about 80% of the earth inhabitants mainly lean on traditional medicines for their health care[2]. Plants have been the origin of the traditional medicine that has survived for thousands of years starting from the first records.

The Egyptian pharmaceutical record named (The Ebers Papyrus (2900 B.C.), documented over 700 plant-based drugs ranging from gargles, pills, infusions, to ointments. The eldest records of natural products were painted on clay tablets in cuneiform from Mesopotamia (2600 B.C.) which authenticated oils from *Cupressus sempervirens* (Cypress) and *Commiphora* species (myrrh) that are used till today to treat coughs, colds and inflammation[3].

Furthermore, the Chinese Materia Medica (1100 B.C.) (Wu Shi Er Bing Fang, contains 52 prescriptions), Shennong Herbal (~100 B.C., 365 drugs) and the Tang Herbal (659 A.D., 850 drugs) are certified records of the uses of natural products. The Greek physician, Dioscorides, (100 A.D.), recorded the collection, storage and the uses of medicinal herbs, whilst the Greek philosopher and natural scientist, Theophrastus (~300 B.C.) sort out the medicinal herbs[4].

Through the Dark and Middle Ages, the Arabs preserved the Greco-Roman knowledge and expanded the uses of their own resources, together with Chinese and Indian herbs unfamiliar to the Greco-Roman world. It was the Arabs who were the first to privately

own pharmacies (8th century) with Avicenna, a pharmacist, physician, philosopher and poet, contributing much to the sciences of pharmacy and medicine through works such as the *Canon Medicinae*[5].

According to empirical knowledge, natural product extracts, mainly plant-derived, have formed the basis of traditional medicine systems. The imperative need for new therapeutic alternatives, mainly for the treatment of cancer and infectious diseases, as well as the new chemical entities (NCE) decline in drug development pipelines, led to the rekindling of interest in "rediscovering natural products" focusing on alternative sources[6]. Therefore, there is worldwide attention to the search for new sources of bioactive constituents, as most medicinal plants (~97%) have been totally investigated. So, many other natural sources were being taken into consideration, especially those located in terrestrial and marine habitats.

1.1.1 History of Antibiotics

Some of the most well-known classes of fungal metabolites are the penicillins and the cephalosporins. Penicillin G (**1**), one of the first antibiotics from microorganisms, was discovered and isolated from the filamentous fungus *Penicillium notatum* in 1928 by Fleming, showing a bactericidal activity against the *Staphylococcus* sp. For this great discovery, Fleming, Chian and Florey were honoured with the Nobel Prize in 1945[7].

Since the discovery of penicillin G (**1**) and mycophenolic acid (**2**) before[8], microorganisms, especially fungi and bacteria, played an essential role in the production of antibiotics and other drugs for the treatment of current diseases[9].

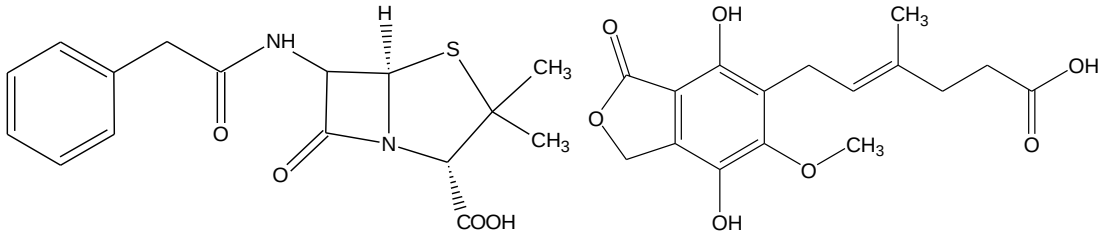

1 **2**

The development of penicillin by Florey and his colleagues opened the door to the "Golden Age of Antibiotics" that has dominated medical practice for several decades. It is an active agent produced by *Penicillium notatum* and has an inhibitory effect against Gram-positive bacteria, including the disease-causing species from the two genera Streptococcus

and Staphylococcus. A post penicillin hunt for further antibiotics began in the 1940s and resulted ultimately in the identification of thousands of microbial metabolites with a broad array of biological properties.

Till the mid-eighties, almost all groups of important antibiotic were discovered: the antibacterial cephalosporin C (**3**), streptomycin, tetracyclines, erythromycin A (**4**), vancomycin, the antifungal amphotericin B, imidazoles, griseofulvin, strobilurins, the antiviral acyclovir (**5**), vidarabine (**6**) and many other compounds that play a role in therapeutics and agriculture[10].

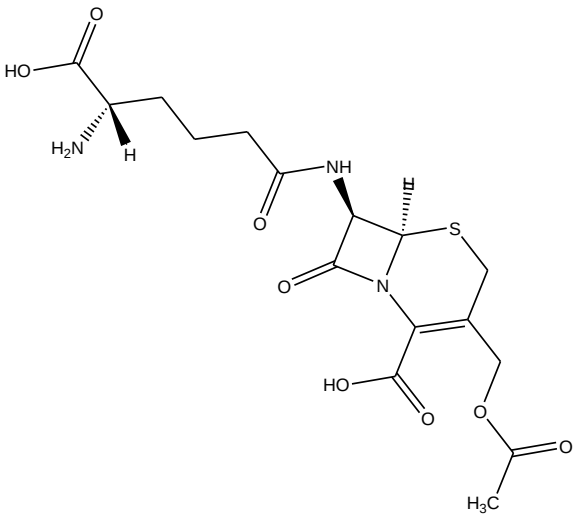

3

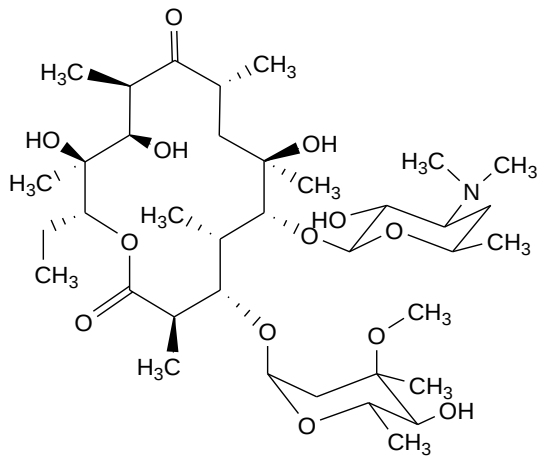

4

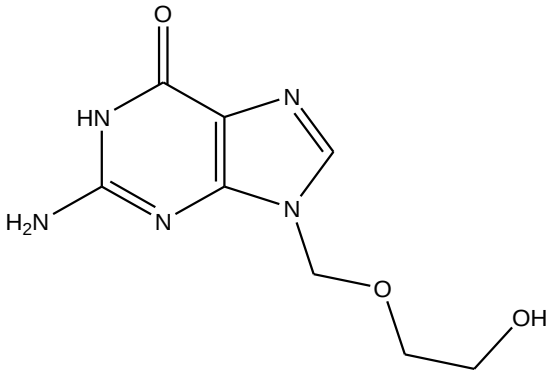

5

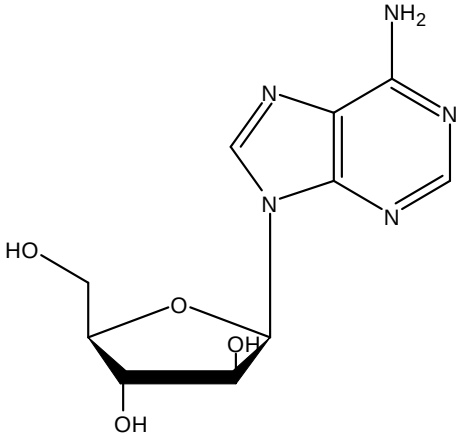

6

The Greek-derived word antibiose had been coined to explain antagonistic effects between microorganisms. In 1941 Waksman defined an antibiotic as a "secondary metabolite, produced by microorganisms, which has the ability to inhibit the growth and even to destroy bacteria and other microorganisms in a very low concentration"[8]. Not all the isolated secondary metabolites act as antibiotics, many of them assist as plant growth factors and enzyme inhibitors[11] and as self-regulating factors in some bacteria (e.g. A Factor; γ-butylrolactone)[12]. The virginiae butanolides induce the production of virginiamycin in *Streptomyces virginiae*, others promote pigment[13] or spore formation and some are cytotoxic or enzyme inhibitors. Zähner et al. proposed the existence of a "playground" of secondary metabolism, which is closely connected to five distinct primary cellular levels. These five levels are: intermediary metabolism, regulation, transport, differentiation and morphogenesis[14].

As a result, the definition of secondary metabolites is not confined to antibiotics but should be extended to all those metabolites, which regulate all physiological and biochemical activities in the life cycle of organisms [15]. It is logically therefore to understand secondary metabolites as 'words' in a language, where chemo ecology is the grammar [16].

1.2 Fungi as a Source of Natural Products.

According to the estimated number of species, Kingdom Fungi is second only to that of Kingdom Animalia. Conservative estimates proposed that there are more than 1.5 million fungal species, of which only approximately 5% have been identified by taxonomists (~72, 000 known species)[17]. Fungi are plentiful, biologically diverse, and play many different roles. For example, they play pivotal roles in both the health and maintenance of ecosystems through their ability to degrade organic waste such as forest leaf litter. Fungi can also act as pathogens, predators, parasites, hosts, and/or symbionts of animals, plants, and other microorganisms[18].

Perhaps more importantly, fungi have long been recognized as possessing the ability to produce novel bioactive secondary metabolites, some of which have facilitated significant advances in human health and agriculture, with vast impacts on societal and economic growth[19]. Although fungi have proven to be prolific producers of diverse bioactive secondary metabolites, a great many fungi remain to be chemically explored. These factors support strongly for continued exploration of fungal chemistry in order to help suffice the increasing demand for new medicinally and agriculturally beneficial agents.

Fungi have garnered a widespread negative connotation since they were first reported to cause disease in 1839. Especially, fungi are known to produce mycotoxins, which have been linked to numerous types of human and animal diseases[20]. On the other hand, fungi can also be used in a profitable manner. For example, some fungi (e.g., yeasts) are used in fermentation processes in the preparation of several foods/drinks, while others are essential in the industrial production of beneficial enzymes[21]. Fungi are often categorized into various ecological groups. Some of these groups include freshwater fungi (fungi isolated from both flowing and still freshwater habitats), fungicolous/mycoparasitic fungi (fungi isolated from tissues of other fungi), endophytic fungi (fungi living symbiotically with plants), and plant pathogenic fungi (fungi that cause disease/damage to host plants)[22].

Endophytic fungi are a further rich source of bioactive compounds.[23,24] Endophytes are microorganisms, which live in the intercellular spaces of host plants without causing any visible signs of their presence.[25] Some of these internal colonizing microorganisms have an excellent potential to promote the plant growth[26], other endophytes are sources of anticancer, antidiabetic, insecticidal and immunosuppressive compounds[27]. The hosts of these microorganisms might be fungi[28], plants[29] and insects,[30] but also algae[31].

Endophytic fungi exhibited biological activity more often than those isolated from soil: 80% of the endophytic fungi from plants inhibited at least one of the test organisms, while only 64% of those from soils did so[32]. There are nearly 300,000 plant species and each plant hosts one or more endophyte[33]. Although scientists claim the discovery of one-hundred thousand fungal species to date, there could however even be over one million species.

1.2.1 Mycotoxins as natural products from fungi

1.2.1.1 Definitions, Etymology, and General Principles

It is difficult to define mycotoxin in a few words. All mycotoxins are low-molecular-weight natural products (i.e., small molecules) produced as secondary metabolites by filamentous fungi. These metabolites constitute a toxigenically and chemically heterogeneous assemblage that are grouped together only because the members can cause disease and death in human beings and other vertebrates. Not surprisingly, many mycotoxins display overlapping toxicities to invertebrates, plants, and microorganisms[34].

The term mycotoxin was coined in 1962 in the aftermath of an unusual veterinary crisis near London, England, during which approximately 100,000 turkey poults died. When this mysterious turkey X disease was linked to a peanut (groundnut) meal contaminated with

secondary metabolites from *Aspergillus flavus* (aflatoxins), it sensitized scientists to the possibility that other occult mold metabolites might be deadly. The period between 1960 and 1975 has been termed the mycotoxin gold rush[35] because many scientists joined the well-funded search for these toxigenic agents. Depending on the definition used, and recognizing that most fungal toxins occur in families of chemically related metabolites, some 300 to 400 compounds are now recognized as mycotoxins, of which approximately a dozen groups regularly receive attention as threats to human and animal health[36].

Mycotoxicoses are animal diseases caused by mycotoxins; mycotoxicology is the study of mycotoxins[37]. While all mycotoxins are of fungal origin, not all toxic compounds produced by fungi are called mycotoxins. The target and the concentration of the metabolite are both important. Fungal products that are mainly toxic to bacteria (such as Penicillin G (**1**)) are usually called antibiotics. Fungal products that are toxic to plants are called phytotoxins by plant pathologists (confusingly, the term phytotoxin can also refer to toxins made by plants[38]. Mycotoxins are made by fungi and are toxic to vertebrates and other animal groups in low concentrations. Other low molecular weight fungal metabolites such as ethanol that are toxic only in high concentrations are not considered mycotoxins[39]. Finally, although mushroom poisons are definitely fungal metabolites that can cause disease and death in humans and other animals, they are rather arbitrarily excluded from discussions of mycotoxicology. Molds (i.e., microfungi) make mycotoxins; mushrooms and other macroscopic fungi make mushroom poisons. The distinction between a mycotoxin and a mushroom poison is based not only on the size of the producing fungus but also on human intention. Mycotoxin exposure is almost always accidental. In contrast, with the exception of the victims of a few mycologically accomplished murderers, mushroom poisons are usually ingested by amateur mushroom hunters who have collected, cooked, and eaten what was misidentified as a delectable species[40].

Mycotoxins are not only hard to define, but they are also challenging to classify. Due to their diverse chemical structures and biosynthetic origins, their myriad biological effects, and their production by a wide number of different fungal species, classification schemes tend to reflect the training of the person doing the categorizing. Clinicians often arrange them by the organ they affect. Thus, mycotoxins can be classified as hepatotoxins, nephrotoxins, neurotoxins, immunotoxins, and so forth. Cell biologists put them into generic groups such as teratogens, mutagens, carcinogens, and allergens. Organic chemists have attempted to classify them by their chemical structures (e.g., lactones, coumarins);

biochemists according to their biosynthetic origins (polyketides, amino acid-derived, etc.); physicians by the illnesses they cause (e.g., St. Anthony's fire, stachybotryotoxicosis), and mycologists by the fungi that produce them (e.g., *Aspergillus* toxins, *Penicillium* toxins)[39].

1.2.1.2 Major Mycotoxins

Aflatoxins

Aflatoxins are a family of toxins produced by certain fungi that are found on agricultural crops such as maize (corn), peanuts, cottonseed, and tree nuts. The main fungi that produce aflatoxins are *Aspergillus flavus* and *Aspergillus parasiticus*, which are abundant in warm and humid regions of the world. Aflatoxin-producing fungi can contaminate crops in the field, at harvest, and during storage.

The four major aflatoxins are called B_1, B_2, G_1, and G_2 based on their fluorescence under UV light (blue or green) and relative chromatographic mobility during thin-layer chromatography. Aflatoxin B_1 (**7**) is the most potent natural carcinogen known and is usually the major aflatoxin produced by toxigenic strains. It is also the best-studied: in a large percentage of the papers published[41]. Aflatoxins are difuranocoumarin derivatives produced by a polyketide pathway by many strains of *Aspergillus flavus* and *Aspergillus parasiticus*; in particular, *Aspergillus flavus* is a common contaminant in agriculture. *Aspergillus bombycis*[42], *Aspergillus ochraceoroseus*[43], *Aspergillus nomius*, and *Aspergillus pseudotamari* are also aflatoxin-producing species, but they are encountered less frequently[44].

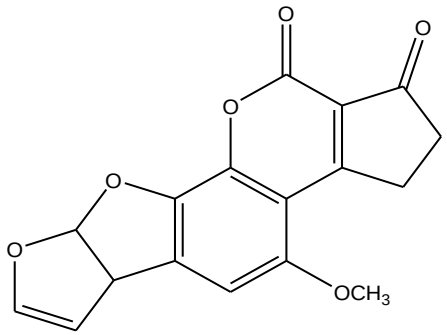

7

Aflatoxins have oncogenic and immunosuppressive properties, inducing infections in people contaminated with these substances. They contribute significantly to increasing the risk of liver cancer in people chronically infected with hepatitis B (VHB)[45] and are considered a risk factor for the development of hepatocellular cancer in Africa and Asia[46].

Aflatoxin is associated with both toxicity and carcinogenicity in human and animal populations[47]. The diseases caused by aflatoxin consumption are loosely called aflatoxicosis. The liver is the primary target organ, with liver damage occurring when poultry, fish, rodents, and nonhuman primates are fed aflatoxin B1.

Ochratoxin A

Ochratoxin A (**8**) was discovered in 1965 as a secondary metabolite from *Aspergillus ochraceus* during studies aimed to identify new mycotoxin molecules[48]. Its chemical structure has a similarity with those of aflatoxins, being represented by an isocoumarin substitute bound to an L-phenylalanine group.

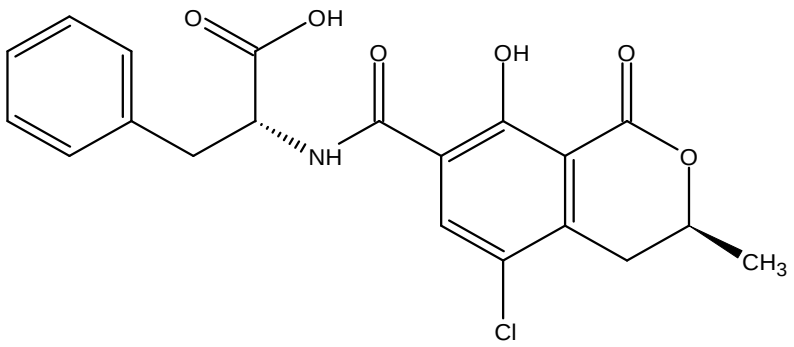

8

Not only *Aspergillus ochraceus* species are capable of producing ochratoxin A, but also this species, *Aspergillus alliaceus*[49], *Aspergillus auricomus*[50], *Aspergillus carbonarius*[51], *Aspergillus glaucus*[52], *Aspergillus niger*[53] and *Aspergillus ochraceopetaliformis*[54] as well as *Penicillium nordicum* and *Penicillium verrucosum*[55], are producers of ochratoxin A.

Ochratoxin A (**8**) has been found in oats, barley, wheat, coffee grains and other products for human and animal consumption. There is also concern that this mycotoxin may be present in wines if the vine fruits are infected by *A. carbonarius*[56]. Ochratoxin A is associated with nephropathy in all animals studied to date. In humans, it is commonly found in serum[57] since this substance has a long half-life in relation to its elimination. Besides being recognized as nephrotoxic, ochratoxin A also shows hepatoxic, immunosuppressive, teratogenic and carcinogenic behaviour[58,59]. Additionally, it has been found in the blood and other tissues of animals and in milk, including human milk[60]. The International Cancer Research Agency has classified ochratoxin A as a possible human carcinogen (category 2B)[**Error! Bookmark not defined.**].

Ergot alkaloids

These compounds are among the most interesting secondary metabolites of fungi, and their production occurs in the scleroids of several species of the genus *Claviceps*. They are classified as indole alkaloids and are derived from a tetracyclic ergoline ring system. Lysergic acid, a structure common to all ergot alkaloids, was first isolated in 1934. The clavines have ergoline as a basic structure but lack peptide components; the lysergic acid alkaloids include ergotamine (**9**) and ergometrine (**10**)[61]. These compounds are produced as a toxic cocktail of alkaloids in the sclerotia of species of *Claviceps*, which are common pathogens of various grass species.

The ingestion of these sclerotia, or ergots, has been associated with diseases since antiquity. Accurately, the effects of these alkaloids on humans have been known since The Middle Ages, a period in which some symptoms were called “Holy Fire” or “St Anthony’s Fire”. In the year 994, in the south of France, thousands of people died after eating cereal grains infected by *Claviceps purpurea*[62].

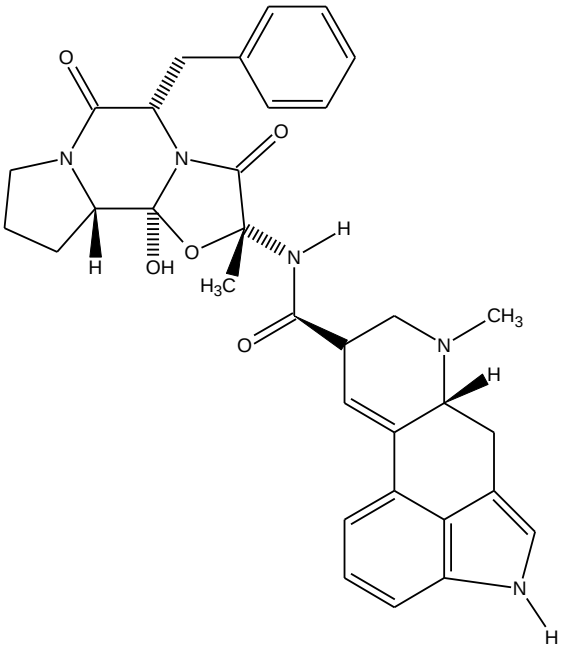

9

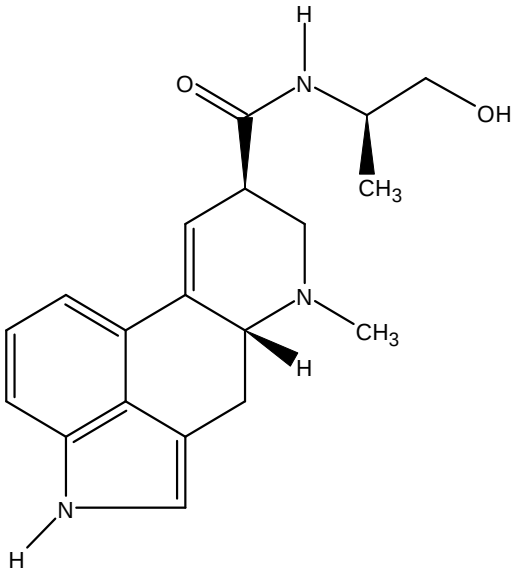

10

Fumonisins

Fumonisins, one of the relevant secondary metabolites, were first described and characterized in 1988[63]. Fumonisins are produced by some *Fusarium* species, notably *Fusarium verticillioides* (formerly *Fusarium moniliforme = Gibberella fujikuroi*), *Fusarium proliferatum*, and *Fusarium nygamai*, as well as *Alternaria alternata* [64].

Fumonisins are classified into three types, FB_1, FB_2, and FB_3. They are thought to be synthesized by condensation of the amino acid alanine into an acetate-derived precursor[65]. FB_1 (**11**) is the most toxic of all fumonisins and the most predominant contaminant of small grain cereals especially maize, and other grains such as (wheat, oats, rye….etc)[66-69]. Unlike most known mycotoxins, which are soluble in organic solvents, fumonisins are hydrophilic which makes hinders to their study.

Usually, they are extracted in aqueous methanol or aqueous acetonitrile[70]. High-performance liquid chromatography with fluorescent detection is the most widely used analytic method[71]. The fumonisin story raises the spectre that there may be many other occult but toxic products of fungal metabolism that have not yet been discovered because of their hydrophilic nature.

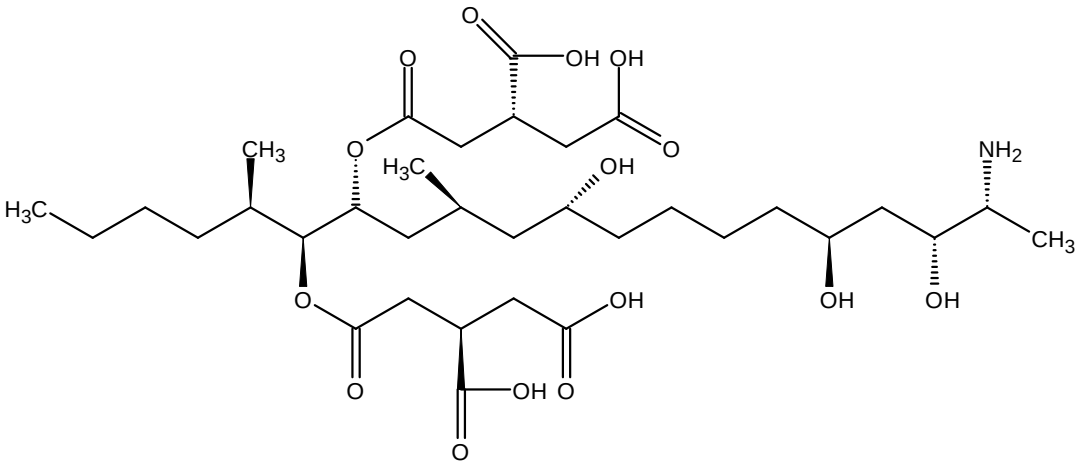

11

Citrinin

Citrinin (**12**) was first isolated as a secondary metabolite from *Penicillium citrinum* prior to World War II[72], subsequently, it was produced in many species of *Penicillium* and several species of *Aspergillus* (e.g., *Aspergillus terreus* and *Aspergillus niveus*)[73], including certain strains of *Penicillium camemberti* (used to produce cheese) and *Aspergillus oryzae* (used to produce sake, miso, and soy sauce)[74].

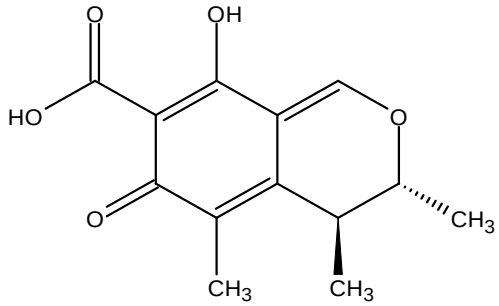

12

Furthermore, citrinin found to be a nephrotoxin with various acute toxicity in different species in all animal species tested[75]. Also, citrinin showed to have an association with another mycotoxin which is also nephrotoxic, ochratoxin A to depress RNA synthesis in murine kidneys[76].

Patulin

Patulin (**13**) is produced by many different molds but was first isolated as an antimicrobial active compound in around 1940, from the fungus *Penicillium patulum*, later called *Penicillium urticae* and currently known as *Penicillium griseofulvum*. Patulin was also isolated later from other species and received the names clavacin, claviformin, expansin, mycoinc, and penicidin[77]. It was used as a nose and throat spray in the treatment of the common cold and as an ointment for the treatment of skin infections[78]. However, during the 1960s it became clear that it was toxic to animals and plants. After these revelations it was reclassified as a true mycotoxin[79]. Chemically, patulin is known as 4-hydroxy-4H-furo[3, 2-c]pyran-2(6H)-one.

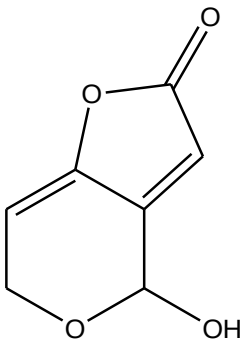

13

The “blue mold” disease, which is common in apple, cherry, pear and other fruits, is caused by the fungus *Penicillium expansum*, currently considered the most efficient

producer of patulin in nature along with the species *Aspergillus clavatus*, *Aspergillus giganteus* and *Aspergillus terreus* which also producers of patulin[80]. Patulin is commonly found in non-fermented apple juice, but it is not resistant to fermentation in products derived from cider, where it is efficiently metabolized by yeasts[81].

Zearalenone

Zearalenone (6-[10-hydroxy-6-oxo-trans-1-undecenyl]-B-resorcyclic acid lactone) (**14**)[82], previously known as F-2 toxins, is the group of toxins produced by all toxigenic and pathogenic species of *Fusarium*, mainly *Fusarium graminearum*, *Fusarium crookwellemse*, *Fusarium culmorum*, and *Fusarium semitectum*[83]. It was given the trivial name zearalenone as a combination of G. zeae, resorcylic acid lactone, -ene (for the presence of the C-1' to C-2 double bond), and -one, for the C-6' ketone[84]. Most probably simultaneously, a second group isolated and studied the metabolic properties of the same compound and named it F-2. The classification of zearalenone as a toxin is considered inappropriate since, although biologically potent, it is rarely toxic. Its structure resembles 7b-estradiol, the main hormone produced in the human female ovary. Zearalenone would better fit the classification of a non-steroidal estrogen or a mycoestrogen. Different derivatives of zearalenone, including α-zearalenol, β-zearalenol, monohydroxylated, dihydroxylated and formylated zearalenone, have been isolated from cultures of Fusarium.[83]

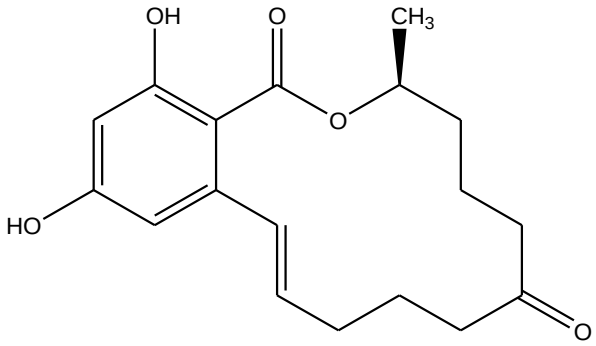

14

Zearalenone is less toxic than trichothecenes. It has an LD_{50} value of 1-10 g/kg body weight of mice[85]. The estimated safe intake of zearalenone for humans has been reported to be 0.05 µg/kg of body weight/day[86]. Nevertheless, because of its genuine biological potency and regular dietary cooccurrence with true mycotoxins such as the fumonisins and trichothecenes, it would not be prudent to ignore the potential of zearalenone to cause adverse health effects.

1.2.1.3 Trichothecenes

Trichothecenes are mycotoxins, named in the year 1948 after the discovery of the antifungal compound 'trichothecin' from the fungus *Trichothecium roseum*[87,88]. They produced by several fungal genera, including *Myrothecium*, *Fusarium*, *Trichoderma*, *Trichothecium Phomopsis*, *Stachybotrys* and others[89]. Many plant species such as *Baccharis coridiofolia* and *Baccharis artemisioides* also produce macrocyclic trichothecenes[90]. Trichothecenes are secondary metabolites produced from the isoprenoid metabolism and have a tricyclic nucleus with an epoxide function[91].

More than 200 molecules are classified as trichothecenes[92]. They are cyclic terpenoids with a common tricyclic 12,13-epoxytrichothec-9-ene, the core structure characterized by the presence of a double-bound between carbons 9 and 10 as well as, an epoxide group between carbons 12 and 13 (**Figure 1**), both being essential for their activity. Although all trichothecenes share this common core structure, they also possess unique substitution groups at carbons 3, 4, 7, 8 and 15, allowing their classification as type A, B, C or D. Types A, B and C differ in the substitution present at carbon 8 (**Figure 1**, **Table 1**).

In type A trichothecenes (e.g. T-2 toxin (**15**), HT-2 toxin (**16**), neosolaniol, and diacetoxyscirpenol (DAS) (**17**)) substitution groups of carbon 8 are either hydroxyl group, an ester group or no substitution.

In type B trichothecenes, a substituent group corresponds to the carbonyl function (**Figure 1**). This subtype of trichothecenes includes five structurally related congeners: nivalenol (NIV) (**21**), deoxynivalenol (DON) (**22**) DON, 3-acetyldeoxynivalenol (3-ADON) (**23**), 15-acetydeoxynivalenol (15-ADON) (**24**) and fusarenon-x (**25**). Some transformations produce mycotoxin derivatives, also called "masked/modified mycotoxins" that are undetectable by conventional analytical techniques. These derivatives result from changes in the "native mycotoxin" structure after transformation by process, bacteria or plants[93,94]. Some plants also have the ability to transform mycotoxins. For example, DON-3-b-glucoside (D3G) results from enzymatic conjugation of glucose to DON by plant[95]. Generally, this biotransformation results in a decrease in toxicity[96].

Type B group are the most common trichothecenes contaminating wheat, and therefore, the trichothecenes of most concern[97]. Type C trichothecenes including crotocin (**26**) are characterized by the presence of a second epoxide group between carbon 7 and 8 (**Figure 2**). Finally, type D trichothecenes (e.g. satratoxins (**27**), roridins, and verrucarins) possess an additional ring between carbon 4 and carbon 15, which is why they are also

called “macrocyclic” trichothecenes, whereas types A, B and C trichothecenes are called “simple” trichothecenes.

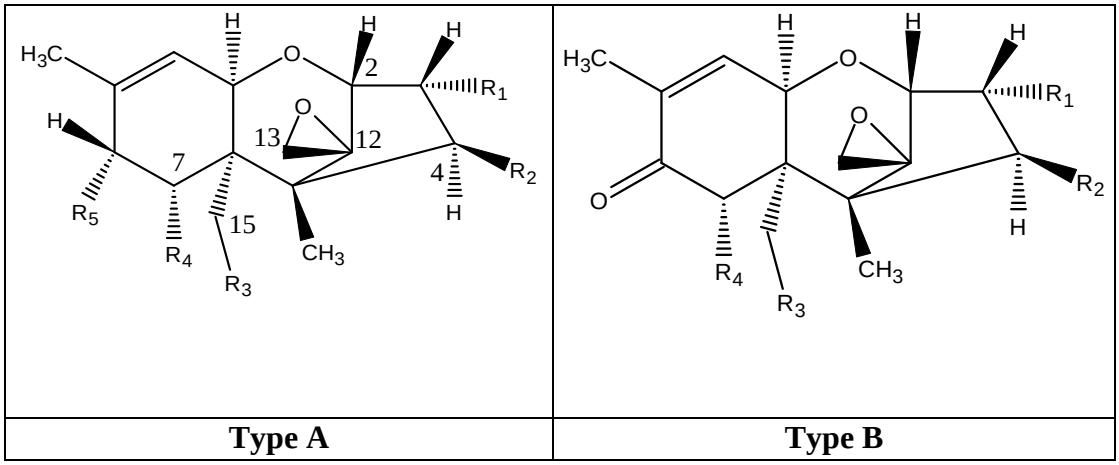

Type A | **Type B**

Figure 1: Chemical structures of type A and B trichothecenes.

Table 1: Substituent patterns of different Type A and B trichothecenes.

Trichothecene	R1	R2	R3	R4	R5
TYPE A					
T-2 toxin (**15**)	-OH	-OAc	-OAc	-	-OIsoval
HT-2 toxin (**16**)	-OH	-OH	-OAc	-H	-OIsoval
DAS (**17**)	-OH	-OAc	-OAc	-H	-H
NX-2 toxin (**18**)	-OAc	H	-OH	-OH	-H
NX-3 toxin (**19**)	-OH	H	-OH	-OH	-H
TYPE B					
Trichothecene (**20**)	-H	-OIsoval	-H	-H	=O
NIV (**21**)	-OH	-OH	-OH	-OH	=O
DON (**22**)	-OH	-H	-OH	-OH	=O
3-ADON (**23**)	-OAc	-H	-OH	-OH	=O
15-ADON (**24**)	-OH	-H	-OAc	-OH	=O
Fusarenon-X (**25**)	-OH	-OAc	-OH	-OH	=O

OAc = O-acetyl, OIsoval = O-isovalerate.

Type C	Type D
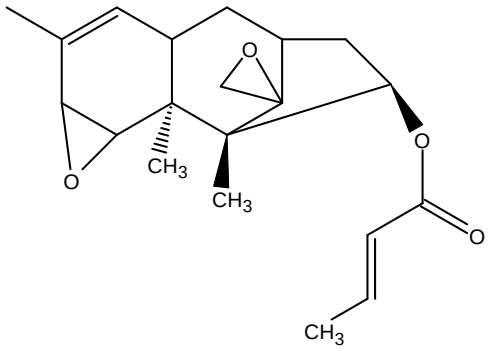	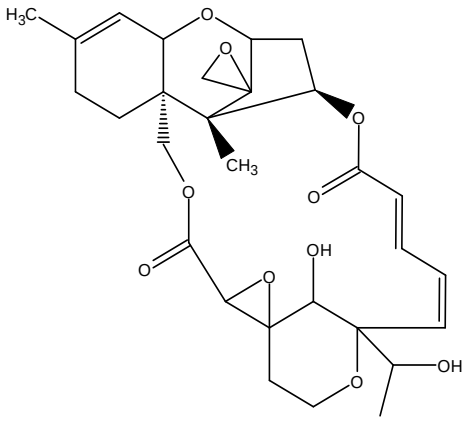
25	**26**

Figure 2: Chemical structures of type C and D trichothecenes.

Toxicity of trichothecenes

Trichothecenes are toxic to all tested animal species, but the sensitivity varies considerably between species and also between the different trichothecenes. The trichothecenes are extremely potent inhibitors of eukaryotic protein synthesis; different trichothecenes interfere with initiation, elongation, and termination stages[98].

Other cellular impacts have been detected on nucleic acid biosynthesis[99], mitosis and membrane/organelle integrity[100], but these are likely all secondary effects of protein synthesis inhibition and ribotoxic stress, and direct interaction between the trichothecenes and cellular components has only been reported for the ribosome[101].

The interaction of trichothecenes with 60S ribosomal subunit through non-covalent hydrogen bonds leads to the so-called ribotoxic stress effect resulting in:

- inhibition of protein synthesis,
- rRNA cleavage
- activation of different cellular signalling pathways, leading to modulation of gene expression and to post-translational protein modifications[102,103].

In parallel to the ribotoxic stress effect, trichothecenes are known to target mitochondria and to cause mitochondrial stress leading to the generation of Radical Oxygen Species (ROS), lipid peroxidation, and oxidative stress that can also cause apoptosis[104].

Trichodermin was the first trichothecene shown to inhibit peptidyl transferase activity[105]. The first reported NIV-mediated inhibition of protein synthesis in rabbit reticulocyte whole cells and cell-free lysates in 1968. Numerous studies on the effect of

various trichothecenes on ribosome activity in mammalian cell extracts followed in the 1970s, with considerable attention on identifying the mode of inhibition[106,107].

The offering produced by various trichothecenes include effects on almost every major system of the vertebrate body; many of these effects are due to secondary processes that are initiated by often poorly understood metabolic mechanisms related to the inhibition of protein synthesis. A greet attempt to compile and interpret the data for different trichothecenes, studied in different organisms, administered by different routes, at different doses, at dissimilar intervals, is given by Beasley[108]. Among the naturally occurring trichothecenes, T-2 and diacetoxyscirpenol appear to be the most effective in animal studies. Besides their cytotoxic activity, they have an immunosuppressive effect that results in decreased resistance to infectious microbes[109]. They cause a wide range of gastrointestinal, dermatological, and neurologic symptoms.

Structure-Activity Relationship

To understand how trichothecenes interact with cells, we must first have an advanced understanding of their structure and dynamics. Early studies showed that the structural features of trichothecenes that most affect their biological activities are the 12,13-epoxide ring, the double bond at C-9–C-10, the five variable R groups (**Table 1**), the structure and position of a side chain, the presence of a second epoxy ring (type C), and the presence of a macrocycle (type D).

The 12, 13 epoxide group is known to be essential for trichothecene toxicity[110]. Despite, epoxides are highly reactive groups, they are remarkably stable in the trichothecene structure. It was surprising that in the trichothecene bound ribosome crystal structure, no direct interaction was detected between the epoxide ring and ribosomal components[99]. Foroud and coworkers approach that the epoxide ring is required for structural stability to the trichothecene skeleton, herewith rendering it essential for toxicity[111]. A water molecule is always present when the structure of trichothecenes investigated in various hydroscopic solvents[112]. The water is bound to a suc formed between the B- and C-rings and this pocket are fairly rigid with limited torsional flexibility as a result of tension imparted by the epoxide ring, which pulls C12 down to form the base of the suc[113].

The substitution type at the C3, C4, and C15 is deemed to affect the nature of the interaction with water. For example, modifications at C3 may affect the susceptibility of water binding in DON(**22**). Several modifications of C3, such as acetylation[114,115] or glucosylation[116], have been found to minimize or disrupt cytotoxicity. These modifications have also been shown to decrease or prevent the inhibition of protein translation[117].

Interestingly, there are instances where C3 acetylation does not appear to reduce phytotoxicity.

Type A trichothecenes, having a functional group other than carbonyl in the C-8 position, are generally more toxic than type B trichothecenes with a carbonyl in this position. The toxicity of type A trichothecenes decreases in the order of isovaleryl > hydrogen > hydroxyl groups in the C-8 position. The toxicity of type B trichothecenes is influenced by the substitutions in the C-4 position. In lymphocytes, the toxicity of the type B trichothecenes decreases in the order from acetyl > hydroxyl > hydrogen in the C-4 position. Loss of side chains in the C-4, C-8 or C-15 positions decreases the toxicity and the loss of more than one side chain in these positions further decreases the toxicity[118].

The presence and position of a second epoxide on type C trichothecenes have a particularly marked effect on the bioactivities of these molecules. When an epoxy ring was introduced in trichothecene between C-7 and C-8, its ability to inhibit protein synthesis in rabbit reticulocytes dropped. However, the second epoxide at C-9–C-10 in some macrocyclic trichothecenes (e.g., baccharinoids) increases their anti-leukemic activity[119]. Moreover, esterification at C-4, C-8, or C-15 generally increases the toxicity of trichothecenes in an *Arabidopsis thaliana* detached leaf assay[120].

In 2015, Appell and Bosma performed a Quantitative Structure Activity Relationship (QSAR) study on 35 trichothecenes using density functional theory. There were distinct quantum-based differences between the type A and type B trichothecenes, including in their frontier molecular orbital and natural bond orbital properties. The type B trichothecenes had significantly larger electrophilicity indices than the type A trichothecenes that were studied. Certain hydroxyl groups of T-2 toxin (**15**), NIV(**21**) and DON (**22**) exhibited considerable rotation during the molecular dynamics simulations. The models suggested that electronegativity and several 2-D topological descriptors significantly affect trichothecene cytotoxicity, phytotoxicity, immunochemical detection, and cross-reactivity[121]. In recent years, in silico analysis has turned out to be an effective tool for analyzing the interactions between mycotoxins and their biological targets, including the interaction between trichothecenes and ribosomes[96].

Biosynthesis of trichothecenes

Trichothecene biosynthesis and regulatory genes (*TRI* genes), can be found in clusters on the genome; this is the case for *Fusarium* species as well as other trichothecene producing genera[122,123]. The core cluster in *Fusarium* includes the majority of the *TRI* genes[124], while four remaining genes are located at three different loci: the *TRI*1-*TRI*16 two gene cluster[125] and two independent loci for *TRI*101[126] and *TRI*15[127].

The initial step in the biosynthesis of type B trichothecenes is the sesquiterpene cyclization of farnesyl diphosphate to trichodiene. This reaction is catalyzed by the enzyme trichodiene synthase, which is encoded by the *TRI*5 gene[91,128]. Next, trichodiene undergoes four oxygenation reactions catalyzed by the multifunctional cytochrome P450 monooxygenase encoded by *TRI*4. This enzyme adds three oxygens at C-2, C-3, C-11, and the epoxidation at C-12/C-13 to form isotrichotriol[129]. Isotrichotriol is non-enzymatically converted to isotrichodermol. During this step, the oxygen at the C-2 position becomes the pyran ring oxygen and the hydroxyl group at C- 11 is lost[130] (**Scheme 1**). Isotrichodermol undergoes acetylation on the C-3-hydroxyl by the acetyltransferase encoded by *TRI*101 to produce isotrichodermin[91].

The next step is the addition of another hydroxyl group to C-15 by a cytochrome P450 encoded by *TRI*11. This hydroxyl group is then acetylated by an acetyltransferase encoded by *TRI*3 to form calonectrin[91]. Calonectrin is later modified by the addition of hydroxyl groups at the C-7 and C-8 positions by the product of *TRI*1. Subsequently, the hydroxyl group at the C-8 position is converted to the keto form, producing 3,15-acetyldeoxynivalenol (3,15ADON) (**Scheme 2**). From here, the pathway branches and NIV-producing strains hydroxylate the C-4 position by a reaction catalyzed by the cytochrome P450 monooxygenase encoded by *TRI*13. Conversely, DON-producing strains lack a functional *TRI*13 and are unable to add a hydroxyl group at C-4.

The last step in the biosynthesis of type B trichothecenes is the selective removal of an acetyl group, either on C-3 or C-15, depending on the activity of the esterase encoded by *TRI*8. Alexander and coworkers notified that the *TRI*8 gene from 3-ADON (**23**) producer 22 strains encode a C-15 deacetylase, whereas the *TRI*8 gene from 15-ADON (**24**) producers encodes a C-3 deacetylase.

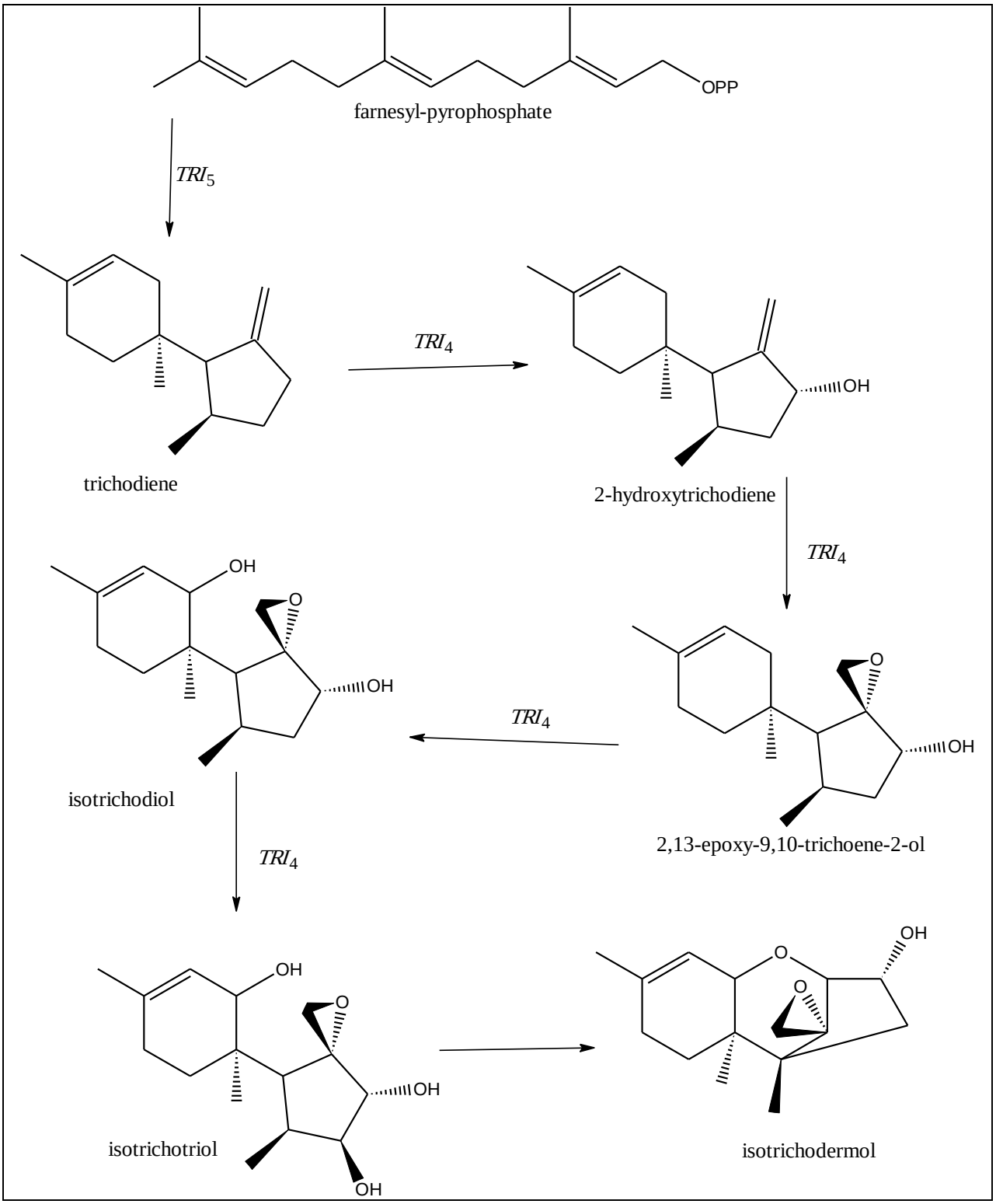

Scheme 1: The proposed biosynthetic pathway for trichothecene, a: First steps

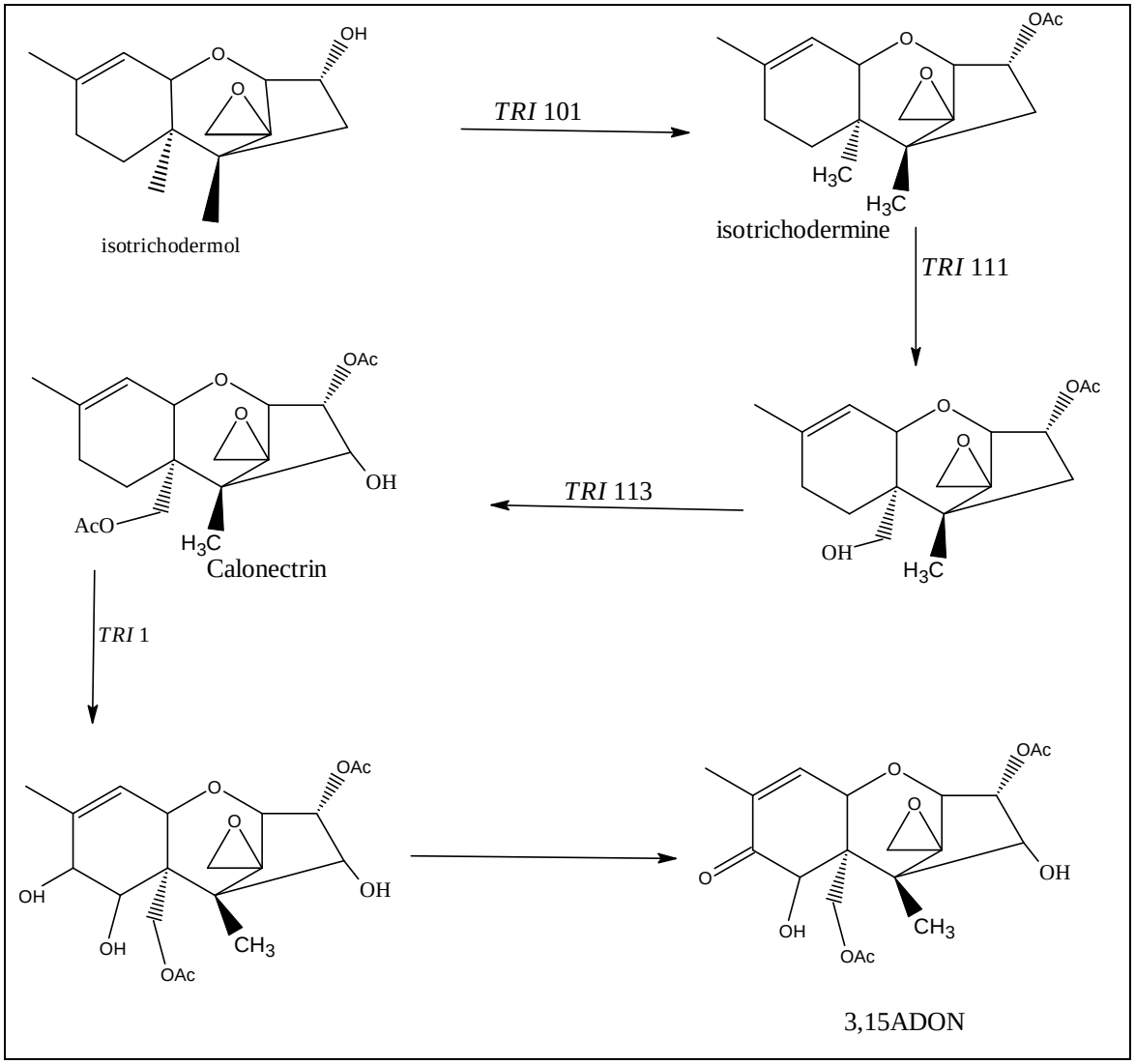

Scheme 2: The proposed biosynthetic pathway for trichothecene, b: Last steps

1.2.1.3.1 Macrocyclic trichothecenes (type D)

Type D trichothecenes were first reported in 1946 when the antifungal antibiotic glutinosin was isolated from a fungus identified as *Metarrhizium glutinosum*[131] which later recognized as *Myrothecium verrucaria*[132]. They have a cyclic diester or triester linking between C-4 and C-15 and are regarded as one of the most toxic trichothecenes. The macrocyclic derivatives possess besides a large fourth ring, formed by esterification of the hydroxyls at positions 4 and 15 of verrucarol (**27**) with long-chain dicarboxylic acids. The macrocyclic trichothecenes are classified as roridins with C29-skeleton or verrucarins with a C27-skeleton[133]. The unusual structural features of macrocyclic trichothecenes result in increased biological activities relative to the other trichothecenes[134].

Because of their potent biological activities, macrocyclic trichothecenes became the focus of many studies throughout the 1970s and 1980s[135,136].

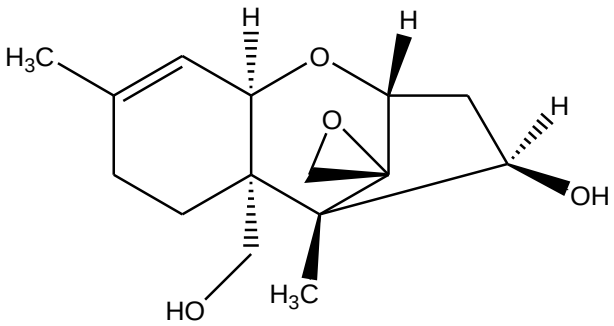

27

Both verrucarins and roridins comprise the sesquiterpene alcohol verrucarol (**27**) and a dicarboxylic acid forming a macrocyclic dilactone. While verrucarins are C27 compounds, roridins are C29-metabolites and many roridins are homologues of verrucarins differing by a C2-side chain at C6'.

Sources of macrocyclic trichothecene

The first macrocyclic trichothecene was discovered from *Myrothecium verrucaria*[137]. Since then several related verrucarins have been described often occurring together in some fungal species including species of *Podostroma*[138] and *Stachybotrys*[139]. Roridins which have a side chain at C6' were described from *Myrothecium*[140], *Podostroma, Stachybotrys*[141], *Calcarisporium*[142], *Cercophora*[143], *Cylindrocarpon*[144], *Dendrodochium*[145] and *Phomopsis*[146] species.

Besides, the *Asteraceae* plant *Baccharis megapotamica* Spreng which causes severe poisoning of cattle in South America produced active compounds that were macrocyclic trichothecenes hitherto only known from this source [147].

The baccharinoids B4 (**28**), B5 (**29**), B6 (**30**), B8 (**31**) and B25 (**32**) are potent antileukemic trichothecenes from *Baccharis megapotamica*. Baccharinoid B4 (**28**) and baccharinoid B25 (**32**) were shown to be esters of 8*β*-hydroxyverrucarol. Baccharinoid B6 (**30**) and baccharinoid B8 (**31**) are the C-13' epimers of baccharinoid B4 (**28**) and baccharinoid B5 (**29**), respectively[148]. Additionally, all of the investigated Brazilian *B. coridifolia* plants produced only roridins[90]. Especially the group of Bruce Jarvis isolated many baccharinoids and elucidated their structures, later they observed that perhaps the

Brazilian strain acquiring roridins from fungal source and then oxygenating to the baccharinoids[149,150].

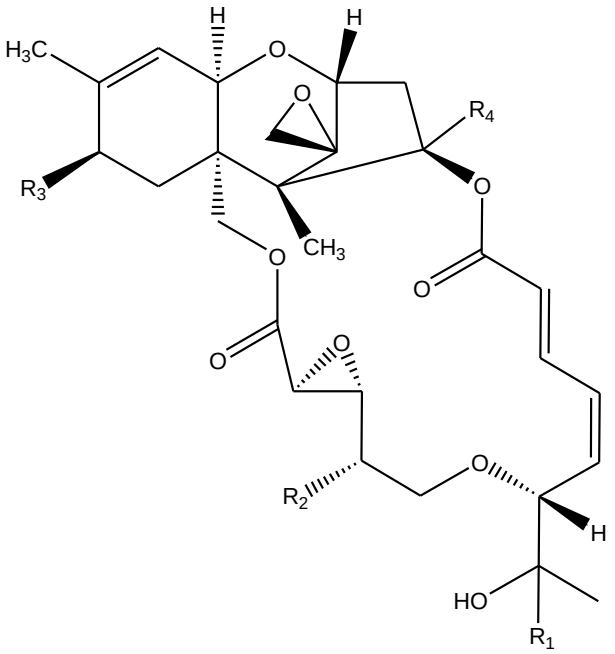

28: R1 = αH, R2 = R3 = OH, R4 = H

30: R1= βH, R2= R3 = OH, R4 = H

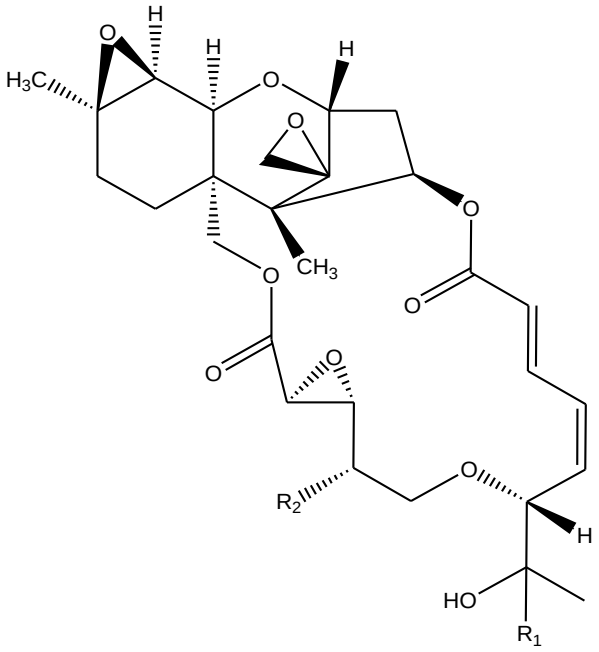

29: R1= βH, R2 = OH

31: R1= αH, R2 = OH

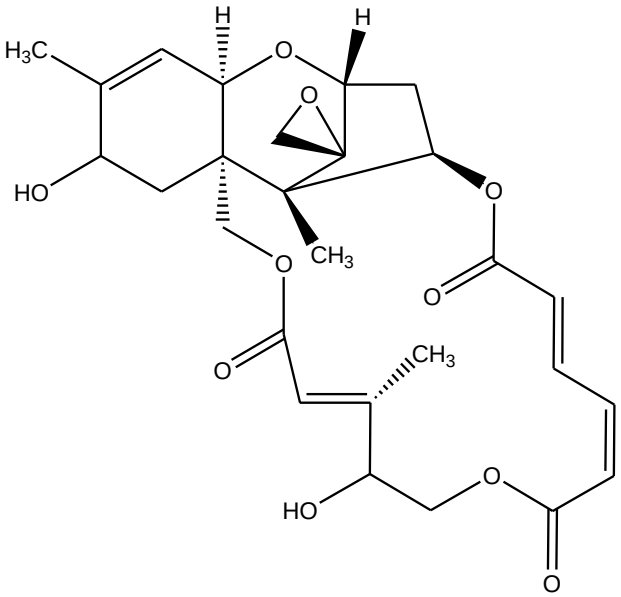

32

Toxicological effects of type D trichothecenes

Macrocyclic trichothecenes (e.g., roridins, verrucarins and satratoxins) are considered to be some of the most toxic trichothecenes and are generally more toxic than simple trichothecenes[151]. Datum has confirmed the capability of type D trichothecenes to inhibit protein synthesis through ribotoxic effects [152,153], causing the activation of Mitogen-Activated Protein (MAP) kinases, inflammation and cell toxicity/apoptosis.

Exposure to type D trichothecenes happens mostly through inhalation and is associated with the so-called damp building-related illnesses that produce respiratory, immunological, and neurological symptoms[154]. Although part of the inhaled type D trichothecenes can reach the blood flow and activate circulating immune cells such as macrophages and trigger the production of anorectic cytokines[155], these toxins are rapidly cleared from the systemic circulation, suggesting rather a local effect on nasal/airway tissues[156]. Type D trichothecenes cause neurotoxic, inflammatory and local mucosecretory responses in the airways of animals exposed to these toxins[157].

Several studies mentioned on effects of macrocyclic trichothecenes on immune functions by using a mitogen-induced blastogenesis assay. Both verrucarins and roridins were able to inhibit B- and T-cell subsets after induction with leukoagglutinin, concanavalin A, or pokeweed mitogen[151]. In 2003, evaluation of some macrocyclic trichothecenes against cancer cell lines was done by Wolf-Rainer Abraham and coworkers[134,158].

There are also some reports on other antimicrobial and phytotoxic effects of macrocyclic trichothecenes. Roridins and verrucarins inhibited the hemorrhagic fever causing arenavirus Junin while not affecting cell viability. IC_{50} (concentration causing 50 % inhibition) values were in the range 1.2 - 4.9 ng ml^{-1}. The trichothecenes lacked virucidal effects on the virions and it could be concluded that a late stage in the replication cycle was inhibited[159].

2. Aim of the investigation

At the beginning of the era of antibiotics, it seemed that all diseases could be medicated soon, whilst, extended use of antibiotics made them insensitive, due to drug resistance phenomena. For this reason, there is a worldwide urgent need now for new medicinal sources. Fungi as aforesaid, are believed to be a treasure fund of bioactive natural products and are expected to provide novel chemical structures for drug discovery for combating emerging diseases.

Accordingly, the main objective of the present investigation is concerned with the isolation and structure elucidation of new and preferably biologically active secondary metabolites from fungi out of different environmental habitats. To achieve this aim, chemical and biological screenings should be applied in such a way, which is in a minimum of time a maximum of results is obtained. For this reason, a 'horizontal screening' should be applied: With a few biological tests using Gram-positive and Gram-negative bacteria, fungi, the antibacterial, antifungal, and cytotoxic activities are covered, and results can be used as a lead for further detailed investigations. The established chemical screening should be applied additionally, extended by using an LC-MS screening (**Figure 3**).

The individual steps can be summarized as follows:

- *Microbiological part*: Collection of strains by carefully selected Habitats, preferably in cooperation with microbiologists. Optimization of fermentation conditions and small scale cultivations.
- *Pre-screening*: Fermentation in a 1 L-scale and horizontal screening. Selection of suitable strains for in-depth explorations
- *Up-scaling*: A large-scale fermentation of selected strains is usually required to obtain sufficient amounts of metabolites; for strains with low productivity, an optimization (pH, fermentation time, medium type) may be needed.
- *Isolation*: The fermentation broths are subjected to exhaustive extraction using either liquid-liquid (solvents) or liquid-solid (Amberlite-XAD) extraction techniques. Chromatographic methods are used to deliver the pure constituents.

- *Dereplication*: Chemical tests (colour reactions), ^{1}H NMR and mass spectra are used to gain preliminary structural information for a dereplication of known compounds with databases.
- *Structure Elucidation*: Novel compounds will be elucidated preferably by using spectroscopic techniques and – if possible – crystal structure analysis.
- *Biological Activity*: Depending on the results of our horizontal screening, new and promising known compounds will be investigated in cooperation with industrial partners for potential use in medicine or agriculture

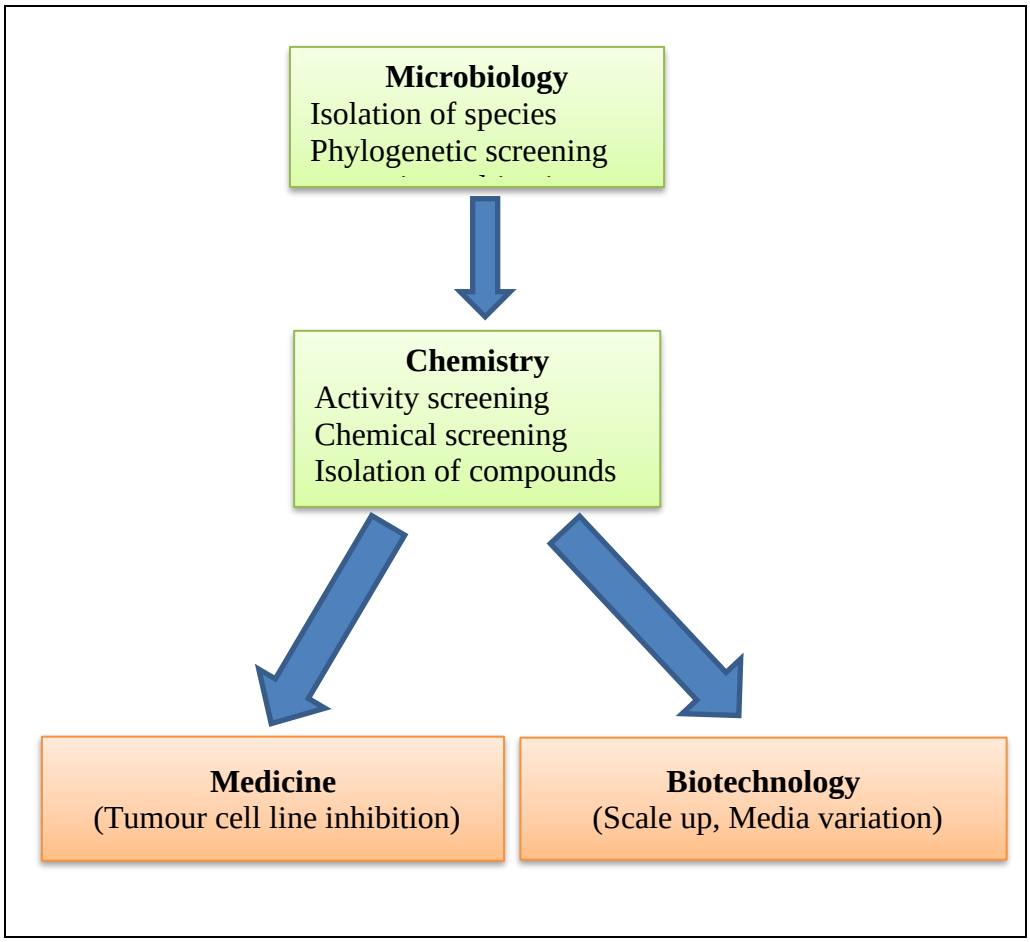

Figure 3: Integrated approach to explore the metabolic capabilities of selected strains for the production of bioactive compounds.

3. General Techniques

3.1 Collection of strains

In this study, the search for bioactive constituents from fungi was continued. For this purpose, the microbial strains were obtained in cooperation with the following microbiological institutions:

- The terrestrial fungus *Aspergillus ochraceopetaliformis* ASAI was obtained from a soil sample collected from Giza, Egypt by Dr. Ahmed S. Abdel-Razek, Microbial Chemistry Department, National Research Centre, Egypt.
- The endophytic fungus *Myrothecium verrucaria* was collected from Wady Al-Asuity, Assiut, Egypt by Dr. Ismail R. Abdel-Rahim, microbiology department, Assiut University, Egypt.

The isolated strains will be described at the material and method part, based on colour, morphological characteristics, etc. The taxonomy was fully determined on the RNA level.

3.2 Work-up Procedure for Selected Fungal Strains

The selection of promising fungal strains producing biologically active and new secondary metabolites depends on two different types of assays: the biological and the chemical screening, which are combined in the so-called pre-screening.

3.3 Pre-screening

Initially, the strains were sub-cultured on agar plates for 3-7 days and microscopically examined for contaminations. Small pieces of the agar culture were then used to inoculate 1 L Erlenmeyer flasks, each containing ~250 ml of medium, for small-scale cultivation, followed by incubation on a rotary shaker at 28 ºC. The culture broth was then lyophilised, and the dried residue was extracted with ethyl acetate. The obtained crude extract was used for the biological and chemical pre-screening (**Figure 4**). Promising strains are selected for chemical in-depth investigation.

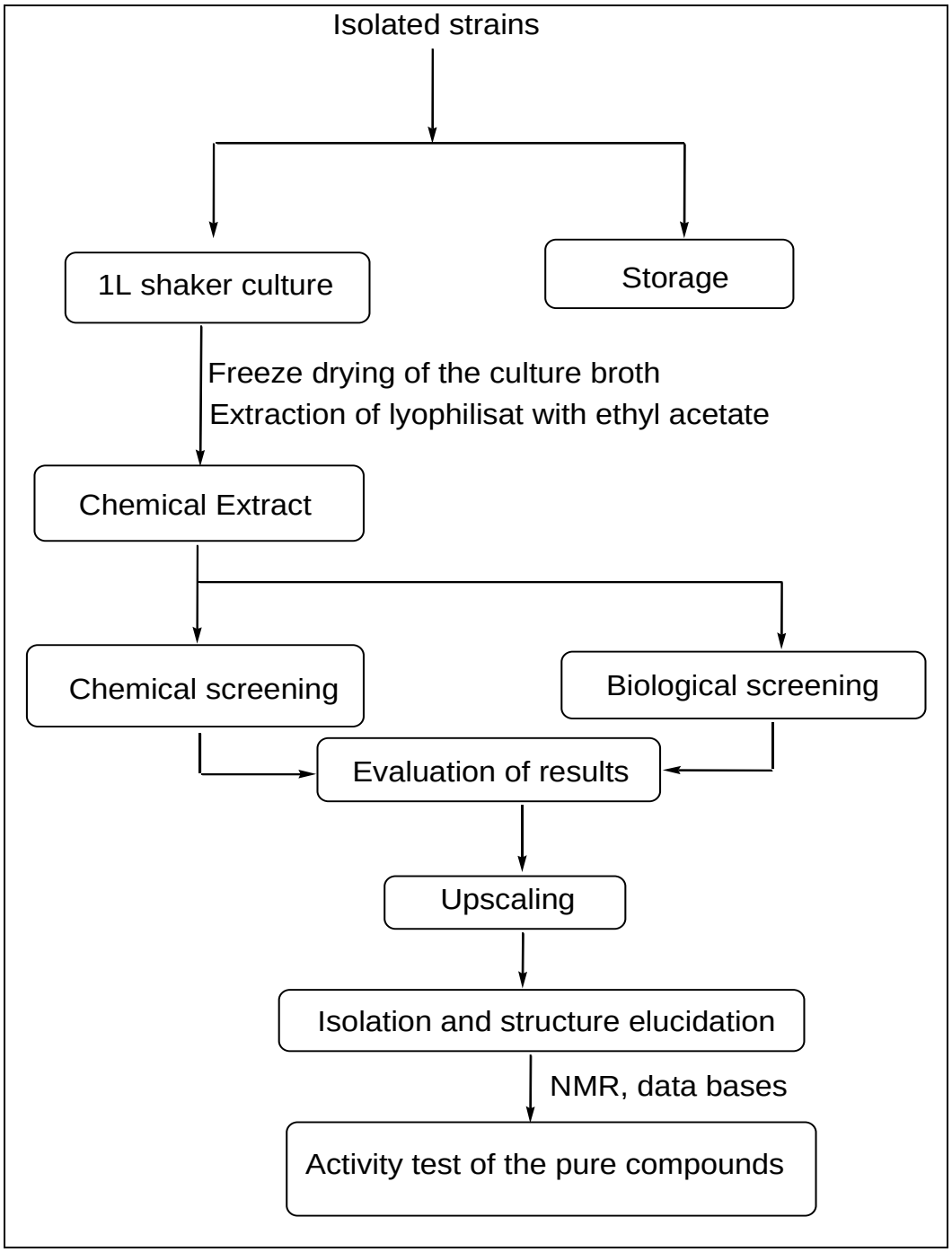

Figure 4: General screening and working up of the selected strains.

3.3.1 Chemical Screening

The isolation of pure bioactive compounds from microbial strains is a multiple-stage procedure and an expensive task. For this reason, it is important to avoid the re-isolation of known metabolites from the crude extract or a partially purified fraction. Chemical screening is one of the economical methods, which allows reaching this aim at an early stage of separation.

The Thin Layer Chromatography (TLC) is one of the simplest and cheapest methods for such a screening. In comparison with other methods (like HPLC-MS), TLC is easier, quicker, and simpler to perform, and is sufficiently reproducible. A spot of the crude extract is developed on a TLC with a suitable solvent system. The developed TLC plate is visualized under UV light, and interesting zones are further localized by exposure to spray reagents. Several spraying reagents are available for the detection, some specific, other universal. In our research group, the following reagents are used intermittently:

- Anisaldehyde/sulphuric acid spray reagent gives different colour reactions with many structural elements and is a universal reagent.
- Dragendorff's reagent is a colour reagent to detect alkaloids in a test sample. Alkaloids, if present in the solution of the sample, will react with Dragendorff's reagent and produce an orange or orange-red precipitate.
- Concentrated sulphuric acid is especially used for polyenes. Short conjugated chains are showing a brown or black colour, carotenoids develop a blue or green colour.
- Ehrlich's reagent is a specific reagent used to determine indoles and some other nitrogen-containing compounds; indoles turn pink, blue or violet, pyrroles and furans become brown, anthranilic acid derivatives change to yellow.
- Ninhydrin is used to detect terminal amino groups of amino acids and peptides.
- NaOH is used for the detection of *peri*-hydroxy-quinones, which turn red, blue or violet. The deep red prodigiosins are showing the colour of the yellow in a free base.
- Vaniline/sulphuric acid gives different colour reactions with many structural elements.

3.3.2 Pharmacological and Biological Assays

As there is still no general way to derive the biological activity of metabolites reliably solely from their structures, a multitude of pharmacological test systems has been developed. They can be subdivided into defined and complex systems: The defined systems are often using highly sophisticated receptor tests; they are often expensive, sometimes highly specific and therefore are giving low response rates, sometimes as low as 1: 20.000 and even 1: 80.000 (as in the case of platensimycin). Receptor tests are therefore less suitable for use in universities, where a quick, sensitive affordable test is required. The selectivity should be low so that broad ranges of activities can be covered; a response rate of 10-20 % is suitable.

The resulting 'horizontal screening' can be realized best with microorganisms, i.e. by the use of complex systems. Based on the agar diffusion method, the crude extracts are tested in this work against different microorganisms, the test bacterial pathogens were Gram positive bacteria *Bacillus subtilis* and *Bacillus cereus*, Gram negative bacteria *Pseudomonas areuginosa* and *Escherichia coli*, while the pathogenic yeasts were *Candida albicans*, *Saccharomyces cerevisiae* and *Trichosporon Jirovecii*. On the other hand, the plant fungal pathogens were *Botrytis cinerea* and *Alternaria porri*.

Moreover, evaluation of tyrosinase inhibitory potential and acetylcholinesterase inhibitory activity were performed using mushroom tyrosinase and L-DOPA and acetylcholinesterase enzyme solution respectively.

3.4 Large Scale Cultivation and Extraction

Generally, there is a minimum amount needed for the structure elucidation of a new compound, which is with our equipment near 1-5 mg, depending on the complexity of the structure. As additional quantities are needed for biological tests, 5-10 mg are desirable. As most strains are producing only metabolite concentrations of 0.1 – 1 mg/L, fermentation in a 10~40 L scale is necessary.

According to the pre-screening, the interesting strains were scaled up for further investigation. In some cases, in order to improve the microbial production of the interesting compounds, the optimisation of the culture conditions may be done. Well-grown agar sub-cultures were monitored and finally selected for performing the subsequent inoculation. A number of usually 100 Erlenmeyer flasks (1 L) each containing 250 ml culture medium (pH 7.5) were used for the inoculation and propagation of the bacteria on a linear shaker (28 °C). After four to five days, the culture broths were harvested, mixed with Celite (diatomaceous earth as filter aid) and filtered under pressure (filter press). The latter step is necessary to separate the water phase, which was successively adsorbed on Amberlite adsorption resin XAD-16 and the latter finally extracted with methanol. The biomass remaining after filtration was exhaustively extracted with ethyl acetate and acetone. Finally, the organic phases are evaporated to dryness, giving the desired residue for further separations. Storing extracts in the moist ethyl acetate at room temperature could result in decomposition products due to the formation of acetic acid. So, solutions should be evaporated as soon as possible, and it is strongly recommended to store the residues at low temperature to minimize degradation reactions.

3.5 Isolation methods

According to the amount of the obtained crude extracts, a suitable isolation method will be determined, with respect to the polarity of the compounds of interest. Extracts from the water phase and cell mass are combined if the composition is similar; otherwise, they are separated independently. For separation of accompanying fats, the crude extract is firstly defatted by cyclohexane, and then two preliminary separation systems are commonly used in our group:

- Centerfuginal Partition Chromatography (CPC) or flash silica gel chromatography by using a gradient of increasing polarity of various solvent systems. However, the contact with silica gel may rearrange, oxidise, cleave or even destroy the adsorbed metabolites.
- Size-exclusion chromatography (Sephadex LH-20), where the compounds are separated depending on molecular size differentiation. This technique offers the advantage of a higher recovery rate than silica gel and minimizes the destruction of compounds. It is used preferentially when the amount of the crude component is less than 3 mg.

Fractions which obtained from CPC or flash silica gel chromatography are monitored by TLC to decide the next isolation steps. The next stages of isolation could be achieved using Prep.TLC, silica gel column chromatography, Sephadex LH-20. Further purification can be done with the aid of HPLC loaded with Normal Phase (NP) or Reverse Phase (RP) columns.

3.6 Dereplication Concept and Partial Identification

The development of screening steps for the discovery of biologically active compounds has resulted in a need to prioritise those samples, which are deemed ‘active’. When these samples are derived from different natural product sources, it is estimated that it takes $50.000 and 3 months of work to isolate, identify and elucidate such an active compound and there will be a distinct sense of ‘wasted’ effort if the isolate is a well-known compound [160]. So the term *dereplication* is commonly used in the natural products community to define the complementary processes of rapid identification of natural compounds.

This might be carried out by comparing the UV[161] or MS data and HPLC retention times with appropriate reference data collections. This method needs only negligible sample amounts and affords reliable results if authentic samples had been available to measure the reference data. UV data and MS fragmentation patterns are also useful to identify unknown

metabolites if these show similar chromophores or fragmentation patterns as known analogues. As it will never be possible to collect a complete sample set and to measure all experimental data under identical conditions, reference values from the literature have to be used. If NMR data are selected, results from 1D measurements can be translated into substructures, which then will be used for a database search. In this case, normally sufficiently pure samples are required. Databases with the NMR or UV data and a variety of other molecular descriptors can be searched using computers[162]. The most comprehensive data collection of natural compounds is the Dictionary of Natural Products (DNP), which compiles metabolites from all natural sources, including plants.

As most compounds of interest are thermally labile, HPLC-ESI MS/MS would be the method of choice to identify known molecules from multi-component mixtures with high selectivity and sensitivity. The absolute configuration of the pure components can be confirmed by application of circular dichroism (CD) spectroscopy[163] and – if possible – crystal structure analysis.

4. Materials and Methods

4.1 Materials

4.1.1 General laboratory equipments

Autoclave	Varioklav, H&P
Balances	ADAM Equipment
Centrifuge	Biofuge pico, Heraeus
Clean Bench	Virkus Labco
Digital pH meter	420Aplus, Orion
Freeze dryer (Lyophilizer)	Zirbus Technology, Germany
Hot plate	Camag**,** Thermo Scientific, USA
Laminar-Flow-Box	Kojar KR-125, GmbH, Germany
Petri dishes	94 mm diameter, 16 mm height
Rotary evaporator	Buchi R-120 (BUCHI Labortechnik AG, Flawil, Switzerland
Sonicator	Elmasonic S100H, Germany
Sterile filters	Rephile, 0.2 μm, (PTFE, PES, NYLON and PVDF)
Syringes	Hamilton
Ultra-Pure Water	Evoqua LaboStar®, Pittsburgh, USA
UV Lamp	Camag (254 and 366), Switzerland
Vortex	Medline scientific, UK

4.1.2 Recipes

All cultures were autoclaved at 1.2 bar and 120 ºC. Sterilisation time for 1 L shaker culture: 33 min, 2 L concentrated medium for fermentor: 50 min and fermentor containing 16 l water: 82 min.

Artificial Seawater

Iron citrate	2.0 g (powder)
NaCl	389 g
$MgCl_2 \cdot 6H_2O$	176 g
Na_2SO_4	68.8 g
$CaCl_2$	36.0 g
Na_2HPO_4	0.16 g
SiO_2	0.30 g
trace element stock soln.	20 mL
stock soln.	200 mL
tap water	ad 20 L

Trace element stock solution

H_3BO_3	0.611 g
$MnCl_2$	0.389 g
$CuSO_4$	0.056 g
$ZnSO_4.7\ H_2O$	0.056 g
$Al_2(SO_4)_3.18\ H_2O$	0.056 g
$NiSO_4.6\ H_2O$	0.056 g
$CO(NO_3)_3.6\ H_2O$	0.056 g
TiO_2	0.056 g
$(NH_4)_6Mo_7O_{24}.4\ H_2O$	0.056 g
LiCl	0.028 g
$SnCl_2$	0.028 g
KI	0.028 g
tap water	ad 1 L

Stock solution

KCl	110 g
$NaHCO_3$	32 g
KBr	16 g
$SrCl_2 . 6H_2O$	6.8 g (dissolved separately)
H_3BO_3	4.4 g
NaF	0.48 g
NH_4NO_3	0.32 g
tap water	ad 2 L

4.1.3 Media

Composition of malt agar (MA) medium

MA medium was used for short term storage of fungal cultures or fresh seeding for the preparation of liquid cultures.

Agar-agar	15 g
Malt extract	15 g
Distilled water	to 1000 ml
pH	7.4 - 7.8

Composition of potato dextrose agar (PDA) medium

Potato infusion [a]	200 g
Dextrose	20 g
Agar	20g
Artificial seawater	500 ml
Distilled water	500 ml
pH	7.2

[a] Potato infusion: The potatoes (200 g) were first washed and cut into small pieces, then boiled in 1000 mL distilled water for 1 hour and filtered to get the potato infusion.

Composition of International Streptomyces Project-2 (ISP2) medium

Malt extract	10 g
Glucose	4 g
Yeast extract	4 g
Artificial seawater	500 ml
Tap water	500 ml
pH	7.8

Composition of rice medium for solid cultures

Rice	100 g
Distilled water	75 ml
Artificial seawater	75 ml

Water was added to the rice and kept overnight before autoclaving.

Composition of Medium Test Agar (for test organisms *Escherichia coli*, *Bacillus subtilis*, *Staphylococcus aureus*)

Malt extract	10 g
Yeast extract	4 g
Glucose	4 g
Bacto agar	4 g
Malt extract	20 g
Demineralised water	1000 ml

The pH was adjusted to 7.8 using 2N NaOH.

Composition of Sabouraud-Agar (for test organism *Candida albicans*)

Glucose	40 g
Bacto peptone	10 g
Bacto agar	20 g
Demineralised water	1000 ml

The pH was adjusted to 7.8 using 2N NaOH.

4.1.4 Chemicals

4.1.4.1 General laboratory chemicals

(-)-2-Butanol	
Acetic anhydride	
Anisaldehyde (4-methoxybenzaldehyde)	
Concentrated ammonia solution	
Concentrated sulphuric acid	Merck KGaA (Darmstadt, Germany
Dimethylsulfoxide	
Formaldehyde	
Hydrochloric acid	
L-(+)-Ascorbic acid	
Potassium hydroxide	
Pyridine	
Sodium hydroxide	
Trifloroacetic acid (TFA)	Merck KGaA (Darmstadt, Germany
Vanillin	Merck KGaA (Darmstadt, Germany

4.1.4.2 Chemicals for culture media

Acetylthiocholine iodide (ATCI)	Sigma-Aldrich
Acetylcholinesterase (AChE)	Sigma-Aldrich
Agar-agar	Galke
Galanthamine hydrobromide	Sigma-Aldrich
Glucose	Caelo
L-DOPA	Sigma-Aldrich
Malt extract	Merck
NaCl	Merck
Peptone	BD
Streptomycin	Sigma
Yeast extract	Sigma
5,5′-dithio-bis(2-nitrobenzoic acid)	Sigma-Aldrich

4.1.5 Chromatography

Pre-coated TLC plates, Silica Gel 60 F254, layer thickness 0.2 mm	Merck
Silica Gel 60, 0.04 - 0.063 mm mesh size	Merck
Pre-coated TLC plates, RP-18, F254 S, layer thickness 0.25 mm	Merck
RP-18, 0.04 - 0.063 mm mesh size	Merck
Sephadex LH 20, 0.25 - 0.1 mm mesh size	Merck

4.1.6 Spray reagents

The reagents were stored in amber-coloured bottles and kept refrigerated until use. TLC was used to monitor the identity of each of the fractions and the qualitative purity of the isolated compounds. It was also utilized to optimize the solvent system that would be applied for column chromatography.

Anisaldehyde/sulphuric acid: 1 ml anisaldehyde was added to 100 ml of a stock solution containing 85 ml methanol, 14 ml acetic acid and 1 ml sulphuric acid.

Dragendorff's reagent: is a solution of potassium bismuth iodide composing of basic bismuth nitrate ($Bi(NO_3)_3$), tartaric acid, and potassium iodide (KI), and when contact with alkaloids it produces an orange or orange red precipitate.

Ehrlich's reagent: 1.0 gm (4-dimethylaminobenzaldehyde) was dissolved in a mixture of 25 ml hydrochloric acid (37%) and 75 ml methanol, give red colouration with indol and yellow for other N-heterocycles.

Ninhydrin: 0.3 g ninhydrin (2,2- dihydroxyindan-1,3-dione) was dissolved in 95 ml isopropanol. The mixture was added to 5 ml collidin (2,4,6-trimethylpyridin) and 5 ml acetic acid (96%). This re- agent gave a blue to a violet colouration with amino acids, peptides and polypeptides with free amino groups. Ninhydrin in ethanol (0.1 %) was also directly used.

NaOH or KOH: 2 N NaOH or KOH solutions are used to identify *peri*- hydroxyquinones by deepening the colour from orange to violet or blue.

Vanillin/ sulphuric acid: stock a: Vanillic acid (5.0 g) was dissolved in100 ml of methanol. Stock b: 5 ml concentrated sulfuric acid added slowly to 95 ml of methanol. When used, equal quantities are added and mixed well.

4.1.7 Solvents

General solvents

Acetone, acetonitrile, dichloromethane, ethanol, ethyl acetate, n-hexane, n-butanol and methanol were used. The solvents were purchased from Fisher Scientific, Loughborough, UK. They were distilled before using and special grades were used for spectroscopic measurements.

Solvents for HPLC

Acetonitrile	Fisher Scientific, Loughborough, UK
Cyclohexane	CARLO ERBA, France
Chloroform	Fisher, UK
Ethyl acetate	CARLO ERBA, France
Isopropanol	Fisher, UK
Methanol	Fisher, UK
Nano pure water	Distilled and heavy metals free water obtained by passing distilled water through nano- and ion exchange filter cells (Barnstead, France)

Solvents for LC-MS

MeOH LC-MS grade	LiChrosolv® Fisher Scientific, Loughborough, UK
ACN LC-MS grade	LiChrosolv® Fisher Scientific, Loughborough, UK
Formic acid (FA)	Fisher Scientific, Loughborough, UK
Trifluoroacetic acid (TFA)	Fisher Scientific, Loughborough, UK

Solvents for NMR

Acetone-*d6*	Merck, Darmstadt, Germany
Chloroform-*d*	Merck, Darmstadt, Germany
DMSO-*d6*	Merck, Darmstadt, Germany
Methanol-*d4*	Merck, Darmstadt, Germany
Pyridine-*d5*	Merck, Darmstadt, Germany

4.2 Methods

4.2.1 Isolation, Purification and cultivation of fungal strains

Aspergillus ochraceopetaliformis

The fungal strain was obtained from a soil sample collected at Giza province, Egypt, in 2015. The sediment sample was suspended in sterile water and incubated into a reciprocal water bath at 30 ºC for 30 min, and then the samples have been serially diluted under aseptic conditions. 100 µl from each dilution have been plated on PDA medium (**Figure 5**). The plates were then incubated at 35 ºC for 6-8 weeks, then the strain was isolated, transferred onto freshly prepared solid media and. deposited in a refrigerator at 4 ºC at Microbial Chemistry Department, National Research Centre (NRC), Egypt until use.

The spore suspension of the selected strain ASAI was inoculated into 100 mL of ISP2 medium and incubated at 30 ºC for 3 days as seed culture. 5 mL of previously prepared seed culture were used to inoculate 5× 1L sterilized Erlenmeyer flasks (each 5 flasks) containing rice. The flasks were incubated for 14 days at 35 ºC[164].

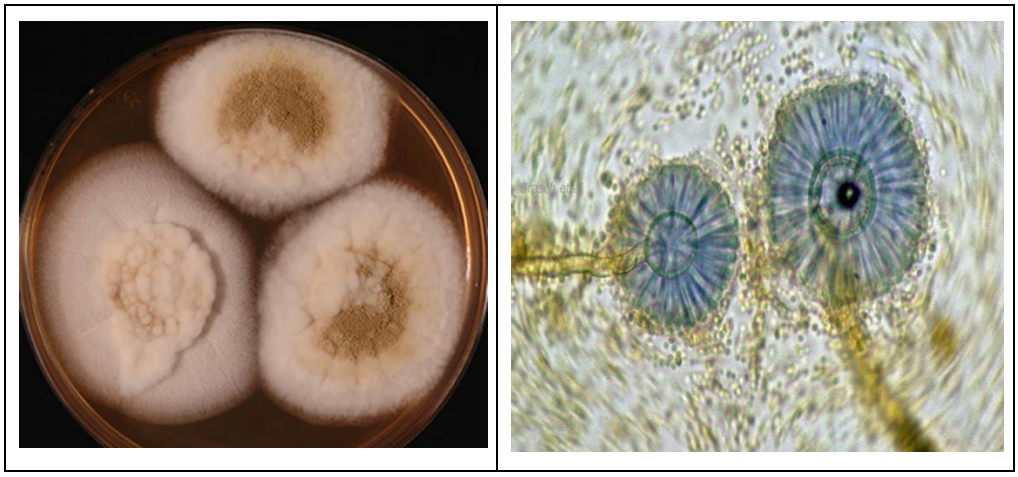

Figure 5: A: colony after 7 days on PDA medium; B: scanning electron micrograph photo of conidia

Myrothecium verrucaria

Ten samples of healthy wild medicinal plant *datura* (*Datura stramonium L.*) were collected from Wadi El Assuity, protective area, Assiut Governorate, Upper Egypt in 2015. The collected samples were packed into sterilized polyethylene bags and directly transferred to the mycological laboratory at Botany and Microbiology Department, Assiut University, Egypt. Plant leaves were thoroughly washed with running tap water to remove dust and spores deposited from the air, washed several times with sterilized distilled water and then dried thoroughly using a sterilized paper towel.

Endophytic fungi were isolated through surface sterilization technique. Datura leaves were sterilized using 75% ethanol for 1 min, followed by immersion in 1% sodium hypochlorite for 5 min and again in 75% ethanol for 30s. Leaves were washed by sterilized distilled water, dried thoroughly between the sterilized paper towel and cut into segments (1 cm^2) in a laminar airflow chamber. For each sample, twenty leaf segments were placed on the surface of the PDA medium and then they were incubated at 25°C for 3 days. The count of endophytic fungi was calculated as colony-forming units (CFU) per 200 leaf segments (**Table 2**). Fungi emerging out of the plant tissues were purified using a hyphal tip technique.

Preliminary, the purified fungi were identified according to their macroscopic and microscopic characteristics described in different mycological keys (**Figure 6**). The fungus was cultivated on Erlenmeyer flasks (250 mL) containing 100 mL of potato dextrose broth and then incubated for 30 days at 25 ºC with agitation (150 rpm/min). The fungal pellets were discarded, while the culture broth was filtered through Seitz filter 0.20 μm.

Table 2: Endophytic fungi associated with leaves of *Datura stramonium* using PDA medium at 25 ± 1 ºC.

Fungal species	**TC**	**%TC**	**%F**
Alternaria alternata (Fr.) Keissler	23	11.92	30
Aspergillus niger Tiegh.	17	8.81	20
Chaetomium globosum Kunze	16	8.29	20
Cladosporium sphaerospermum Penzig	25	12.95	30
Fusarium oxysporum Schlecht	16	8.29	20
Gliocladium roseum Bainier	5	2.59	10
Myrothecium verrucaria (Alb. & Schwein.) Ditmar	39	20.21	50
Nigrospora sphaerica (Sacc.) Mason	16	8.29	20
Penicillium duclauxii Delacroix	5	2.59	10
Stemphylium vesicarium (Wallr.) Simmons	18	9.33	30
Torula graminis Desmazieres	3	1.55	10
Trichoderma harzianum Rifai	10	5.18	20
TC (CFU / 200 leaf segments)		**193**	
Number of genera		**12**	
Number of species		**12**	

TC: total fungal count (CFU / 200 leaf segments); %TC: percentage of total fungal count; %F: % frequency of fungi per 10 collected samples.

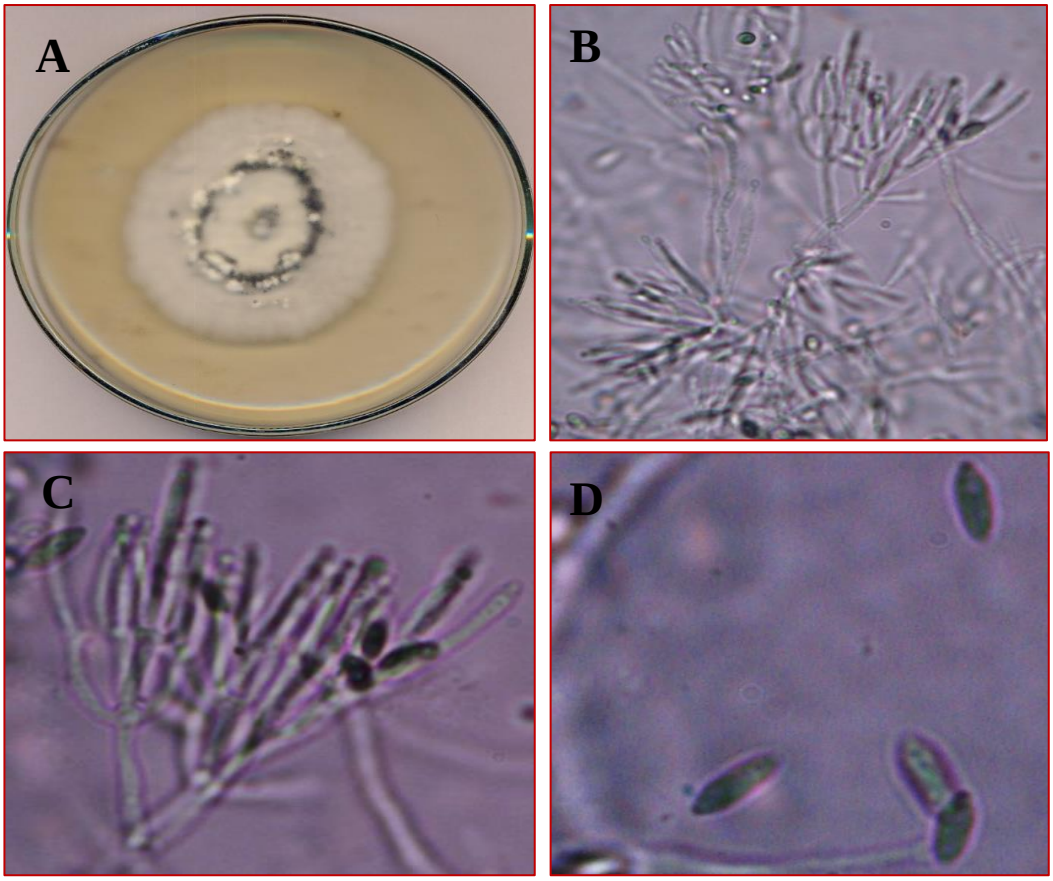

Figure 6: A: The colony was 4.5 cm after 7 days on PDA medium at 25℃ and whitish with black sporodochia. B: Conidiophores were repeatedly branched and compacted. C: Phialides were lanceolate or cylindrical, compacted and closely packed in a parallel layer forming sporodochia. D: Conidia were broadly fusiform with the pointed apical end and bulged basal end.

4.2.2 Identification of fungal strains and their taxonomy

4.2.2.1 Fungal identification

Fungal strains were identified using a molecular biological protocol by DNA amplification and sequencing of the internal transcribed spacer (ITS) region.

Aspergillus ochraceopetaliformis

The DNA concentration was 100 ng/µl, Volume 20 µl. The PCR product was detected by agarose gel and visualized by (UV) fluorescence after ethidium bromide staining[165]. The results of 18S rRNA sequence were compared to the available database at GenBank using BLAST software (blastn) on National Centre Biotechnology Information (NCBI). Based on the morphological, 18S rRNA gene sequence and phylogenetic data the

fungus ASAI was taxonomically characterized *Aspergillus ochraceopetaliformis* (accession no. MN611443).

Myrothecium verrucaria

For DNA extraction, the fungus was grown on PDA media and incubated at 25 °C for 3 days and then fungal growth was scraped and suspended in 100µl of distilled water and boiled at 100 ºC for 15 minutes and stored at -80 ºC. DNA was extracted from fungal cultures using the genomic DNA Prep kit (SolGent, Daejeon, Korea) according to SDS/CTAB lysis and phenol/chloroform extraction method[166].

The ribosomal rRNA gene was amplified via the polymerase chain reaction (PCR) using primer pair ITS1 (5'-CTTGGTCATTTAGAGGAAGTAA-3') and ITS4 (5'-TCCTCCGCTTATTGATATGC-3')[167]. Fungal DNA (1 µl) was amplified in a 25 µl reaction mixture with Solgent EF-Taq as follows: 10X EF-Taq buffer 2.5 µl, 10 mM dNTP (T) 0.5 µl, primer (Forward-10 picomol) 1.0 µl, primer (Reverse -10 picomol) 1.0 µl, E(2.5U) 0.25µl, Distilled Water (to 25µl). The thermocycling conditions included an initial denaturation for 15 s at 95 ºC, followed by 30 cycles of denaturation for 20 s at 95 ºC, annealing for 30 s at 55 ºC and extension for 60 s at 72 ºC, and a final extension of 10 min at 72 ºC. The PCR product was separated by gel electrophoresis on 1% agarose gel run for 75 min in buffer TAE (40 mM Tris, 20 mM sodium acetate, 1 mM EDTA, pH 7.2) and visualized using a UV illuminator. The PCR product corresponding to ribosomal ITS, according to electrophoretic migration, was eluted from the gel and then purified using a SolGent PCR purification kit (SolGent, Daejeon, South Korea) according to the manufacturer's instructions.

The amplified ribosomal ITS region was sequenced in the sense and antisense directions using ITS1 and ITS4 primers and dideoxynucleotides (dd NTPs) in the reaction mixture. Sequences were analyzed using the BLAST search program at National Center for Biotechnology Information (at the NCBI website: http://blast.ncbi.nlm.nih.gov/Blast.cgi). Multiple sequence alignment and molecular phylogeny were performed using CLUSTALW program (http://clustalw.ddbj.nig.ac.jp/top-ehtml). The phylogenetic tree was constructed with referential strains from GenBank using MegAlign software (DNAStar 5.01). Successively, the amplified and sequenced fragment of the 18S ribosomal DNA gene (536 base pair) confirmed that *M. verrucaria* strain ASU7 has a 99.7% similarity to *M. verrucaria* strain I-5 (KT305924). Next, the obtained sequence of *M. verrucaria* strain ASU7 was deposited in the GenBank nucleotide sequence database under accession number KX611156.

4.2.2.2 Taxonomy

Aspergillus ochraceopetaliformis

The fungal strain was isolated from a soil sample collected at Giza province, Egypt. Taxonomically, the strain was identified as *Aspergillus ochraceopetaliformis* on the bases of phenotypic and genotypic characterizations

Taxonomy

Domain: Eukaryota
Kingdom: Fungi
Phylum: Ascomycota
Subphylum: Pezizomycotina
Class: Eurotiomycetes
Subclass: Eurotiomycetidae
Order: Eurotiales
Genus: *Aspergillus*
Species: *Aspergillus ochraceopetaliformis*

Myrothecium verrucaria

The fungus *Myrothecium verrucaria* was isolated from fresh leaves of healthy wild medicinal plant datura (*Datura stramonium* L.) which collected from Wadi El Assuity, protective area, Assiut Governorate, Upper Egypt at 2015.

Taxonomy

Domain: Eukaryota
Kingdom: Fungi
Phylum: Ascomycota
Subphylum: Pezizomycotina
Class: Sordariomycetes
Subclass: Hypocreomycetidae
Order: Hypocreales
Genus: *Myrothecium*
Species: *Myrothecium verrucaria*

4.2.3 Extraction of fungal liquid cultures

After harvesting, the culture broth was mixed with methanol and filtered under vacuum. The filtered aqueous methanol was concentrated in vacuo, and the remaining water residue was re-extracted by an equal volume of ethyl acetate using a separation funnel. Then the organic layers were combined, dried through anhydrous sodium sulfate and filtered. The solvent was evaporated under vacum.

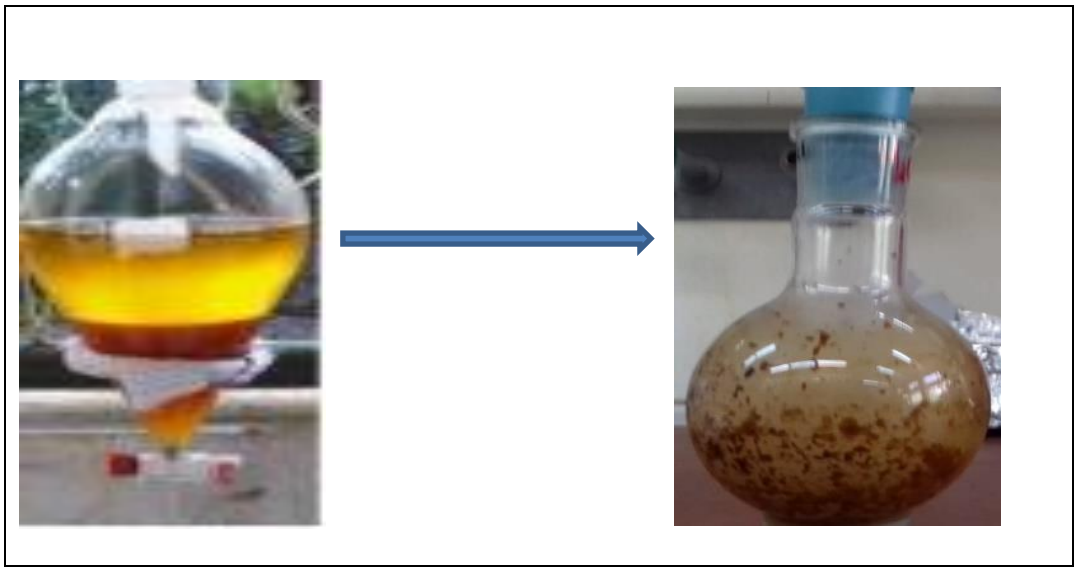

Figure 7: Extraction of fungal liquid cultures using ethyl acetate separation funnel.

4.2.4 Isolation and purification of secondary metabolites

4.2.4.1 Isolation of the secondary metabolites from *A. ochraceopetaliformis*

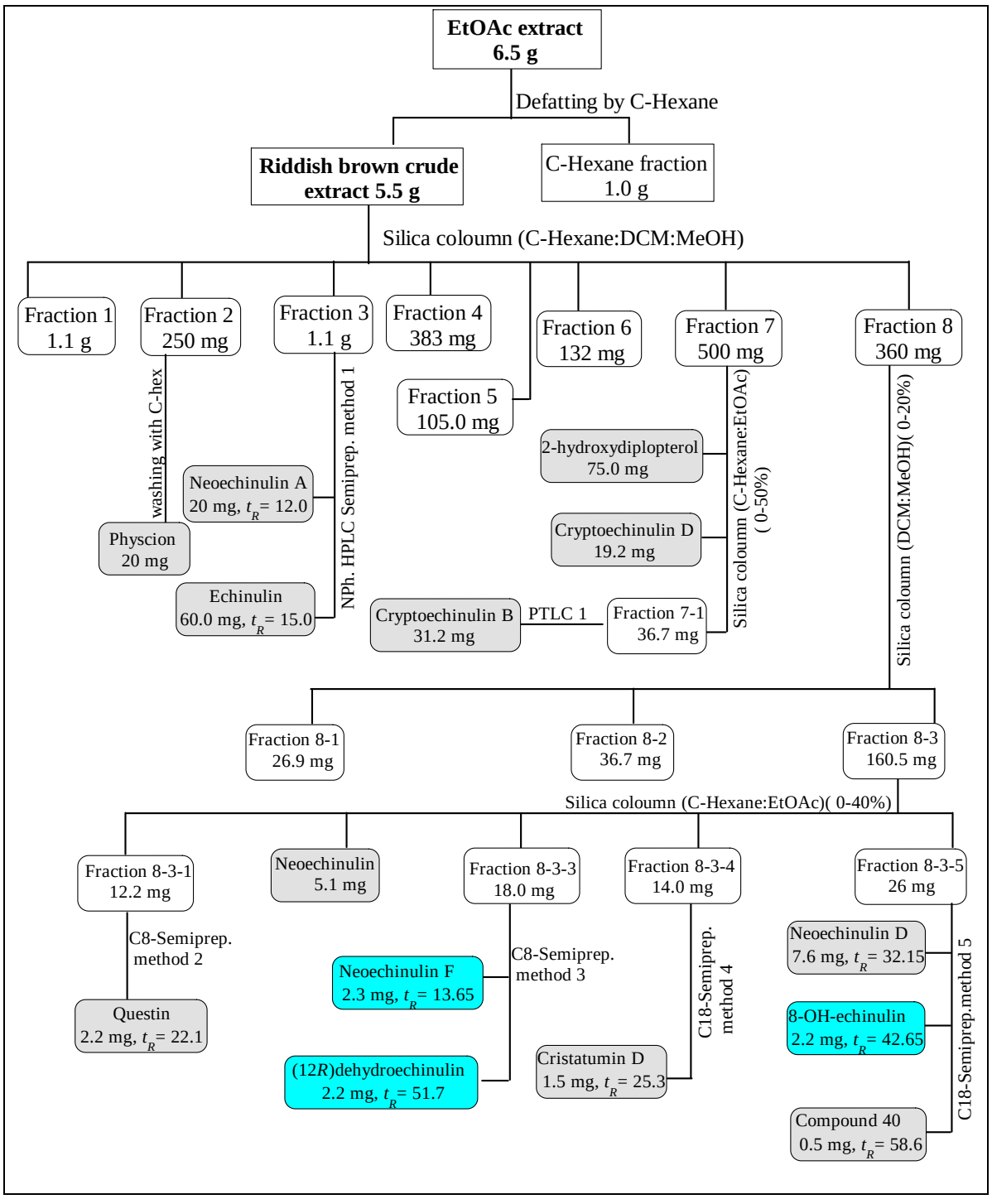

Figure 8: Work-up procedure of *Aspergillus ochraceopetaliformis*, part one

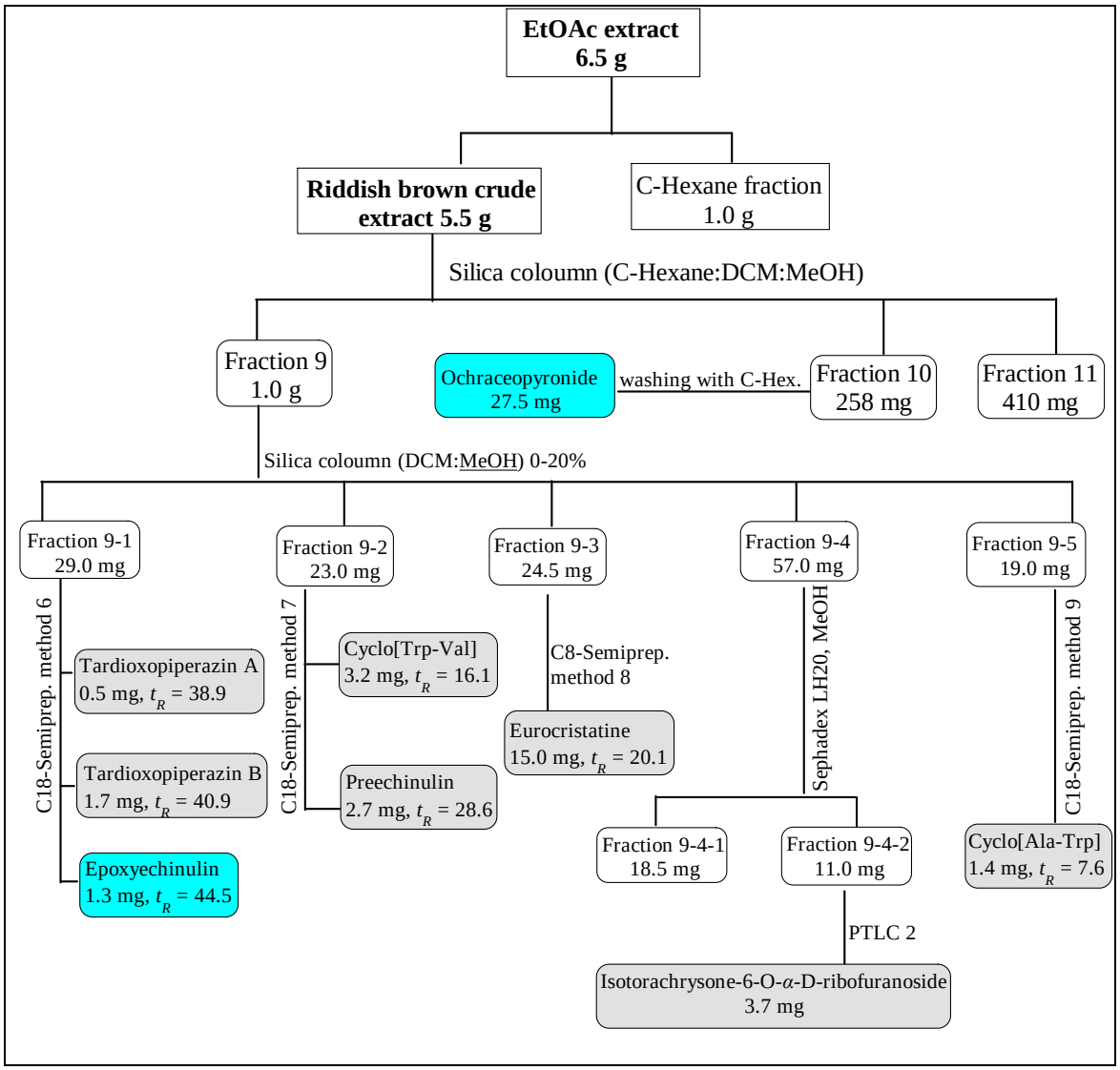

Figure 9: Work-up procedure of *Aspergillus ochraceopetaliformis*, part two.

Table 3: Characteristics of HPLC methods used for the isolation of *Aspergillus ochraceopetaliformis* metabolites

No	Column	Method	Solvent System	Flow rate (ml/min)	Time (min)
1	Silica, semiprep.	isocratic	(EtOAc/$CHCl_3$/Isopropanol) (30/65/5)	3.0	25
2	C8 semiprep.	Gradient	H_2O/MeOH (65/35), (25/75), (20/80) (5/95) and (65/35)	1.5	55
3	C8 semiprep.	Gradient	H_2O/MeOH (65/35), (25/75), (20/80) (5/95) and (65/35)	1.5	70
4	C-18, semiprep.	Gradient	H_2O/MeOH (65/35), (25/75), (20/80) (5/95) and (65/35)	1.5	55
5	C-8, semiprep.	Gradient	H_2O/MeOH (60/40), (25/75), (20/80) (5/95) and (65/35)	1.5	70
6	C-18, semiprep.	Gradient	H_2O/MeOH (60/40), (20/80), (10/90), and (60/40),	2.0	55
7	C-18, semiprep.	Gradient	H_2O/MeOH (50/50), (30/70), (20/80) (2/98), and (50/50)	2.0	60
8	C-8, semiprep.	Gradient	H_2O/MeOH (50/50), (35/65), (25/75) (5/95), and (50/50)	1.8	55
9	C-18, semiprep.	Gradient	H_2O/MeOH (50/50), (30/70), (20/80) (2/98), and (50/50)	2.5	55

PTLC 1: The eluent was (DCM/MeOH 7%)

PTLC 2: The eluent was (DCM/MeOH 7%)

4.2.4.2 Isolation of the secondary metabolites from *Myrothecium verrucaria*

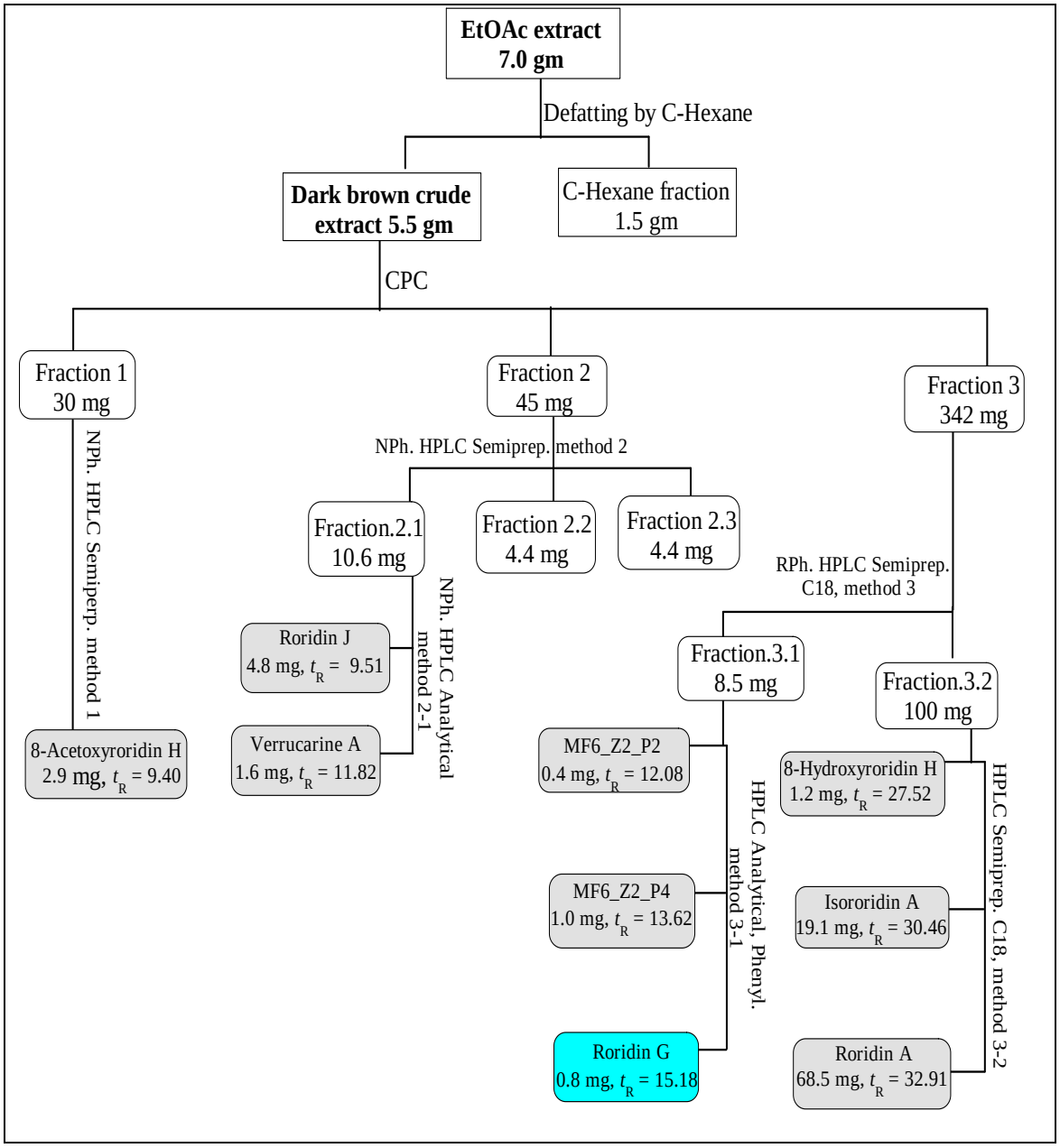

Figure 10: Work-up procedure of *Myrothecium verrucaria*, part one.

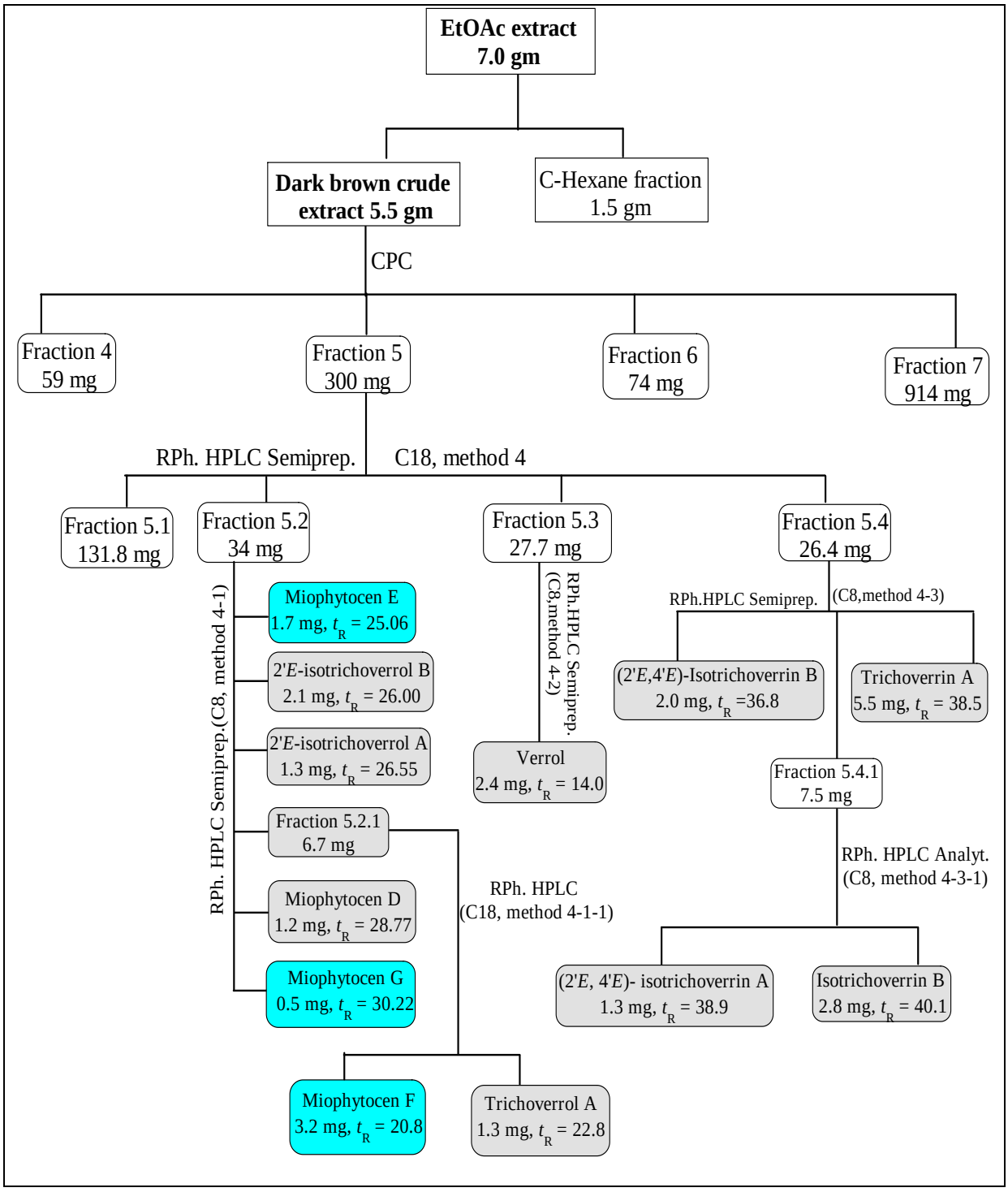

Figure 11: Work-up procedure of *Myrothecium verrucaria*, part two.

Table 4: Characteristics of HPLC methods used for the isolation of *Myrothecium verrucaria* metabolites

No	Column	Method	Solvent System	Flow rate (ml/min)	Time (min)
1	Silica, semiprep.	isocratic	(C-Hex/EtOAc/$CHCl_3$/Isopropanol) (60/28/9/3)	3.0	25
2	Silica, semiprep.	isocratic	(C-Hex/EtOAc/$CHCl_3$/Isopropanol) (50/30/15/5)	2.0	30
2-1	Silica, semiprep.	isocratic	(C-Hex/EtOAc/$CHCl_3$) (72/23/5)	1.2	20
3	C18 semiprep.	Isocratic & Gradient	H_2O/MeOH (50/50), (5/95) and (95/5)	4.0	30
3-1	Phenyl, Analytic.	Gradient	H_2O/MeOH/ACN (70/15/15), (5/50/45), and (70/15/15)	1.0	20
3-2	C-18, semiprep.	Isocratic & Gradient	H_2O/MeOH (60/40), (5/95) and (60/40)	3.0	60
4	C-18, semiprep.	Gradient	H_2O/MeOH (98/2), (35/65), (2/98), and (98/2)	2.0	55
4-1	C-8, Analytic.	Gradient	H_2O/ACN (98/2), (35/65), (2/98), and (98/2)	2.0	50
4-1-1	C-18, semiprep.	Gradient	H_2O/MeOH (70/30), (50/50), (30/70), and (70/30)	4	37
4-2	C-8, semiprep.	isocratic	H_2O/MeOH (55/45)	4.0	50
4-3	C-8, semiprep.	Gradient	H_2O/ACN (98/2), (35/65), (2/98), and (98/2)		50
4-3-1	C-8, Analytic	Gradient	H_2O/ACN (98/2), (35/65), (2/98), and (98/2)		50

4.2.5 Chromatographic methods

4.2.5.1 Centrifugal Partition Chromatography (CPC)

General aspects and principles

Centrifugal Partition Chromatography (CPC) is one of the embodiments of Counter-Current Chromatography (CCC) introduced by Wataru Murayama and co-workers in 1982[168] and refers to a particular type of support-free liquid-liquid chromatographic technique[169,170]. The separation mechanism in CPC is based on differences in distribution coefficients (KD) of analytes between two immiscible solvent systems. While one liquid remains in the column as the stationary phase by conforming to the application of a centrifugal field, the other is pumped through as the mobile phase. A CPC column consists of a series of partition cells connected together by narrow ducts. These partition cells and ducts are engraved in polymeric or stainless steel partition disks connected and stacked to form the chromatographic column also called the rotor[171].

Due to the liquid nature of the stationary phase and the absence of any solid support, this technique provides many advantages over conventional liquid chromatographic techniques such as high selectivity attained by the skilled design of a solvent system, high loading capacity, low solvent consumption, high sample recovery, no adsorption onto a solid support, and relatively easy scale-up[172,173]. Therefore, CPC serves as an efficient alternative liquid chromatographic technique for preparative separations and purifications at a laboratory scale. In addition to the advantages of the CPC technique, with the wide variety of solvent combinations available to form a biphasic solvent system and skilled design of such systems, high selectivity for the targeted compounds can be obtained. Once the solvent combination for a freely soluble analyte has been determined in both organic and aqueous phases, it is important to adjust the solvent ratio to obtain a KD of the target analyte between 0.5 and 2.0[174].

The industrialization of CPC or CCC processes involves four main aspects: the development of production-scale equipment, separation process intensification, scale-up rules knowledge, and environmental and regulatory aspects. As mentioned above, industrial devices are available on the market for both CCC and CPC devices. The information collected from CPC or CCC users of pilot or production apparatus and various published results[175] show that the scaling up is quite straightforward when the process is well developed at the lab-scale, with even sometimes a positive effect on the quality of separation. Concerning the last point, whereas the environmental impact of the technology

is positive, due to reduced consumption of the solvents, the regulatory constraints have not yet been delineated, as no industrial process, using CPC or CCC, has yet been implemented.

Figure 12: CPC instrument used in our group.

The crucial point concerns the intensification of the process at a laboratory scale because this step conditions the economic viability of the process as well as the optimal capacity of the column. In this optimization process, some aspects are specific to the support-free chromatographic techniques insomuch as they are based on the use of two liquid phases in thermodynamic equilibrium. The introduction of a sample in the biphasic solvent system necessarily disturbs this equilibrium, especially when amass overload is applied, resulting often in a partial or total loss of stationary phase. This aspect has been studied for the purification of 5-n-alkylresorcinols for which the construction of the "mobile phase/stationary phase/sample" ternary diagram allowed characterization of the effect of the injected solution on both mobile and stationary phases[176].

The position of the binodal curve maximum of the pseudo ternary diagram indicates whether the biphasic system is "robust" toward a large injection or not, and this simple tool can be used for the determination of both the maximum mass concentration and the optimal (mobile phase)/ (stationary phase) ratio in the injection volume. Moreover, it is necessary to check the impact of the sample on the physicochemical properties (mainly density and viscosity) of the phases. For instance, increasing the concentration of the sample in the biphasic system can increase the density of the upper phase and thus reduce or even reverse the density difference between the two phases.

Solvent selection strategy

The solvent system plays a critical role in the selectivity of compounds separated in CPC The selection of a solvent system for CPC is similar to the selection of a column and mobile phase for HPLC[177]. Each of the solvents used must fully dissolve the sample without compromising its stability. Additional criteria for the selection of appropriate CPC solvents include volatility, toxicity, availability, environmental friendliness, and cost. Hoppman et al. discussed the selection of "good solvents" for a target analyte isolated using CCC/CPC[178].

Once good solvents with high solvent solubility and capacity have been selected, options for the biphasic liquid solvent system (i.e. the liquid mobile phase and stationary phase) can be considered. Then, solvent optimization is performed by adjusting the solvent composition to ensure the distribution ratio of the solutes falls into a useful range of values; this generally centers KD near 1, in contrast to more conventional chromatographic methods [177]. The most commonly used biphasic solvent systems in CCC and CPC experiments are made of three solvents (ternary solvent systems). A large choice of ternary solvent systems is available in the literature, and sometimes several systems can be suitable for the same application[179]. The solvent systems composed of an organic phase and an aqueous phase are the most popular in conventional CCC or CPC processes. Three types of ternary solvent systems can be distinguished according to their phase diagrams Type 0 solvent systems are composed of three solvents fully miscible by pairs but for which a zone exists in the ternary diagram where a biphasic system occurs. This is the case of the solvent system composed of tetrahydrofuran (THF), dimethylsulfoxide (DMSO) and water[180].

Most solvent systems are conformed to type 1 (for instance chloroform/methanol/water), composed of one solvent miscible to the two other immiscible solvents. In the corresponding ternary diagrams (**Figure 13**). The binodal is the borderline separating the monophasic and the biphasic zones. Along the tie-line, any point corresponds to the same composition of the left and right phases, but with different volume ratios. The plait point indicates that the compositions of the left and right phases become identical and partition coefficients converge to 1. A few systems composed of three solvents result in type 2 ternary diagram. This is the case for instance of ethyl acetate/*n*-butanol/water for which the binodal is in two parts without plait point.

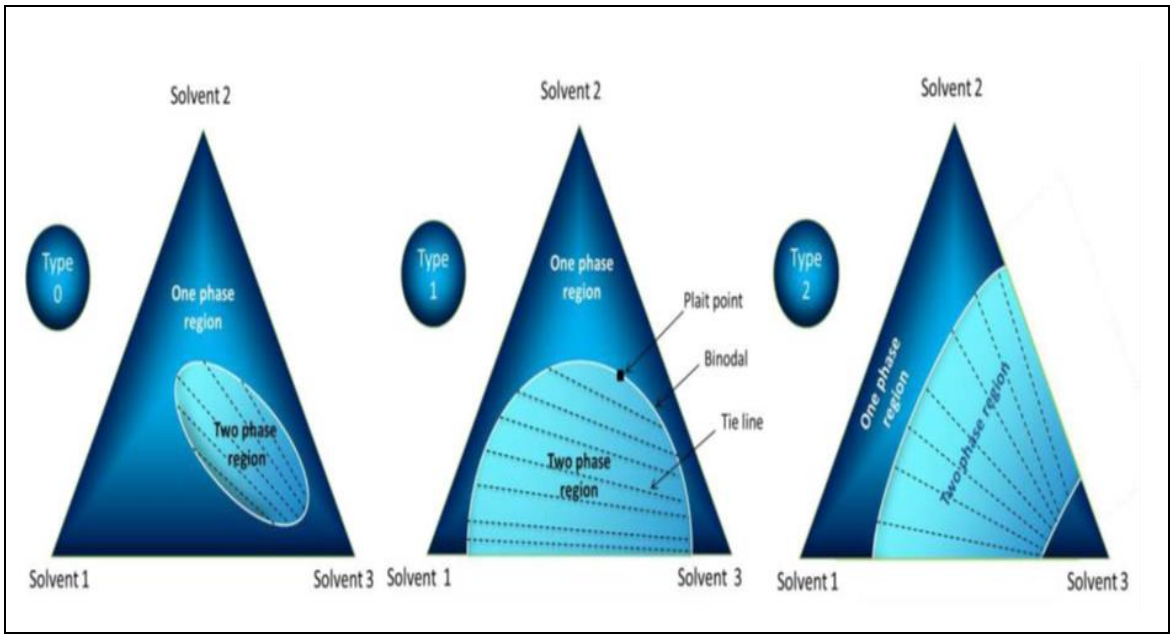

Figure 13: Phase diagrams for ternary solvent systems: equilateral triangle representation.

The most widely applied biphasic solvent systems for CPC include: the "Arizona" system (also referred to as HEMW at, rep-resenting heptane (or hexane), ethyl acetate, methanol and water)[181]; the Oka scale (as named after Oka et al.) which is composed of hexane, ethyl acetate, n-butanol, methanol, and water[182]; and the acetone scale which is composed of heptane, toluene, acetone, and water[183]. The biphasic liquid solvent systems for CPC often contain a mixture of three or four solvents, and the number of options for implementing biphasic systems is vast. This makes CPC a versatile and powerful method for the separation of a wide variety of compounds; however, the development of a small set of useful phases to fit with a given application remains challenging. The development of a biphasic CPC solvent system is similar to the selection of an HPLC column and eluents.

In our work, we used this technique with the crude extract of *Myrothecium verrucaria*. The biphasic solvent systems were detected after many trials with the solvent systems and the best was a gradient system. The selected solvent system of heptane/ethyl acetate/ n-butanol/ methanol/ water was used at ratios as in (**Table 5**) and prepared by mixing the solvents in a separatory funnel. After that, the solvent mixture was vigorously shaken, and allowed to settle at room temperature for at least 1 h or until both phases became transparent. The solvent system was freshly prepared immediately before use.

Fast Centrifugal Partition Chromatography (FCPC) was performed on a Rousselet-Robatel Kromaton FCPC system (Annonay, France), equipped with 1 L column, a Lab Alliance pump and a Buchi C-660 fraction collector (**Figure 12**).

Table 5: Gradient system used for CPC of *Myrothecium verrucaria* crude extract.

Heptane	Ethyl acetate	n-butanol	Methanol	Water
4	2	0	2.5	3.5
2	4	0	2.5	3.5
1	4.5	0.5	2.5	3.5
0.5	3	2.5	2.5	3.5
0.5	2	3.5	2.5	3.5

Table 6: Characteristic of the used method

Mode	Ascending
Mobile Phase	Organic Phase (UP)
Stationary Phase	Aqueous Phase (LP)
Sample weight	1.0gm in 15 mL UP 13mL LP
V_{COLUMN}	200 mL
V_M	75 mL
V_S	200-75 = 125 mL = 65 % SP retention
Flow rate	25 mL/ min for loading SP; 10 mL/min for equilibration and elution; 25 mL for extrusion
RPM	500 rpm for loading SP; 1500 rpm for equilibration, elution and extrusion

4.2.5.2 Thin Layer Chromatography (TLC)

Chromatography refers to any separation method in which the components are distributed between the stationary phase and mobile phase. The separation occurs because sample components have different affinities for the stationary and mobile phases and therefore move at different rates along the TLC plates and the column. TLC was performed on pre-coated TLC plates with silica gel 60 F254 (layer thickness 0.2 mm, E. Merck, Darmstadt, Germany) with the following eluents:

For polar compounds EtOAc:MeOH:H_2O (30:5:4, 30:6:5 and 30:7:6)

For semi-polar compounds DCM:MeOH (95:5, 90:10, 85:15, 80:20 and 70:30)

DCM:MeOH:EtOAc (90:10:5 and 80:20:10)

$CHCl_3$:EtOAc:Isopropanol (55:40:5)

For non-polar compounds n-Hexane:EtOAc (95:5, 90:10, 85:15, 80:20 and 70:30)

n-Hexane:MeOH (95:5 and 90:10)

TLC on reversed-phase RP18 F_{254} (layer thickness 0.25 mm, Merck, Darmstadt, Germany) was used for polar substances and using the different solvent systems of MeOH:H_2O (90:10, 80:20, 70:30 and 60:40). The band separation on TLC was detected under UV lamp at 254 and 366 nm, followed by spraying the TLC plates with anisaldehyde/H_2SO_4 or vaniline/H_2SO_4 reagent and subsequent heating at 110 ºC.

4.2.5.3 Column chromatography

The crude extract of *Aspergillus ochraceopetaliformis* was subjected to open column chromatography on silica gel (100 x 5 cm, 150 gm of silica) and gradually eluted with cyclohexane(C-Hex)–CH_2Cl_2–MeOH. According to TLC monitoring, eleven fractions were obtained and then subjected to repeated separation through column chromatography using appropriate stationary and mobile phase solvent systems previously determined by TLC. The following separation systems were used:

I. Normal phase chromatography using a polar stationary phase, typically silica gel, in conjunction with a non-polar mobile phase (e.g. *n*-hexane, DCM) with gradually increasing amounts of a polar solvent (e.g. EtOAc or MeOH). Thus hydrophobic compounds elute more quickly than do hydrophilic compounds.

II. Size exclusion chromatography involves separations based on the molecular size of compounds being analyzed. The stationary phase consists of porous beads (Sephadex LH-20). The larger compounds will be excluded from the interior of the bead and thus will elute first. The smaller compounds will be allowed to enter the beads and elute according to their ability to exit from the small-sized pores they were internalized through. Elution was performed using MeOH or MeOH: DCM (1:1).

4.2.5.4 High Pressure Liquid Chromatography (HPLC)

HPLC system consisting of an ECOM ECP2010 Pump coupled with an ECB2004 gradient box with degasser (ECOM, Prague, Czech Republic), a MISTRAL oven (Spark Holland, Emmen, Holland), an ALIAS autosampler (Spark Holland, Emmen, Holland), an ECOM ECDA2800 Diode Array Detector (DAD) and ECF 200 fraction collector (Prague, Czech Republic) and a SOFTA Model 300S ELSD (Teledyne Isco, Nebraska, USA).

Semi-Preparative High Pressure Liquid Chromatography

This process was used for the isolation and purification of compounds from fractions previously separated using column chromatographic separation. The most appropriate solvent systems were determined before running the HPLC separation. The mobile phase combination was MeOH or acetonitrile and nanopure H_2O pumped in gradient or isocratic manner depending on the compounds retention time. Each injection consisted of 5-10 mg of the fraction dissolved in 1 mL of the solvent system. The solvent system was pumped through the column at a rate of 2-4 mL/min. The eluted peaks were detected by the online UV detector and collected separately in Erlenmeyer flasks.

The separation columns: associated with a sample loop 500 ml

Normal Phase: 100 Si (250 × 10 mm× 5µm), MZ Analasentichnik, Germany.

Reverse Phase: C18, (250 mm × 10 mm × 5µm), Dr. Maisch GmbH, Germany.

C8 (250 × 10 mm × 5µm), Dr. Maisch GmbH, Germany.

Phenyl (250 × 10 mm × 5µm), Dr. Maisch GmbH, Germany

Diphenyl (250 × 10 mm × 5µm), Fortis Technologies Ltd., UK

Analytical High Pressure Liquid Chromatography

Analytical HPLC was used to identify the distribution of peaks either from extracts or fractions, as well as to evaluate the purity of isolated compounds. The solvent gradient used started with MeOH:nanopure H_2O (10:90) and reached to (95:5). The autosampler injected 25 µL sample. All peaks were detected by UV-VIS photodiode array detector. HPLC instrument consists of the pump, the detector, the injector, the separation column and the reservoir of mobile phase.

The separation columns: associated with a sample loop 100 ml

Normal Phase: 100 Si 5µm (250 × 4.6 mm), MZ Analasentichnik, Germany

Reverse Phase: C18 (250 × 4.6 mm × 5µm), Supelco Analytical, USA

C8 (250 × 4.6 mm × 5µm), Fortis Technologies Ltd., UK

Phenyl (250 × 4.6 mm × 5µm), Fortis Technologies Ltd., UK

Cyano (250 × 4.6 mm × 5µm), Fortis Technologies Ltd., UK

4.2.6 Structure elucidation methods

4.2.6.1 Infrared Spectrometer (IR)

Infrared (IR) Spectroscopy is the analysis of infrared light interacting with a molecule. IR spectroscopy is useful for finding out what kinds of bonds are present in a molecule, and knowing what kinds of bonds are present is a good start towards knowing what the structure could be. It measures the vibrations of atoms, and based on this it is possible to determine the functional groups. Generally, stronger bonds and light atoms will vibrate at a high stretching frequency (wavenumber).

4.2.6.2 Nuclear magnetic resonance spectroscopy (NMR)

Nuclear magnetic resonance is a phenomenon that occurs when the nuclei of certain atoms are immersed in a static magnetic field and exposed to a second oscillating magnetic field. Some nuclei experience this phenomenon, and others do not, dependent upon whether they possess a property called spin. It is used to study the physical, chemical, and biological properties of matter. As a consequence, NMR spectroscopy finds applications in several areas of science. NMR spectroscopy is routinely used by chemists to study chemical structure using a simple one-dimensional technique. Two-dimensional techniques are used to determine the structure of more complicated molecules. NMR spectra were recorded at 298º K on a Bruker Avance III 600 MHz spectrometer (600.23 MHz for ^{1}H, 150.93 MHz for ^{13}C) equipped with a PABBI inverse detection probe with a z-axis gradient coil and a B-ACS 60 autosampler and (400MHz for ^{1}H, 100 MHz for ^{13}C) equipped with a PABBI inverse detection probe with a z-axis gradient coil

All 1D and 2D spectra were obtained using the standard Bruker software. The samples were dissolved in different solvents, the choice of which was dependent on the solubility of the samples. Residual solvent signals were used as internal standards (reference signal) $CDCl_3$ (δ_H 7.26 ppm and δc 77.0), CD_3OD-d_4 (δ_H 3.31 ppm and δ_C 49.0 ppm), $(CD_3)_2CO$-d_6 (δ_H 2.05 ppm and δ_C 29.84 ppm) and DMSO-d_6 (δ_H 2.50 ppm and δ_C 39.52). The observed chemical shift (δ) values were given in ppm and the coupling constants (J) in Hz.

4.2.6.3 Mass spectrometry (MS)

Mass spectrometers use the difference in a mass-to-charge ratio (m/z) of ionized molecules to separate them from each other. Mass spectrometry is therefore useful for the quantification of atoms or molecules and also for the determination of chemical and structural information of molecules. A mass spectrometer consists of an ion source, ion

detector and mass-selective analyzer. The output of mass spectrometers shows a plot of relative intensity vs. the mass-to-charge ratio (*m/z*).

Electrospray ionization mass spectrometry (ESI-MS)

A mass spectrometer is an analytical instrument used to determine the molecular weight of a compound. Basically, mass spectrometers are divided into three parts; ionization source, analyzer and detector, which should be maintained under high vacuum conditions in order to maintain the ions travel through the instrument without any hindrance from air molecules. Once a sample was injected into the ionization source, the molecules are ionized. The ions were then passed and extracted into the analyzer. In the analyzer, the ions were separated according to their mass (*m*) to charge (*z*) ratio (*m/z*). Once the separated ions flow into the detector, the signals are transmitted to the data system where the mass spectrum is recorded.

Ultra Performance Liquid Chromatography mass spectrometry (UPLC/MS)

UPLC is a modern technique that gives a new direction for liquid chromatography, is a specialized chromatographic method that runs faster, resolves better and uses less solvent than HPLC. UPLC accomplishes this by using a smaller column packed with smaller particles (usually less than 2 µm in diameter). It is a powerful method for the separation of complex mixtures, especially when many of the components may have similar polarities. If a mass spectrum of each component can be recorded as it elutes from the LC column, quick characterization of the components is greatly facilitated. Usually, ESI-MS is interfaced with LC to make an effective on-line LC/MS. The samples were dissolved in water/MeOH mixtures and injected to UPLC/ESI-MS set-up.

UPLC/ESI-MS was carried out using two different instruments, the first was a Dionex Ultimate 3000 UHPLC system (Thermo Scientific™Dionex™, Sunnyvale, CA, USA) was employed. A Hypersil Gold UPLC C18 (2.1×150 mm, 1.9µm) reversed phased column (Thermo Fisher Scientific, San Jose, CA, USA). The second one was an HPG-3400 pump (Dionex Ultimate 3000 RSLC, Thermo Fischer Scientific, Dreieich, Germany) coupled to a QTOF mass spectrometer (Maxis Impact, Bruker Daltonics, Bremen, Germany) was equipped for the screening analysis.

High Resolution Mass Spectrometry (HR-MS)

High resolution is achieved by passing the ion beam through an electrostatic analyzer before it enters the magnetic sector. In such a double-focusing mass spectrometer, ion masses can be measured with an accuracy of about 1 ppm. With the measurement of this

accuracy, the atomic composition of the molecular ions can be determined. HRESI-MS was measured on a Q-Exactive Orbitrap platform (Thermo Fisher Scientific, San Jose, CA, USA) connected to a Dionex Ultimate 3000 UHPLC system (Thermo Scientific™Dionex™, Sunnyvale, CA, USA) was employed. A Hypersil Gold UPLC C18 (2.1×150 mm, 1.9μm) reversed phased column (Thermo Fisher Scientific, San Jose, CA, USA) was used.

For positive ionization mode, the mobile phases were water/methanol 90/10 (solvent A) and methanol (solvent B) both amended with 5mM ammonium formate and 0.01% formic acid. The adopted gradient elution program starts with 1% B with a flow rate of 0.2 mL min-1 for 1 min and it increases to 39 % in 2 min (flow rate 0.2 mL min-1), and then to 99.9 % (flow rate 0.4 mL min-1) in the following 11 min. Then it keeps constant for 2 min (flow rate 0.48 mL min-1), then initial conditions were restored within 0.1 min, kept for 3 min and then the flow rate decreased to 0.2 mL min-1. The injection volume was set up to 5 μL.

4.2.6.4 X-Ray analysis

Iso-Roridin-A was crystallized in the orthorhombic lattice, space group $P2_12_12_1$, with unit cell dimensions a=9.302 (3) Å, b=15.412 (6) Å, c=20.191 (8) Å, $\alpha=\beta=\gamma=90°$ and one (1) molecule per asymmetric unit.

The equipment used for the experimental work involved:

- A Leica MZ16 polarizing stereomicroscope equipped with a digital camera
- An In house X-ray generator: microfocus sealed tube, Rigaku (former Agilent/Oxford Diffraction), CuKα radiation, λ=1.54 Å, equipped with a kappa goniometer and a charged coupled detector, diameter 135 mm. The X-rays were generated at power settings of 50 kV and 0.8 mA.

4.2.6.5 Optical activity

Optically active compounds contain at least one chiral center. Optical activity is a microscopic property of a collection of these molecules that arises from the way they interact with light. Optical rotation was determined on a Perkin-Elmer-341 MC polarimeter. The substance was stored in a 0.5 mL cuvette with 0.1 dm length. The angle of rotation was measured at the wavelength of 589 nm of a mercury vapour lamp at room temperature (25 ºC). The specific optical rotation was calculated using the expression:

$$[\alpha]_D^T = \frac{100\alpha}{l\,c}$$

Where

$[\alpha]_D^T$ = the specific rotation at the wavelength 589 nm, at certain temperature T.

α = the measured angle of rotation in degrees,

l = the length in dm of the polarimeter tube,

c = the concentration of the substance expressed in g/100 mL.

The optical activity of the molecules was carried out using a PERKIN ELMER 341 polarimeter, the concentration was given in [mg/ml].

4.2.6.6 Determination of absolute stereochemistry by Marfey's reaction

Marfey's method[184] has emerged as a popular and effective procedure for determining the absolute configurations of hydrolytically accessible amino acid residues in natural products. This method was employed via four steps:

(i) The natural product to be analyzed is subjected to acid hydrolysis (6 M HCl) to release amino acid residues.

(ii) The hydrolysate is derivatized under alkaline conditions (1 M $NaHCO_3$) with Nα-(2,4-dinitro-5-fluorophenyl)-L-alaninamide (L-FDAA) or the enantiomer Nα-(2,4-dinitro-5-fluorophenyl)-D-alaninamide (D-FDAA).

(iii) The neutralized derivatized analyte is subjected to HPLC-UV (340 nm) analysis.

(iv) HPLC retention times of derivatized amino acids in the analyte are compared with those of derivatized L and D amino acid standards.

4.2.7 Testing the biological activity

Finding biologically important compounds from fungi is only achieved if, and when, assay systems have been devised that will allow for successful biologically guided fractionation of the culture extracts.

4.2.7.1 Antimicrobial assay

4.2.7.1.1 Agar diffusion assay

This method was used to detect the capability of a substance to inhibit the growth of microorganisms by measuring the diameter of the inhibition zone around a tested compound on the agar plate. The agar diffusion assay was performed according to the test[185, 186].

Microorganisms

Crude extracts and isolated pure compounds were tested for activity against the following standard strains: Gram positive bacteria *Bacillus subtilis* and *Bacillus cereus*, Gram negative bacteria *Pseudomonas areuginosa* and *Escherichia coli*, while the

pathogenic yeasts were *Candida albicans*, *Saccharomyces cerevisiae* and *Trichosporon Jirovecii*. On the other hand, the plant fungal pathogens were *Botrytis cinerea* and *Alternaria porri*.

Culture preparation

Prior to testing, bacterial liquid cultures were prepared by subculture of a few colonies (3 to 10) of the organism to be tested in 4 mL semi-liquid medium (containing only 0.01% agar) followed by incubation to allow the growth of organisms. The liquid cultures were then separately mixed in the Ultraturrax to produce suspensions of moderate cloudiness. The suspension was diluted with sterile saline solution to a density visually equivalent to that of $BaSO_4$ standards, prepared by adding 0.5 mL of 1% BaCl2 to 99.5 mL of 1% H_2SO_4 (0.36 N). The prepared broth was inoculated onto agar plates using an Eppendorf pipette and homogenously dispersed by means of a sterile spatula.

For the preparation of fungal cultures mycelia of *C. cucumerinum* and *C. herbarum* (after growing the fungi for about one month) were put into a fresh fungal medium (**see section 4.1.3**) and destroyed using Ultraturax. The cell debris (extracted mycelium) was removed by vacuum filtration and the filtrate (medium containing fungal spores) was then used for the next steps of the assay.

Assay

The applied media in this test were nutrient agar (for bacterial pathogens) and PDA (for fungal pathogens). Spore suspensions were prepared from the pathogenic microorganisms containing approximately 2 $x10^8$ cell/ml (for bacteria), 2 $x10^6$ cell/ml (for yeasts) and 2 $x10^5$ conidia/ml. 500 µl of the pathogen spore suspension were added to sterilized Petri plates and then the media were poured. Thereafter, the plates were maintained for 20 min at room temperature for solidification. Subsequently, wells (5 mm diameter) were perforated with a sterilized cork borer. One hundred microliter of the tested extract were loaded into the well, while wells loaded with 100 µl of DMSO represent a control. Thereafter, the plates were incubated for 48 h at 37 °C for bacterial pathogens and at 28 °C fungal pathogens. The antimicrobial impact was demonstrated by the measurement the diameter of the inhibition zone in mm[187].

4.2.7.2 Antioxidant activity using DPPH

Evaluation of antioxidant potential of selected extracts and pure compounds was performed using the DPPH (2,2-diphenyl-1-picrylhydrazyl) radical scavenging assay in 96-well plate. DPPH is a stable, synthetic radical that does not disintegrate in water, methanol, or ethanol. The working solution of DPPH (314µM) was prepared by diluting 12.4 mg in

100 mL of ethyl alcohol (EtOH absolute), vortexed and kept in dark at ambient temperature until its use. Gallic acid (final concentration=29.4 μM) was used as a positive control.

The fungal extracts were diluted in DMSO at final concentrations of 100 and 200 μg/mL. In a 96-well plate, 190 μL of DPPH solution and 10 μL of gallic acid/sample were added. When DPPH reacts with an antioxidant compound, which can donate hydrogen, it is reduced. The changes in colour (from deep violet to light yellow) were read [Absorbance (Abs)] at 517 nm after 30 min of incubation (dark, room temperature) using the reader Infinite 200 PRO series (Tecan).

The experiment was done in triplicate for each sample. A negative control containing 10 μL DMSO and 190 μL DPPH was performed each time. Blanks contained 190 μL EtOH and 10 μL sample. All materials were purchased from Sigma-Aldrich. The radical scavenging activity percentage (AA%) was determined as follow:

AA% = [100-[(A sample-Ablank)/Acontrol]]*100

Where A control is the absorbance of negative control, A sample is the absorbance after the reaction of the sample with DPPH, Ablank is the absorbance of the sample with EtOH instead of DPPH.

4.2.7.3 Anti-enzymes activity

4.2.7.3.1 Antityrosinase activity

Evaluation of tyrosinase inhibitory potential of selected extracts and pure compounds was performed using mushroom tyrosinase and L-DOPA, as a substrate purchased from Sigma-Aldrich Chemical Co. The enzyme, the substrate and all the samples were diluted in phosphate-buffered saline (pH 6,7). The evaluation was performed in a 96-well plate and wells were divided into four groups containing the following:

(A) 120μl phosphate buffer (1/15M, pH 6,7) and 40μl mushroom tyrosinase (92 Units/ml in phosphate buffer), in triplicate, as control.

(B) 160μl phosphate buffer, in one well, as blank of control.

(C) 80μl phosphate buffer, 40μl of sample dissolved in phosphate buffer (containing up to 3% DMSO) and 40μl mushroom tyrosinase (92 Units/ml in phosphate buffer), in triplicate.

(D) 120μl phosphate buffer and 40μl of sample dissolved in phosphate buffer (containing up to 3% DMSO), in one well, as blank of sample.

The contents of each well were incubated for 10 minutes at room temperature before 40μl of L-DOPA (2.5mM in phosphate buffer) were added. After incubating at room temperature for 5 minutes, the absorbance at 475nm was measured. Kojic acid (KA2) and *Glycyrrhiza*

glabra (Gly5) methanolic extract from roots were used as positive control. The percentage inhibition of tyrosinase activity was calculated by the following equation:

$$\%\ inhibition\ of\ Tyrosinase\ = \frac{(OD\_A - OD\_B) - (OD\_C - OD\_D)}{(OD\_A - OD\_B)} \times 100$$

4.2.7.3.2 Antiacetylcholinesterase activity

The acetylcholinesterase inhibitory activity of some compounds was evaluated based on the method described by Hasnat *et al.*[188]. In a 96 well microplate 150 μL of 0.1 M sodium phosphate buffer (pH 8.0) 10 μL of tested compound solutions and 20 μL of enzyme solution (0.1 units/mL) were mixed and incubated for 15 min at 25 °C. Then, 10 μL of the chromophore DTNB (10 mM) were added and the reaction initiated by the addition of 10 μl of the substrate solution ATCI (14 Mm). The mixture was incubated for 10 min at 25 °C and the formation of the coloured product, 5-thio-2-nitrobenzoate anion, was measured at 410 nm. The hydrolysis of ATCI by the enzyme leads to the release of thiocholine which reacts with the DTNB, forming the coloured product 5-thio-2-nitrobenzoate anion. All tested compounds were evaluated at 100 μM, galanthamine hydrobromide was used as a positive control at final concentrations 25 and 1 μM and AChE percentage inhibition was calculated by the equation:

.

$$\%\ inhibition\ activity\ = \frac{\text{Absorbance of control}\ -\ \text{Absorbance of sample}}{\text{Absorbance of control}} \times 100$$

4.2.7.4 Docking studies

The crystal structure of the target protein MurF. (PDB ID: 4CVL, resolution: 2.98 Å) was downloaded from Protein Data Bank (http://www.pdb.org). Molecular Operating Environment (MOE) was used for the docking analysis[189]. In these studies, the free energies and binding modes of the examined molecules against the target protein were determined. At first, the water molecules were removed from the crystal structures of target proteins, retaining only one chain which essential for binding. The Co-crystallized ligand (ACP) was used as a reference ligand. Then, the protein structure was protonated and the hydrogen atoms were hidden. Next, the energy was minimized and the binding pocket of the target protein was defined[190].

The structures of the examined compound and the co-crystallized ligand were drawn using ChemBioDraw Ultra 14.0 and saved as SDF formats. Then, the saved files were opened using MOE software and 3D structures were protonated. Next, the energy of the

molecules was minimized[191]. MMFF94X has applied a force field and ASE as a scoring function. The docking procedure was carried out utilizing a default protocol. In each case, 30 docked structures were generated using genetic algorithm searches. The output from MOE software was further analyzed and visualized using Discovery Studio 4.0 software [192,193].

5. Investigation of Selected Microbial Strains

5.1 *Aspergillus ochraceopetaliformis* ASAI

The fungal strain was obtained from a soil sample collected at Giza province, Egypt. The identification of *Aspergillus ochraceopetaliformis* was done using molecular protocol by DNA amplification and sequencing of Internal Transcribed Spacer (ITS) region. Based on the morphological, 18S rRNA gene sequence and phylogenetic data the fungus ASAI was taxonomically characterized *Aspergillus ochraceopetaliformis* (accession no. MN611443).

The spore suspension of the selected strain ASAI was inoculated into 100 mL of ISP2 medium and incubated at 30 ºC for 3 days as seed culture. 5 mL of previously prepared seed culture were used to inoculate 5× 1L sterilized Erlenmeyer flasks (each 5 flasks) containing rice medium composition: 100 g commercial rice; 150 mL of 50% seawater. The flasks were incubated for 14 days at 35 °C. After harvesting, the culture was mixed with methanol and filtered under vacuum. The filtered aqueous methanol was concentrated in vacuo, and the remaining water residue was re-extracted by ethyl acetate, and then concentrated to dryness to afford 5.50 gm of a dark green crude extract.

Based on paper-disk diffusion assay[194], the fungal extract exhibited significant antimicrobial activity against several pathogenic test microorganisms: of test microorganisms comprising Gram positive bacteria *Bacillus subtilis* ATCC 6633, Gram negative bacteria *Pseudomonas areuginosa* ATCC 27853, yeasts (*Candida albicans* ATCC 10231, *Saccharomyces cerevisiae* ATCC 9080), and the fungus *Aspergillus niger* NRRL A-326 (**Figure 14**).

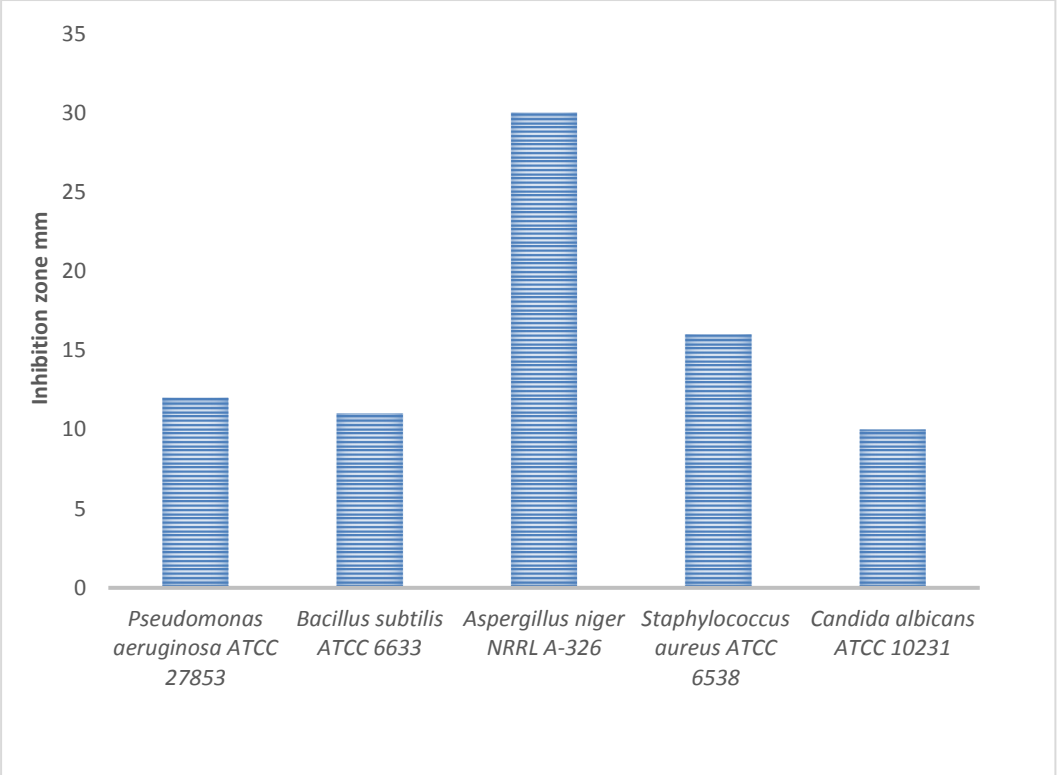

Figure 14: Antimicrobial activities of the fungal strain extract in agar diffusion assays.

In the TLC screening, the extract showed a low polar yellow band. In addition, numerous UV absorbing and fluorescent zones were observed, which were coloured orange to violet when sprayed with anisaldehyde/sulphuric acid, or pink to blue with Ehrlich's reagent.

The extract was defatted using cyclohexane and the methanolic part was pre-separated by column chromatography using silica gel (100 x 5 cm, 150 gm of silica) and gradually eluted with cyclohexane(C-Hex)–CH_2Cl_2–MeOH. According to TLC monitoring, eleven fractions were obtained (**see section 4.2.4.1**). Further purification on Sephadex LH-20, by PTLC and HPLC, afforded 24 compounds, belonging to different chemical families are described as shown below.

5.1.1 Isolated metabolites from *Aspergillus ochraceopetaliformis*

5.1.1.1 Cyclo[Ala-Trp]

Compound (**33**) was obtained as a white powder (1.4 mg) and had the molecular formula $C_{14}H_{15}N_3O_2$ deduced by the positive-ion mode HRESIMS data. It showed UV absorbances at 226, 280 and 288 nm, indicative of an indole chromophore.

The ^{1}H NMR spectrum of (**33**) (**Table 7**) showed three signals attributed to NH group at δ_H 10.86 (1H, s, H-1), 7.96 (1H, br d, J = 1.5 Hz, H-14), and 7.87 (1H, br d, J = 1.5 Hz, H-11), as well as, five aromatic protons at δ_H 7.56 (1H, br d, J = 7.9 Hz, H-4), 7.31 (1H, br d, J = 7.9 Hz, H-7), 7.02 (br td, J = 7.9, 1.1 Hz, H-6), and 6.94 (1H, br td, J = 7.9, 1.1 Hz, H-5) were characteristic for a 1,2-disubstituted aromatic ring. The fifth proton at δ_H 7.05 showed a small long-range coupling constant (^3J = 2.3 Hz) confirming the indole skeleton substituted at 3-position. In the aliphatic region, two oxygenated or aminated methines at δ_H 4.11 (1H, m, H-9) and 3.60 (1H, br q, J = 7.0 Hz, H-12), one methylene at δ_H [3.24 (1H, dd, J = 14.5, 4.3 Hz, H-8a), 3.02 (1H, dd, J = 14.5, 4.6 Hz, H-8b)] and one methyl at 0.48 (d, J = 7.0 Hz, H_3-15) were observed.

The structure of (**33**) was further elucidated by analysis of 2D NMR data including the ^{1}H-^{1}H COSY and HMBC spectra (**Figure 15**). The ^{1}H-^{1}H COSY spectrum of (**33**) revealed connectivity of structural fragments: a (NH-1 to H-2), b (H-4 to H-7), c (H-8 to H-9 and NH-14), and d (NH-11 to H-12 and H_3-15). Interpretation of the HMBC spectrum showed that CH_2-8 correlated to C-3, C-3a, C-9 as well as C-10, confirming the 3-substituted indole structure. Moreover, both CH_2-8 and H-9 showed HMBC correlations to an oxygenated carbon signal at δ_C 166.8 (C-10), thereby establishing the C9-C10 bond and the tryptophane substructure.

Furthermore, the COSY spectrum showed a saturated spin system (d) composed of an aliphatic methyl group detected at δ_H 0.45 (d, J = 7.0 Hz, H_3-15), a broad quartet at δ_H 3.60 (J = 7.0 Hz, H-12) and a signal at δ_H 7.87 (br d, J = 1.5 Hz, NH-11). All the latter proton signals showed HMBC correlations to an oxygenated carbon atom appearing at δ_C 167.7 (C-13), thus confirming an alanine substructure. The HMBC correlation between NH-11 and C-9 as well as the pronounced upfield shift of the methyl group indicated that both amino acids were arranged into a cyclic dipeptide or diketopiperazine.

The evidence mentioned above indicated that this metabolite was alanyl-tryptophan anhydride. The clear NOESY correlation between H-9 and H-12, suggested the co-facial correlation which means the configuration of the two amino acids might be D-Tryptophane and D-Alanine) or (L-Tryptophane and L-Alanine).

Table 7: NMR spectroscopic data for (**33**) (600 and 150 MHz, δ ppm) [a]

Position	^{1}HNMR (*J* in Hz)	^{13}CNMR	COSY	HMBC	NOESY
1-NH	10.86 s	-	2	3, 7a	-
2	7.05 (d, 2.3)	124.2	1	3, 3a	8, 9, 15
3	-	108.3	-	-	-
3a	-	127.8	-	-	-
4	7.56 (br d, 7.9)	118.7	5	3, 3a, 6	8, 9, 14
5	6.94 (td,7.9, 1.1)	118.1	4, 6	3a, 7	-
6	7.02 (td, 7.9, 1.1)	120.5	5, 7	5, 7a	8, 9, 14
7	7.31 (br d, 7.9)	110.9	6	3a, 4, 7a	-
7a	-	135.8	-	-	-
8	3.02 (dd, 4.6, 14.5) 3.24(dd, 4.3, 14.5)	28.6	9	2, 3, 3a, 9, 10	9
9	4.11, m	55.2	8, 14	3, 8, 10	4, 12
10-CO	-	166.8	-	-	-
11-NH	7.87 (br d, 1.5)	-	12	9, 13	
12	3.60 (br q, 7.0)	49.6	11, 15	13, 15	9
13-CO	-	167.7	-	-	-
14	7.96 (br d, 1.5)	-	9	10, 12	2, 8
15	0.45 (d, 7.0)	19.2	12	12, 13	2, 4, 11

[a] The assignments were based on DEPT, ^{1}H-^{1}H COSY, HSQC, and HMBC experiments, and recorded in DMSO-d_6.

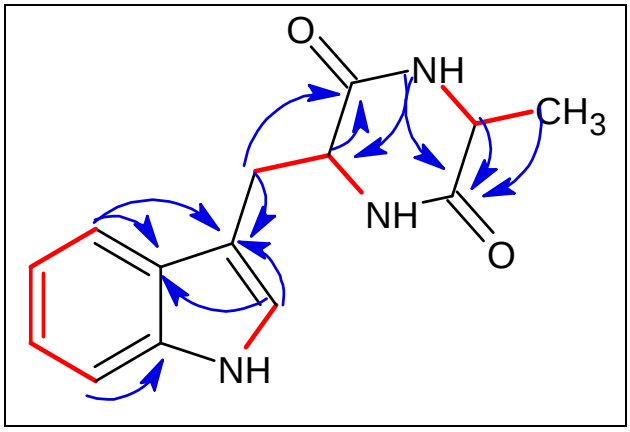

Figure 15: Key COSY (▬) and selected HMBC(⟶) correlations for (**33**).

Due to the Marfey's analysis and comparing the specific rotation of (**33**) $[\alpha]_D^{22} = +60$ (c 0.5 EtOH) with the published data[195], the configuration confirmed to be (L-Trp and L-Ala).

The obtained UV, ^{1}H, ^{13}C NMR and mass spectral data were identical to published data for cyclo[L-Aal-L-Trp] previously isolated from *Aspergillus sp.*[196].

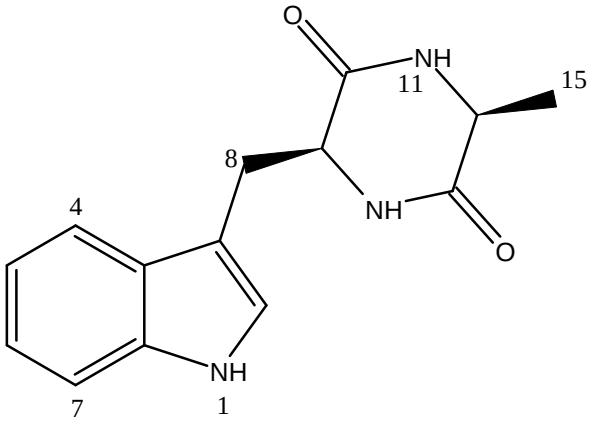

33

5.1.1.2 Preechinulin

Preechinulin (**34**) was isolated as white solid (2.7 mg). The Positive HRESI-MS exhibited a strong peak at *m/z* 326.1862 $[M+H]^+$ indicating a molecular formula of $C_{19}H_{23}N_3O_2$ (calculated 326.1869), required 10 degrees of unsaturation.

The ^1H NMR spectrum of (**34**) (**Table 8**) showed high similarity to those of alanyl-tryptophan anhydride (**33**) especially the existence of three amid signals and four aromatic protons. The sole difference was the presence of two singlet signals attributed for two methyl groups at δ_H 1.49 and 1.48, as well as one olefinic methine at δ_H 6.18 (1H, dd, J = 10.6, 17.5 Hz), and exocyclic methylene protons at δ_H [5.07 (1H, dd, J = 17.5, 1.0 Hz) and 5.04 (1H, dd, J = 10.6, 1.0 Hz)], indicated the existence of reverse prenyl group.

This observation was supported by both instances ^1H-^1H COSY and HMBC correlations (**Figure 16**), established that the low-field olefinic proton (H-16), resonating at δ_H 6.18 (1H, dd, J = 17.5, 10.6 Hz), exhibited a clear COSY correlation with the exocyclic methylene protons H_2-17 at δ_H [5.07 (1H, dd, J = 17.5, 1.0 Hz) and 5.04 (1H, dd, J = 10.6, 1.0 Hz)] and HMBC correlations to the carbons at δ_C 38.9 (C-15) and 27.9 (C-18 and 19). Due to the HMBC correlation between the methyls at δ_H 1.48 and 1.49 with the quaternary carbon at δ_C 141.6 (C-2), the connection of the reverse prenyl group with the indole moiety over C-2 was established. Furthermore, the diagnostic HMBC cross-peaks from H_2-8 to the carbons at δ_C 59.2 (C-9), 108.6 (C-3), 128.8 (C-3a), 144.0 (C-2), and 169.5 (C-10) estimated the connection between the indole moiety and diketopiperazine side.

Concerning to the stereochemistry, the configuration of the alanine amino acid residue found to be L-alanine due to the enhancement of CH_3-20 after irradiation of H-8a in 1D NOE experiment (**Appendix 3**) and from the specific rotation $[\alpha]_D^{22} = -100$ (c 0.2 MeOH).

The structure was then confirmed by comparison of ^{1}H, ^{13}C NMR and mass spectral data with the published data for preechinulin which previously reported from *Aspergillus ruber*[197].

Table 8: NMR spectroscopic data for preechinulin (**34**), (400 and 100 MHz, δ ppm)[a]

Position	^{1}HNMR (*J* in Hz)	^{13}CNMR	COSY	HMBC
1-NH	10.51 s	-	-	2, 3, 3a, 7a
2	-	141.6	-	-
3	-	104.9	-	-
3a	-	128.8	-	-
4	7.43 (br d, 7.8)	117.8	5	3, 3a, 5, 7a
5	6.93 (td,7.8, 1.0)	118.2	4, 6	3a, 7
6	7.02 (td, 7.8, 1.0)	120.3	5, 7	4, 7a
7	7.32 (br d, 7.8)	110.7	6	3a, 6
7a	-	134.9	-	-
8	a 3.08 (dd, 9.0, 14.7) b 3.35(dd, 4.6, 14.7)	30.9	9	2, 3, 3a, 9, 10
9	3.97 m	55.5	8, 14	3, 8, 10
10-CO	-	167.7	-	-
11-NH	8.13 (d, 3.0)	-	12	9, 13
12	3.79 (qd, 7.0, 3.0)	50.4	11, 20	13, 15
13-CO	-	168.0	-	
14-NH	7.51 (d, 3.0)	-	9	10, 12
15	-	38.9	-	-
16	6.18 (dd, 10.6, 17.5)	146.6	17	15,18,19
17	5.04 (dd, 10.6, 1.0) 5.07 (dd, 17.5, 1.0)	110.9	16	15, 16, 18, 19
18	1.48 s	27.9	-	2, 15, 17, 19
19	1.49 s	27.9	-	2, 15, 17 18
20	1.23 (d, 7.0)	20.6	12	12, 13

[a] The assignments were based on DEPT, ^{1}H-^{1}H COSY, HSQC, and HMBC experiments, and recorded in DMSO-d_6.

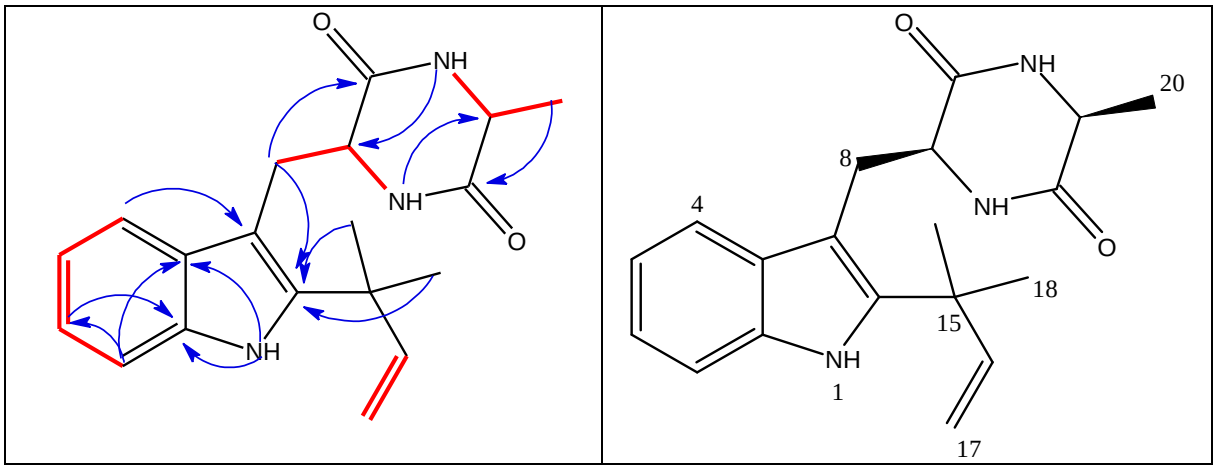

Figure 16: Key COSY (▬), selected HMBC(→) correlations and structure of (**34**).

5.1.1.3 Tardioxopiperazine B

Compound (**35**) was isolated as pale yellow solid (1.5 mg). The Positive HRESI-MS exhibited a strong peak at *m/z* 394.2490 $[M+H]^+$ indicating a molecular formula of $C_{24}H_{31}N_3O_2$ (calculated 393.2495), implied 11 degrees of unsaturation.

The ^1H and ^{13}C NMR spectrum of (**35**) (**Table 9**) revealed the same characteristics of indole diketopiperazine similar to those of preechinulin (**34**). However, the differences were observed, the existence of another prenyl moiety indicated from the presence of two singlet signals attributed for two methyl groups at (δ_H 1.80, s; δ_C 18.0) and (δ_H 1.77, s; δ_C 25.9), as well as one olefinic methine at δ_H 5.39 (1H, br tq, J = 7.3, 1.3 Hz; δ_C 123.9), and methylene protons at δ_H 3.59 (2H, d, J = 7.3 Hz; δ_C 30.8). Additionally, the presence of three aromatic protons at δ_H [7.36 (1H, d, J = 7.8 Hz; δ_C 117.1), 6.95 (1H, t, J = 7.4 Hz; δ_C 120.6), and 6.88 (1H, d, J = 7.4 Hz; δ_C 122.0)] instead of four aromatic protons in (**34**), supposed that the connection of the prenyl group must be at the C-4 or C-7 position.

Detailed investigation of ^1H-^1H COSY and HMBC correlations (**Figure 17**) established the gross structure. The COSY correlation between H-6 and H_2- 21 along with the HMBC cross-peaks from H-6 to C-21 and from CH_2-21 to C-6 confirmed that the prenyl group connected with the indole moiety through C-7.

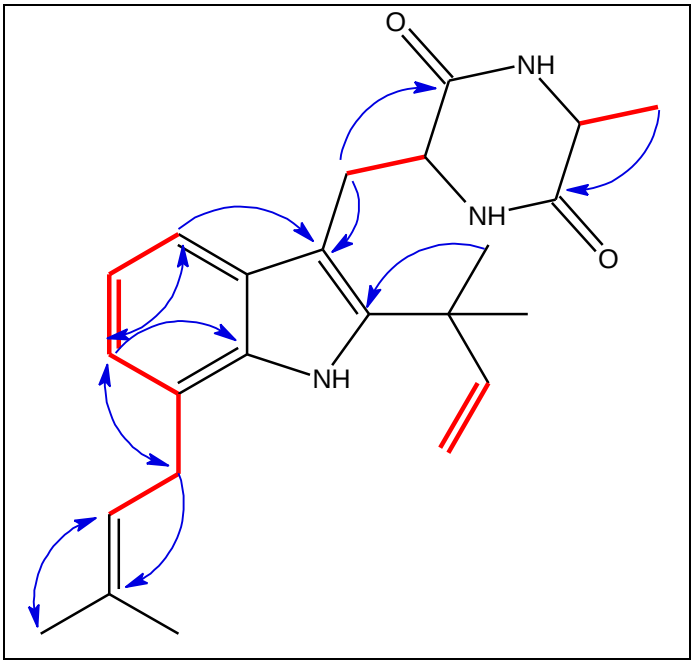

Figure 17: Key COSY (▬) and selected HMBC (⟶) correlations for (**35**).

Table 9: NMR spectroscopic data for tardioxopiprazine B (**35**), (400 and 100 MHz)[a]

Position	^{1}HNMR (*J* in Hz)	^{13}CNMR	COSY	HMBC
1-NH	-	-	-	-
2	-	142.6	-	-
3	-	106.2	-	-
3a	-	130.5	-	-
4	7.36 (d, 7.8)	117.1	5	3, 3a, 6, 7, 7a
5	6.95 (t, 7.4)	120.6	4, 6	3a, 4, 6, 7
6	6.88 (d, 7.4)	122.0	5, 21	4, 7a, 21
7	-	125.1	-	-
7a	-	135.5	-	-
8	3.28 (dd, 9.7, 14.6) 3.54 (dd, 3.8, 14.6)	32.3	9	2, 3, 3a, 9, 10
9	4.26 (dd, 3.8, 9.7)	57.2	8	3, 8, 13
10-CO	-	170.1	-	-
11-NH	-	-	-	-
12	3.94 (q, 7.2)	52.2	20	13, 20
13-CO	-	170.7		-
14-NH	-	-	-	-
15	-	40.4	-	-
16	6.23(dd, 10.6, 17.5)	148.1	17	2, 15, 18, 19
17	5.13 (br dd, 10.6, 1.0) 5.17 (br dd, 17.5, 1.0)	112.1	16	2, 15, 16, 18
18	1.57 s	28.6	-	2, 15, 16, 17, 19
19	1.58 s	28.7	-	2, 15, 16, 17, 18
20	1.31 (d, 7.2)	21.1	12	12, 13
21	3.59 (d, 7.3)	30.8	22	6, 22, 23
22	5.39 (tq, 7.3, 1.3)	123.9	21	21, 24, 25
23	-	133.6	-	-
24	1.77 s	25.9	21, 22	22, 23, 25
25	1.80 s	18.0	21, 22	22, 23, 24

[a] The assignments were based on DEPT, ^{1}H-^{1}H COSY, HSQC, and HMBC experiments, and recorded in MeOD-*d4*.

With regard to the stereochemistry, the enhancement of CH_3-20 after irradiation of H-8a in 1D NOE experiment (**Appendix 5**), suggested the co-facial correlation which means the configuration of the two amino acids might be D-Tryptophane and D-Alanine or L-Tryptophane and L-Alanine. Marfey`s analysis (**Appendix 6**) confirmed the absolute configuration of the alanine residue to be L-Alanine (9*S*,12*S*). The specific rotation of (**35**) was $[\alpha]_D^{22} = +150$ (c 0.2 $CHCl_3$).

Finally, the structure was confirmed by comparison of the NMR and mass spectral data with published data for tardioxopiperazine B which was previously reported as (9*S*,12*S*)) from an ascomycete, *Microascus tardifaciens*[198].

5.1.1.4 Tardioxopiperazine A

Compound (**36**) was isolated as a faint yellow substance (0.5 mg). The Positive HRESI-MS exhibited a strong peak at *m/z* 394.2490 $[M+H]^+$ indicating a molecular formula of $C_{24}H_{31}N_3O_2$ (calculated 393.2495), suggesting a similar structure to tardioxopiperazine B (**35**) with 11 degrees of unsaturation.

The ^{1}H NMR spectrum of (**36**) (**Table 10**) revealed the same characteristics of prenylated indole diketopiperazine like (**35**), However, the pivotal differences were observed, the presence of three aromatic protons at δ_H [7.29 (1H, s), 7.24 (1H, d, J = 8.2 Hz), and 6.89 (1H, d, J = 8.2 Hz)], suggested that the connection of the prenyl group should be at the C-5 or C-6 position. Detailed investigation of ^{1}H-^{1}H COSY and HMBC correlations (**Table**), confirmed that the connection of the prenyl group with the indole moiety through C-5. The COSY spectrum confirmed that the isoprenyl group was attached to the aromatic side of the indole substructure since H-4 exhibited long-range correlations to both CH_2-21 and H-6. Besides, in the HMBC spectrum (**Table 10**) a correlation of H-4 to C-3 was detected.

The configuration of the amino acid residue confirmed to be L-Alanine (9*S*,12*S*) by elaborating Marfey's analysis (**Appendix 8**) and the specific rotation of (**36**) was measured $[\alpha]_D^{22} = -80$ (c 0.1 $CHCl_3$) . Finally, The structure was confirmed by comparison of the NMR and mass spectral data with the published data for tardioxopiperazine A which was previously reported from an ascomycete, *Microascus tardifaciens*[198].

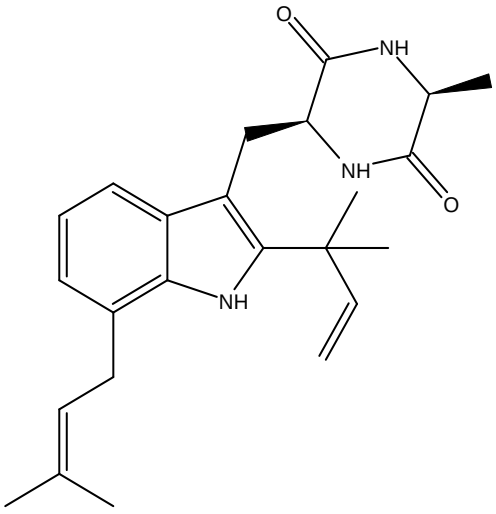

35

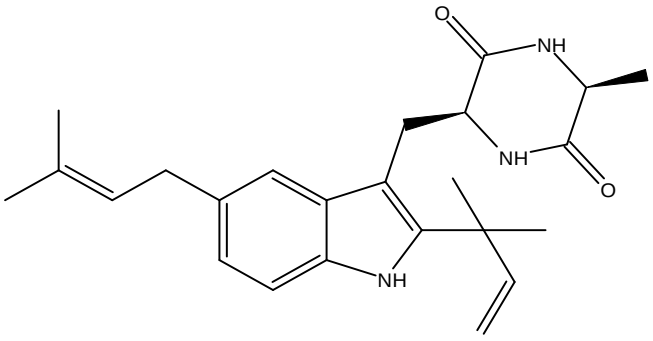

36

Table 10: NMR spectroscopic data for tardioxopiprazine A **(36)** (600 and 150 MHz)[a]

Position	^{1}HNMR (*J* in Hz)	^{13}CNMR	COSY	HMBC
1-NH	-	-	-	-
2	-	143.5	-	-
3	-	105.2	-	-
3a	-	130.8	-	-
4	7.29 s	118.3	6, 21	3, 6, 7a, 21
5	-	133.4	-	-
6	6.89 (d, 8.2)	123.2	4, 7	4, 7, 7a, 21
7	7.24 (d, 8.2)	111.6	6	3a, 4, 5
7a	-	135.5	-	-
8	3.22 (dd, 10.1, 14.7) 3.53 (dd, 3.7, 14.7)	32.4	9	2, 3, 3a, 9, 10
9	4.26 (dd, 3.7, 10.1)	57.2	8	3, 8, 10
10-CO	-	170.3	-	-
11-NH	-	-	-	-
12	3.97 (q, 7.1)	52.2	20	13, 20
13-CO	-	170.9	-	-
14-NH	-	-	-	-
15	-	40.5	-	-
16	6.20(dd, 10.6, 17.5)	148.2	17	2, 15, 18, 19
17	5.09 (br dd, 10.6, 1.0) 5.13 (br dd, 17.5, 1.0)	112.0	16	15, 16, 18, 19
18	1.54 s	28.7	-	2, 15, 16, 17, 19
19	1.55 s	28.7	-	2, 15, 16, 17, 18
20	1.39 (d, 7.1)	21.5	12	12, 13
21	3.40 (d, 7.1)	35.5	22, 24	4, 5, 6, 22
22	5.38 (br t, 7.1)	126.1	21, 24	24, 24
23	-	132.5	-	-
24	1.74 s	26.2	21	22, 23, 25
25	1.75 s	18.0	22	22, 23, 24

[a] The assignments were based on DEPT, ^{1}H-^{1}H COSY, HSQC, and HMBC experiments, and recorded in MeOD-d_4.

To the best of our knowledge, these two metabolites (**35**) and (**36**) were isolated biosynthetically by using two prenyltransferases from *Aspergillus ruber* to control the echinulin biosynthesis via exceptional sequential prenylations[197].

5.1.1.5 Echinulin

Echinulin (**37**) was isolated as a white powder (60.0 mg), it showed an absorbing band at 254 nm and turned into faint blue on spraying with vanillin reagent and heating. R_f = 0.32 (DCM/MeOH 5%). The Positive and negative HRESI-MS exhibited a strong peak at *m/z* 462.3103 $[M+H]^+$ and *m/z* 460.2946 $[M-H]^+$ indicating a molecular formula of $C_{29}H_{39}N_3O_2$, bearing 12 degrees of unsaturation.

The ^{1}HNMR spectral data (**Table 11**) exhibited signals attributed to NH groups at δ_H 8.05, 1H, s, H-1), 5.90 (1H, s, H-11) and 5.64 (1H, s, H-14), as well as, two aromatic H-atoms at δ_H 7.11 (1H, s, H-6) and δ_H 6.78 (1H, s, H-4) indicated the presence of an aromatic ring with *meta* disubstituted equal groups. Additionally, the spectrum revealed five olefinic H-atoms at δ_H 5.40 (1H, br t, *J* = 7.4 Hz, H-22), δ_H 5.33 (br t, *J* = 7.4 Hz, H-27), 4.08 (1H, br q, *J* = 6.9 Hz, H-12), 4.39 (1H, br d, *J* = 11.3 Hz, H-9) and 6.08 (1H, dd, *J* = 17.4, 10.4 Hz, H-16), moreover, seven methyl groups at δ_H 1.85 (3H, s, H_3-24), 1.79 (3H, br q, *J* = 1.1 Hz, H_3-25), 1.72 (3H, s, H_3-29), 1.71 (3H, br q, *J* = 1.1 Hz, H_3-30), 1.51 (3H, d, *J* = 7.1 Hz, H_3-20),1.49 (6H, s, H_3-18), and 1.48 (3H, s, H_3-19) were observed.

From ^{13}C NMR (**Table 11**), two amid carbonyl groups appeared at δ_C 168.3 and 167.7, sex quaternary carbons of the indole moiety were shown at δ_C 141.4, 133.9, 131.6, 129.0, 122.9 and 104.0, as well as one sp^2 carbon for methylene group at δ_C 112.4. In the aliphatic region, three methylene carbons at δ_C 31.4, 34.6 and 29.4 and seven methyl carbons at δ_C 27.9, 27.8, 25.8, 25.7, 19.9 and two signals at 17.9 were observed. The ^{13}C NMR spectrum with the aid of HSQC DEPT revealed carbons comprising two pairs of methyl (δ_C 17.9, 2CH_3 / δ_C 25.7, 25.8), two methine sp^2 (δ_C 123.4, 124.5), two quaternary sp^2 (δ_C 132.2, 132.9) and two methylene sp^3 (δ_C 31.4, 34.6) carbons which in combination with the presence of the methyl groups at δ_H 1.85, 1.79, 1.72, and 1.71, a two methine triplets at δ_H 5.40, and 5.39, and two methylene doublets at δ_H 3.42 and 3.56, confirmed the existence of another two prenyl groups in the molecule.

The analysis of ^{1}H–^{1}H COSY and HMBC data (**Table 11**) afforded two substructures, A, and B, as shown in (**Figure 18**). The COSY cross-peaks data afforded couplings of the olefinic proton at δ_H 6.08 (dd, *J* = 17.4, 10.6 Hz; δ_C 145.7) to the methylene sp^2 protons at δ_H 5.13, (dd, *J* = 17.4, 0.9 Hz; H-17a) and 5.14 (dd, *J* = 10.6, 0.9 Hz; H-17b).

Table 11: NMR spectroscopic data for echinulin (**37**) (600 and 150 MHz, δ ppm)[a]

Position	^{1}HNMR (*J* in Hz)	^{13}CNMR	COSY	HMBC	NOESY
1-NH	8.05 s	-	-	2, 3, 3a	21, 20
2	-	141.4	-	-	-
3	-	104.0	-	-	-
3a	-	129.0	-	-	-
4	7.11 s	115.1	-	3, 6, 7a, 21	21, 26
5	-	133.9	-	-	-
6	6.78 s	122.9	-	4, 7a, 21, 26	8, 9, 14, 26
7	-	122.9	-	-	-
7a	-	131.6	-	-	-
8	3.64 (dd, 3.7, 14.8) 3.17 (dd, 11.7, 14.8)	29.4	9	2, 3, 9, 10	8, 9, 20 8, 18, 19
9	4.39 (br dd, 3.7, 11.7)	54.5	8, 14	10, 12	6, 8, 12, 14, 20
10-CO	-	168.3	-	-	-
11-NH	5.90 s	-	12	9, 12, 13	12, 20
12	4.08 (br qt, 7.0, 1.2)	50.8	11, 20	13, 20	11, 20
13-CO	-	167.7	-	-	-
14-NH	5.64 s	-	9	12, 13	9, 20
15	-	39.0	-	-	-
16	6.08 (dd, 10,4, 17,4)	145.7	17	15, 18. 19	17, 20
17	5.14 (dd, 0.9, 17.3) 5.13(dd, 0.9, 10.4)	112.4	16	15, 16	16, 18, 19
18	1.49 s	27.9	-	2, 15, 16, 19	1, 8, 14, 16, 17
19	1,49 s	27.8	-	2, 15, 16, 18	-
20	1.51 (d, 7.0)	19.9	12	12, 13	12
21	3.51 (d, 7.4)	31.4	22	22, 23	1, 4, 24
22	5.40 (tq, 7.4, 1.4)	123.4	21	21, 24, 25	25, 26
23	-	132.2	-	-	-
24	1.85 s	17.9	-	22, 23, 25	21
25	1.79 (br q, 1.1)	25.7	-	22, 23, 24	22
26	3.37 (d, 7.4)	34.6	27	6, 26, 27, 28	4, 6, 26
27	5.33 (tq, 7.4, 1.4)	124.5	26	26, 29, 30	21, 29
28	-	132.9	-	-	-
29	1,72 s	17.9	-	27, 28, 30	26
30	1.71 (br q, 1.1)	25.8	-	27, 28, 29	26

[a] The assignments were based on DEPT, HSQC, and HMBC experiments, and recorded in $CDCl_3$.

Since the HMBC spectrum displayed correlations of the olefinic proton H-16 to the quaternary sp^3 carbon (C-15) and the methyl carbons (C-18) and (C-19), of the methylene protons at H_2-17 to the carbons (C-16) and (C-15), and of the methyl protons H_3-18 and H_3-19 to the carbons (C-15) and (C-16), the presence of (1-dimethylbuten-3-yl) "commonly named reverse prenyl" moiety was confirmed. The HMBC correlations of NH-1 to C-2, C-3 and C-3a confirmed the presence of (2,3-disubstituted 2,3-dihydro-1H-indole). Consequently, the other two prenyl substituents were placed on C-5 (δ_C 133.9) and C-7 (δ_C

122.9) of the benzene ring of the 2,3-dihydro-1H-indole moiety due to the HMBC correlations of H-4 to C-3, C-6, C-7a, and C-21, of H-6 to C-4, C-7a, C-21 and C-26.

Likewise, the COSY spectrum showed the continuous coupling system of the singlet at δ_H 5.90, the quartet triplet at δ_H 4.08 (1H, J = 7.0, 1.4 Hz; δ_C 50.8) and the methyl doublet at δ_H 1.51 (3H, J = 7.0 Hz; δ_C 19.9). On the other hand, both the singlets at δ_H 5.90 and 5.64 exhibited the HMBC cross-peaks to the methine sp^3 carbon C-9 and the carbonyl C-12, while the methylene H_2-8 gave HMBC cross-peaks to the carbons C-2, C-3, C-9, and C-12, confirmed the presence of substructure B (1,4-diketopiperazine with substituents on C-2 and C-5).

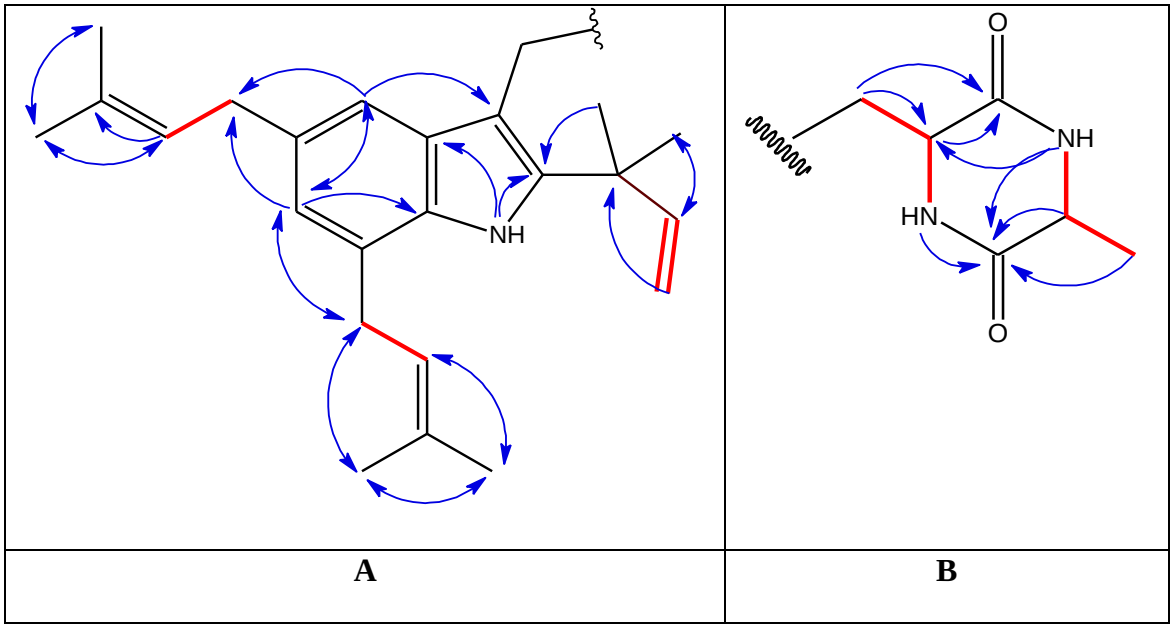

Figure 18: Key COSY (▬) and selected HMBC(⟶) correlations for echinulin (**37**).

The weak long-range ^5JH,H coupling constant of 1.2 Hz observed for H-9 and H-12 was consistent with the *cis* relationship between these protons[199], this observation was supported by the NOESY correlations from H-9 to H-12.

From the above evidence and NOESY correlations, the structure of (**37**) identified to be echinulin. The compound was further confirmed by comparison with published data on the literature[200, 201]. Since the specific rotation of (**37**) equal zero, therefore, the compound found to be a racemic mixture in the solution.

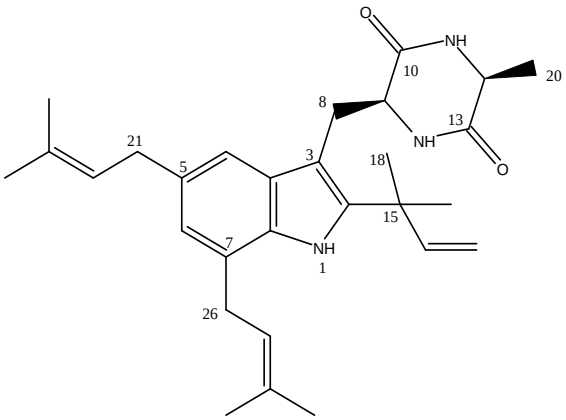

37a

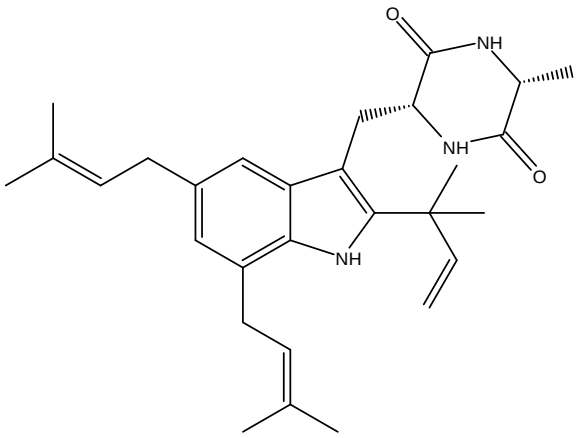

37b

In fact, echinulin is a common prenylated indolopiperazine derivative, first isolated from *Aspergillus amstelodami* in 1961[202], and later from various sources such as its teleomorph *Eurotium amstelodami*[203], as well as from several other species from the genus *Eurotium*[204,205]. Echinulin was also identified from cultures of different fungal species such as *Aspergillus variecolor*[206] and *Penicillium griseofulvum*[207], as well as from different plants of *Anacardiaceae*, *Cucurbitaceae* and *Orchidaceae* families[208].

5.1.1.6 8-Hydroxyechinulin

Compound (**38**) was obtained as a dark brown solid (2.3 mg). The molecular formula $C_{29}H_{39}N_3O_3$ was deduced based on the basis of HRESIMS (*m/z* 500.2900 calcd. 500.2891 $[M + Na]^+$, suggesting 12 degrees of unsaturation.

The ^{1}H NMR spectrum in (MeOD-d_4) (**Table 12**) displayed signals for two aromatic protons [δ_H 7.49 (1H, s, H-4) and 6.71 (1H, s, H-6)], and five olefinic protons [δ_H 6.23 (1H, dd, *J* = 17.5, 10.6 Hz, H-16), 5.36 (1H, m, H-22), 5.37 (1H, m, H-27), 5.21 (1H, dd, *J* = 17.5, H-17a) and 5.12 (1H, d, *J* = 10.5 Hz, H-17b)]. Furthermore, three methine protons including one oxygenated [δ_H 5.54 (1H, d, *J* = 7.7 Hz, H-8), 4.56 (1H, br dd, *J* = 7.7, 0.9 Hz, H-9), and 3.94 (1H, q, *J* = 7.1 Hz, H-12)], two methylene protons [δ_H 3.56 (2H, d, *J* = 7.2 Hz, H-21), and 3.37 (2H, m, H-26)], and seven methyl protons [δ_H 1.79 (3H, s, H_3-24), 1.77 (3H, s, H_3-29), 1.75 (3H, s, H_3-25), 1.73 (3H, s, H_3-30), 1.56 (3H, s, H_3-18), 1.55(3H, s, H_3-19), and 1.13 (3H, d, *J* = 7.1 Hz, H_3-20)] were observed.

The ^{13}C NMR spectroscopic data (**Table 12**) exhibited 29 carbon signals that were assigned to seven methyls, three methylene, eight methines among them one oxygenated and two nitrogen-containing tertiary, two amide carbonyl, and nine quaternary carbons.

Interpretation of the ^{1}H-^{1}H COSY NMR data of (**38**) (**Figure 19**) identified four isolated proton spin systems corresponding to the C-4–C-29 (via C-5 and C-7), C-16–C-17, C-8–C-9, and C-12-C-20) fragments.

HMBC correlations from H_3-24 and H_3-25 to C-22 and C-23, H-22 to C-24 and C-25, as well as correlations of both H_3-29 and H_3-30 to C-27 and C-28, H-27 to C-29 and C-30, established the two prenyl subunits (C-21–C-25 and C-26–C-30). While those from H_3-18 and H_3-19 to C-15 and C-16, H-17 to C-15 and C-16, and from H-16 to C-18 and C-19 completed the reverse prenyl C-15–C-19 substructure of (**38**). The tetrasubstituted indole moiety of (**38**) was deduced by HMBC correlations from H-4 to C-3, C-3a, C-6, C-7a, and C-21 and from H-6 to C-4, C-5, C-7, C-21, and C-26, together with the ^{1}H-^{1}H COSY correlation between H-4 and H-6. HMBC cross-peaks from H_2-21 to C-4, C-5, and C-6, from H_2-26 to C-6 and C-7a indicated that C-21 and C-26 were attached to C-5 and C-7, respectively. HMBC correlations from H-16, H_3-18, and H_3-19 to C-2 led to the connection of C-2 to C-15.

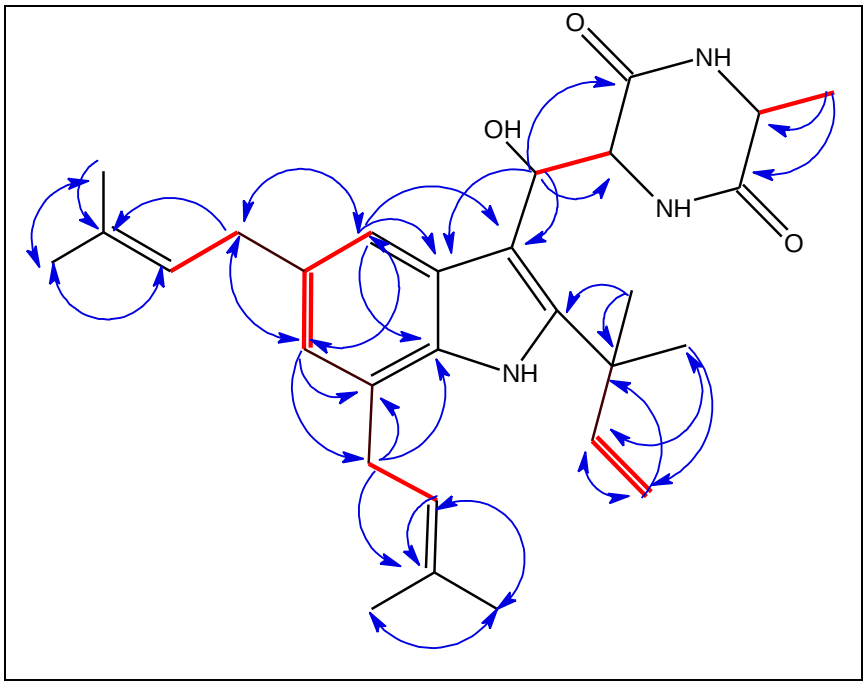

Figure 19: Key COSY (▬) and selected HMBC(⟶) correlations for (**38**).

Table 12: NMR spectroscopic data for 8-Hydroxyechinulin **(38)** (600 MHz, 150MHz)[a]

Position	^{1}HNMR (*J* in Hz)	^{13}CNMR	COSY	HMBC	NOESY
1-NH	-		-	-	-
2	-	144.1	-	-	-
3	-	109.1	-	-	-
3a		128.5	-	-	-
4	7.49 s	119.3	6	3, 3a, 6, 7a, 21	9, 21
5	-	133.7	-	-	-
6	6.71 s	123.0	4	4, 5, 7, 21, 26	21, 26
7	-	134.1	-	-	-
7a	-	134.2	-	-	-
8	5.54 (d, 7.7)	71.0	9	2, 3, 3a, 9, 10	9, 18
9	4.56 (br dd, 7.7, 0.9)	59.6	8	3, 8, 10	4
10-CO	-	169.6	-	-	-
11-NH	-		-	-	-
12	3.94 (br qd, 7.1, 0.9)	51.9	20	13, 20	-
13-CO	-	170.4	-	-	-
14-NH	-		-	-	-
15	-	40.3	-	-	-
16	6.23 (dd, 10.6, 17.5)	148.0	17	2, 17, 18, 19	-
17	5.12 (d, 10.6)	112.2	16	15, 16	-
	5.22 (d, 17.5)				
18	1.56 s	29.0	-	2, 15, 16, 19	-
19	1.55 s	28.8	-	2, 15, 16, 18	-
20	1.13 (d, 7.1)	20.3	12	12, 13	-
21	3.37 m	35.7	22	4, 22, 23	-
22	5.36 m	126.3	21	24, 25	-
23	-	133.7	-		-
24	1.73 s	26.0	21, 22	22, 23, 25	-
25	1.75 s	18.0	22	24	-
26	3.56 (d, 7.2)	30.8	27, 29	27, 28	6
27	5.37	123.9	26	7, 29, 30	-
28	-	133.4	-	-	-
29	1.77 s	18.0	26	30	-
30	1.79 s	26.0	27	27, 28	-

[a] The assignments were based on DEPT, HSQC, and HMBC experiments, and recorded in MeOD-d_4.

The above data revealed that (**38**) is a prenylated dioxopiperazine alkaloid similar to echinuline (**37**) except for the presence of an oxygenated methine at C-8 [δ_H 5.54 (1H, d, J = 7.7 Hz; δ_C 70.7)], instead of the two methylene protons. This observation was supported by both instances ^{1}H-^{1}H COSY and HMBC correlations (**Figure 19**) established that the low-field proton (H-8), resonating at δ_H 5.54 exhibited a clear COSY correlation with H-9 (δ_H 4.56) and HMBC correlations to the carbons at δc 59.2 (C-9), 108.6 (C-3), 128.8 (C-3a), 144.0 (C-2), and 169.5(C-10).

The relative configuration of (**38**) was assigned by NOESY experiments due to the correlation between H_3-20 and H-8, as well as the weak long-range ^5JH,H coupling constant of 0.9 Hz observed for H-9 and H-12 was consistent with the *cis* relationship between these protons[199]. Marfey's analysis (**Appendix 18**) allowed the assignment of L-configuration for the alanine residue. Moreover, the optical rotation was measured as $[\alpha]_D^{22}$ = -150 (c 0.2, MeOH). The configuration at position C-8 was not assigned. All the aforementioned evidence characterized compound (**56**) as a new prenylated indole diketopiperazine with the name 8-hydroxyechinulin.

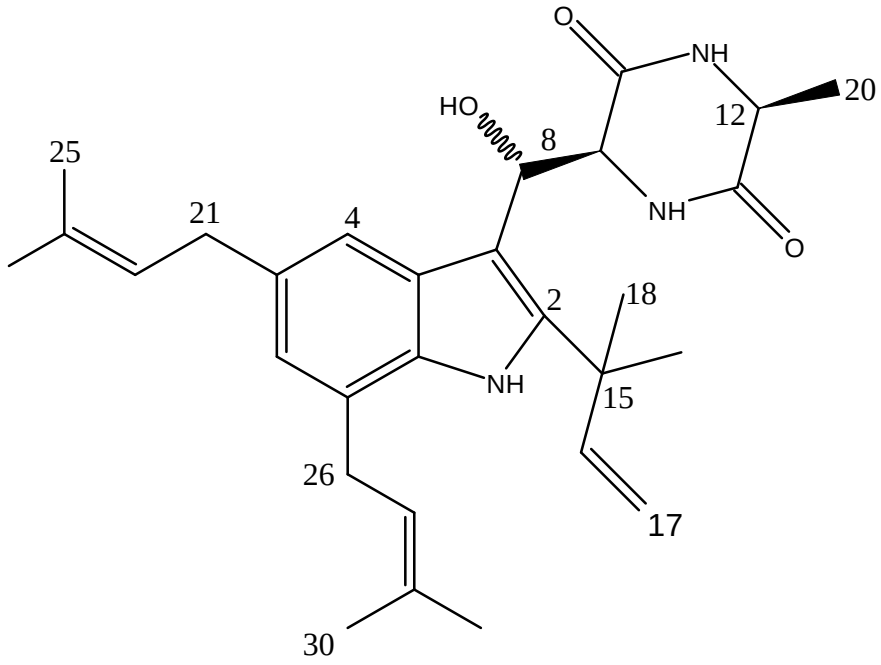

38

5.1.1.7 27-28-Epoxyechinulin

Compound (**39**) was obtained as a brown amorphous solid (1.3 mg) and showed the same molecular formula of $C_{29}H_{39}N_3O_3$ based on HR-ESIMS of the quasi molecular ion $[M+H]^+$ (*m/z* 478.3085 calcd. 478.3081), suggesting a similar structure to (**38**) with twelve degrees of unsaturation. This information, coupled with the ^{13}C NMR data, suggested that (**39**) contained two carbonyl groups, six double bonds, and four rings.

Carefully comparing the NMR spectra of (**39**) (**Table 13**) with those of (**38**) indicated that one of the prenyl groups had two upfield shifted methyl singlets at (δ_H 1.35 and 1.47) instead of (δ_H 1.77 and 1.79), as well as one oxygenated methine at (δ_H 3.02, t, J = 8.7 Hz) instead of the olefinic methine, and two methylene protons appeared at δ_H 3.00, ovlp and 3.13, m. Moreover, sp^3 quaternary carbon at δ_C 61.0 instead of sp^2 quaternary at (δ_C 133.4 in **38**) was observed in the ^{13}C NMR spectrum. These data indicated that an oxiran ring was formed between C-27 and C-28. This conclusion was confirmed by the key HMBC correlations (**Figure 20**) between H_2-26 with C-28 (δ_C 60.8), C-27 (δ_C 66.1), C-6 (δ_C 123.8) and C-7a (δ_C 134.2), between H-27 with C-30 (δ_C 19.1), C-29 (δ_C 25.0), C-26 (δ_C 33.1) and C28 (δ_C 61.0). The epoxy unit was also corroborated with the unsaturation degrees and molecular weight.

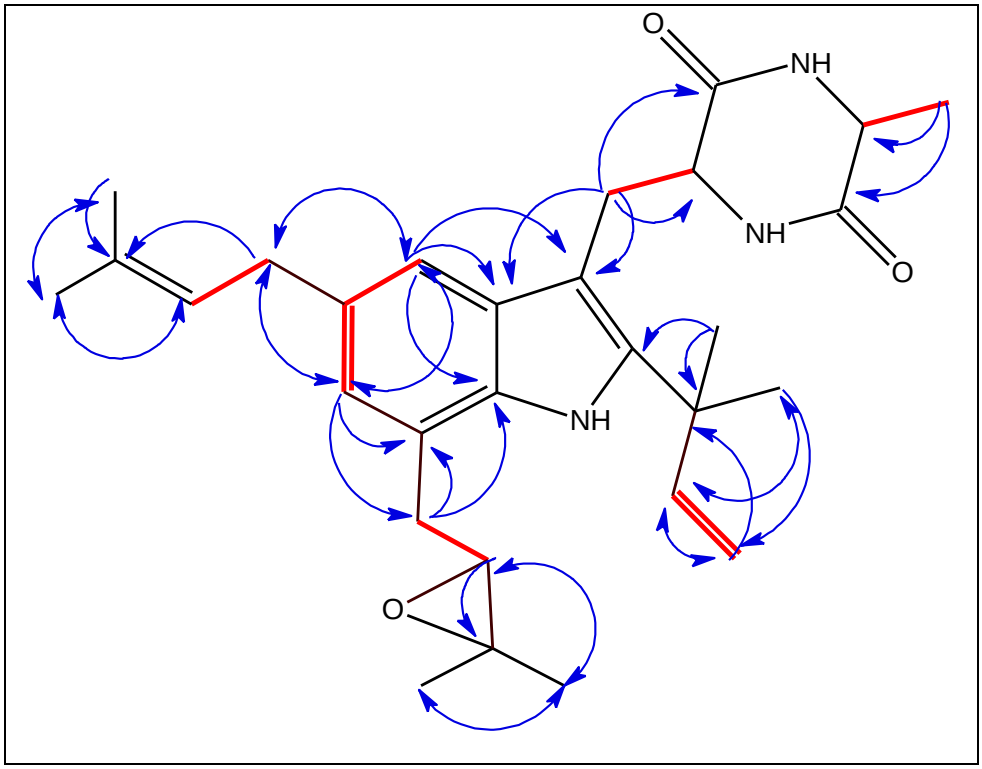

Figure 20: Key COSY (▬) and selected HMBC(⟶) correlations for (**39**)

Table 13: NMR spectroscopic data for epoxyechinulin (**39**), (400 and 100 MHz, δ ppm) [a]

Position	^{1}HNMR (*J* in Hz)	^{1}HNMR (*J* in Hz)[b]	^{13}CNMR	COSY	HMBC	NOESY[b]
1-NH	-	9.84 br s	-	-	-	-
2	-	-	143.0	-	-	-
3	-	-	105.9	-	-	-
3a	-	-	130.7	-	-	-
4	7.21 s	7.10 s	117.0	6, 21	3, 6, 7, 21	
5	-	-	134.0	-	-	-
6	6.79 s	6.71 s	123.8	4	4, 5, 7, 21, 26	
7	-	-	133.9	-	-	-
7a	-	-	134.2	-	-	-
8	3.22 (dd, 9.9, 14.5)	3.32 ovlap	32.1	9	2, 3, 3a, 9, 10	20, 30
	3.52 (dd, 3.9, 14.5)	3.02 (br dd, 6.6, 14.6)				
9	4.26 (dd, 3.9, 14.5)	3.92 m	57.2	8	3, 8, 13	18, 29
10-CO	-	-	170.2	-	-	-
11-NH	-	8.19 (br d, 3.0)		-	-	12, 20
12	3.94 (q, 7.0)	3.82 (qd, 7.0, 3.0)	52.1	20	13, 20	11, 20
13-CO	-	-	170.3	-	-	-
14-NH	-	7.48 (br d, 3.0)		-	-	4, 8, 16
15	-	-	40.3	-	-	-
16	6.20(dd, 10.6, 17.4)	6.20(dd, 10.6, 17.4)	147.8	17	2, 15, 18, 19	
17	5.12 (br dd, 10.6, 1.0)	5.03 (br dd, 10.6, 1.0)	112.1	16	2, 15, 16, 17, 18	
	5.16 (br dd, 17.4, 1.0)	5.07 (br dd, 17.4, 1.0)				
18	1.567 s	1.50 s	28.5	-	2, 15, 16, 19	
19	1.57 s	1.51	28.6	-	2, 15, 16, 18	
20	1.40 (d, 7.0)	1.32 (d, 7.0)	21.2	12	12, 13	4, 11, 12
21	3.40 (d, 6.9)	3.00 ovlp.	35.5	22, 25	4, 22, 23	
22	5.38 (tq, 6.9, 1.3)	5.31 (tq, 6.9, 1.3)	126.0	21, 25	21, 24, 25	
23	-	-	132.1	-	-	-
24	1.746 s	1.70 s	26.0	21, 22	22, 23, 25	
25	1.75 s	1.69 s	17.9	21, 22	22, 23, 24	
26	3.00 ovlp	2.99 ovlap	33.1	27	6, 7a, 27, 28	
	3.13 m	3.16				
27	3.02 (t, 8.7)	3.05	66.1	26	26, 28, 29, 30	
28	-	-	61.0	-	-	-
29	1.35 s	1.23 s	25.0	30	27, 28, 30	
30	1.47 s	1.27	19.1	29	27, 28, 29	

[a] The assignments were based on DEPT, ^{1}H-^{1}H COSY, HSQC, and HMBC experiments, and recorded in MeOD-d_4. [b] The assignments were recorded in DMSO-d_6

The other indication was the replacement of the oxygenated methine at C-8 [δ_H 5.54 (1H, d, J = 7.7 Hz; δ_C 70.7)] by methylene protons at [(δ_H 3.22, 1H, dd, J = 14.5, 9.9 Hz) and 3.52 (1H, dd, J = 14.5, 3.9 Hz; δ_C 32.1)]. The gross structure of (**39**) was completely assigned by a detailed analysis of its COSY and HMBC data (**Table 13**). The relative configuration of (**39**) could not be directly assigned by NOESY experiments due to the lack of enhancement between H-9 and H-12. However, the co-facial stereo-relation between the 20-CH_3 and 8-CH_2 was deduced by the observed enhancement of the H_3-20 signal (1.40 ppm) after irradiation of H-8a (3.22 ppm) in the selected 1D NOE (**Appendix 26**).

Marfey's analysis (**Appendix 27**) allowed the assignment of L-configuration for the alanine residue of (**39**). The specific rotation was measured $[\alpha]_D^{22}$ = -200 (c 0.2, MeOH).

Furthermore, the ^{13}C NMR chemical shifts of C-27 and C-28 were 66.1 and 61.0 ppm respectively, which suggested that the relative configuration of C-27 of the epoxide ring was (*S*) like isoechinulin D[209]. But due to the lack of the compound quantity, we could not confirm that.

All the above data supported the compound to be a new diketopiperazine alkaloid with the name 27-28-epoxyechinulin.

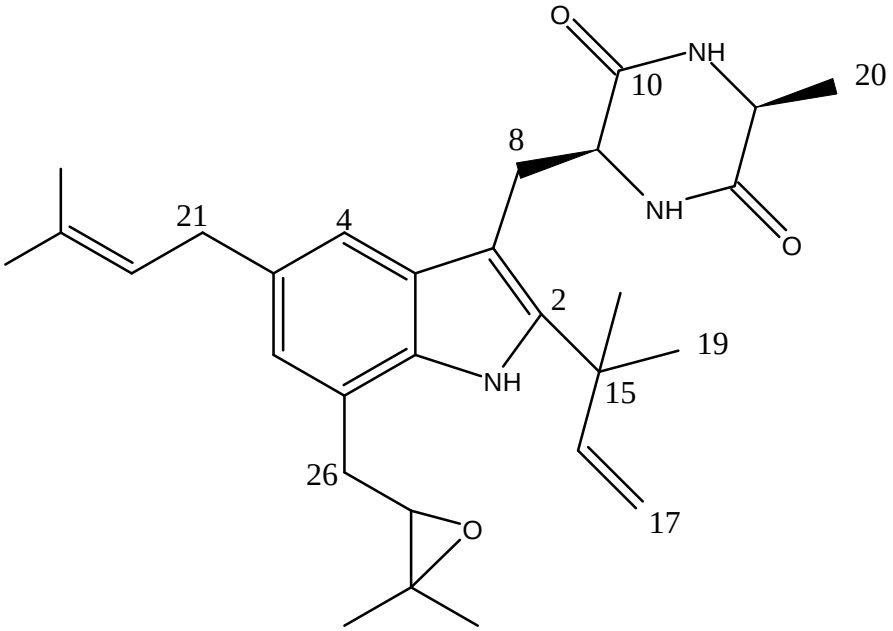

39

5.1.1.8 Cyclo-L-2-tert-DMA-4,5,7-tri-DMA-Trp-L-Ala

Compound (**40**) was obtained as a white amorphous solid (0.5 mg) and showed the molecular formula of $C_{34}H_{47}N_3O_2$ based on HRESIMS (*m/z* 530.3750 $[M+H]^+$ calcd. 529.3747), suggesting twelve degrees of unsaturation.

The ^1H NMR spectrum (**Table 14**) displayed singlet signal for one aromatic protons at δ_H 6.73 (1H, s, H-6), and six olefinic protons [δ_H 6.23 (1H, dd, *J* = 17.5, 10.6 Hz, H-16), 5.36 (1H, m, H-22), 5.37 (1H, m, H-27), 5.37 (1H, m, H-27), 5.21 (1H, dd, *J* = 17.5 Hz, H-17a) and 5.12 (1H, d, *J* = 10.5 Hz, H-17b)]. Furthermore, two methine protons at δ_H 4.30 (1H, br dd, *J* = 11.0, 3.9 Hz, H-9), and 4.00 (1H, q, *J* = 6.9 Hz, H-12)], four methylene protons [δ_H 3.71 (2H, m, H_2-31), [3.67 (1H, dd, *J* = 15.1, 3.9 Hz, H-8a), 3.31 (1H, ovlap, H-8b)], 3.54 (2H, d, *J* = 7.1 Hz, H_2-26), and 3.31 (2H, d, *J* = 7.1 Hz, H_2-21), and nine methyl protons [δ_H 1.82 (3H, s, H_3-29), 1.79 (3H, s, H_3-30), 1.75 (3H, s, H_3-34), 1.71 (3H, s, H_3-

24), 1.70 (3H, s, H_3-25), 1.66 (3H, s, H_3-35), 1.58 (3H, s, H_3-18), 1.56 (3H, s, H_3-19), and 1.46 (3H, d, J = 6.9 Hz, H_3-20)] were observed.

Table 14: NMR spectroscopic data for (**40**) (600 and 150 MHz, δ ppm)[a]

Position	^{1}HNMR (J in Hz)	^{13}CNMR	COSY	HMBC
1-NH	-	-	-	-
2	-	142.7	-	-
3	-	106.3	-	-
3a	-	126.1	-	-
4	-	134.6	-	-
5	6.73 s	124.5	-	4, 7, 21, 26
6	-	133.8	-	-
7	-	130.0	-	-
7a	-	131.8	-	-
8	3.67 (dd, 3.9, 15.1)	32.6	9	3, 10
	3.32 ovlp			3, 3a
9	4.30 (dd, 11.0, 3.9)	56.6	8	3a, 10
10-CO	-	169.8	-	
11-NH	-	-	-	-
12	4.00 (q, 6.9)	51.3	20	13, 20
13-CO	-	170.5	-	-
14-NH	-	-	-	-
15	-	40.3	-	-
16	6.21 (dd, 10.6, 17.5)	147.8	17	18, 19
17	5.12 (d, 10.6)	111.9	16	15, 16
	5.17 (d, 17.5)			
18	1.56 s	28.1	-	2, 15, 16, 19
19	1.58 s	28.1	-	2, 15, 16, 18
20	1.46 (d, 6.9)	19.6	12	12, 13
21	3.32 ovlp	32.6	22	3, 3a, 5, 23
22	5.20 (br t, 7.1)	126.1	21	21, 25
23	-	131.3	-	-
24	1.71 s	18.0	-	23, 25
25	1.70 s	25.5	-	23, 24
26	3.54 (d, 7.1)	30.5	27	27, 28
27	5.39 (br t, 7.1)	123.9	26	30
28	-	133.4	-	-
29	1.82, s	18.0	-	27, 28, 30
30	1.79, s	25.5	-	27, 28, 29
31	3.71 m	28.4	32	-
32	4.95 (br t, 7.0)	125.6	31	7, 34
33	-	132.5	-	-
34	1.75, s	18.0	-	32, 33, 35
35	1.66, s	25.5	-	32, 33, 34

[a] The assignments were based on DEPT, HSQC, and HMBC experiments, and recorded in MeOD-d_4

The ^{13}C NMR data (**Table 14**) assigned by the aid of HSQC and HMBC exhibited 34 carbon signals that were assigned to nine methyls, four methylene, seven methines among them two nitrogen-containing tertiary, two amide carbonyl, and eleven uncharacteristic carbons. Characteristic triplets for olefinic protons of three regular prenyl moieties were observed at δ_H 5.39, 5.20, and 4.95 ppm, respectively. Interpretation of the ^{1}H-^{1}H COSY NMR data of (**40**) (**Figure 21**) identified six isolated proton spin systems corresponding to H-8/H-9, H-12/H-20, H-16/H-17, H-21/H-22, H-26/H-27, and H-31/H-32 fragments.

A close comparison of these signals with those of echinulin (**37**) suggested that the three regular residues of (**40**) are located at C-4, C-6 and C-7 of the indole ring. This was further verified by the HMBC correlation of H-21 to C-3, C-3a, C-6, and C-23, in addition to the observation of only one singlet signal for one aromatic proton at δ_H 6.73 ppm, which correlated with C-4, C-7, C-21, and C-26

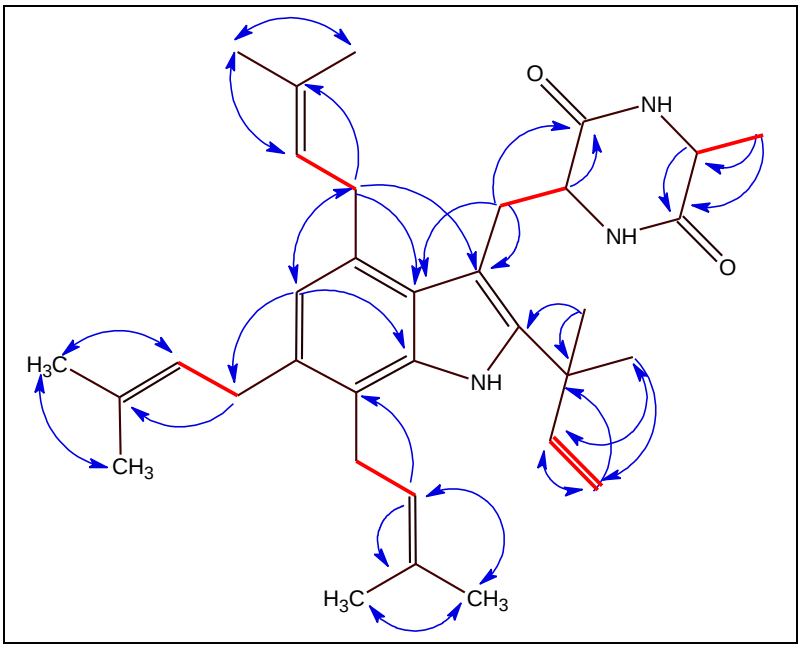

Figure 21: Key COSY (▬) and selected HMBC(⟶) correlations for (**40**)

Based on Marfey's analysis (**Appendix 30**), the absolute configuration of the alanine residue (**40**) was found to be L (C-9*S*, C-12*S*). The specific rotation was measured $[\alpha]_D^{22}$ = -80 (c 0.2, MeOH). All the above-mentioned witness characterized compound (**40**) as a prenylated indolediketopiperazin with the name Cyclo-L-2-tert-DMA-4,5,7-tri-DMA-Trp-L-Ala. Compound (**40**) was isolated only one time before as a minor compound during a biosynthetic experiment using two prenyltransferases from *Aspergillus ruber*[197] supported only ^{1}H NMR data in $CDCl_3$.

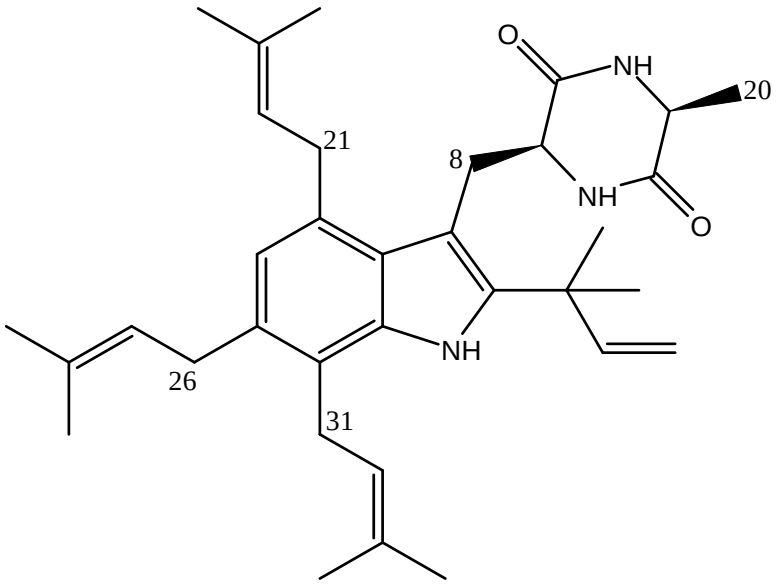

40

5.1.1.9 Cyclo[Trp-Val]

Compound (**41**) was obtained as white amorphous (3.2 mg) and its molecular formula was deduced as $C_{16}H_{19}N_3O_2$ based on the (+)-HR-ESIMS exhibited the *m/z* 286.1553 $[M+H]^+$, Calcd. 286.1556), required 9 degrees of unsaturation.

The ^{1}H NMR spectrum of compound (**41**) (**Table 15**) recorded in (MeOD-d_4), showed only 16 hydrogens, which suggested the presence of at least three exchangeable protons. Furthermore, the data indicated that (**41**) contained an indole ring owing to the presence of 5 protons in the aromatic region at δ_H (7.62, dt, J = 7.9, 1.0 Hz; δ_C 119.5), 7.32 (dt, J = 8.2, 1.0 Hz; δ_C 111.9), 7.08 (ddd, J = 8.2, 6.9, 1.0 Hz; δ_C 122.2), 7.08 (s; δ_C 125.6) and 7.00 (dt, J = 7.9, 1.0 Hz; δ_C 119.8), in addition to one methylene δ_H [3.20 (dd, J = 14.7, 4.5 Hz), 3.42 (dd, J = 14.7, 4.5 Hz; δ_C 30.5), three methines at δ_H 4.25 (td, J = 4.5, 1.0 Hz; δ_C 56.5), 2.91 (dd, J = 2.9, 1.0 Hz; δ_C 60.2), and 2.10 (m; δ_C 32.4), as well as, two methyl protons at δ_H 0.83 (d, J = 7.2 Hz; δ_C 18.1), and 0.81 (d, J = 6.8 Hz; δ_C 16.2).

The ^{13}C NMR data assigned by the aid of HSQC and HMBC of compound (**41**) exhibited 16 resonances, two of which were attributable to carbonyl carbons at (δ_C 170.8 and 170.1), three quaternary carbons at (δ_C 137.7, 128.7, and 108.4), and the 11 remainings corroborated the features deduced by analysis of the ^{1}H NMR spectroscopic data. The

mentioned spectroscopic data proposed compound (**41**) to be a 2,5-dioxopiperazine resulting from the condensation of tryptophan and valine.

Table 15: NMR spectroscopic data for Cyclo[Trp-Val] (**41**) (600 and 150 MHz, δ ppm) [a]

Position	^{1}HNMR (*J* in Hz)[b]	^{1}HNMR (*J* in Hz)	^{13}CNMR	COSY	HMBC	NOESY
1-NH	10.89 s	-	-	-	-	-
2	7.07 (d, 2.2)	7.08 s	125.6	-	3, 8, 9	8, 9
3	-	-	108.4	-	-	-
3a	-	-	128.7	-	-	-
4	7.60 (d, 7.9)	7.62 (dt, 7.9, 1.0)	119.5	5	3, 3a, 6, 7a	8
5	7.00 (dt, 7.9, 1.0)	7.00 (dt, 7.9, 1.0)	119.8	4, 6	3a, 7, 7a	-
6	7.08 (td, 7.9, 1.0)	7.08 (ddd, 8.2, 6.9 1.0)	122.2	5, 7	3a, 4, 7, 7a	12
7	7.30 (d, 7.9)	7.32 (dt, 8.2, 1.0)	111.9	6	3a, 4	-
7a	-	-	137.7	-	-	-
8	3.26 (dd, 4.5, 14.5)	3.20 (dd, 4.5, 14.7)	30.5	9	2, 3,3a, 9, 10	4, 6, 9
	3.03 m	3.42 (dd, 4.5, 14.7)				
9	4.12 (br t, 4.5)	4.25 (td, 4.5, 1.0)	56.5	8	3a, 8, 13	2, 4, 17
10-CO	-	-	170.8	-	-	-
11-NH	7.85, br s	-	-	-	-	-
12	3.03 m	2.91 (dd, 2.9, 1.0)	60.2	15	13, 15, 17	15, 17
13-CO	-	-	170.1	-	-	-
14-NH	8.01,br s	-	-	-	-	-
15	2.03 m	2.10 m	32.4	12	12, 13, 17	17
16	0.81 (d, 7.2)	0.83 (d, 7.2)	18.1	15	12, 15, 17	12
17	0.76 (d, 6.8)	0.81 (d, 6.8)	16.2	15	12, 15, 16	9, 12

[a] The assignments were based on DEPT, ^{1}H-^{1}H COSY, HSQC, and HMBC experiments, and recorded in MeOD-d_4; [b] assignments were recorded in DMSO-d_6

The relative configuration of (**41**) was determined to be C-9*S*, C-12*R* by the aid of NOESY correlation (**Table 15**), the specific rotation $[\alpha]_D^{22}$ = -143 (c 0.28, MeOH), and a comparison of its spectroscopic data with those found in the literature[210].

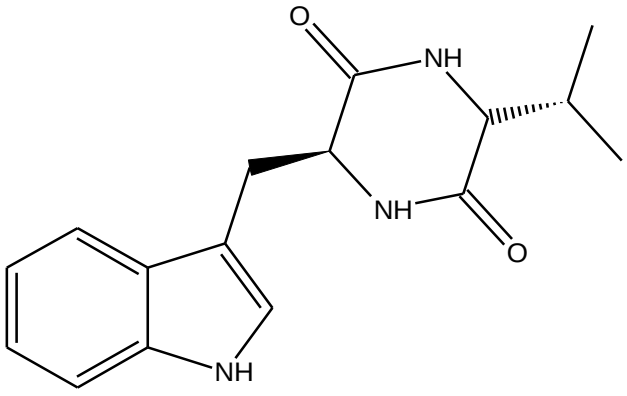

41

5.1.1.10 Eurocristatine

Compound (**42**) was isolated as white solid (15.0 mg) and its molecular formula was deduced as $C_{32}H_{36}N_6O_4$ based on the (+)-HR-ESIMS exhibited the *m/z* 569.2905 $[M+H]^+$, required 18 degrees of unsaturation.

The ^{13}C NMR (**Table 16**) displayed sixteen carbon signals which were categorized, according to HSQC as two amide carbonyls (δ_C 168.5, 167.6), two quaternary sp^2 (δ_C 149.1, 130.5), four methine sp^2 (δ_C 128.8, 124.5, 118.1, 109.0), one quaternary sp^3 (δ_C 59.8), four methine sp^3 (δ_C 78.9, 62.3, 55.8, 32.1), one methylene sp^3 (δ_C 37.3) and two methyl (δ_C 19.0, 18.0) carbons. However, the (+)-HR-ESIMS exhibited the molecular formula $C_{32}H_{36}N_6O_4$, implying that each carbon signal must correspond to two carbon atoms.

The analysis of $^1H-^1H$ COSY (**Figure 22**) afforded coupling system of the aromatic protons at δ_H 7.38 (d, J = 7.5 Hz), 7.02 (t, J = 7.8 Hz), 6.64 (t, J = 7.5, Hz), and 6.61 (d, J = 7.8 Hz), which revealed the presence of one 1,2-disubstituted benzene ring. This was confirmed by the HMBC cross-peaks of the doublet at δ_H 7.38 (J = 7.5 Hz; δ_C 124.5) to the carbons at δ_C 128.8 and 149.1, of the triplet at δ_H 6.64 (J = 7.5, Hz; δ_C 118.0) to the carbons at δ_C 109.0 and 130.5, of the triplet at δ_H 7.02 (J = 7.8, Hz; δ_C 128.8) to the carbons at δ_C 124.5 and 149.1, and of the doublet at δ_H 6.61 (J = 7.8 Hz; δ_C 109.0) to the carbons at δ_C 118.0 and 130.5. Moreover, the doublet at δ_H 7.39 (J = 7.5 Hz; δ_C 124.5) also showed HMBC cross-peaks to the quaternary sp^3 carbon at δ_C 59.8, while the amide singlet at δ_H 6.72, displayed HMBC cross-peaks to the aromatic carbons at δ_C 130.5 and 149.1 as well as to the quaternary sp^3 carbon at δC 59.8 and the methine sp^3 carbon at δ_C 78.9. These correlations confirmed that the 1,2-disubstituted benzene ring was a part of an indole moiety in the molecule.

The COSY spectrum also showed that another part of the molecule consisted of three coupling systems, i.e., of the methylene protons at δ_H 2.40 [(dd, J = 14.0, 9.3 Hz) and 3.12 (dd, J = 14.0, 9.3 Hz); δ_C 37.3)] to the methine proton at δ_H 4.12 (t, J = 9.0 Hz; δ_C 55.8), of the amide proton at δ_H 8.27 (d, J = 4.2 Hz) to the methine proton at δ_H 3.38 (br dd, J = 2.0, 5.7 Hz; δ_C 62.3), of the methine proton at δ_H 3.38 to the methine proton at δ_H 1.95 (m; δ_C 32.0), and of the methine proton at δ_H 1.95 to the methyl protons at δ_H 0.80 (d, J = 6.9 Hz; δ_C 19.0) and 0.70 (d, J = 6.7 Hz; δ_C 18.0). The HMBC spectrum showed cross-peaks of the amide proton at δ_H 8.25 (d, J = 4.3 Hz) to the methine carbon signals at δ_C 55.8, 62.3 and the amide carbonyl carbons at δ_C 168.5 and 167.6, indicating that another portion of the molecule was a 1,4-diketopiperazine system.

Table 16: NMR spectroscopic data for eurocristatine (**42**) (400 and 100 MHz, δ ppm) [a]

Position	^{1}HNMR (*J* in Hz)	^{13}CNMR	COSY	HMBC	NOESY [b]
1-NH	6.72 s	-	2	3, 4, 8, 9	
2	4.92 s	78.9	1	3, 4, 9	11, 12b, 19
3	-	59.8	-	-	-
4	-	130.5	-	-	-
5	7.38 (d, 7.5)	124.5	6	3, 4, 7, 9	6, 11, 12
6	6.64 (br t, 7.5)	118.1	5, 7	4, 8, 9	-
7	7.02 (t, 7.8)	128.8	6, 8	4, 5, 8, 9	-
8	6.61 (d, 7.8)	109.0	7	4, 5, 9	-
9	-	149.1	-	-	-
11	4.12 (t, 9.0)	55.8	12	12, 13	2, 5, 12b, 17, 19
12	2.40 (dd, 9.3, 14.0)	37.3	11	3, 4, 11, 13	
	3.12 (dd, 9.3, 14.0)				2
13-CO	-	168.5	-	-	-
14-NH	8.25 (d, 4.3)	-	15	11, 13, 15, 16	
15	3.38 (br dd, 2.0, 5.7)	62.3	14, 17	13, 16, 17, 18	17, 18, 19
16-CO	-	167.6	-	-	-
17	1.95 m	32.1	15, 18, 19	15, 16, 18, 19	15, 18
18	0.80 (d, 6.9)	19.0	17	15, 17, 19	15, 17
19	0.70 (d, 6.7)	18.0	17	15, 17, 18	11, 15, 17

[a] The assignments were based on DEPT, ^{1}H-^{1}H COSY, HSQC, and HMBC experiments, and recorded in DMSO-d_6; [b] recorded in MeOD-d_4

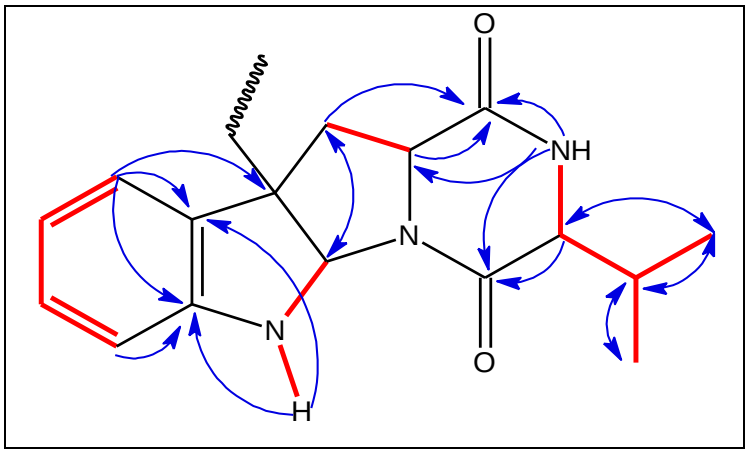

Figure 22: Key COSY (▬) and selected HMBC(→) correlations in the monomer (A).

Additionally, the HMBC cross-peaks of the triplet at δ_H 3.39 (J = 5.0 Hz; δ_C 62.3) to the carbon at δ_C 32.1 and the methyl carbons at δ_C 19.0 and 18.0, and of the multiplet of the methine proton at δ_H 1.94 (δ_C 32.0) to the amide carbonyl carbon at δ_C 167.5, to the methine carbon at δ_C 62.3 and methyl carbons at δ_C 19.0 and 18.0, indicated that the isopropyl moiety was placed on C-15 (δ_C 62.3) of the diketopiperazine ring.

That the 1,4 diketopiperazine ring moiety was linked to the indole ring system through C-2 (δ_C 78.9) of the latter and N-10 of the former, and through the methylene group

on C-3 (δ_C 59.8) of the latter and C-11 (δ_C 55.7) of the former, was evidenced by COSY correlations discussed above, as well as the HMBC correlations of the methylene proton at δ_H 2.39, to the carbons at δ_C 59.8, 130.5 and 168.5

Considering altogether the NMR data, the partial structure A ($C_{16}H_{18}N_3O_2$) was proposed as in (**Figure 22**). Due to the (+)-HR-ESIMS which gave the molecular formula $C_{32}H_{36}N_6O_4$, the complete structure of (**42**) must include two A units connected through the carbon at δ_C 59.8. The specific rotation of (**42**) was measured as $[\alpha]_D^{22}$ = +273 (c 0.3, MeOH), The compound was further confirmed by comparison with authentic data in the literature[211].

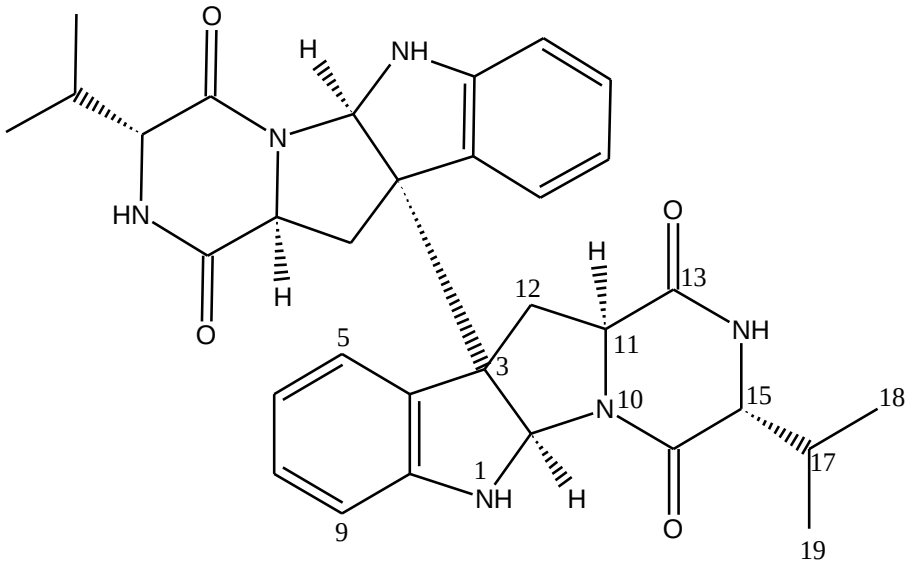

42

Recently, two diketopiperazine dimers whose structures closely resemble to eurocristatine (**42**), were reported. Interestingly, the first isomer which named Homodimer was reported synthetically[212], whereas the second isomer cristatumin E, was isolated from the algicolous *Eurotium herbariorum* HT-2[213].

Biosynthetically, compounds (**41**) and (**42**) are derived from different biosynthetic pathways. The biosynthesis of the prenylated indole derivatives, including diketopiperazine derivatives, has been reviewed[214].

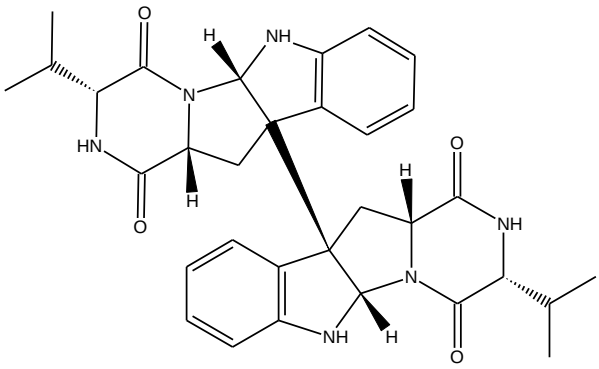

Homodimer

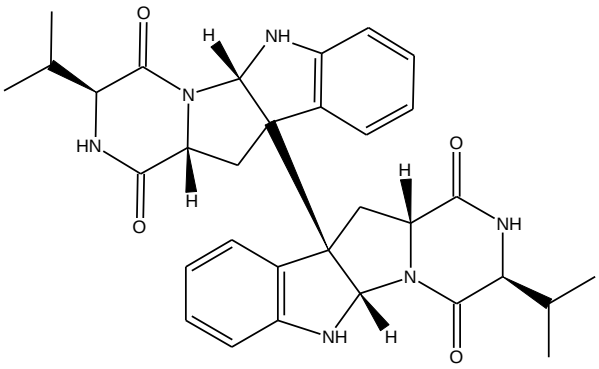

Cristatumin E

While cyclo-[D-tryptophyl-D-alanyl) (**33**) derives from a simple cyclization of D-tryptophan and D-alanine, echinulin (**37**) and its analogues correspond to mono- (**34**), di- (**36**), tri (**38**, **39**) or tetra (**40**) prenylated derivatives of a cyclic dipeptide consisting of L-tryptophan and L-alanine. Eurocristatine (**42**) is a dimerized cyclic dipeptide derived from two molecules of L-tryptophan and two molecules of L-valine. Despite the limited number of reports concerning the biosynthesis of dimerized cyclodipeptides, recently a plausible and unifying hypothesis was proposed for the biosynthetic pathway of dimeric diketopiperazines joined through C3/C3' bond[215]. Thus the structure of eurocristatine (**42**) suggests that it was derived from a common biosynthetic pathway proposed in **Scheme 3**.

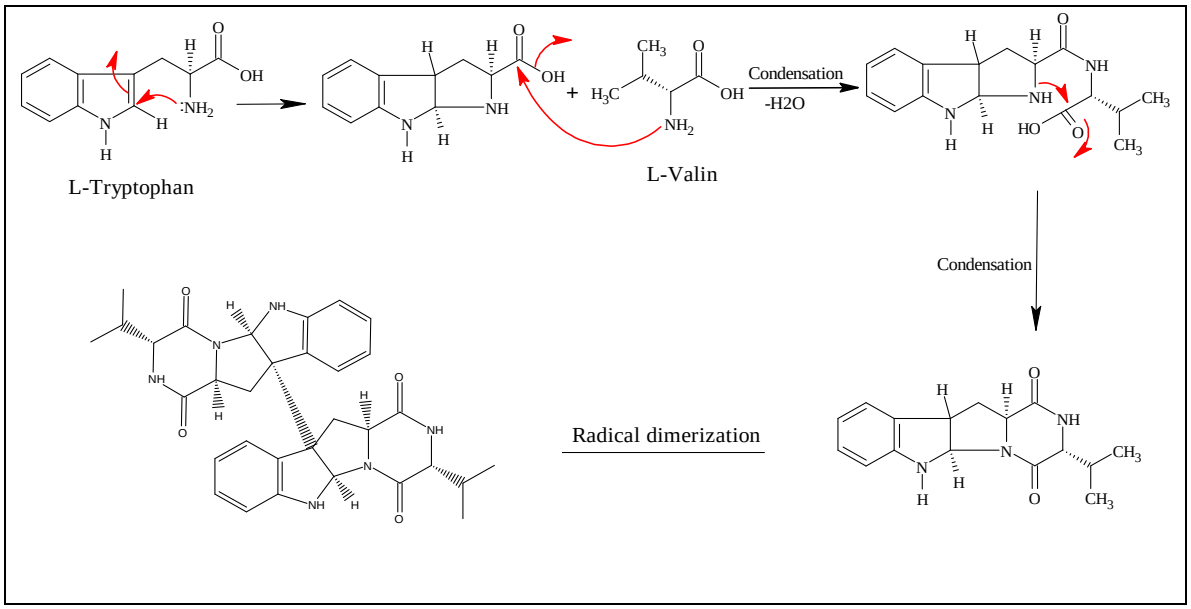

Scheme 3: Proposed biosynthetic pathway for eurocristatine (**42**)

5.1.1.11 Neoechinulin A

Neoechinulin A (**43**) was isolated as a yellow solid (20 mg). it showed an absorbing band at 254 nm and turned into green after spraying with vanillin reagent and heating. R_f = 0.29 (DCM/MeOH 5%). The Positive and negative HRESI-MS exhibited a strong peak at *m/z* 324.1700 $[M+H]^+$ and *m/z* 322.1554 $[M-H]^+$ indicating a molecular formula of $C_{19}H_{21}N_3O_2$, required 11 of unsaturation.

The ^1H NMR and HSQC spectra (**Table 17**) exhibited the presence of signals attributable to three NH protons at δ_H [8.30 (1H, s, NH-1), 7.44 (1H, s, NH-11), and 6.29 (1H, s, NH-14)], and four aromatic protons at δ_H 7.37 (1H, br dd, *J* = 7.9, 1.0 Hz, H-7), 7.28 (d, *J* = 7.9 Hz, H-4), 7.16 (1H, ddd, *J* = 7.9, 7.0, 1.0 Hz, H-5) and 7.19 (1H, ddd, *J* = 7.9, 7.0, 1.0 Hz, H-6). The ^{13}C NMR spectrum with the aid of HSQC DEPT revealed the presence of two amide carbonyls (δ_C 166.7, 159.7), six methines sp^2 (δ_C 144.3, 122.4, 121.1, 118.9, 111.3, 112.0), five quaternary sp^2 (δ_C 143.8, 134.3, 126.1, 124.5, 103.0), one methylene sp^2 (δ_C 113.4), one methine sp^3 (δ_C 51.7), one quaternary sp^3 (δ_C 39.2) and three methyl carbons at (δ_C 27.3, 27.4, 20.9).

The analysis of $^1H–^1H$ COSY and HMBC data afforded three substructures, A, B and C as shown in (**Figure 23**). The COSY cross-peaks between the aromatic protons H-4/H-5/H-6/ and H-7, along with the HMBC correlations of H-4 to C-3a and C-7a, of H-5 to C-3a and C-7, of H-6 to C-3a, C-5, C-7 and C-7a, of H-7 to C-3a and C-5, and of NH-1 to C-3, C-3a, and C-7a confirmed the presence of the substructure A (2,3-disubstituted 2,3-dihydro-1H-indole). Furthermore, the COSY spectrum also revealed couplings of the olefinic proton at δ_H 6.08 (dd, *J* = 17.4, 10.6 Hz; δ_C 144.3) to the methylene sp^2 protons at δ_H [5.24, dd (*J* = 10.6, 0.6 Hz; H-17a), and 5.21(d, *J* = 17.4 Hz; H-17b)]. Due to the diagnostic HMBC correlations of the olefinic proton H-16 to the quaternary sp^3 carbon at δ_C 39.2 and the methyl carbons at δ_C 27.4, 27.3, of the methylene protons at H_2-17 to the carbons at δ_C 144.3 and 39.2, as well as, of the methyl protons at δ_H 1.53, s (δ_C 27.4) and 1.53, s (δ_C 27.3) to the carbons at δ_C 39.2 and 144.3, the presence of substructure B (1-methylbuten-3-yl) moiety was confirmed.

Table 17: NMR spectroscopic data for neoechinulin A (**43**), (600 and 150 MHz)[a]

Position	^{1}HNMR (*J* in Hz)	^{13}CNMR	COSY	HMBC
1-NH	8.30, s	-	-	3, 3a, 7a
2	-	143.8	-	-
3	-	103.0	-	-
3a	-	126.1	-	-
4	7.28 (d, 7.9)	118.9	5	3a, 7a
5	7.16 (ddd, 7.9, 7.0 1.0)	122.4	4, 6	3a, 7
6	7.19 (ddd, 7.9, 7.0 1.0)	121.1	5, 7	3a, 5, 7, 7a
7	7.37 (br dd, 7.9, 1.0)	111.3	6	3a, 5
7a	-	134.3	-	-
8	7.21 s	112.0	-	2, 3a, 10
9	-	124.5	-	-
10-CO	-	159.7	-	-
11-NH	7.44 s		12	10, 12, 13
12	4.31 (qd, 7.0, 1.7)	51.7	11, 20	10, 13
13-CO	-	165.7	-	-
14-NH	6.29 s	-	-	9, 13
15	-	39.2	-	-
16	6.08 (dd, 17.4, 10.6)	144.3	17	15, 17, 18, 19
17	5.24 (dd, 10.6, 0.6) 5.21 (dd, 17.4, 0.6)	113.4	16	15, 16
18	1.53 s	27.3	-	2, 15, 19
19	1.53 s	27.4	-	2, 15, 18
20	1.61 (d, 7.0)	20.9	12	12, 13

[a] The assignments were based on DEPT, ^{1}H-^{1}H COSY, HSQC, and HMBC experiments, and recorded in $CDCl_3$.

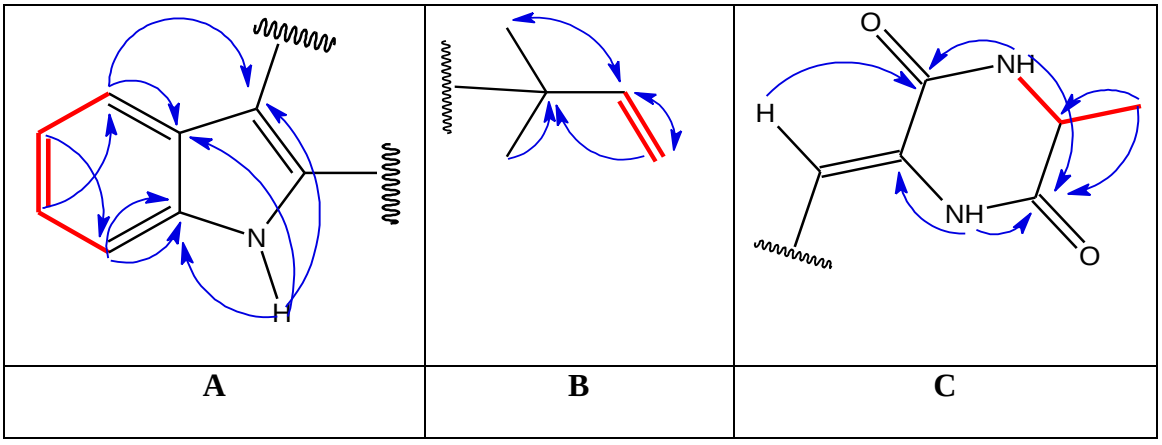

Figure 23: Key COSY (▬) and selected HMBC (→) correlations for neoechinulin A (**43**)

Likewise, the COSY spectrum showed the continuous coupling system of the singlet at δ_H 6.29, the quartet doublet at δ_H 4.31 (1H, J = 7.0, 1.7 Hz; δ_C 51.7) and the methyl doublet at δ_H 1.61 (3H, J = 7.0 Hz; δ_C 20.9). On the other hand, the singlet at δ_H 6.29 exhibited the HMBC cross-peaks to the quaternary sp^2 carbon at δ_C 124.5 and the carbonyl at δ_C 165.7, while the broad singlet at δ_H 7.44 gave HMBC correlations to the carbons at δ_C 165.7, 159.7 and 51.7. Since the singlet of the olefinic proton at δ_H 7.21 (δ_C 112.0) showed also cross-peaks to the carbonyl at δ_C 159.7, and the quaternary sp^2 carbons at δ_C 143.8 and 126.1, the presence of substructure C (1,4-diketopiperazine with substituents on C-2 and C-5), was confirmed.

The connection between the three substructures A, B and C was established by the aid of HMBC correlations (**Figure 24**), due to the HMBC correlations of the methyl groups H_3-18, 19 and the olefinic proton H-16 to the quaternary sp^2 carbon C-2 at δ_C 143.8, the 1-methylbuten-3-yl moiety was attached to C-2 (δ_C 143.8) of the indole ring system. Additionally, the HMBC cross peak of the methine singlet H-8 to the carbons of the indole ring system C-2 and C-3a confirmed the attachment of the substituted 1,4-diketopiperazine moiety to 2,3-dihydro-1H-indole portion through the carbon at δ_C 112.0 (C-8) of the former and the carbon at δ_C 103.0 (C-3) of the latter.

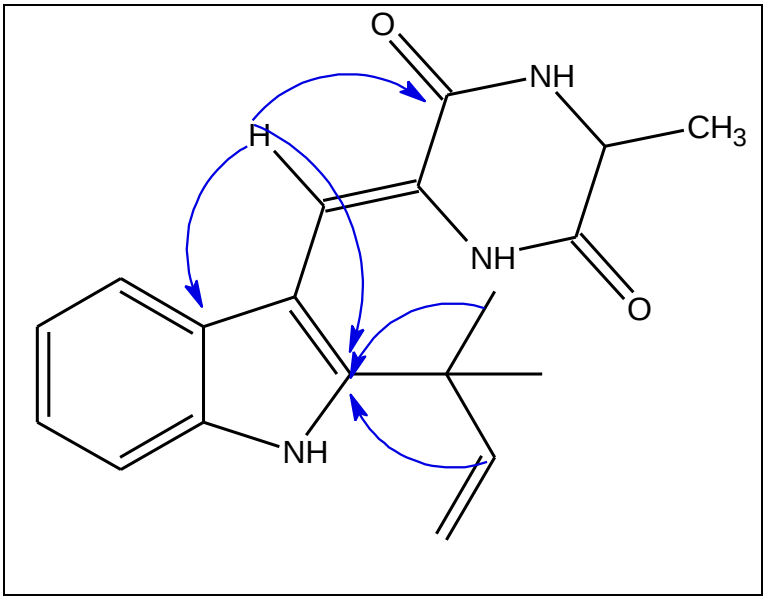

Figure 24: Selected HMBC (⟶) correlations for neoechinulin A (**43**).

Finally, the *Z*-geometry of the Δ^8 double bond was deduced from the downfield shift of H-8 (δ_H 7.21) attributed to the deshielding effect of the carbonyl group on the β-vinyl protons[216]. Marfey's analysis indicated that the absolute configuration of the alanine residue was L, as well as the specific rotationwas measured $[\alpha]_D^{22}$ = -50 (c 0.2, MeOH). Therefore, the structure of **(43)** was proposed as (3*Z*)-3-[[2-(1,1- dimethylallyl)-1H-indol-3-yl]methylene]-6-methyl-piperazine-2,5-dione which is commonly known as neoechinulin A[217].

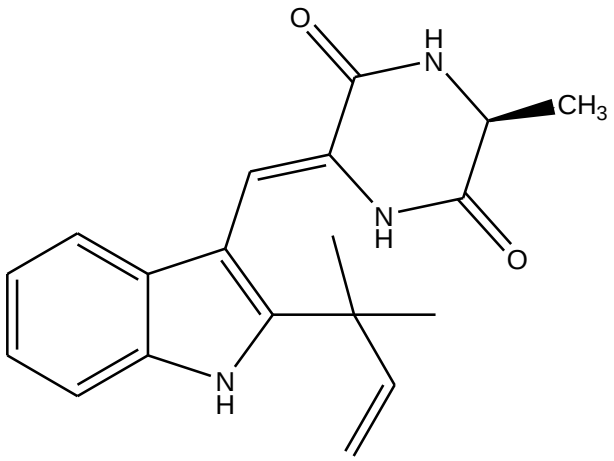

43

Neoechinulin A has been widely reported from several species of fungi, both from marine and terrestrial environments, essentially from species of the genus *Eurotium*[218, 219] and *Aspergillus*[220]as well as from the higher plants *Bridelia ferruginea*[221] and *Cyrtomium fortumei*[222].

5.1.1.12 Variecolorin G

Compound (**44**) was isolated as a red amorphous solid (1.0 mg), the positive HRESI-MS exhibited a strong peak at *m/z* 392.2330 $[M+H]^+$ (calcd for 391.2338) indicating a molecular formula of $C_{24}H_{29}N_3O_2$ with 12 degrees of unsaturation.

The ^{13}C NMR (**Table 18**) displayed twenty-four carbon signals which were categorized, according to HSQC as nine quaternary sp^2 (δ_C 164.6, 159.0, 142.0, 133.0, 132.3, 125.3, 123.4, 122.0, 102.4), one quaternary sp^3 (δ_C 38.3), six methine sp^2 (δ_C 143.5, 121.5, 120.9, 120.2, 115.9, 111.3), one methine sp^3 (δ_C 50.7), one methylene sp^2 (δ_C 112.2), one methylene sp^3 (δ_C 30.2) and five methyl (δ_C 26.2, 26.2, 24.5, 19.7, 16.8) carbons.

These ^{13}CNMR data was similar to that of neoechinulin A (**43**) except for the presence of additional two methyl carbons at δ_C 18.0 and 24.5, one methylene sp^3 at δ_C 30.2, one methine sp^2 at δ_C 121.5 and one quaternary sp^2 at δ_C 132.3, suggested the existence of another prenyl group

The COSY spectrum (**Table 18**) displayed correlations of the olefinic proton at δ_H 5.44 (1H, m; δ_C 121.5) to the methylene protons at δ_H 3.58 (2H, d, J = 7.3 Hz; δ_C 30.2) and the methyl protons at δ_H 1.82 (3H, s; δ_C 24.5), and 1.87 (3H, s; δ_C 16.8), indicated that the additional five carbons were 3-methyl-2-butenyl moiety. This was further confirmed by the HMBC cross-peaks of the doublet of the methylene protons at δ_H 3.58 (H_2-21) to the methine sp^2 carbon at δ_C 121.5 (C-22) and the quaternary sp^2 carbon at δ_C 132.3 (C-23), of the multiplet at (δ_H 5.44, H-21) to the methyl carbons at δ_C 24.5 (C-25) and 16.8 (C-24), and of the singlet at δ_H [1.82 (CH_3-25) and 1.87 (CH_3-24)] to the quaternary sp^2 carbon at δ_C 132.3 (C-23) and the methine sp^2 carbon at δ_C 121.5 (C-22) (**Figure 25**).

Unlike neoechinulin A (**43**), the ^1H NMR data of (**44**) displayed three aromatic protons at δ_H 7.13 (1H, d, J = 7.8 Hz), 7.08 (1H, br t, J = 7.2 Hz), and 6.99 (1H, br d, J = 7.2 Hz), suggesting the presence of a substituent on C-4 or C-7 of the benzene ring of the 2,3-dihydro-1H-indole portion. Since the doublet at δ_H 7.13 (J = 7.8 Hz; δ_C 115.9) exhibited a clear HMBC correlation to the carbons at δ_C 102.4 and 133.0, which were assigned to C-3 and C-7a of the indole moiety, the substituent indicated to be on C-7 (δ_C 122.2) of the benzene ring. The connection of the substituent with C-7 was further supported by the HMBC cross-peaks of H-6 to the methylene carbon C-21, as well as of H_2-21 to the aromatic carbons C-7 and C-7a.

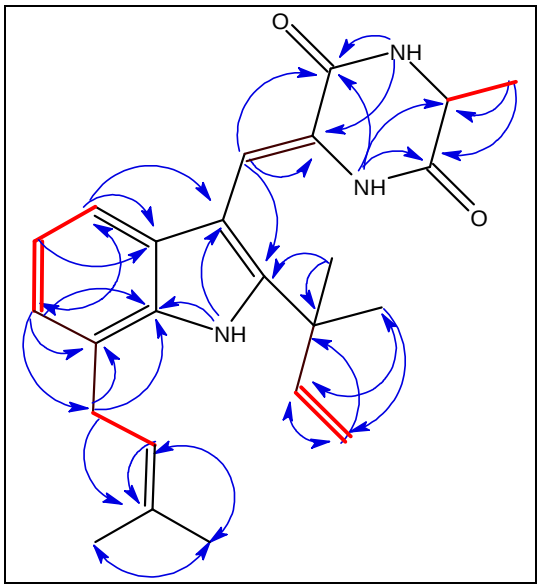

Figure 25: Key COSY (▬) and selected HMBC (→) correlations for variecolorin G (**44**)

Table 18: NMR data for Variecolorin G (**44**) (400 and 100 MHz, δ ppm) [a]

Position	^{1}HNMR (*J* in Hz)	^{13}CNMR	COSY	HMBC
1-NH	8.38 s	-	-	2, 3, 3a, 7a
2	-	142.0	-	-
3	-	102.4	-	-
3a	-	125.3	-	-
4	7.13 (br d, 7.8)	115.9	5	3, 6, 7a
5	7.08 (br t, 7.2)	120.2	4, 6	3a, 6
6	6.99 (br d, 7.2)	120.9	5, 21	3a, 4, 7a, 21
7	-	122.2	-	-
7a	-	133.0	-	-
8	7.21 s	111.3	-	10, 12, 13
9	-	123.4	-	-
10-CO	-	164.6	-	-
11-NH	6.12 br s	-	12	9, 10
12	4.29 (qd, 2.0, 7.0)	50.7	11, 20	10, 13, 20
13-CO	-	159.0	-	-
14-NH	7.43 s	-	-	10, 12, 13
15	-	38.3	-	-
16	6.06 (dd, 10.5, 17.4)	143.5	17	2, 15, 18, 19
17	5.19 (dd, 0.9, 17.4)	112.2	16	15, 16, 18, 19
	5.22 (dd, 0.9, 10.5)			
18	1.51 s	26.2	-	15, 16, 17, 19
19	1.51 s	26.2	-	15, 16, 17, 18
20	1.59 (d, 7.0)	19.7	12	12, 13
21	3.58 (d, 7.3)	30.2	6, 22, 24, 25	7, 22, 23, 25
22	5.44 m	121.5	21, 24, 25	21, 24, 25
23	-	132.3	-	-
24	1.87 s	16.8	21, 22	22, 23, 25
25	1.82 s	24.5	21, 22	22, 23, 24

[a] The assignments were based on DEPT, HSQC, and HMBC experiments, and recorded in $CDCl_3$

According to the aforementioned arguments, the structure established for (**44**) corresponded to variecolorin G, a prenylated indolopiperazine derivative previously reported from the fungi *Aspergillus*[223] and *Eurotium* sp. SCSIO F452[224]. Due to the optical rotation of (**44)** that was mesured as $[\alpha]_D^{22}$ = 0 (c 0.1, MeOH) variecolorin G was isolated as a racemic mixture.

To the best of our knowledge, racemic variecolorin G has been isolated only once before from the soft coral-associated epiphytic fungus *Aspergillus* sp. EGF 15-0-3.

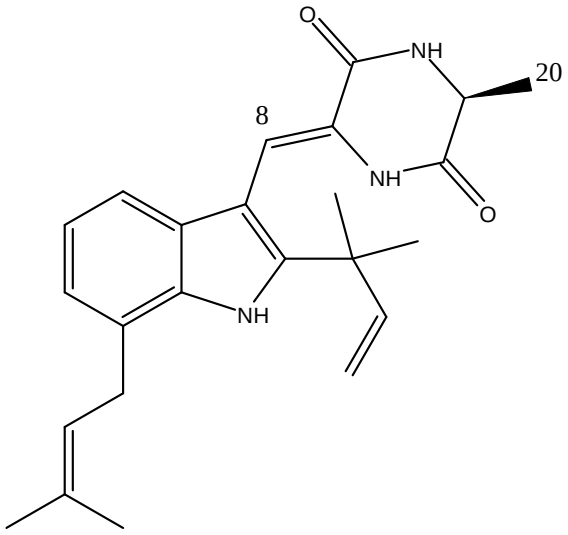

44a

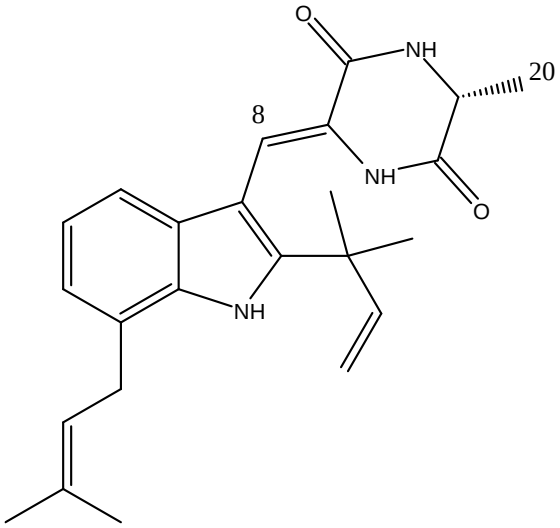

44b

5.1.1.13 Neoechinulin

Compound (**45**) was isolated as a red amorphous solid (5.1 mg) and showed an absorbing band at 254 nm and turned into faint green on spraying with vanillin reagent and heating. R_f = 0.34 (DCM/MeOH 5%). The Positive HRESI-MS exhibited a strong peak at *m/z* 392.1983 [M+H]+ (calcd. for 392.1974) indicating a molecular formula of $C_{23}H_{25}N_3O_3$.

The ^{13}C NMR (**Table 19**) displayed twenty-three carbon signals which were categorized, according to HSQC DEPT as ten quaternary sp^2 (δ_C 158.1, 155.1, 150.8, 146.0, 137.3,134.7, 132.5, 123.2, 121.4, 102.8), six methine sp^2 (δ_C 144.2, 123.7, 123.6, 120.0, 119.0, 111.3), one methylene sp^2 (δ_C 114.2), one quaternary sp^3 (δ_C 39.0), one methylene sp^3 (δ_C 34.6) and four methyl (δ_C 27.9, 27.9, 25.9, 18.0) carbons. These ^{1}H and ^{13}C NMR data was very similar to that of (**44**), however, the differences were observed.

Table 19: NMR spectroscopic data for neoechinulin (**45**) (600 and 150 MHz, δ ppm)[a]

Position	^{1}HNMR (*J* in Hz)	^{13}CNMR	COSY	HMBC
1 –NH	8.41 s	-	-	2, 3, 3a, 7a
2	-	146.0	-	-
3	-	102.8	-	-
3a	-	123.2	-	-
4	7.22 (d, 8.2)	119.0	5	3, 6, 7a
5	7.07 (d, 8.2)	123.6	4	3a, 4, 7, 20
6	-	137.3	-	-
7	7.21 s	111.3	-	4, 5, 20
7a	-	134.7	-	-
8	7.61 s	120.0	-	2, 3a, 10, 13
9	-	121.4	-	-
10-CO	-	158.1	-	
11-NH	8.23 s	-	-	10, 12
12-CO	-	155.1	-	-
13-CO	-	150.8	-	-
14-NH	8.73 s	-	-	9, 13
15	-	39.0	-	-
16	6.06 (dd,10.6, 17.5)	144.2	17	2, 15, 18, 19
17	5.22 (br dd, 17.5, 0.9)	114.2	16	15, 16
	5.27 (br dd, 10.6, 0.9)			
18	1.54 s	27.9	-	2, 15, 16, 17, 19
19	1.54 s	27.9	-	2, 15, 16, 17,18
20	3.44 (d, 7.4)	34.6	21, 23	6, 7, 21, 22, 23
21	5.36 br (t, 7.4)	123.7	20	20, 23, 24
22	-	132.5	-	-
23	1.77 s	25.9	-	21, 22, 24
24	1.75 s	18.0	-	21, 22, 23

[a] The assignments were based on DEPT, ^{1}H-^{1}H COSY, HSQC, and HMBC experiments, and recorded in $CDCl_3$.

The absence of the methyl signals (δ_H 1.61, 3H; δ_C 20.9, CH_3-20) and methine signals (δ_H 4.31; δ_C 51.7, CH-12) in (**44**), instead, an additional carbonyl carbon signal (δ_C 155.1) was observed in the 1D NMR of (**45**). Shifts of about -1.6 and -14.9 ppm for C-10 and C-13 were also observed respectively. These observations indicated that the methyl on C-12 of (**44**) is substituted by oxygen in (**45**). Furthermore, the presence of three aromatic protons at δ_H [7.23 (1H, d, *J* = 8.2 Hz), 7.21 (1H, s), and 7.07 (1H, d, *J* = 8.2 Hz)], suggested that the connection of the prenyl group should be at the C-5 or C-6 position. Detailed investigation of ^{1}H-^{1}H COSY and HMBC correlations (**Figure 26**), confirmed that the connection of the prenyl group with the indole moiety was through C-6. The COSY spectrum confirmed that the isoprenyl group was attached to the aromatic side of the indole substructure since H-5 exhibited long-range correlations to both CH_2-20 and H-4. Besides,

in the HMBC spectrum a clear correlation of H-4 to C-3, C-6, and C-7a, of H-5 to C-3a, C-4, C-7, and C-20, and of H_2-20 to both C-5 and C-7 were detected

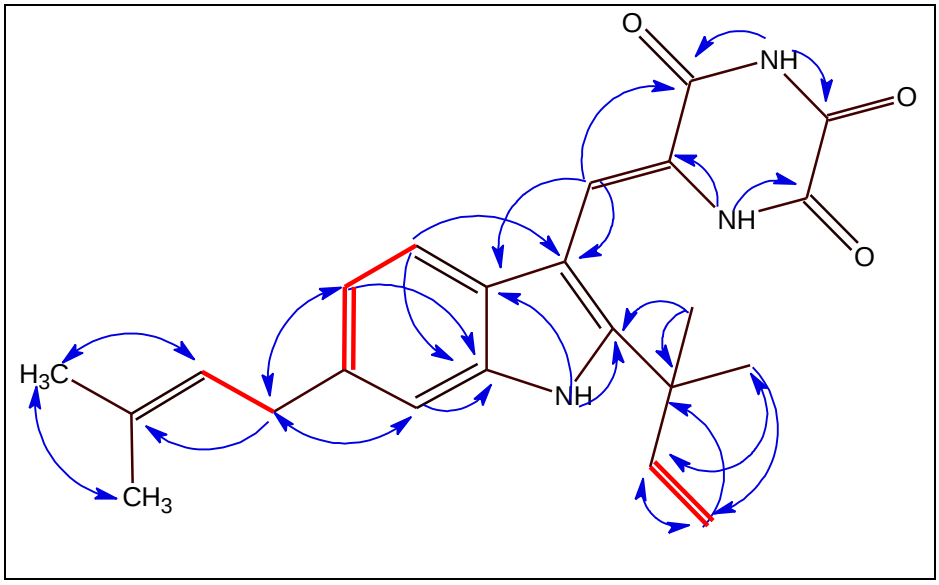

Figure 26: Key COSY (▬) and selected HMBC (→) correlations for neoechinulin (**45**)

Therefore, the structure established for (**45**) corresponded to neoechinulin, a prenylated indolopiperazine derivative previously reported from the fungi *Aspergillus amstelodami*[225].

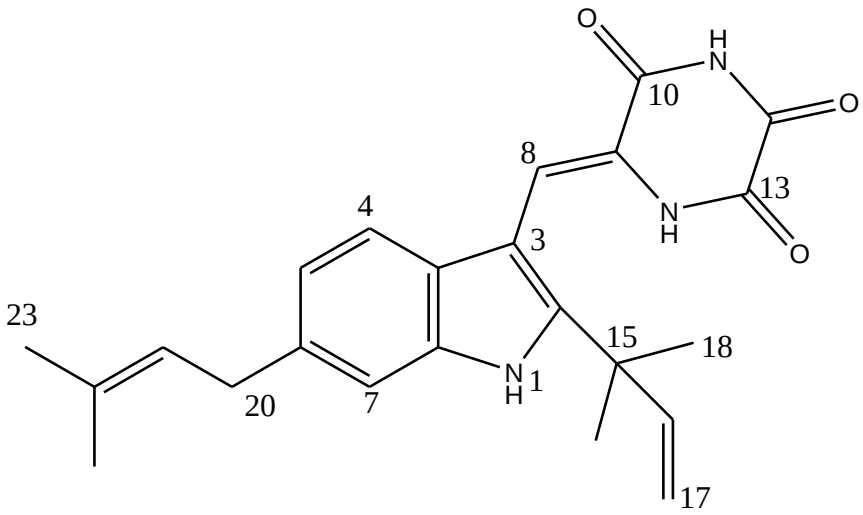

45

5.1.1.14 Neoechinulin F

Compound (**46**) was isolated as an orange-red solid (2.3 mg), its molecular formula was deduced as $C_{18}H_{18}N_4O_2$ based on the (+)-HR-ESIMS which exhibited a strong quasi ion peak at *m/z* 340.2590 $[M+NH_4]^+$, (calcd. 340.2602) required 12 degrees of unsaturation.

The ^{1}H NMR with the aid of HSQC spectra (**Table 20**) exhibited the presence of signals attributable to four NH protons at δ_H 11.21 (1H, s, NH-1), 9.63 (1H, s, NH-14), 7.98 (1H, s, NH-20a), and 7.66 (1H, s, NH-20b), four aromatic protons at δ_H 7.37 (1H, br dd, *J* = 7.9 Hz, H-7), 7.19 (d, *J* = 7.9 Hz, H-4), 7.03 (1H, ddd, *J* = 7.9, 7.0, 1.0 Hz, H-5) and 6.88 (1H, ddd, *J* = 7.9, 7.0, 1.0 Hz, H-6). Moreover, the proton of the vinylic methine (H-8) was observed at δ_H 7.77 (1H, s). Additionally, the presence of singlet signal (6H) accounted for two methyl groups at δ_H 1.51, along with one olefinic methine at δ_H 6.13 (1H, dd, *J* = 17.3, 10.5 Hz), and exocyclic methylene protons at δ_H [5.13 (1H, dd, *J* = 17.3, 1.0 Hz) and 5.12 (1H, dd, *J* = 10.5, 1.0 Hz)], indicated the existence of reverse prenyl group in the molecule.

The ^{13}C NMR spectrum revealed the presence of two amide carbonyls (δ_C 165.1, 161.5), six quaternary sp^2 (δ_C 158.2, 146.1, 135.0, 125.6, 125.6, 105.9), one quaternary sp^3 (δ_C 39.2), six methines sp^2 (δ_C 144.3, 122.4, 120.9, 120.1, 119.1, 111.6), one methylene sp^2 (δ_C 111.9), and two methyl carbons at (δ_C 27.9). The ^{1}H and ^{13}C NMR spectra of (**46**) (**Table 20**) closely resembled those of neoechinulin A **(43)** in DMSO-d_6[226], nevertheless, some differences were observed. The absence of the methyl signals (δ_H 1.61, 3H; δ_C 20.9, CH_3-20) and methine signals (δ_H 4.31; δ_C 51.7, CH-12) in (**46**), instead, a pair of protons appeared as two singlet signals resonating at δ_H 7.98 and 7.66. Interestingly these two protons revealed a clear key COSY correlation to each other and exhibited HMBC correlations with the quaternary carbons at δ_C 161.5 and 158.2, respectively (**Figure 27**), suggesting the existence of an amino group attached to the C-12. This was further supported by the absence of the usual amide proton NH-11.

Contrary to neoechinulin A (**43**), the olefinic proton H-8 of a trisubstituted double bond and the broad singlet of the amide hydrogen NH-14 appeared at higher frequencies (δ_H 7.77, s; δ_C 129.7) / δ_H 9.63), respectively. Whilst, similar to neoechinulin A (**43**), the olefinic proton at δ_H 7.77 exhibited HMBC cross-peaks to the carbons at δ_C 125.6 (C-3a) and 146.1 (C-3) of the 2,3-dihydro-1H-indole moiety, in addition to the amide carbonyl at δ_C 165.1 (C-10).

Table 20: NMR spectroscopic data for neoechinulin F (**46**) (400 and 100 MHz, δ ppm) [a]

Position	^{1}HNMR (*J* in Hz)[b]	^{1}HNMR (*J* in Hz)	^{13}CNMR	COSY	HMBC
1-NH	-	11.21 s	-	-	2, 3, 3a, 7a
2	-	-	146.1	-	-
3	-	-	105.9	-	-
3a	-	-	125.6	-	-
4	7.41 (br d, 7.9)	7.19 (d, 7.9)	120.1	5	3, 3a, 6, 7, 7a
5	7.12 (td, 7.9, 1.3)	7.03(td, 7.9, 1.3)	119.1	4, 6	3a, 6, 7, 7a
6	7.16 (td, 7.9, 1.3)	6.88 (td, 7.9, 1.3)	120.9	5, 7	3a, 6, 7, 7a
7	7.45 (d, 7.9)	7.37 (d, 7.9)	111.6	6	3a, 5
7a	-	-	125.6	-	-
8	7.54 s	7.77, s	129.7	9	2, 3a, 10
9	-	-	-	-	-
10-CO	-	-	165.1	-	-
11	-	-	-	-	-
12	-	-	158.2	-	-
13-CO	-	-	161.5	-	-
14-NH	-	9.63, s	-	8	8, 10, 12
15	-	-	40.4	-	-
16	6.13 (dd, 17.310.6)	6.13 (dd, 17.3,10.6)	145.0	15	2, 15, 18, 19
17	5.14 (dd, 17.3, 0.8) 5.16 (dd, 10.6,0.8)	5.13 (dd, 17.3, 0.8) 5.12 (dd, 10.6,0.8)	111.9	15	15, 16, 18, 19
18	1.57 s	1.51 s	27.9		2, 15, 16, 19
19	1.57 s	1.51 s	27.9		2, 15, 16, 18
20-NH_2	-	7.98 s 7.66 s	-	20	12 12, 13

[a] recorded in DMSO, [b]recorded in MeOD

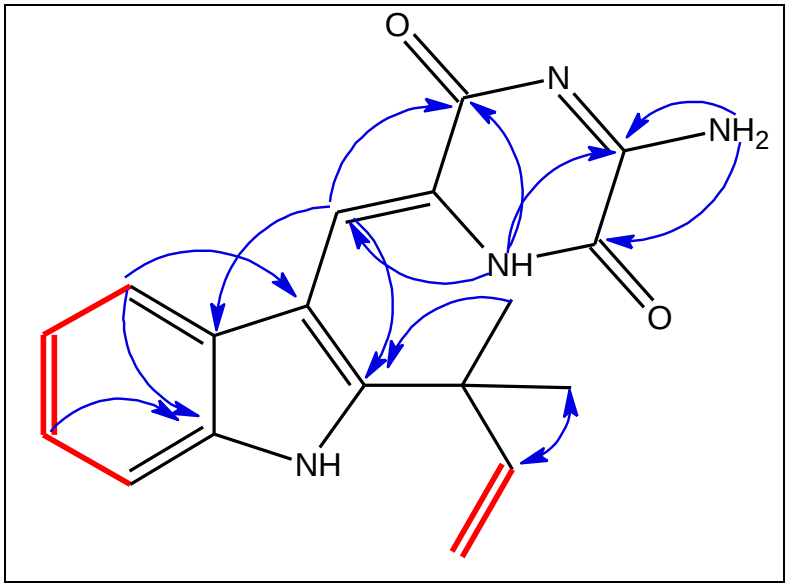

Figure 27: Key COSY (▬) and selected HMBC (→) correlations for (**46**)

Considering the chemical shift value of the carbons and protons, as well as the HMBC correlations and after studying the literature the compound (**46**) was confirmed to be a new indole diketopiperazine alkaloid which we named neoechinulin F.

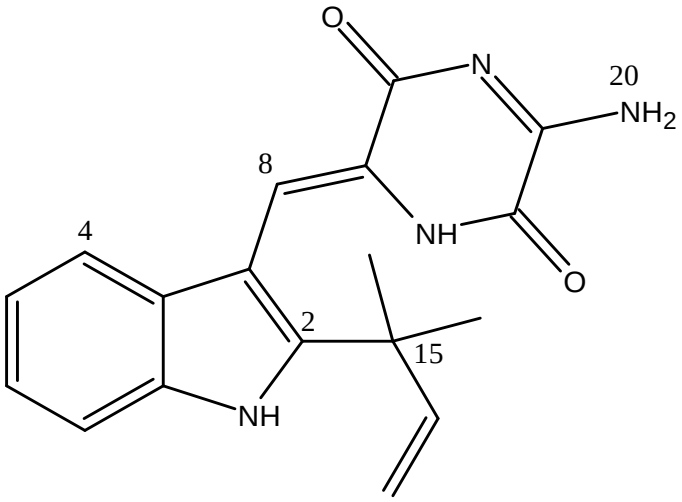

46

5.1.1.15 Neoechinulin D

Compound (**47**) was isolated as a brown solid (7.6 mg), its molecular formula was determined as $C_{24}H_{29}N_3O_2$ according to the positive HRESIMS peak at *m/z* 392.2333[M + H]$^+$ (calcd 392.2338).

The ^{1}H NMR spectrum of compound (**47**) (**Table 21**) recorded in (MeOD-d_4), showed only 26 hydrogens, which suggested the presence of at least three exchangeable protons. Furthermore, the ^{1}H NMR spectrum showed also the characteristic 2,3-disubstituted indole signals, as also observed in the spectrum of neoechinulin A (**43**), namely the aromatic spin system appearing at δ_H 7.23 (1H, br d, J = 1.3 Hz, H-7), 7.15 (1H, d, J = 8.3 Hz, H-4), and 6.92 (1H, dd, J = 8.3, 1.3 Hz, H-5), as well as, the proton of the vinylic methine (H-8) was observed at δ_H 7.20 (1H, s). The presence of singlet signal attributed for two methyl groups at δ_H 1.53, as well as one olefinic methine at δ_H 6.10 (1H, dd, J = 10.5, 17.3 Hz), and exocyclic methylene protons at δ_H [5.10 (1H, dd, J = 17.3, 1.0 Hz) and 5.09 (1H, dd, J = 10.5, 10 Hz)], indicated the existence of reverse prenyl group in the molecule.

The ^{13}C NMR (**Table 21)** displayed 24 carbon signals which were categorized, according to HSQC as two amide carbonyls (δ_C 168.7, 162.3), six methines sp^2 (δ_C 146.3, 125.4, 122.3, 119.7, 114.6, 111.9), seven quaternary sp^2 (δ_C 146.6, 137.2, 136.6, 132.7, 125.4, 124.4, 104.1), one methylene sp^2 (δ_C 112.5), one methylene sp^3 (δ_C 35.4), one methine sp^3 (δ_C 52.6), one quaternary sp^3 (δC 40.4) and five methyl carbons at (δ_C 28.2, 28.16, 25.9, 20.7, 17.9). Furthermore, aromatic protons and carbon resonances had chemical shifts and multiplicities consistent with the presence of either a 2,3,5- or a 2,3,6-trisubstituted indole residue, since the aromatic multiplet signals clearly indicated a 1,2,4-trisubstituted phenyl substructure. The presence of a 2-methyl-but-2-enyl (= isoprenyl) substituent was also established by a metastable ion observed in the mass spectrum indicating the loss of a neutral fragment of 69 mass units.

In addition, the ^{1}H NMR spectrum indicated that the olefinic proton (H-22) at δ_H 5.36 was allylically coupled to the methyl protons at δ_H 1.75 and vicinally coupled to the methylene group (CH_2-21) at δ_H 3.42. From the COSY spectrum, the attachment of the isoprenyl side chain to the aromatic side of the indole substructure (either at C-5 or C-6) was evident by long-range correlations of CH_2-21 to both H-5 and H-7. Most diagnostics for unambiguously deducing the position of the isoprenyl side chain proved a correlation of H-4 to C-3 in the HMBC spectrum (**Figure 28**), the corresponding proton signal was the

one exhibiting the meta-coupling, thus representing the proton immediately adjacent to the substituent.

Table 21: NMR spectroscopic data for neoechinulin D (**47**) (400 and 100 MHz, δ ppm) [a]

Position	^{1}HNMR (*J* in Hz)	^{13}CNMR	COSY	HMBC
1-NH	-	-	-	-
2	-	146.6	-	-
3	-	104.1	-	-
3a	-	124.4	-	-
4	7.15 (d, 8.3)	119.7	5	3, 3a, 6
5	6.92 (dd, 8.3, 1.3)	122.3	4, 7	3a, 6, 7, 21
6	-	136.6	-	-
7	7.23 (br d, 1.3)	111.9	5	5, 21
7a	-	137.2	-	-
8	7.20 s	114.6	-	2, 3a, 10
9	-	125.4	-	-
10-CO	-	162.3	-	-
11-NH	-	-	-	-
12	4.21 (q, 7.0)	52.6	20	10, 13, 20
13-CO	-	168.7	-	-
14	-	-	-	-
15	-	40.4	-	-
16	6.10 (dd, 10,7, 17,3)	146.3	17	2, 15, 18, 19
17	5.09 (dd, 17.3, 1.0) 5.10 dd (10.5, 1.0)	112.5	16	2, 15, 18, 19
18	1.53 s	28.16	-	3a, 15, 16, 17, 19
19	1,53 s	28.2	-	3a, 15, 16, 17, 18
20	1.52 d (7.0)	20.7	12	12, 13
21	3.42 d (7.4)	35.4	22	5, 6, 7, 22, 23, 25
22	5.36 t (7.4)	125.4	21	6, 21, 24, 25
23	-	132.7	-	-
24	1.75 s	17.9	22	22, 23, 25
25	1,75 s	25.9	22	22, 23, 24

[a] The assignments were based on DEPT, ^{1}H-^{1}H COSY, HSQC, and HMBC experiments, and recorded in MeOD-d_4

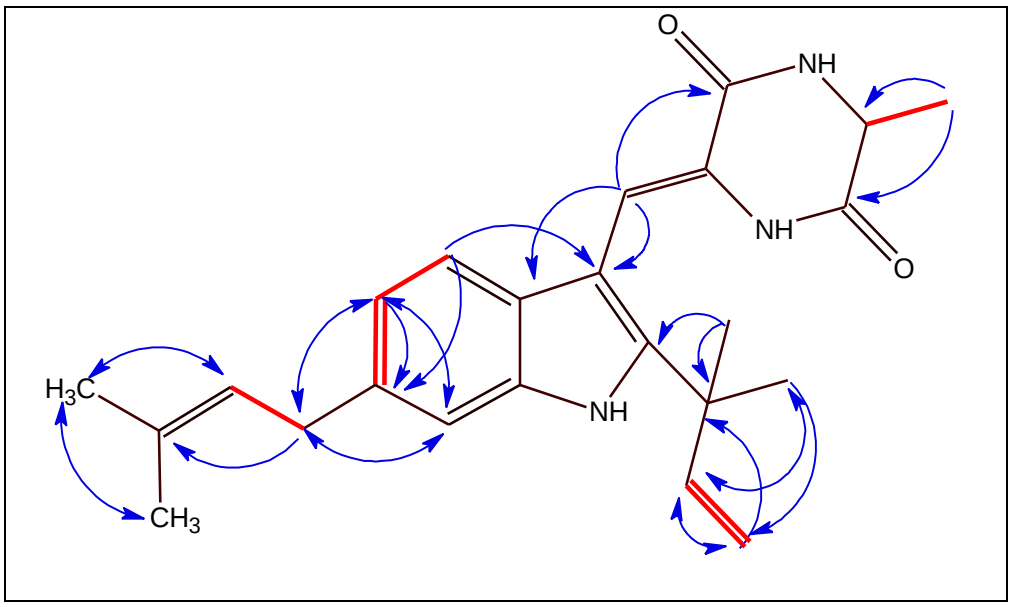

Figure 28: Key COSY (▬) and selected HMBC (→) correlations for (**47**).

According to the literature, the identification of (**47**) was confirmed by comparison of ^{1}H, ^{13}C NMR, specific rotation $[\alpha]_D^{22}$ = -14 (c 0.7, MeOH), and mass spectral data with published data for neoechinulin D which was previously reported from *Aspergillus amstelodami*[227].

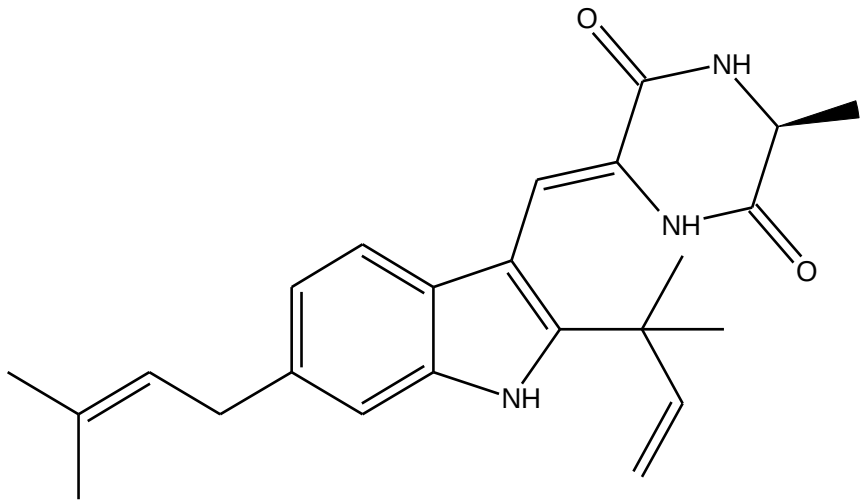

47

5.1.1.16 Cristatumin D

Compound (**48**) was obtained as a white amorphous solid and its molecular formula was deduced as $C_{19}H_{21}N_3O_4$ based on the (+)-HR-ESIMS exhibited the *m/z* 356.1605 $[M+H]^+$, calcd. 365.1625) and required 10 degrees of unsaturation.

The ^1H NMR spectrum of compound (**48**) (**Table 22**) recorded in (MeOD-d_4), showed only 17 hydrogens, which recommended the presence of at least three exchangeable protons. Furthermore, proton decoupling experiments indicated that (**48**) contained an indole ring owing to the presence of 5 hydrogens in the aromatic region at δ_H [7.35(1H, br dt, J = 8.0, 1.0 Hz; δ_C 112.3), 7.20 (1H, br dt, J = 8.0, 1.0 Hz; δ_C 121.0), 7.06 (ddd, J = 8.0, 6.9, 1.0 Hz; δ_C122.3), and 6.96 (1H, ddd, J = 8.0, 6.9, 1.0 Hz; δ_C 120.9), were characteristic for an 1,2-disubstituted aromatic ring. The fifth proton at δ_H 8.00 (1H, s; δ_C 131.7) confirmed the indole skeleton substituted at 3-position. Additionally, the presence of singlet signal attributed for two methyl groups at δ_H 1.58, one olefinic methine at δ_H 6.17 (1H, dd, J = 10.5, 17.4 Hz; δ_C 146.2), and exocyclic methylene protons at δ_H [5.19 (1H, dd, J = 17.5, 1.0 Hz) and 5.17 (1H, dd, J = 10.6, 1.0 Hz); δ_C 112.5], indicated the existence of reverse prenyl group. The down-filed singlet attributed for one methoxy group at (δ_H 3.84; δ_C 52.4) suggested the existence of one methoxy group in the molecule.

Elaborating the 1D and 2D NMR in (DMSO-d6) (**Table 22**) confirmed the presence of the exchangeable protons at δ_H [11.21 (1H, s, NH-1), 9.63 (1H, s, NH-14), 7.98 (1H, s, NH-20a), and 7.66 (1H, s, NH-20b)]. Interestingly, the two singlets at 7.98 and 7.66 revealed clear COSY connectivity to each other. Besides, these two protons showed a diagnostic HMBC cross-peaks to the quaternary carbons at δ_C 158.2 (C-12) and 161.5 (C-13), while the methoxy protons exhibited an HMBC correlation with the quaternary carbon at δ_C 165.1 (C-10) (**Figure 29**). All the discussed data supported that (**48**) was a ring-opened diketopiperazine.

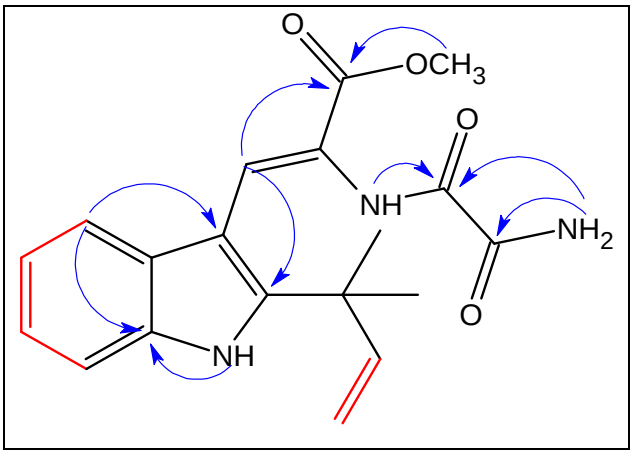

Figure 29: Key COSY (▬) and selected HMBC (→) correlations for (**48**).

Table 22: NMR spectroscopic data for cristatumin D (**48**) (600 and 150 MHz, δ ppm) [a]

Position	^{1}HNMR (*J* in Hz)[b]	^{1}HNMR (*J* in Hz)	^{13}CNMR	COSY	HMBC
1-NH	-	11.21 s	-	-	2, 3, 3a, 7a
2	-	-	146.1	-	-
3	-	-	105.9	-	-
3a	-	-	125.6	-	-
4	7.20 (br dt, 8.0, 1.0)	7.19 (d, 7.9)	120.1	5	3, 3a, 6, 7, 7a
5	6.96 (ddd, 8.0, 6.9, 1.0)	7.03(td, 7.9, 1.3)	119.1	4, 6	3a, 6, 7, 7a
6	7.06 (ddd, 8.0, 6.9, 1.0)	6.88 (td, 7.9, 1.3)	120.9	5, 7	3a, 6, 7, 7a
7	7.36 (br dt, 8.0, 1.0)	7.37 (d, 7.9)	111.6	6	3a, 5
7a	-	-	125.6	-	-
8	8.00 s	7.77, s	129.7	9	2, 3a, 10
9	-	-	-	-	-
10-CO	-	-	165.1	-	-
11-NH_2	-	7.98 s	-	-	12
		7.66 s			13
12-CO	-	-	158.2	-	-
13-CO	-	-	161.5	-	-
14-NH	-	9.63, s	-	-	8, 10, 13
15	-	-	40.4	-	-
16	6.17 (dd, 10.5, 17.4)	6.13 (dd, 17.3,10.6)	145.0	17	2, 15, 18, 19
17	5.19 (dd, 17.4, 0.8)	5.13 (dd, 17.3, 0.8)		16	15, 16, 18, 19
	5.17 (dd, 10.5,0.8)				
18	1.58 s	5.12 (dd, 10.6,0.8)	111.9	-	2, 15, 16, 19
19	1.58 s			-	2, 15, 16, 18
O-CH3	3.84 s	3.72 s	51.9	--	10

[a] The assignments were based on DEPT, ^{1}H-^{1}H COSY, HSQC, and HMBC experiments, and recorded in DMSO-d6. [b]Recorded in MeOD-*d*$_4$

The structure was confirmed by comparison of UV, ^{1}H, ^{13}C NMR and mass spectral data with published data for cristatumin D previously isolated from the marine-derived endophytic fungus *Eurotium cristatum* EN-220[228].

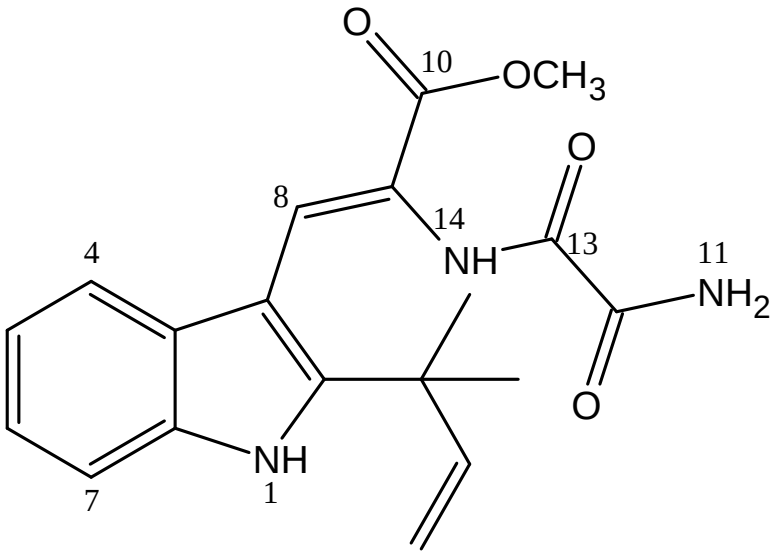

48

5.1.1.17 (12*R*)dehydroechinulin

Compound (**49**) was obtained as a colourless amorphous powder (1.8 mg). The molecular formula was determined as $C_{29}H_{37}N_3O_2$ based on the positive HR-ESI-MS (*m/z* 460.2973 ($[M+H]^+$, calcd. 460.2964), which was in agreement with the ^1H and ^{13}C NMR spectral data (**Table 23**).

Detailed examination of the NMR spectral data and comparison with those reported for echinulin (**37**), showed that the structures of these two compounds are very similar. However, in the ^1H-NMR spectrum, the aliphatic methylene proton signals at δ_H [(3.64 (1H, dd, *J* = 3.7, 14.8 Hz), 3.17 (1H, dd, *J* = 11.7, 14.8 Hz) H_2-8)] and the aliphatic methine at δ_H 4.39 (br dd, 3.7, 11.7 Hz, H-9) in (**37**) disappeared in (**49**). Instead, an olefinic methine proton δ_H 7.19 (s, H-8) was observed. This observation was supported by the fact that the aliphatic methylene and methine carbons at δ_C (29.4, C-8) and (54.5 C-9) in (**37**) were replaced by the olefinic methine and the quaternary C-atoms at δ_C (114.2, C-8) and (126.9, C-9) in (**49**), respectively. The placement of the C=C bond at C-8 and C-9 was further confirmed by the observed HMBC correlations from H-8 resonating at δ_H 7.19 to C-2, C-9 and C-10 at δ_C 145.0, 126.9, and 161.8 respectively (**Figure 30**).

The lower-field-shifted CH at 7.19 (1H, s, H-8) implied that H-8 was influenced by the deshielding effect of the C=O group, which suggested the double bond between C-8 and C-9 to have *Z*-geometry. The absolute configuration at C-12 was assigned as *R* by Marfey's analysis (**Appendix 49**). The specific rotation of (**49**) was measured $[\alpha]_D^{22}$ = +200 (c 0.1, $CHCl_3$)

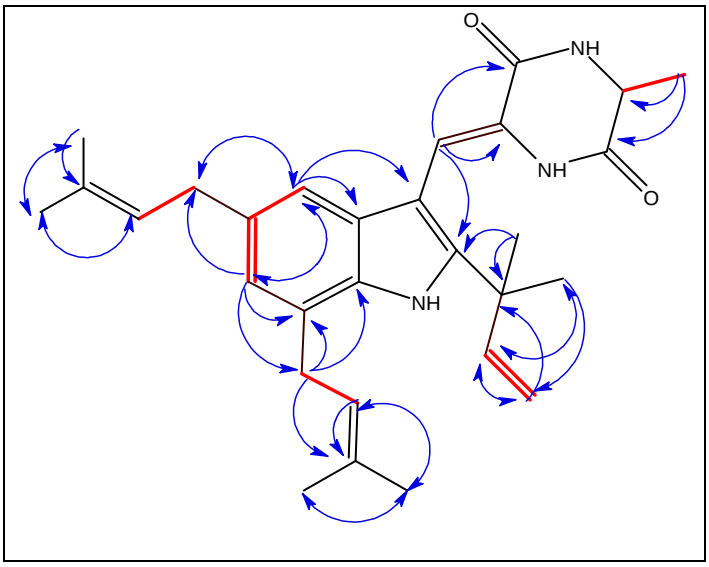

Figure 30: Key COSY (▬) and selected HMBC (⟶) correlations for (**49**).

Table 23: NMR spectroscopic data for dehydroechinulin (**49**) (400 and 100 MHz, δ ppm)[a]

Position	^{1}HNMR (*J* in Hz)[b]	^{1}HNMR (*J* in Hz)	^{13}CNMR	COSY	HMBC
1-NH	10.20 s	-	-	-	-
2	-	-	145.0	-	-
3	-	-	104.2	-	-
3a	-	-	126.9	-	-
4	6.76 s	6.85 br s	116.5	-	3, 3a, 6, 7a, 21
5	-	-	134.9	-	-
6	6.68 s	6.77 br s	123.2	-	4, 7, 21, 26
7	-	-	133.4	-	-
7a	-	-	133.4	-	-
8	6.85 s	7.19 s	114.2	-	2, 9, 10
9	-	-	126.9	-	-
10-CO	-	-	161.8	-	-
11-NH	8.33 (br d, 4.8)	-	-	-	-
12	4.10 (br q, 6.5, 2.0)	4.21 (q, 7.0)	52.4	20	10, 13, 20
13-CO	-	-	168.3	-	-
14-NH	8.62 s	-	-	-	-
15	-	-	40.0	-	-
16	6.11 (dd, 10.7, 17.3)	6.13 (dd, 10.7, 17.3)	146.4	17	2, 15, 18, 19
17	5.00 (dd, 17.3, 0.8) 5.02 (dd, 10.5, 0.8)	5.12 (dd, 17.3, 0.8) 5.13 dd (10.5, 0.8)	112.4	16	15, 16
18	1.48 s	1.548 s	27.8	-	2, 15, 16, 19
19	1.49 s	1.55 s	27.8	-	2, 15, 16, 18
20	1.38 (d, 6.5)	1.53 (d, 7.0)	20.6	12	12, 13
21	3.29 (d, 7.3)	3.36 (d, 7.3)	35.2	22	4, 5, 22, 23
22	5.25 (br t, 7.3)	5.34 (br t, 7.3)	125.4	21	-
23	-	-	132.0	-	-
24	1.64 s	1.73 s	25.6	21	22, 23, 25
25	1.74 s	1.70 s	17.6	22	22, 23, 24
26	3.61 (d, 7.3)	3.61 (d, 7.3)	30.3	27	6, 27, 28
27	5.39 (br t, 7.3)	5.42 (br t, 7.3)	123.6	26	-
28	-	-	133.2	-	-
29	1.65 s	1.79 s	25.6	27	27, 28, 30
30	1.74 s	1.80 s	17.6	26	27, 28, 29

[a] The assignments were based on DEPT, ^{1}H-^{1}H COSY, HSQC, and HMBC experiments, and recorded in (MeOD-d_4). [b] recorded in (DMSO, d_6).

From the above deductions, the structure of (**49**) was assigned to be a new metabolite with the name (12*R*)dehydroechinulin. To the best of our knowledge (12*S*)dehydroechinulin previously reported from the marine mangrove derived endophytic fungus *Eurotium rubrum*[229].

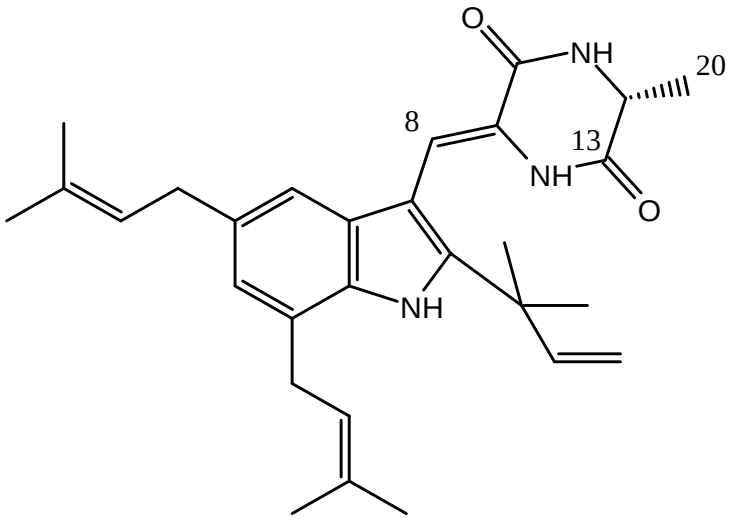

49

5.1.1.18 Cryptoechinuline D

Cryptoechinulin D (**50**) was isolated as a yellow solid, it showed an absorbing band at 254 nm and turned into white on spraying with vanillin reagent and heating. R_f = 0.25 (DCM/MeOH 5%). The molecular formula was determined as $C_{38}H_{41}N_3O_5$ according to the positive HRESIMS peak at *m/z* 620.3110 $[M + H]^+$ (calcd. 620.3120).

The ^{1}H NMR spectrum of (**50**) (**Table 24**) showed the presence of 41 hydrogen atoms, in agreement with the molecular composition ($C_{38}H_{41}N_3O_5$) determined by exact mass measurements. The l H singlet signals at δ_H 10.06, 7.37, and 6.54 suggest the presence of one aldehydic and two amid protons. Moreover, the l H singlet signal at δ_H 8.29 is in the range expected for tryptophan NH. The ^{13}C NMR (**Table 24**) assigned by the aid of HSQC and HMBC, displayed 43 carbon signals which were categorized as one aldehydic carbon at (δ_C 195.3), two amid carbonyl at (δ_C 166.9 and 161.7), 11 quaternary sp^2 (δ_C 155.1, 145.3, 143.8, 133.7, 133.6, 130.5, 125.7, 124.4, 124.1, 116.5 and 102.6), two quaternary sp^3 (δ_C 60.1 and 38.7), twelve methine sp^2 (δ_C 143.5, 136.7, 133.7, 126.0, 125.7, 123.3, 121.6, 120.6, 120.2, 117.8, 111.6, 110.5), two methine sp^3 at (δ_C 45.1 and 27.3), one methylene sp^2 (δ_C 114.2), two methylene sp^3 (δ_C 38.0 and 26.5), as well as, five methyl (δ_C 26.4, 26.4, 24.9, 21.0, 17.0) carbons.

Comparing the ^{1}HNMR with those of neoechinulin A (**43**) we observed that the compound consists of an indole diketopiprazine beside another moiety. These observation indicated the presence of one methyl carbon at (δ_H 1.26 d, J = 7.3 Hz; δ_C 21.0), one methylene sp^3 at [δ_H (1.86 dd, J = 14.0, 3.5 Hz), 2.49 (dd, J = 14.0, 8.0 Hz) δ_C 38.0], three methines one of them sp^3 at δ_C 45.1 and the others sp^2 at δ_C 123.3 and 133.7 suggesting that

the presence of substituted cyclohexene moiety. This suggestion was confirmed by the ^{1}H-^{1}H COSY correlations of the olefinic proton at δ_H 5.73 (dt, J = 10.1, 2.5 Hz) to the methines at δ_H 5.95 (dt, J = 10.1, 2.8 Hz) and 3.68 m, of the multiplet at δ_H 2.69 to one of the methylene protons at δ_H 2.49 (dd, J = 14.0, 8.0 Hz) along with the methyl at δ_H 1.26.

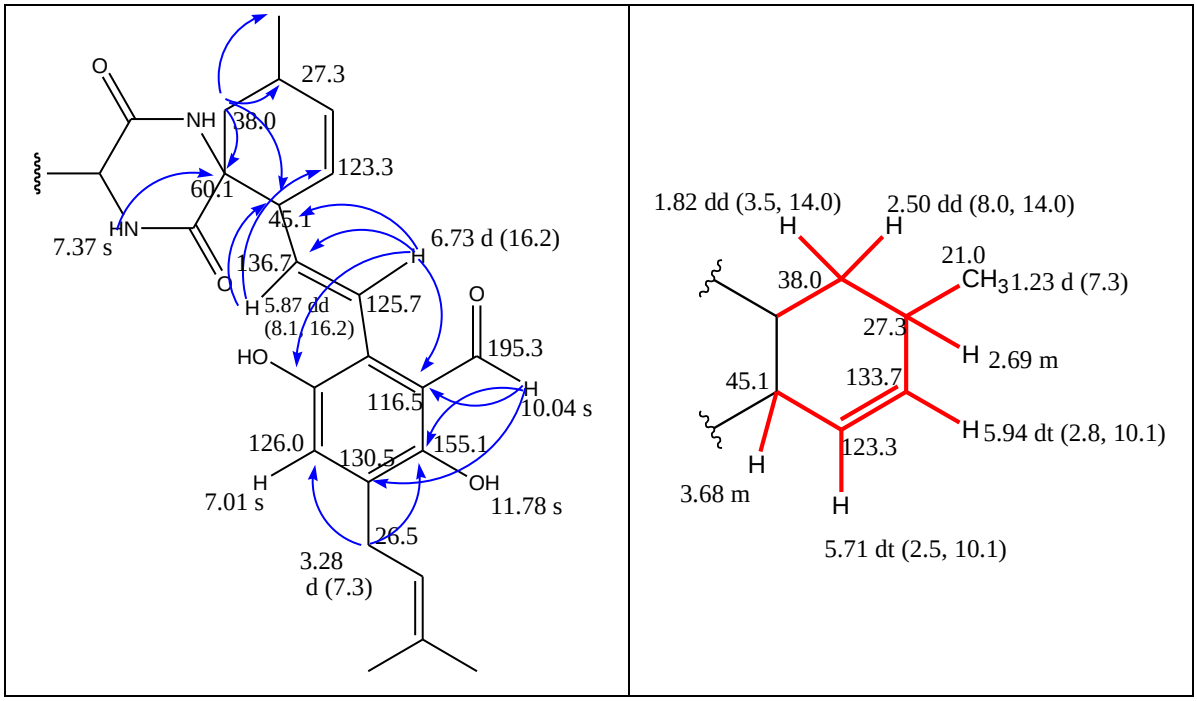

Figure 31: Selected COSY (▬) and HMBC (→) correlations for cryptoechinuline D (**50**)

The appearance of the hydrogen-bonded proton at δ_H (11.80, s), aldehydic proton at δ_H (10.06, s; δ_C 195.3), trans vinylic protons at δ_H [6.76 (d, J = 16.2 Hz; δ_C 125.7) and 5.89 (dd, J = 16.2, 8.1 Hz; δ_C 136.7)] and aromatic proton at δ_H 7.02 (s; δ_C 126.0), provided that the compound consists of an aromatic ring with five substitutions. The HMBC cross-peaks between the methylene of the prenyl group at δ_H 3.30 (d, J = 7.3 Hz) and the two quaternary sp^2 carbons at δ_C 155.1 and 130.5 supplied that the prenyl group is connected with the aromatic ring.

Based on ^{1}H-^{1}H COSY and HMBC correlations (**Figure 31**), the correlations with the quaternary sp^3 at δ_C 60.1 from the methylene protons at δ_H [1.86 (dd, J = 14.0, 3.5 Hz), 2.49 (dd, J = 14.0, 8.0 Hz)], the methine proton at δ_H 5.73 (dt, J = 10.1, 2.5 Hz) and the singlet proton at δ_H 7.39, indicated that the connection between the indole diketopiperazine moiety and the cyclohexene moiety was over the quaternary carbon at δ_C 60.1.

Table 24: NMR spectroscopic data of cryptoechinulin D (**50**) (600 and 150 MHz, δ ppm)[a]

Position	^{1}HNMR (*J* in Hz)	^{13}CNMR	COSY	HMBC
1-NH	8.29 s	-	-	3, 3a, 7a
2	-	143.8	-	-
3	-	102.6	-	-
3a	-	125.7	-	-
4	7.10, ovlp	121.6	5	3a, 5, 7a
5	7.08, ovlp	117.8	4, 6	-
6	7.18 (ddd, 7.2, 7.5, 8.1)	120.6	5, 7	3a, 7, 7a
7	7.32 (br d, 8.1)	110.5	6	3a, 6
7a	-	133.6	-	-
8	7.18 s	111.6	-	2, 12
9	-	124.4	-	-
10-CO	-	167.8	-	-
11-NH	6.54 s	-	-	-
12	-	60.1	-	-
13-CO	-	161.7	-	9, 10
14-NH	7.39 s	-	-	12, 13
15	-	38.7	-	-
16	6.00 (dd, 10.5, 17.4)	143.5	17	18, 19
17	5.19 (dd, 0.8, 10.5)	112.5	16	15, 16
	5.13 (dd, 0.8, 17.4)			15, 16, 19
18	1.41 s	26.4	-	2, 15, 19
19	1.40 s	26.4	-	2, 15, 18
20	-	116.5	-	-
21	-	155.1	-	-
22	-	130.5	-	-
23	7.02 s	126.0	-	21, 25, 24, 35
24	-	145.3	-	-
25	-	124.1	-	-
26	6.76 (d, 16.2)	125.7	27	20, 24, 27, 28
27	5.89 (dd, 8.1, 16.2)	136.7	26, 28	28, 29
28	3.69 m	45.1	27	-
29	5.73 (dt, 2.5, 10.1)	123.3	28, 30	12, 28, 31
30	5.95 (dt, 2.8, 10.1)	133.7	29	28
31	2.70 m	27.3	30, 33	-
32	1.86 (dd, 3.5, 13.7)	38.0	31	12, 28, 31, 33
	2.49 (dd 8.0, 14.0)			
33	1.26 d (7.3)	21.0	31	12, 30, 31, 32
34	10.06 s	195.3	-	20, 21, 22
35	3.30 (d 7.3)	26.5	36	21, 23, 36, 37
36	5.26 b (tq, 1.4, 8.8)	120.2	35	38, 39
37	-	133.7	-	-
38	1.68 s	17.0	-	36, 37, 39
39	1.74 (d, 0.9)	24.9	-	36, 37, 38
OH-21	11.80 s	-	-	20, 21, 22
OH-24	nd	-	-	

[a] The assignments were based on DEPT, ^{1}H-^{1}H COSY, HSQC, and HMBC experiments, and recorded in $CDCl_3$. nd: not detected.

Additionally, the vinylic protons at δ_H 5.89 (dd, J = 16.2, 8.1 Hz) exhibited a clear COSY correlation with both δ_H 3.68 m and 6.76 (d, J = 16.2 Hz), as well as, HMBC cross-peaks with the methine carbons at δ_C 45.1 and 123.3. Furthermore, the other vinylic proton δ_H 6.76 (d, J = 16.2 Hz) revealed a cross-peaks with two quaternary sp^2 at δ_C 116.5, 145.3 along with the methines at δ_C 45.1, 136.7 which confirmed that the vinylic protons are the intermediate between the aromatic moiety and cyclohexene moiety.

The specific rotation of (**50**) $[\alpha]_D^{22}$ = 0 (c 0.5, MeOH), indicated that we isolated the compound as a racemic mixture. From all of the above proofs and by comparing the NMR data with literature data[230] the structure of (**50**) was confirmed to be cryptoechinuline D.

Cryptoechinuline D (**50**) could be biosynthesized by an enzyme-catalyzed regiospecific [4+2] Diels–Alder reaction. Similar Diels–Alder biosynthetic reaction has already been suggested such as dihydrocryptoechinuline D[231], yaoshanenolides[232] and lanceolatins[233]. Cryptoechinuline D (**50**) was firstly obtained from *Aspergillus amstelodami* [234] and then from *Eurotium rubrum*[235]. Cryptoechinuline D (**50**) was synthesized by the Diela-Alder reaction and its relative stereochemistry was determined[236].

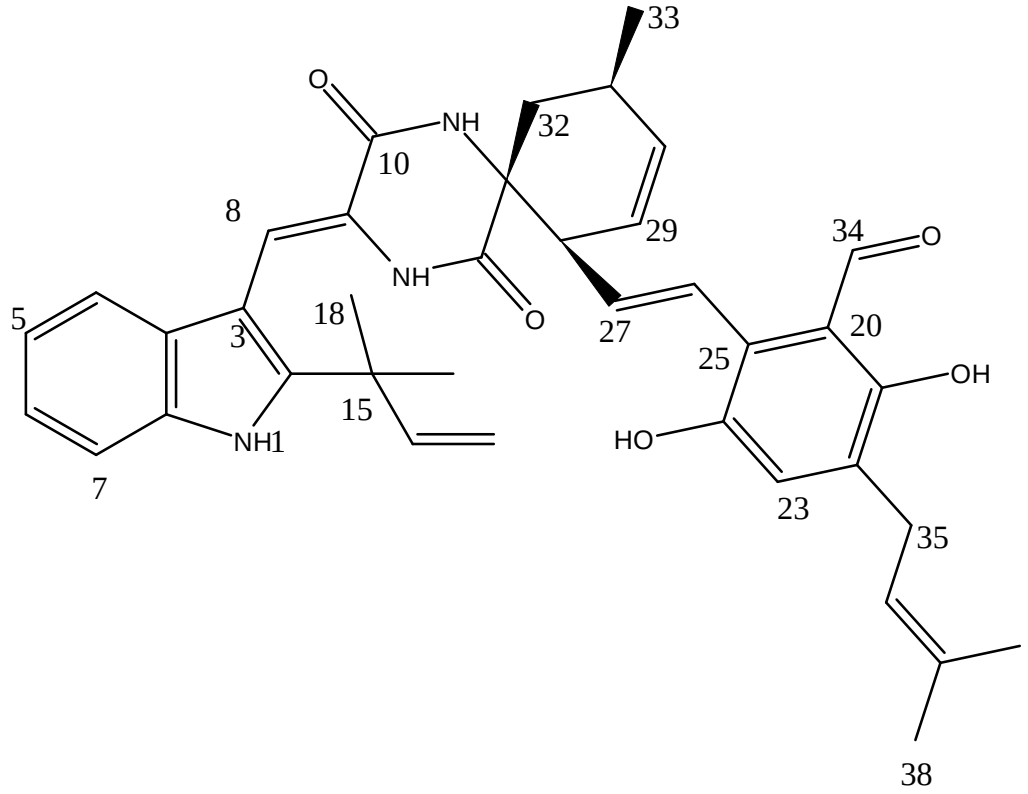
33
O
NH
32
10
8
29
34
O
NH
O
5
18
3
27
20
25
OH
15
HO
NH1
7
23
35
38

50a

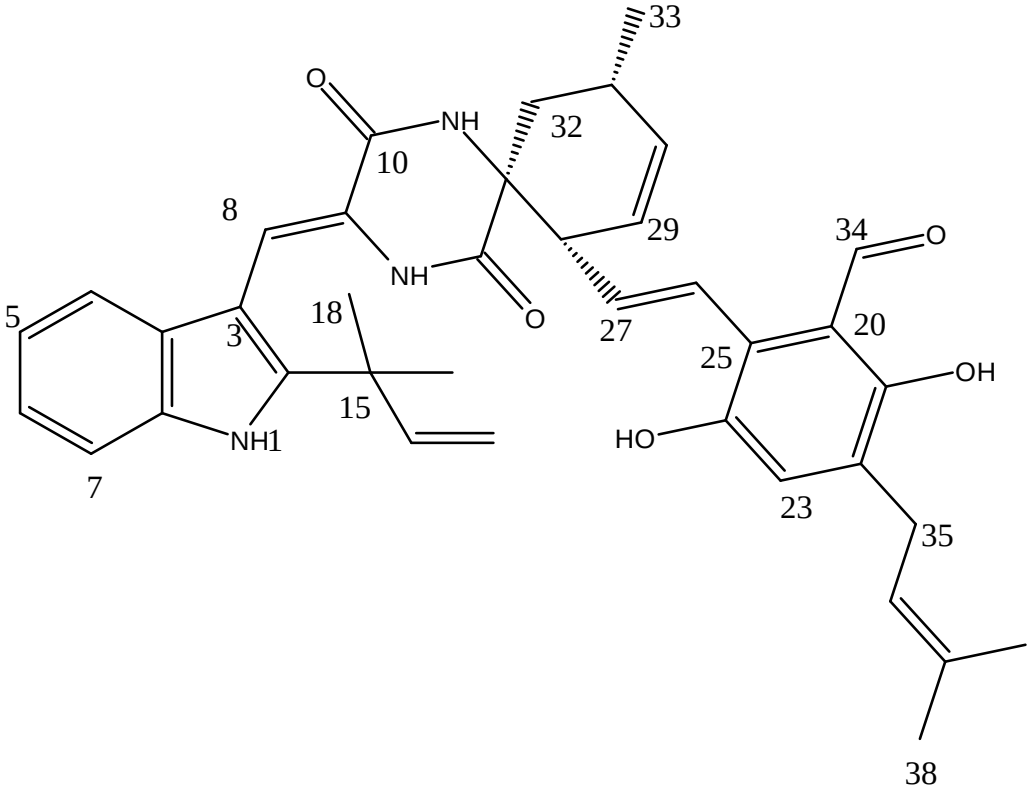
33
O
NH
32
10
8
29
34
O
NH
O
5
18
3
27
20
25
OH
15
HO
NH1
7
23
35
38

50b

5.1.1.19 Cryptoecinuline B

Compound (**51**) was isolated as a yellow solid (31.2 mg), it showed an absorbing band at 254 nm and turned into white on spraying with vanillin reagent and heating. R_f = 0.27 (DCM/MeOH 5%). Its molecular formula was determined as $C_{43}H_{49}N_3O_5$ according to the negative HR-ESIMS peak at *m/z* 686.36244 $[M-H]^+$ (calcd. 686.36240).

The ^{1}H NMR data of (**51**) (**Table 25**) was highly similar to those of cryptoecinuline D (**50**), however, some differences were observed. The existence of two methyls singlet resonating at δ_H 1.74 and 1.75 and a (-CH_2-CH=) pattern at δ_H 3.41 (2H, d, *J* = 7.5 Hz) and 5.35 (1H, br tq, *J* = 7.5 Hz). Furthermore, the aromatic absorption of the tryptophan unit was reduced to an ABX system similar to that in neoechinulin D (**47**).

Based on ^{1}H-^{1}H COSY and HMBC correlations, the methylene protons at δ_H 3.41 (d, *J* = 7.5 Hz) revealed an HMBC cross-peaks with the aromatic methine sp^2 carbons at δ_C (135.1, 122.5, and 110.8) along with the vinylic methine carbons at δ_C 132.1, moreover, the aromatic protons resonating at δ_H 6.94 (1H, dd, *J* = 1.4, 8.2 Hz, H-5) and 7.14 (1H, br s, H-7) exhibited a clear correlation with the methylene at δ_C 34.7. All these facts point to the presence of the dimethylallyl chain in position 6.

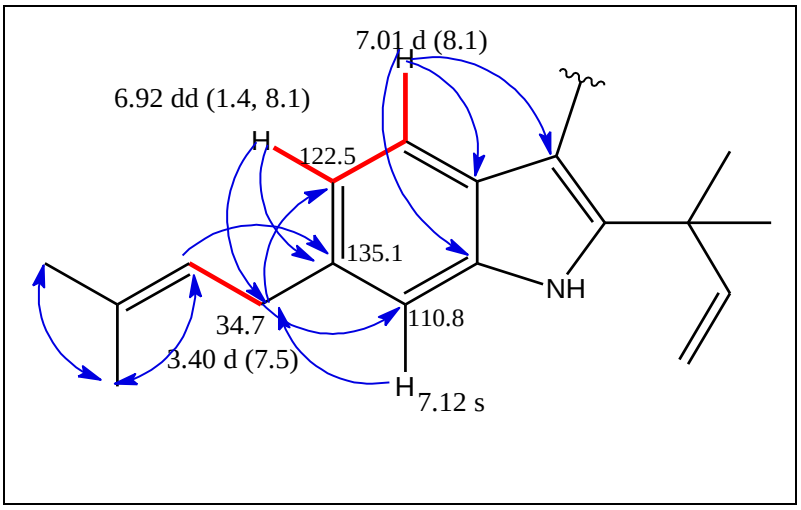

Figure 32: Selected COSY (▬) and HMBC (→) correlations for cryptoechinuline B (**51**)

According to the above spectroscopic data, compound **(51)** was preliminarily identified as a cryptoecinuline D derivative and finally by comparison with literature data confirmed as (6-isopentylcryptoecinuline D) which has the trivial name cryptoecinuline B.

The specific rotation $[\alpha]_D^{22}$ = 0 (c 0.5, MeOH) indicated that (**51**) was a racemic mixture.

Table 25: NMR spectroscopic data for (**51**) (600, 150 MHz, $CDCl_3$, δ ppm)[a]

Position	^{1}HNMR (*J* in Hz)	^{13}CNMR	COSY	HMBC
1-NH	8.15 s	-	-	2, 3, 3a, 7a
2	-	143.3	-	-
3	-	102.4	-	-
3a	-	123.9	-	-
4	7.01 (d, 8.1)	118.8	5	3, 6, 7
5	6.94 (dd, 1.4, 8.2)	122.5	4	3a, 7, 40
6	-	135.1	-	-
7	7.14 br s	110.8	-	5, 6, 40
7a	-	134.3	-	-
8	7.18 s	113.0	-	2, 3a, 10
9	-	123.7	-	-
10-CO	-	161.7	-	-
11-NH	7.41 s	-	-	10, 13
12	-	60.1	-	-
13-CO	-	167.0	-	-
14-NH	6.28 s	-	-	10, 13
15	-	38.7	-	-
16	5.98 (dd, 10.5, 17.4)	144.7	17	15, 18, 19
17	5.11 (dd, 0.8, 10.5)	113.5	16	15, 16
	5.16 (dd, 0.8. 17.4)			
18	1.37 s	27.5	-	2, 15, 19
19	1.38 s	27.5	-	15, 18, 32
20	-	116.5	-	-
21	-	155.1	-	-
22	-	130.7	-	-
23	7.02 s	127.1	-	21, 24, 25, 35
24	-	145.2	-	-
25	-	123.9	-	-
26	6.75 (d, 16.3)	126.8	27	20, 24, 27, 28
27	5.88 (dd. 8.0, 16.2)	137.8	26, 28	25, 28
28	3.69 m	46.3	27	
29	5.72 (dt, 2.5, 10.1)	124.4	28, 30	12, 28, 31
30	5.96 (dt, 2.9, 10.6)	134.7	29, 31	32
31	2.73 m	28.1	30, 32, 33	
32	1.85 (dd, 3.4, 14.0)	39.0	31	12, 13, 28, 30, 31, 33
	2.53 (dd, 8.0, 14.0)			
33	1.26 (d, 7.3)	22.1	31	12, 30, 31, 32
34	10.05 s	195.3	-	20, 21, 22
35	3.30 (d, 7.5)	27.5	36	21, 22, 23, 36, 37
36	5.27 (b tq, 1.4, 7.4)	121.2	35	38, 39
37	-	133.7	-	-
38	1.68 s	18.0	-	36, 37, 39
39	1.74 s	26.1	-	36, 38
40	3.41 (d, 7.5)	34.7	41	42, 5, 6, 7
41	5.35 (br tq, 1.4, 7.4)	123.9	40	40, 43, 44
42	-	132.1	-	-
43	1.74 s	18.0	-	42, 44
44	1.75 s	26.1	-	41, 43
OH-21	11.80 s	-	-	20, 21, 22
OH-24	nd	-	-	-

During our study, another research work was published isolating also the racemic cryptoecinuline B, in that study the two enantiomers were separated by using chiral HPLC chromatography[237]. However, we present in this study the whole NMR data (COSY, HSQC and HMBC) (**Table 25**) for cryptoecinuline B (**51**) in $CDCl_3$ for the first time.

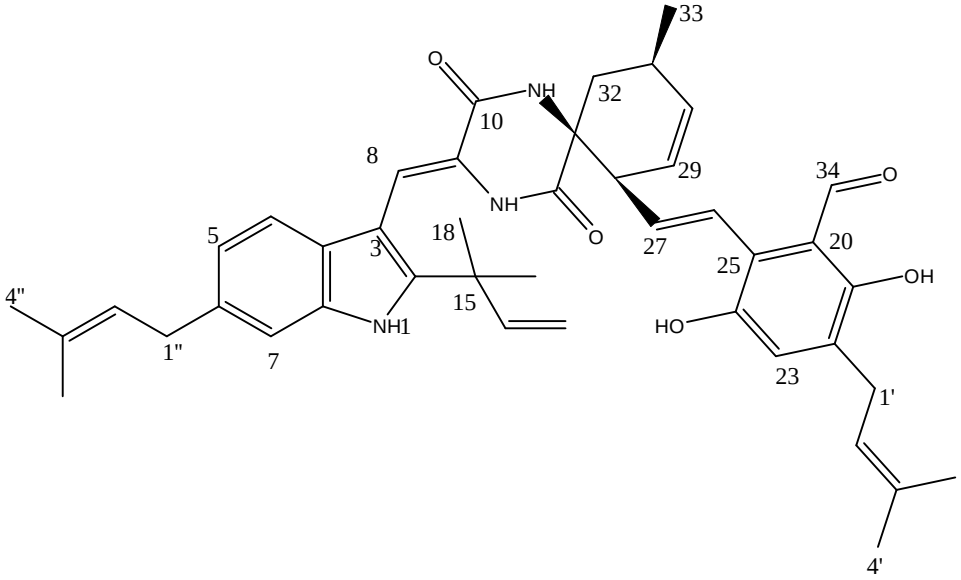

51a

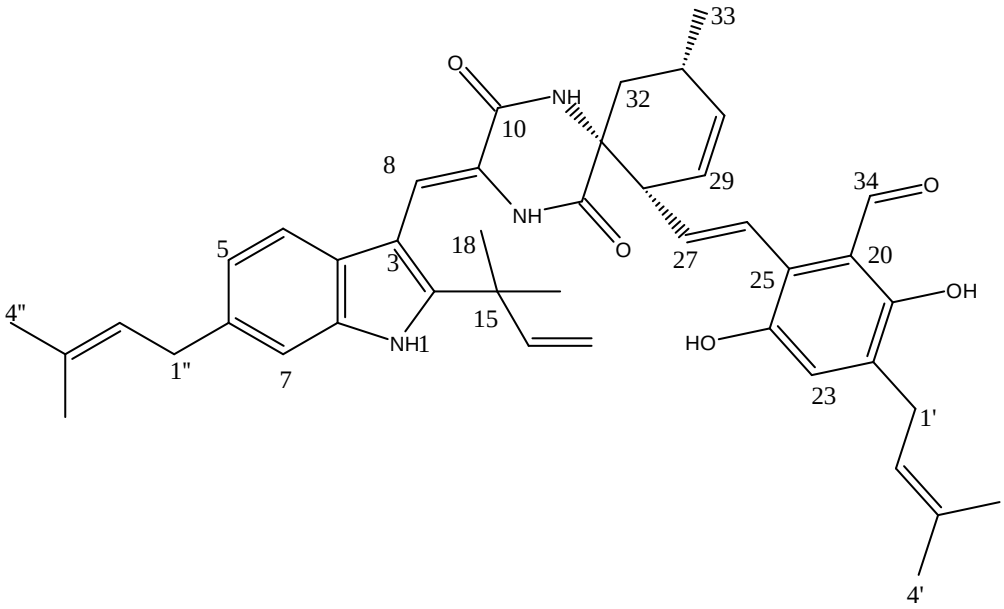

51b

To the best of our knowledge, spiro-polyketide-diketopiperazines are rare in nature. Only a few examples belonging to this kind of spirocyclic alkaloids, variecolortides A–C[223] and cryptoechinuline D[262] have been reported. The synthesis of racemic variecolortide A and B has been recently reported by exploiting a hetero Diels–Alder reaction of a 1,4-anthraquinone with a didehydrodiketopiperazine to form the central spirocyclic core[238].

5.1.1.20 Ochraceopyronide

Ochraceopyronide (**52**) was isolated as a dark brown, optically active, amorphous solid, it showed an absorbing band at 254 nm and turned into white on spraying with vanillin reagent and heating. R_f = 0.42 (DCM/MeOH 5%). Its molecular formula $C_{10}H_{12}O_7$ was determined based on the HR-ESI(+)-MS pseudo molecular ion peak [M+H]+ at *m/z* 245.0767 amu (calcd for $C_{10}H_{13}O_7$, 245.0760 amu), a formula indicating 5 degrees of unsaturation (5 DBE's).

The IR spectrum exhibited absorption bands for hydrogen-bonded hydroxyl groups at 3466 cm^{-1} (broad), bands indicative for α,β unsaturated ester or lactone carbonyl moiety (1637, 1695 cm^{-1}) and a band for aromatic O-H at 1384 cm^{-1}. The UV absorption bands at 218 and 262 nm supported the presence of the conjugation in the structure.

In the ^{1}H NMR spectrum of (**52**) in DMSO-d_6 (**Table 26**), two groups of proton signals that were not interrelated in the ^{1}H-^{1}H COSY spectrum were observed. The first one consisted of three oxymethine protons at δ_H 4.00 (1H, br t, *J* = 3.5 Hz, H-2'), 3.90 (1H, br t, *J* = 3.7 Hz, H-3'), 3.73 (1H, br.q, *J* = 4.65 Hz, H-4'), two oxymethylene protons at δ_H 3.58 (1H, dd, *J* = 11.5, 4.6 Hz, H-5'a) and 3.62 (1H, dd, *J* = 11.5, 4.6 Hz, H-5'b), and a low-field oxymethine proton doublet at δ_H 6.00. Within the same group there were detected the signals of three hydroxyl protons, resonating at δ_H 5.56, 5.43 and 5.01 as broad singlets, having weak but discernible COSY correlations with the oxymethines at δ_H 4.0 (H-2'), 3.90 (H-3') and the oxymethylene at δ_H 3.62 (H-5'b) respectively. The above data suggested the presence of a pentoside moiety in the molecule, with the oxymethine proton doublet at δ_H 6.00 (1H, d, *J* = 4.5 Hz, H-1') being the anomeric proton.

The anomeric H-1' was attached to a carbon resonating at 85.0 ppm. The high field chemical shift of the anomeric carbon was indicative of a furanose instead of a pyranose sugar ring, connecting with a C- instead of an O-glycosidic bond to the aglycon moiety [239]. The furanose nature of the sugar ring was further supported by a weak but diagnostic HMBC cross peak from H-4 to the anomeric carbon C-1'[240] (**Figure 33**).

The second group consisted of three proton signals. We detected two olefinic methines of a disubstituted double bond – with a cis geometry - at δ_H 7.62 (1H, d, *J* = 8.1 Hz, H-4; δ_C 142.3) and 5.55 (1H, d, *J* = 8.1 Hz, H-3; δ_C 100.0 ppm) and an isolated aromatic or enolic hydroxyl proton at δ_H 11.22 attached to a carbon resonating at 150.5 ppm. The downfield shifts of H-4/C-4 can be well explained when the double bond is conjugated to an ester or lactone carbonyl and this was secured by the HMBC correlations of both H-4 and H-3 with a carbonyl moiety at δ_C 163.4 (C-2).

Based on the above NMR data and taking into account the 5 DBE's of the molecular formula we concluded the gross structure of (**52**), which was confirmed by the ^{1}H-^{1}H-COSY and HMBC experiments (**Table 26**). By the combined study of ^{1}H-^{1}H-COSY and HSQC-DEPT experiments, starting from the anomeric proton, we assigned all the sugar methines and their corresponding carbons.

The extended π-conjugation which takes place in the 6-OH-*α*-pyrone ring, incorporating the enol-keto equilibrium, probably accounts for the unusual downfield shift of the anomeric proton H-1'. In our case because of a clear HMBC cross-peak between H-1' and C-6, the most abundant tautomer of (**52**) in DMSO-d_6 solution at 25 °C, corresponds to (**52**) rather than to (**52a**) (**Figure 34**).

Table 26: NMR spectroscopic data for ochraceopyronide (**52**) (600 and 150 MHz)[a]

Position	^{1}HNMR (*J* in Hz)	^{13}CNMR	COSY	HMBC	NOESY
2-CO	-	163.4	-	-	-
3	5.55, d (8.1)	100.0	4	2, 4	4
4	7.62, d (8.1)	142.3	3	2, 3, 6, 1'	3, 1', 2', 3', 4', H-5'
5	-	nd	-	-	-
6	-	150.5	-	-	-
6-OH	11.22, s	-	-	-	2', 3' 2'-OH, 3'-OH, 5'-OH
1'	5.99, d (4.4)	84.7	2'	4, 6, 2'	4, 2', 3'(w), 4'
2'	4.00, br t (3.4)	75.2	1', 3'	7, 9	1', 3', 4', 2'-OH, 3'-OH, 5'-OH (w)
2'-OH	5.43, br s	-	-	-	2', 3', 3'-OH, 5'-OH, 6-OH
3'	3.90, br t (3.2)	75.5	2', 4'	2', 4', 5'	4, 2', 1', 4', 5', 2'-OH, 3'-OH, 5'-OH
3'-OH	5.56, br s	-	-	-	2', 3', 2'-OH, 3'-OH, 6-OH
4'	3.74, q (4.7)	85.1	5'a, 5'b	3', 5'	4(w), H-1', H-2', 3', 5'
5'	a- 3.57, dd (5.5, 11.7) b- 3.62, dd (5.5, 11.7)	60.7	4'	3', 4'	4, 3', 4'
5'-OH	5.01, br s	-	-	-	2', 3', 2'-OH, 3'-OH, 6-OH

[a] The assignments were based on DEPT, ^{1}H-^{1}H COSY and HMBC experiments, and recorded in DMSO-d_6.

Surprisingly, we detected only 9 carbon signals in the ^{13}C-NMR spectrum, with the missing one being C-5 of the 6-OH-*α*-pyrone ring. The same phenomenon had been reported in 2001 for Tetillypyrone and nor-Tetillyapyrone, two 5-C-(2'-deoxy)-furanosyl-6-hydroxyl-*α*-pyrones, isolated from a sponge, collected in Thailand waters[241]. The authors attributed the lack of observation, in both compounds, of a distinct signal of the same carbon C-5 in the ^{13}CNMR spectrum to the coincidental superimposition of the signals of C-5 and C-3, even though C-3 is an sp^2 methine in nor-Tetillyapyrone and an sp^2 quaternary carbon in Tetillyapyrone.

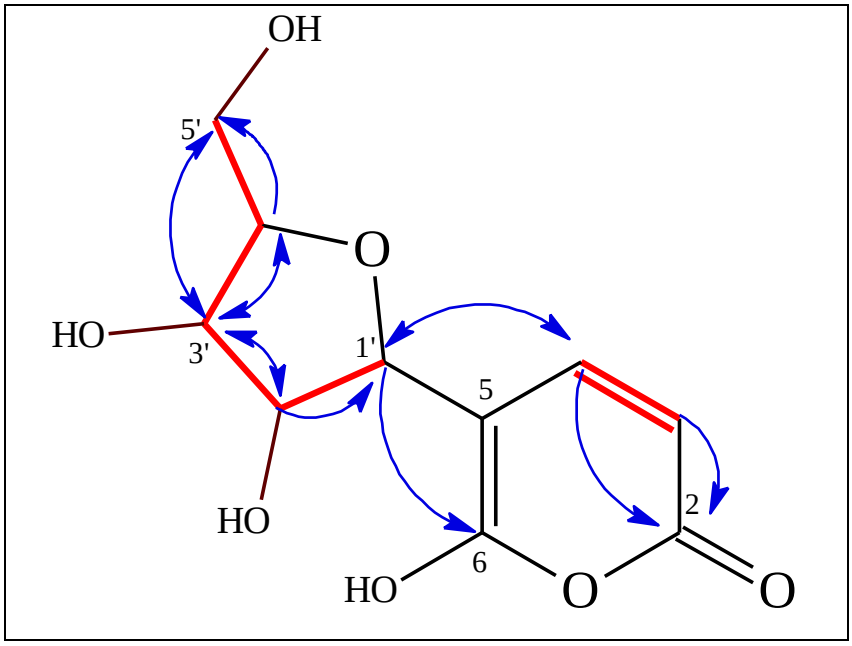

Figure 33: Key COSY (▬) and selected HMBC(⟶) correlations for compound **(52)**

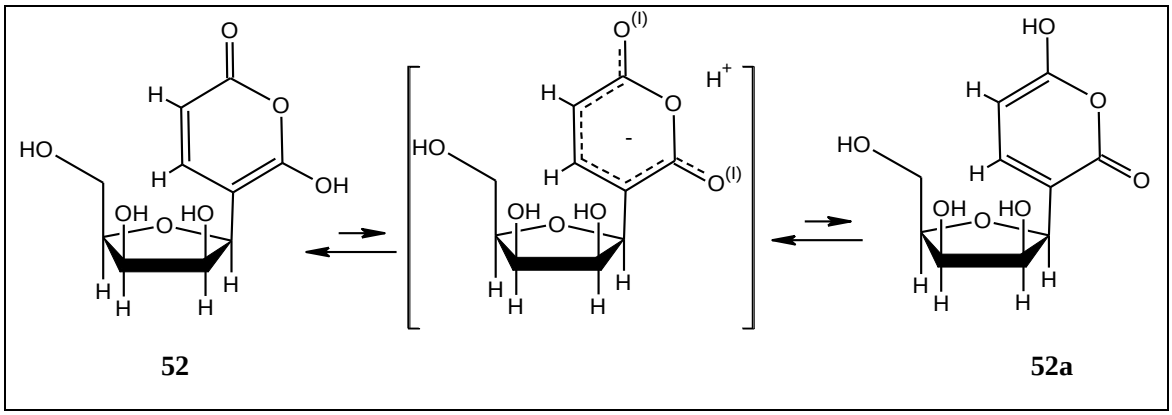

Figure 34: Tautomerization in Ochraceopyronide (**52**).

Assuming that the invisibility of the C-5 resonance in the ^{13}C NMR spectrum of (**52**) at 25 °C is due to the splitting of its signal into several ones, corresponding to different conformers generated by the hindered rotation through the C-1'-C-5 single bond[242, 243], we run ^{13}C NMR experiments at elevated temperatures in DMSO-d_6. Unfortunately, we were not able to detect any average carbon signal for C-5 not even at 80 °C.

Concerning the relative configuration of the furanose sugar moiety we utilized the results from the NOESY experiment combined with the ^{3}J coupling constants data and theoretical calculations.

Five membered tetrahydrofuran rings are known to adopt in solution several puckered conformations from a sum of 10 Envelope (E) and 10 Twisted (T) combinations. These conformers interconvert through pseudorotation and their stability/abundancy depends on the substituents, the solvent and the temperature[244]. In contrast to the 6-membered pyranose rings in which the assignment of the stereochemistry of the sugar carbons can more easily be relied on the spin-spin coupling constants of their vicinal protons, due to the predominance of one of usually two stable, rigid conformers ($^{4}C_{1}$ or $^{1}C_{4}$), in furanose sugars, the flexibility of the ring prevents the direct correlation of the magnitude of the 3JH-H values with the cis or trans geometry of the vicinal protons.

The observed splitting patterns of the furanose oxymethines are the weighted averages of those of each one of all the existing conformers in the solution. This is the reason why relative configuration in furanosides has been based mainly on NOESY or ROESY data[245, 246].

In the NOESY spectrum of (**52**) we detected the correlations of the anomeric proton H-1' with H-4', H-3' and H-2' and those between all three hydroxyl groups of the sugar moiety with each-other. Two more sets of cross peaks in the same experiment secured the relative stereochemistry of (**52**) providing also important information concerning the inherent conformational flexibility of the 5-membered sugar ring. The first one showed correlations of the H-4 of the pyrone ring with H-1', H-2' but also with H-3', H-4' and H-5'a/H-5'b. The second one included the NOE correlations of the enolic 6-OH with all three sugar hydroxyl groups 2'-OH, 3'-OH and 5'-OH (**Figure 35**). This stereo-relation between the furanose HO-groups and the enolic 3-OH allows the development of multiple intramolecular hydrogen-bonds which in turn could explain not only the shift of the enol-keto equilibrium of the *α*-pyrone ring in favour of (**52**) but also the stabilization of the several preferred conformers (**Figure 36**) that could split the ^{13}C signal of C-5, thus accounting for its invisibility in the ^{13}CNMR spectrum even at higher temperatures.

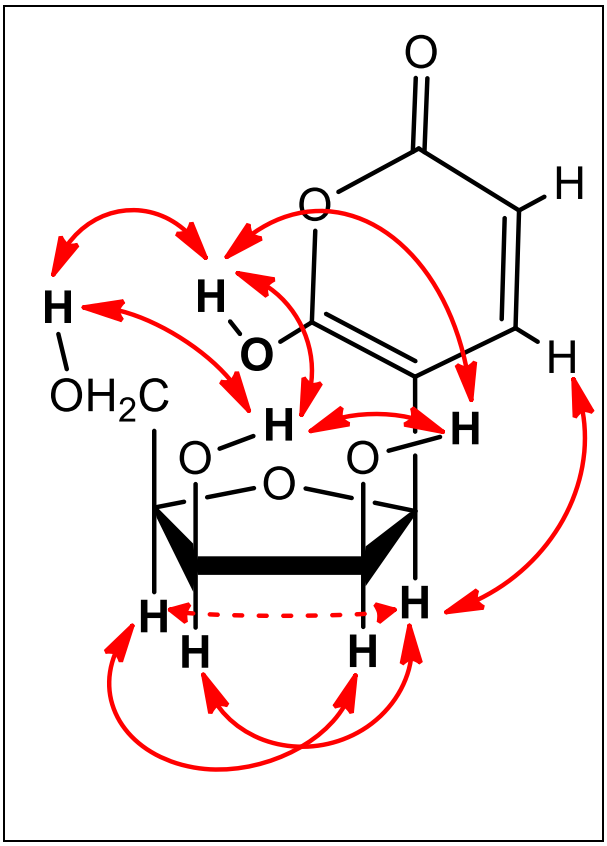

Figure 35: Key NOE correlations for compound (**52**).

Based on the above results the sugar residue of (**52**) is, therefore, a β-$_D$-C-lyxofuranoside or its enantiomer β-$_L$-C-lyxofuranoside.

In two relatively recent articles involving coupling constant computational studies in 5-membered homo and heterocycles, there has been proposed an unequivocal relation between $^3J_{H\text{-}H}$ and relative configuration, although confined to *trans* vicinal protons[247]. The authors have found a $^3J_{H\text{-}H}$ threshold of 2 Hz for H-1/H-2 and H-3/H-4 and a threshold of 3.5 Hz for H-2/H-3, under of which the geometry of the above vicinal proton pairs should always be *trans*.

In these theoretical calculations the model compounds that were used were the known methoxy-α/β-*D*-furanosides (ribo-, xylo-, arabino-, lyxo-) or methyl/methoxy oxolanes, while for the measurements for the dihedral angles and the $^3J_{H\text{-}H}$'s only the E conformers of the furanoside/oxolane rings were considered.

In **52**, none of the $^3J_{H\text{-}H}$ of the oxymethines H-1' (d, J = 4.5 Hz), H-2' (br.t, J = 3.6 Hz), H-3' (br.t, J = 3.7 Hz), H-4' (br q, J = 4.6 Hz) that we measured in DMSO-d6 (20 °C) were lower than 3.5 Hz, in alignment with the conclusions of the previously published theoretical work. We also undertook a computational study, in order to calculate the dihedral angles of the furanose ring and the corresponding vicinal oxymethine coupling constants of the

theoretically more abundant conformations, detecting any impact of the α-pyrone ring, and compare them with our experimental $^{3}J_{H\text{-}H}$'s and nOe correlations.

Initially, we designed the β-L and β-D enantiomers of Ochraceopyronide (**52**) using the Maestro Software (Schrödinger Release 2020-2: Maestro, Schrödinger, LLC, New York, NY, 2020). We generated all possible conformations of the furanose ring based on the pseudorotation equation for torsion angles by Altona and Sundaralingam[247], resulting in 20 conformers, (10E and 10T) for each enantiomer. Next, each conformer was solvated on a periodic box with explicit TIP3P water molecules. The GLYCAM_06 and GAFF2 forcefield were applied and we run 10ns of Molecular Dynamic (MD) simulation with AMBER18 software. We analyzed the resulted trajectories by identifying the furanose ring puckering and the variation of all torsion angles between H1'-C1'-C2'-H2', H2'-C2'-C3'-H3' and H3'-C3'-C4'-H4'.

Although we started from all possible E and T conformations, the D enantiomer was mainly populated from ^{3}E to $^{0}T_{4}$ and E_1 to E_3 conformers (**Figure 36E)**, while the L enantiomer was mainly populated from $^{3}T_{2}$ to ^{3}E, E_3 to $^{4}T_{0}$ and ^{1}E to E_2 conformers (**Figure 36F**). The α-pyrone substituent seems to disturb the free conformation change on the furanose ring. Furthermore, we explored the theoretical ^{3}J coupling of H1'-H2', H2'-H3' and H3'-H4' by calculating the torsion angles Φ of H1'-C1'-C2'-H2', H2'-C2'-C3'-H3' and H3'-C3-C4'-H4' respectively. All torsion angles were within the range of -60° to + 60° as expected for all vicinal protons being *cis* oriented. Each torsion angle Φ passed through the Altona Equation to predict the theoretical $^{3}J_{HH}$ coupling constant. The deviation of each torsion angle was ±20° for each unique sugar conformation leading to ± 2 Hz deviation in $^{3}J_{HH}$ prediction. Using the appropriate substituents on carbon atoms C1', C2' C3' and C4' the theoretical $^{3}J_{HH}$ values were calculated[248] and presented in **Figure 36A** for the D-enantiomer and **Figure 36B** for the L-enantiomer**.** The distribution of each torsion angle Φ is depicted in (**Figure 36C and D)** for D- and L- enantiomer respectively**.**

***β*-D-C-lyxofuranoside residue of** (**52**). For $^{3}J_{H1\text{-}H2}$ the majority of conformers resides on Φ = 30 to 50 (^{3}J= 4.3-1.4), and Φ = -20 to 5 (^{3}J=7.7-8.7), for $^{3}J_{H2\text{-}H3}$ on Φ= -20 to -50 (7.1–3.5 Hz) and Φ = 20 to 50 (7.1 – 3.6 Hz) and for $^{3}J_{H3\text{-}H4}$ on Φ = -30 to -50 (4.2 - 1.4 Hz) and Φ = 10 to 40 (8.4 – 6.8Hz).

***β*-L-C-lyxofuranoside residue of** (**52**). For $^{3}J_{H1\text{-}H2}$ the majority of conformers resides on Φ = 0 to 30 (8.1– 8.8Hz), and Φ = -20 to -50 (5.8–1.4 Hz) for $^{3}J_{H2\text{-}H3}$ on Φ = -20 to -40 (7.1–4.8 Hz) and Φ = 25 to 55 (6.6 –2.9 Hz) and for $^{3}J_{H3\text{-}H4}$ on Φ = -10 to -40 (8.3 - 6.7 Hz) and Φ = 30 to 50 (4.2 –1.5 Hz).

The above results show that only a combination of several existing conformers in solution for (**52**) with different abundancies/stabilities, would account for better proximity between theoretical and experimental $^{3}J_{H\text{-}H}$ values. This could also explain the numerous correlations we observed in the NOE spectrum between protons that are spatially close to each other in some conformations but far apart in others.

We present in (**Figure 37A**) a representative theoretical conformer for *β*-D-C-lyxofuranoside residue of (**52**) (^{2}E) and in (**Figure** 37B) a representative theoretical conformer for *β*-L-C-lyxofuranoside residue of (**52**) ($^{2}T_{3}$). Both belong to the group of theoretical conformers with the closest values of $^{3}J_{H\text{-}H}$ with the experimental ones.

To the best of our knowledge, this is the first C-lyxofuranoside isolated from Nature. Lyxosides, in general, are rare as natural products, encountered only as *O*-pyranosides[249, 250], while there are some synthetic works including *O*-lyxofuranosides or *O*-lyxopyranosides as intermediates or targets for finding routes to interconvert sugars[251], or for theoretical NMR and physicochemical calculation purposes[252, 253, 254].

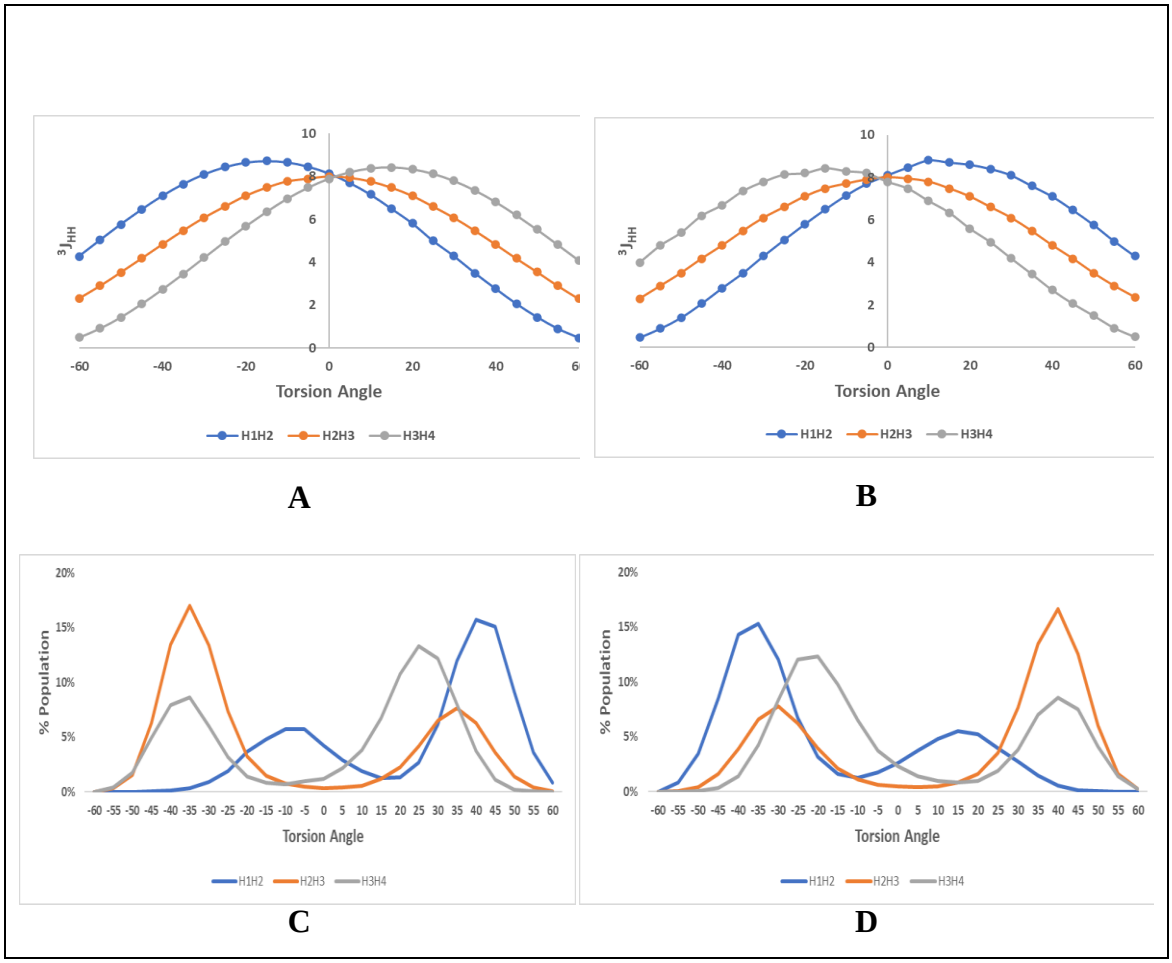

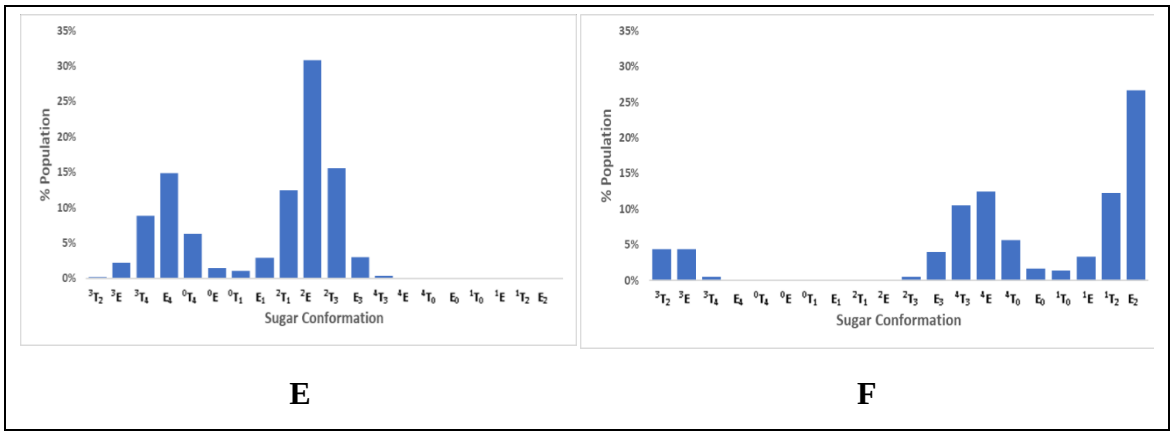

Figure 36: A,B) Theoretical $^{3}J_{HH}$ coupling constants distribution, C,D) Distribution of $^{3}J_{HH}$ coupling after MD. E,F) Distribution of furanose conformers of *β*-D- and β-L-C-lyxofuranoside residues of Ochraceopyronide (**52**) respectively.

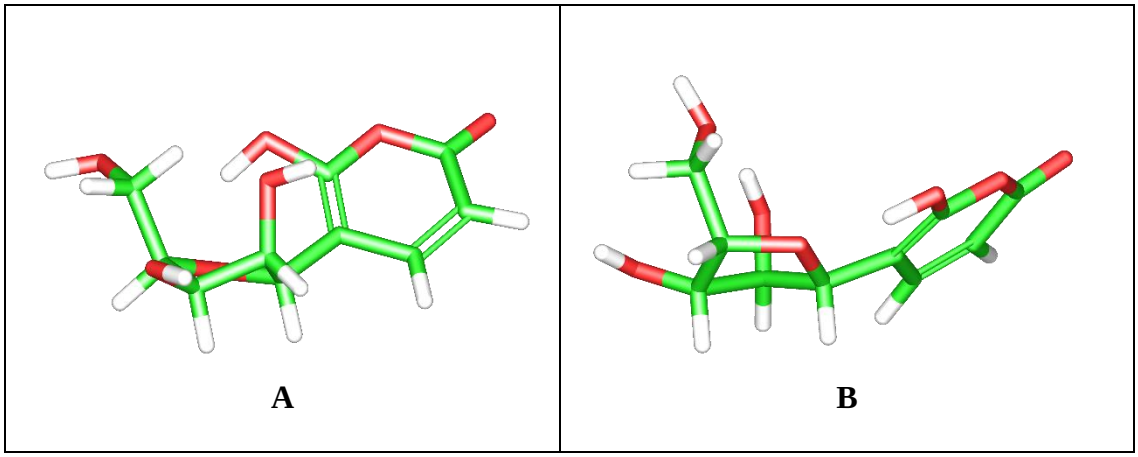

Figure 37: Representative conformers (^{2}E for *β*-D-C-lyxofuranoside (**A**) and $^{2}T_{3}$ for *β*-L-C-lyxofuranoside (**B**)) for the two enantiomers of Ochraceopyronide (**52**).

To the best of our knowledge, this is the first C-lyxofuranoside isolated from nature. Lyxosides, in general, are rare as natural products, encountered only as *O*-pyranosides [255,256], while there are some synthetic works including *O*-lyxofuranosides or *O*-lyxopyranosides as intermediates or targets for finding routes to interconvert sugars[257] or for theoretical NMR or physicochemical calculations[258,259,260].

5.1.1.21 Isotorachrysone-6-O-*α*-D-ribofuranoside

Compound (**53**) was obtained as a red amorphous powder (3.7 mg), it showed an absorbing band at 254 nm and turned into white on spraying with vanillin reagent and heating. R_f = 0.77 (DCM/MeOH 5%). its molecular formula $C_{19}H_{22}O_8$ was determined by HRESIMS (*m/z* 377.1254 $[M-H]^-$, calcd. 377.1236), which required 9 degrees of unsaturation.

The ^{1}H-NMR data (**Table 27**) revealed the presence of three aromatic H-atoms, two of them appeared at δ_H 7.00 and 6.78 as a pair of *meta*-coupled signals (d, *J* = 2.1 Hz), and a singlet at δ_H 7.01, as well as, aromatic methyl, acetyl methyl, and methoxy signals at δ_H 2.29, 2.59, and 4.08, respectively, along with a sugar residue at δ_H [4.24 (1H, dd, *J* = 4.5, 6.5 Hz), 4.17 (1H, br q, *J* = 3.5 Hz), 4.13 (1H, dd, *J* = 3.1, 6.5 Hz), and (3.72 (1H, d, *J* = 3.5, 12.1 Hz) and 3.69 (1H, d, *J* = 4.0, 12.1 Hz)].

According to the above NMR features and taking into account the 9 degrees of unsaturation of the molecular formula, we proposed that (**53**) consist of two fused benzene ring with sugar moiety. The structure of (**53**) was further elucidated by analysis of 2D NMR data including the ^{1}H-^{1}H COSY and HMBC spectra (**Figure 38**). Besides the fact that the two *meta*-coupled protons are in the same benzene ring, the ^{1}H-^{1}H COSY spectrum of (**53**) revealed a long-range correlation between the methyl singlet at δ_H 2.29 and the aromatic proton at δ_H 7.01(H-4), moreover, the HMBC exhibited a clear correlation between both methyls at δ_H 2.29, 2.59 with the quaternary sp^2 carbon at δ_C 124.0, indicating that these two methyls were in the other benzene ring. On the other hand, the correlation between the methoxy protons at δ_H 4.08 to the quaternary carbon at δ_C 159.2 (C-8), made the position of the methoxy unambiguous.

^{1}H-^{1}H COSY spectrum showed also connectivity between three oxymethine protons at δ_H 4.24 (1H, dd, *J* = 6.5, 4.5Hz, H-2"), 4.13 (1H, dd, *J* = 6.5, 3.1, H-3"), 4.17 (1H, br q, *J* = 3.5 Hz, H-4"), oxymethylene protons at δ_H 3.69 (1H, dd, *J* = 12.1, 4.0 Hz, H-5'a) and 3.72 (1H, dd, *J* = 12.1, 3.5 Hz, H-5'b), and a low-field oxymethine proton at δ_H 5.77 (1H, d, *J* = 4.5 Hz, H1"). The above data suggested the presence of a pentoside moiety in the molecule, with the oxymethine proton doublet at δ_H 6.00 (1H, d, *J* = 4.5 Hz, H-1") being the anomeric proton.

The anomeric H-1" was attached to a carbon resonating at 101.9 ppm, the downfield chemical shift of the anomeric carbon was indicative of a furanose instead of a pyranose sugar ring, connecting with an O-glycosidic bond to the aglycon moiety. The furanose

nature of the sugar ring was further supported by the diagnostic HMBC cross peak from H-4" to the anomeric carbon C-1" (**Figure 38**).

Table 27: NMR spectroscopic data for (**53**) (400 and 100 MHz, δ ppm) [a]

Position	^{1}HNMR (*J* in Hz)	HSQC	COSY	HMBC
1	-	154.2	-	-
2	-	124.0	-	-
3	-	135.8	-	-
4	7.01 s	120.3	3'	1, 2, 3', 5, 9, 10
5	7.00 (d, 2.1)	104.6	7	4, 6, 7, 9
6	-	158.5	-	-
7	6.78 (d, 2.1)	99.8	5	5, 6, 9
8	-	159.2	-	-
9	-	110.0	-	-
10	-	139.2	-	-
1'	-	206.8	-	-
2'	2.59 s	32.3	-	2, 1'
3'	2.29 s	19.9	4	2, 3, 4
4'	4.08 s	56.8	-	8
1"	5.77 (d, 4.5)	101.9	2"	4", 6
2"	4.24 (dd, 4.5, 6.5)	73.2	1"	3"
3"	4.13 (dd, 3.1, 6.5)	71.1	2	1", 2", 5"
4"	4.17 (br q, 3.5)	87.7	5"	-
5"	3.72 (d, 12.1, 3.5) 3.69 (d, 12.1, 4.0)	63.1	4"	-

[a] The assignments were based on DEPT, HSQC, and HMBC experiments recorded in MeOD-d_4.

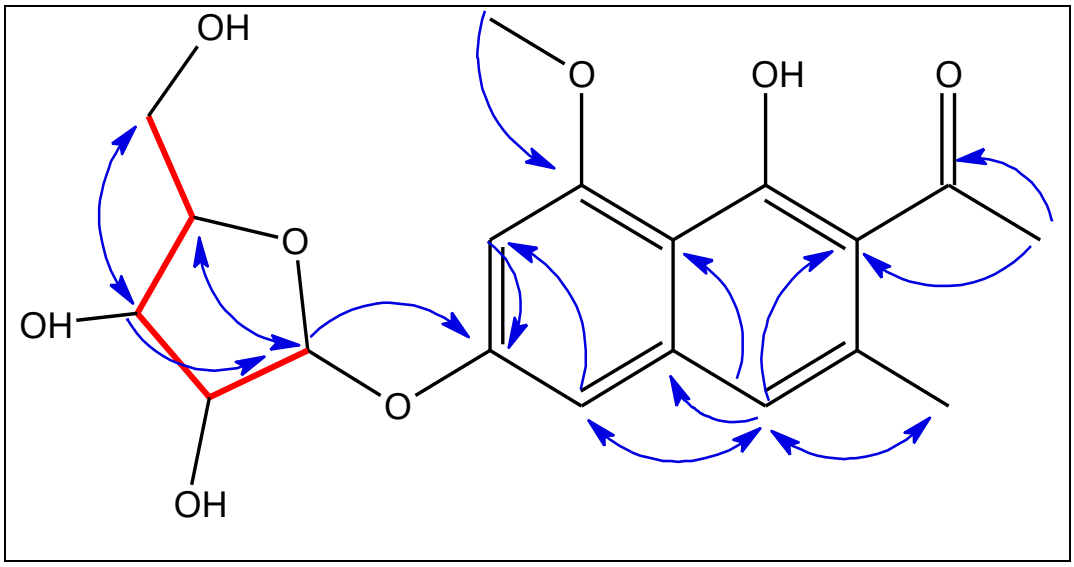

Figure 38: Key COSY (▬) and selected HMBC(⟶) correlations for (**53**).

Finally, the sugar moiety was determined as α-D-ribofuranose by comparison of the $J_{1'',2''}$ (4.5 Hz) with those of the methyl-α-D-ribofuranoside ($J_{1,2}$ = 4.3 Hz) and methyl- β-D-ribofuranoside ($J_{1,2}$ = 1.2 Hz)[261].

Based on the above chromatographic, spectroscopic data of compound (**53)** and by direct comparison with the authentic spectral data[262], the compound (**53**) was further confirmed to be Isotorachrysone-6-O-α-D-ribofuranoside.

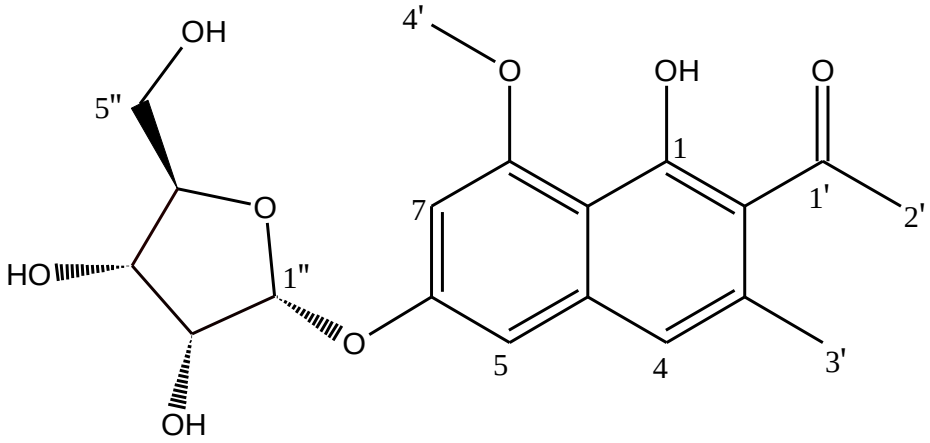

53

To the best of our knowledge compound (**53**) was isolated for the first time from the marine-derived fungus *Aspergillus glaucus*[263], after that, it has been reported many times from several fungi especially from marine origin[264].

5.1.1.22 2-Hydroxydiplopterol

2-Hydroxydiplopterol (**54**) was obtained as orange crystals (75.0 mg), showed an absorbing band at 254 nm and turned into deep violet on spraying with vanillin reagent and heating. R_f = 0.51 (DCM/MeOH 5%). Its molecular formula was determined as $C_{30}H_{52}O_2$ by its HR-ESIMS at *m/z* 467.3865 $[M+Na]^+$ (calcd. 467.3863), bearing 5 double bond equivalents (DBE).

Detailed analysis of the ^{13}C NMR (**Table 28**) displayed thirty carbon signals which were categorized, according to HSQC as eight methyls at δ_C (33.5, 30.9, 28.7, 22.4, 17.0, 16.9, 16.8 and 16.1), six methine carbons at δ_C (49.8, 55.5, 53.9, 51.1, 50.3, and one oxygenated at δ_C 65.4), ten methylenes at δ_C (55.5, 51.2, 49.7, 41.2, 34.4, 33.1, 26.6, 24.0, 21.9, 21.04, 18.4), as well as, six quaternary carbons one oxygenated δ_C 73.94 and the others at δ_C (44.1, 41.9, 41.9, 39.2, 35.0), this means that we had triterpene skeleton.

Except for an oxygenated methine signal (δ_H 3.87 and δ_C 65.4) instead of methylene (δ_C 18.7), these NMR data were quite similar to those of diplopterol (= hopanol)[265], suggesting that (**54**) is a hydroxylated diplopterol. Besides, +9.0, +8.8, +1.6, and +1.4 ppm of shift effects for C-1, C-3, C-4 and C-10 were observed respectively, indicating that the hydroxylation occurs at C-2 of diplopterol. This determination was further supported by ^1H-^1H COSY and HMBC experiments (**Figure 39**) which displayed COSY cross-correlations between the oxymethine at δ_H 3.87(tt, *J* = 11.4, 4.1 Hz, H-2) with the methylene at δ_H [(0.67 (br td, *J* = 12.5, 2.0 Hz), 2.04 (dq, *J* = 11.4, 2.0 Hz), H_2-1)] and (1.06 (t, *J* = 12.0 Hz), 1.72 m), H_2-3], and key HMBC correlations from H_3-25 (δ_H 0.86) to C-1 (δ_C 49.6), C-5 (δ_C 55.5), C-9 (δ_C 50.3) and C-10 (δ_C 39.1), from H_3-23 (δ_C 0.92) to C-3 (δ_C 51.2), C-4 (δ_C 35.0), C-5 (δ_C 55.5), and C-24 (δ_C 22.4).

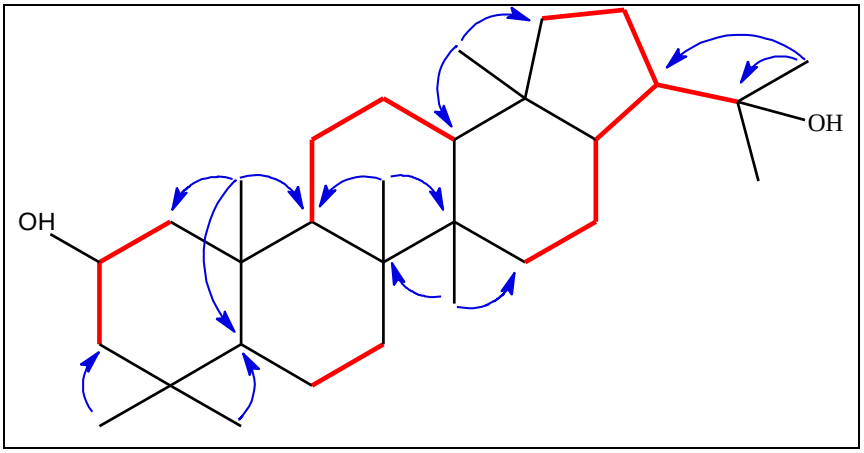

Figure 39: Key COSY (▬) and selected HMBC(⟶) correlations for (**54**).

Table 28: NMR spectroscopic data for (**54**), (400 and 100 MHz), δ ppm)[a]

Position	^{1}HNMR (*J* in Hz)	^{13}CNMR	COSY	HMBC	NOESY
1	0.67 (dd, 2.0, 12.5) 2.04 (dq, 2.0, 11.4)	49.7	2, 3	2, 3, 5, 10	11
2	3.87 (tt, 4.1,11.4)	65.4	1, 3		24
3	1.06 (t, 12.0) 1.72 m	51.2	2, 1	1, 2, 4, 23, 24	7, 20
4	-	35.0	-	-	-
5	0.68 s	55.5	6	2, 9, 10, 24	
6	1.30 (d, 3.9) 1.50 m	18.4	7	5, 7, 8, 9	24
7	1.22 m 1.36 d (3.2)	33.1	6	5, 8	
8	-	41.9	-	-	-
9	1.28 (br t, 4.3)	50.3	11	10, 11, 14, 27	
10	-	39.2	-	-	-
11	1.31 (d, 3.8) 1.54 (d, 4.3)	21.04	9, 12	7, 9, 12	1, 26
12	1.41 (br d, 3.8) 1.48 (br t, 4.3)	24.0	11, 13	11, 13, 14, 28	
13	1.34 (br d, 3.8)	49.8	12	7, 9, 12, 14	
14	-	41.9	-	-	-
15	1.20 m 1.44 m	34.4	16	14, 27	
16	1.56 (dd, 3.6, 12.9) 1.91 (dt, 2.4, 12.9)	21.9	15, 17	15, 17, 18	
17	1.43 (br t, 3.6)	53.9	16, 21	14, 16, 21, 28	
18	-	44.1	-	-	-
19	0.92 m 1.51 m	41.2	20	17, 20, 21, 28	
20	1.47 m 1.73 m)	26.6	19, 21	18, 21	
21	2.20 (br q, 9.0)	51.1	17, 20, 22	17, 18, 20, 22, 29, 30	17, 29
22	-	73.94	-	-	-
23	0.90 (3H, s)	33.5	-	3, 4, 5, 24	19
24	0.82 (3H, s)	22.4	-	3, 4, 5, 23	6
25	0.84 (3H, s)	17.0	-	1, 5, 9, 10	
26	0.93 (3H, s)	16.9	-	13, 14	11
27	0.93 (3H, s)	16.8	-	13, 14	
28	0.74 (3H, s)	16.1	-	13, 17, 18, 19	
29	1.16 (3H, s)	28.7	-	21, 22, 30	
30	1.19 (3H, s)	30.9	-	21, 22, 29	

[a] The assignments were based on DEPT, ^{1}H-^{1}H COSY, HSQC, and HMBC experiments, and recorded in $CDCl_3$.

The absolute configuration of C-2 was assigned as 2*S*- by NOESY correlations between H-2 and CH_3-24 (**Table 28**) and the comparison of the specific rotation $[\alpha]_D^{22}$ = +38 (c 0.13, $CHCl_3$), 1D/2D NMR data with the authentic data[266]. Thus, the structure of (**54**) was unambiguously elucidated as 2*S*-hydroxydiplopterol, i.e. hopan-2*S*,22-diol.

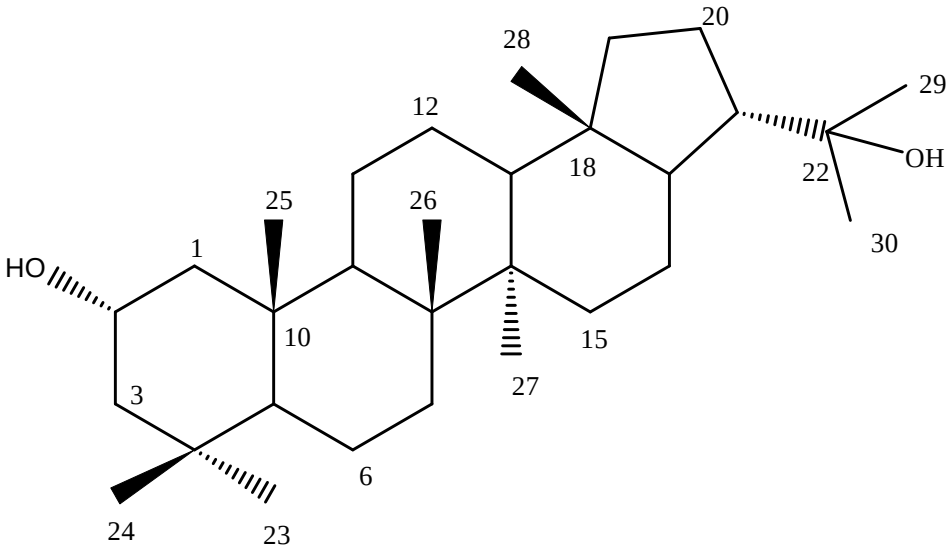

54

5.1.1.23 Questin

Compound (**55**) was obtained as orange crystals (2.1 mg) showing a green UV fluorescence. There was no colour changing with conc. sulphuric acid or sodium hydroxide solution, i.e. a *peri*-hydroxyquinone or benzopyrone were excluded. The molecular formula of $C_{16}H_{12}O_5$ was assigned based on HR-EIMS $[M+H]^+$, *m/z* 284.0685; calcd. for $C_{16}H_{12}O_5$, 284.0679), implying 10 degrees of unsaturation.

The ^{1}H NMR spectrum (**Table 29**) confirmed the existence of an acidic proton at δ_H 11.33, four aromatic protons appeared as a pair of *meta* coupled at δ_H 7.50 (br d (*J* = 1.7 Hz), 7.35 (d, *J* = 2.3 Hz), 7.11 (br d, *J* = 1.7 Hz) and 6.95 (d, *J* = 2.3 Hz), as well as, two singlet signals attributed for one methoxy group at δ_H 3.99 and one aromatic methyl at δ_H 2.44. The ^{13}CNMR spectrum displayed sixteen carbon signals which were categorized, according to HSQC DEPT as four methine sp^2 (δ_C 125.3, 120.6, 108.4, 105.7), one methoxy (δ_C 56.8) and one methyl (δ_C 21.9), and ten uncharacterized carbons at (δ_C 184.0, 184.0, 166.2, 165.5, 163.7, 148.3, 138.8, 133.9, 116.0, 114.5). Based on the ^{1}H and ^{13}C NMR data,

(**55**) is constituted of two substituted aromatic rings connected by carbonyl groups forming an anthraquinone.

Table 29: NMR spectroscopic data for questin (**55**) (400 and 100 MHz, δ ppm) [a]

Position	^{1}HNMR (*J* in Hz)[b]	^{1}HNMR (*J* in Hz)	^{13}CNMR	COSY	HMBC
1	-	-	163.7	-	-
2	7.11 (br d, 1.7)	7.08 s	125.3	4, 3-Me	4, 9a, 3-Me
3	-	-	148.3	-	-
4	7.50 (br d, 1.7)	7.51 s	120.6	2, 3-Me	2, 9a, 10, 3-Me
4a	-	-	133.9	-	-
5	7.35 (d, 2.3)	7.28 (d, 2.3)	108.4	7	7, 8a, 10
6	-	-	165.2	-	-
7	6.95 (d, 2.3)	6.83 (d, 2.3)	105.7	5, 8-OMe	5, 8, 8a
8	-	-	166.2	-	-
8a	-	-	114.5	-	-
9-CO	-	-	184.0	-	-
9a	-	-	116.0	-	-
10-CO	-	-	184.0	-	-
10a	-	-	138.8	-	-
1-OH	11.33 s	-	-	-	-
3-CH_3	2.44 s	2.40 s	21.9	2, 4	2, 3, 4
8-OCH_3	3.99 s	3.97 s	56.8	7	8

[a] The assignments were based on DEPT, ^{1}H-^{1}H COSY, HSQC, and HMBC experiments, and recorded in MeOD-d_4, [b] recorded in acetone-d_6

The structure of was further deduced from ^{1}H-^{1}H COSY and HMBC correlations (**Figure 40**), both instances established that the low-field proton (H-4), resonating at δ_H 7.50 exhibited a clear COSY correlation with H-2 (δ_H 7.11) along with the methyl at (δ_H 2.44) and HMBC correlations to the carbons at δc 21.9 (C-3-Me), 116.0 (C-9a), 125.3 (C-2), 184.0 (C-9, and or C-10). Additionally, an HMBC cross-peaks of the aromatic proton at δ_H 7.11 with the carbons at δc 21.9 (C-3-Me), 120.6 (C-4), and 116.0 (C-9a), and of the methyl protons at (δ_H 2.44) to the carbons at δ_C 148.3 (C-3), 125.3 (C-2), and 120.6 (C-4), confirmed the first part of the anthraquinone.

Likewise, the COSY connectivity between the two aromatic protons resonating at δ_H (7.35, H-5, and 6.95, H-7), moreover the HMBC correlation from H-5 to the carbons at δ_C 184.0 (C-10), 114.5 (C-8a), and 105.7 (C-7), from H-7 to the carbons at δ_C 166.2 (C-8), 114.5 (C-8a), and 108.4 (C-5), and from the methoxy protons to the carbon at δ_C 166.2 (C-8) confirmed the other part of the anthraquinone (**Figure 40**).

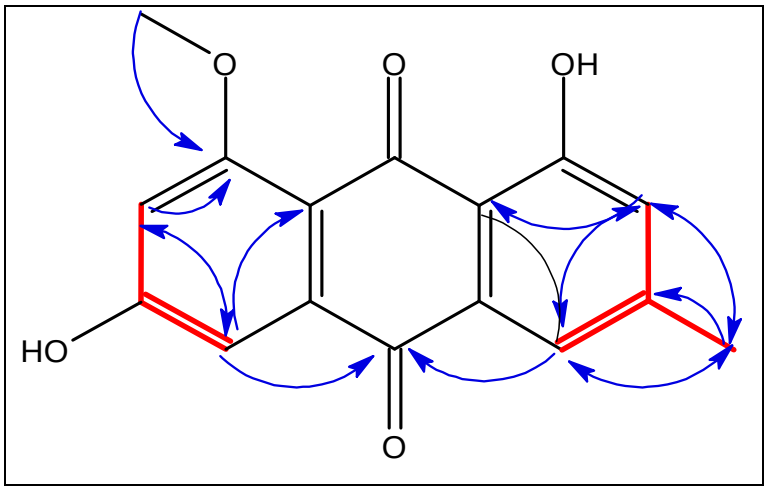

Figure 40: Key COSY (▬) and selected HMBC(⟶) correlations for (**55**).

Consequently, the structure of (**55**) was established as 1,6-dihydroxy-8- methoxy-3-methyl-9,10-anthracene-9,10-dione, commonly known as questin[267]. Questin has been previously reported from several species of *Eurotium*[203], *Astragalus membranaceus*[268] as well as from plants belonging to the genera *Cassia*[269] and *Polygonum*[270].

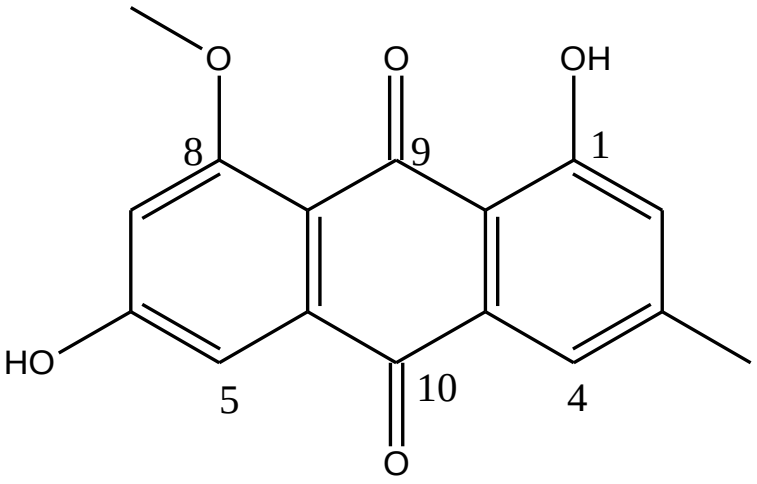

55

5.1.1.24 Physcion

Physcion (**56**) was obtained as an orange solid (20.0 mg), its molecular formula was determined based on HR-EIMS [M+H]+, *m/z* 284.0685; calcd for $C_{16}H_{12}O_5$, 284.0679), implying 10 degrees of unsaturation.

The general features of its MS and ^{1}H NMR spectra closely resembled those of (**56**). However, the ^{1}H NMR spectrum in (DMSO-d_6) (**Table 30**) revealed the presence of two singlet signals attributed for two chelated hydroxyl groups at δ_H 12.30 and 12.10, four aromatic protons at δ_H 7.55 (br d, J = 1.4 Hz), 7.22 (br d, J = 1.4 Hz), 7.21 (d, J = 2.5 Hz), and 6.89 (d, J = 2.5 Hz), furthermore, one methoxy group at δ_H (3.94, s) and one aromatic methyl at δ_H (2.43, s). The ^{13}CNMR spectrum displayed also sixteen carbon signals which were categorized as four methines, one methoxy, one methyl, and ten quaternary carbons, suggesting the anthraquinone nucleus.

Table 30: NMR spectroscopic data for physcion **(56)** (600 and 150 MHz, δ ppm) [a]

Position	^{1}HNMR (J in Hz)[b]	^{1}HNMR (J in Hz)	^{13}CNMR	COSY	HMBC
1	-	-	161.6	-	-
2	7.06 br s	7.22 (br d, 1.4)	124.2	4, 3-Me	1, 4, 9a, 3-Me
3	-	-	148.5	-	-
4	7.60 br. s	7.55 (br d, 1.4)	120.5	2, 3-Me	2, 9a, 10, 3-Me
4a	-	-	nd	-	-
5	7.34 d (2.5)	7.21 d (2.5)	107.5	7	4, 6, 8a, 10
6	-	-	166.2	-	-
7	6.67 d (2.5)	6.89 d (2.5)	106.5	5	5, 8, 8a
8	-	-	165.3	-	-
8a	-	-	110.1	-	-
9-CO	-	-	181.6	-	-
9a	-	-	113.5	-	-
10-CO	-	-	181.6	-	-
10a	-	-	nd	-	-
1-OH	12.10 s	12.10 s	-	-	-
3-CH3	2.43 s	2.43 s	21.4	4	2, 3, 4
6-OCH3	3.91 s	3.94 s	56.2	-	6
8-OH	12.30 s	12.30 s	-	-	-

[a] The assignments were based on DEPT, ^{1}H-^{1}H COSY, HSQC, and HMBC experiments, and recorded in DMSO-d_6, [b]recorded in $CDCl_3$

Further investigation using ^{1}H-^{1}H COSY and HMBC correlations revealed that one of the substituted benzene rings was a 1-hydroxy-3-methoxybenzene ring of the anthraquinone corroborated not only by the chemical shift values of the aromatic protons and their corresponding carbons (δ_H 6.89 (d, J = 2.5 Hz; δ_C 106.5) / δ_H 7.21 (d, J = 2.5 Hz; δ_C 107.5), but also by the HMBC correlations of the aromatic proton at δ_H 6.89 to the carbon

at δ_C 165.3 (C-8), 107.5 (C-5) and 110.1 (C-8a), and of the aromatic proton at δ_H 7.21 to the carbons at δ_C 166.2 (C-6), 120.5 (C-4), 110.1 (C-8a) and the carbonyl carbon at δ_C 181.6 (C-9).

The other part of the anthraquinone was a 1-hydroxy-3-methylbenzene, supported by the presence of the methyl singlet at δ_H 2.46 (δ_C 22.2) which, in turn, gave HMBC correlations to the carbons at δ_C 148.5 (C-3). Moreover, the HMBC correlations of the doublet of the aromatic proton at δ_H 7.55 to the carbonyl at δ_C 181.6 (C-10), the methyl carbon at δ_C 21.4 (3-CH_3), and the aromatic carbons at δ_C 124.2 (C-2) and 113.5 (C-9a).

According to the aforementioned data, the structure of (**56**) was proposed as 1,8-dihydroxy-6-methoxy-3-methylanthracene-9,10-dione. The ^{1}H and ^{13}C NMR data of (**56**) was compatible with those of physcion[271], the pigment isolated from several species of the genus *Aspergillus*[272, 273].

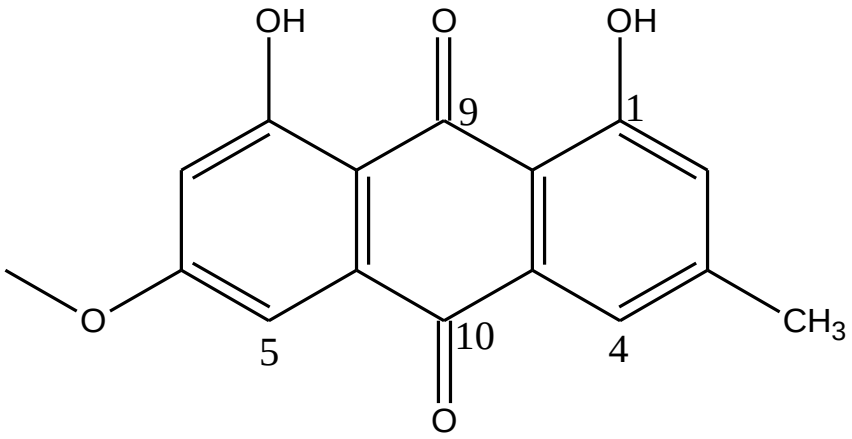

56

Anthraquinones are aromatic polyketides produced by repetitive Claisen condensations of an acyl CoA starting unit with malonyl-CoA elongations units. Biosynthesis of questin (**55**) and physcion (**56**) is shown in (**Scheme 4**)[274].

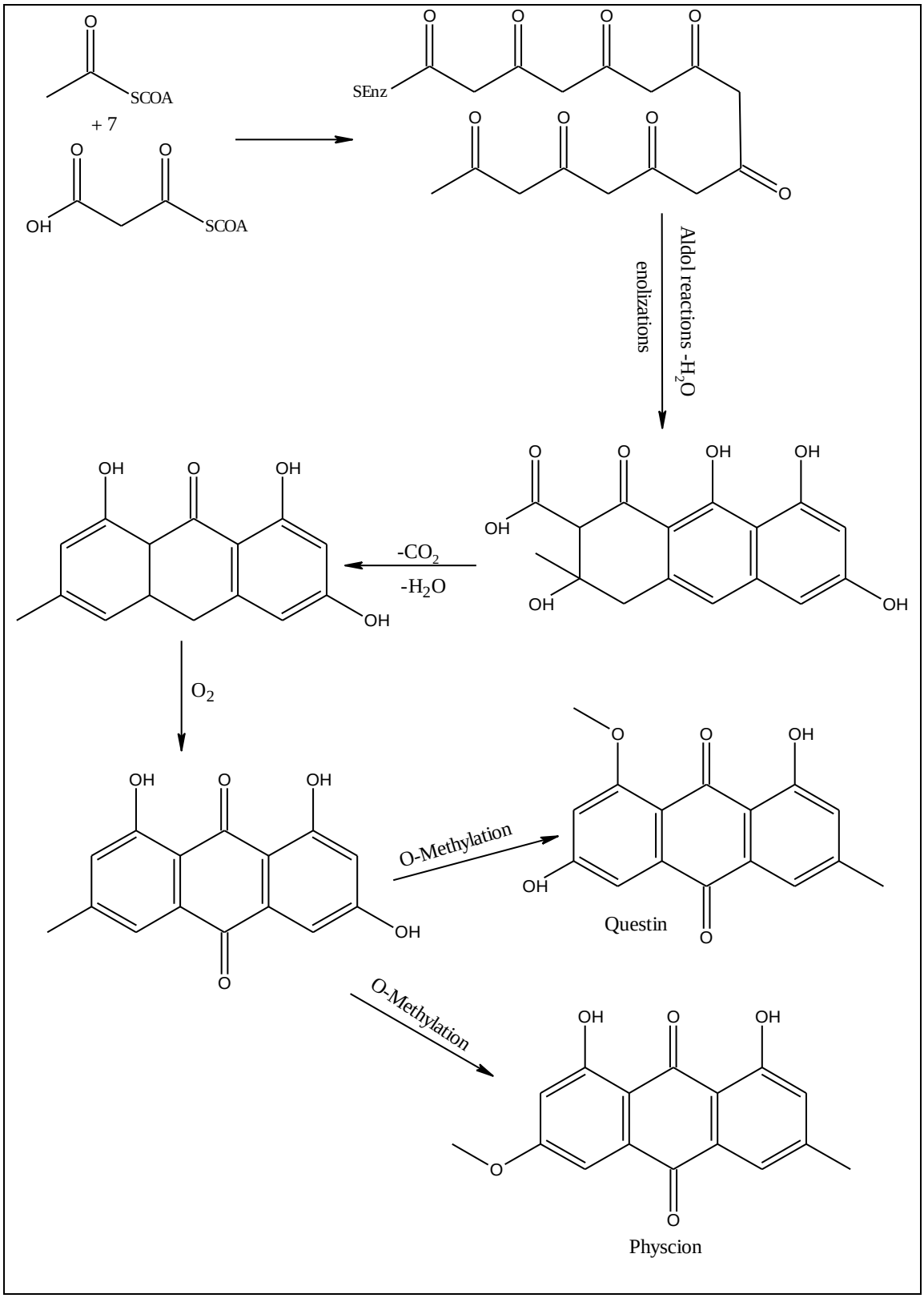

Scheme 4: Biosynthetic pathway of the anthraquinones (**55**) and (**56**).

5.1.2 Bioactivity assay of isolated compounds from *A. Ochraceopetaliformis*

5.1.2.1 Antimicrobial Activity

Antimicrobials are probably one of the most successful forms of chemotherapy in the history of medicine. There are 3 main classes of antimicrobials – disinfectants, antiseptics, and antibiotics. Disinfectants (which include bleach and common household cleaning materials) are non-selective agents that kill microbes on non-living surfaces, preventing their spread. Antiseptics are applied to living tissue during surgery, reducing microbial infection. Antibiotics are drugs that are used to destroy microbes within the body by either killing them or slowing their development and growth.

The term "antibiotics" is used to specifically refer to antibacterials but in recent years it has been expanded to include drugs that treat all forms of microbe. It also used to only describe drugs that were derived from living microorganisms but now includes synthetic formulations such as fluoroquinolones and sulfinamides.

Antimicrobial Activity Evaluation

The isolated compounds were evaluated for their antibacterial activity against two Gram positive bacteria: *Staphylococcus aureus* (ATCC 25923) and *Staphylococcus epidermidis* (ATCC 12228); four Gram negative bacteria: *Escherichia coli* (ATCC 25922), *Enterobacter cloacae* (ATCC 13047), *Klebsiella pneumoniae* (ATCC 13883) and *Pseudomonas aeruginosa* (ATCC 227853); as well as they were were evaluated for their antifungal activity against three pathogenic fungi: *Candida albicans* (ATCC 10231), *Candida tropicalis* (ATCC 13801) and *Candida glabrata* (ATCC 28838),
as shown in (**Table 31**). The antimicrobial studies showed that all the new compounds 8-hydroxyechinulin (**38**), epoxyechinulin (**39**), neoechinulin F (**46**), (12R)dehydroechinulin (**49**) and ochraceopyronide (**52**) had a mild activity against the Gram- positive bacteria, whereas they were inactive against the tested Gram-negative bacteria and the human pathogenic fungi. It is noteworthy that compounds neoechinulin (**45**), Isotorachrysone-6-O-α-D-ribofuranoside (**53**), 2-hydroxydiplopterol (**54**) and physcion (**56**) exhibited the strongest antibacterial and antifungal activity (minimal inhibition concentration (MIC) values 0.09 – 0.87 mg/mL).

Table 31: : Antimicrobial activity of the isolated compounds (MIC mg/ml, n = 3).

Microbe / Compound	*S. aureus*	*S. epidermidis*	*P. aeruginosa*	*K. pneumoniae*	*E. cloacae*	*E.coli*	*C. albicans*	*C. tropicalis*	*C. glabrata*
33	9/1.25	9/1.15	na	na	na	na	na	na	na
34	10/1.25	10/1.18	na	na	na	na	na	na	na
35	16/0.04	17/0.02	9/1.00	9/1.15	9/1.24	13/0.65	na	na	na
37	10/1.30	9/1.28	8/1.75	8/1.90	8/2.15	8/2.30	na	na	na
38	9/1.19	9/1.15	na	na	na	na	na	na	na
39	9/1.12	9/1.20	na	na	na	na	na	na	na
41	10/0.95	9/1.10	na	na	na	na	na	na	na
42	9/1.00	9/0.95	na	na	na	na	na	na	na
43	10/1.15	9/1.32	8/1.85	8/2.0	8/1.77	8/1.84	na	na	na
44	8/1.17	9/1.12	na	na	na	na	na	na	na
45	10/1.12	9/1.20	8/1.98	8/1.77	8/1.85	8/1.87	10	10	11
46	9/1.30	10/1.21	na	na	na	na	na	na	na
47	8/1.30	8/1.28	na	na	na	na	na	na	na
49	8/1.22	9/1.15	na	na	na	na	na	na	na
50	10/1.48	9/1.55	8/1.70	na	8/2.10	8/2.22	9	10	10
51	9/1.79	9/1.65	8/1.90	na	8/2.00	8/1.94	9	10	10
52	9/1.19	9/1.22	na	na	na	na	na	na	na
53	16/0.10	17/0.09	12/0.45	13/0.50	13/0.47	13/0.42	11	12/0.90	13/0.72
54	15/0.23	16/0.25	12/0.52	13/0.61	13/0.65	13/0.47	12/0.87	12/0.82	12/0.7 8
55	8/1.22	9/1.12	na	na	na	na	na	na	na
56	10/1.35	9/1.25	8/1.62	-	8/1.97	8/1.90	9	10	10
Netilmicin	20/0.2 $x10^{-3}$	26	21	24	21	23	nt	nt	nt
Amoxicillin	22	24	25	23	22	22	nt	nt	nt
5-fluocytocin	nt	nt	nt	nt	nt	nt	22	22	24
Amphotericin B	nt	nt	nt	nt	nt	nt	24	24	25

na: not active, nt: not tested

5.1.2.2 Antioxidant activity

Evaluation of antioxidant potential of selected pure compounds was performed using the DPPH radical scavenging assay in 96-well plate, however, none of the tested compounds exhibited antioxidant activity.

Table 32: Antioxidant activity of some of the isolated metabolites (100µM)

Test / Compound	DPPH	
	% INHIB.	SEM
37	-5.27	0.94
43	-1.69	0.32
45	5.65	2.85
50	2.78	1.34
51	0.95	0.83
52	-3.18	0.87
53	-2.38	0.98
54	-11.35	3.30
56	8.78	7.80

5.1.2.3 Antienzymatic activity

Some of the isolated compounds had been tested against tyrosinase and acetylcholine-esterase in a 96 well microplate as in (**Table 33** and **Table 34**)

Table 33: Antityrosinase activity of some of the isolated metabolites (100µM)

Test / Compound	TYROSINASE INHIBITION	
	% INHIB.	SEM
37	14.27	2.33
43	-2.41	3.42
45	32.66	1.28
50	-2,10	2.06
51	-4.31	3.75
52	-7.02	3.64
53	4.17	3.17
54	7.99	4.89
56	-14.99	0.40

Table 34: Anti acetylcholinesterase activity of some of the isolated metabolites (100µM)

	100µM		**50µM**	
Compound	AVERAGE	STDEV	AVERAGE	STDEV
37	**64.44**	4.13	**61.45**	1.09
42	13.94	0.84	12.09	2.05
43	15.92	1.35	20.93	7.19
51	3.18	2.73	8.89	4.89
52	5.31	1.04	21.62	1.53
54	13.36	3.47	23.15	2.74
55	**26.87**	2.83	**22.06**	1.22
56	7.24	1.72	7.97	3.32
	25 µM		**1µM**	
	AVERAGE	STDEV	AVERAGE	STDEV
GALANTHAMINE	**94.87**	**0.22**	**52.30**	**0.68**

In the Evaluation of tyrosinase inhibitory, all of the tested compounds were inactive except neoechinulin (**45**) which inhibited the enzyme activity 32,66% at the concentration of 100µM. While, in the acetylcholinesterase activity echinulin (**37**) was characterized as the most potent inhibitor, inhibiting the enzyme's activity 64.44% at 100µM.

5.1.3 Molecular docking study

The peptidoglycan (PG or murein) is an essential component of the bacterial cell wall consisting of polysaccharides with alternating *N*-acetylmuramic acid (MurNAc) and *N*-acetylglucosamine (GlcNAc) in addition to an attached pentapeptide to the MurNAc moiety. The biosynthesis of different enzymes in the peptidoglycan (PG) has been a novel target for a new antimicrobial drug. The synthesis process starts in the cytoplasm by the formation of the nucleotide precursors (UDP-GlcNAc) from fructose-6-phosphate under the effect of the Glm enzymes. UDP-GlcNAc is the precursor of UDP-N-acetylmuramyl-pentapeptide (UDP-Mpp) that produced by different Mur enzymes (MurA, MurB, MurC, MurD, MurE and MurF)[275, 276].

The PG synthesis process is a crucial target to discover new highly specific antimicrobial agents due to its essential role for bacterial survival while it has no homologs in humans. PG synthesis includes the formation of different precursor such as lipid

intermediates (Lipid I and Lipid II), UDP-N-acetylglucosamine (GlcNAc), UDP-N-acetylmuramic acid (MurNAc). The process catalyzed at first by several enzymes like GlmS, GlmM, GlmU enzyme, then Mur Ligases (MurA MurF) and finally by MraY and MurG. Consequently, Mur enzymes can be considered as a promising target for new selective antimicrobial agent development[277].

Molecular docking studies were performed aiming to get further insight into the binding modes and orientations of the most active compound against MurF. The target proteins were retrieved from Protein Data Bank (PDB ID: 4CVL). The co-crystalized ligand (ACP) was used as a reference ligand. The study was designed to evaluate how our small molecule and the target macromolecule (MurF) fit together. Docking studies were carried out using MOE Software.

Two reasons encouraged us to run this study. Firstly, the antibacterial effect of the isolated compounds. Secondly, the isolated compounds have some sort of structural similarity with phosphomethylphosphonic acid adenylate ester (ACP, the co-crystallized ligand of MurF, PDB ID: 4CVL). As shown in Fig. 1, ACP has two main pharmacophores: lipophilic part (6-amino-9H-purine) and hydrophilic part (ribose and triphosphate derivative). It was found that neoechinulin (**45**) has the two main parts: 1) lipophilic part (1H-indole derivative) and hydrophilic part (piperazine-2,3-dione). This great similarity drove us to carry the docking studies for neoechinulin (**45**) against MurF.

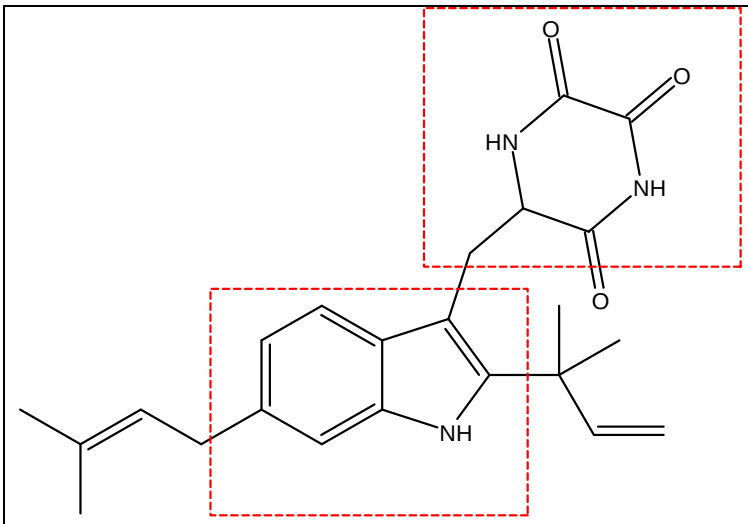

hydrophilic part

lipophilic part

Neoechinulin (45)

hydrophilic part

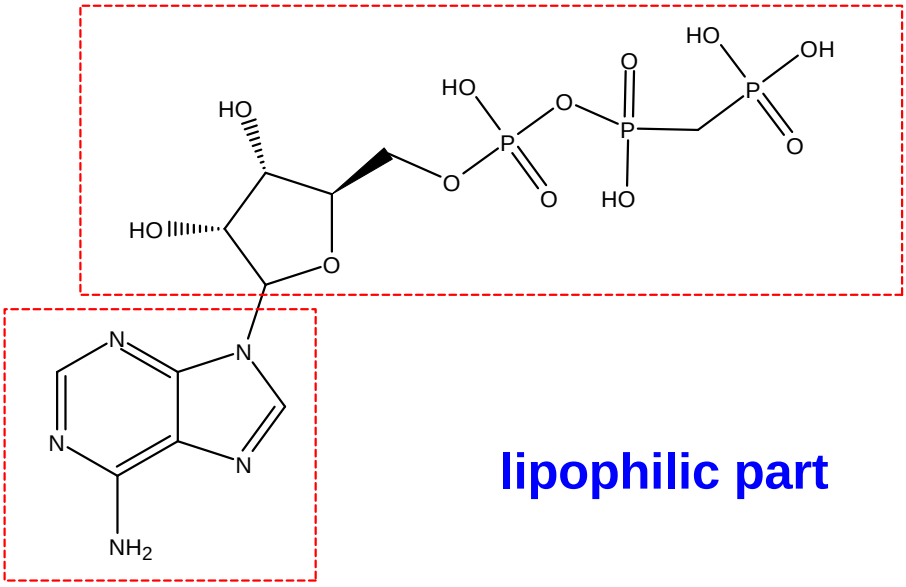

lipophilic part

ACP

Flexible alignment

3D- flexible alignment of neoechinulin (**45**) with the co-crystallized ligand (ACP) was presented in **Figure 41.** In the figure is possible to observe that, in general, the structure of neoechinulin (**45**) has a good overlapping with the reference molecules (ACP).

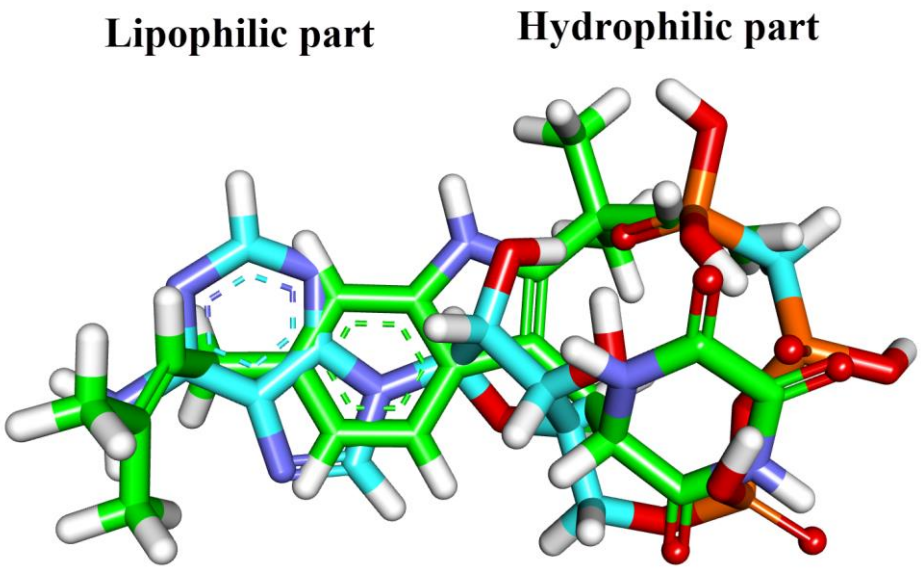

Figure 41: Flexible alignment of neoechinulin (**45**) (carbon atoms in green) with the co-crystallized ligand (ACP) (carbon atoms in turquoise).

Molecular docking studies

The co-crystallized ligand (ACP**)** exhibited a binding affinity value of -10.77 kcal/mol against MurF. The terminal hydrophilic part (triphosphate derivative) was oriented into the hydrophilic region of the target macromolecule forming eight hydrogen bonds with Asn142, Thr114, Thr115, Lys113, Gly112. Besides, it formed two electrostatic interactions with Lys113. Furthermore, the 6-amino-9H-purine moiety was inserted in the hydrophobic region of the target receptor forming two hydrogen-bonding interactions with Asn292 (**Figure 42**).

Table 35: The docking binding free energies (kcal/mol) of (**45**) and the co-crystallized ligand (**ACP**)

Compounds	**Free energies (kcal/mol)**
Neoechinulin (45)	-13.72
(**ACP)**	-10.77

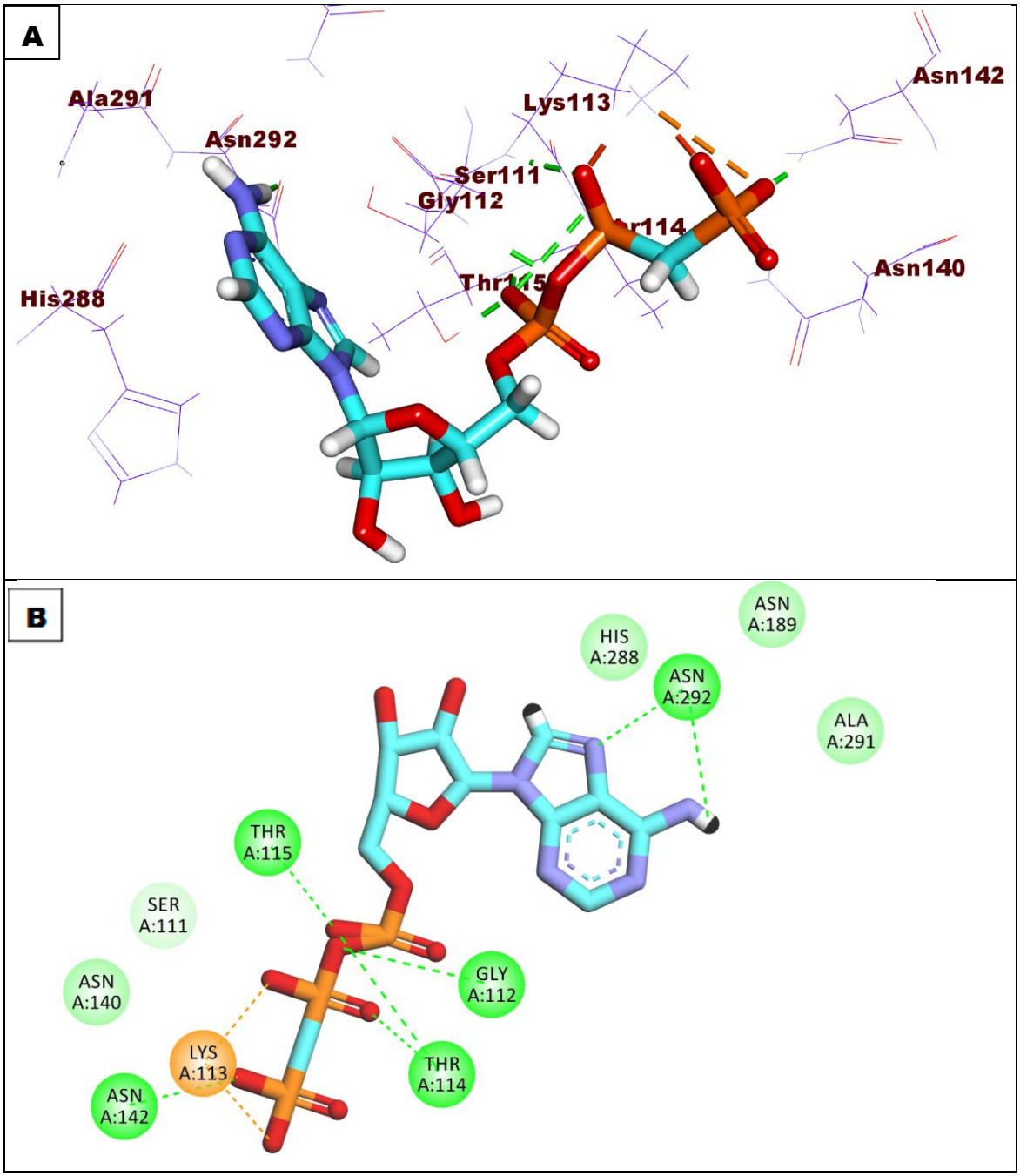
A
Ala291
Asn292
Lys113
Asn142
Ser111
Gly112
Asn140
His288
B
ASN A:189
HIS A:288
ASN A:292
ALA A:291
THR A:115
SER A:111
GLY A:112
ASN A:140
LYS A:113
THR A:114
ASN A:142

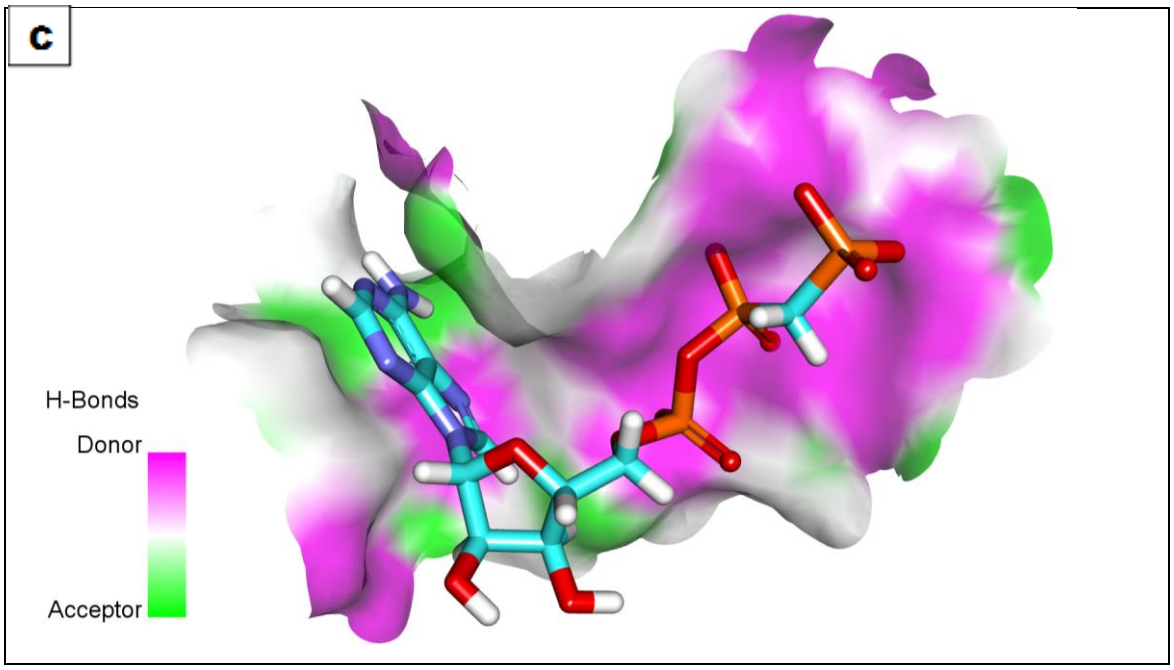

Figure 42: A) 3D of co-crystallized ligand (ACP) docked into the active site of MurF. B) 2D of co-crystallized ligand (ACP) docked into the active site of MurF. C) Mapping surface showing Co-crystallized ligand **(**ACP**)** occupying the active pocket of MurF.

The most active neoechinulin (**45**) exhibited a binding mode like that of the reference molecule with a higher affinity value of -13.72 kcal/mol against MurF**.** The hydrophilic part (piperazine-2,3-dione) was oriented into the hydrophilic region of the target macromolecule forming six hydrogen bonds through its two carbonyl groups. The amino acid residues which were involved in such hydrogen bonding interactions are Gly112, Thr114, Thr115. Furthermore, the lipophilic part of this molecule was buried in the hydrophobic region of the target receptor forming six hydrophobic interactions with His288, Ala349, and Arg323 (**Figure 43**).

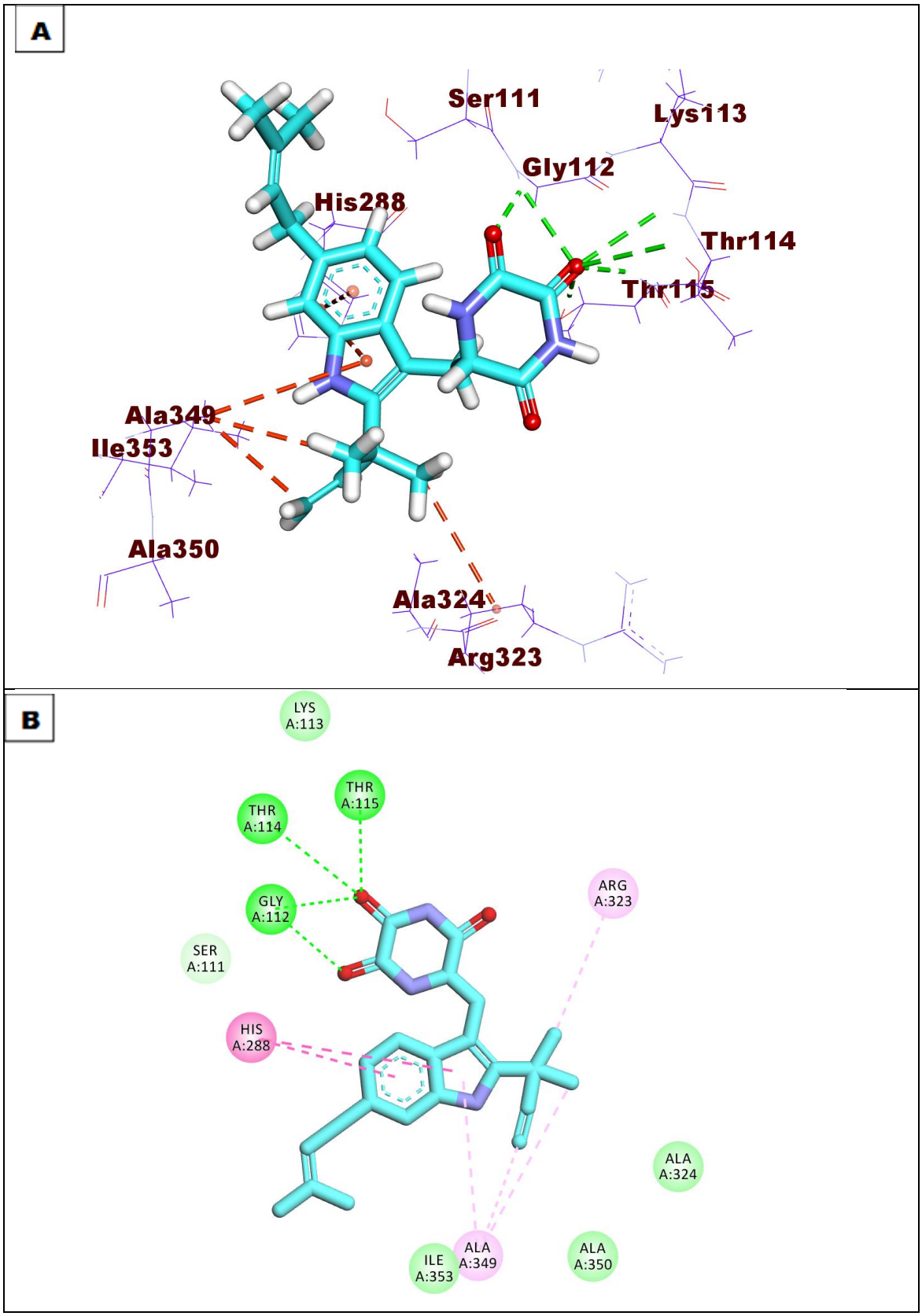
A
Ser111
Lys113
Gly112
His288
Thr114
Thr115
Ala349
Ile353
Ala350
Ala324
Arg323
B
LYS A:113
THR A:115
THR A:114
GLY A:112
SER A:111
HIS A:288
ARG A:323
ALA A:324
ILE A:353
ALA A:349
ALA A:350

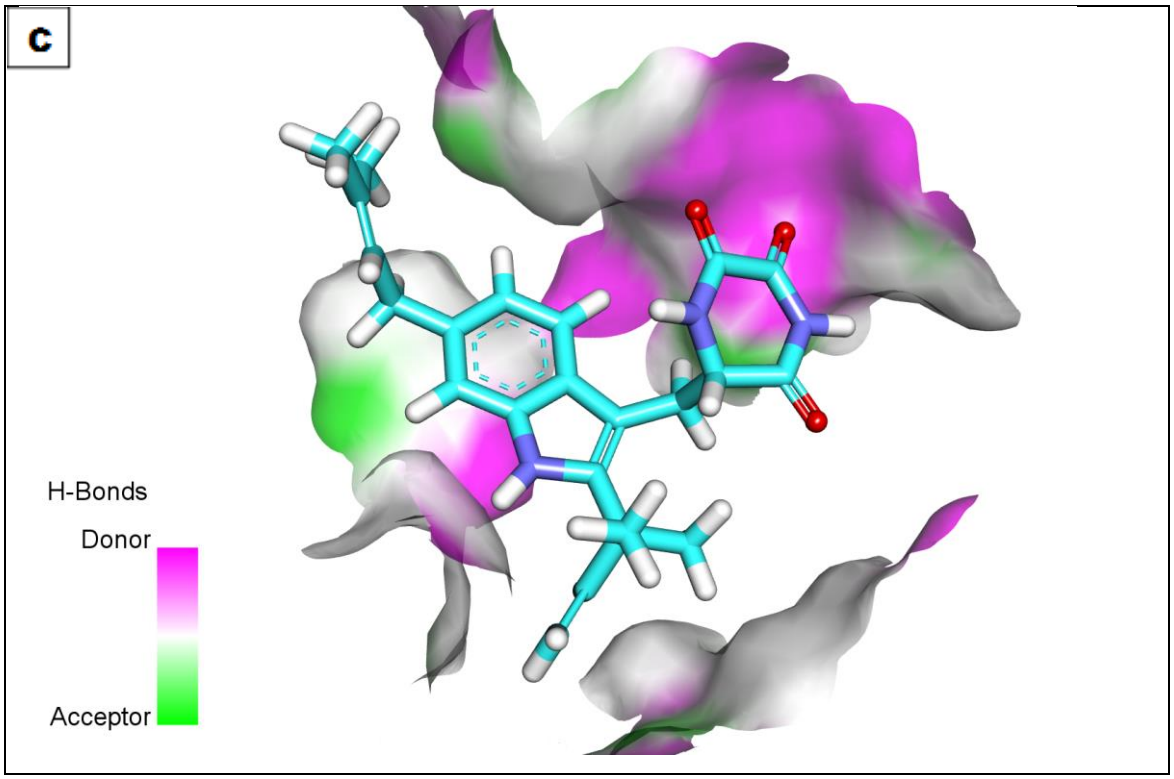

Figure 43: A) 3D of neoechinulin (**45**) docked into the active site of MurF. B) 2D of (**45**) docked into the active site of MurF. C) Mapping surface showing (**45**) occupying the active pocket of MurF.

5.2 *Myrothecium verrucaria* ASU7

This endophytic fungal strain was isolated from healthy wild medicinal plant datura (*Datura stramonium L.*) which collected from Wadi El Assuity, protective area, Assiut Governorate, Upper Egypt in 2015. The identification of *Myrothecium verrucaria* strain ASU7 was preliminary based on culture and microscopic characteristics next, the obtained sequence of *M. verrucaria* strain ASU7 was deposited in the GenBank nucleotide sequence database under accession number KX611156.

The pure fungal strain was cultivated on PDA medium and incubated for 30 days at 25ºC with agitation (150 rpm/min). The culture broth was extracted three times with an equal volume of ethyl acetate using a separation funnel. Then the organic layers were combined, dried through anhydrous sodium sulfate and filtered to afford 7.0 gm of dark brown extract.

In the primary screening, the ethyl acetate extract of the endophytic *Myrothecium verrucaria* ASU7showed interesting characteristics during TLC. Moreover, the extract showed significant antimicrobial activity against six pathogenic microorganisms using agar well diffusion method (**Figure 44**). The test bacterial pathogens were *Bacillus cereus* and *Escherichia coli*, while the pathogenic yeasts were *Candida albicans* and *Trichosporon Jirovecii*. On the other hand, the plant fungal pathogens were *Botrytis cinerea* and *Alternaria porri*.

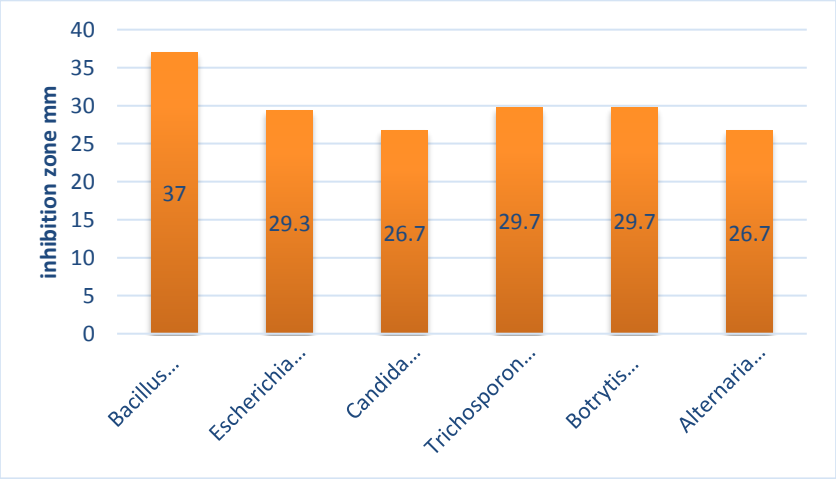

Figure 44: Antimicrobial activity of *Myrothecium verrucaria* ASU7crude extract.

For further investigation, the obtained EtOAc extract was defatted by cyclohexane and subjected to CPC for fractionation (**see section 4.2.5.1**). After several injections using CPC, seventy tubes were collected, then according to the pre-screening via TLC monitoring, fifteen fractions were obtained and proceeded for the profiling using High Performance Thin Layer Chromatography (HPTLC) analysis (**Figure 45**).

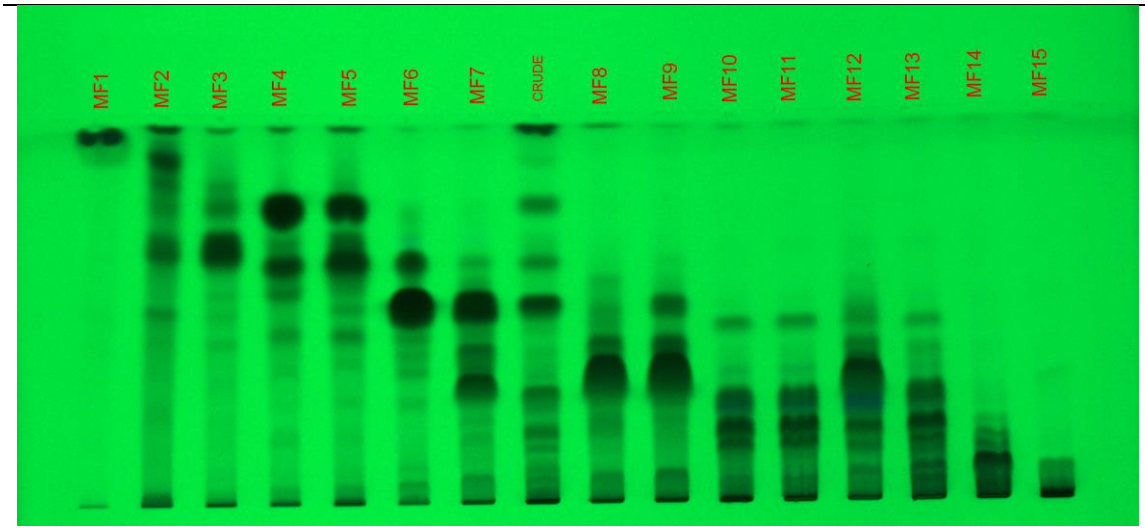

A

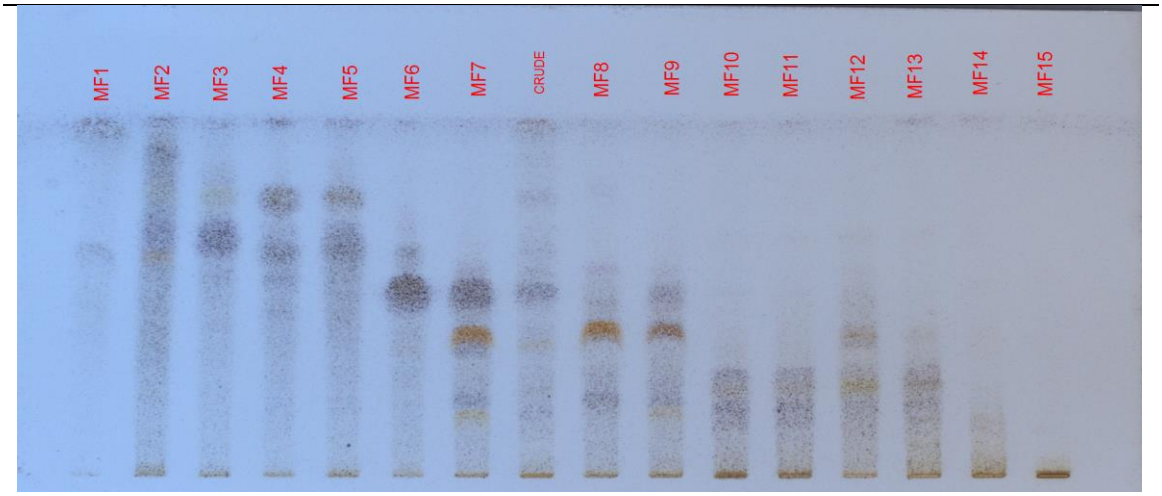

B

Figure 45: HPTLC of the CPC fractions; A: at 254nm, B: after spraying with vanillin/ sulphuric acid, elution system ($CHCl_3$:EtOAc: Isopropanol 55:40:5)

According to the HPLC profiling of the fractions, the similar fractions were added together (MF6+MF7), (MF8+MF9), (MF10+MF11+MF12+MF13) to get seven fractions overall (**see section 4.2.4.2**). Further purification on HPLC afforded 19 compounds (**Figure 10, Figure 11**), and **Table 4**, which are described as shown below.

5.2.1 Isolated metabolites from *Myrothecium verrucaria*

5.2.1.1 Roridin A

Roridin A (**57**) was isolated as white crystals (68.5 mg). It displayed Positive ESI-MS showed a molecular ion peak at *m/z* 571.2312 $[M+K]^+$ (calculated for $C_{29}H_{40}O_9$, 571.2304) indicated that it had 10 degrees of unsaturation.

The ^{1}H NMR data (**Table 36**) of (**57**) showed four methyls at [δ_H 0.79 (3H, s, H-14), 1.07 (3H, d, *J* = 6.9 Hz, H-14′), 1.18 (3H, d, *J* = 6.1 Hz, H-12'), 1.72 (3H, s, H-16)], oxygenated methylenes and methines at δ_H 3.30−5.60 ppm, and five olefinic protons [δ_H 4.08 (1H, dd, *J* = 6.9, 3.1 Hz, H-2′), 5.78 (1H, d, *J* = 11.5 Hz, H-10′), 5.98 (1H, dd, *J* = 15.5, 3.1 Hz, H-7′), 6.64 (1H, t, *J* = 11.5 Hz, H-9′), 7.64 (1H, dd, *J* = 15.5, 11.5 Hz, H-8′)]. The ^{13}C NMR data (**Table 36**), displayed the resonances of four methyls at (δ_C 7.4, 14.7, 18.2, and 23.2), seven methylenes at (δ_C 20.2, 27.6, 32.9, 34.8, 47.7, 64.8, and 69.8), 12 methines at (δ_C 37.1, 67.1, 70.7, 74.2, 75.5, 79.0, 83.9, 117.4, 118.2, 126.1, 139.2, and 143.8), and six uncharacterized carbons at (δ_C 43.7, 49.3, 65.2, 140.9, 166.4, and 174.8). Detailed inspection of ^{1}H and ^{13}C NMR data speculated that the structure of (**57**) was a macrocyclic trichothecene analogue.

The analysis of ^{1}H−^{1}H COSY and HMBC data afforded two substructures, A and B, as shown in **Figure 46**. Substructure A was identified to be a trichothecene sesquiterpene moiety, whereas the vicinal proton correlations (H-4′/H-5′ and H-10′/H-9′/H-8′/H-7′/H-6′/H-13′/H-14′) in the ^{1}H−^{1}H COSY spectrum and HMBC cross-peaks (H-2′/C-1′, C-3′, C-4′, and C-12′, H-5′/C-6′, H-9′/C-11′, H-10′/C-11′, and H-12′/C-2′, C-3′, and C-4′) led to the establishment of substructure B.

Key HMBC correlations of H-13/C-2, C-5, C-6, and C-12 led to the assignment of the epoxide, commonly present in trichothecene analogues at C-12. Finally, the substructures A and B were assembled by HMBC correlations of H-4/C-11′ and H-15/C-1′, which completed the planar structure of (**57**).

The relative configuration of the rearranged trichothecene moiety was identified by the analysis of NOESY correlations of H-2/H-13b, H-3*β*/H-14, H-3*α*/H-4, H-4/H-11, H-4/H-15a, and H-13*β* /H-14. The geometries of two disubstituted double bonds in the macrocyclic ring were confirmed using coupling constants ($^3J_{7',8'}$ = 15.6 Hz; *E*-geometry, and $^3J_{9',10'}$ = 11.5 Hz; *Z*- geometry) of olefinic protons and the NOESY correlation between H-9′ and H-7′.

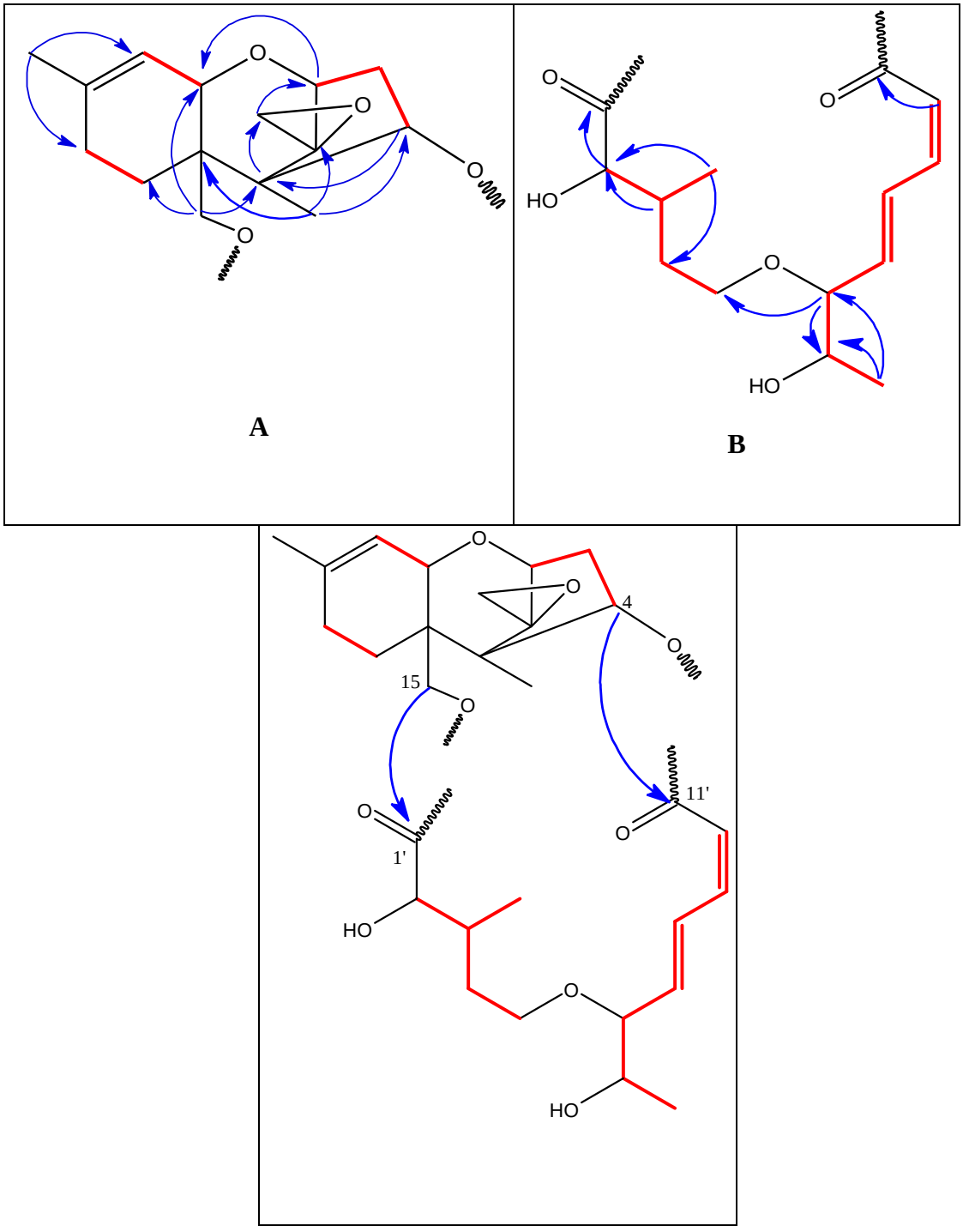

Figure 46: Key COSY (▬) and selected HMBC(→) correlations for roridin A (**57**)

Table 36: NMR spectroscopic data for Roridin A (**57**) (400 and 100 MHz, δ ppm)[a]

Position	^{1}HNMR (*J* in Hz)	^{13}CNMR	COSY	HMBC	NOESY
2	3.84 (d, 5.1)	79.0	3, 4	4, 5, 11	3β 13b, 13'
3	α 2.43 (dd, 8.3, 15.3) β 2.19 (dt, 4.5, 9.3, 15.3)	34.8	2, 4	2, 5, 12 4	4 13'
4	5.76 (dd, 4.5, 8.3)	74.2	3	2, 5, 6, 12, 11'	11
5	-	49.3	-	-	-
6	-	43.7	-	-	-
7	1.75 m 1.88 m	20.2	8	6, 8, 11 15	13b, 14
8	1.85 (br d, 3.0) 1.97 (dd, 4.1, 11.4)	27.6	7	6, 9, 10	13a, 15
9	-	140.9	-	-	-
10	5.41 (d, 5.1)	118.2	11, 16	6, 8, 11, 16	15
11	3.57 Ovlp.	67.1	10	6, 8, 10, 16	10'
12	-	65.2	-	-	-
13	a 2.78 (d, 4.1) b 3.10 (d, 4.1)	47.7	-	2, 3, 5, 12	14, 13' 2', 12', 13'
14	0.79 s	7.4	-	4, 5, 6, 12	3', 15, 8', 12'
15	4.42 s	64.5	-	5, 6, 7, 11, 1'	10, 14, 12'
16	1.72 s	23.2	9, 10	7, 8, 9, 10	10
1'-CO	-	174.8	-	-	-
2'	4.08 (dd, 3.1, 6.9)	75.5	3'	1', 3', 4', 12'	12'
3'	2.01 m	37.1	2', 12'	1', 4', 12'	14, 5', 8'
4'	1.61 m 1.78 m	32.9	3', 5', 12'	3', 5', 12' 2', 3'	5', 8', 14'
5'	3.51 (dd, 5.0, 7.4)	69.8	4'	3', 4', 6'	3', 8', 12'
6'	3.64 m	83.9	7', 8', 13'	7', 8', 13', 14'	3α, 13a, 7'
7'	5.98 (dd, 3.1, 15.6)	139.2	6', 8'	6', 8', 9'	14'
8'	7.64 (dd, 11.5, 15.6)	126.0	7', 9'	6', 9', 10'	3', 5', 12'
9'	6.63 (t, 11.5)	143.8	8', 10'	7', 8', 11'	7'
10'	5.78 (d, 11.5)	117.4	9'	8', 11'	15, 8'
11'-CO	-	166.4	-	-	-
12'	1.07 (d, 6.9)	14.7	3'	2', 3', 4'	7'
13'	3.58 Ovlp	70.7	6', 14'	6', 7', 14'	2, 15
14'	1.18 (d, 6.2)	18.2	6', 13'	6', 13'	13, 14, 15, 2', 5', 8'
2'-OH	2.95 (dd, 2.2, 6,9)	-	2'	1', 2', 3'	13'

[a] The assignments were based on DEPT, ^{1}H-^{1}H COSY, HSQC, and HMBC experiments, and recorded in $CDCl_3$.

The stereochemistry at C2' and C3' was assigned as *S* and *R* respectively based on the comparison of the ^{1}H and ^{13}C chemical shifts with published data for Roridin A. In addition, the remaining stereochemistry at C6' and C13' was determined by employing diagnostic ^{1}H NMR parameters summarized in (**Table 37**)[158]. Unfortunately, the multiplicity of H-13' was not clear (overlapped with another signal) in both $CDCl_3$ and MeOD-d_4, however, the coupling constant of H-6′/H-7′ (^{3}J H-6′, ^{3}J H-7′ = 3.1 Hz). Moreover, the carbon chemical shift difference between C-7′ and C-8′ ($\Delta\delta$ C-7′/C-8′ = 13.2 ppm) pointed out that the configuration of C6' was *R*. The stereochemistry of C13' was indirectly assigned as *R* after comparison with the next isolated compound Isororidin A (**58**) for which we confirmed its relative configuration by Xray crystallography. The obtained ^{1}H, ^{13}C NMR and mass spectral data were found to be identical with the published data for roridin A[278].

Table 37: Diagnostic 1D NMR parameters to define the absolute configuration of C6' and C13'

H-13'multiplicity	^{3}J 6',7'(in Hz)	^{13}C $\Delta\delta$ 7',8'	Configuration
quintet	3.0	11.7	6' R, 13' R
dq	7.8	2.9	6' S, 13' R
qd	3.2	10.9	6' R, 13' S
five-line multiplet	3.0	11.5	6' R, 13' R
five-line multiplet	6.0	4.2	6' S, 13' S
eight-line multiplet	6.0	3.7	6' S, 13' R

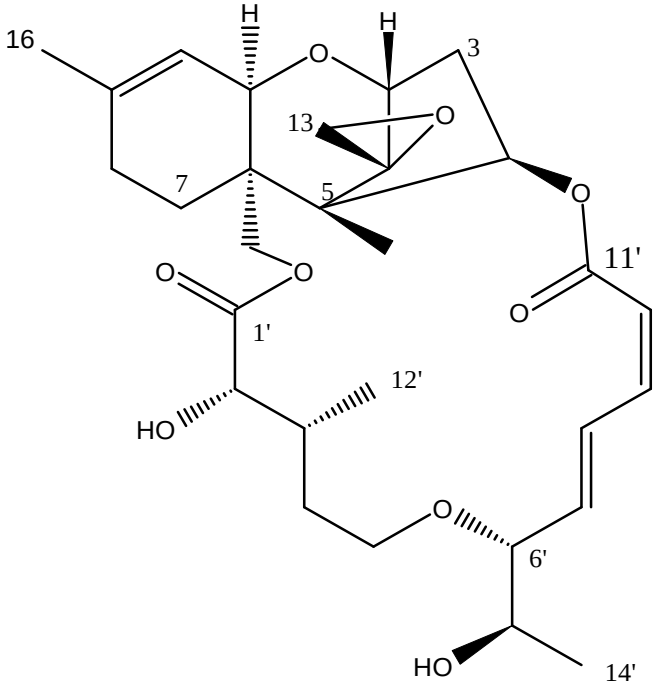

57

5.2.1.2 Isororidin A

Compound (**58**) was isolated as colourless crystals (19.5 mg). It displayed (+) HR-ESIMS showed a molecular ion peak at *m/z* 571.2312 $[M+K]^+$ (calculated for $C_{29}H_{40}O_9$, 571.2304) indicated that it had 10 degrees of unsaturation.

The ^{1}H NMR data in (MeOD-d_4) (**Table 38**) of (**58**) revealed four methyls at [δ_H 0.81 (3H, s, H-14), 1.09 (3H, d, J = 6.8 Hz, H-12'), 1.16 (3H, d, J = 6.4 Hz, H-14′), 1.72 (3H, s, H-16)], oxygenated methylenes and methines at δ_H 3.30−5.60 ppm, and five olefinic protons [δ_H 4.04 (1H, d, J = 4.0 Hz, H-2′), 5.76 (1H, d, J = 11.2 Hz, H-10′), 6.17 (1H, dd, J = 15.4, 3.0 Hz, H-7′), 6.75 (1H, t, J = 11.4 Hz, H-9′), 7.60 (1H, ddt, J = 15.4, 11.4, 1.1 Hz, H-8′)]. In conjunction with the HSQC data, the 28 carbon signals in its ^{13}C NMR spectrum were attributed to four methyls at (δ_C 8.0, 15.1, 18.4, and 23.3), seven methylenes at (δ_C 21.3, 28.7, 34.9, 35.7, 48.5, 64.8, and 70.9), 12 methines at (δ_C 37.7, 68.5, 71.0, 76.0, 76.7, 80.4, 84.6, 117.9, 119.7, 126.8 142.3, and 145.5), and six uncharacterized carbons at (δ_C 45.0, 50.5, 66.4, 141.7, 168.1, and 175.6). Subsequently, detailed examination of ^{1}H and ^{13}C NMR data estimated that the structure of (**58**) was a macrocyclic trichothecene analogue similar to roridin A (**57**).

A further study of the ^{1}H−^{1}H COSY and HMBC data (**Table 38**) led to the establishment of the gross structure of (**58**) and by comparing the spectroscopic values of (**58**) with those of roridin A (**57**) in (MeOD-d_4) (**Appendix 68Appendix 69**), where minor ambivalences were observed. The high shift of C-13' at 71.0 ppm instead of 68.5 in roridin A, supposed the epimerization at C-13'.

The relative configuration of (**58**) was revealed based on the coupling constant of geminal and vicinal protons and NOESY analysis. In sesquiterpenoid moiety, the NOESY correlations of H-11/H-4, and H-11/H-3α demonstrated that these groups were co-facial, while H-2, H-13, and CH_3-14 were speculated to be co-facial but oriented in the opposite direction according to the NOE signals of H-2/H-3β, H-2/H-13β, and CH_3-14/H-7β. The ^{1}H chemical shifts of H2', H3', and H312'were almost identical with those of Roridin A, thus we defined the stereochemistry at C2' and C3' as *S* and *R* respectively. Additionally, the coupling constants between H9'-H10' ($^3J_{9',10'}$ = 11.4 Hz) and H7'-H8' ($^3J_{7',8'}$ = 15.4 Hz) proposed the *Z*/*E* geometry for $\Delta^{9'}$ and $\Delta^{7'}$ respectively The remaining stereochemistry at C6' and C13' could not be directly confirmed by NOESY analysis nevertheless, it was proposed to be (C6' *R*, C13' *S*) due to the NOESY correlations between both H-6' and H-13' with H-7', H-8' and H-14'.

Finally, the absolute configuration was confirmed by X-ray crystallographic analysis of the colourless needle-like crystals obtained from slow evaporation of (ether/$CHCl_3$ in the atmosphere of hexane) solution (**Figure 47**)

Table 38: ^{1}H and ^{13}C NMR data for Isororidin A (**58**) (400 and 100 MHz, δ ppm)[a]

Position	^{1}HNMR (*J* in Hz)	^{13}CNMR	COSY	HMBC	NOESY
2	3.74 (d, 5.1)	80.4	3, 4	4, 5, 12	3*β*, 13b, 3'
3	α 2.47 (dd, 8.2, 15.2)	35.7	2, 4	2, 5, 12	4
	β 2.14 (br t, 4.5)			2, 4	2
4	5.84 (dd, 4.5, 8.2)	76.0	3	2, 3, 5, 6, 12, 11'	11
5	-	50.5	-	-	-
6	-	45.0	-	-	-
7	1.87 (dd, 8.0, 11.4)	21.3	8	6, 8, 9, 11	13, 14
8	1.93 (d, 8.0)	28.7	7	6, 7, 9, 10	
	1.98 m				
9	-	141.7	-	-	-
10	5.41 (d, 5.4)	119.7	11, 16	6, 8, 11, 16	
11	3.72 (br d, 5.4)	68.5	10	7, 10, 15	4
12	-	66.4	-	-	-
13	a 2.86 (d, 4.0)	48.5	-	2, 5, 12	14
	b 3.05 (d, 4.0)				
14	0.81 s	8.0	-	4, 5, 6, 12	2', 3', 15, 12'
15	a 4.32 (d, 12.2)	64.8	-	5, 6, 7, 1'	
	b 4.46 (d, 12.2)			5, 6, 7, 11, 1'	14
16	1.72 s	23.3	10	8, 9, 10	
1'-CO	-	175.6	-	-	-
2'	4.04 (d, 4.0)	76.7	3'	1', 4', 12'	14, 16, 3', 12'
3'	2.08 m	37.7	2', 12'	1', 2'	14, 2', 5', 8'
4'	1.58 m	34.9	3', 5'	3', 5', 12'	5', 8', 14'
	1.73 m			2', 3', 5'	
5'	3.50 (ddd, 5.2, 8.7, 9.1)	70.9	4'	3', 4', 6'	3', 8', 12'
	3.58 (ddd, 5.2,9.6, 9.8)				
6'	3.82 m	84.6	7', 8'	5', 7', 8', 14'	7', 8', 14'
7'	6.17 (dd, 3.0, 15.4)	142.3	6', 8'	6', 8', 9'	13', 14'
8'	7.60 (ddt, 11.4, 15.4, 1.1)	126.8	7', 9'	6', 9', 10'	14, 3', 10', 12'
9'	6.75 (t, 11.4)	145.5	8', 10'	7', 8', 11'	7'
10'	5.76 (d, 11.4)	117.9	9'	8', 9', 11'	14
11'-CO	-	168.1	-	-	-
12'	1.09 (d, 6.8)	15.1	3'	2', 3', 4'	14, 2', 3', 5'
13'	3.69 (dq, 6.4, 3.2)	71.0	14'	6', 14'	7', 8', 14'
14'	1.16 (d, 6.4)	18.4	6', 13'	6', 13'	6', 7', 8',13'

[a] The assignments were based on DEPT, ^{1}H-^{1}H COSY, HSQC, and HMBC experiments, and recorded in MeOD-d_4.

To the best of our knowledge Isororidin A was isolated before[279] but this the first time for detection of the absolute configuration of isororidin A by using X-ray analysis.

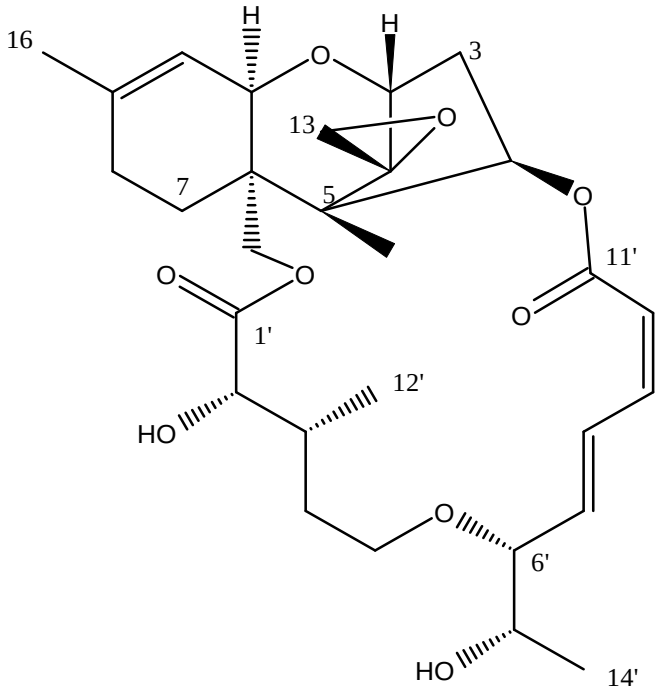

58

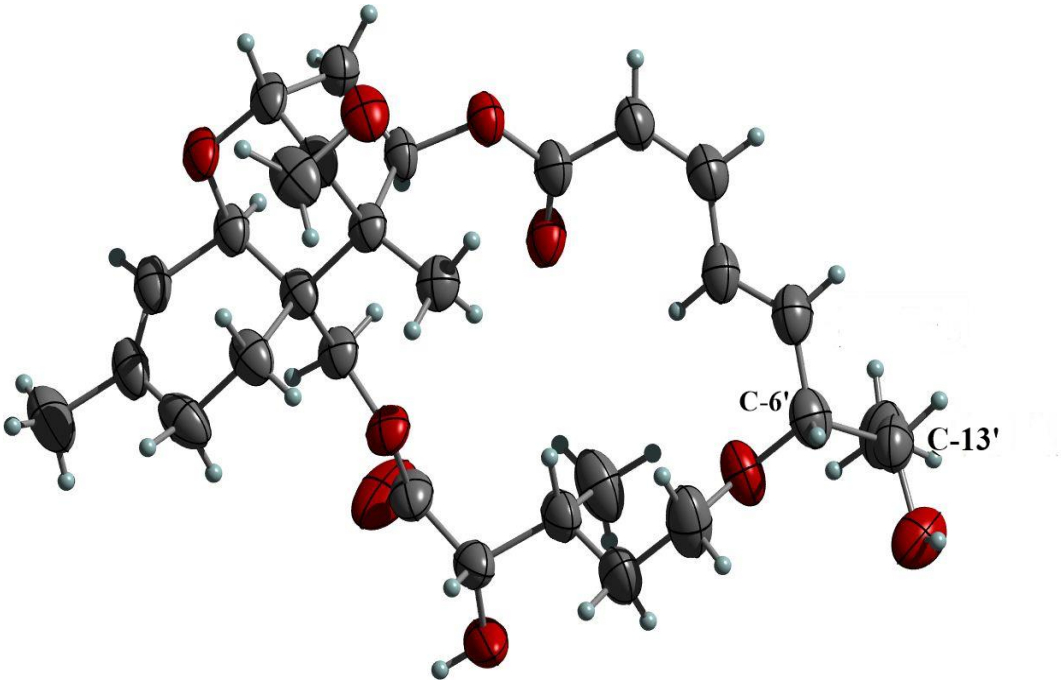

Figure 47: X-ray molecular structure of Isororidin A

5.2.1.3 Miophytocen D

Miophytocen D (**59**) was obtained as a white powder (1.2 mg) and had the molecular formula $C_{29}H_{40}O_9$ which deduced by the positive-ion mode HR-ESIMS data. showed a molecular ion peak at m/z 550.3019 $[M+NH_4]+$ (calcd. 550.3011)

The ^1H NMR data (**Table 39**) of (**59**) displayed four methyls [δ_H 1.01 (3H, s, H-14), 1.21 (3H, d, J = 6.5 Hz, H-14′), 1.24 (3H, s, H-16), 2.23 (3H, br d, J = 1.2 Hz, H-12′)], oxygenated methylenes and methines at δ_H 3.30−5.60 ppm, and five olefinic protons [δ_H 5.74 (1H, d, J = 11.0 Hz, H-10′), 5.87 (1H, dd, J = 15.5, 3.0 Hz, H-7′), 5.91 (1H, br d, J = 1.2, H-2′), 6.61 (1H, t, J = 11.0 Hz, H-9′) and 7.37 (1H, dd, J = 15.5, 11.0 Hz, H-8′)]. The ^{13}C NMR data, assigned by the aid of HSQC and HMBC spectra, afforded the resonances of four methyls (δ_C 10.0, 18.5, 19.6, and 28.0), seven methylenes (δ_C 28.1, 28.4, 30.9, 38.8, 41.2, 68.8 and 71.6), eleven methines (δ_C 44.2, 69.3, 70.3, 78.1, 80.7, 84.2, 118.1, 118.5, 128.1, 135.8, and 142.6) and seven uncharacterized carbons (δ_C 44.4, 51.6, 73.6, 78.6, 156.1, 165.1, and 166.8). Detailed investigation of ^1H and ^{13}C NMR data suggested that the structure of (**59**) was a macrocyclic trichothecene analogue.

The data of $^1H-^1H$ COSY and HMBC (**Table 39**) led to the establishment of substructure A and substructure B and by comparing the spectroscopic values of (**59**) with those of roridin A (**57**), where minor discrepancies were observed. The most distinctive feature of substructure B in (**59**) was the presence of olefinic proton at δ_H 5.91 (br d, J = 1.2 Hz, δ_C 118.1) instead of an oxymethine and the absence of the epoxide signals, commonly present in trichothecene analogues at C-12. Key HMBC correlations of H-13/C-2, C-5, C-6, C-9, and C-12 led to the assignment of a carbon−carbon linkage between C-10 and C-12 via the bridged methylene carbon C-13 [δ_H 1.43 (1H, dd, J = 14.7, 5.5 Hz, H-13a), and 1.62 (1H, dd, J = 14.0, 5.5 Hz, H-13b); δ_C 28.1] as shown in **Figure 48**.

The presence of an oxygenated carbon (δ_C 73.6) at C-9 was unambiguously established from HMBC correlations of H-8, H-13, and H-16 with C-9, moreover, the chemical shift of the methyl group C-12' (δ_C 19.6 ppm) and the influence on the protons in the vicinity of the C2'-C3' double bond supported the geometry of the $\Delta^{2'}$ to be (*E*). In the case of macrocyclic trichothecenes, the proton shifts, especially of H_2-15, H_2-4', and H_2-5', are strongly dependent on the geometry of the $\Delta^{2'}$ double bond[280].

Table 39: NMR spectroscopic data for miophytocen D (**59**) (400 and 100 MHz, δ ppm)[a]

Position	^{1}HNMR (*J* in Hz)	^{13}CNMR	COSY	HMBC
2	4.02 (d, 4.2)	80.7	3, 4	4, 5, 11, 13
3	2.00, m 2.33 (dd, 8.4, 15.7)	38.8	2, 4	4 2.5, 12
4	5.81 (dd, 2.7, 8.4)	78.1	3	2, 5, 6, 12, 11'
5	-	44.4	-	-
6	-	51.6	-	-
7	2.15 m 1.94 m	28.4	8	6, 8, 11 15
8	1.76 (dd, 4.9, 14.4) 1.37 (dd, 4.9, 14.4)	30.9	7	6, 9, 10
9	-	73.6	-	-
10	2.17, m	44.2	11, 16	6, 8, 11, 16
11	3.63 (d, 3.5)	69.3	10	6, 8, 11, 13 16
12	-	78.6	-	-
13	1.61 (dd, 5.5, 14.7) 1.43 (dd, 5.5, 14.0)	28.1	10	2, 5, 6, 9, 12
14	1.01 s	10.0	-	4, 5, 6, 12
15	3.70 (d, 11.7) 4.69 (d, 11.7)	71.6	-	5, 6, 7, 11, 1'
16	1.24 s	28.0	9, 10	7, 8, 9, 10
1'-CO	-	166.8	-	-
2'	5.91 (br d, 1.2)	118.1	-	1', 3', 4', 12'
3'	-	156.1	-	-
4'	2.44 m 2.52 m	41.2	5', 12'	3', 4', 12' 2', 3'
5'	3.61 ovlp 3.90 (ddd, 4.1, 8.5, 9.5)	68.8	4'	3', 4', 6'
6'	3.65 m	84.2	7',8', 13'	7', 8', 13', 14'
7'	5.87 (dd, 3.4, 15.6)	135.8	6', 8'	6', 8', 9'
8'	7.37 (dd, 11.0, 15.6)	128.1	7', 8'	6', 9', 10'
9'	6.63 (t, 11.0)	142.6	8', 9'	7', 8', 11'
10'	5.76 (d, 11.0)	118.5	9'	8', 11'
11'-CO	-	165.1	-	-
12'	2.23 (br d, 1.2)	19.6	-	2', 3', 4'
13'	3.64 Ovlp	70.3	6', 14'	6', 7', 14'
14'	1.21 (d, 6.9)	18.5	6', 13'	6', 13'

[a] The assignments were based on DEPT, ^{1}H-^{1}H COSY, HSQC, and HMBC experiments, and recorded in $CDCl_3$.

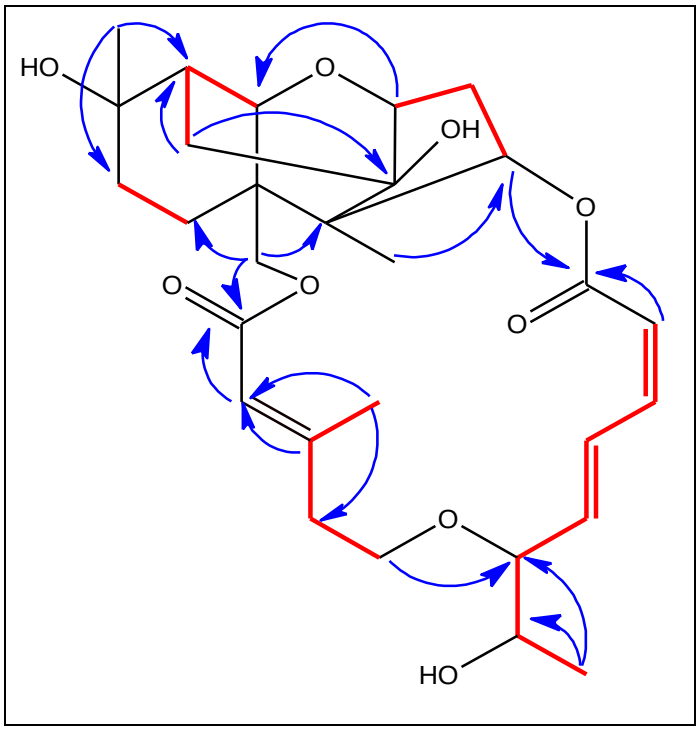

Figure 48: Key COSY (▬) and selected HMBC (→) correlations for miophytocin D (**59**)

The assignment of the relative configurations of the stereogenic centres of (**59**) was utilized based on the combined study of coupling constants of geminal and vicinal protons (**Table 39**), and by comparing the ^{1}H and ^{13}C chemical shifts of (**59**) with those of Roridin A (**57**), Isororidin A (**58**) (in $CDCl_3$) and Miophytocen subgroup of MTs isolated from the Brazilian plant *Baccharis coridifolia* in the 1980s [282].

Concerning the configuration of C6' and C13' of the macrocyclic ring, the C6' was assigned the *R* absolute configuration by measuring the $\Delta\delta_{C7'\text{-}C8'}$ (7.7 ppm) and the $^{3}J_{H6',H7'}$ (3.4 Hz). Because of the severe overlapping in the region 3.6-3.7 ppm in the ^{1}HNMR spectrum, we couldn't unambiguously assign the absolute configuration of C13'. Nevertheless, by inspecting the ^{13}C NMR of C6' and C-13' and C14' in the Roridin E complex of diastereomers[144] we observed a pattern of lower field chemical shifts for those carbons in the *threo* derivatives (C6'*R*/C13'*R* or C6'*S*/C13'*S*) in comparison with the respective carbons in the *erythro* derivatives (C6'*R*/C13'*S* or C6'*S*/C13'*R*) in the same solvent. The magnitude of the difference was in the range of 1-2 ppm. Based on this comparison we tentatively attributed the *R* configuration at C13'.

The geometries of two disubstituted double bonds from C-7′ to C-10′ were determined by coupling constants ($^{3}J_{7',8'}$ = 15.6 Hz; *E*-form, and $^{3}J_{9',10'}$ = 11.0 Hz; *Z*-form) of the olefinic protons.

A literature search with the discussed spectroscopic data and the molecular weight of (**59**) pointed to miophytocin D, which is reported once only during this study from the MeOH extract of a plate culture of the fungus *Podostromacornu-damae*, a deadly poisonous mushroom[281] therefore, this is the first isolation of miophytocin D from *Myrothecium verruacria*.

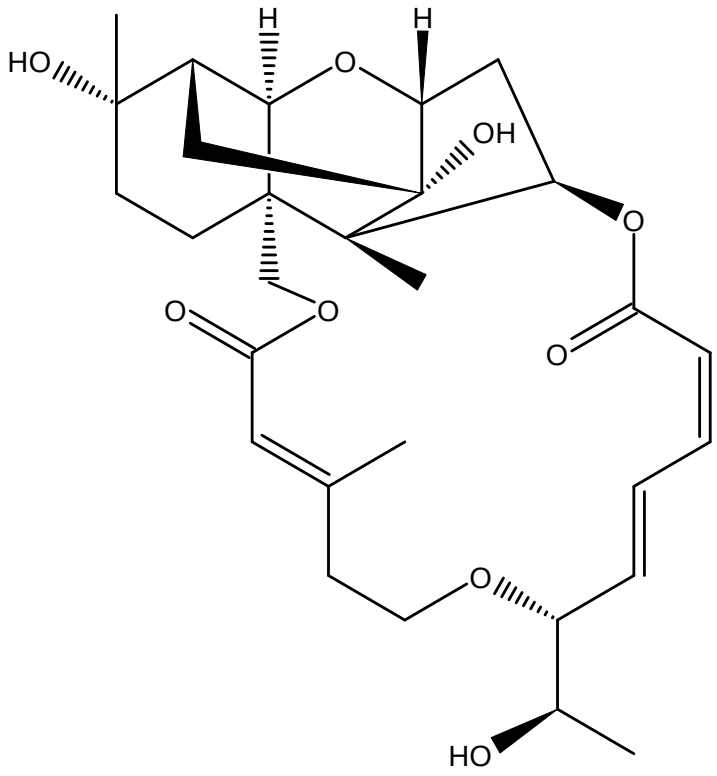

59

To the best of our knowledge, macrocyclic trichothecenes with the rearranged pentacyclic trichothecene core, miophytocens A−C and myrothecines A−C, have been reported,[158,282] and particularly, the absolute configurations of myrothecines A−C were elucidated by a combination of 1D and 2D NMR spectroscopic experiments, CD data, Mosher's esterification analysis, and single-crystal X-ray diffraction[283].

5.2.1.4 Miophytocen E

Miophytocen E (**60**) was isolated as a colourless solid (1.7 mg) and its (+)-HR-ESIMS *m/z* 568.3126 $[M+NH_4]^+$ (calculated for $C_{29}H_{42}O_{10}$; 568.3122) indicated that it had 9 degrees of unsaturation.

The ^{1}H NMR data in MeOD-d_4 (**Table 40**) of (**60**) showed four methyls [δ_H 1.06 (3H, s, H-14), 1.09 (3H, d, J = 6.7 Hz, H-12′), 1.12 (3H, d, J = 6.2 Hz, H-14'), 1.19 (3H, s, H-16)], oxygenated methylenes and methines at δ_H 3.30−5.60 ppm, and five olefinic protons [δ_H 4.24 (1H, d, J = 2.5, H-2′), 5.81 (1H, d, J = 11.2 Hz, H-10′), 6.06 (1H, dd, J = 15.8, 3.3 Hz, H-7′), 6.73 (1H, t, J = 11.2 Hz, H-9′), 7.66 ((1H, ddt, J = 15.8, 11.2, 1.2 Hz, H-8′)]. The ^{13}C NMR data (**Table 40**), revealed the resonances of four methyls (δ_C 10.3, 18.0, 18.5, and 27.3), seven methylenes (δc 28.1, 28.4, 31.3, 35.5, 40.2, 70.6, and 74.5), 12 methines (δ_C 36.2, 45.0, 70.9, 71.2, 75.5, 79.0, 81.8, 84.5, 118.5, 128.2, 138.7 and 143.4), and six quaternary carbons (δ_C 44.8, 51.8, 73.6, 77.7, 164.4, and 175.1).

Detailed check of ^{1}H and ^{13}C NMR data indicated that the structure of (**60**) was a macrocyclic trichothecene analogue. Most of the signals resembled those of miophytocin D (**59**), except for the presence of the two methines; one oxymethines at δ_H 4.24 (1H, d, J = 2.5 Hz; δ_C 75.5) and one tertiary aliphatic at δ_H 2.29 (1H, m; δ_C 36.2) instead of the olefinic proton at δ_H 5.91(1H, br d, J = 1.2 Hz; δ_C 118.1), showing the hydration of the C2'-C3' double bond in (**60**). The ^{1}H-^{1}H COSY and HMBC correlations (**Figure 49**) of the oxymethine proton at C-2′ (δ_C 75.5) indicated the occurrence of the cleavage. Additionally, the assignment of a carbon−carbon linkage between C-10 and C-12 via the bridged methylene carbon C-13 [δ_H 1.54 (1H, dd, J = 14.6, 5.5 Hz, H-13a), 1.85 (1H, m, H-13b), δ_C 29.6] was detected.

The relative configuration of (**60**) was elucidated based on the NOESY correlations and the coupling constant data of geminal and vicinal protons. In trichothecane core moiety, the NOESY correlations of H-4/H-3α and H-4/H-15a demonstrated that these groups were co-facial, while H-2, H-13, and CH_3-14 were speculated to be oriented in the opposite direction. Overall, the analysis of all the cross-peaks in the NOESY showed that the stereochemistry of the trichothecene moiety of (**60**) was similar to that of miophtocen D (**59**) based on the same spectroscopic values and the aspect of common biosynthetic origin. The geometries of two disubstituted double bonds from C-7′ to C-10′ were determined by coupling constants (^3J 7′,8′ = 15.8

Hz; *E*-form, and ^{3}J 9′,10′ = 11.2 Hz; *Z*-form) of the olefinic protons as well as NOESY correlations of H-7′/H-9′.

Table 40: NMR spectroscopic data for miophytocen E (**60**) (400 and 100 MHz, δ ppm)[a]

Position	^{1}HNMR (*J* in Hz)	^{13}CNMR	COSY	HMBC	NOESY
2	3.94 (d, 4.1)	81.8	3, 4	3, 5, 11, 13	3*β*, 13b
3	α 2.19 (dd, 8.3, 15.1)	40.2	2, 4	2, 6, 12	4
	β 1.99 (dt, 4.0 15.1)			2, 5, 12	15β
4	5.64 (dd, 2.7, 8.3)	79	3	6, 12, 11'	3*α*, 15a
5	-	44.8	-	-	-
6	-	51.8	-	-	-
7	1.46 (br dd, 4.5, 14.5)	28.4	8	5, 6, 8, 15	11
	2.06 (br d, 4.5)			5, 9, 10	14
8	1.37 (dd, 4.5, 14.5)	31.3	7	9, 10	
	1.77 m			7	14, 2'
9	-	73.6	-	-	-
10	2.10, m	45.0	11, 13	5, 6, 8, 9	16
11	3.56 (d, 3.6)	71.2	10	5, 6, 9, 13, 16	7a, 10, 15
12	-	77.7	-	-	-
13	a 1.54 (dd, 5.5, 14.6)	28.1	10	2, 5, 6, 9, 12	14, 16
	b 1.85 m			2, 9, 12	2
14	1.06 s	10.3	-	5, 6, 12	2, 13a, 10'
15	a 4.52 (d, 11.7)	74.5	-	5, 6, 7, 11, 1'	4, 7, 11
	b 3.88 (d, 11.7)			6, 7, 1'	
16	1.19 s	27.3	10	8, 9, 10	7, 8, 13a
1'-CO	-	175.1	-	-	-
2'	4.24 (d, 2.5)	75.5	3'	1', 3', 12'	5', 8', 12'
3'	2.29 m	36.2	4', 12'	-	4, 5', 8'
4'	1.67 m	35.5	3', 5',		2', 14
	1.78 m		12'	12'	
5'	3.49 m	70.6	4'	3', 4', 6'	3', 6', 8'
	3.66 m				
6'	3.77 m	84.5	7', 13'	7', 8', 13'	15b, 7', 8', 14'
7'	6.06 (dd, 3.3, 15.8)	138.7	6', 8'	6', 9'	9', 12'
8'	7.66 (ddt, 11.2, 15.6, 1.2)	128.2	7', 9'	6', 9', 10'	14, 3', 5''
9'	6.73 (t, 11.2)	143.4	8', 10'	7', 11'	7'
10'	5.81 d (11.2)	118.5	9'	8', 11'	12'
11'-CO	-	164.4	-	-	-
12'	1.09 (d, 6.7)	18.5	3'	2', 4'	2', 5'
13'	3.71 (dq 3.3, 6.2)	70.9	6', 14'	6', 7', 14'	7', 14'
14'	1.12 (d, 6.2)	18.0	6', 13'	6', 13'	7'

[a] The assignments were based on DEPT, ^{1}H-^{1}H COSY, HSQC, and HMBC experiments, and recorded in MeOD-d_4.

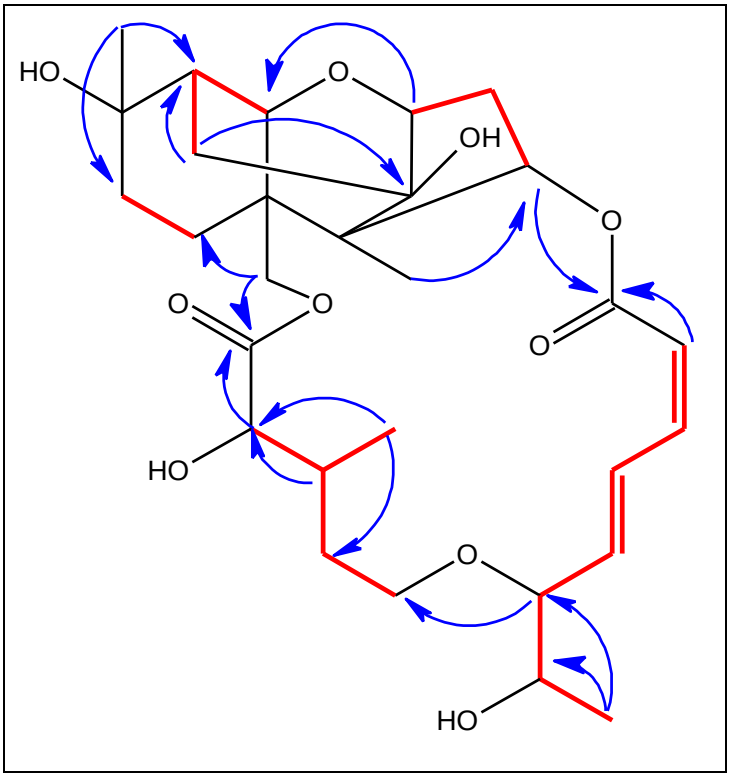

Figure 49: Key COSY (▬) and selected HMBC (→) correlations for miophytocen E (**60**)

Concerning the assignment of configuration at C2′ and C3′ of (**60**) we propose the retention of configuration as *S* and *R* respectively, as it occurs in the other isolated macrocyclic trichothecenes (Roridin A (**57**) /Isororidin A (**58**)) based on the observance of the same NOE correlation between H-2′ and H_3-12′ in all three compounds (in MeOD-d_4) and their common biosynthetic origins. The notable differences in the ^{1}HNMR and ^{13}CNMR for C2′, C3′, C12′ between (**57**), (**58**) and (**60**) are not only attributed to changes in the configuration on either of the C2′/C3′ but also changes of the conformation of the macrocyclic ring due to substitution of the usual 12-13 epoxide in (**57**), (**58**) with the C10-C13-C12 bridge in (**60**) (**Table 41**).

The coupling constant of H-6′/H-7′ ($^{3}J_{H6',H7'}$ = 3.3 Hz) and the carbon chemical shift difference between C-7′ and C-8′ ($\Delta\delta_{C\text{-}7'/C\text{-}8'}$ = 10.5 ppm) verified the *R* absolute configuration for C6′. In the ^{1}HNMR spectrum, we managed to discern the splitting pattern of H13' as a dq/8 line multiplet ($^{3}J_{H13',H14'}$ = 6.2 Hz, $^{3}J_{H13',H6'}$ = 3.3 Hz), revealing the absolute configurations of C-13′ as *S*. Thus compound (**60**) is a C6'*R*, C13'*S* (C6'/C13') *erythro* derivative like Isororidin A (**58**)) based on chemical shift trends described in (**Table 37**).

Table 41: Comparison of ^{13}CNMR data for (**57**), (**58**), (**59**) in MeOD-d_4

Position	Roridin A (57)	Isororidin A (58)	Miophytocen E (60)
2	80.4	80.4	81.8
3	35.7	35.7	40.2
4	76.0	76.0	79.0
5	50.5	50.5	44.8
6	45.0	45.0	51.8
7	21.3	21.3	28.4
8	28.7	28.7	31.3
9	141.7	141.7	73.6
10	119.6	119.7	45.0
11	70.8	68.5	71.2
12	66.4	66.4	77.7
13	48.4	48.5	28.1
14	8.0	8.0	10.3
15	64.8	64.8	74.5
16	23.3	23.3	27.3
1'-CO	175.6	175.6	175.1
2'	76.6	76.7	75.5
3'	37.6	37.7	36.2
4'	34.8	34.9	35.5
5'	70.5	70.9	70.6
6'	84.4	84.6	84.5
7'	141.3	142.3	138.7
8'	127.4	126.8	128.2
9'	145.3	145.5	143.4
10'	117.9	117.9	118.5
11'-CO	168.0	168.1	164.4
12'	15.0	15.1	18.5
13'	68.5	71.0	70.9
14'	18.3	18.4	18.0

According to the above-mentioned data (**60)** was identified as a new natural product with the name miophytocen E

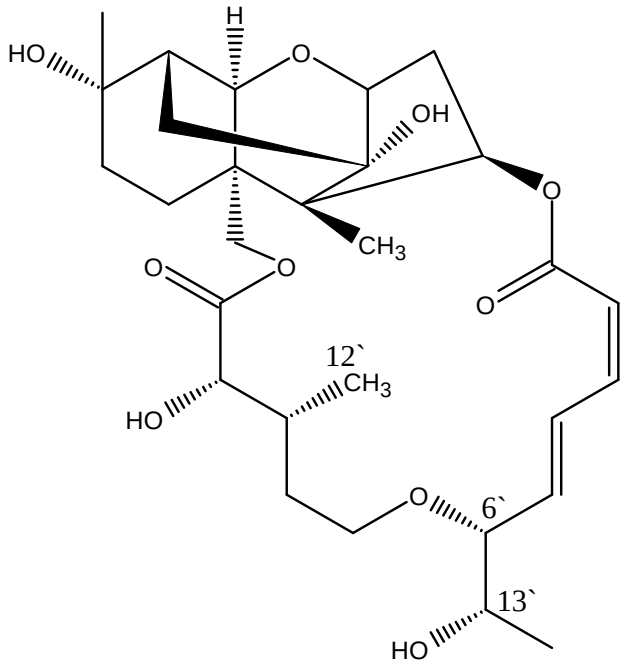

60

With regard to a plausible biosynthetic pathway, the π electrons of the $\Delta^{9/10}$ double bond in isororidin A (**58**), an expected biogenetic precursor, attack the C-13 of the epoxide as an electrophilic addition, and then a tertiary carbocation simultaneously occurs at C-9 (**Scheme 5**). Successively, this carbocation is stable by the substitution of a hydroxy group, which gives the rearranged pentacyclic trichothecene sesquiterpene moiety.

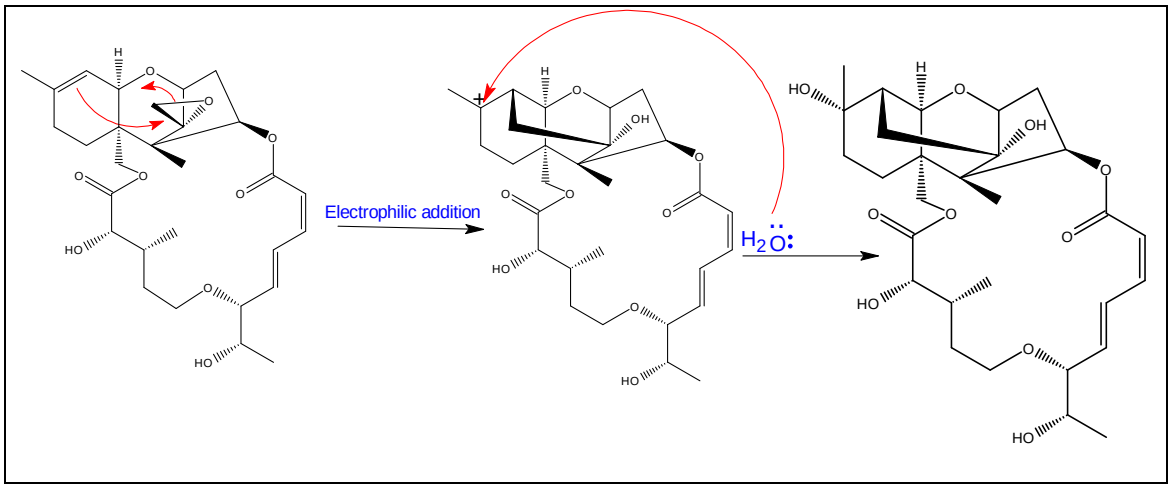

Scheme 5: Plausible biosynthetic pathway of miophytocen E (**60**)

5.2.1.5 Roridin J

Roridin J (**61**) was obtained as a white powder (4.8 mg) and had the molecular formula $C_{29}H_{36}O_9$ as deduced by the positive-ion mode HRESIMS data, $[M+NH_4]^+$ at *m/z* 546.2697 (calcd. 546.2690), required 12 degrees of unsaturation.

The ^{1}H NMR data (**Table 42**) displayed four methyls [δ_H 0.85 (3H, s, H-14), 1.37 (3H, d, *J* = 6.0 Hz, H-14′), 1.71 (3H, s, H-16), 2.27 (3H, d, *J* =1.2 Hz, H-12′)], oxygenated methylenes and methines at δ_H 2.80−5.60 ppm, and six olefinic protons [δ_H 5.44 (br d, *J* = 5.2 Hz, H-10), 5.76 (1H, br q, *J*= 1.2 Hz, H-2′), 5.79 (1H, d, *J* = 11.3 Hz, H-10′), 5.92 (1H, dd, *J*= 2.5, 15.4 Hz , H-7′), 6.65 (1H, t, *J* = 11.3 Hz, H-9′) and 7.65 (1H, dd, *J* = 15.4, 11.3 Hz, H-8′)]. The ^{13}C NMR with the aid of HSQC DEPT spectra, established the presence of four methyls, five methylenes, thirteen methines, as well as seven quaternary carbons atoms including two carbonyls. This gave altogether 29 carbons, pointing to a roridins type macrocyclic trichothecene structure.

The structure of (**61**) was further elucidated by analysis of 2D NMR data including the ^{1}H-^{1}H COSY and HMBC spectra. The ^{1}H-^{1}H COSY spectrum of (**61**) revealed connectivity of structural fragments: a (C-2 to C-4), b (C-7 to C-8), c (C-10 to C-11), d (C-4' to C-5') and e (C-13' to C-6' and C-14', C-6' to C-10'). To accommodate the molecular formula and the degree of unsaturation, the macrocyclic ring must close through a ring containing two oxygens. The downfield chemical shifts of C-6' and C-13' (δ_C 82.2, and 76.4) respectively, indicated each is oxygenated and the chemical shift of C-5' (δ_C 100.8) suggested it had two oxygen substituents. Therefore, there was a secondary cyclization inside the macrocyclic ring, which contained an acetal system.

The aforementioned data along with the acetal signal at (δ_H 5.53, dd, *J* = 8.3, 3.0 Hz; δ_C 100.8) made it clear that compound (**61)** closely resembled roridin H[144], except for the following differences. The presence of the doublet signal at [δ_H 3.83(1H, d, *J* = 7.0 Hz; δ_C 79.7)] attributed for oxygenated methine instead of the methylene at (δ_H 2.64, 2H, d; δ_C 47.7 in roridin H), moreover the downfield of the acetal carbon C-5' chemical shift from (δ_C 100.8 in roridin H) to (δ_C 103.3 in (**61**)), as well as the upfield of H-5' from (δ_H 5.58 in roridin H) to (δ_H 5.25, d, *J* = 7.0 Hz in (**61**)). This observation was confirmed by the ^{1}H-^{1}H COSY correlation between H-4' and H-5' and the Key HMBC cross-peaks of H-4'/C-2', C-3', C-5', and C-12', and between H-5'/C-4' and C-13' (**Figure 50**).

Table 42: NMR spectroscopic data for roridin J (**61**) (400 and 100 MHz, δ ppm)[a]

Position	^{1}HNMR (*J* in Hz)	^{13}CNMR	COSY	HMBC	ROESY
2	3.84 (d, 5.2)	79.1	3, 4	4, 5, 11, 12	3*β*, 13b, 2'
3	α 2.47 (dd, 8.4, 15.4) β 2.18 (br dd, 4.6, 15.4)	34.7	2, 4	2, 4 2, 5, 12	11
4	5.89 (dd, 4.6, 8.4)	73.8	3	2, 6, 7, 12, 11'	11, 15*α*
5	-	49.1	-	-	-
6	-	43.1	-	-	-
7	1.87 m	20.3	8	6, 8, 9, 11, 15	13, 14
8	2.00 m	27.6	7	6, 7, 9, 10	14, 15
9	-	140.5	-	-	-
10	5.44 (br d, 5.2)	118.6	11, 16	6, 8, 11, 16	11, 16
11	3.63 (d, 5.2)	67.8	10, 16	7, 9, 10, 15	3*α*, 4, 4'
12	-	65.5	-	-	-
13	a 2.82 (d, 4.0) b 3.12 (d, 4.0)	47.9	-	2, 5, 12	7, 8, 14 2, 7, 14
14	0.85 s	7.3	-	4, 5, 6, 12	4, 7, 13, 15, 2'
15	a 4.01 (d, 12.5) b 4.40 (d, 12.5)	63.4	-	5, 6, 7, 11, 1'	7, 8
16	1.71 s	23.3	10, 11	8, 9, 10	2'
1'-CO	-	166.2	-	-	-
2'	5.76 (br q, 1.2)	119.9	12'	1', 2', 3', 4'	14
3'	-	155.3	-	-	-
4'	3.83 (d, 7.0)	79.7	5'	2', 3', 5', 12'	2'
5'	5.25 (d, 7.0)	103.3	4'	4', 13'	6', 12', 14'
6'	4.08 (dt, 2.8, 8.8)	82.2	7', 13'	7', 8', 13', 14'	5', 7', 14'
7'	5.92 (dd, 2.5, 15.4)	134.5	6', 8'	6', 8', 9'	14'
8'	7.65 (br dd, 11.3, 15.4)	126.0	7', 9'	6', 9', 10'	2'
9'	6.65 (t, 11.3)	143.1	8', 10'	7', 11'	7'
10'	5.79 d (11.3)	118.6	9'	8', 11'	14, 4'
11'-CO	-	165.9	-	-	-
12'	2.27 (d, 1.2)	13.0	2'	1', 2', 3', 4'	2', 5'
13'	3.65 ovlp.	76.4	6', 14'	6', 7'	4'
14'	1.37 d (6.0)	15.9	6', 13'	6', 13'	5',6', 7'

[a] The assignments were based on DEPT, ^{1}H-^{1}H COSY, HSQC, and HMBC experiments, and recorded in $CDCl_3$.

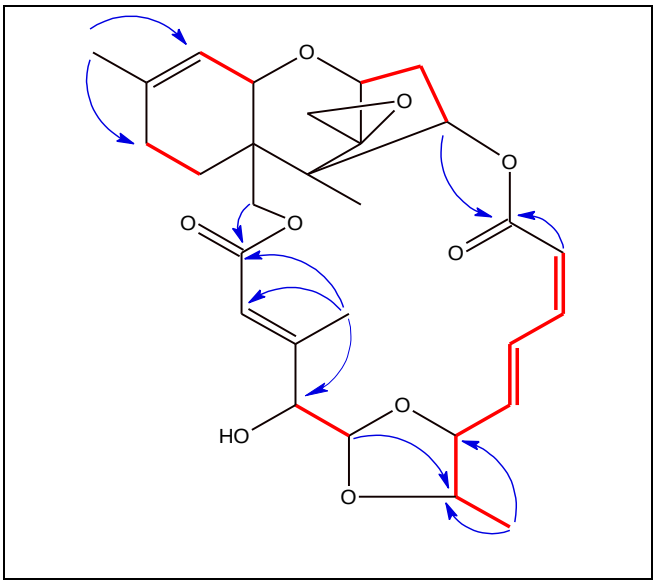

Figure 50: Key COSY (▬) and selected HMBC (→) correlations for roridin J (**61**).

The chemical shift of the methyl group C-12' (δ_C 13.0 ppm) supported the configuration at C-2' to be *E* form by taking account of the steric compression effect due to the C-1' carbonyl group[284]. Finally, the configuration of the C-4' was detected to be *R* based on the ROESY correlation between H-4 and H-2' (**Table 42**). The structure was further confirmed by comparison of ^{1}H, ^{13}C NMR and mass spectral data with the published data for roridin J[285].

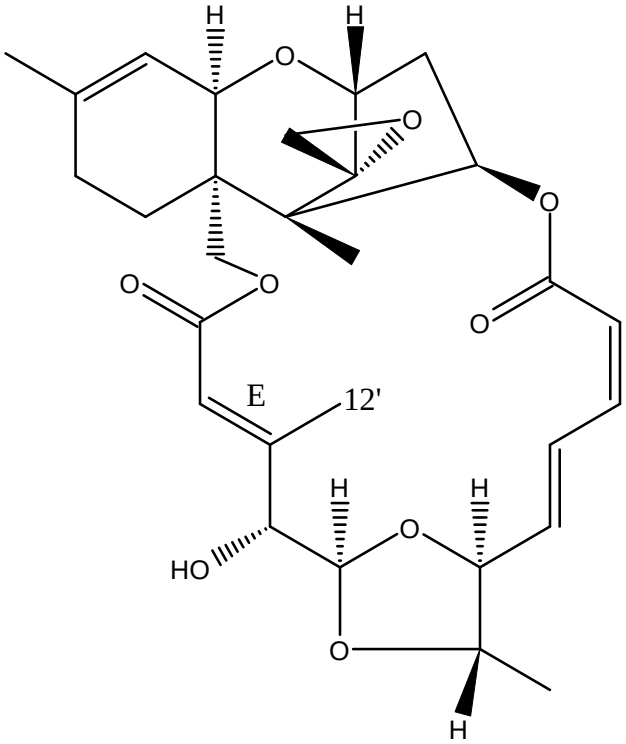

61

5.2.1.6 8*α*-Hydroxyroridin H

8*α*-Hydroxyroridin H (**62**) was obtained as a white solid (1.2 mg) and had the molecular formula $C_{29}H_{36}O_9$ deduced by the positive-ion mode HR-ESIMS data, $[M+NH_4]^+$ at *m/z* 546.2710 (calcd. for $C_{29}H_{40}NO_9$, 546.2703), suggesting 12 degrees of unsaturation.

The ^{1}H NMR data (**Table 43**) displayed four methyls [δ_H 0.88 (3H, s, H-14), 1.34 (3H, d, *J* = 6.1 Hz, H-14′), 1.86 (3H, s, H-16), 2.27 (3H, s, H-12′)], oxygenated methylenes and methines at 3.30−5.60 ppm, and five olefinic protons [δ_H 5.80 (1H, d, *J* = 11.4 Hz, H-10′), 5.95 (1H, overlap., H-7′), 5.70 (1H, br s, H-2′), , 6.56 (1H, t, *J* = 11.4 Hz, H-9′) and 7.70 (1H, dd, *J* = 15.5, 11.4 Hz, H-8′)]. The ^{13}C NMR data assigned by the aid of HSQC DEPT and HMBC spectra, afforded the resonances of four methyls, five methylenes, thirteen methines as well as seven uncharacterized carbons consist of two carbonyls. The structure of (**62**) was further elucidated by analysis of 2D NMR data including the ^{1}H-^{1}H COSY and HMBC spectra. The ^{1}H-^{1}H COSY spectrum of (**62**) revealed connectivity of structural fragments: a (C-2 to C-4), b (C-7 to C-8), c (C-10 to C-11), d (C-4' to C-5') and e (C-13' to C-6' and C-14', C-6' to C-10').

Detailed inspection of ^{1}H and ^{13}C NMR data speculated that the structure of (**62**) was a macrocyclic trichothecene analogue quite similar to those of roridin J (**61**), especially the existence of the acetal signal at (δ_H 5.53, dd, *J* = 3.0, 8.3 Hz, δ_C 100.8). However, the crucial differences between compound (**62**) and roridin J (**61**) were the chemical shift of C-8 at δ_C 66.8 which showed a significant downfield shift than that of roridin J (**61**) at δ_C 27.6, suggesting the presence of a hydroxyl group at C-8. Moreover, instead of the oxygenated methine H-4' at (δ_H 3.83; δ_C 79.7), two methylene protons at [δ_H 2.26 (br dd, *J* = 12.9, 6.8 Hz) and 2.63 (dd, *J* = 12.9, 3.0 Hz); δ_C 47.4] were observed.

In the HMBC spectrum (**Figure 51**), H-8 (δ_H 4.12, br d, *J* = 5.3 Hz) showed long-range correlations with the carbon signals of C-6, C-9 and C-10, which supported the presence of a hydroxyl group at C-8. The configuration of the hydroxyl group at C-8 was assigned as *α* according to the bibliography. The introduction of a hydroxyl group at C-8 (either *α* or *β*) causes a downfield shift in the H_3-16 vinyl methyl resonance in the ^{1}H NMR spectrum of ca. 0.2 ppm. The C-16 carbon - in the sesquiterpene core of the MTs - resonance in the ^{13}C NMR spectra shifts upfield by ca. 2-3 ppm in the C-8 *α*-hydroxyl derivatives and upfield by ca. 4-5 ppm in the C-8 *β*-hydroxyl derivatives.[286, 287].

Table 43: NMR spectroscopic data for (**62**) (400 and 100 MHz, δ ppm)[a]

Position	^{1}HNMR (*J* in Hz)	^{13}CNMR	COSY	HMBC
2	3.82 (d, 5.2)	79.0	3	4, 5, 11
3	2.16 (dd, 4.9, 9.6)	34.9	2, 4	2, 4, 12
	2.50 (dd, 8.3, 15.4)			2, 5, 12
4	5.93 ovlp	73.3	3	2, 5, 6, 12, 11'
5	-	49.1	-	-
6	-	42.5	-	-
7	2.08 (br d, 14.7)	29.5	8	6, 8, 9, 11, 15
	2.19 (dd, 5.3, 9.8)			
8	4.12 (br d, 5.3)	66.8	7	6, 9, 10
9	-	139.8	-	-
10	5.56 (d, 5.2)	121.0	11, 16	6, 11, 16
11	3.76 (d, 5.2)	67.4	10	6, 7, 9, 10, 15
12	-	65.4	-	-
13	2.84 (d, 4.0)	47.9	-	2, 5, 12
	3.13 (d, 4.0)			
14	0.88 s	7.1	-	4, 5, 6, 12
15	4.40 s	64.9	-	5, 6, 7, 11, 1'
16	1.86 s	20.5	8, 10	9, 10, 11
1'-CO	-	166.1		
2'	5.70 br s	119.0	12'	1', 3', 4', 12'
3'	-	154.9	-	-
4'	2.26 (br dd, 6.8, 12.9)	47.4	5', 12'	2', 3', 5', 12'
	2.63 (dd, 3.0, 12.9)			
5'	5.53 (dd, 3.0, 8.3)	100.8	4'	3', 4', 13'
6'	4.06 (br dt, 2.4, 8.5)	81.9	7', 13'	8', 13'
7'	5.95 ovlap	134.9	6', 8'	6', 8', 9'
8'	7.70 (dd, 11.4, 15.5)	126.1	7', 9'	6', 7'
9'	6.56 (t, 11.4)	142.9	8', 10'	7', 8',11'
10'	5.80 (d, 11.4)	118.4	9'	8', 11'
11'-CO	-	166.1	-	-
12'	2.27 s	18.3	2', 4'	1', 2', 3', 4'
13'	3.66 (dq, 6.1, 8.5)	76.6	6', 14'	7'
14'	1.34 (d, 6.1)	16.3	6', 13'	6', 13'

[a] The assignments were based on DEPT, ^{1}H-^{1}H COSY, HSQC, and HMBC experiments, and recorded in $CDCl_3$.

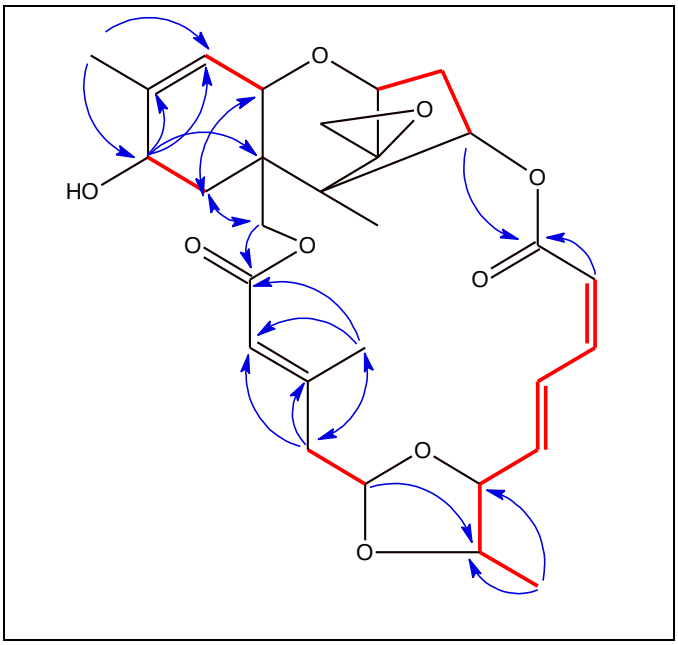

Figure 51: Key COSY (▬) and selected HMBC (→) correlations for (**62**)

Concerning the stereochemistry, the relative configuration of (**62**) was deduced to be the same as roridin J (**61**) based on the $^{1}H/^{13}C$ chemical shifts, the coupling constants of geminal and vicinal protons and the aspect of common biosynthetic origin. The chemical shift of the methyl group C-12' (δ_C 18.3 ppm) supported the configuration at C-2' to be of *E* form.

Carefully comparison of NMR data with those of relative compounds in the literature (**Table 44**) supported that compound (**62**) was isolated and elucidated before with the name of 8α-Hydroxyroridin H[140].

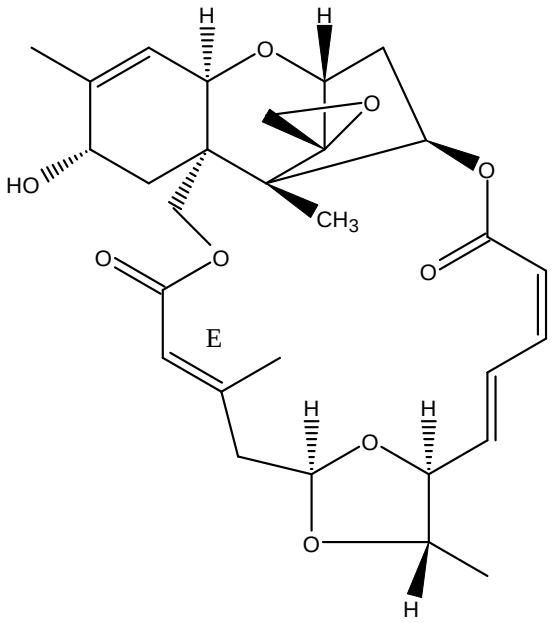

62

5.2.1.7 8*α*-Acetoxyroridin H

8*α*-Acetoxyroridin H (**63**) was obtained as a white solid (2.9 mg) and its molecular weight indicated as $C_{31}H_{38}O_{10}$ based on (+) HR-ESIMS at *m*/*z* 571.2550 $[M+H]^+$ calcd. 571.2543). According to the molecular formula of $C_{31}H_{38}O_{10}$, compound (**63**) must contain 13 degrees of unsaturation. The presence of 5 methyls, 5 methylenes, 13 methines, 5 quaternary carbons, and 3 ester carbonyls were deduced from a combination of 1D and 2D NMR experiments.

Additionally, six spin systems were identified from ^{1}H-^{1}H COSY experiment as shown in (**Figure 52**), moreover, long-range HMBC correlations were used to establish the connectivities of the various spin systems of the compound. A macrocyclic lactone ring is formed through ester linkages at C-4 and C-15 of the trichothecane ring system, also the ester linkage at C-15 is supported by the correlation of the C-15 methylene protons to C-1' and the downfield chemical shift of C-15 (δ_C 64.9). The correlations of H-2' to C-1' and C-3' and the correlations of the C-12' methyl protons to both C-2' and C-3' along with the carbon chemical shifts of C-2' and C-3' (δ_C 118.8 and 155.4 ppm respectively) indicate the presence of an *α, β*-unsaturated ester with a methyl group off the *β*-position.

Further investigation of NMR data speculated that the structure of (**63**) was a macrocyclic trichothecene analogue resembled those of 8*α*-hydroxyroridin H (**62**), except for the presence of the acetoxy group at C-8 instead of the hydroxyl group. This observation was confirmed by the downfield chemical shift of both C-8 at (δ_H 5.18, br d, J = 5.0 Hz, δ_C 68.8) and C-10 (δ_H 5.69 d, J = 5.5 Hz, δ_C, 124.1) as well as the HMBC correlations of H-8 and the H_3-18 at (δ_H 1.75 s, δ_C 20.5) to CO-17(δ_C 171.0). The stereochemistry at C-8 was assigned as *α* according to the former evidences discussed in 8*α*-Hydroxyroridin H (**62**). Based on the detailed spectroscopic data 8*α*-Acetoxyroridin H (**63**) was identified and this conclusion was further confirmed by comparison with the literature.[288]

It should be noted that the first isolation of this compound from *Myrothecium sp.* was done by Melissa M. Wagenaar and Jon Clardy in 2001 and detected again in 2002 from the cultured mycelia of *Calcarisporium arbuscula* Preuss by Hai-Yan Lu team and named by mistake as a new compound calcarisporin B1[289].

Table 44: Comparison of ^{1}H and ^{13}C NMR data for (**62**), (**63**) and roridin H

	8*α*-Acetoxyroridin H (63)[a]		**8*α*-Hydroxyroridin H (62)[a]**		**roridin H[b]**
Position	^{1}HNMR (*J* in Hz)	^{13}CNMR	^{1}HNMR (J in Hz)	^{13}CNMR	^{13}CNMR
2	3.83 (d, 5.0)	79.1	3.82 (d, 5.2)	79.0	79.0
3	2.19 (dd, 4.6, 8.5) 2.47 (dd, 8.3, 15.4)	34.7	2.16 (dd, 4.9, 9.6) 2.50 (dd, 8.3, 15.4)	34.9	34.8
4	5.90 (dd, 4.6, 8.4)	73.5	5.93 ovlp	73.3	74.0
5	-	49.1	-	49.1	48.9
6	-	42.5	-	42.5	43.2
7	2.15 (br d, 5.0) 2.17 (dd, 5.0, 9.8)	26.5	2.08 (br d, 14.7) 2.19 (dd, 5.3, 9.8)	29.5	20.5
8	5.18 (br d, 5.0)	68.8	4.12 (br d, 5.3)	66.8	27.6
9	-	139.8	-	139.8	139.9
10	5.69 (d, 5.5)	124.1	5.56 (d, 5.2)	121.0	118.6
11	3.75 (d, 5.5)	67.3	3.76 (d, 5.2)	67.4	67.6
12	-	65.4	-	65.4	65.3
13	2.83 (d, 4.0) 3.10 (d, 4.0)	48.0	2.84 (d, 4.0) 3.13 (d, 4.0)	47.9	47.3
14	0.83 s	7.1	0.88 s	7.1	7.0
15	4.40 (d, 12.2) 4.36 (d, 12.2)	64.9	4.40 s	64.9	63.0
16	1.92 s	21.0	1.86 s	20.5	22.9
17-CO	-	171.1	-	-	-
18	1.75 s	20.5	-	-	-
1'-CO	-	166.1	-	166.1	166.0
2'	5.53 br s	118.8	5.70 br s	119.0	119.0
3'	-	154.9	-	154.9	154.4
4'	2.24 (br dd, 3.9, 12.5) 2.64 (dd, 3.0, 12.5)	47.7	2.26 (br dd, 6.8, 12.9) 2.63 (dd, 3.0, 12.9)	47.4	47.7
5'	5.52 (dd, 3.4, 8.6)	100.9	5.53 (dd, 3.0, 8.3)	100.8	100.8
6'	4.07 (br dt, 2.5, 8.6)	82.0	4.06 (br dt, 2.4, 8.5)	81.9	81.9
7'	5.94 (2.5, 15.5)	135.0	5.95 ovlap	134.9	134.6
8'	7.65 (dd, 11.3, 15.5)	126.1	7.70 (dd, 11.4, 15.5)	126.1	126.2
9'	6.56 (t, 11.3)	143.3	6.56 (t, 11.4)	142.9	142.5
10'	5.79 (d, 11.3)	118.4	5.80 (d, 11.4)	118.4	118.9
11'-CO	-	166.1	-	166.1	166.0
12'	2.27 s	18.2	2.27 s	18.3	18.2
13'	3.67 (qd, 6.0, 8.5)	76.6	3.66 (dq, 6.1, 8.5)	76.6	76.8
14'	1.34 (d, 6.1)	16.5	1.34 (d, 6.1)	16.3	16.3

[a] The assignments were based on DEPT, ^{1}H-^{1}H COSY, HSQC, and HMBC experiments, and recorded in$CDCl_3$. (400 and 100 MHz, δ ppm)
[b] signals detected by C. Tamm[278]

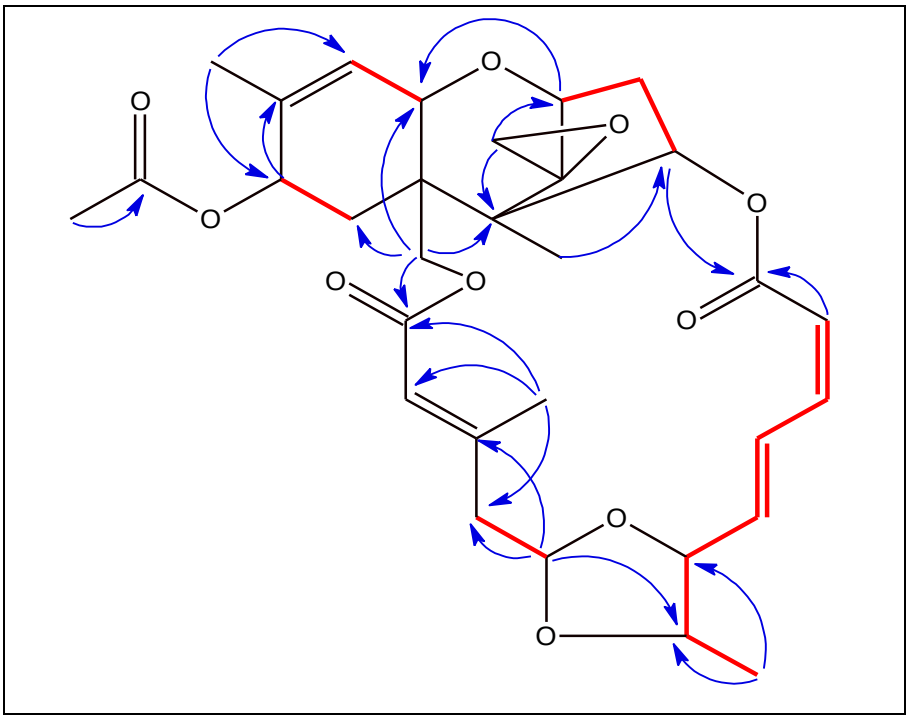

Figure 52: Selected key COSY (▬) and HMBC (→) correlations for (**63**)

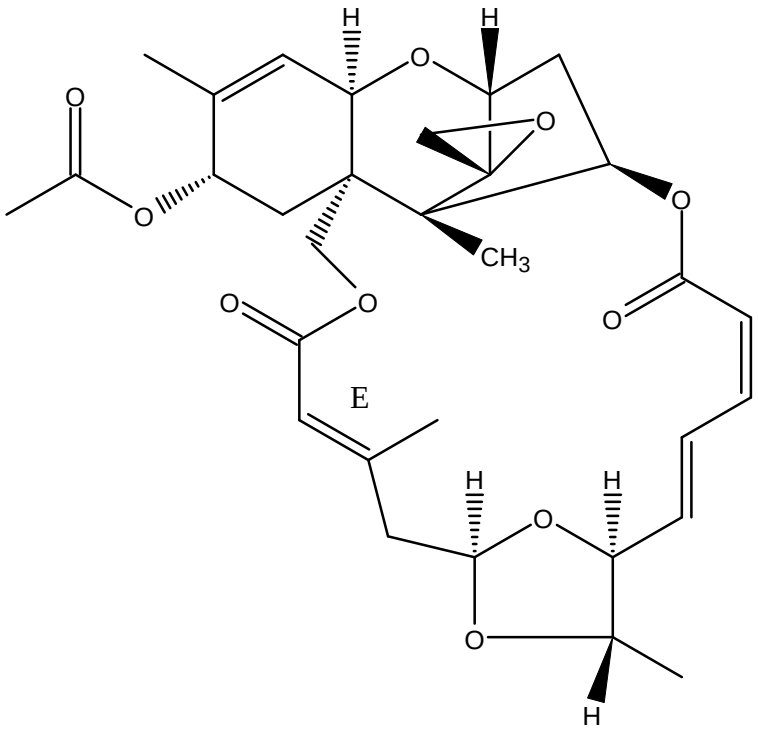

63

5.2.1.8 Miophytocen F

Compound (**64**) was obtained as a white powder (3.2 mg). The HR-ESI-MS exhibited a strong peak at *m/z* 564.2803[M+NH_4]$^+$ indicating a molecular formula of $C_{29}H_{38}O_{10}$, (calcd. 564.2792) with 10 degrees of unsaturation.

The ^{1}H NMR spectrum (**Table 45**) exhibited four methyl signals at [δ_H 1.06 (3H, s, H-14), 1.24 (3H, s, H-16), 1.39 (3H, d, *J* = 6.0 Hz, H-14′), and 2.29 (3H, d, *J* =1.2 Hz, H-12′)], oxygenated methylenes and methines at δ_H 3.55−5.72 ppm, and five olefinic protons [δ_H 5.76 (1H, d, *J* = 10.9 Hz, H-10′), 5.96 (1H, dd, *J* = 2.4, 15.4 Hz , H-7′), 5.91 (1H, br q, *J* = 1.2 Hz, H-2′), , 6.64 (1H, t, *J* = 11.2 Hz, H-9′) and 7.97 (1H, dd, *J* = 15.4, 11.2 Hz, H-8′)]. The ^{13}C NMR and HSQC DEPT spectra revealed the presence of four methyls, five methylenes, thirteen methines as well as seven quaternary carbons atoms consist of two carbonyls. All the aforementioned evidence characterized compound (**64**) as a macrocyclic trichothecene.

The structure of (**64**) was further elucidated by analysis of 2D NMR including the ^{1}H-^{1}H COSY, and HMBC spectra. The ^{1}H-^{1}H COSY spectrum of revealed connectivity of structural fragments: a (C-2 to C-4), b (C-7 to C-8), c (C-10 to C-13), d (C-4' to C-5') and e (C-13' to C-6' and C-14', C-6' to C-10').

Comparison of the NMR data of (**64**) with those of roridin J (**61**) showed that the major change occurred in the sesquiterpene core of the molecule. The characteristic methylene protons of the 12-13 epoxide were missing, as well as, in the A-ring the signals of the double bond at C9-C10 in roridin J (**61**) were replaced by a quaternary oxygenated carbon C-9 (δ_C 73.6) and an adjacent sp^3 methine C-10 (δ_H 2.18, m, δ_C 44.3). Therefore, the oxymethylene signals of C-13 was replaced by an sp^3 methylene (δ_H 1.55, 1H, dd, *J* = 5.5, 14.9 Hz, and 1.89, 1H, br d, *J*= 5.5Hz, δ_C 28.1). The ^{1}H-^{1}H COSY showed the cross-peaks of H-11/H-10/H-13 and the HMBC exhibited the correlation of H-13 with C-2, C-5, C-9, C-10 and C-12 (**Figure 53**). The aforementioned data suggested the connectivity of C11-C10-C13, indicating that (**64**) possessed the same A, B and C rings as miophytocen D (**59**).

Table 45: NMR spectroscopic data for miophytocen F (**64**) (400 and 100 MHz)[a]

Position	^{1}HNMR (*J* in Hz)	^{13}CNMR	COSY	HMBC	NOESY
2	4.00 (d, 3.9)	80.7	3, 4	4, 5, 11	3*β*, 12'
3	*α* 2.30 (dd, 8.8, 13.1) β 1.91 (br dd, 3.6, 5.5)	38.7	2, 4	2, 4, 5, 6, 12 2, 5, 12	4 2
4	5.74 (dd, 3.2, 8.5)	77.9	3	2, 5, 6, 12, 11'	11
5	-	51.2	-	-	-
6	-	44.2	-	-	-
7	2.16 Ovlp. 1.94 (d, 4.4)	28.4	8	6, 8, 9, 11	14, 16
8	1.77 (dd, 4.9, 14.4) 1.36 (dd, 4.9, 14.4)	31.3	7	6,7, 9, 10	14
9	-	73.6	-	-	-
10	2.18, m	44.3	11, 13	6, 7, 8, 9, 11, 15	14
11	3.62 (d, 3.5)	69.2	10	6, 8, 11, 13 16	13a, 15a
12	-	78.1	-	-	-
13	a 1.55 (dd, 5.5, 14.9) b 1.89 (br d, 5.5)	28.1	10	2, 5, 6, 9, 12	11 14, 16
14	1.06 s	10.2	-	4, 5, 6, 12	3', 15, 8', 12'
15	a 4.69 (d, 11.7) b 3.62 (d, 11.7)	71.6	-	5, 6, 7, 11, 1'	10, 14, 12'
16	1.24 s	28.0	10	8, 9, 10	7, 8, 2', 13b
1'-CO	-	165.8	-	-	-
2'	5.91 (br q, 1.2)	121.7	12'	1', 3', 4', 12'	14, 4', 10'
3'	-	153.6	-	-	-
4'	3.81 (d, 7.6)	79.1	5'	2', 3', 5', 12'	2'
5'	5.35 (d, 7.6)	103.8	4'	3', 4', 6'	6', 12'
6'	4.14 (dt, 2.4, 8.6)	82.4	7', 13'	8', 13', 14'	5', 7', 14'
7'	5.96 (dd, 2.4, 15.4)	134.2	6', 8'	6', 8', 9'	9', 14'
8'	7.97 (br ddq, 1.0, 11.2, 15.4)	126.9	7', 9'	6', 9', 10'	4'
9'	6.64 (t, 11.2)	142.9	8', 10'	7', 11'	7'
10'	5.76 d (10.9)	118.4	9'	8', 11'	14
11'-CO	-	165.2	-	-	-
12'	2.29 (d, 1.2)	12.6	2'	1', 2', 3', 4'	2, 3*β*, 2', 5'
13'	3.70 m	76.5	6', 14'	7'	7', 14'
14'	1.39 d (6.0)	15.9	6', 13'	6', 13'	6', 7'

[a] The assignments were based on DEPT, ^{1}H-^{1}H COSY, HSQC, and HMBC experiments, and recorded in $CDCl_3$

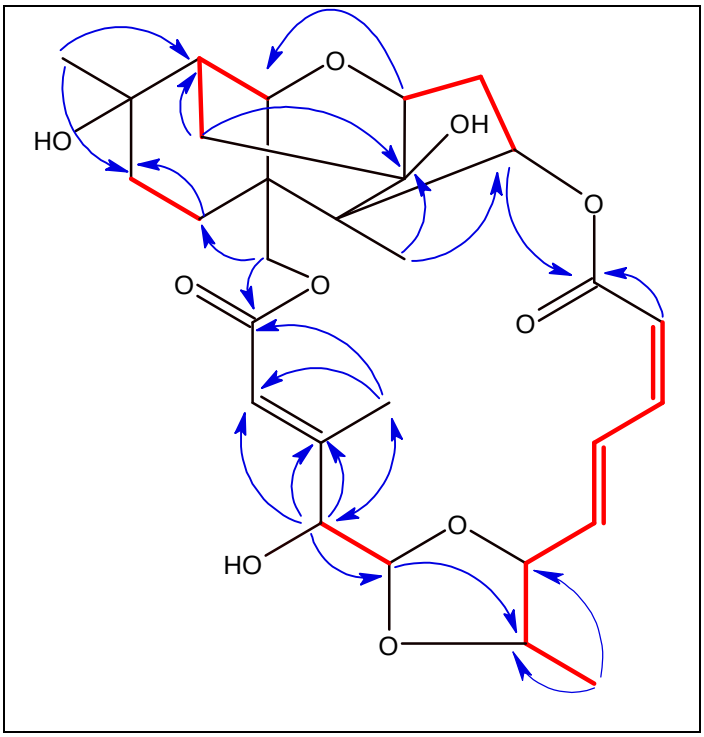

Figure 53: Key COSY (▬) and selected HMBC (→) correlations for (**64**).

The relative configuration of (**64**) was deduced based on the NOESY data and coupling constants of geminal and vicinal protons (**Table 45**). Moreover, the stereochemistry of the trichothecene moiety of (**64**) was similar to that of miophtocen D (**59**) based on the following characters and the aspect of common biosynthetic origin. The correlation of H-15α to H-11 suggested the presence of the cis-fused A/B ring system. The NOE correlation of H-4 with H-15a and H-11 indicated that they took the α configuration. In addition, the correlations of CH_3-14 with H-7b, H-13b, and of H-2 with H-13b suggested that all these protons were on the opposite side with the β orientation. The low-field chemical shift of the methyl group C-12' (δ_C 12.6 ppm) supported the configuration at C-2' to be *E* form. 9α-OH orientation was determined based on the cross peak between CH_3-16 and H-7b.

Besides that, the configuration of C6' and C13' was further determined to be both *S* by the NOESY correlation of H-6' with H-5' and 14'-CH_3 which revealed that H-5', H-6' and 14'-CH_3 were on the same face. The similarity of the NMR data for (**64)** with roridin J (**61**), provided additional proofs for the aforementioned assignment of the relative configuration.

The structure of compound (**64**) was then established as a new compound with the name of miophytocen F.

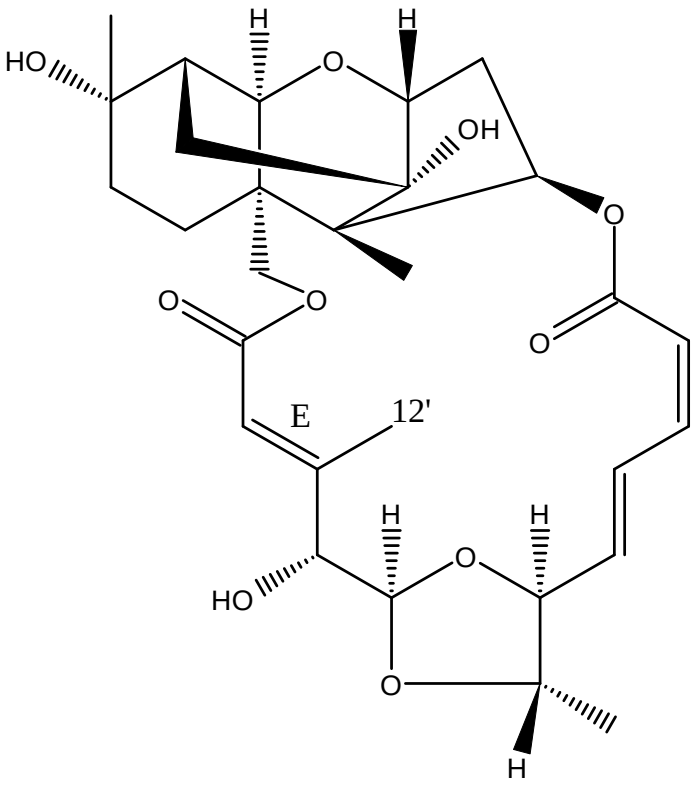

64

To the best of our knowledge, this is the first example of (roridin H-type) macrocyclic trichothecenes with the rearranged pentacyclic trichothecene core, however, a plausible biosynthetic pathway was proposed starting from roridin J (**61**) as in **Scheme 6**.

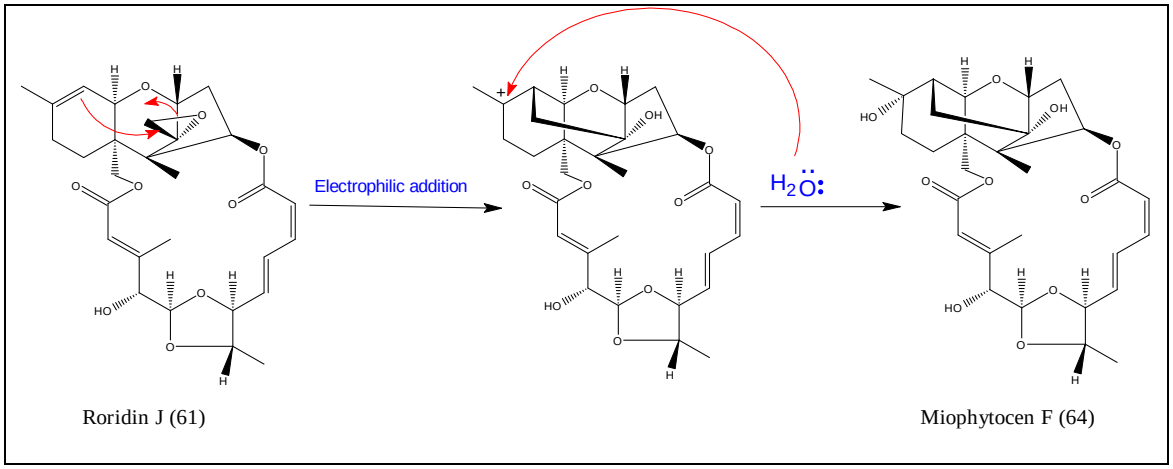

Scheme 6: Plausible biosynthetic pathway of miophytocen F (**64**)

5.2.1.9 Miophytocen G

Compound (**65**) was isolated as a colourless amorphous solid (0.5 mg) and its (+)-HR-ESIMS at *m/z* 564.2812 $[M+NH_4]^+$ indicating a molecular formula of $C_{29}H_{38}O_{10}$, (calcd for 564.2809).

The ^1H and ^{13}C NMR spectrum of (**65**) (**Table 46**) exhibited a high similarity in its pattern to miophytocen F (**64**), it displayed the same trichothecane moiety attached with the macrocyclic and acetal rings. However, the sole differences between (**65**) and (**64**) were the chemical shift of C-8 at δ_C 66.8 which showed a significant downfield shift than that of (**64**) at δ_C 31.3, suggesting a hydroxyl substitution at C-8. This observation was conducted over ^1H-^1H COSY connectivity between H-8 and H_2-7, between H_2-4' and H-5'. Further confirmation was done via HMBC correlation of H_2-7/C-8 and of H_3-16 C-8 (**Figure 54**). Additionally, the absence of the hydroxyl at C-4' was proposed due to the presence of methylene protons at [δ_H 2.32 (1H, br dd, J = 8.1, 4.3 Hz) and 2.58 (1H, br d, J = 13.5 Hz); δ_C 47.7]

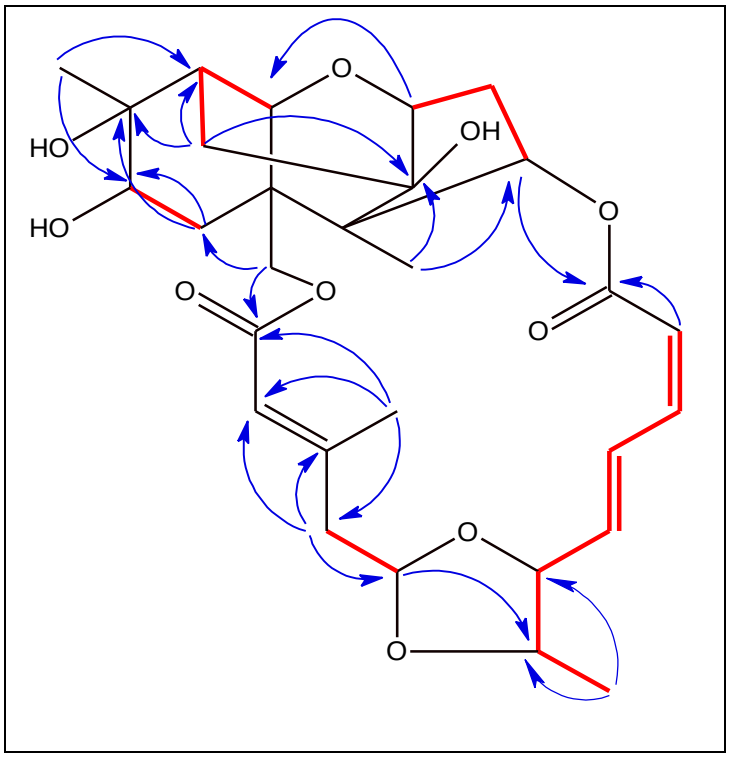

Figure 54: Key COSY (▬) and selected HMBC (→) correlations for (**65**).

Table 46: NMR spectroscopic data for miophytocen G (**65**) (600 and 150 MHz, δ ppm)[a]

Position	^{1}HNMR (*J* in Hz)	^{13}CNMR	COSY	HMBC	NOESY
2	4.00 (d, 4.0)	80.2	3	3, 4, 5	3β, 7', 12'
3	α 2.30 (dd, 8.3, 15.1) β 1.93 (t, 3.7)	38.3	2, 4	2, 4, 5, 6 2, 4, 5, 12	13' 4
4	5.75 (dd, 2.8, 8.3)	77.2	3	5, 12, 11'	3α, 15a
5	-	50.6	-	-	-
6	-	45.9	-	-	-
7	1.37 ovlp 2.40 (br dd, 4.5, 14.5)	37.1	8	5, 6, 8, 9	13b, 14
8	3.86 (dd, 5.4, 11.3)	68.1	7	-	13b, 14, 16
9	-	73.6	-	-	-
10	2.36, m	43.6	11, 13	7, 9	15, 16
11	3.67 (d, 5.2)	67.9	10	2, 7, 13	14', 15a
12	-	77.7	-	-	-
13	a 1.95 m b 1.51 (dd, 5.9, 14.6)	26.3	10	 2, 6, 9, 10, 12	2, 2' 8
14	1.10 s	10.1	-	5, 6, 12	8, 2'
15	a 4.56 (d, 11.7) b 3.66 (d, 11.7)	71.1	-	5, 6, 7, 1' 6, 7	12' 2
16	1.29 s	23.1	-	8, 9, 10	8, 10, 14
1'-CO	-	165.7	-	-	-
2'	5.75ovlp	118.2	4'	4', 12'	12, 9'
3'	-	153.4	-	-	-
4'	2.32 (br dd, 4.3, 8.1) 2.58 (br d, 13.5)	47.7	5'	2', 3', 5', 12' 2', 5'	
5'	5.66 (dd, 2.9, 9.4)	101.1	4'	4'	6'
6'	4.11 (dt, 2.3, 8.3)	81.7	7', 13'	8, 13', 14'	5', 7', 14'
7'	5.99 (dd, 2.5, 15.3)	134.7	6', 8'	6', 9'	13', 14'
8'	7.98 (br dd, 11.2, 15.3)	126.2	7', 9'	-	6', 13'
9'	6.65 (t, 11.2)	142.6	8', 10'	7', 11'	7'
10'	5.76 ovlp	118.2	9'	8', 11'	14, 15b
11'-CO	-	164.8	-	-	-
12'	2.30 s	16.8	2', 4'	1', 2', 3', 4', 5'	2
13'	3.73 m	76.1	6', 14'	-	12', 7'
14'	1.36 (d, 6.0)	16.0	13'	6', 13'	6', 7'

[a] The assignments were based on DEPT, ^{1}H-^{1}H COSY, HSQC, and HMBC experiments, and recorded in $CDCl_3$.

Based on the NOESY data (**Table 46**) and coupling constants of geminal and vicinal protons, the relative configuration of (**65**) was deduced to be the same as (**64**). The stereochemistry at C-8 was assigned as *α* according to the observed NOESY correlations between H-8/H_3-14 and the former evidence which discussed in 8*α*-Hydroxyroridin H (**62**). Besides that, the NOESY correlation of H-6' with H-5' and 14'-CH_3 which revealed that H-5', H-6' and 14'-CH_3 were on the same face indicated the configuration (C-6'*S*, C-13'*S*) of C-6' and C-13'

All the above-mentioned data characterized compound (**65**) as a new macrocyclic trichothecene which we named miophytocen G.

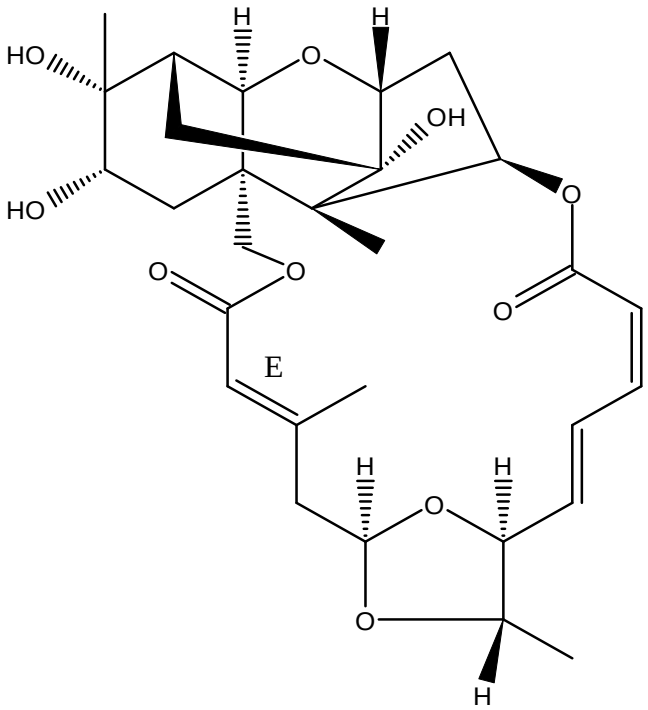

65

With regard to a plausible biosynthetic pathway, the expected biogenetic precursor is 8-*α*-Hydroxyroridin H (**62**) and the proposed plausible biosynthetic pathway in **Scheme 7**.

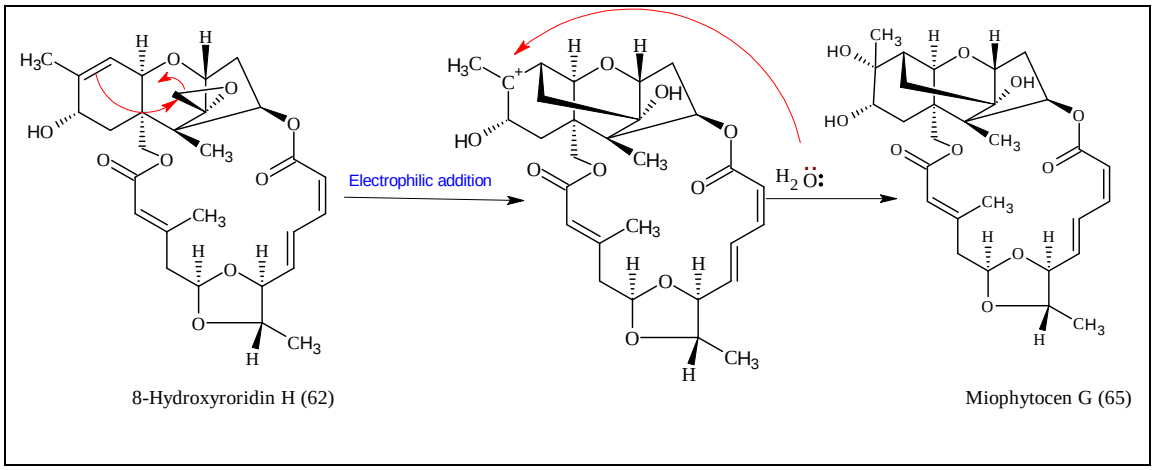

Scheme 7: Plausible biosynthetic pathway of miophytocen G (**65**)

5.2.1.10 Verrucarin A

Verrucarin A (**66**) was isolated as white solid (1.6 mg), its molecular formula was determined to be $C_{27}H_{34}O_9$ by HR-ESIMS at *m/z* 503.2290 $[M+H]^+$ (calcd. 503.2281) indicating 11 degrees of unsaturation.

^{1}H NMR and HSQC experiments (**Table 47**) revealed the presence of five vinylic protons, congruent with three double bonds, and three aliphatic methyl groups. The ^{1}H NMR data also highlighted seven methylene and one methine protons, along with twelve protons on carbons adjacent to an oxygen. Splitting patterns of olefinic protons at [δ_H (8.05, 1H, ddd, J = 1.0, 11.3, 15.6 Hz), (6.67, 1H, t, J = 11.3 Hz), (6.15, 1H, d, J =11.3 Hz), and (6.05, 1H, d, J = 15.6 Hz)] suggested the presence of a muconic acid moiety.

^{13}C NMR data showed the existence of 27 carbons, inclusive of three carbonyl, six vinylic, eight oxygenated, and ten aliphatic carbons. The DEPT edited HSQC experiment noted 14 diastereotopic protons, which resembled the structure of verrucarins and indicated a macrocyclic trichothecene. ^{1}H-^{1}H COSY correlations were used to confirm a macrocyclic trichothecene core (**Figure 55**), and in doing so, COSY correlations confirmed the connectivity through the spin systems of H-2′ to H-3′ to H_2-4′ to H_2-5′ and of H-3′ to H_3-12′.

The configuration of (**66**) was elucidated by the analysis of coupling constants and ^{1}H chemical shifts and by considering its biosynthesis. The obtained ^{1}H, ^{13}C NMR and mass spectral data were found to be identical with the published data for verrucarin A. [278,290].

Table 47: ^{1}H, ^{13}C NMR and COSY data for verrucarin A (**66**) (400 and 100 MHz, δ ppm)[a]

Position	^{1}HNMR (*J* in Hz)	^{13}CNMR	COSY
2	3.86 (d, 5.1)	78.9	3
3	2.22 (dt, 4.1, 15.4) 2.48 (dd, 8.1, 15.4)	34.9	2, 4
4	5.81 (dd, 4.1, 8.1)	75.5	3
5	-	49.5	-
6	-	44.2	-
7	1.70 ovlp 1.90 ovlp	20.0	8
8	1.93 ovlp	27.5	7
9	-	141.2	-
10	5.43 (d, 5.1)	117.9	11, 16
11	3.57 (d, 5.1)	66.9	10, 16
12	-	65.2	-
13	2.80 (d, 4.0) 3.12 (d, 4.0)	47.8	-
14	0.85 s	7.3	-
15	4.21 (d, 12.2) 4.80 (d, 12.2)	63.5	-
16	1.75 s	23.3	10
1'-CO	-	174.7	-
2'	4.14 br s	74.2	2'-OH
3'	2.36 m	33.2	2', 12'
4'	1.79 ovlp 1.94 ovlp	32.2	5'
5'	3.98 m 4.51 m	61.1	4'
6'-CO	-	165.5	-
7'	6.05 (d, 15.6)	127.5	8'
8'	8.05 (ddd, 1.0, 11.3, 15.6)	138.8	7', 9'
9'	6.67 (t, 11.3)	138.9	8', 10'
10'	6.15 (d, 11.3)	125.8	9'
11'	-	166.1	-
12'	0.88 (d, 6.8)	14.7	3'
2'-OH	2.66 br s	-	2'

[a] The assignments were based on DEPT, ^{1}H-^{1}H COSY, HSQC, and HMBC experiments, and recorded in $CDCl_3$

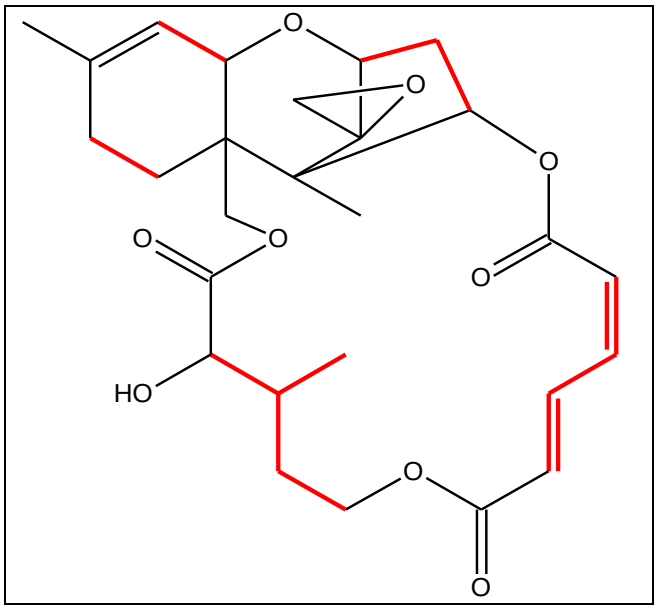

Figure 55: ^{1}H-^{1}H COSY (▬) correlations of verrucarin A (**66**).

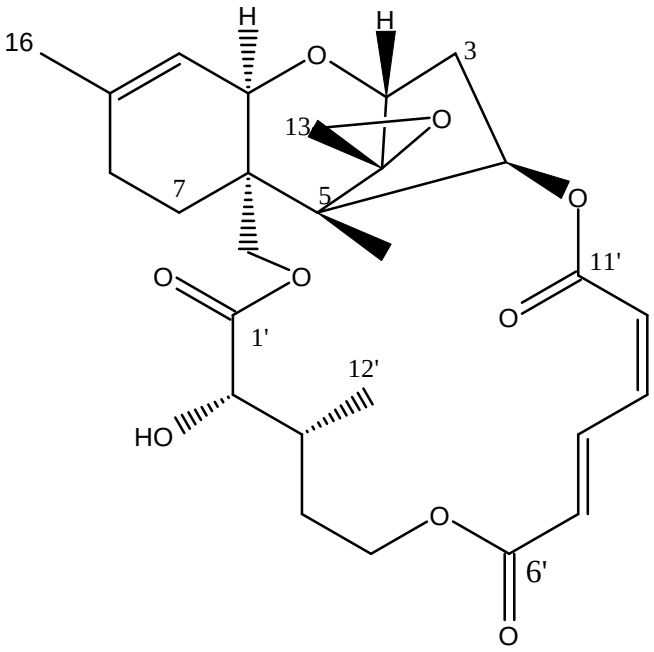

66

Verrucarin A (**66**) was the first macrocyclic trichothecene discovered from *Myrothecium verrucaria*, its structure was firstly elucidated by chemical degradation and confirmed by X-ray crystallography, which also established the absolute configuration[137]. It was reported that roridin A (**57**) may be the precursor of the respective verrucarin A (**66**) because the C-2 side chain at C-6' of roridins might be cleaved by oxidation to form verrucarins[279].

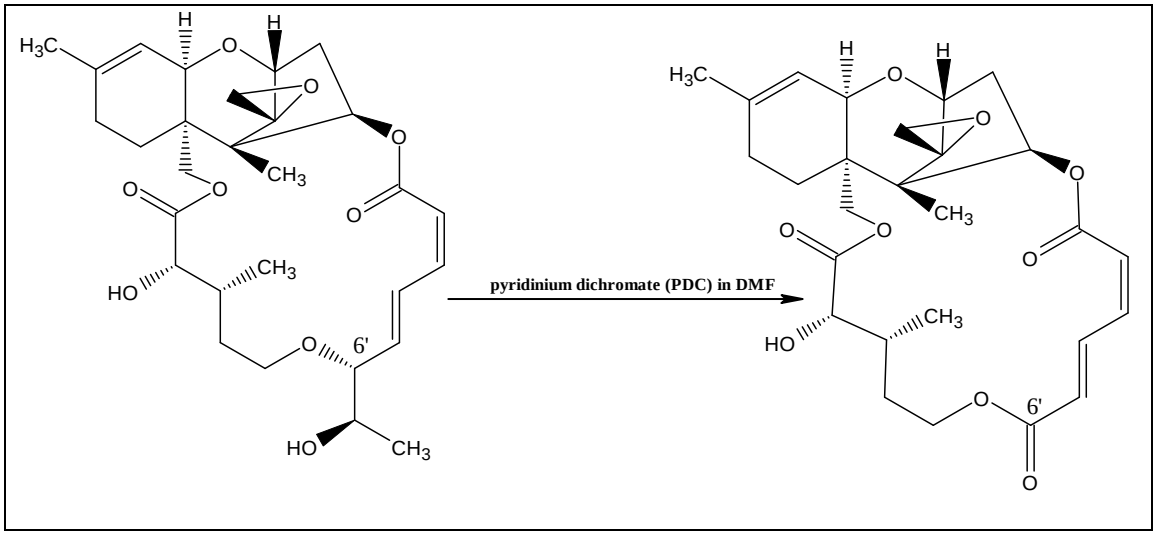

Scheme 8: Oxidation of roridin A (**57**) to verrucarin A (**66**) using PDC in DMF.

5.2.1.11 Roridin G

Roridin G (**67**) was obtained as white solid (0.8 mg), it had the molecular formula $C_{30}H_{44}O_{10}$ from the positive-ion mode HR-ESIMS at *m/z* 565.3021 $[M+H]^+$ (calcd. 565.3013).

The ^{1}H NMR data (**Table 48**) of (**67**) displayed five methyls [δ_H 0.86 (3H, s, H-14), 0.88 (3H, d, *J* = 6.9 Hz, H-12′), 1.12 (3H, d, *J* = 6.4 Hz, H-14′), 1.71 (3H, s, H-16), and 3.74 (3H, s,11'-OMe)], oxygenated methylenes and methines at δ_H 3.30−5.60 ppm, and five olefinic protons [δ_H 4.16 (1H, br d, *J* = 3.3 Hz, H-2′), 5.97 (1H, d, *J* = 15.4 Hz, H-10′), 6.09 (1H, dd, *J* = 15.4, 7.3 Hz, H-7′), 6.49 (1H, dd, *J* = 15.4, 11.1 Hz, H-8′), and 7.32 (1H, dd, *J* = 15.4, 11.1 Hz, H-9′)]. The ^{13}C NMR data assigned with the aid of HSQC and HMBC spectra afforded the resonances of five methyls, seven methylenes, eleven methines, and seven uncharacterized carbons.

The NMR data of (**67**) in (MeOD-d_4) was quite similar to those of roridin A (**57**) (in MeOD-d_4) especially the signals of the sesquiterpenoid core, however, the following differences were observed. The existence of the methoxy group at δ_H 3.73 in (**67**), and the HMBC correlation from these methoxy protons to C-11′ (δ_C 167.6) supported that the occurrence of a methyl ester functionality in (**67**) (**Figure 56**). In addition, the upfield chemical shift of CH-4 [δ_H 4.49 (1H, dd, *J* = 7.7, 3.7 Hz); δ_C 74.5] compared to that of roridin A (**57**) [δ_H 5.84 (1H, dd, *J* = 8.3, 4.2 Hz); δ_C 76.0] and HMBC correlations from H-2, H-3, and H_3-14 to C-4 (δ_C 72.9) suggested that the ester linkage between C-4 and C-11′ was cleaved in (**67**).

Table 48: NMR spectroscopic data for roridin G (**67**) (600 and 150 MHz, δ ppm)[a]

Position	^{1}HNMR (*J* in Hz)	^{13}CNMR	COSY	HMBC
2	3.69 (d, 5.2)	80.6	3	4, 5, 11, 12
3	1.87 (dt, 3.7, 5.2)	39.8	2, 4	
	2.47 (dd, 7.7, 15.3)			2, 5, 12
4	4.49 (dd, 3.7, 7.7)	74.5	3	
5	-	49.9	-	-
6	-	44.4	-	-
7	1.89 m	21.7	8	6, 8
	1.97 m			
8	2.00 m	28.7	7	6, 7
9	-	140.8	-	-
10	5.38 (d, 5.3)	119.3	11, 16	16
11	3.67 (br d, 5.3)	67.7	10	6, 7, 9, 10, 16
12	-	65.2	-	-
13	2.80 (d, 4.0)	48.0	-	-
	3.02 (d, 4.0)			
14	0.86 s	9.4	-	5, 6, 12
15	4.19 (d, 12.2)	62.2	-	5, 6, 7, 1'
	4.03 (d, 12.2)			5, 6, 11, 1'
16	1.71 s	23.6	10	8, 9, 10
1'-CO	-	173.5	-	-
2'	4.16 (d, 3.3)	73.7	3'	3'
3'	2.20 m	34.6	2', 12'	-
4'	1.58 m	33.7	5'	2', 3', 5', 12'
	1.76 m			2', 3', 5', 12'
5'	3.44 m	68.0	4'	3', 4', 6'
	3.61 m			
6'	3.70 m	85.7	7', 8'	5', 8', 13'
7'	6.09 (dd, 7.3, 15.4)	141.4	6', 8'	9'
8'	6.49 (dd, 11.1, 15.4)	132.2	7', 9'	6'
9'	7.32 (dd, 11.1, 15.4)	145.6	8', 10'	7'
10'	5.97 (d, 15.4)	122.3	9'	8', 11'
11'-CO	-	167.6	-	-
12'	0.88 (d, 6.9)	14.4	-	2', 3', 4'
13'	3.76 (dq, 6.3)	70.0	14'	7'
14'	1.12 (d, 6.3)	18.8	13'	6', 13'
11'-OMe	3.74 s	50.1	-	11'

[a] The assignments were based on DEPT, ^{1}H-^{1}H COSY, HSQC, and HMBC experiments, and recorded in MeOD-d_4

The other distinct difference was related with the chemical shift and the coupling constant of the sp^2 methines H-7', H-8', H-9' and H-10' at δ_H 6.09 (1H, dd, J = 15.4, 7.3 Hz; δ_C 141.4), 6.49 (1H, dd, J = 15.4, 11.1 Hz; δ_C 132.2), 7.32 (1H, dd, J = 15.4, 11.1 Hz; δ_C 145.6), and 5.97 (1H, d, J = 15.4 Hz; δ_C 122.3) respectively, confirmed the geometries of the two disubstituted double bonds from C-7′ to C-10′ as 7'*E*, 9'*E* form. Detailed 2D NMR data analysis led to the confirmation of the gross planar structure of (**67**).

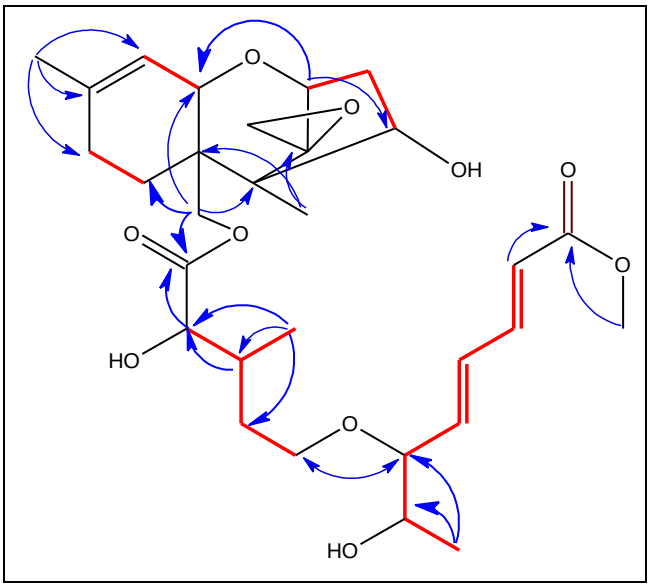

Figure 56: Key COSY (▬) and selected HMBC (→) correlations for (**67**).

The relative configuration of (**67**) was elucidated based on the comparison of NMR data and coupling constants of geminal and vicinal protons (**Table 48**) with those of roridin A (**57**). The stereochemistry of the sesquiterpene moiety was identical to that of (**57**) based on the same spectroscopic values and the aspect of common biosynthetic origin. The configuration at C-2′ and C-3′ could be the same as Roridin A (**57**) and Isororidin A (**58**) (2′*S*, 3′*R*) based on the same biosynthetic origin, but since we lack hard experimental evidence we omitted the assignment.

The *threo* configuration of C-6′/C-13′ was deduced from the characteristic five-line multiplets of H-13′, resonating at δ_H 3.76 (dq, J = 6.3, 6.3 Hz) revealed that the relative configurations of C-6′ and C-13′ were either both *R* or *S*.

Thus, (**67**) was identified as a new natural product for which we suggest the name roridin G.

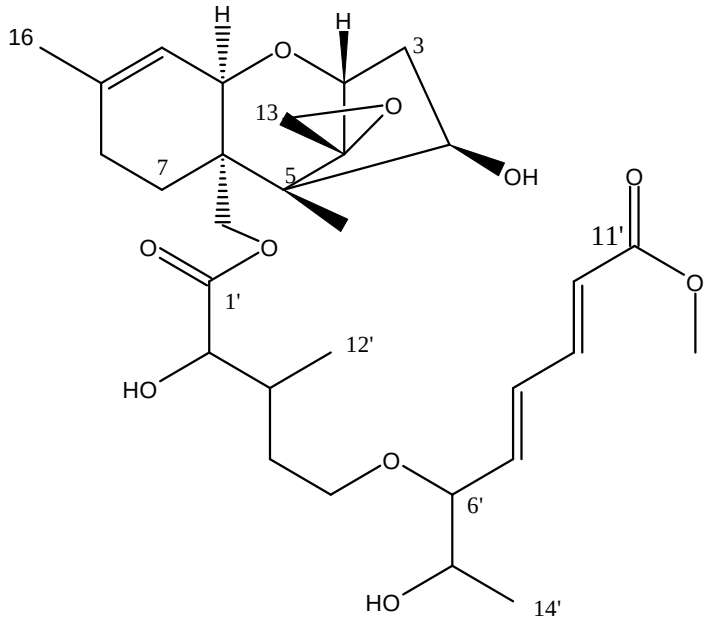

67

5.2.1.12 Verrol

Verrol (**68**) was obtained as a white solid (16.6 mg). The Positive HRESI-MS exhibited a strong peak at *m/z* 396.2387 $[M+NH_4]^+$ indicating a molecular formula of $C_{21}H_{30}O_6$ (calcd. 396.2381), bearing 7 double bond equivalents (DBE).

The ^{1}H NMR and HSQC data (**Table 49**), exhibited the presence of thirty protons attributed for three methyls at δ_H 2.21 (3H, d, *J* = 1.1 Hz, H-6'), 1.70 (3H, s, H-16) and 0.87 (3H, s, H-14), seven methylene protons at δ_H (4.15 (1H, d, *J* =12.4 Hz, H-15a), 3.94 (1H, d, *J* =12.4 Hz, H-15b), 3.80 (2H, t, *J* = 6.3 Hz, H-5'), 2.42 (2H, t, *J* = 6.3 Hz, H-4'), (2.59 (1H, dd, *J* = 15.8, 7.5 Hz, H-3a), 1.90 (1H, dd, *J* = 5.1, 3.0 Hz, H-3b), (3.11 (1H, d, *J* = 4.0 Hz, H-13a), 2.81 (1H, d, *J* = 4.0 Hz, H-13b) and 2.00 (2H, m, 1.77 m, H_2-7), as well as the overlapped signals at δ_H (1.98, 2H, m, H_2-8). Additionally, five methines are detected three of them are oxygenated at δ_H 4.53 (1H, dd, *J* = 7.5, 3.0 Hz, H-4), 3.82 (1H, d, *J* = 5.1 Hz, H-2), and the doublet at 3.64 (1H, d, *J* = 5.3 Hz, H-11) and two vinylic methines at 5.73 (1H, d, *J* =1.1 Hz, H-2') and 5.41 (1H, d, *J* = 5.3 Hz, H-10).

The structure of (**68**) was further elucidated by analysis of 2D NMR data including the ^{1}H-^{1}H COSY and HMBC spectra. The ^{1}H-^{1}H COSY data of (**68**) revealed connectivity of structural fragments: a (C-2 to C-4), b (C-7 to C-8), c (C-10 to C-11), and d (C-4' to C-5'). The molecular weight of (**68**) along with the above NMR indications, revealed that this compound has trichodermol moiety and six-carbon acrylic acid ester side chain. Obviously, it lacks the right-hand dienic portion of the other

trichoverroids, roridins and verrucarins, as evidenced by the absence of downfield signals between (5.80-8.00 ppm) and existent of the upfield signal at δ_H (4.53 (1H, dd, J = 7.5, 3.0 Hz, H-4); δ_C 73.8). The HMBC correlations (**Figure 57**) showed that the trichodermol moiety and the ester side chain are attached through the oxymethylene at [δ_H (4.15 (1H, d, J =12.4 Hz), 3.94 (1H, d, J =12.4 Hz); δ_C 62.2)].

Table 49: NMR spectroscopic data for verrol (**68**) (400 and 100 MHz, δ ppm) [a]

Position	^{1}HNMR (J in Hz)	^{13}CNMR	COSY	HMBC	NOESY
2	3.82 (d, 5.1)	78.1	3a	4, 5, 11	3β, 13β
3	α 2.59 (dd, 7.5, 15.8)	39.2	2, 3b, 4	2, 5, 12	11
	β 1.90 (dd, 3.0, 5.1)			4	2
4	4.53 (dd, 3.0, 7.5)	73.8	3	2, 5, 6, 12	11, 15α
5	-	48.3	-	-	-
6	-	42.0	-	-	-
7	2.00 m	20.6	8	5, 8, 9, 15	14
	1.77 m				
8	1.98 ovlp	27.4	7	7, 10	14
9	-	140.3	-	-	-
10	5.41 (d, 5.3)	117.9	8, 11, 16	6, 8, 11, 16	16
11	3.64 (d, 5.3)	66.0	10	2, 8, 10, 11, 15	3α, 4, 15α
12	-	64.9	-	-	-
13	α 3.11 (d, 4.0)	47.0	-	2, 5, 12	8, 14
	β 2.81 (d, 4.0)				2, 8
14	0.87 s	6.5	-	4, 5, 6, 12	13, 15, 2', 6'
15	α 4.15 (d,12.4)	62.2	-	5, 6, 7, 11, 1'	11
	β 3.94 (d,12.4)				
16	1.70 s	22.6	8, 10, 11	8, 9, 10	8, 10
1'-CO	-	165.4	-	-	-
2'	5.73 (d, 1.1)	116.6	4', 6'	1', 3', 4', 6'	4', 5', 14
3'	-	156.7	-	-	-
4'	2.42 (t, 6.3)	43.2	2', 5'	2', 3', 5'	2'
5'	3.80 (t, 6.3)	59.5	4'	3', 4'	2', 6'
6'	2.21 (d, 1.1)	18.1	2'	1', 2', 3', 4'	4', 5'

[a] The assignments were based on DEPT, ^{1}H-^{1}H COSY, HSQC, and HMBC experiments, and recorded in $CDCl_3$

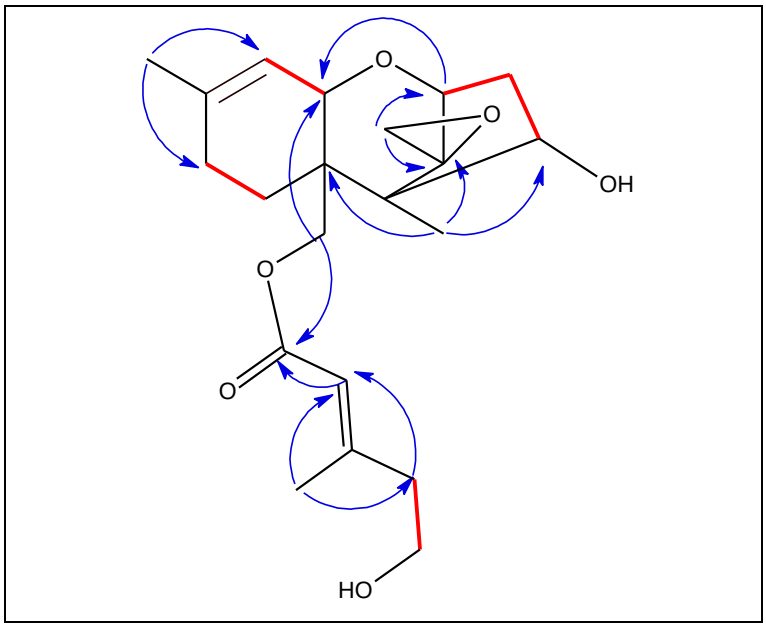

Figure 57: Key COSY (▬) and selected HMBC (→) correlations for verrol (**68**)

The relative configuration of (**68**) was revealed based on NOESY analysis. In trichothecene part, the NOESY correlations of H-11/H-4, H-11/H-15*α*, and H-11/H-3*α* demonstrated that these groups were co facial, while H-2, H-13, and CH_3-14 were speculated to be oriented in the opposite direction according to the NOE signals of H-2/ H-3*β*, H-2/H-13*β*, and CH_3-14/H-2' and CH_3-14/CH_3-6'. The configuration at C-2' supported to be *Z* due to the chemical shift of the methyl group C-6' (δ_C 18.1 ppm) like the normal roridins. According to all of the above indications, the structure corresponds to that of verrol which previously reported from *Myrothecium verrucaria* [291].

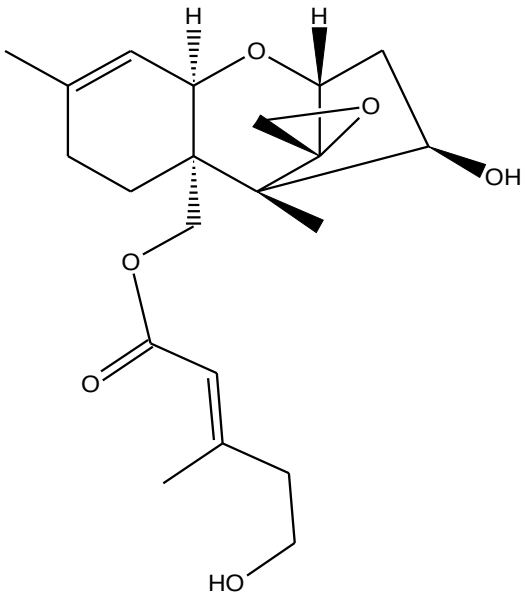

68

5.2.1.13 Trichoverrol A

Trichoverrol A (**69**) was obtained as white solid (1.3 mg), the Positive HRESI-MS exhibited a strong peak at *m/z* 438.2486 $[M+NH_4]^+$ indicating a molecular formula of $C_{23}H_{32}O_7$ (calcd. 438.2480) bearing 8 double bond equivalents (DBE).

The ^{1}H NMR with the aid of HSQC spectrum (**Table 50**) exhibited the presence of 32 protons attributed for three methyls at δ_H [0.84 (3H, s, H-14), (1.72, 3H, s, H-16) and 1.21 (3H, d, *J* = 6.3 Hz, H-8')], five methylenes at δ_H [1.58 (1H, m), 1.95 (1H, m), H_2-8), 2.00 (2H, m, H_2-7), 2.13 (1H, br dd , *J* = 5.1, 3.8 Hz and 2.52 (1H, dd, , *J* = 15.4, 8.0 Hz), H_2-3], moreover the epoxide protons at δ_H [(2.85, 1H, d, *J* = 4.0 Hz), 3.18 (1H, d, *J* = 4.0 Hz), H_2-13] and oxymethylen at δ_H [3.83(1H, d, *J* = 12.0 Hz), 3.67, 1H, d, *J* =12.0 Hz), H_2-15].

Additionally, ten methines are detected five of them are oxygenated at δ_H [(3.70, 1H, br d, *J* = 6.3 Hz, H-7'), (3.87 (1H, d, *J* = 5.1 Hz, H-2), (3.93, 1H, d, *J* = 5.5 Hz, H-11), (4.05, 1H, m, H-6') and 6.16 (1H, dd, *J* = 8.0, 3.8 Hz, H-4) and others are vinylic methines at δ_H [5.50 (1H, d, *J* = 5.5 Hz, H-10), 5.73 (1H,d, *J* = 11.3 Hz, H-2'), (6.08 (1H, br dd, *J* = 15.5, 5.6 Hz, H-5'), 6.64 (1H, t, *J* = 11.3 Hz, H-3') and 7.62 (1H, br dd, *J* = 15.5, 11.3 Hz, H-4')]. The molecular weight of (**69**) along with the 1D NMR data revealed that the compound is not a macrocyclic trichothecene, but still contain trichothecane moity.

The structure was fully confirmed by 2D NMR correlations (**Figure 58**). The data of ^{1}H−^{1}H COSY and HMBC led to the establishment of the dienic ester (the right side chain). Further on, the absence of the HMBC correlation between the methylene protons CH_2-15 at [δ_H 3.83 (1H, d, *J* = 12.0 Hz), 3.67 (1H, d, *J* =12.0 Hz; δ_C 62.5)] with any carbons above 150 ppm indicated the absence of the left ester side chain. The chemical shifts and the coupling constant of the sp^2 methines H-2', H-3' and H-4' at [δ_H (5.73, d, *J* = 11.3 Hz; δ_C 118.0), (6.64, t, *J* = 11.3, Hz; δ_C 143.4), and (7.62, dd, *J* = 15.5, 11.3 Hz; δ_C 127.5)] respectively, indicated the presence of (2' *Z*, 4' *E*) form.

Table 50: NMR spectroscopic data for trichoverrol A (**69**) (400 and 100 MHz, δ ppm)[a]

Position	^{1}HNMR (*J* in Hz)	^{13}CNMR	COSY	HMBC
2	3.87 (d, 5.1)	78.9	3	4, 12, 13
3	2.13 (br dd, 3.8, 5.1) 2.52 (dd, 8.0, 15.4)	35.6	2, 4	 2, 5, 12
4	6.16 (dd, 3.8, 8.0)	74.8	3	6, 1'
5	-	47.9	-	-
6	-	43.3	-	-
7	2.00 m	21.0	8	6, 15
8	1.58 m 1.95 m	27.9	7	9 6, 10, 15
9	-	140.1	-	-
10	5.50 (d, 5.5)	118.2	11, 16	6, 16
11	3.93 (d, 5.5)	66.5	10	9, 10
12	-	65.6	-	-
13	2.85 (d, 4.0) 3.18 (d, 4.0)	48.1	-	12 2, 12
14	0.84 s	6.1	-	2, 4, 6, 12, 13
15	3.83 (d, 12.0) 3.67 (d, 12.0)	62.5	-	 5, 11, 12
16	1.72 s	23.1	10	8, 9, 10
1'-CO	-	166.0	-	-
2'	5.73 (br d, 11.3)	118.0	3'	1', 4'
3'	6.64 (t, 11.3)	143.4	2', 4'	1', 5'
4'	7.62 (br dd, 11.3, 15,5)	127.5	3', 5'	3', 6'
5'	6.08 (br dd, 5.6, 15.5)	141.8	4', 6'	3', 6
6'	4.05 m	76.2	5', 7'	7'
7'	3.70 (m,5 lines, 6.3)	70.2	8'	-
8'	1.21 (d, 6.3)	18.5	7'	6', 7'

[a] The assignments were based on DEPT, ^{1}H-^{1}H COSY, HSQC, and HMBC experiments, and recorded in $CDCl_3$

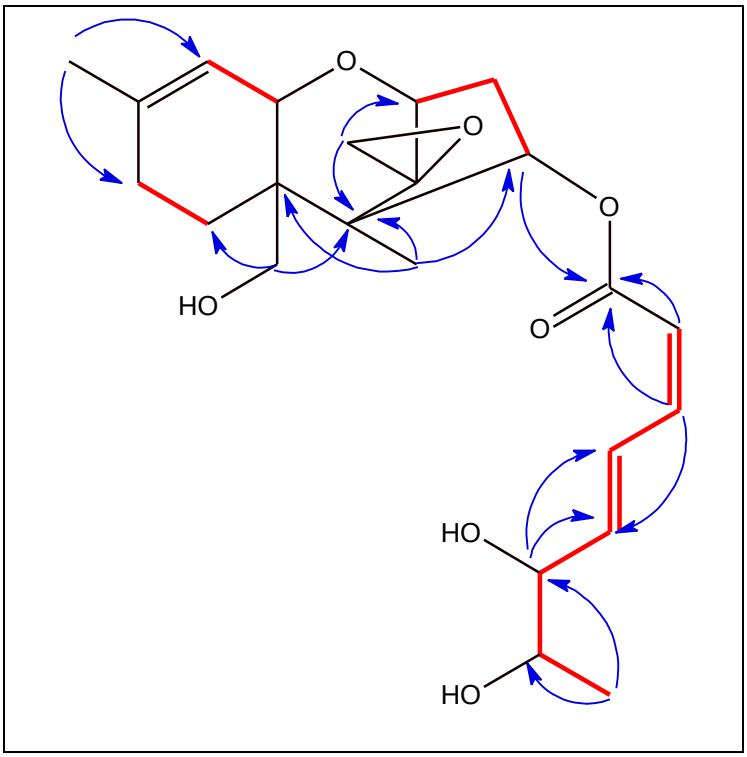

Figure 58: Key COSY (▬) and selected HMBC (→) correlations for trichoverrol A (**69**)

The relative configuration of (**69**) was deduced based on the coupling constants of geminal and vicinal protons (**Table 50**). Besides that, the remaining stereochemistry at C6' and C7' was determined to be both *S* by employing diagnostic ^{1}H NMR parameters summarized in (**Table 51**)[292]. The diagnostic pattern of a five-line multiplet at H-7' indicated *threo* configuration. Thus, (**69**) was identified as trichoverrol A, and its ^{1}H, ^{13}C NMR and mass spectral data were in agreement with published data[286].

Table 51: Diagnostic ^{1}H NMR parameters to define the absolute configuration of C6' and C7'

H-6' multiplicity	^{3}J 5',6'(in Hz)	^{3}J 6',7'(in Hz)	Epimer series	configuration
five-line multiplet	6.5	6.5	A epimers, (*threo*)	C6'- (*S*),C7'(*S*)
				C6'- (*R*),C7'(*R*)
eight-line multiplet	3.3	6.5	B epimer (*erythro*)	C6' (*S*),C7' (*R*) C6' (*R*),C7' (*S*)

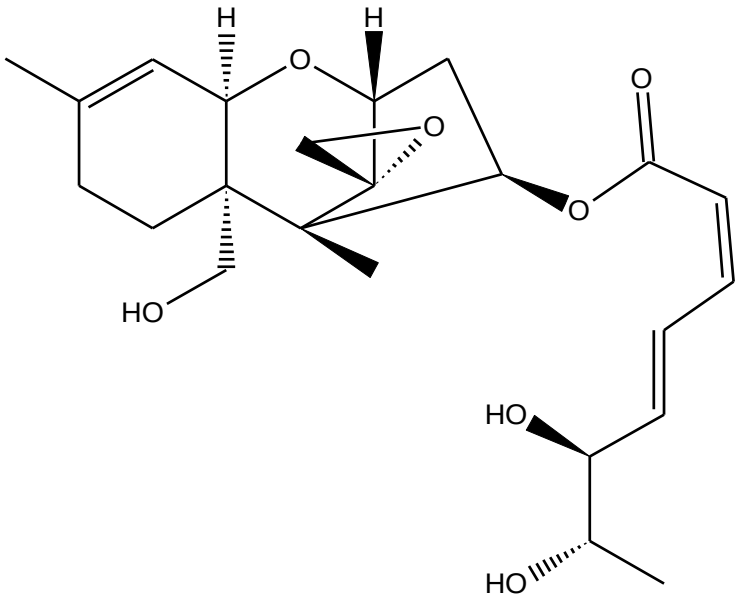

69

The trichoverroids lie along the biosynthetic path leading from the simple to the macrocyclic trichothecenes. The two principal types of trichoverroids are the trichoverrols, which are C8 monoesterified of the simple trichothecenes at carbon C-4, and the trichoverrins, which are simple trichothecenes esterified at both C-4 and C-15. The A series of compounds is *L-threo* and the B series is *D-erythro*, making these compounds epimeric at C7' and of the *S* configuration at C6'. This difference does not seem to be associated with an effect of the macrocyclic ring.

5.2.1.14 2'*E*-isotrichoverrol A (C6'*R*, C7'*R*)

Compound (**70**) was obtained as white solid (1.3 mg), the Positive HRESI-MS exhibited a strong peak at *m/z* 421.2230 $[M+H]^+$ indicating a molecular formula of $C_{23}H_{32}O_7$ (calcd. 421.2221), bearing 8 double bond equivalents (DBE).

The ^{1}H NMR data (

Table 52) showed a similarity with that of trichoverrol A (**69**) especially for the signals of the trichothecane moiety which appeared at δ_H 3.85 (1H, d, *J* = 5.0 Hz, H-2), (2.13, 1H, br dd, *J* = 5.0, 3.9 Hz and 2.50 (1H, dd, *J* = 15.3, 8.2 Hz) H_2-3), 6.14 (1H, dd, *J* = 8.2, 3.2 Hz, H-4), (1.58 (1H, m) and 1.96 (1H, dd, *J* = 12.0, 6.0 Hz) H_2-7), 2.00 (2H, m, H_2-8), 5.50 (1H, d, *J* = 5.6 Hz, H-10), 3.94 (1H, d, *J* = 5.6 Hz, H-11), and the two methyls at δ_H (0.84, s, H-14) and (1.72, s, H-16). Moreover, the epoxide protons at δ_H [2.82 (1H, d, *J* = 4.0 Hz), 3.14 (1H, d, *J* = 4.0 Hz) H_2-13]) and oxymethylen at δ_H [3.67, 1H, d, *J* =12.0 Hz, 3.83(1H, d, *J* = 12.0 Hz), H_2-15]. Along with the lack of the ester side chain on the left hand, the chemical shift and the coupling constant of the sp^2 methines H-2', H-3' and H-4' at [δ_H (5.97, 1H, d, *J* = 15.3 Hz; δ_C 121.7), (7.31, 1H, dd, *J* = 15.3, 11.0 Hz; δ_C 144.4), and (6.48, 1H, dd, *J* =15.3, 11.0 Hz; δ_C 129.7)] respectively, indicated the (2'*E*, 4' *E*) form.

The molecular weight of (**70**) along with the 1D NMR data led to the establishment of the planner structure. The relative configuration of (**70**) was revealed based on ROESY analysis. In the trichothecene part, the ROESY correlations of H-11/H-4, H-11/H-15*α*, and H-11/H-3*α* demonstrated that these groups were co facial, while H-2, H-13, and CH_3-14 were speculated to be oriented in the opposite direction according to the ROE signals of H-2/ H-3b, and H-2/H-13b. Moreover, the *threo* configuration of C-6′/C-7′ was deduced from the characteristic five-line multiplets at H-7′, the chemical shift of C-6' and C-7' which resonance at (δ_H 4.01, 1H, br t, *J* = 6.0 Hz, δ_C 77.2) and (δ_H 3.70, 1H, qd, *J* = 8.8, 6.3 Hz; δ_C 70.6) respectively, along with the ROESY correlations between H-6'/H-8' confirmed the *R* configuration at C-6' and C7'

According to all of the above data, the structure corresponds to that of 2'*E*-isotrichoverrol A which previously reported once from *Myrothecium verrucaria*[292].

Table 52: NMR spectroscopic data for (**70**) (400 and 100 MHz, δ ppm)[a]

Position	^{1}HNMR (*J* in Hz)	^{13}CNMR	COSY	HMBC	ROESY
2	3.85 d (5.0)	79.0	3	4, 5, 6, 12	3β, 13β
3	α 2.50 (dd, 8.2, 15.3) β 2.13 (br dd, 3.9, 5.0)	35.9	2, 4	2, 5, 12 2, 4	11, 4 2
4	6.14 (dd, 3.2, 8.2)	75.6	3	1', 6, 12	11, 15α
5	-	48.2	-	-	-
6	-	44.2	-	-	-
7	1.55 m 1.96 (dd, 6.0, 12.0)	21.3	8	9 6, 8, 15	
8	2.0 m	28.0	7, 16	7, 9, 10, 15	14
9	-	140.5	-	-	-
10	5.50 (br d, 5.6)	118.8	11, 16	6, 11, 16	16
11	3.94 (d, 5.6)	66.6	10	7, 9, 10	3α, 4
12	-	65.6	-	-	-
13	α 2.82 (d, 4.0) β 3.14 (d, 4.0)	48.0	-	2, 5, 12	14
14	0.82 s	6.4	-	4, 5, 6, 12	8, 13β, 15
15	α 3.82 (d, 11.8) β 3.67 (d, 11.8)	63.0	-	5, 6, 7, 11	 14
16	1.72 s	23.3	10, 11	8, 9, 10	10
1'-CO	-	167.8	-	-	-
2'	5.97 (d, 15.3)	121.7	3'	1', 4'	14
3'	7.31 (dd, 11.0, 15.3)	144.4	2', 4'	1', 2', 4', 5'	
4'	6.48 (dd, 11.0, 15.3)	129.7	3', 5'	2', 3', 6'	2', 6'
5'	6.13 (dd, 6.0, 15.3)	141.4	4', 6'	3', 6'	
6'	4.01 (br t, 6.0)	77.2	5', 7'	4', 5', 7'	4'
7'	3.70 (m, 5 lines, 6.3)	70.6	6', 8'	-	4, 6'
8'	1.22 (d, 6.3)	19.1	-	6', 7'	4'

[a] The assignments were based on DEPT, ^{1}H-^{1}H COSY, HSQC, and HMBC experiments, and recorded in $CDCl_3$

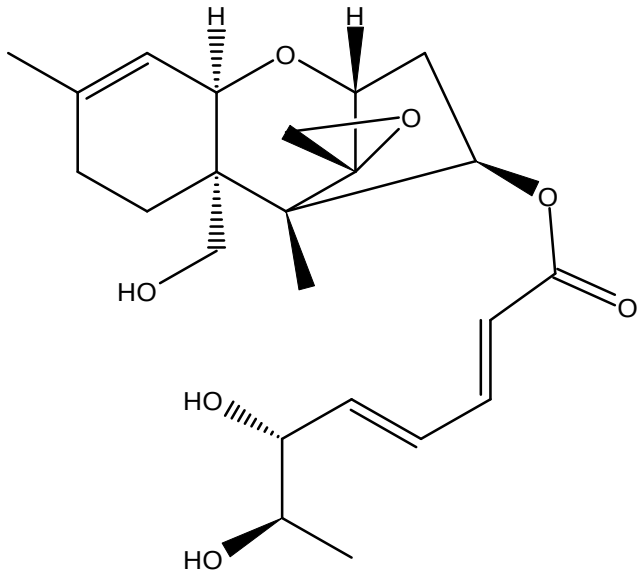

70

5.2.1.15 2'*E*-isotrichoverrol B (C6'*R*, C7'*S*)

Compound (**71**) was obtained as a white amorphous solid (2.1 mg), the positive HRESI-MS exhibited a strong peak at *m/z* 421.2230 $[M+H]^+$ indicating a molecular formula of $C_{23}H_{32}O_7$ (calcd. 420.2221), bearing 8 double bond equivalents (DBE).

The ^1H NMR spectrum of (**71**) exhibited a high similarity in its pattern to 2'*E*-isotrichoverrol A (**70**), it displayed the same trichothecane moiety attached with the ester side chain at C-4. The *E* form of the vinylic protons observed also due to the coupling constant of H-2', H3' and H-4' which resonating at [δ_H (5.97, 1H, d, J = 15.3, δ_C 121.5), (7.32, 1H, dd, J = 15.3, 11.1 Hz, δ_C 145.9), and (6.45, 1H, dd, J = 15.3, 11.1 Hz; δ_C 129.7)] respectively. Moreover, COSY and HMBC spectra showed the same set of correlations as observed for (**70**) (**Table 53**).

The sole difference was found at C-6', which shifted down-field to δ_H (4.24, 1H, br t, J = 4.8 Hz; δ_C 76.6), while in the case of 2'*E*-isotrichoverrol A (**70**), it was found at δ_H 4.01 (1H, br t, J = 6.0 Hz; δ_C 77.2), this observation supplied that these two compounds are epimers. The relative configuration of (**71**) was deduced based on the NOESY correlations and coupling constants of geminal and vicinal protons. The five-lines multiplets of H-7' (in MeOD-d_4) and the observed NOESY correlation between H-6' and H-7' established the stereochemistry at C-6', C-7' as *erythro* (C-6' *R*, C-7' *S*), the same as is found in the B-series trichoverroids.

Table 53: NMR spectroscopic data for (**71**) (600 and 150 MHz, δ ppm)[a]

Position	^{1}HNMR (*J* in Hz)[b]	^{1}HNMR (*J* in Hz)	^{13}CNMR	COSY	HMBC	NOESY [b]
2	3.85 (d, 4.9)	3.73 (d,(5.2)	80.0	3	4, 5, 11, 12	3β, 13β
3	α 2.50 (br dd, 8.0, 15.2) β 2.13 (br t, 4.9)	1.92 (t, 4.4) 2.51 (br dd, 7.5, 15.5)	37.3	2, 4	4, 6 2, 5, 12	4 2
4	6.14 (br dd (3.4, 8.7)	5.95 (br d, 3.0, 7.8)	76.9.1	3	6, 12	3α, 11
5	-	-	49.9	-	-	-
6	-	-	45.3	-	-	-
7	1.75 (dd,5.9, 12.4) 1.89 (dd, 5.9, 12.4)	1.75 (dd, 5.9, 12.4) 1.89 (dd, 5.9, 12.4)	21.5	8	8, 11 6, 15	14
8	α 1.54 m β 1.96 (dd, 5.9, 12.0)	2.11 (br dd, 5.9, 12.4) 2.14 m	28.7	7	9, 10	14
9	-	-	141.6	-	-	-
10	5.50 (br d, 5.4)	5.41 (d, 5.2)	119.4	11, 16	6, 8, 16	16
11	3.95 ovlp	3.77 (d, 5.2)	68.2	10	7, 9, 10, 16	3α
12	-	-	66.5	-	-	-
13	α 2.82 (d, 4.0) β 3.14 (d, 4.0)	2.88 (d, 4.0) 3.09 (d, 4.0)	48.6	-	12	3β, 14
14	0.82 s	0.88 s	6.9	-	4, 5, 6, 12	4, 8β, 13β, 15β
15	α 3.83 (d, 12.2) β 3.67 (d, 12.2)	3.50 (d, 12.0) 3.82 (d, 12.0)	62.0	-	5, 6, 7, 11	14
16	1.72 s	1.72 s	22.8	10	8, 9, 10	7, 10
1'-CO	-	-	168.1	-	-	-
2'	5.97 (d, 15.3)	5.93 (d, 15.2)	121.5	3'	1', 4'	14, 4'
3'	7.32 dd (11.1, 15,3)	7.35 (dd, 11.1, 15,2)	145.9	2', 4'	1', 5'	14, 5'
4'	6.45 dd (11.1, 15,3)	6.48 (dd, 11.1, 15,2)	129.7	3', 5'	2', 3', 6'	2', 6', 8'
5'	6.17 dd (6.0, 15.3)	6.28 (dd, 5.7, 15.2)	143.9	4', 6'	3', 6, 7'	8'
6'	4.24 (br t, 4.8)	4.01 (t, 5.7)	76.6	5', 7'	4, 5', 7', 8'	4',5', 7', 8'
7'	3.93 ovlp	3.69 (m, 5 lines)	71.1	6'	5', 8'	6', 8'
8'	1.15 (d, 6.5)	1.16 (d, 6.5)	18.3	7'	6', 7'	5', 6'

[a] The assignments were based on DEPT, ^{1}H-^{1}H COSY, HSQC, and HMBC experiments, and recorded in MeOD-d_4. [b] The assignments were recorded in $CDCl_3$.

The structure was further confirmed by comparing ^{1}HNMR, mass spectral data with published data for 2'*E*-isotrichoverrol B, previously reported once from *Myrothecium verrucaria*[292].

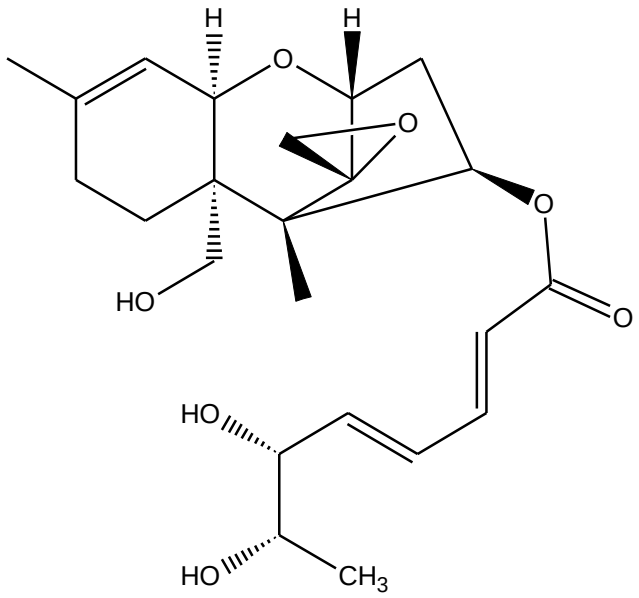

71

5.2.1.16 Trichoverrin A

Trichoverrin A (**72**) was obtained as white solid (5.5 mg), the Positive HR-ESI-MS exhibited a strong peak at *m/z* 550.3011 $[M+NH_4]^+$ indicating a molecular formula of $C_{29}H_{40}O_9$ (calcd. 550.2998) bearing 10 double bond equivalents (DBE). Compound (**72**) has 94 amu higher than trichoverrol A (**69**), which suggested the presence of the two sides of ester at C-4 and C-15.

The ^{13}C NMR data (**Table 54**), assigned by the aid of HSQC and HMBC spectra, displayed the resonances of four methyls (δ_C 6.5, 18.7, 19.0, and 23.0), seven methylenes (δ_C 21.7, 27.7, 36.7, 43.4, 48.4, 59.4 and 63.3), eleven methines (δ_C 66.4, 70.2, 74.8, 76.2, 78.8, 116.7, 118.0, 118.4, 127.3, 142.1, and 143.8) and seven uncharacterized carbons (δ_C 42.7, 48.5, 65.8, 140.5, 157.1, 165.9, and 166.1).

Additionally, six spin systems were identified from ^{1}H-^{1}H COSY experiment as shown in **Figure 59**, moreover, long-range HMBC correlations were used to establish the connectivities of the various spin systems.

Table 54: NMR spectroscopic data for trichoverrin A (**72**) (400 and 100 MHz)[a]

Position	^{1}HNMR (*J* in Hz)	13CNMR	COSY	HMBC	NOESY
2	3.87 (d, 5.2)	78.9	3	4, 5, 11, 12	13β, 14, 6"
3	α 2.58 (br dd, 7.7, 15.7) β 1.97 (br dd,3.3, 5.2)	36.7	2, 4	2, 5, 12 4, 6	2 4
4	6.25 (dd, 3.3, 7.7)	74.8	3	6, 12, 1'	3α, 11, 15α
5	-	48.5	-	-	-
6	-	42.7	-	-	-
7	1.56 m 2.11 m	21.7	8	6, 9,12 6, 10, 15	14
8	2.01 (br dd, 3.2, 5.2)	27.7	7	6, 7, 9, 10	14
9	-	140.5	-	-	-
10	5.49 (br d, 5.4)	118.4	11, 16	6, 8, 16	16
11	4.01 (br d, 6.3)	66.4	10, 16	7, 9, 10, 15	3α, 4, 15α
12	-	65.8	-	-	-
13	α 3.18 (d, 4.0) β 2.85 (d, 4.0)	48.4	-	2, 5, 12	14
14	0.81 s	6.5	-	2, 4, 5, 6, 12	8β, 13β, 15β, 4', 2"
15	α 4.14 (d, 12.4) β 4.11 (d, 12.4)	63.3	-	5, 6, 7, 11, 1"	2, 14, 6"
16	1.72 s	23.0	10, 11	8, 9, 10	10
1'-CO	-	166.1	-	-	-
2'	5.70 (d, 11.3)	118.0	3'	1', 3', 4'	14
3'	6.61 (d, 11.3)	143.8	2', 4'	1', 5'	5'
4'	7.57 (br dd, 11.3, 15.5)	127.3	3', 5'	2', 3', 6'	14
5'	6.08 (dd, 5.3, 15.5)	142.1	4', 6'	3', 4', 6'	7', 8'
6'	4.05 (br d, 6.3)	76.2	5', 7'	5', 7', 8'	4', 8'
7'	3.68 m (5 lines *J*=6.3)	70.2	6', 8'	5', 6', 8'	11, 5'
8'	1.21 (d, 6.3)	18.7	7'	6', 7'	5', 6'
1"-CO	-	165.9	-	-	-
2"	5.88 (br d, 1.1)	116.7	6"	1", 3", 4", 6"	2, 14, 6"
3"	-	157.1	-	-	-
4"	2.42 (t, 5.7)	43.4	5"	2', 3", 5", 6'	2", 6"
5"	3.79 m 3.86 (br dd 2.4, 5.7)	59.4	4"	3", 4"	6" 14
6"	2.20 (br d, 1.1)	19.0	2"	1", 2", 3", 4"	2", 4"

[a] The assignments were based on DEPT, ^{1}H-^{1}H COSY, HSQC, and HMBC experiments, and recorded in $CDCl_3$

The right side ester chain is formed through ester linkages at C-4 of the trichothecane ring system due to the cross-peaks from H-4 to C-1', also the ester linkage at C-15 is supported by the correlation of the H_2-15 methylene protons to C-l" and the downfield chemical shift of C-15 (δ_C 63.3). The correlations of H-2" to C-l" and C-3" and of the C-6" methyl protons to both C-2" and C-3" along with the carbon chemical shifts of C-2" and C-3" (δ_C 116.7 and 157.1 respectively) indicated the presence of an *α, β*-unsaturated ester with a methyl group off the *β*-position. The lack of the HMBC correlation between H_2-5" with C-5' or C-6', and between H-5' or H-6' with C-5", suggested that the macrocyclic ring was opened. This suggestion was confirmed by the upfield chemical shift of the oxymethylene C-5" (δ_C 59.4) which appeared around (δ_C 70.0) in the close macrocyclic compounds like roridin A (**57**). As stated by the aforementioned data the planner structure of (**72**) was established.

The relative configuration of (**72**) was deduced based on the NOESY correlations and coupling constants of geminal and vicinal protons. The H-7' proton in (**72**) appeared as five-line multiplets with J 6',7' = J 7',8' = 6.3 Hz which established the stereochemistry at C-6', C-7' as *threo* (C6' *S*, C7' *S*), the same as is found in the A-series trichoverroids. Compound (**72**) was plausible, showing a close agreement with values of trichoverrin A in the literature data[293, 294].

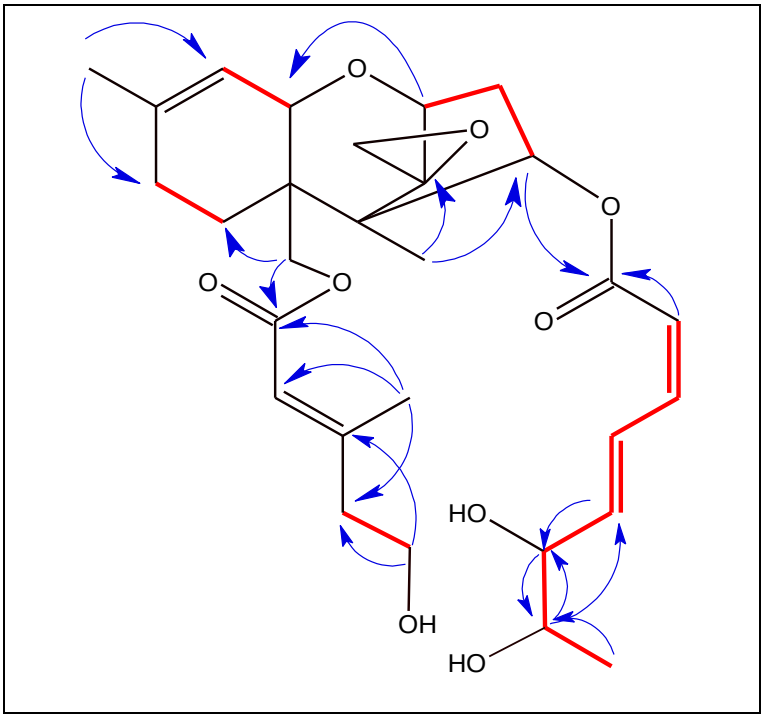

Figure 59: Key COSY (▬) and selected HMBC (→) correlations for trichoverrin A (**72**)

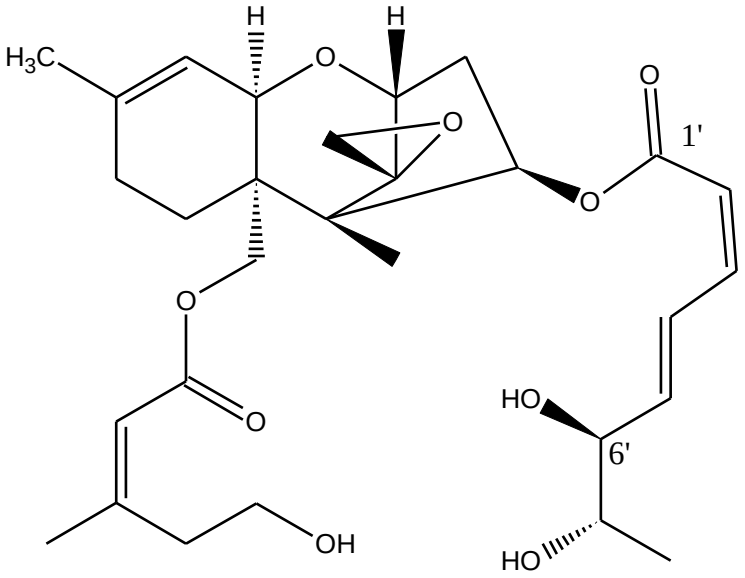

72

5.2.1.17 (2'*E*, 4'*E*)- Isotrichoverrin A

Compound (**73**) was isolated as a white solid (1.3 mg), the Positive HRESI-MS exhibited a strong peak at *m/z* 533.2750 $[M+H]^+$ indicating a molecular formula of $C_{29}H_{40}O_9$ (calcd. 533.2744), bearing 10 double bond equivalents (DBE). Compound (**73**) showed the same molecular weight like trichoverrin A (**72**), which suggest the same skeleton.

The ^{1}H NMR spectrum (**Table 55**) of (**73)** was highly similar to that of trichoverrin A (**72**). Differences, however, were observed in the chemical shifts and the coupling constant of the sp^2 methines H-2', H-3' and H-4' at [δ_H (5.93, 1H, d, J = 15.4 Hz, δ_C 122.1), (7.25, 1H, dd, J = 15.4, 11.2 Hz; δ_C 144.1), and (6.44, 1H, dd, J = 15.4, 11.2 Hz; δ_C 129.8)] respectively, which indicated the presence of (2' *E*, 4' *E*) form. The change of C-2' configuration from *Z* to *E* form affected the chemical shift of the H-4 to be a little upfield at δ_H 6.03 (1H, dd, J = 7.8, 3.2 Hz; δ_C 74.1).

Table 55: NMR spectroscopic data for (**73**), (400 and 100 MHz, δ ppm)[a]

Position	^{1}HNMR (*J* in Hz)	^{13}CNMR	COSY	HMBC	NOESY
2	3.85 (d, 5.1)	79.1	3	4, 5, 12	3*β*, 13*β*
3	α 2.58 (dd, 7.8, 15.6)	36.8	2, 4	2, 4	4
	β 2.01 (br dd, 3.2, 5.1)			2, 5, 12	2
4	6.03 (dd, 3.2, 7.8)	74.1	3	2, 12, 1'	2α, 11
5	-	47.8	-	-	-
6	-	42.5	-	-	-
7	α 1.65 ovlp	21.9	8	6, 10, 15	14
	β 2.10 (dd, 6.3, 12.2)				
8	1.99 m	27.9	7	6, 10	14
9	-	140.3	-	-	-
10	5.47 (br d, 5.3)	118.5	11, 16	6, 7, 16	
11	3.90 (br d, 5.3)	66.8	10	7, 9, 10	4
12	-	65.4	-	-	-
13	α 3.15 (d, 4.0)	48.1	-	2, 12	
	β 2.84 (d, 4.0)				
14	0. 81s	6.6	-	4, 5, 6, 12, 13	13*β*
15	4.14, s	63.1	-	5, 6, 7, 11, 1"	14
16	1.72 s	23.2	8, 10	8, 9, 10	10
1'-CO	-	165.6	-	-	-
2'	5.93 (d, 15.4)	122.1	3'	1', 3'	2
3'	7.25 (dd, 11.2, 15.4)	144.1	4', 2'	1', 4', 5'	5'
4'	6.44 (dd, 11.2, 15.4)	129.8	3', 5'	2', 3', 6'	2', 6'
5'	6.10 (dd, 6.2, 15.4)	141.2	4', 6'	3', 6'	3'
6'	3.98 (t, 6.4)	76.6	5', 7'	4', 5', 7', 8'	4', 8'
7'	3.68 (m, 5 lines 6.4)	70.6	6', 8'	5', 6', 8'	2, 5'
8'	1.20 (d, 6.3)	19.1	7'	6', 7'	6'
1"-CO	-	165.2	-	-	-
2"	5.82 (br d, 0..9)	117.2	4", 6"	3", 4", 6"	14, 4"
3"	-	156.1	-	-	-
4"	2.41 (t, 5.8)	43.8	2", 5"	2", 3", 5", 6"	
5"	(3.76~3.84) m	59.7	3"	3", 4"	
6"	2.20 (br d, 0..9)	19.0	2", 4"	1", 2", 3", 4"	2"

[a] The assignments were based on DEPT, ^{1}H-^{1}H COSY, HSQC, and HMBC experiments, and recorded in $CDCl_3$

The relative configuration of (**73**) was revealed based on NOESY analysis and coupling constants of geminal and vicinal protons. In trichothecane moiety, the NOESY correlations of H-11/H-4, H-11/H-15*α*, and H-11/H-3*α* demonstrated that these groups were co facial, while H-2, H-13, and CH_3-14 were speculated to be oriented in the opposite direction according to the NOE signals of H-2/ H-3*β*, H-13*β*, and H-2'. The H-7' proton in (**73**) appeared at δ_H 3.68 as five-lines multiplets with J 6',7' = J 7',8' = 6.4 Hz, which established the stereochemistry at C-6', C-7' as *threo* (C-6'*R*, C-7'*R*), the same as is found in the A-series trichoverroids. According to all of the above evidences, the

structure corresponds to that of (2' *E*,4' *E*)-isotrichoverrin A which previously reported from *Myrothecium verrucaria*[292].

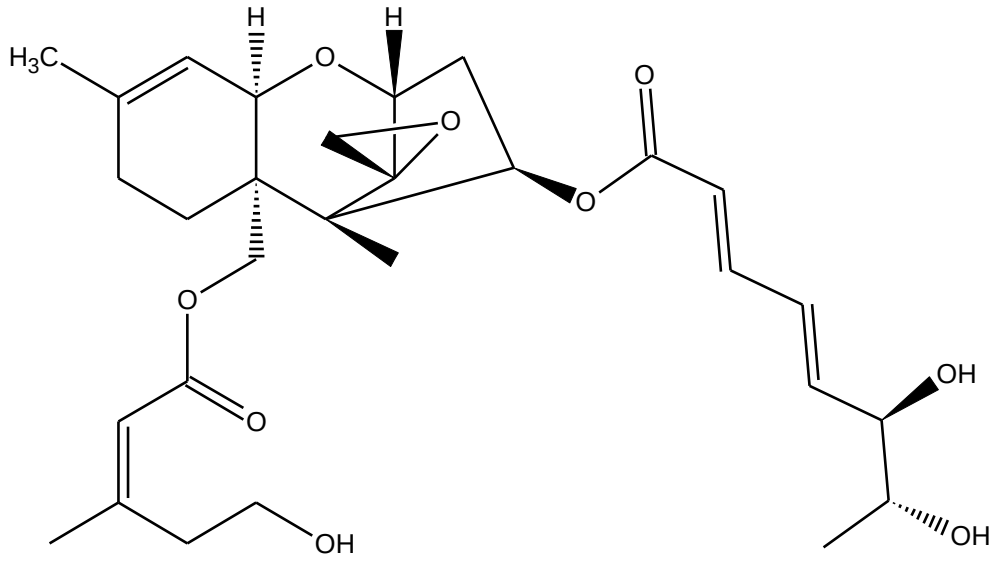

73

5.2.1.18 Isotrichoverrin B

Isotrichoverrin B (**74**) was obtained as a white amorphous solid (2.8 mg), the Positive HR-ESI-MS exhibited a strong peak at *m/z* 550.2690 $[M+NH_4]^+$ indicating a molecular formula of $C_{29}H_{40}O_9$ (calcd. 550.2678), required 10 double bond equivalents (DBE). Compound (**74**) revealed the molecular weight like trichoverrin A (**72**), which suggested the same skeleton.

The ^{1}H NMR spectrum (**Table 56**) of (**74**) was almost identical to that of trichoverrin A (**72**). However, significant differences were observed in the chemical shifts of two protons signals ascribable to the C-6' and C-7' position. Trichoverrin A (**72**), showed at [δ_H 4.05, 1H, br d, J = 6.3 Hz), H-6'] and [δ_H 3.68, 1H, m (5 lines) J = 6.3 Hz, H-7'], while (**74**) gave [δ_H 4.27, 1H, br t, J = 4.6 Hz, H-6'] and [3.92, 1H, m (5 lines, J = 6.3 Hz, H-7'] in their ^{1}H NMR spectra.

Carefully comparison of ^{13}C NMR data (**Table 59**) for (**74**) with those measured for (**72**) showed good accordance except for the signals due to the C-5' and C-6' positions which appeared upfield at (δ_C 141.1, C-5') and (δ_C 75.3, C-6') instead of (δ_C 142.1, C-5') and (δ_C 76.2, C-6') in (**72**).

Table 56: NMR spectroscopic data for **(74)** (400 and 100 MHz, δ ppm)[a]

Position	^{1}HNMR (*J* in Hz)	^{13}CNMR	COSY	HMBC	NOESY
2	3.87 (d, 5.2)	79.1	3	4, 5, 12	8, 13β, 2"
3	α 2.58 (dd, 7.7, 15.5)	36.8	2, 4	2, 4	11
	β 1.97 (br dd, 3.2, 5.2)			2, 5, 12	2
4	6.25 (dd, 3.2, 7.7)	75.0	3	2, 5, 6, 12, 1'	11
5	-	48.5	-	-	-
6	-	43.5	-	-	-
7	α 2.11 m	21.9	8	6, 8, 11, 15	13, 15
	β 1.56 (br dd, 4.9, 12.6)				
8	2.01 m	27.8	7	6,7, 9, 10, 16	15
9	-	140.5	-	-	-
10	5.49 (br d, 5.7)	118.5	11, 16	5, 6, 7, 11, 16	2
11	4.02 (br d, 5.7)	66.6	10	7, 9, 10	3α, 4
12	-	65.8	-	-	-
13	2.85 (d, 4.0)	48.3	-	2, 5, 12	7
	3.18 (d, 4.0)				
14	0. 81s	6.7	-	2, 4, 5, 6, 12, 13	13, 15, 2"
15	4.11 (d, 12.4)	63.5	-	5, 6, 7, 11, 1'	14
	4.15 (d, 12.4)				
16	1.72 s	23.2	8, 10	8, 9, 10	10
1'-CO	-	166.1	-	-	-
2'	5.70 (d, 11.3)	118.0	3'	8', 1'	14
3'	6.63 (t, 11.3)	143.9	2', 4'	7', 1'	
4'	7.55 (dd, 11.3, 15.6)	127.5	3', 5', 6'	2', 3', 6'	14, 6'
5'	6.15 (dd, 5.1, 15.5)	141.1	4', 6'	6'	7', 8'
6'	4.27 (br t, 4.6)	75.3	5', 7'	-	5', 7', 8'
7'	3.92 m	70.2	6', 8'	-	5', 6', 8'
8'	1.16 (d, 6.3)	17.9	7'	6', 7'	5', 6', 7'
1"-CO	-	165.9	-	-	-
2"	5.88 (br d, 0.9)	116.9	4", 6"	1", 3", 4", 6"	2, 14, 6"
3"	-	157.0	-	-	-
4"	2.43 (t, 5.7)	42.8	2", 5"	2", 3", 5", 6"	2, 6"
5"	3.80 (br q 5.7)	59.6	4"	3"	7', 2"
	3.88 ovlp				
6"	2.20 (br d, 0.9)	19.2	2", 4"	1", 2", 3", 4"	14, 2"

[a] The assignments were based on DEPT, ^{1}H-^{1}H COSY, HSQC, and HMBC experiments, and recorded in $CDCl_3$

The ^{1}H and ^{13}C NMR signals ascribable to C-6' and C-7' suggest that (**74**) is an epimer at C-6' position. The multiplicity of H-7' was not clear, therby this assumption was corroborated by carefully coparison of the NMR data of (**74**) with those of (**71**) and (**72**), as well as the NOESY correlations between H-6'/H5', H-7', and H-8', between H7'/H-5', H6', and H-8'.

The compound was thus identified as Isotrichoverrin B (C6' *R*, C7' *S*) which was isolated only one time from *Myrothecium verrucaria*[292,295].

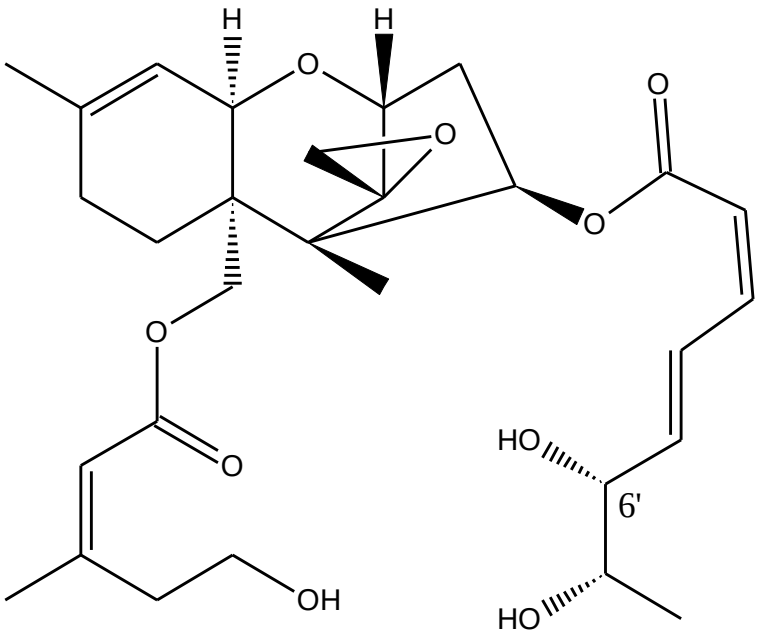

74

5.2.1.19 (2'*E*, *4*'*E*)-Isotrichoverrin B

Compound (**75**) was isolated as a colourless solid (2.0 mg), the Positive HRESI-MS exhibited a strong peak at *m/z* 550.3011 $[M+NH_4]^+$ indicating a molecular formula of $C_{29}H_{40}O_9$ (calcd. 550.2998) bearing 10 double bond equivalents (DBE). Compound (**75**) had the same molecular weight as Isotrichoverrin B (**74**), which suggested the same skeleton.

The ^{1}H NMR spectrum (**Table 57**) of (**75)** was highly similar to that of Isotrichoverrin B (**74**), however, the crucial distinctions were observed in the chemical shifts and the coupling constant of the vinylic methines H-2', H3' and H-4' at [δ_H (5.92, 1H, d, J = 15.3 Hz; δ_C 122.8), (7.26, 1H, dd, J = 15.3, 11.2 Hz; δ_C 144.0), and (6.42, 1H, dd, J =15.3, 11.2 Hz; δ_C 129.9)] respectively, which indicated the presence of (2' *E*, 4' *E*) form.

Table 57: NMR spectroscopic data for (**75**) (400 and 100 MHz, δ ppm)[a]

Position	^{1}HNMR (*J* in Hz)[b]	^{13}CNMR	COSY	HMBC	NOESY [b]
2	3.85 (d, 5.2)	79.2	3	4, 5, 11, 12	3β, 13β
3	α 2.56 (br dd, 7.7, 15.4) β 1.99 (br dd,3.4, 5.2)	36.8	2, 4	4, 6 2, 5, 12	4 2
4	6.03 (dd, 3.4, 7.7)	75.5	3	6, 12, 1'	11
5	-	48.9	-	-	-
6	-	43.1	-	-	-
7	α 1.67 m β 2.08 (dd, 6.1, 12.2)	21.6	8	8, 11 6, 8, 15	13, 15
8	2.00 m	28.0	7	9, 10	-
9	-	140.0	-	-	-
10	5.47 (br d, 5.7)	118.5	11, 16	6, 8, 16	15
11	3.90 (br d, 6.7)	66.6	10, 16	7, 9, 10	3α, 4
12	-	65.5	-	-	-
13	α 3.15 (d, 4.0) β 2.84 (d, 4.0)	48.0	-	2, 5, 12	14
14	0.81 s	6.7	-	4, 5, 6, 12	8, 13β, 15, 3', 2"
15	4.13 s	63.1	-	5, 6, 7, 11, 1"	13, 14
16	1.72 s	23.2	10, 11	8, 9, 10	10
1'-CO	-	166.2	-	-	-
2'	5.92 (d, 15.3)	122.8	3'	1', 4'	14, 4', 4"
3'	7.26 (dd, 11.2, 15.3)	144.0	2', 4'	1', 2', 5'	14, 5'
4'	6.42 (dd, 11.2, 15.3)	129.9	3', 5'	2', 3', 6'	6', 8'
5'	6.15 (dd, 6.3, 15.3)	140.4	4', 6'	3', 6'	3b, 8'
6'	4.22 (br dd, 3.4, 6.3)	75.5	5', 7'	-	4', 8'
7'	3.92 ovlp.	70.2	6', 8'	5'	5'
8'	1.14 (d, 6.4)	17.6	7'	6', 7'	4', 6'
1"-CO	-	166.2	-	-	-
2"	5.82 (br d, 0.9)	117.2	6"	1", 4", 6"	14, 6"
3"	-	157.0	-	-	-
4"	2.41 (t, 5.9)	43.8	5"	2", 3", 5", 6"	2"
5"	3.81 m	59.8	4"	3"	2"
6"	2.20 (br d, 0.9)	18.9	2"	1", 2", 3", 4", 5"	15, 2"

[a] The assignments were based on DEPT, ^{1}H-^{1}H COSY, HSQC, and HMBC experiments, and recorded in $CDCl_3$. [b] data recorded in 600MHz.

The relative configuration of (**75**) was revealed based on NOESY analysis and coupling constants of geminal and vicinal protons. In trichothecane moiety, the NOESY correlations of H-11/H-4, and H-11/H-3α demonstrated that these groups were co facial, while H-2, H-13, and CH_3-14 were speculated to be oriented in the opposite direction according to the NOE signals of H-2/ H-3*β*, H-2/H-13*β*, and CH_3-14/H-2'. The multiplicity of H-7' which resonating at δ_H 3.92 was not clear, however, carefully comparison of the NMR data of (**75**) with those of (**73**) and (**74**) (**Table 58** and **Table 59**), established the stereochemistry at C-6', C-7' as *erythro*, the same as is found in the B-series trichoverroids.

According to all of the above signs, the structure corresponds to that of (2'*E*, 4'*E*)-isotrichoverrin B which previously reported from *Myrothecium verrucaria*.[292].

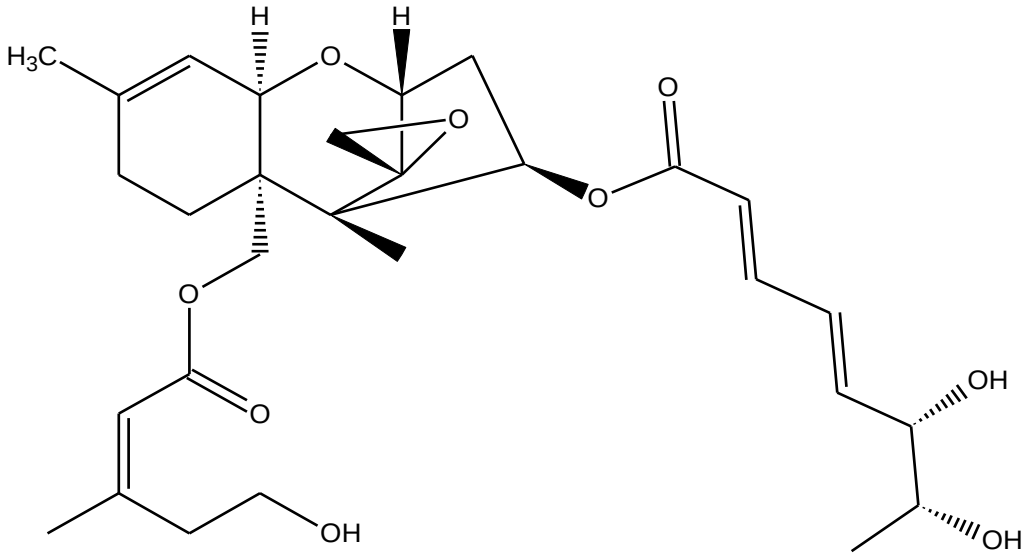

75

Herein we should note that the close structural relationship of these natural products suggested a common biogenetic pathway. The A- and B-series assignments were based on the observed proton couplings between H-6' and H-7'. The 2',4'-diene functionality found in the naturally occurring trichoverroids and macrocyclic trichothecenes nearly always has the 2'*Z*,4'*E* configuration, with the only reported exceptions being the (2'*E*)-isotrichoverrol A (**70**) (2'*E*)-isotrichoverrol B (**71**), (2'*E*)-isotrichoverrin A (**73**) and (2'*E*)-isotrichoverrin B (**75**). The stereochemistry of the diene chains are readily apparent from the analysis of the proton NMR spectra. Thus for the 2'(*E*),4'(*E*)-dienes, $J_{2',3'}$ and $J_{4',5'}$ J = 15-16 Hz (e.g., (**70**) and (**71**), (**Table 58**). For the corresponding congeners with the 2'(*Z*),4' (*E*)- diene configuration, $J_{2',3'}$ = 11.3 Hz and $J_{4',5'}$ = 15.5 Hz (e.g., trichoverrins (**72)**, and (**74**).

In the typical (2'*Z*,4'*E*)- trichoverroids, the H-4' proton is found at highest frequency (around 7.50 ppm) but moves upfield by about 1 ppm in the 2'*E*,4'*E* congeners. In these latter compounds, the H-3' resonance moves downfield by about 1 ppm and becomes the highest-frequency signal in these compounds (see **Table 58**).

Another notable effect is observed in the ^{13}C-NMR spectra of (**73**) and (**75**), where the C-2' resonance shift downfield by about 4 ppm (relative to the carbon signals in the corresponding 2'*Z* congeners; e.g., (**72**) and (**74**) due to the *gauche* effect (**Table 59**). The change of C-2' configuration from *Z* to *E* form affected the chemical shift of the H-4 to be a little upfield at ca. 0.2 ppm.

Table 58: Comparison of ^{1}H NMR assignments for (**72**), (**73**), (**74**), and (**75**)

Position	(72)	(73)	(74)	(75)
2	3.87 (d, 5.2)	3.85 (d, 5.1)	3.87 (d, 5.2)	3.85 (d, 5.2)
3	1.97 (br dd,3.3, 5.2)	2.01 (br dd, 3.2, 5.1)	1.97 (br dd, 3.2, 5.2)	1.99 (br dd,3.4, 5.2)
	2.58 (br dd, 7.7, 15.7)	2.58 (dd, 7.8, 15.6)	2.58 (dd, 7.7, 15.5)	2.56 (br dd, 7.7, 15.4)
4	6.25 (dd, 3.3, 7.7)	6.03 (dd, 3.2, 7.8)	6.25 (dd, 3.2, 7.7)	6.03 (dd, 3.4, 7.7)
5	-	-	-	-
6	-	-	-	-
7	1.56 m	1.65 ovlp	1.56 (br dd, 4.9, 12.6)	1.67 m
	2.11 m	2.10 (dd, 6.3, 12.2)	2.11 m	2.08 (dd, 6.1, 12.2)
8	2.01 (br dd, 3.2, 5.2)	1.99 m	2.01 m	2.00 m
9	-	-	-	-
10	5.49 (br d, 5.4)	5.47 (br d, 5.3)	5.49 (br d, 5.7)	5.47 (br d, 5.7)
11	4.01 (br d, 6.3)	3.90 (br d, 5.3)	4.02 (br d, 5.7)	3.90 (br d, 6.7)
12	-	-	-	-
13	2.85 (d, 4.0)	2.84 (d, 4.0)	2.85 (d, 4.0)	2.84 (d, 4.0)
	3.18 (d, 4.0)	3.15 (d, 4.0)	3.18 (d, 4.0)	3.15 (d, 4.0)
14	0.81 s	0. 81s	0. 81s	0.81 s
15	4.11 (d, 12.4)	4.14, s	4.11 (d, 12.4)	4.13 s
	4.14 (d, 12.4)		4.15 (d, 12.4)	
16	1.72 s	1.72 s	1.72 s	1.72 s
1'-CO	-	-	-	-
2'	5.70 (d, 11.3)	5.93 (d, 15.4)	5.70 (d, 11.3)	5.92 (d, 15.3)
3'	6.61 (d, 11.3)	7.25 (dd, 11.2, 15.4)	6.63 (t, 11.3)	7.26 (dd, 11.2, 15.3)
4'	7.57 (br dd, 11.3, 15.5)	6.44 (dd, 11.2, 15.4)	7.55 (dd, 11.3, 15.6)	6.42 (dd, 11.2, 15.3)
5'	6.08 (dd, 5.3, 15.5)	6.10 (dd, 6.2, 15.4)	6.15 (dd, 5.1, 15.5)	6.15 (dd, 6.2, 15.3)
6'	4.05 (br d, 6.3)	3.98 (t, 6.4)	4.27 (br t, 4.6)	4.22 (br dd, 3.4, 6.3)
7'	3.68 m (5 lines *J*=6.3)	3.68 q (5 lines) 6.4	3.92 m	3.92 (br dd, 3.4, 6.3)
8'	1.21 (d, 6.3)	1.20 (d, 6.3)	1.16 (d, 6.3)	1.14 (d, 6.4)
1"-CO	-	-	-	-
2"	5.88 (br d, 1.1)	5.82 (br d, 0..9)	5.88 (br d, 0..9)	5.82 (br d, 0.9)
3"	-	-	-	-
4"	2.42 (t, 5.7)	2.41 (t, 5.8)	2.43 (t, 5.7)	2.41 (t, 5.9)
5"	3.79 m	(3.76~3.84) m	3.80 (br q 5.7)	3.81m
	3.86 (br dd 2.4, 5.7)		3.88 ovlp	
6"	2.20 (br d, 1.1)	2.20 (br d, 0..9)	2.20 (br d, 0..9)	2.20 (br d, 0.9)

[a] The assignments were recorded in (400 and 125 MHz, δ ppm) $CDCl_3$.

Table 59: Comparison of ^{13}C NMR assignments for (**72**), (**73**), (**74**), and (**75**)[a]

Position	(72)	(73)	(74)	(75)
2	78.9	79.1	79.1	79.2
3	36.7	36.8	36.8	36.8
4	74.8	74.1	75.0	75.5
5	48.5	47.8	48.5	48.9
6	42.7	42.5	43.5	43.1
7	21.7	21.9	21.9	21.6
8	27.7	27.9	27.8	28.0
9	140.5	140.3	140.5	140.0
10	118.4	118.5	118.5	118.5
11	66.4	66.8	66.6	66.6
12	65.8	65.4	65.8	65.5
13	48.4	48.1	48.3	48.0
14	6.5	6.6	6.7	6.7
15	63.3	63.1	63.5	63.1
16	23.0	23.2	23.2	23.2
1'	166.1	165.6	166.1	166.2
2'	118.0	122.1	118.0	122.8
3'	143.8	144.1	143.9	144.0
4'	127.3	129.8	127.5	129.9
5'	142.1	141.2	141.1	140.4
6'	76.2	76.6	75.3	75.5
7'	70.2	70.6	70.2	70.2
8'	18.7	19.1	17.9	17.6
1''	165.9	165.2	165.9	166.2
2''	116.7	117.2	116.9	117.2
3''	157.1	156.1	157.0	157.0
4''	43.4	43.8	42.8	43.8
5''	59.4	59.7	59.6	59.8
6''	19.0	19.0	19.2	18.9

[a] All the assignments were based on DEPT, HSQC, and HMBC experiments, and recorded in (400 and 125 MHz, δ ppm) in $CDCl_3$.

5.2.2 Bioactivity test results for the isolated compounds

From the report of WHO in 2015, lower respiratory tract infection is the third cause of death worldwide, with approximately 3.19 million deaths (http://www.who.int/media-centre/factsheets/fs310/en/). One of the important causes of mortality is antimicrobial resistance which leads to a decrease in the efficacy of antimicrobial agents. The death rate of patients who were infected by MRSA is about 64% higher than non-resistant *S. aureus* infected patients (http://www.who.int/mediacentre/factsheets/fs194/en/). Nowadays, the problem of antimicrobial resistance is growing higher. WHO has been reported that the world is lack of new antibiotics to treat the antimicrobial-resistant pathogens. Therefore, the priority pathogens list (PPL) that includes 12 families of antibiotic-resistant bacteria was published by WHO to guide researchers for new drug discovery and development (http://www.who.int/mediacentre/news/releases/2017/bacteria-antibiotics-needed/en/).

As described in (introduction), macrocyclic trichothecenes (e.g., roridins, verrucarins and satratoxins) are considered to be some of the most toxic trichothecenes and are generally more toxic than simple trichothecenes[296]. Therefore, we decided to test the secondary metabolites we have isolated for their antimicrobial and anticancer activities in our studies.

Antimicrobial activity

Some of the isolated compounds were evaluated for their antibacterial activity against

two Gram positive bacteria: *Staphylococcus aureus* (ATCC 25923) and *Staphylococcus epidermidis* (ATCC 12228); four Gram negative bacteria: *Escherichia coli* (ATCC 25922), *Enterobacter cloacae* (ATCC 13047), *Klebsiella pneumoniae* (ATCC 13883) and *Pseudomonas aeruginosa* (ATCC 227853); as well as they were were evaluated for their antifungal activity against three pathogenic fungi: *Candida albicans* (ATCC 10231), *Candida tropicalis* (ATCC 13801) and *Candida glabrata* (ATCC 28838).

It is clear from the evaluation data that there is no one of the tested compounds inhibited the tested bacterial strains neither Gram positive nor Gram negative, furthermore, they were moderately active against the tested pathogenic fungi (**Table 60**).

Table 60: Antimicrobial activity of some isolated compounds (MIC mg/ml, n = 3).

Microbe / **Compound**	***S. aureus***	***S. epidermidis***	***P. aeruginosa***	***K. pneumoniae***	***E. cloacae***	***E.coli***	***C. albicans***	***C. tropicalis***	***C. glabrata***
57	na	na	na	na	na	na	10/0.92	12/0.78	13/0.70
58	na	na	na	na	na	na	11/0.85	12/0.72	14/0.65
59	na	na	na	na	na	na	10/0.90	10/0.82	11/0.75
61	na	na	na	na	na	na	11/0.82	12/0.70	13/0.61
62	na	na	na	na	na	na	12/0.75	13/0.67	14/0.58
63	na	na	na	na	na	na	10/0.88	12/0.75	13/0.72
66	na	na	na	na	na	na	10/0.94	11/0.85	12/0.70
68	na	na	na	na	na	na	12/0.69	12/0.74	13/0.67
71	na	na	na	na	na	na	10/0.99	11/0.88	12/0.71
72	na	na	na	na	na	na	10/0.87	12/0.65	14/0.520
74	na	na	na	na	na	na	11/0.92	12/0.70	13/0.68
75	na	na	na	na	na	na	11/0.85	12/0.67	13/0.65
Netilmicin	20/0.2 $x10^{-3}$	26	21	24	21	23	nt	nt	nt
Amoxicillin	22	24	25	23	22	22	nt	nt	nt
5-fluocytocin	nt	nt	nt	nt	nt	nt	22	22	24
Amphotericin B	nt	nt	nt	nt	nt	nt	24	24	25

na: not active, nt: not tested

6. Summary

The search for new medically active compounds to overcome the countless diseases is one of the most relevant objectives worldwide. Medicinal plants were used previously in traditional medicine and even now for the treatment of several infections. However, the appearance of new diseases and new drug resistances induced the search for new sources of bioactive agents. Steadily over the years, the focus of interest has been shifted from plants towards microorganisms e.g. bacteria and fungi as a new source of natural products. Fungi play a crucial role in the pharmaceutical industry and agriculture due to their potential to produce secondary metabolites with diverse chemical structures and biological activities.

This dissertation investigates natural products from two fungi isolated from different biological sources. The identification of the purified fungi was preliminary based on culture and microscopic characteristics next, the obtained sequence was deposited in the GenBank nucleotide sequence database with a specific accession number. The isolates were scaled up under standard conditions, and the culture broths were usually extracted with ethyl acetate. The crude extracts were purified using various chromatographic methods, including CPC, silica gel columns, Sephadex LH-20, PTLC and HPLC. The isolated compounds were dereplicated by means of the Dictionary of Natural Products (DNP) and the Chemical Abstracts. Structure elucidation of novel compounds required application of more advanced NMR techniques such as HSQC, HMBC, and NOESY. Assigning absolute configuration was often the most difficult task in characterizing individual metabolites. To assign absolute configuration of the peptides encountered, a process of 2D NOESY and optical rotation were employed.

In general, many of the isolated compounds were investigated for various biological activities (e.g. as antimicrobial, antienzymatic agents,… etc.).

The crude extract of the soil-derived fungus *Aspergillus ochraceopetaliformis* which collected at Giza province, Egypt and cultivated in rice medium, exhibited significant antimicrobial activity against several pathogenic test microorganisms based on paper-disk diffusion assay.

In the TLC screening, the extract showed a low polar yellow band and numerous UV absorbing and fluorescent zones. The extract was defatted using cyclohexane and the methanolic part was pre-separated by column chromatography using silica gel. Further purification on Sephadex LH 20, by PTLC and HPLC, afforded **24** compounds, belonging to different chemical families.

19 alkaloids among them 4 new compounds named 8-OH-Echinulin (**38**), 27-28-epoxyechinulin (**39**), and neoechinulin F (**46**) and (12*R*)dehydroechinulin (**49**), as well as two cyclic peptide compounds Cyclo[Ala-Trp] (**33**), and Cyclo[Trp-Val] (**41**), six prenylated alkaloids (echinulin-type) preechinulin (**34**), tardioxopiperazine B (**35**), tardioxopiperazin A (**36**), echinulin (**37**), and Cyclo-L-2-tert-DMA-4,5,7-tri-DMA-Trp-L-Ala (**40**) which reported only one time as a minor compound and one indole diketopiperazine dimer eurocristine (**42**).

The other alkaloids were (neoechinulin-type) like neoechinulin A (**43**), variecolorin G (**44**), neoechinulin (**45**), neoechinulin D (**47**), dehydroechinulin (**49**), cryptoechinulin D (**50**), and cryptoechinulin B (**51**) and cristatumin D (**48**) which had open ring. Moreover, a new ochraceopyronoid (**52**) which had a rare lyxofuranosid, isotorachrysone-6-O-*α*-D-ribofuranoside (**53**) and the rare triterpene 2-*α*-hydroxydiploptero (**54**) which reported one time only. Besides, two anthraquinone derivatives named questin (**55**), and physcion (**56**) were identified. All of the isolated compounds have been tested for antimicrobial activity against several pathogenic microorganisms.

To the best of our knowledge, all of these metabolites recorded for the first time from *Aspergillus ochraceopetaliformis*

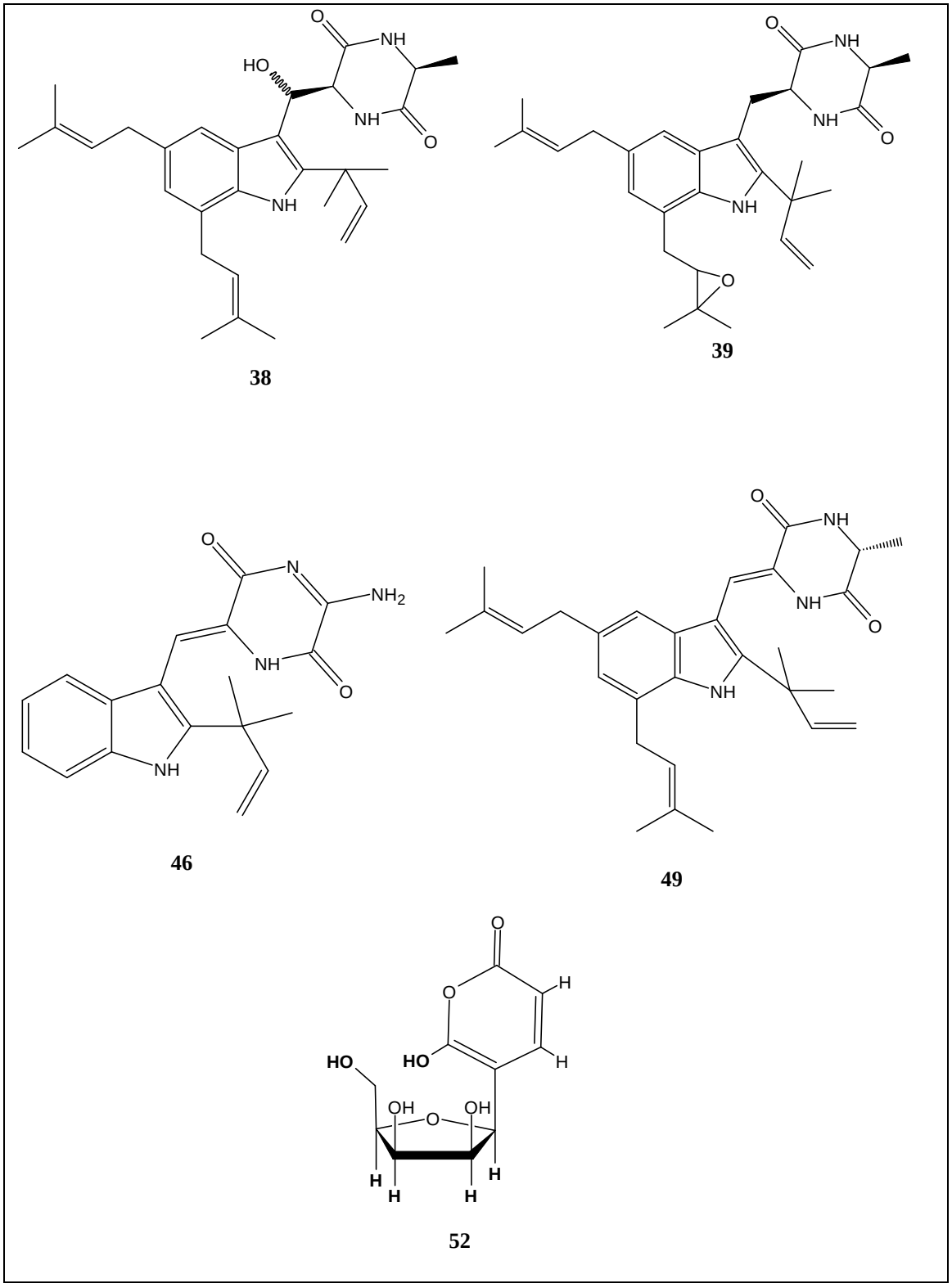

Figure 60: Chemical structures of the new compounds isolated from *Aspergillus* sp.

On the other hand, the endophytic fungal strain *Myrothecium verrucaria* was isolated from healthy wild medicinal plant datura (*Datura stramonium L.*) which collected from Wadi El Assuity, a protective area, Assiut Governorate, Upper Egypt in 2015 and cultivated in PDA medium. In the primary screening, the ethyl acetate extract of the endophytic fungus showed interesting characteristics during TLC. Moreover, the extract showed significant antimicrobial activity against six pathogenic microorganisms using agar well diffusion method. Further isolation and purification using CPC and HPLC afforded 19 compounds

Three new macrocyclic trichothecenes named miophytocen E (**60**), miophytocen F (**64**) and miophytocen G (**65**) were identified, as well as one new non-macrocyclic trichothecene named roridin G (**67**). Additionally, miophytocin D (**59**) was reported here for the first time from *Myrothecium verrucaria* and isolated only one time before.

The rest were known compounds and categorized into two groups: the first is the macrocyclic trichothecenes which have (roridoid type C-27) like roridin A (**57**), isororidin A (**58**), roridin J (**61**), 8-*α*-Hydroxyroridin H (**62**), and 8-*α*-Acetoxyroridin H (**63**), and (verrucaroid type C-29) such verrucarin A (**66**). The second group was non-macrocyclic trichothecenes and consist of trichoverroids like verrol (**68**), trichoverrol A (**69**), 2'*E* isotrichoverrol A (**70**), and 2'*E* isotrichoverrol B (**71**) and trichoverrins such as trichoverrin A (**72**), (2'*E*, 4'*E*) isotrichoverrin A (**73**), isotrichoverrin B (**74**), and (2'*E*, 4'*E*) isotrichoverrin B (**75**).

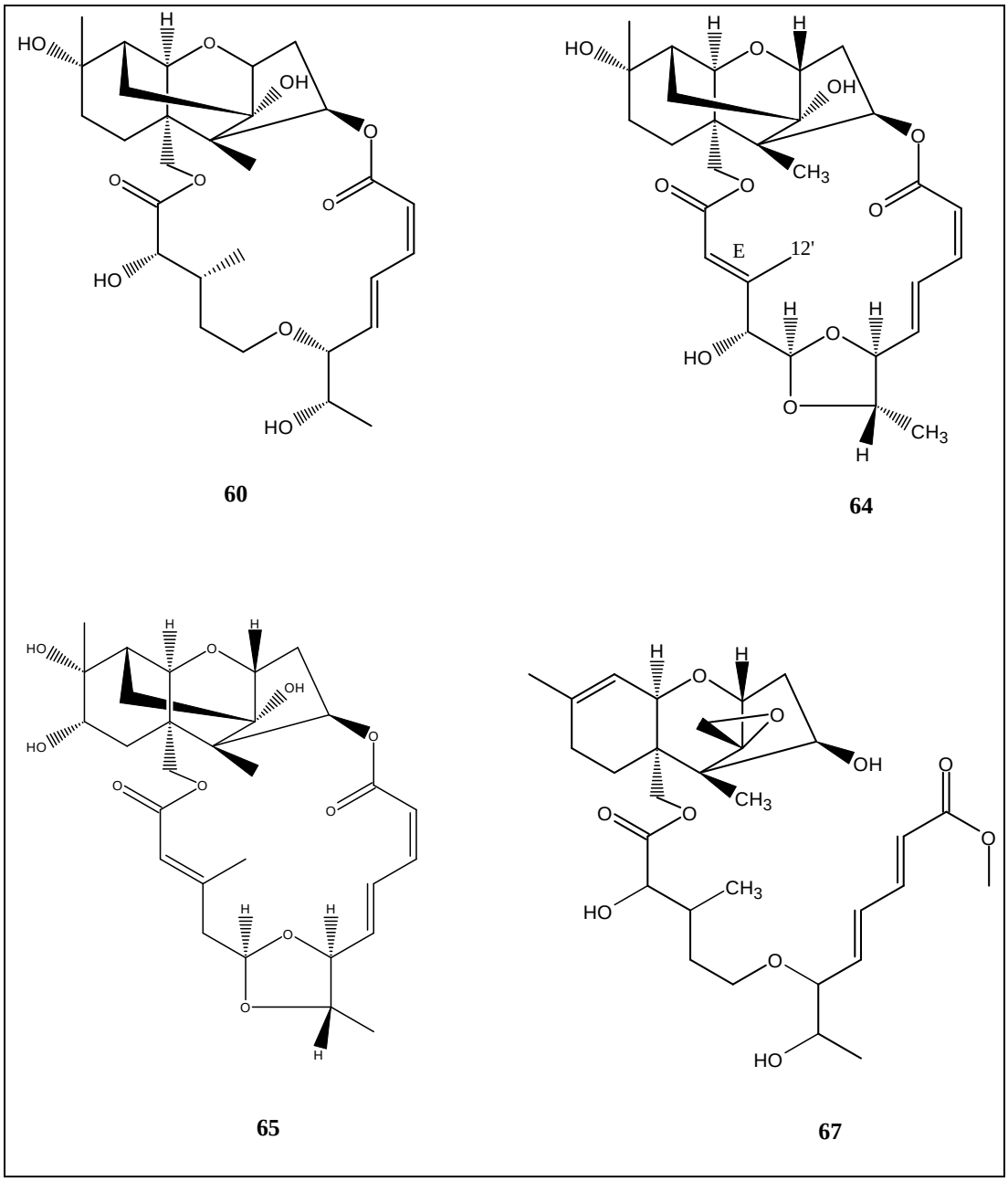

Figure 61: Chemical structures of the new compounds isolated from *Myrothecium* sp.

7. Appendices

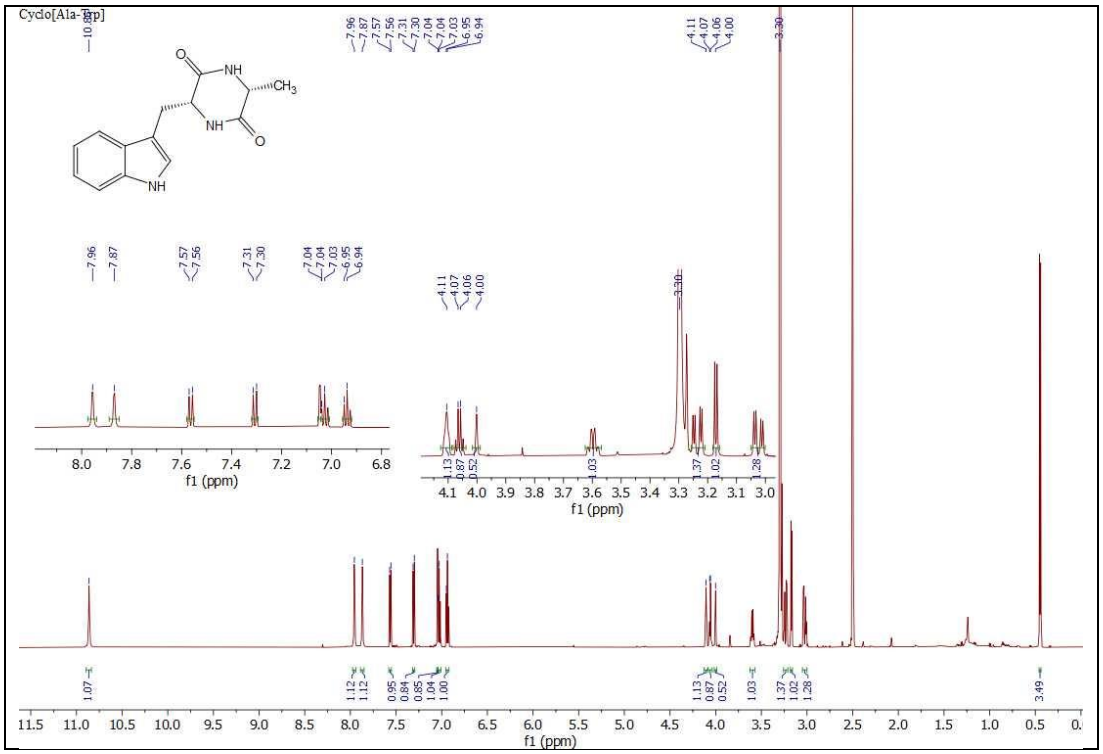

Appendix 1: ^{1}H NMR spectrum of Cyclo[Ala-Trp] (**33**) (DMSO-d_6)

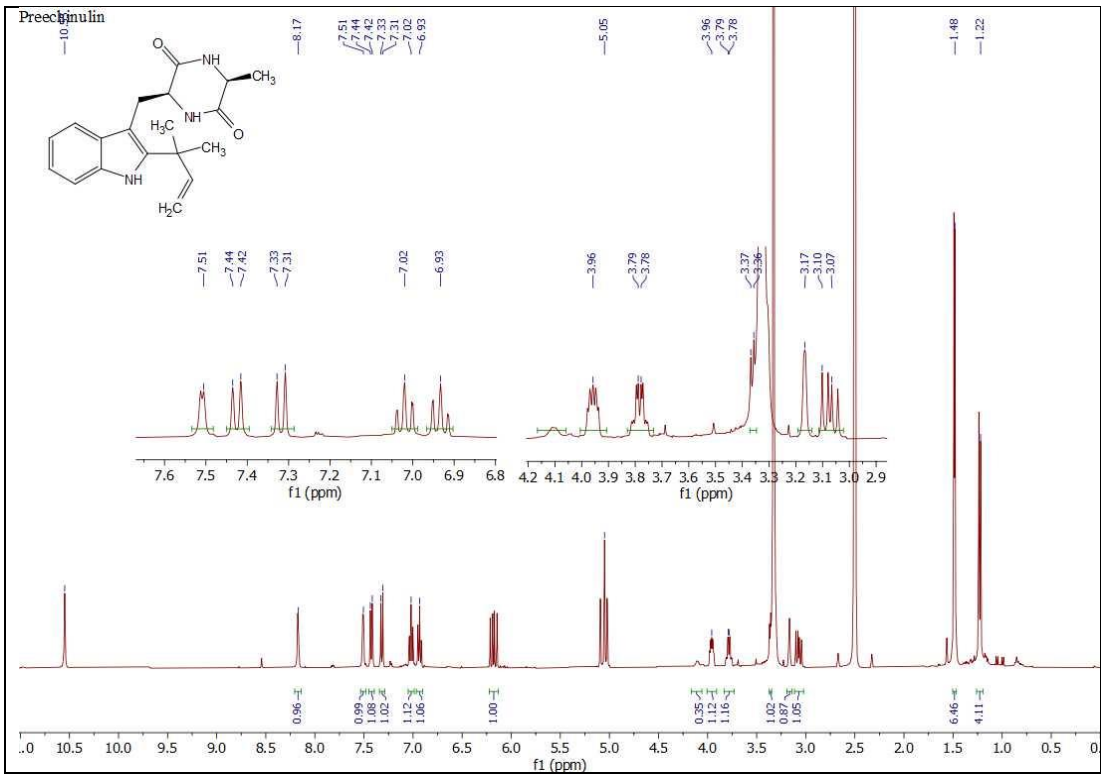

Appendix 2: ^{1}H NMR spectrum of preechinulin (**34**) (DMSO-d_6)

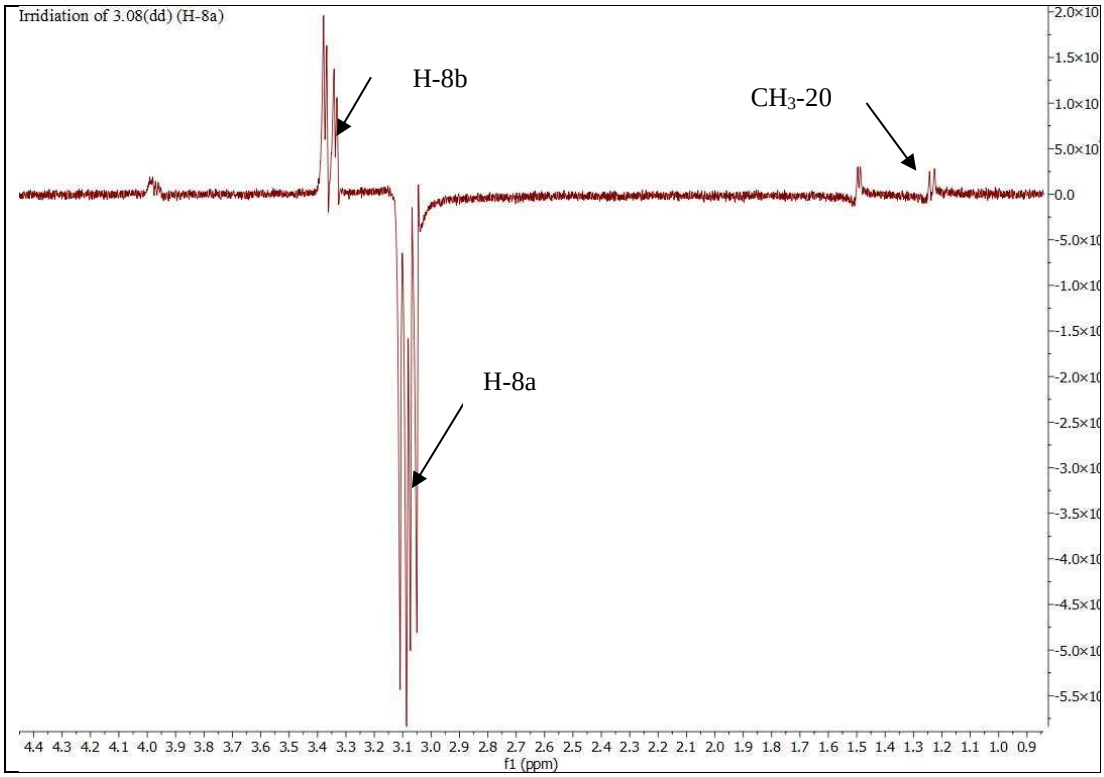

Appendix 3: Selected 1D NOE of preechinulin (**34**) (DMSO-d_6) (400MHz)

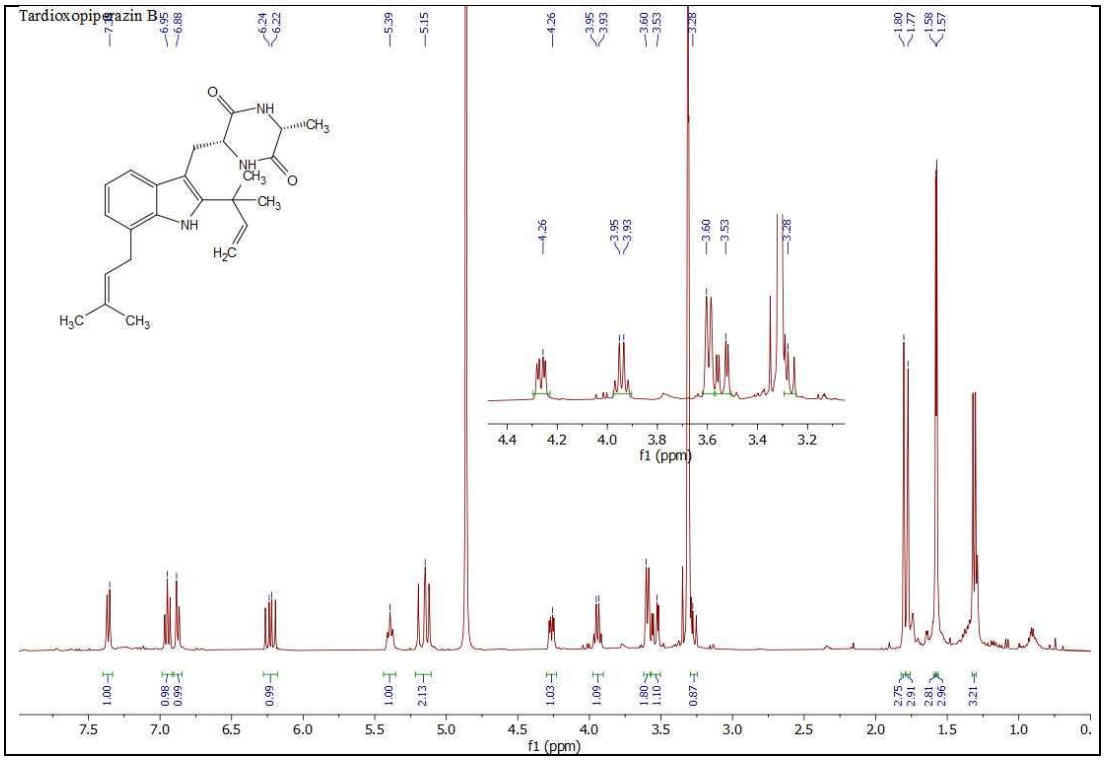

Appendix 4: ^{1}H NMR spectrum of Tardioxopiperazine B (**35**) (MeOD-d_4)

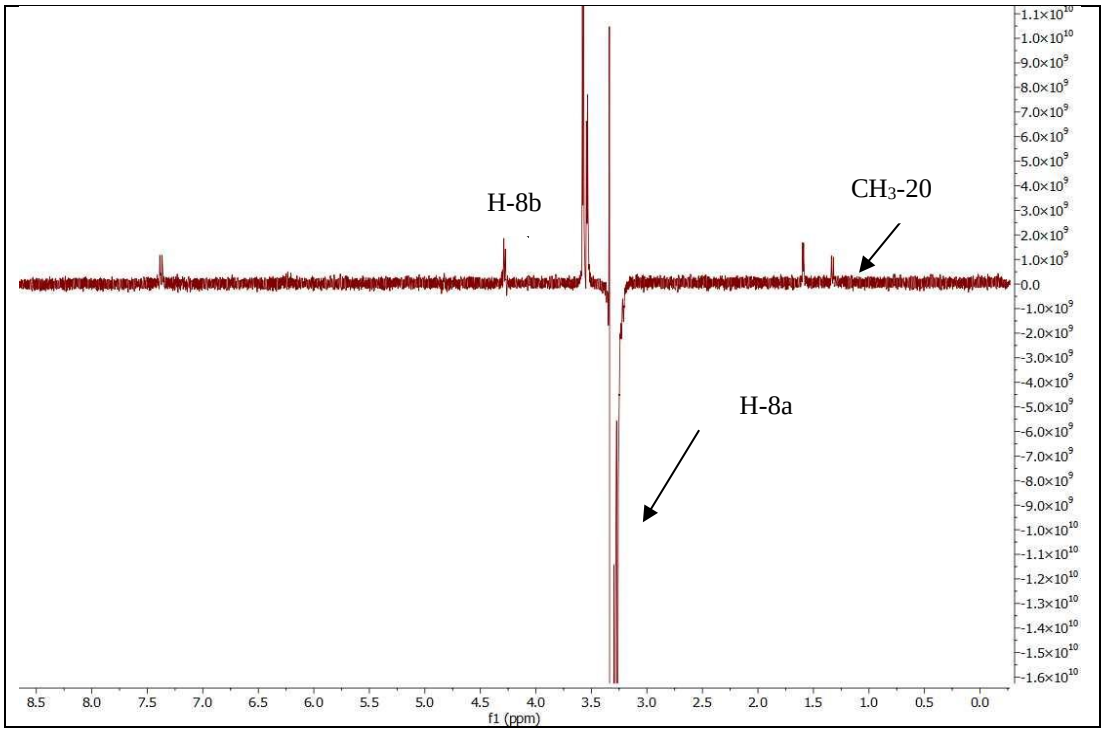

Appendix 5: Selected 1D NOE of Tardioxopiperazine B (**35**) (MeOD-d_4) (400MHz)

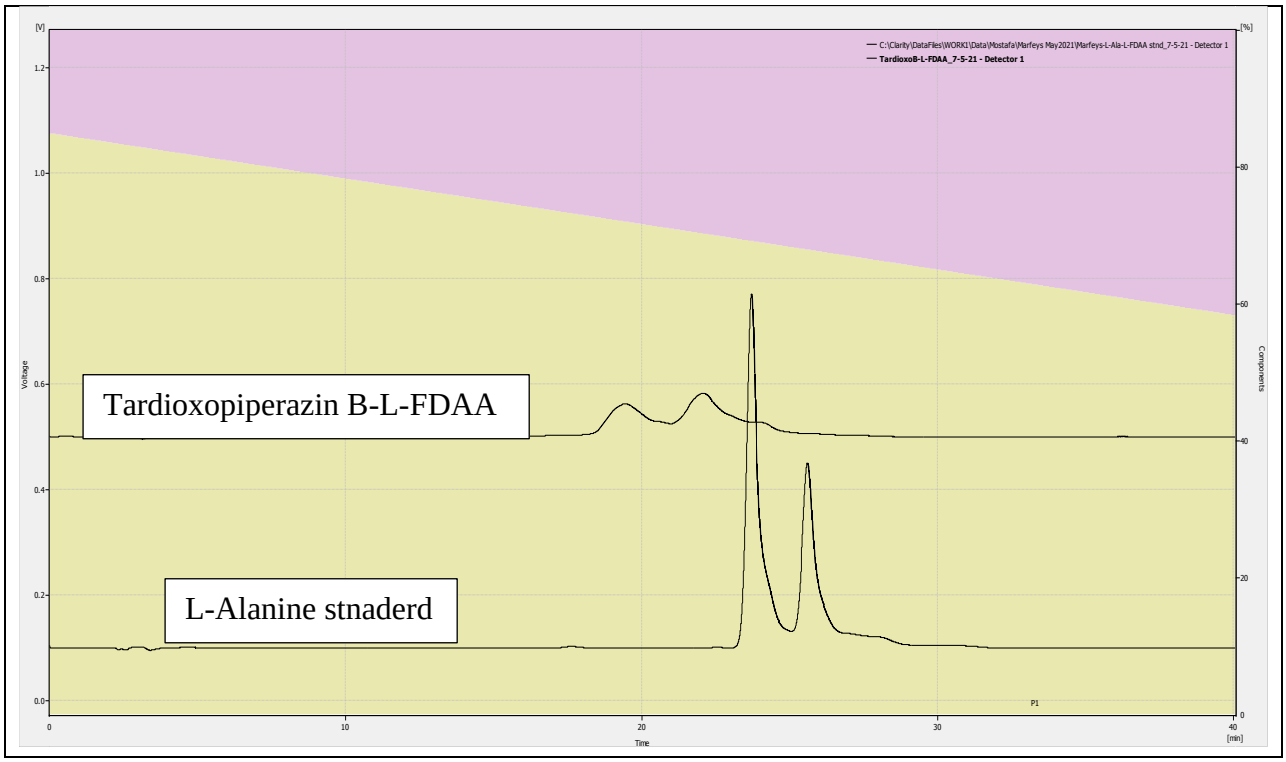

Appendix 6: HPLC analysis of of the acid hydrolyzate of Tardioxopiperazin B (**35**)

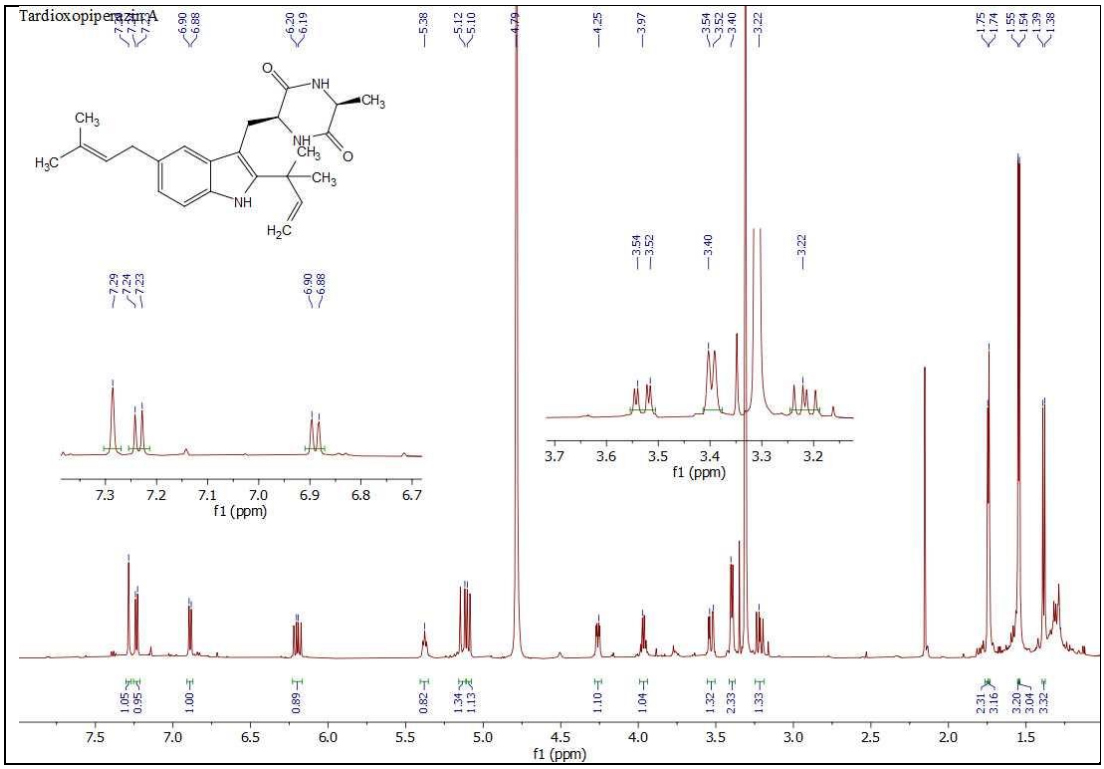

Appendix 7: ^{1}H NMR spectrum of Tardioxopiperazine A (**36**) (MeOD-d_4)

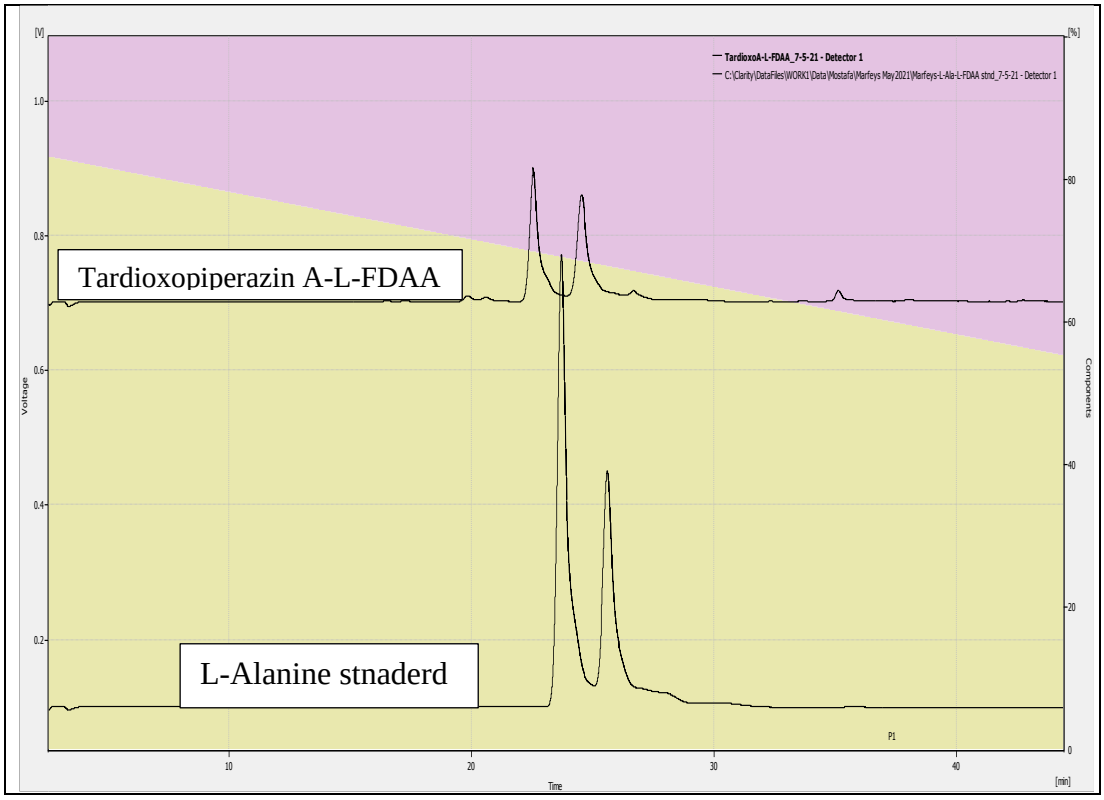

Appendix 8: HPLC analysis of of the acid hydrolyzate of Tardioxopiperazin A (**36**)

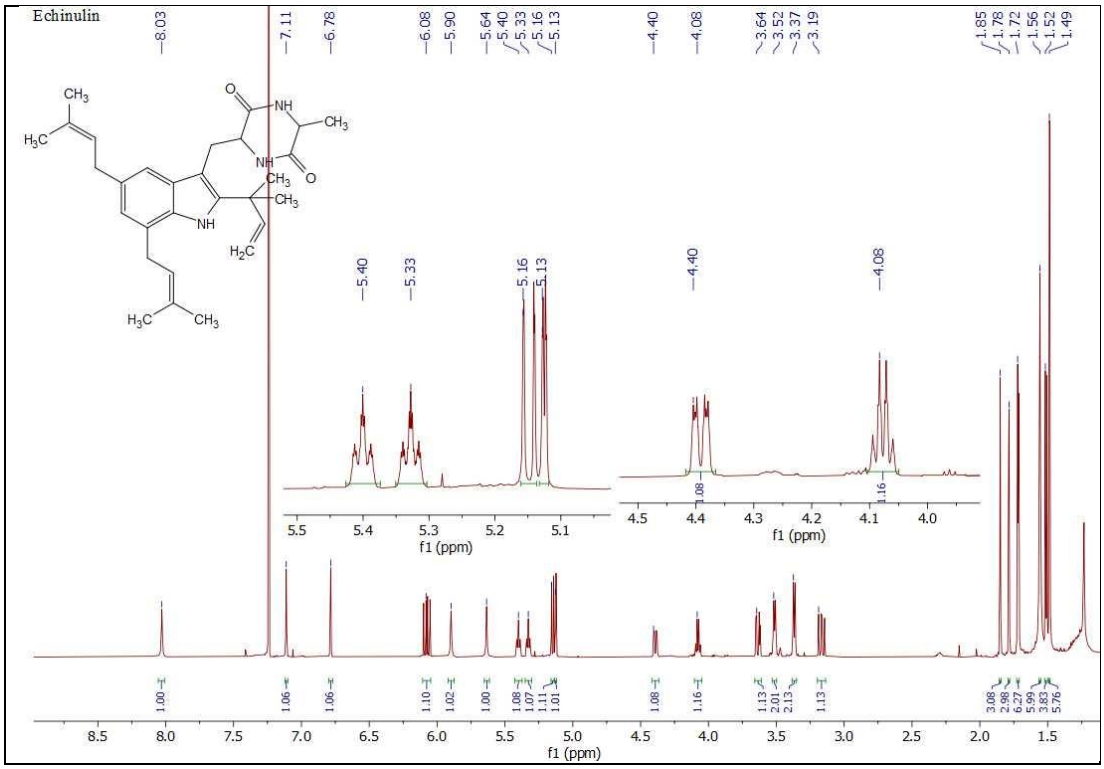

Appendix 9: ^{1}H NMR spectrum of Echinulin (**37**) ($CDCl_3$)

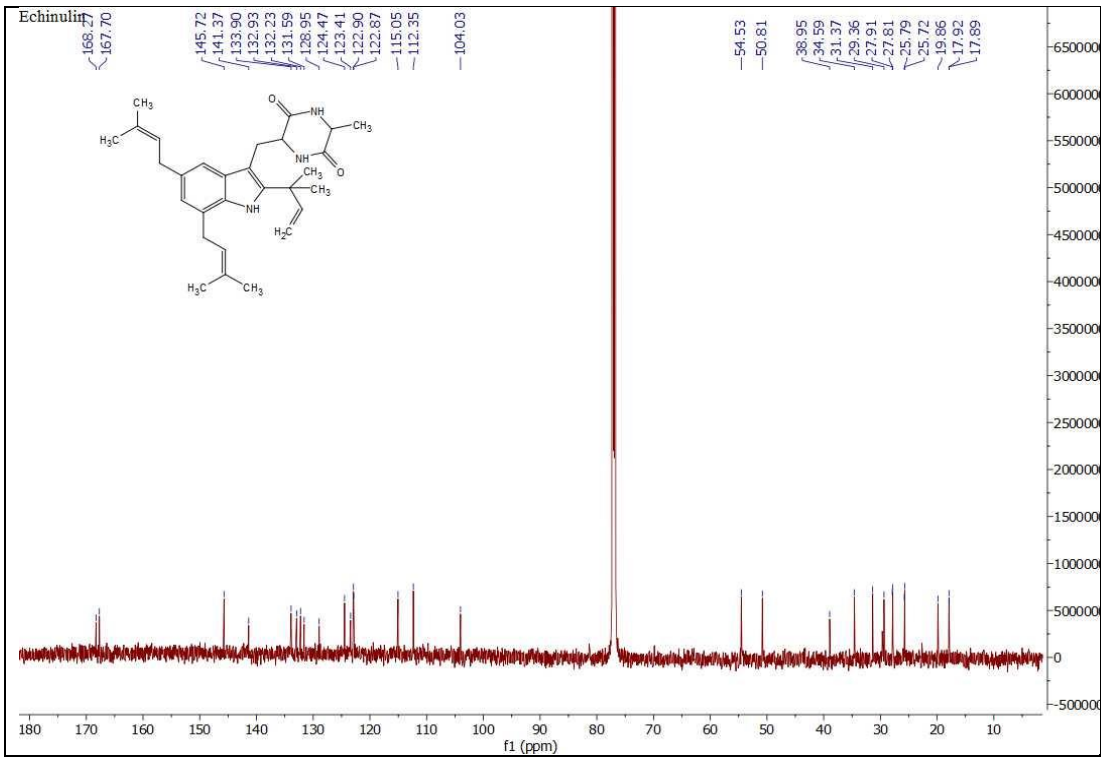

Appendix 10: ^{13}C NMR spectrum of Echinulin (**37**) ($CDCl_3$)

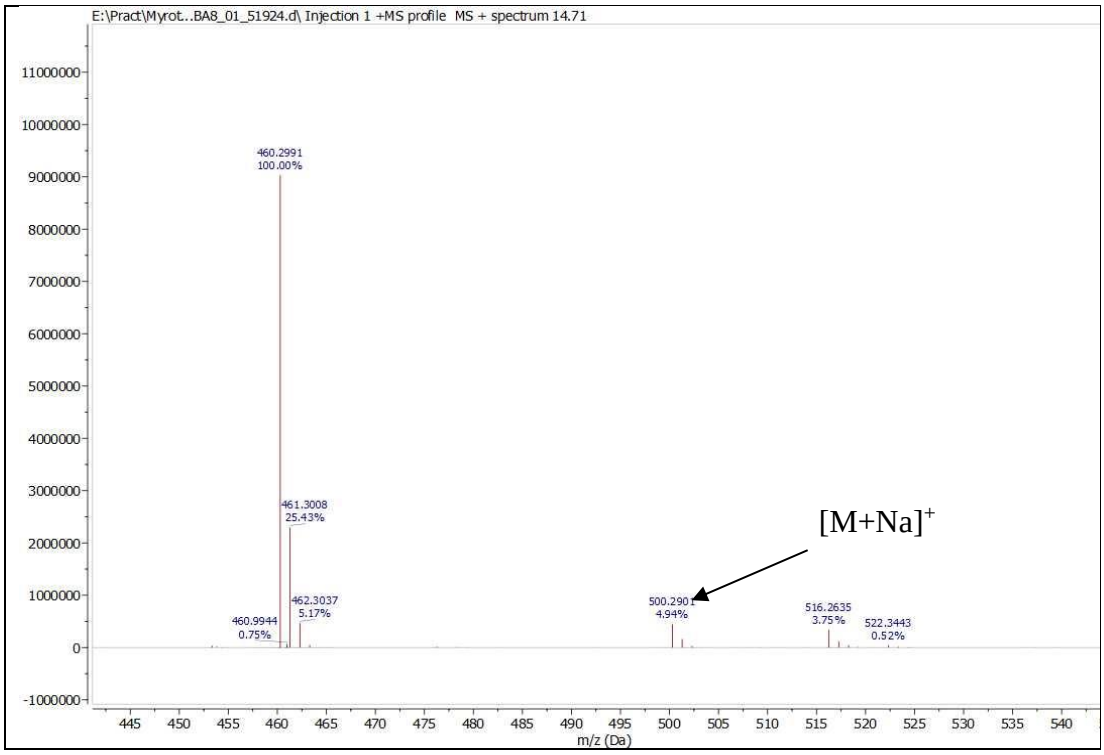

Appendix 11: HR-Mass spectrum of 8-Hydroxyechinulin (**38**)

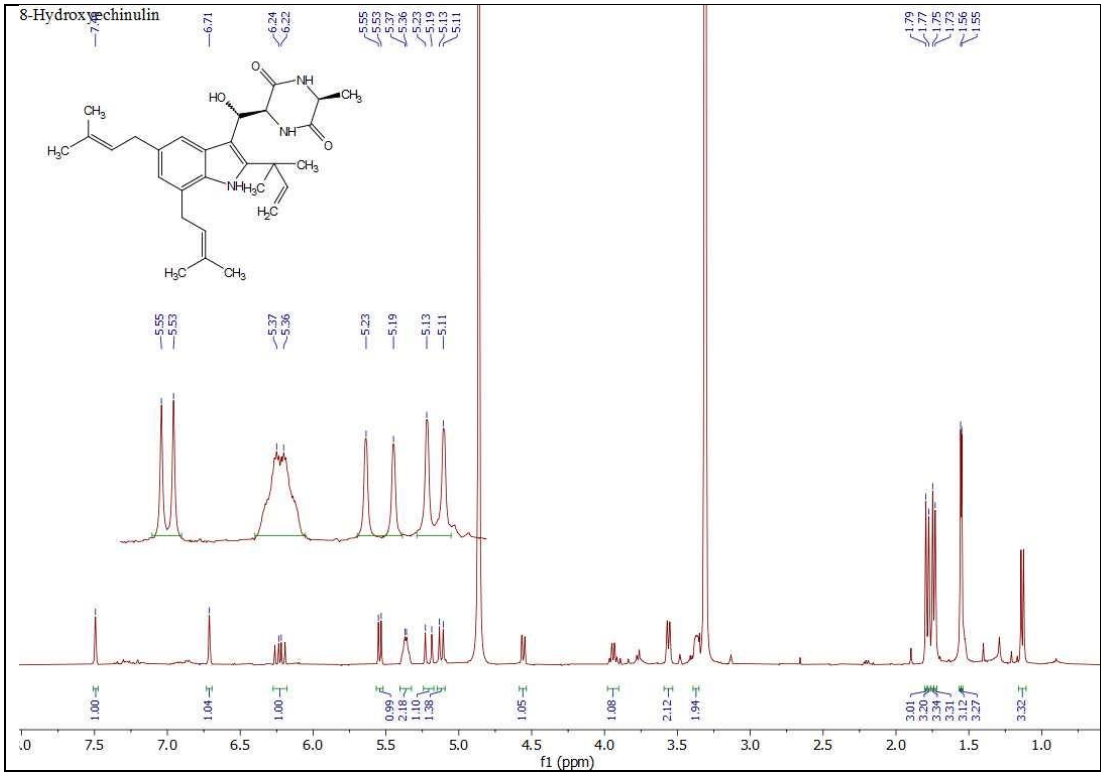

Appendix 12: ^{1}H NMR spectrum of 8-Hydroxyechinulin (**38**) (MeOD-d_4)

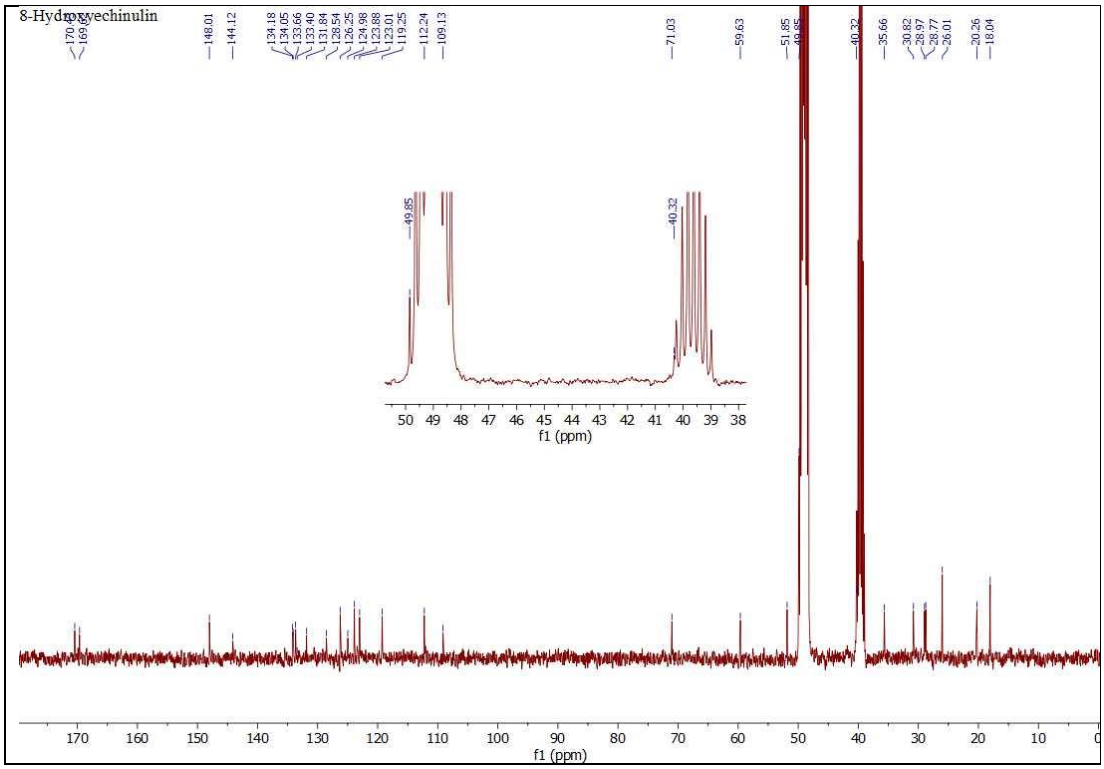

Appendix 13: The ^{13}C NMR spectrum of 8-Hydroxyechinulin (**38**) (MeOD-d_4)

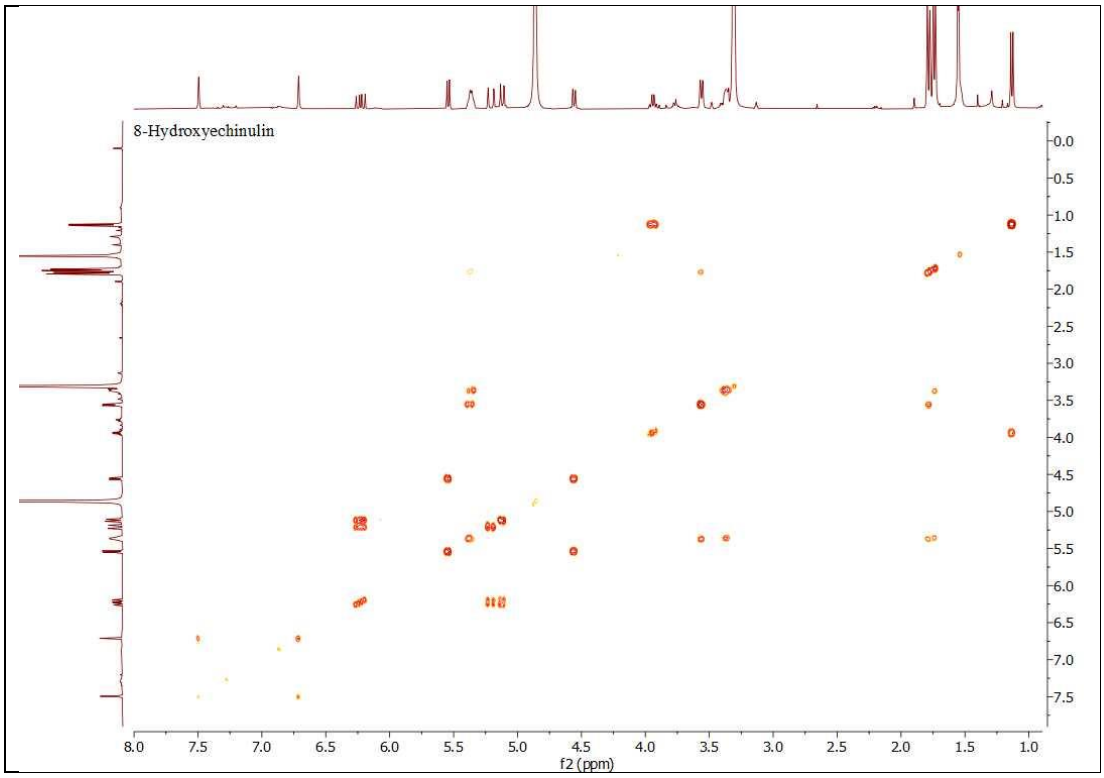

Appendix 14: ^{1}H-^{1}H COSY spectrum of 8-Hydroxyechinulin (**38**) (MeOD-d_4)

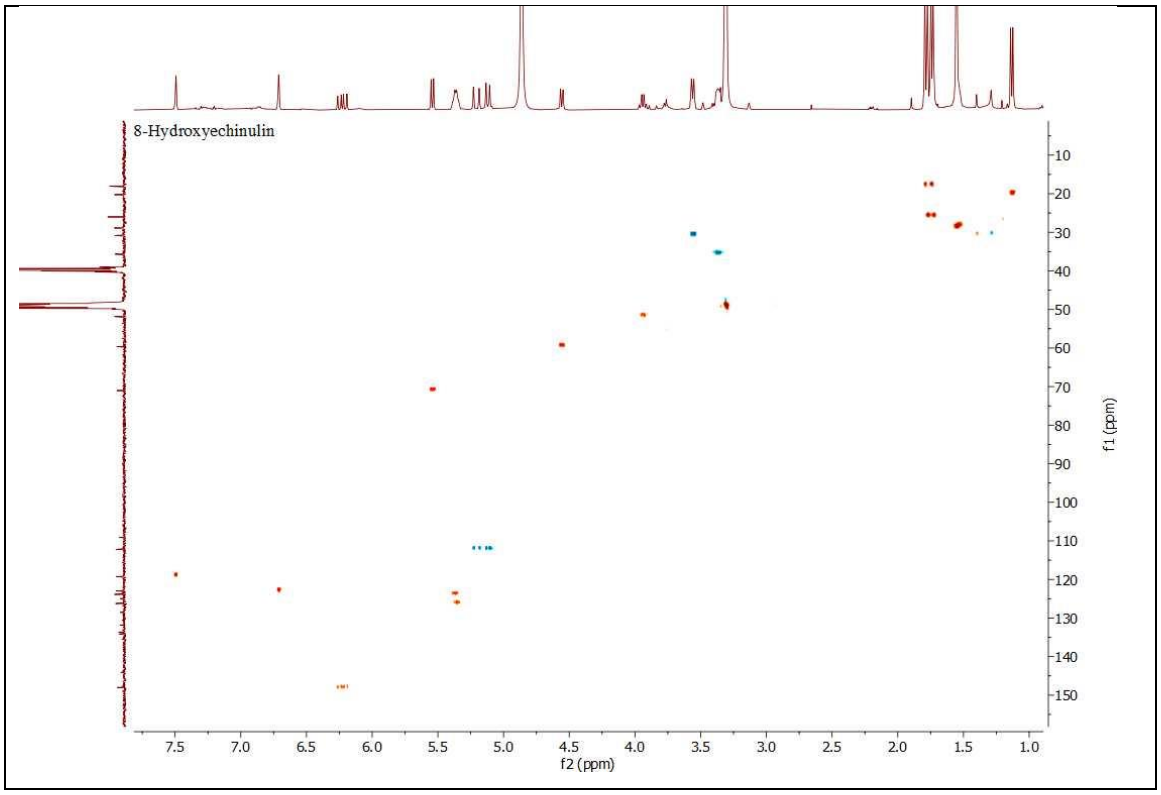

Appendix 15: HSQC spectrum of 8-Hydroxyechinulin (**38**) (MeOD-d_4)

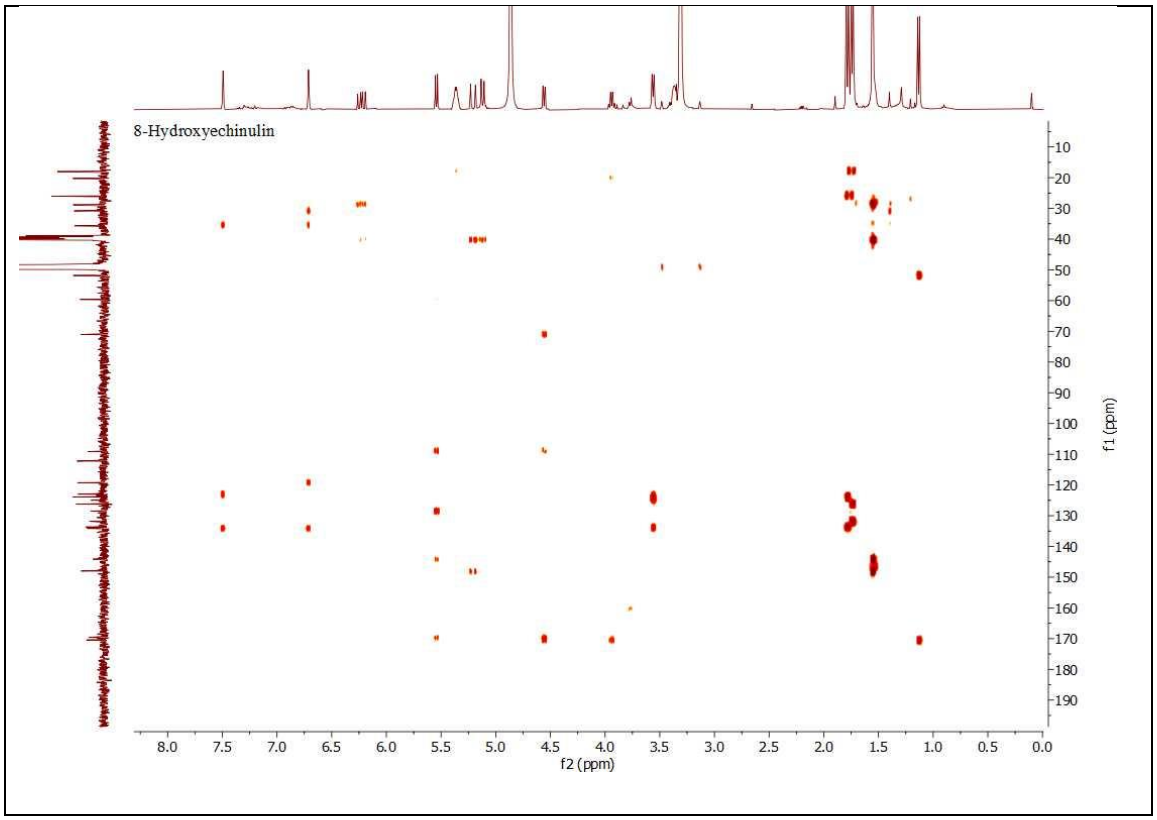

Appendix 16: HMBC spectrum of 8-Hydroxyechinulin (**38**) (MeOD-d_4)

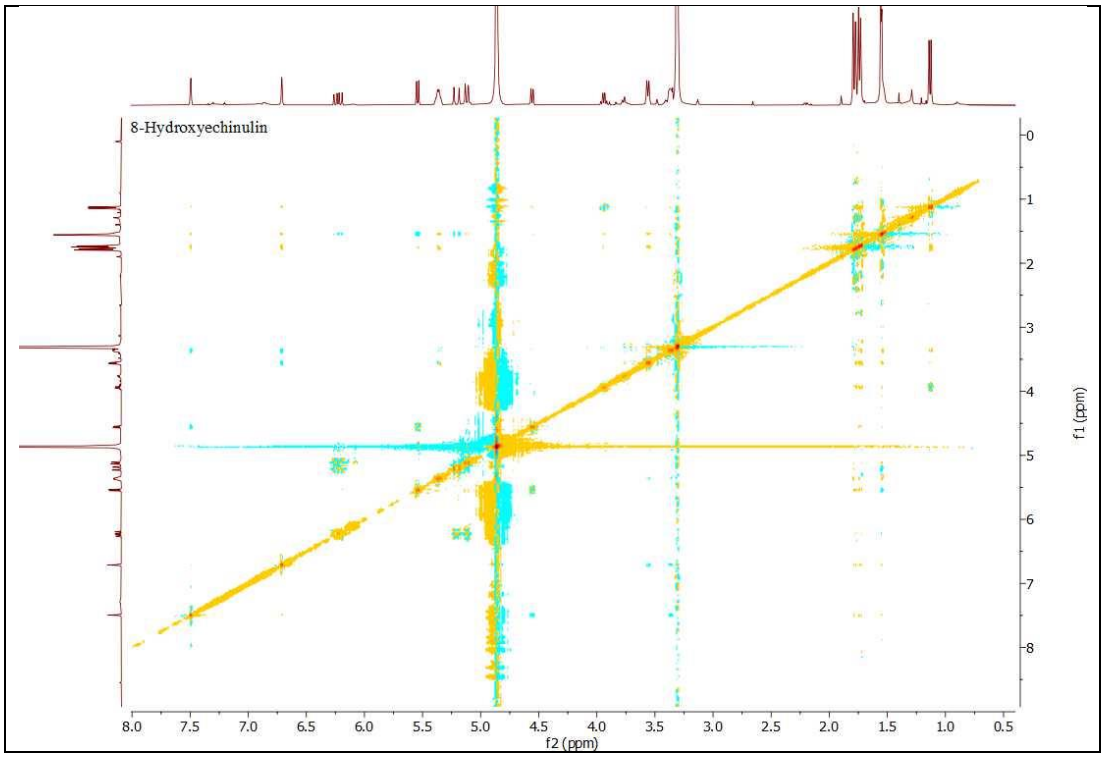

Appendix 17: NOESY spectrum of 8-Hydroxyechinulin (**38**) (MeOD-d_4)

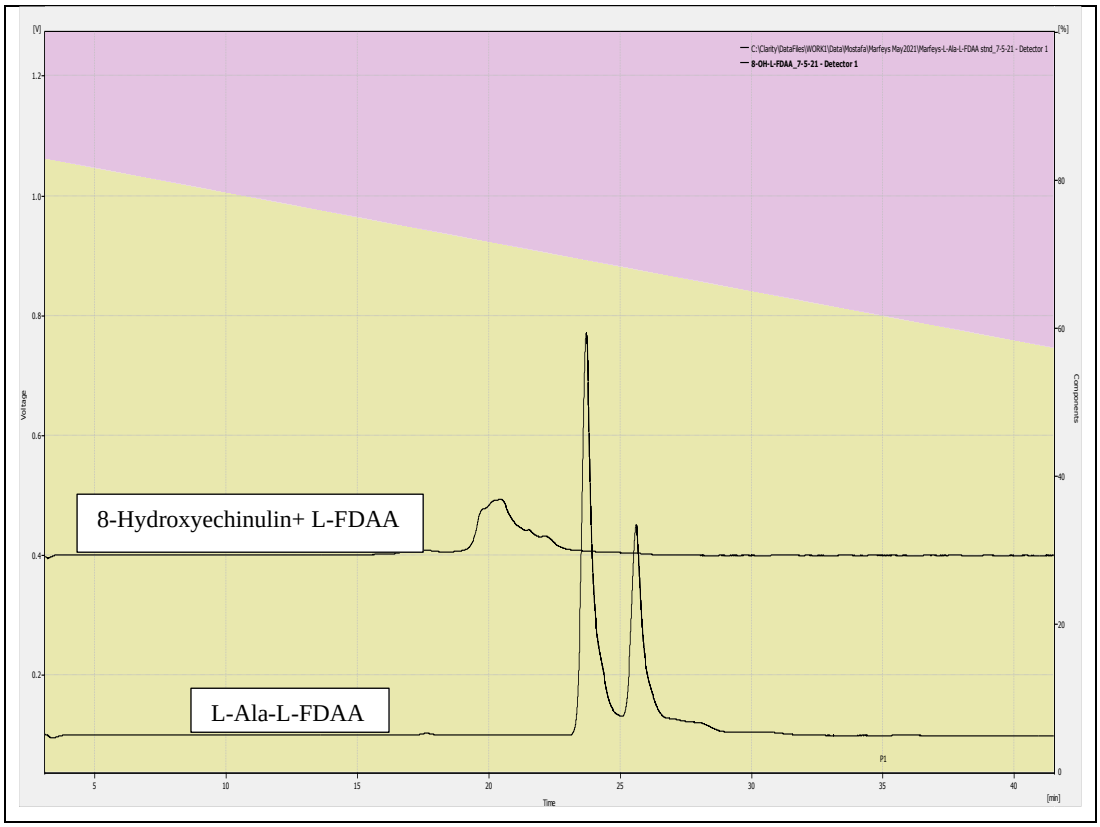

Appendix 18: HPLC analysis of the acid hydrolyzate of 8-Hydroxyechinulin (**38**)

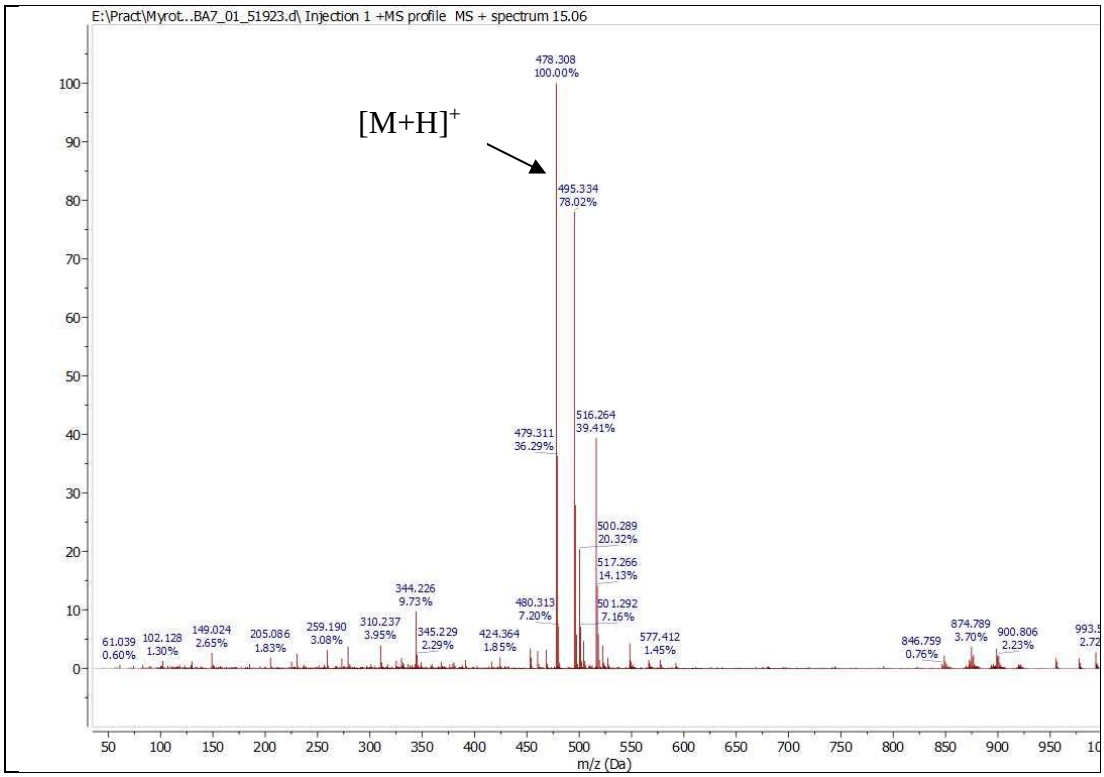

Appendix 19: HR-Mass spectrum of 27-28-Epoxyechinulin (**39**)

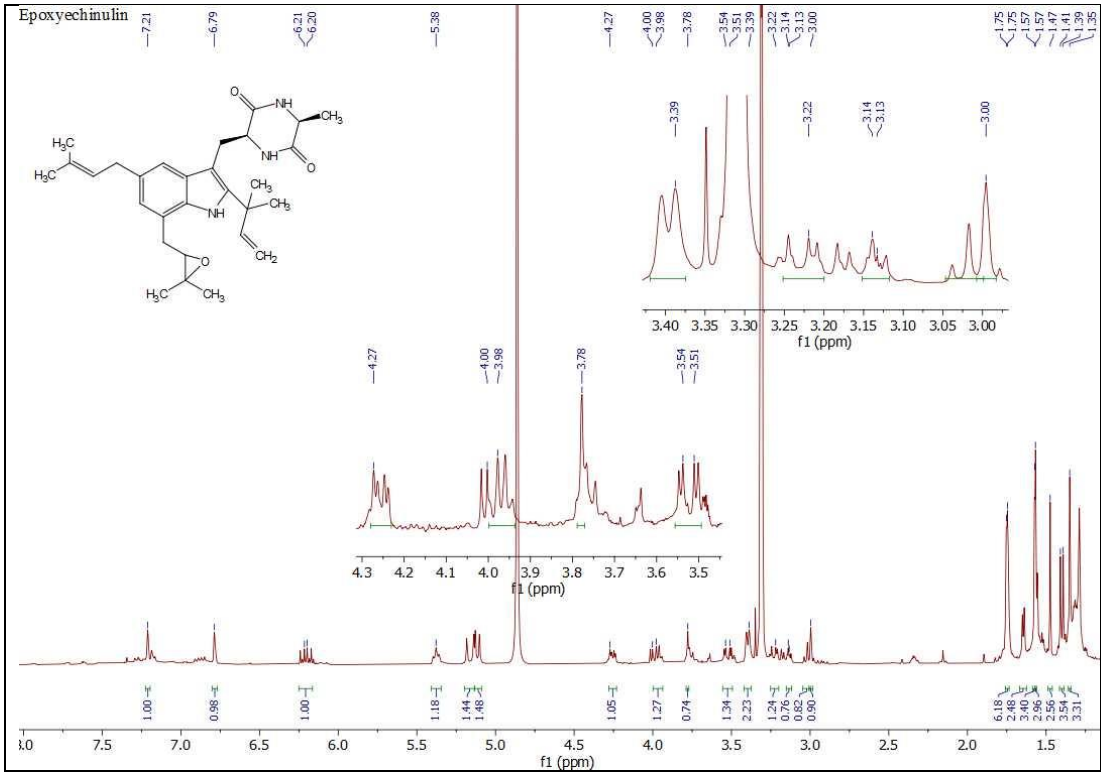

Appendix 20: ^{1}H NMR spectrum of 27-28-Epoxyechinulin (**39**) (MeOD-d_4)

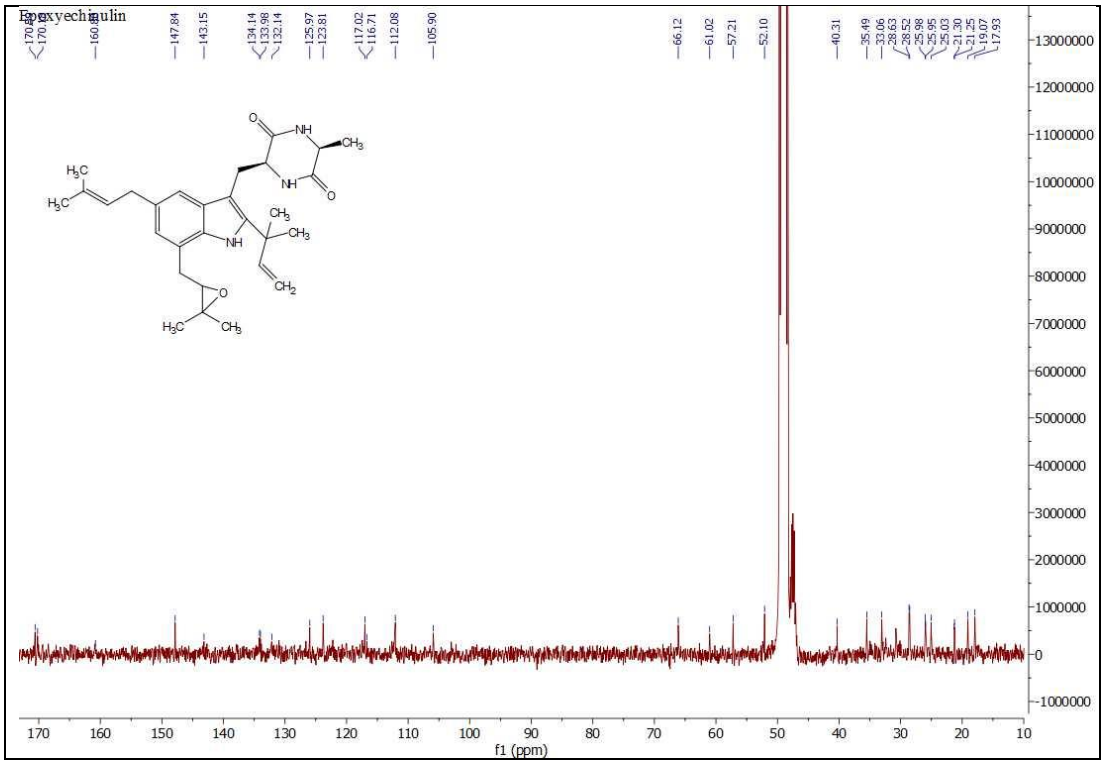

Appendix 21: ^{13}C NMR spectrum of 27-28-Epoxyechinulin (**39**) (MeOD-d_4)

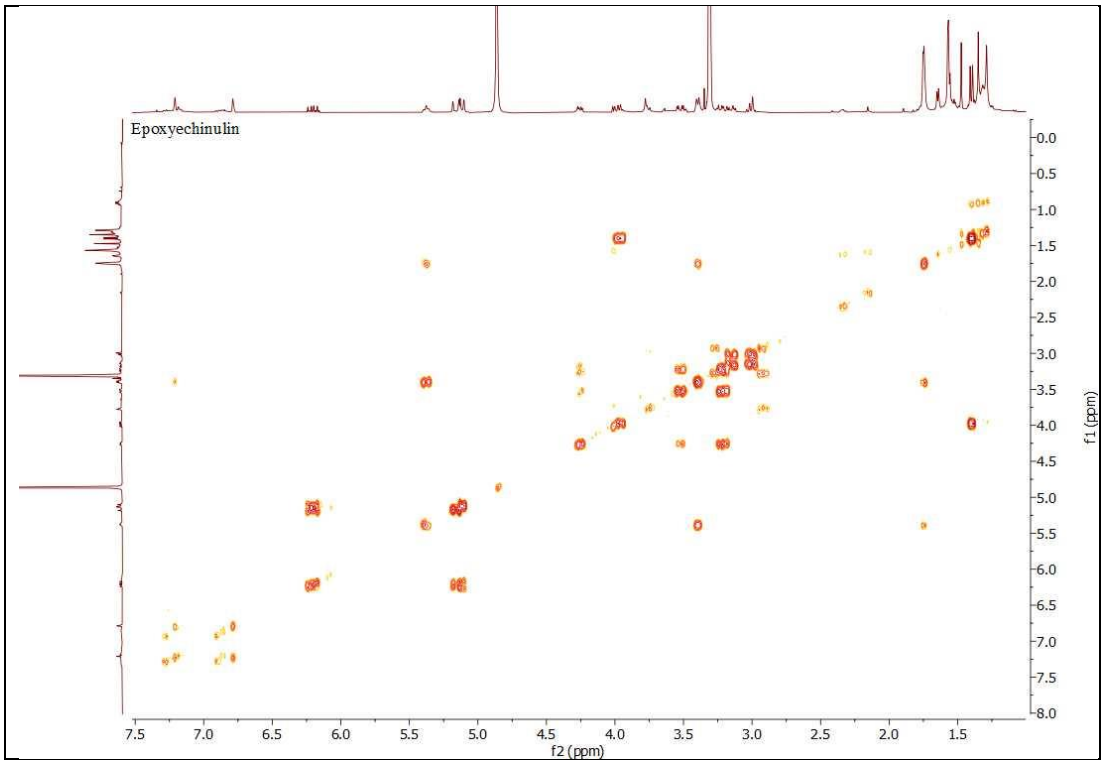

Appendix 22: ^{1}H-^{1}H COSY spectrum of Epoxyechinulin (**39**) (MeOD-d_4)

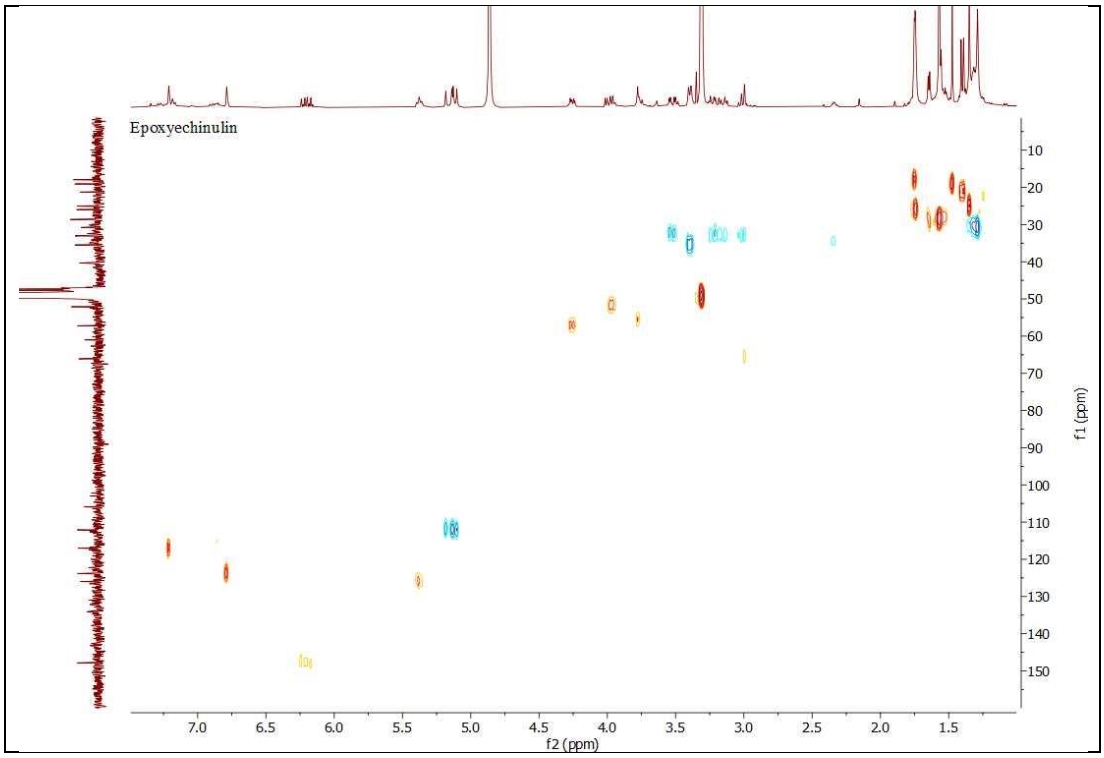

Appendix 23: HSQC spectrum of Epoxyechinulin (**39**) (MeOD-d_4)

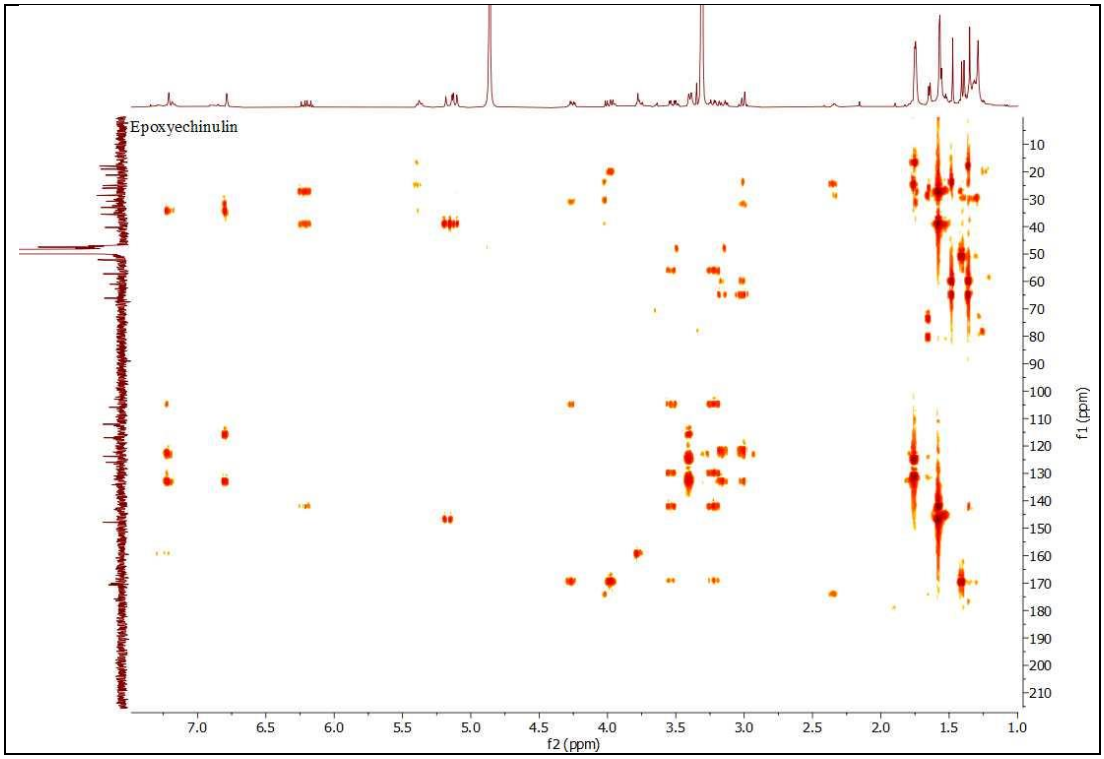

Appendix 24: HMBC spectrum of Epoxyechinulin (**39**) (MeOD-d_4)

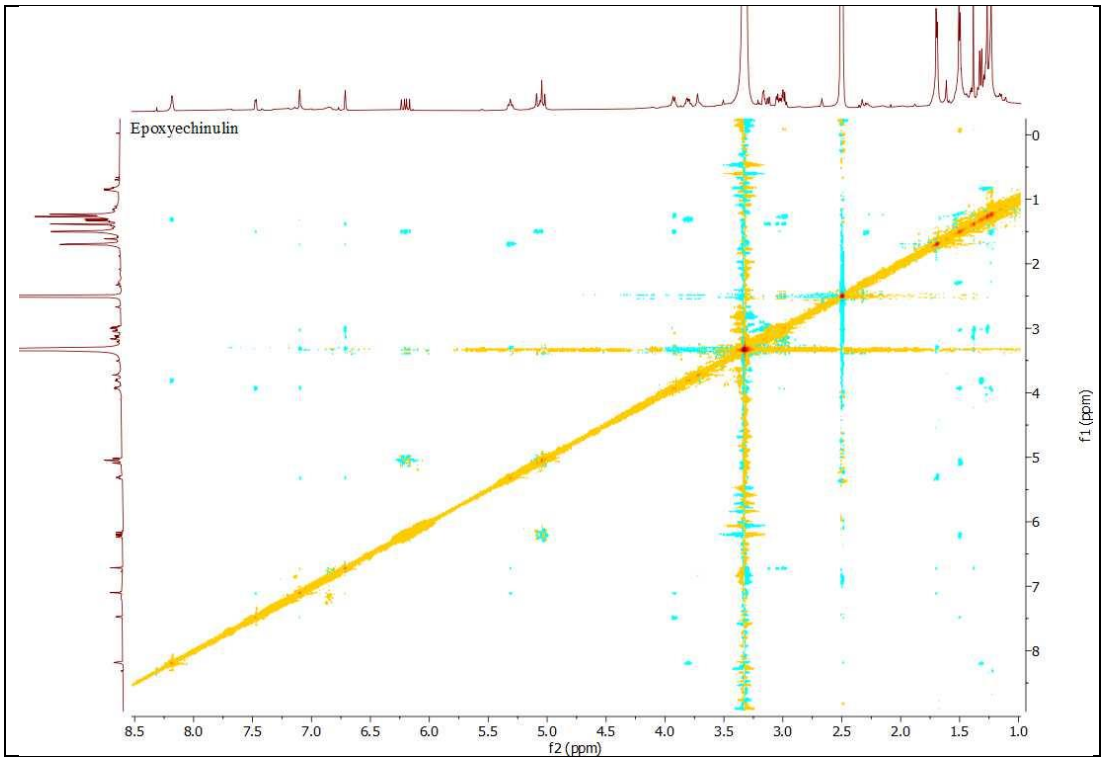

Appendix 25: NOESY spectrum of Epoxyechinulin (**39**) (DMSO-d_6)

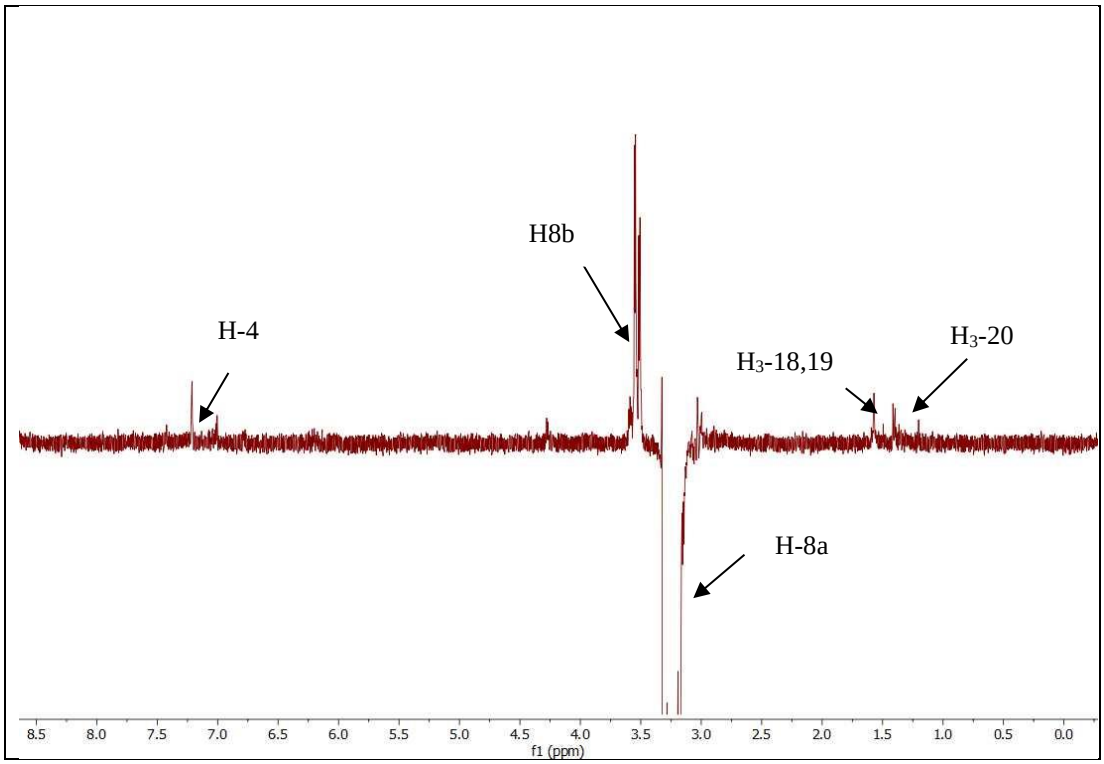

Appendix 26: Selected 1D NOE of Epoxyechinulin (**39**) (MeOD-d_4) (400MHz)

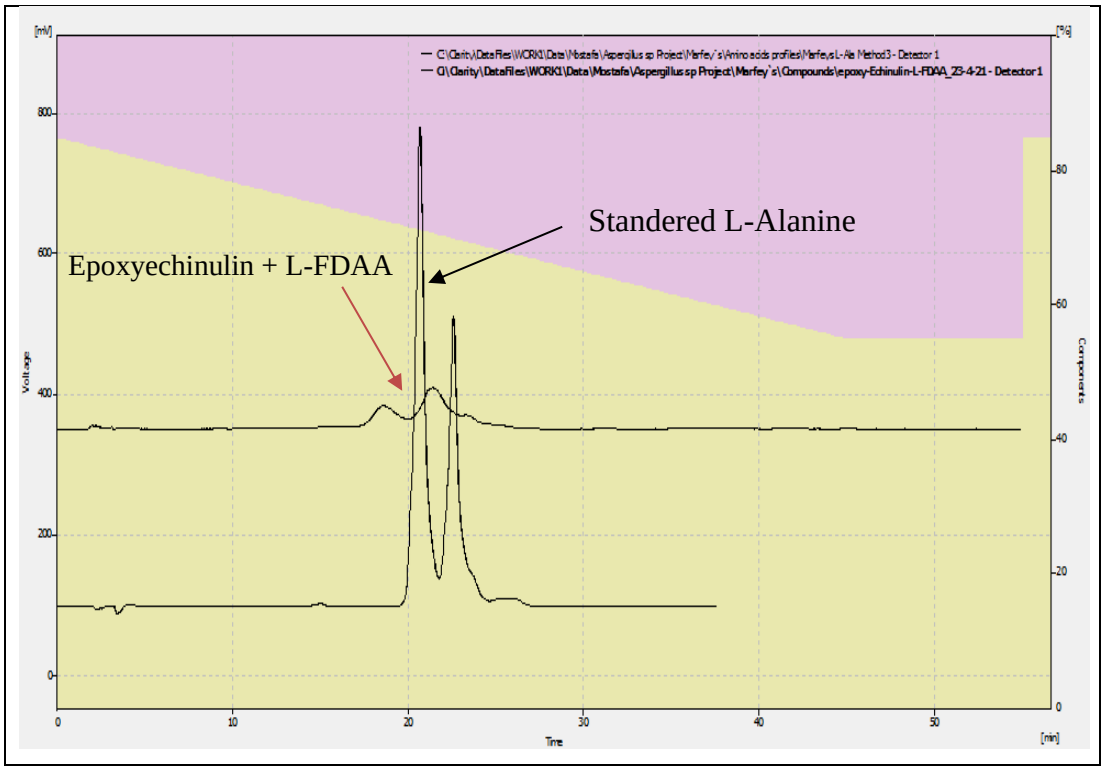

Appendix 27: HPLC analysis of the acid hydrolyzate of (**39**)

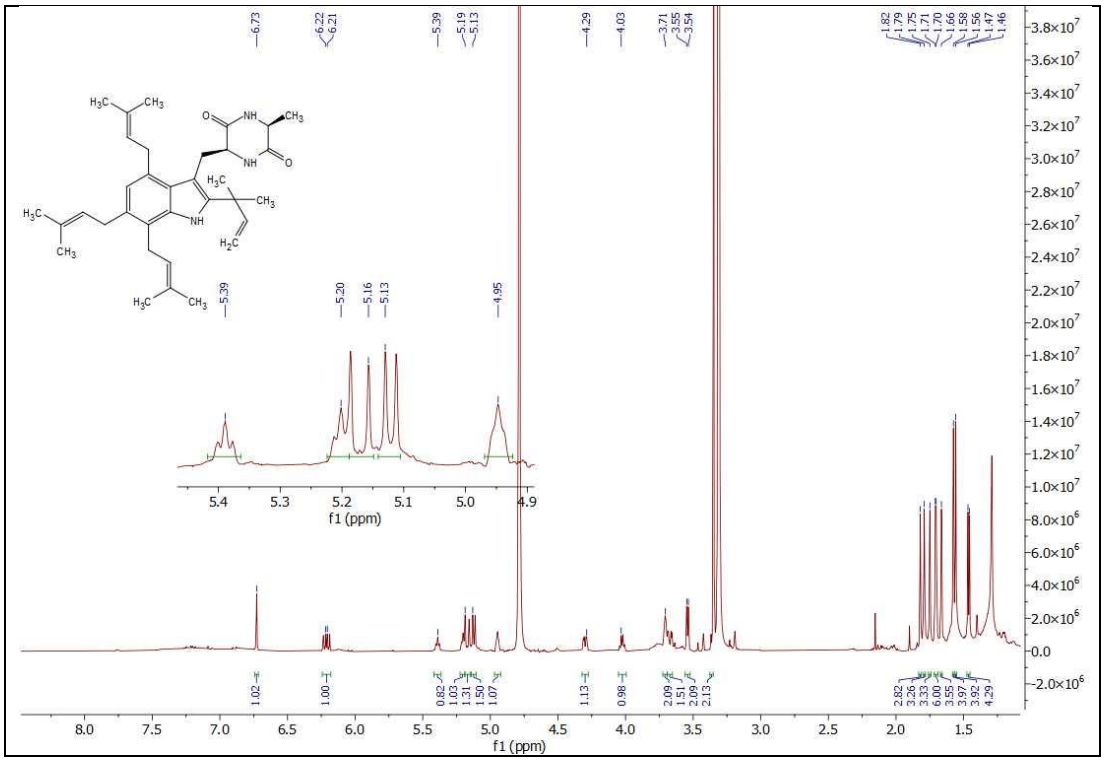

Appendix 28: ^{1}H NMR spectrum of (**40**) (MeOD-d_4)

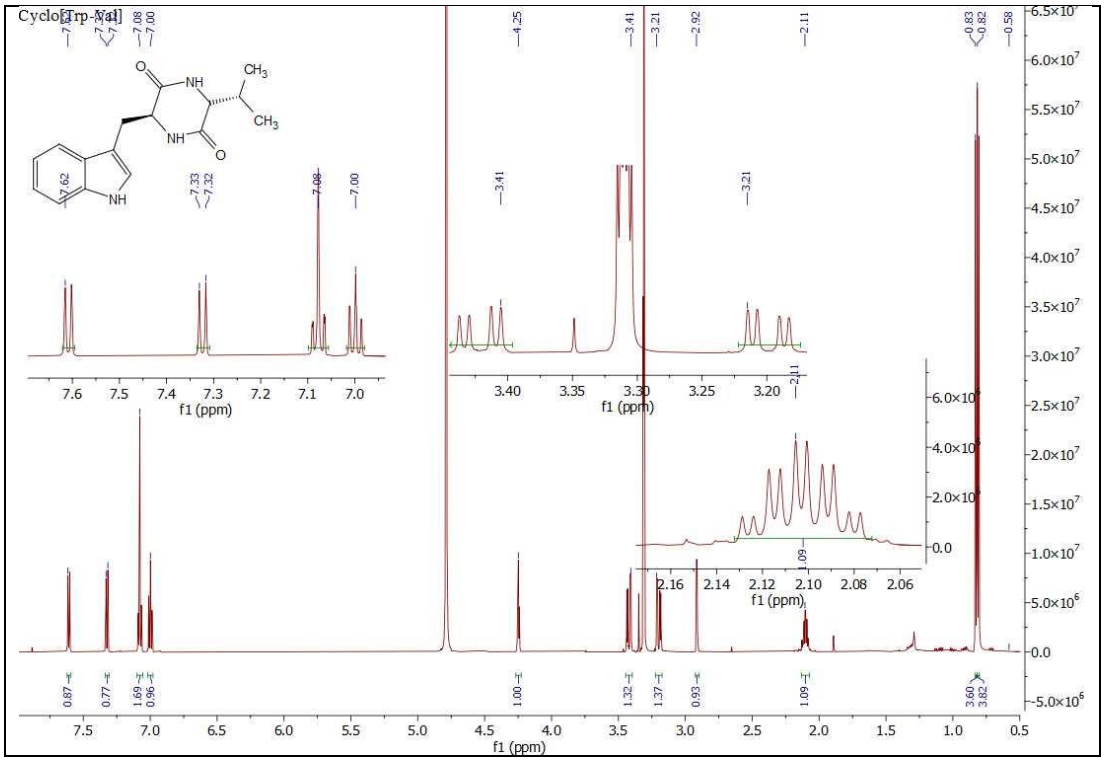

Appendix 29: ^{1}H NMR spectrum of Cyclo[Trp-Val] (**41**) (MeOD-d_4)

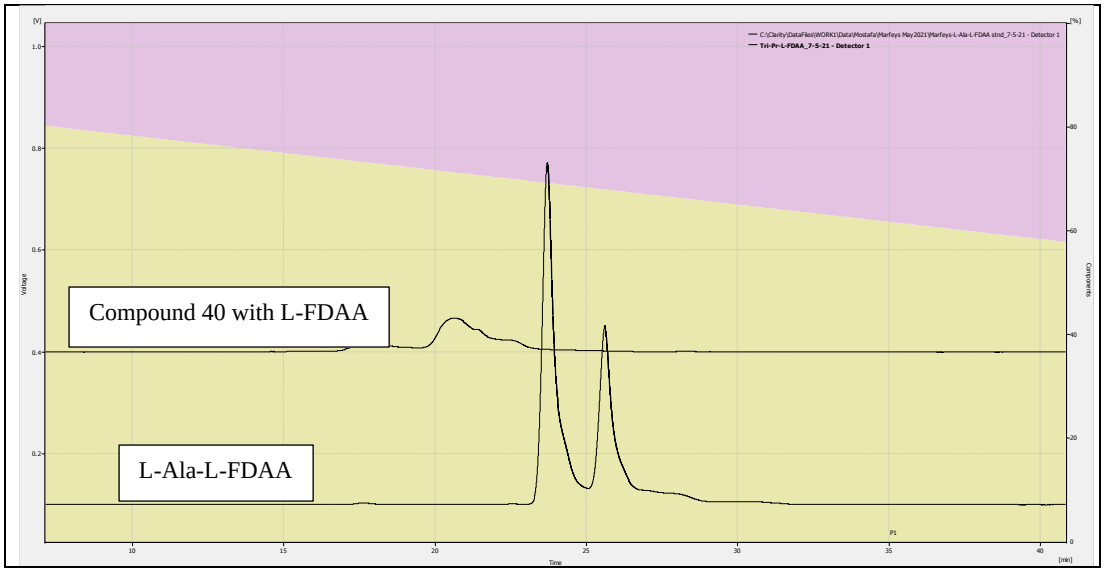

Appendix 30: HPLC analysis of the acid hydrolyzate of (**40**)

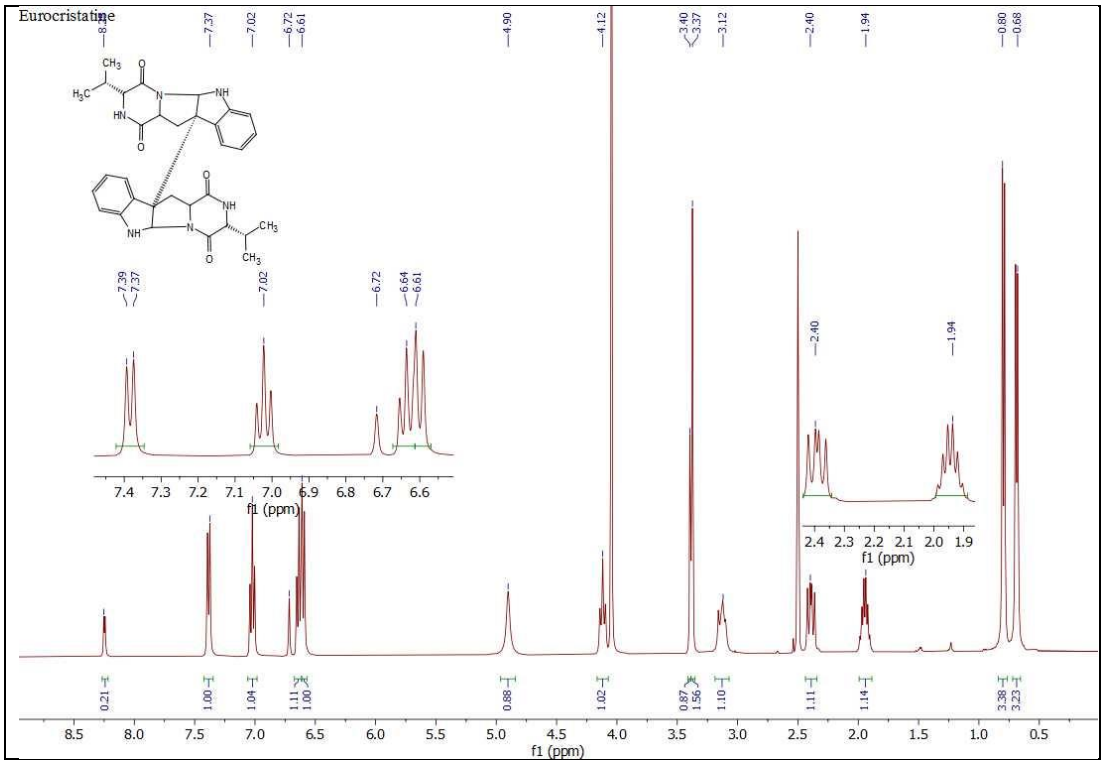

Appendix 31: ^{1}H NMR spectrum of Eurocristatine (**42**) (DMSO-d_6)

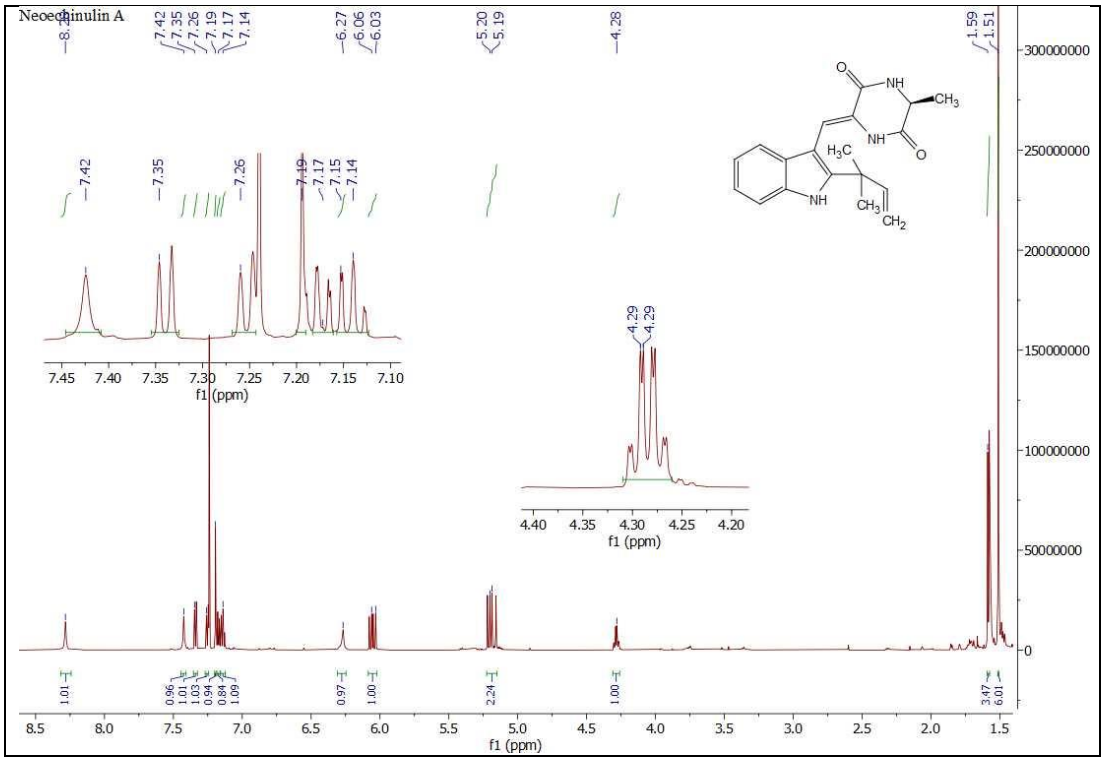

Appendix 32: ^{1}H NMR spectrum of Neoechinulin A (**43**) ($CDCl_3$)

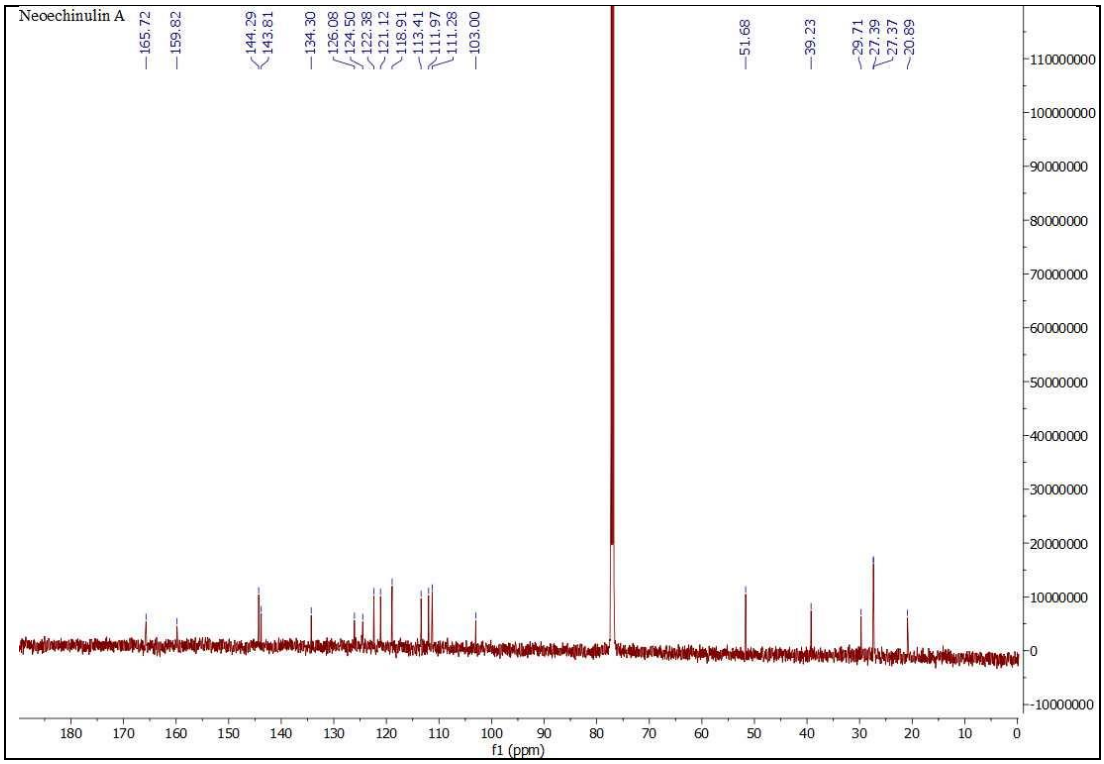

Appendix 33: ^{13}C NMR spectrum of Neoechinulin A (**43**) ($CDCl_3$)

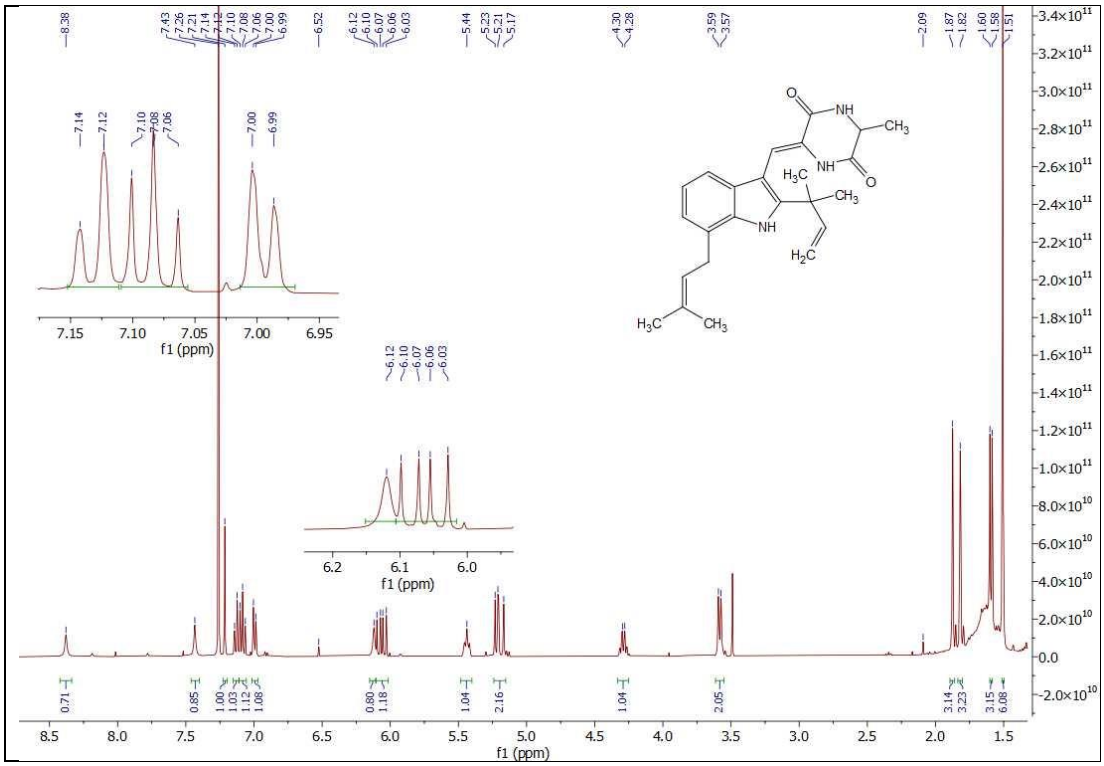

Appendix 34: ^{1}H NMR spectrum of Varicolorin G (**44**) ($CDCl_3$)

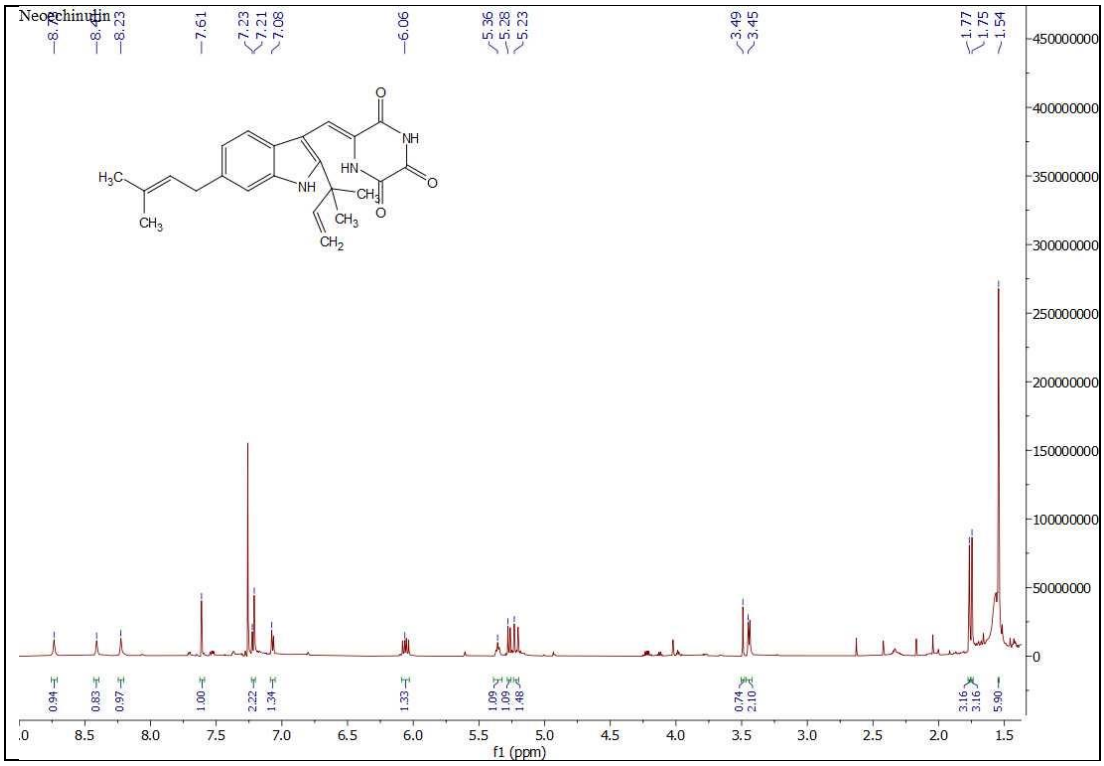

Appendix 35: ^{1}H NMR spectrum of Neoechinulin (**45**) ($CDCl_3$)

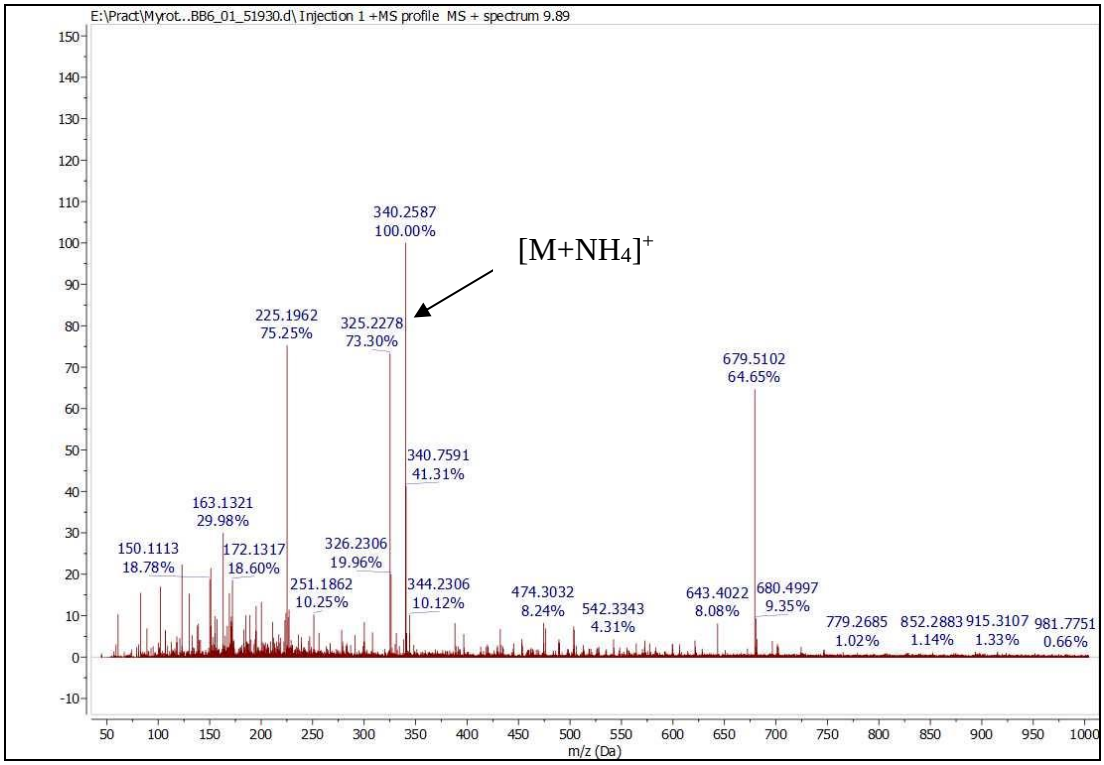

Appendix 36: HR-ESI-MS spectrum of Neoechinulin F (**46**)

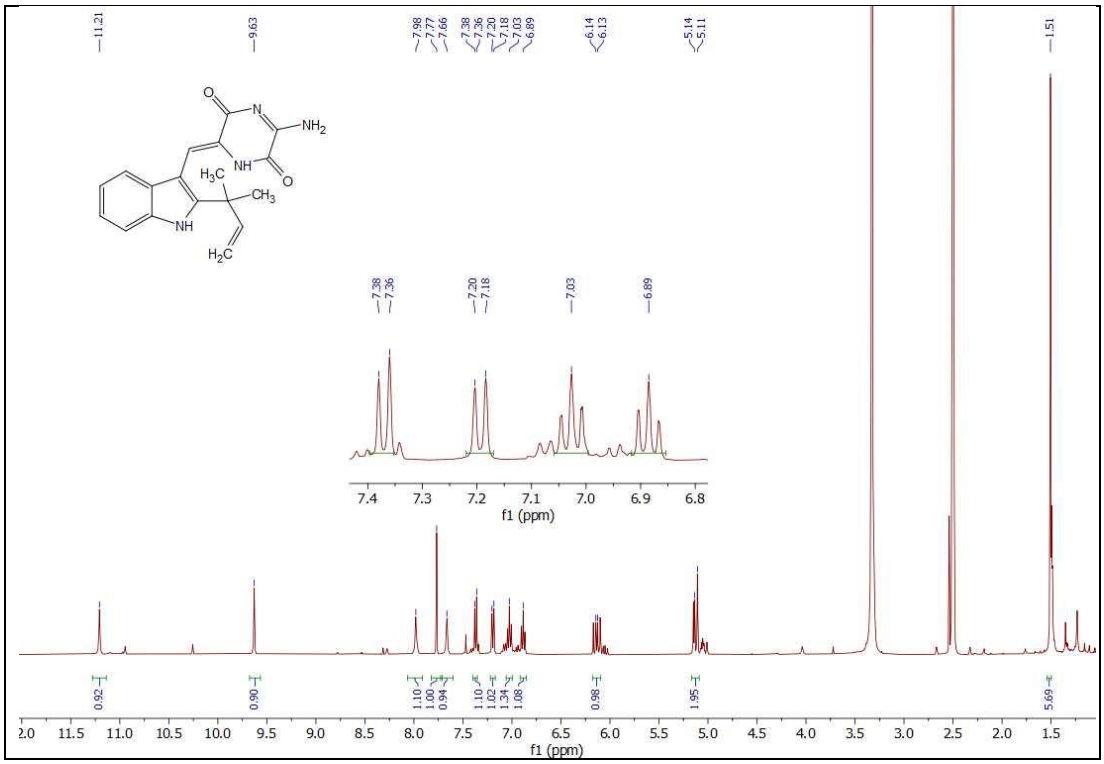

Appendix 37: ^{1}H NMR spectrum of Neoechinulin F (**46**) (DMSO-d_6)

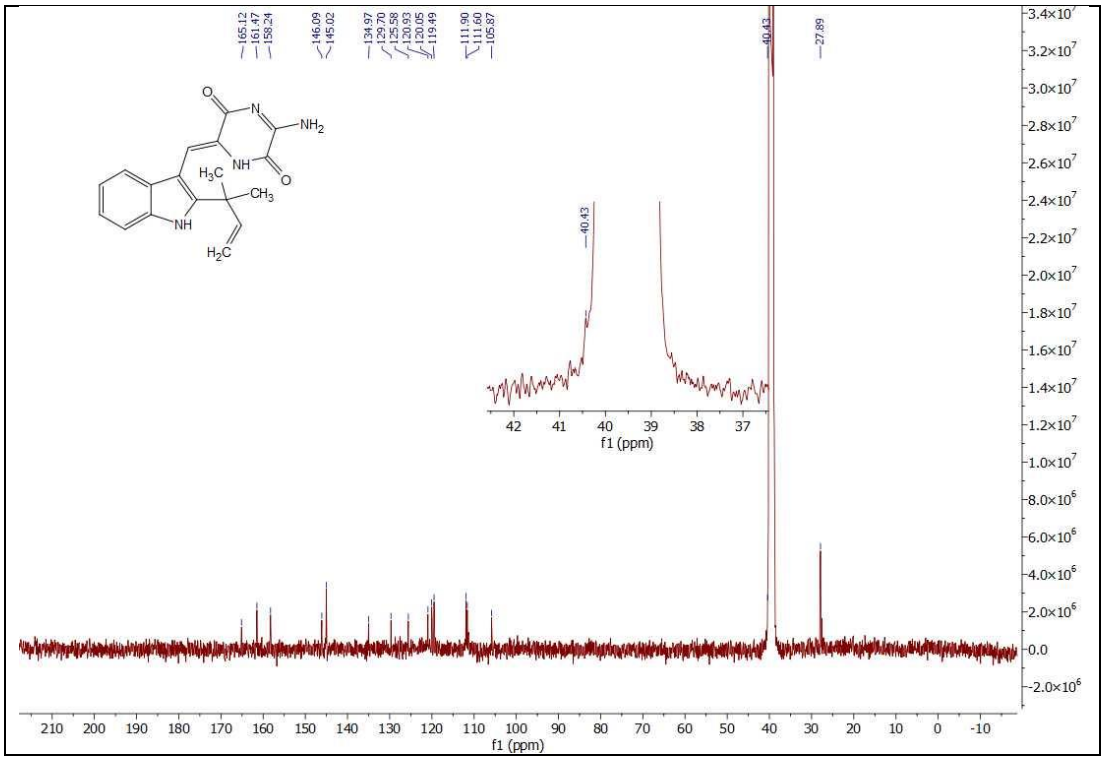

Appendix 38: ^{13}C NMR spectrum of Neoechinulin F (**46**) (DMSO-d_6)

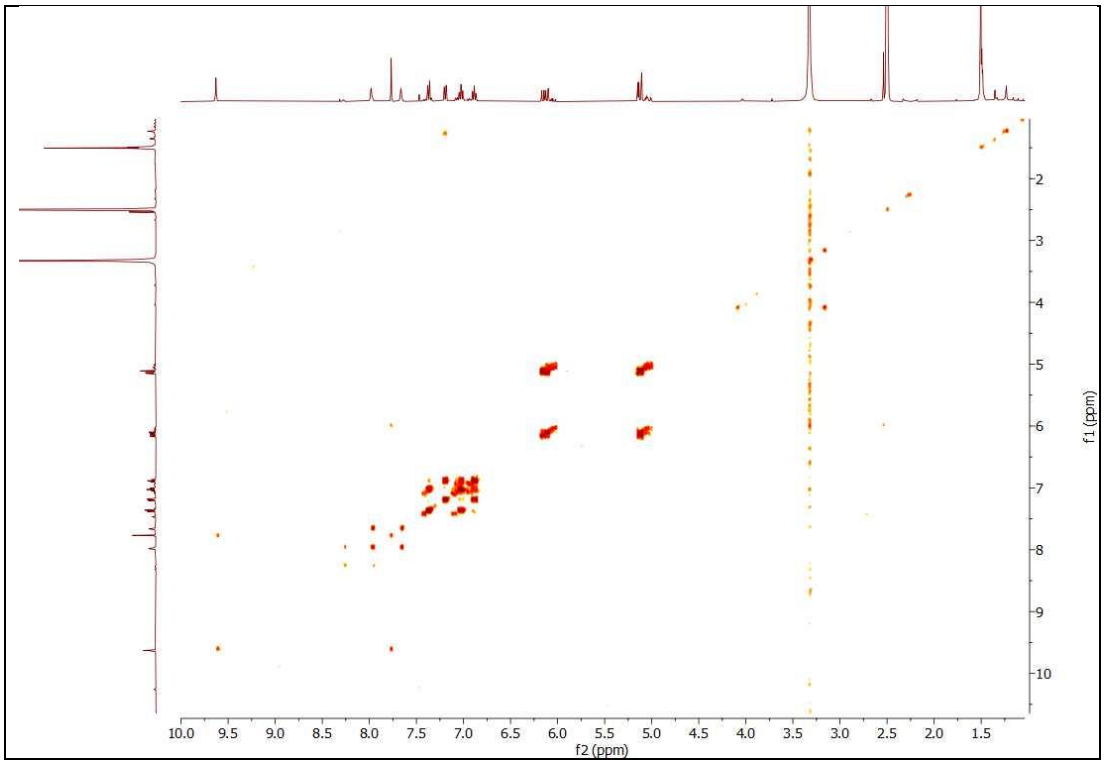

Appendix 39: ^{1}H-^{1}H COSY spectrum of Neoechinulin F (**46**) (DMSO-d_6)

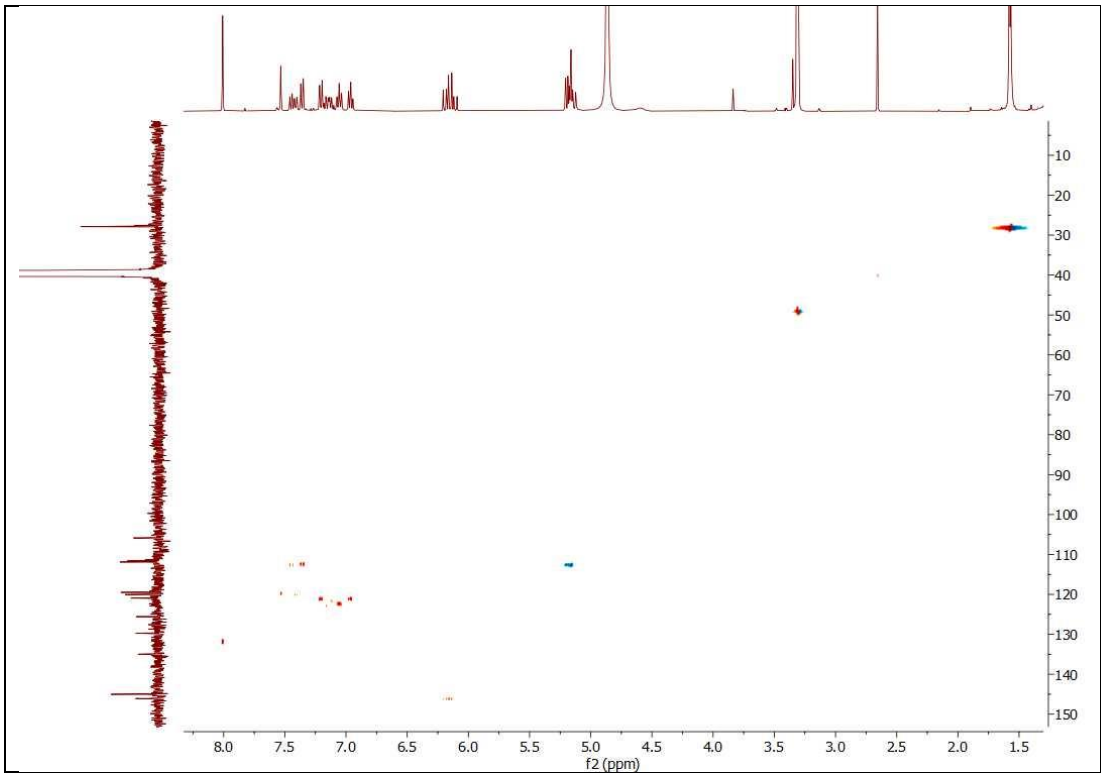

Appendix 40: HSQC spectrum of Neoechinulin F (**46**) (MeOD-d_4)

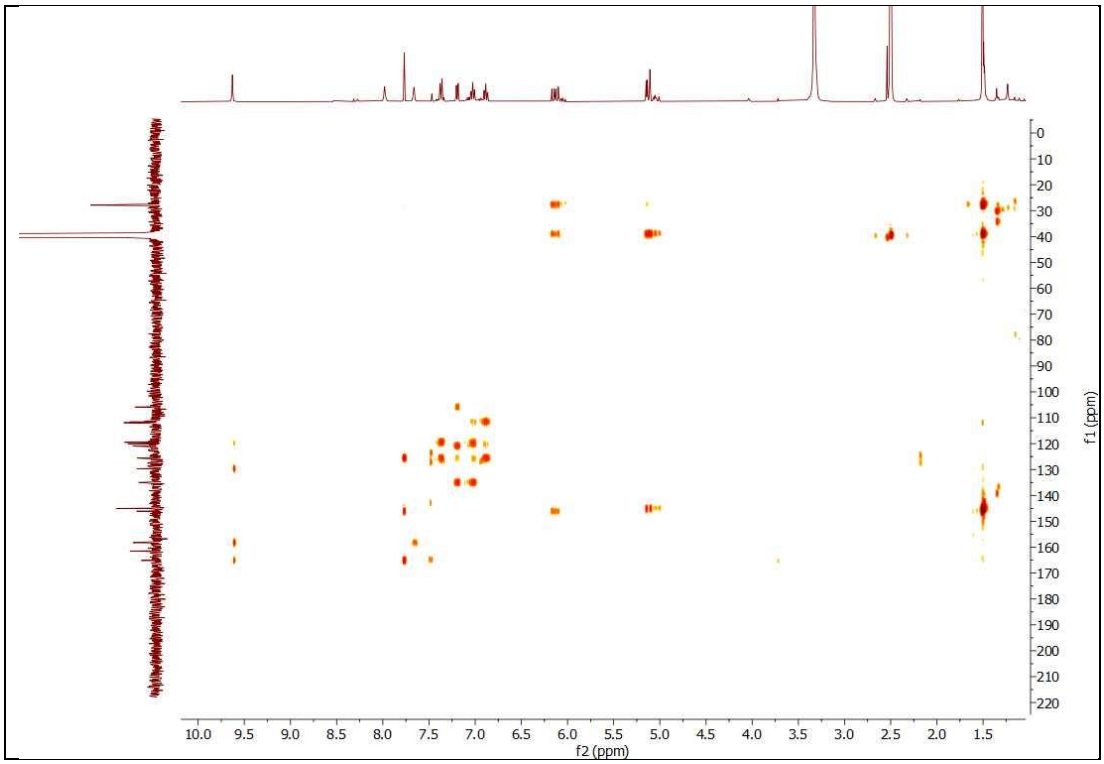

Appendix 41: HMBC spectrum of Neoechinulin F (**46**) (MeOD-d_4)

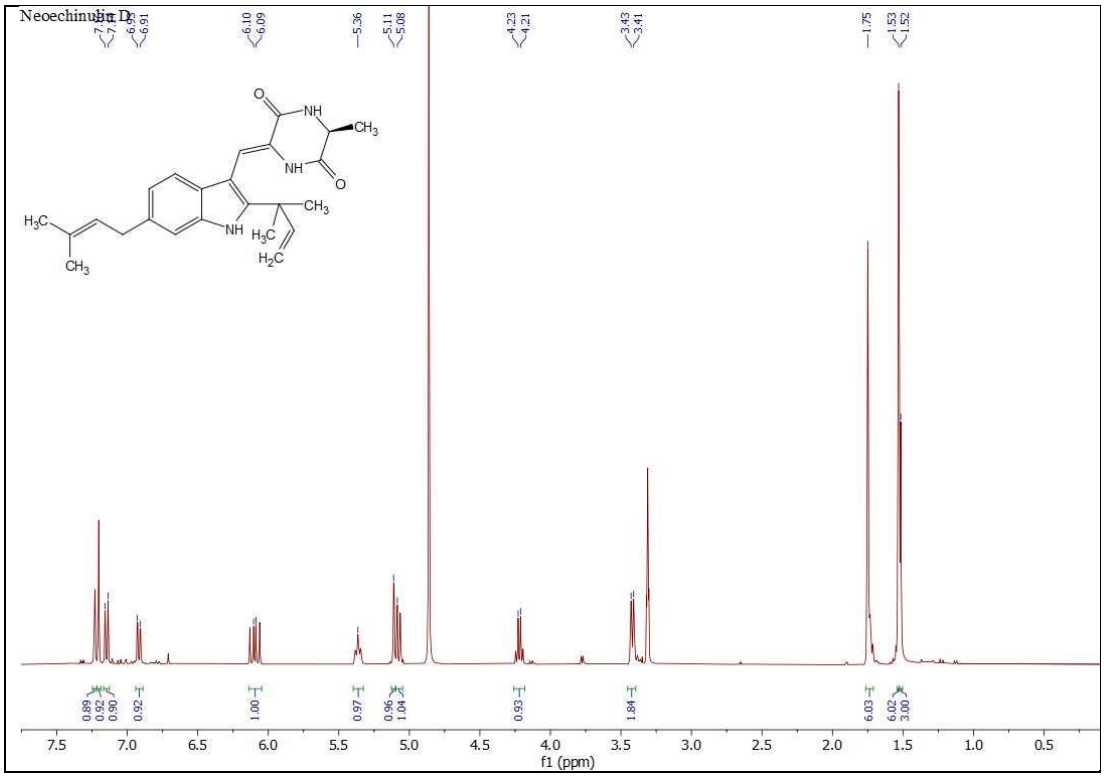

Appendix 42: ^{1}H NMR spectrum of Neoechinulin D (**47**) (MeOD-d_4)

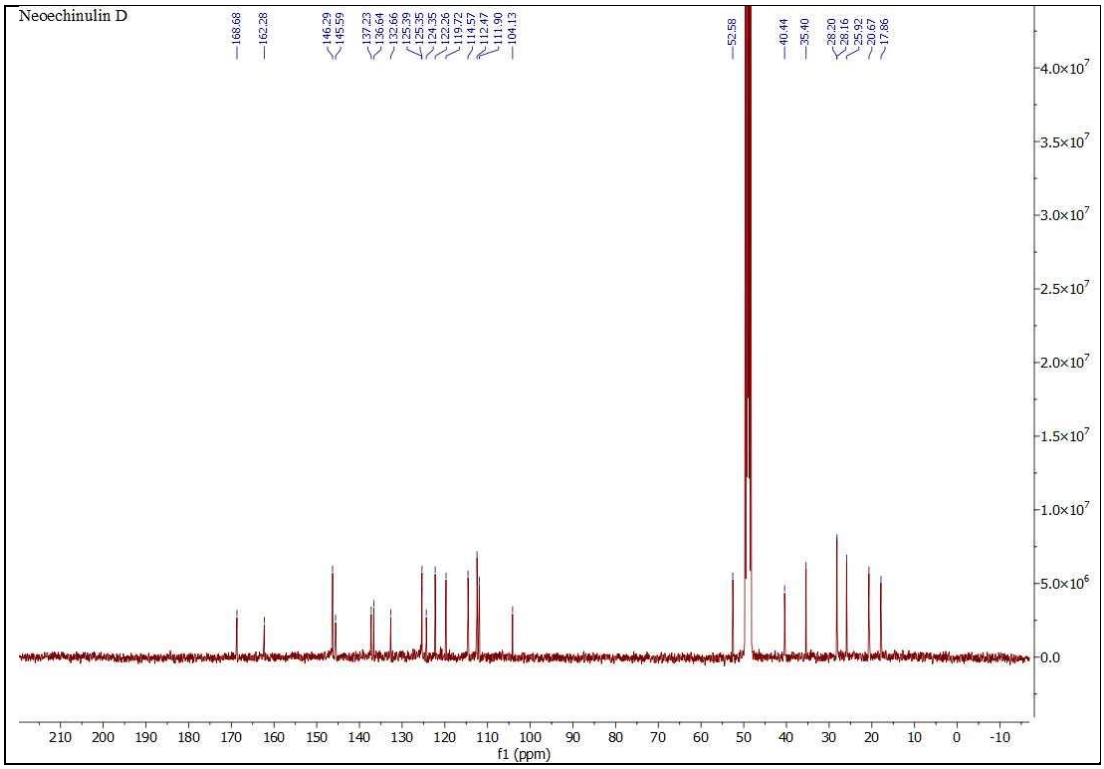

Appendix 43: ^{13}C NMR spectrum of Neoechinulin D (**47**) (MeOD-d_4)

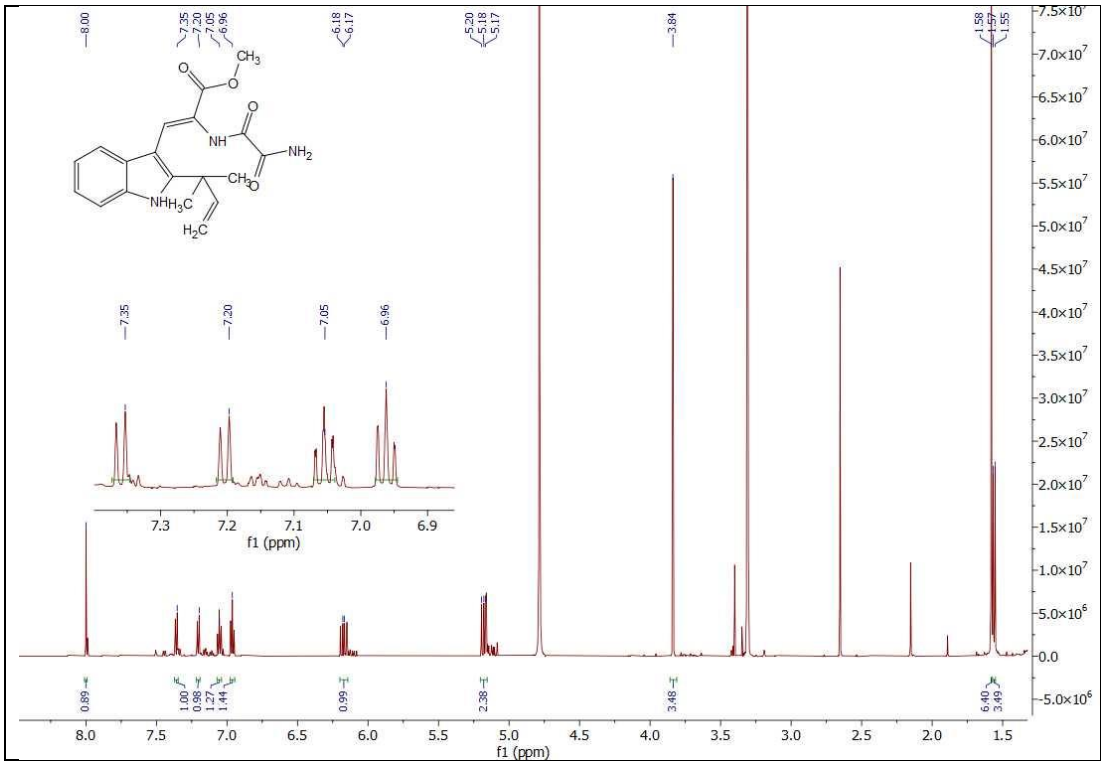

Appendix 44: ^{1}H NMR spectrum of Cristatumin D (**48**) (MeOD-d_4)

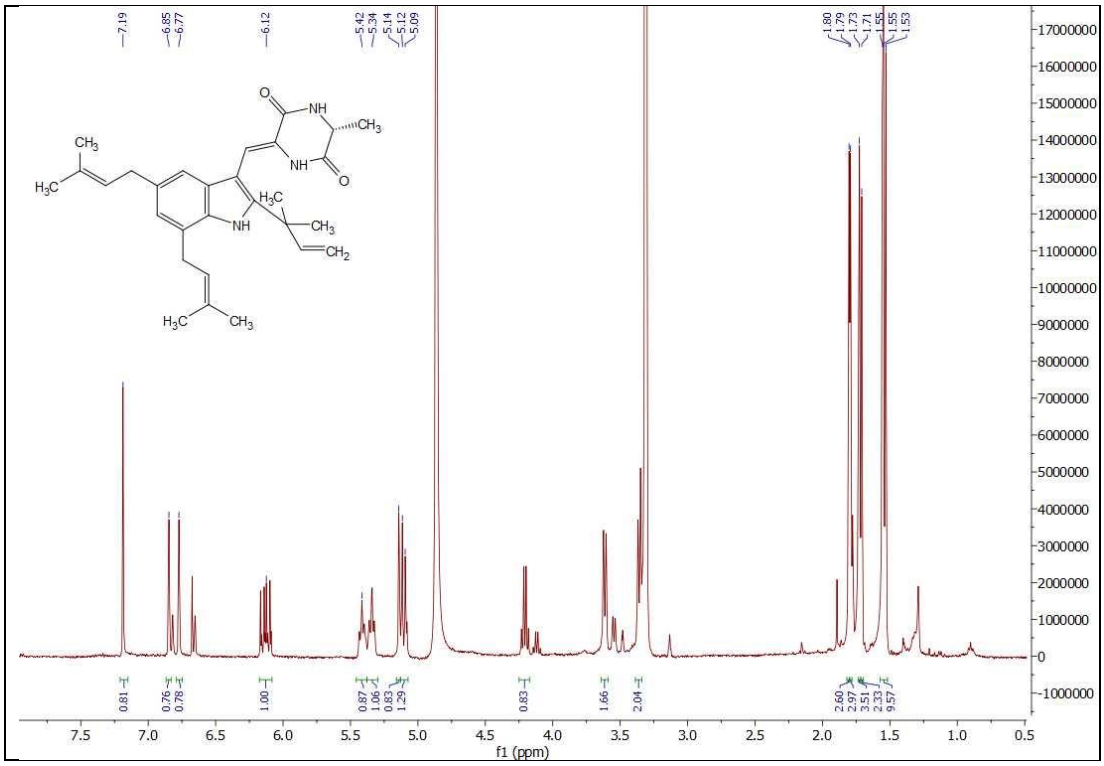

Appendix 45: ^{1}HNMR spectrum of (12*R*)Dehydroechinulin (**49**) (MeOD-d_4)

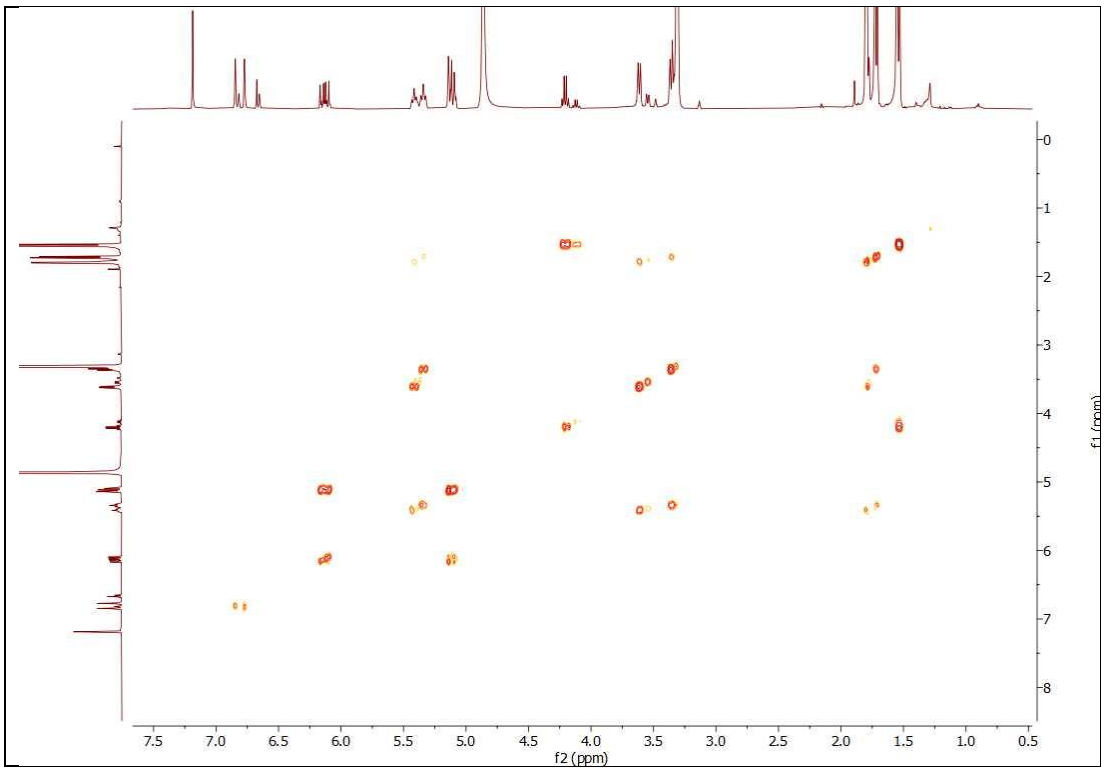

Appendix 46: COSY spectrum of (12*R*)Dehydroechinulin (**49**) (MeOD-d_4)

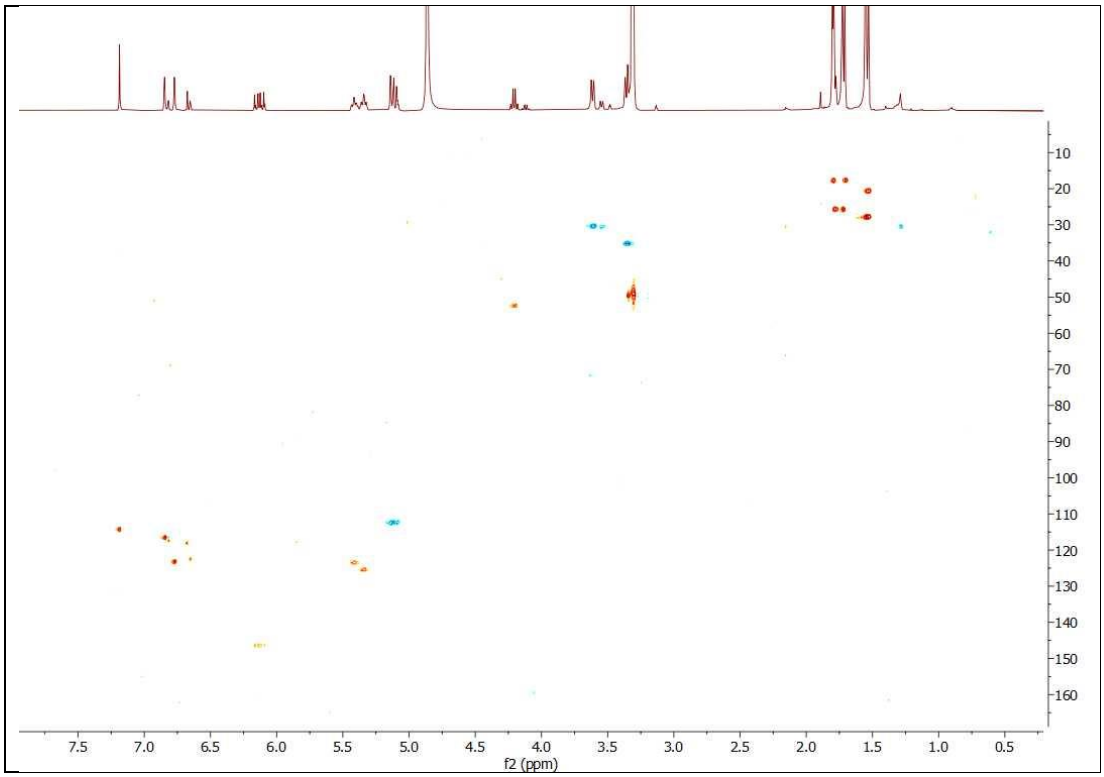

Appendix 47: HSQC spectrum of (12*R*)Dehydroechinulin (**49**) (MeOD-d_4)

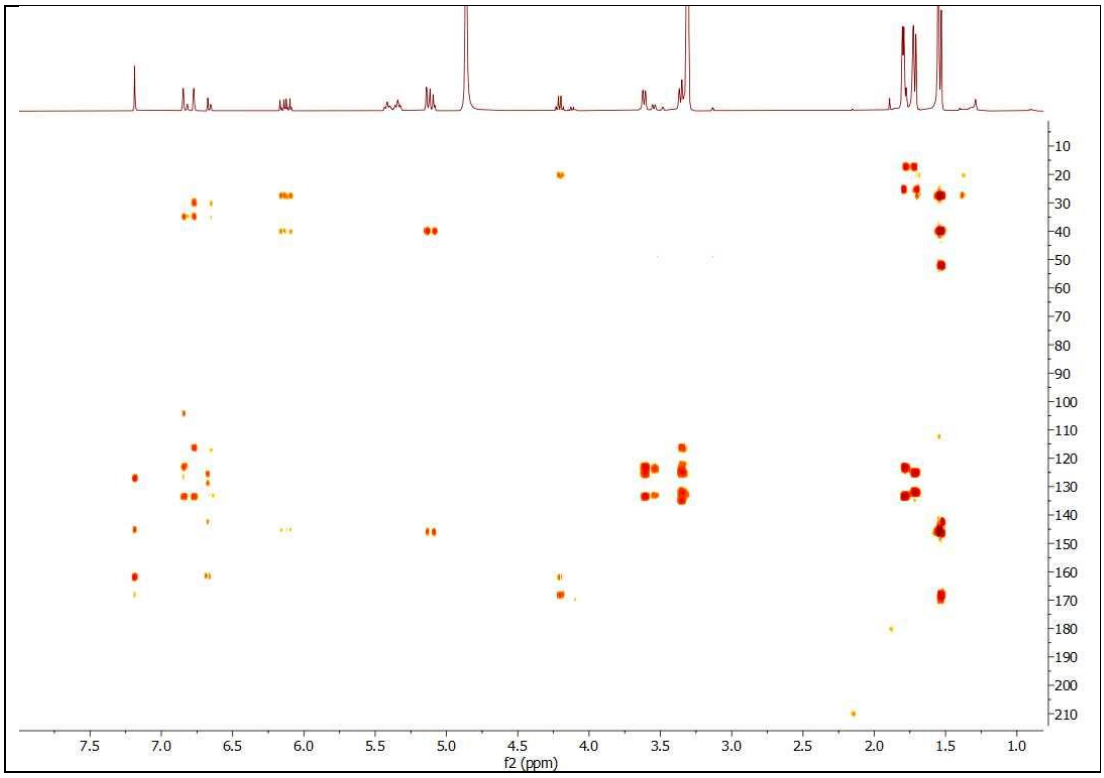

Appendix 48: HMBC spectrum of (12*R*)Dehydroechinulin (**49**) (MeOD-d_4)

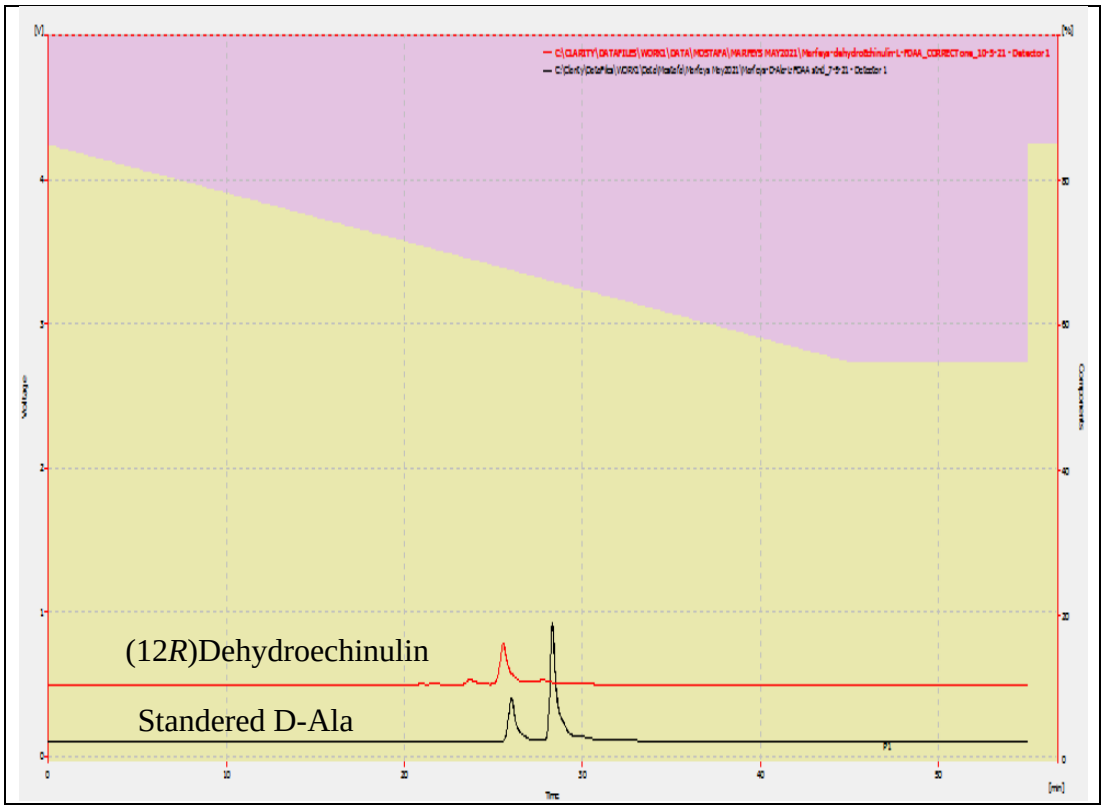

Appendix 49: HPLC analysis of the acid hydrolyzate of (12*R*)Dehydroechinulin (**49**)

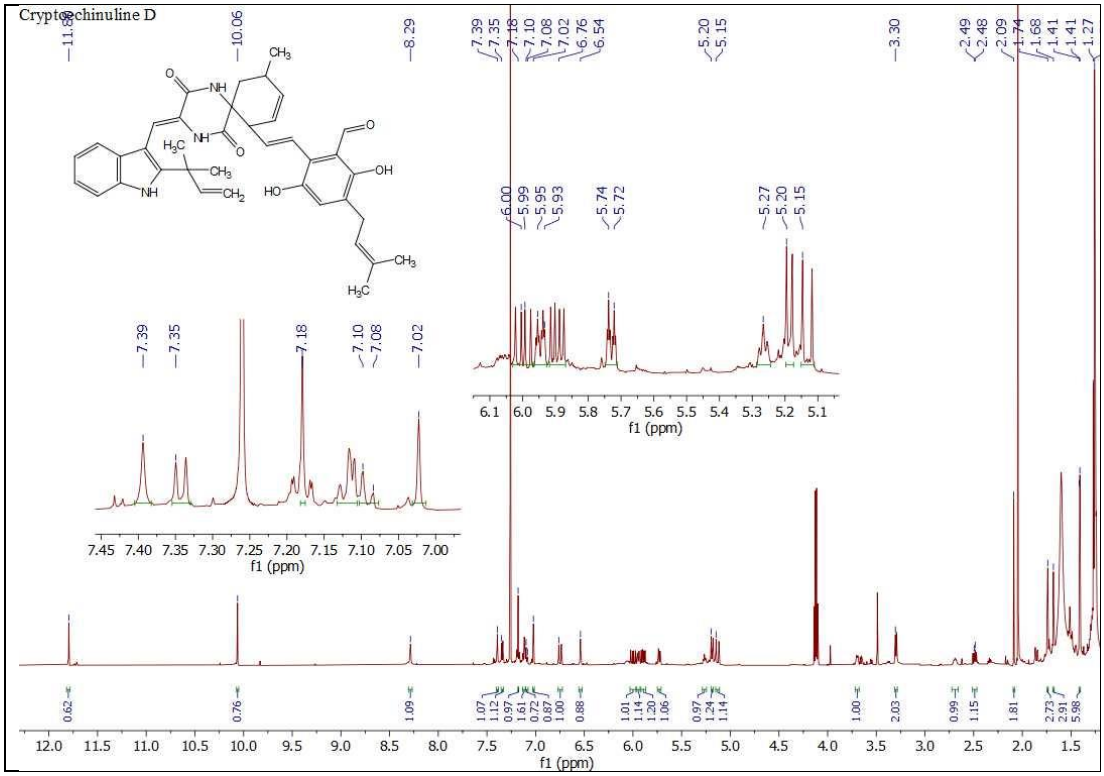

Appendix 50: ^{1}HNMR spectrum of Cryptoechinuline D (**50**) ($CDCl_3$)

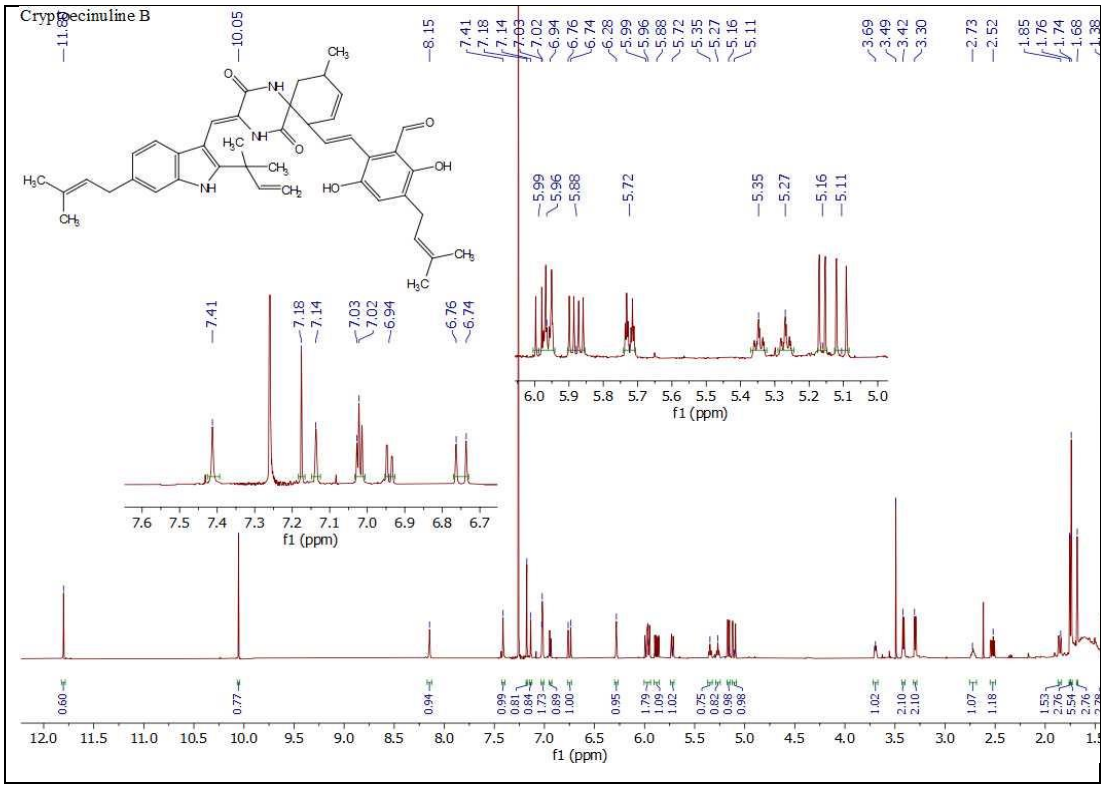

Appendix 51: ^{1}HNMR spectrum of Cryptoechinuline B (**51**) ($CDCl_3$)

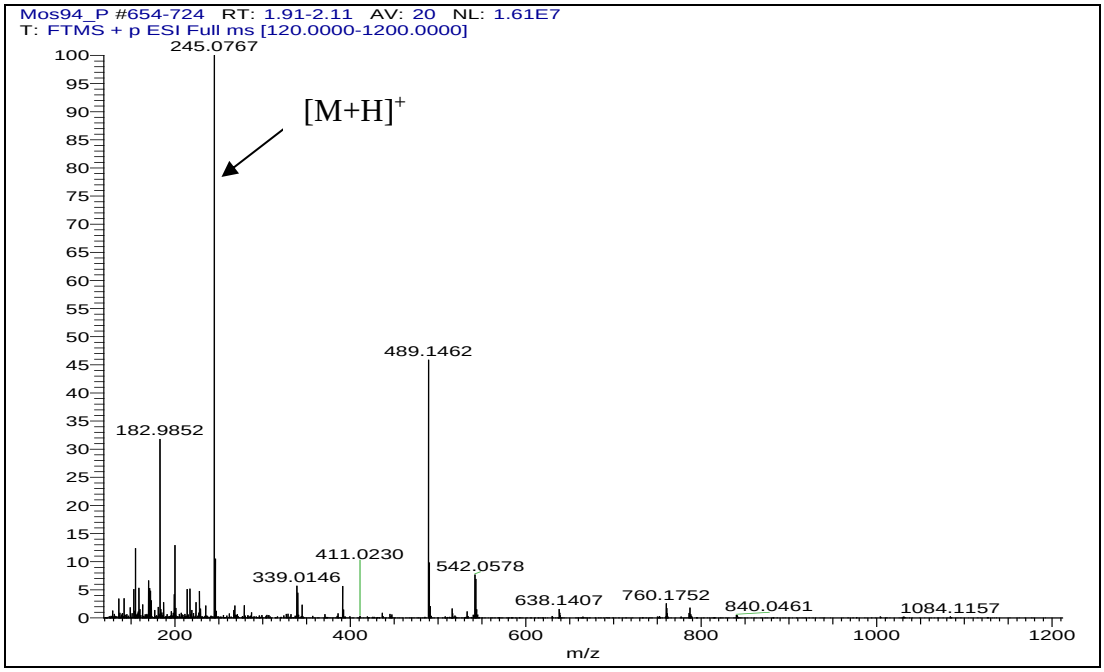

Appendix 52: HR-ESI-MS spectrum of Ochraceopyronoide (**52**)

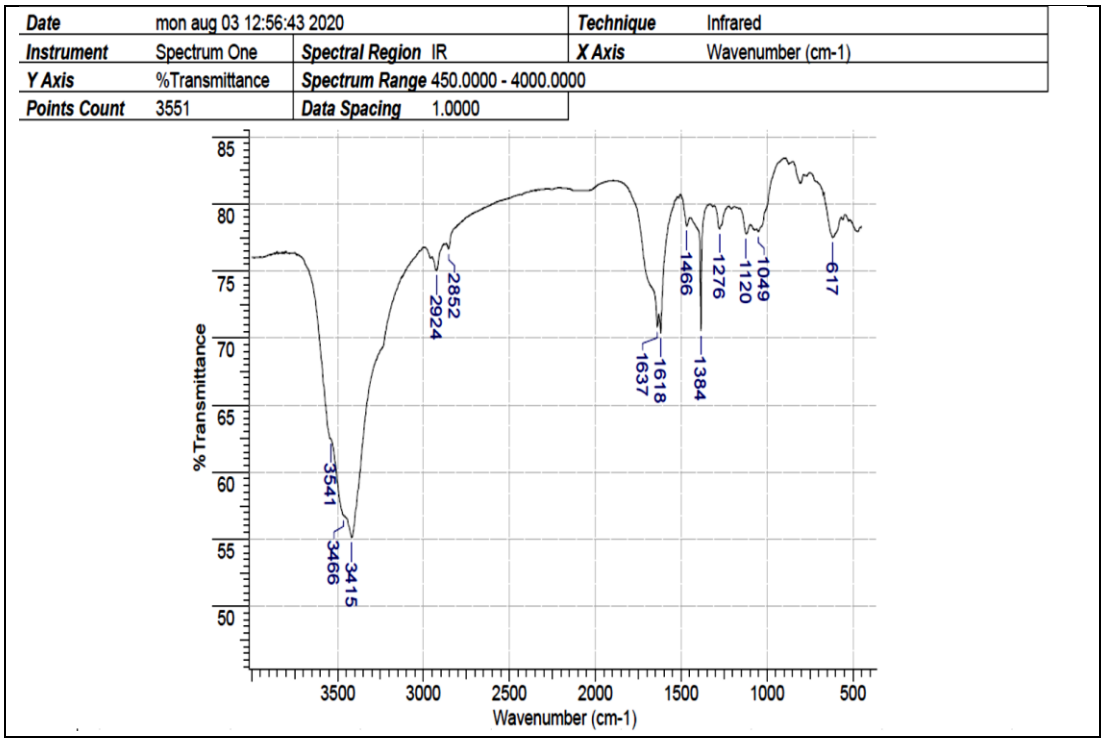

Appendix 53: IR spectrum of Ochraceopyronoide (**52**) (KBr disc)

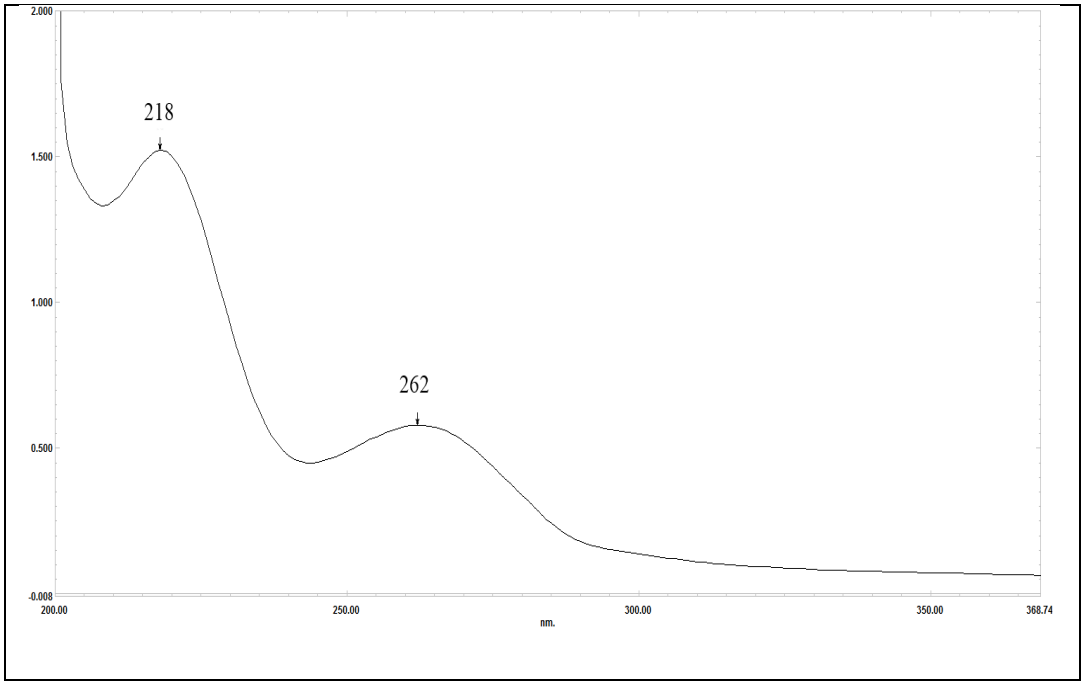

Appendix 54 : UV spectrum of Ochraceopyronoide (**52**) in MeOH

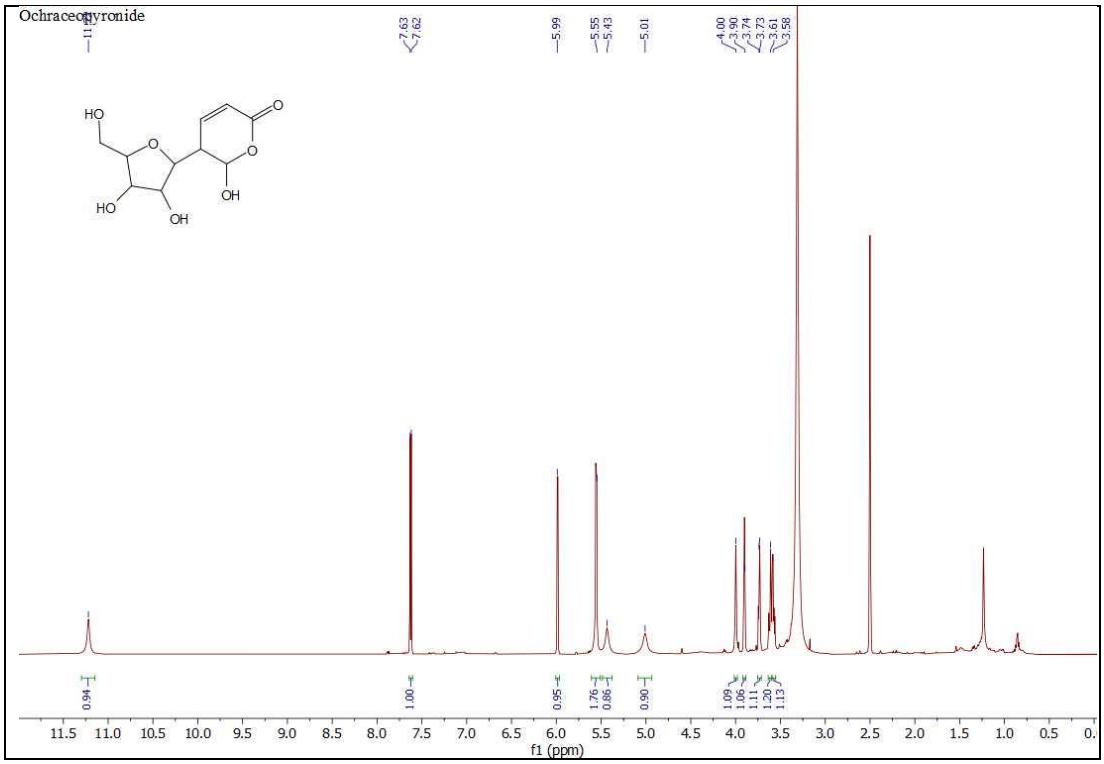

Appendix 55: ^{1}HNMR spectrum of Ochraceopyronoide (**52**) (DMSO-d_6)

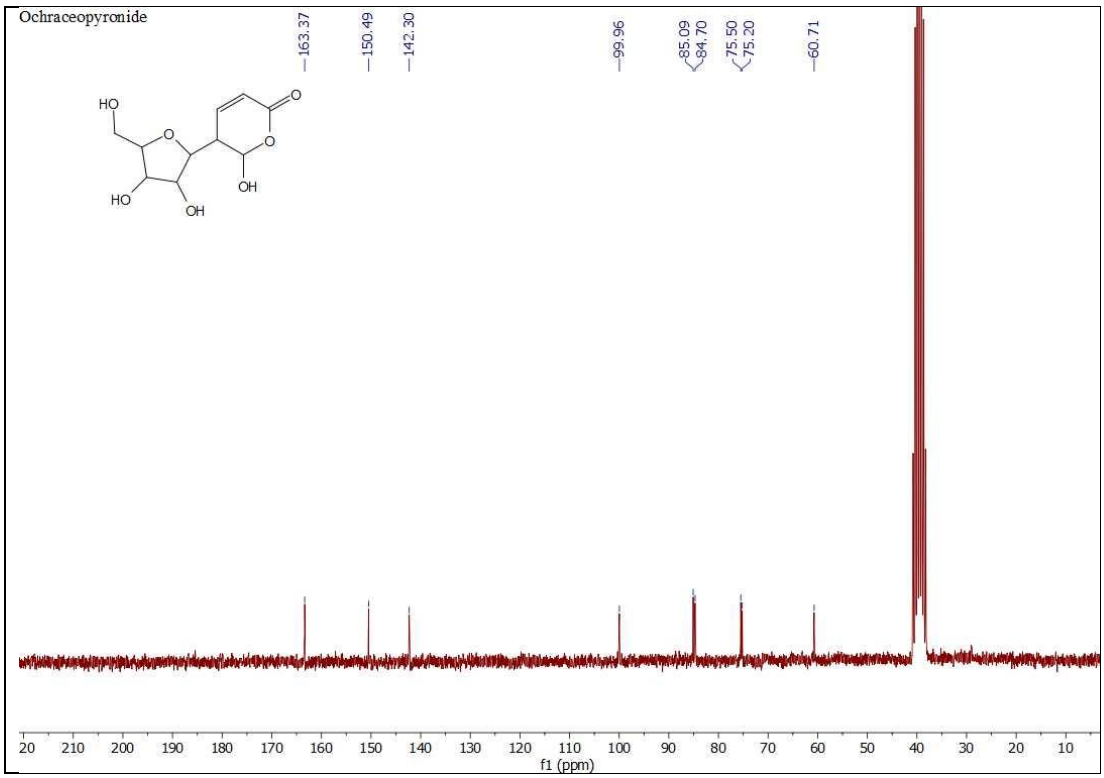

Appendix 56: ^{13}C NMR spectrum of Ochraceopyronoide (**52**) (DMSO-d_6)

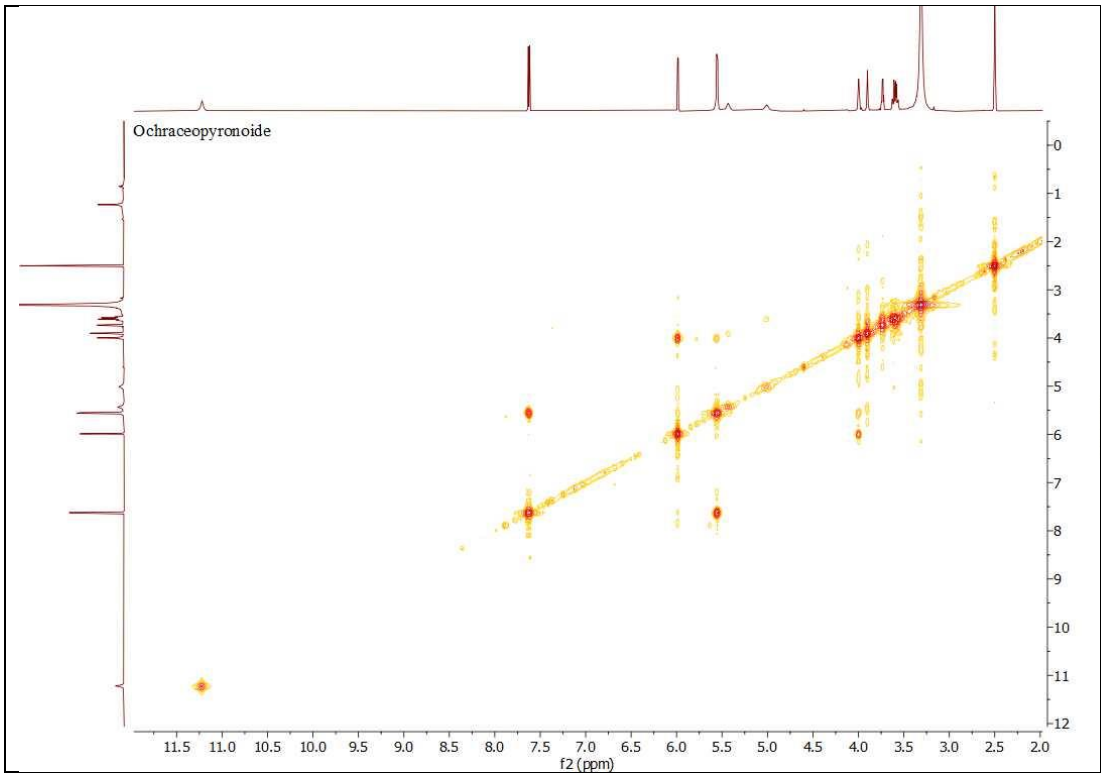

Appendix 57: ^{1}H-^{1}H COSY spectrum of Ochraceopyronoide (**52**) (DMSO-d_6)

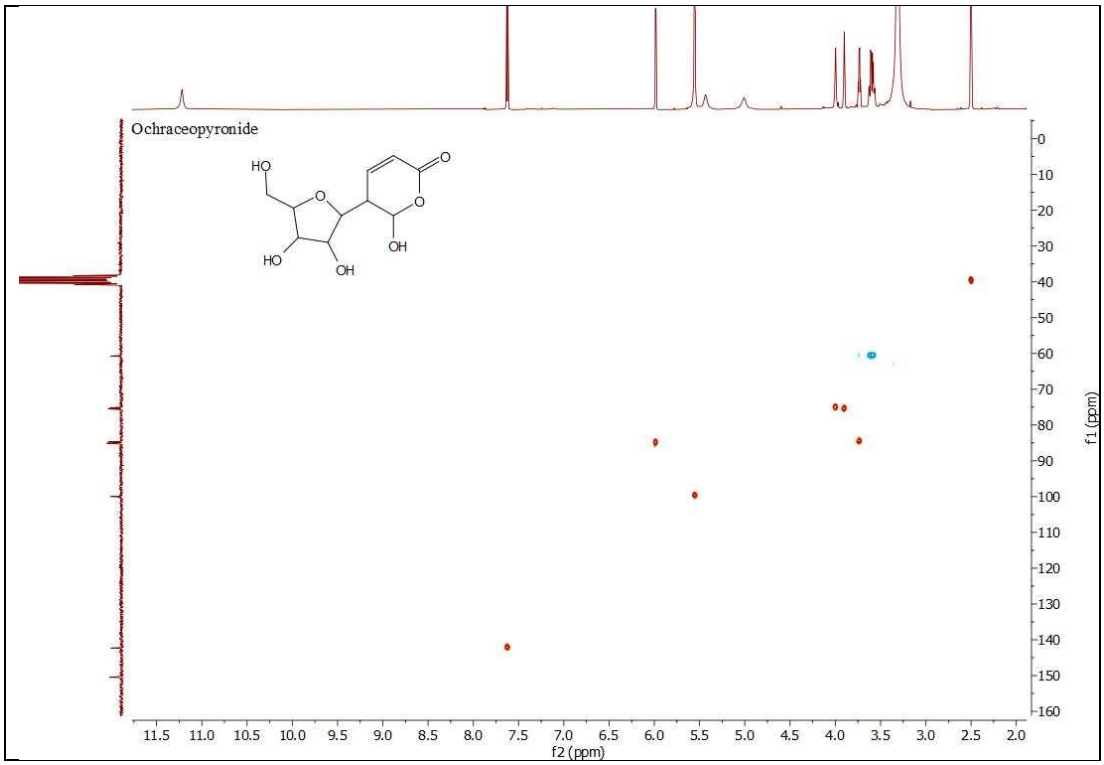

Appendix 58: HSQC spectrum of Ochraceopyronoide (**52**) (DMSO-d_6)

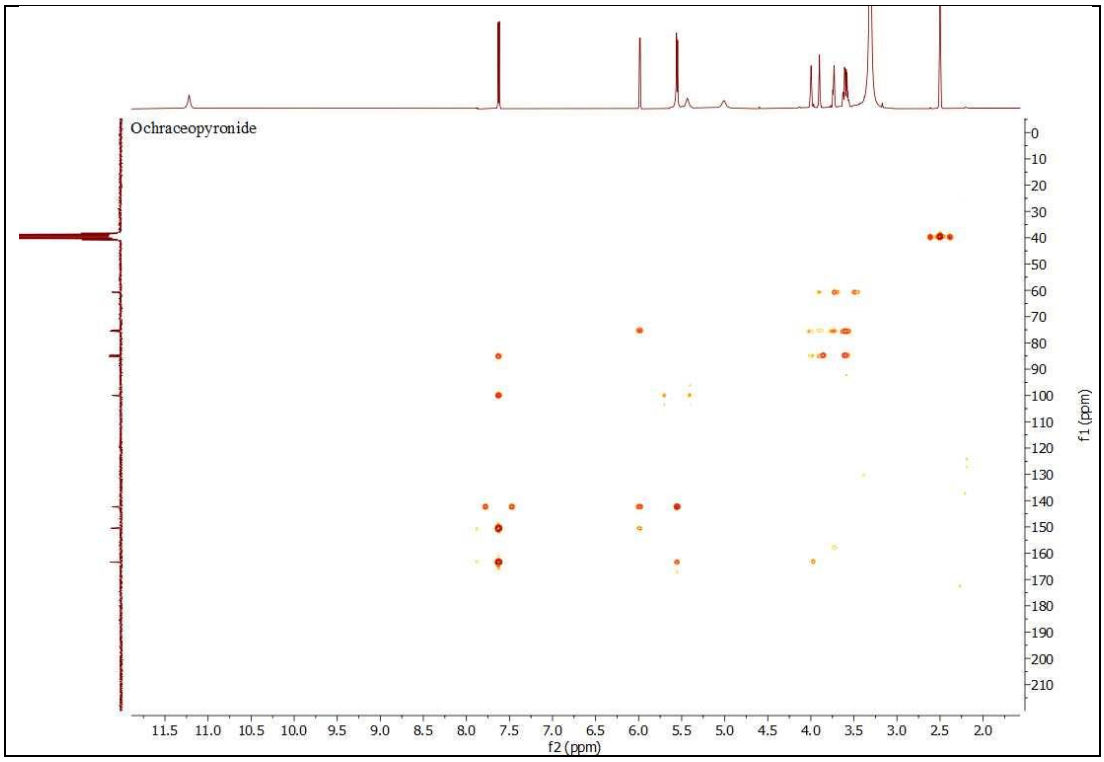

Appendix 59: HMBC spectrum of Ochraceopyronoide (**52**) (DMSO-d_6)

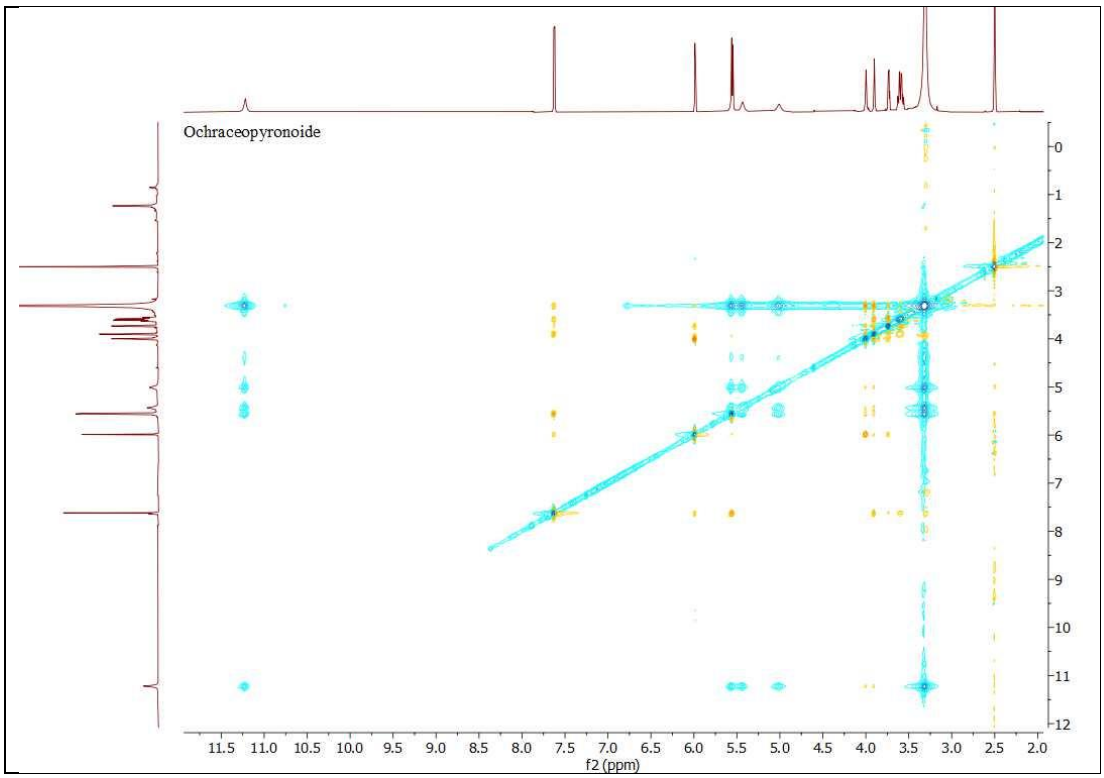

Appendix 60: NOESY spectrum of Ochraceopyronoide (**52**) (DMSO-d_6)

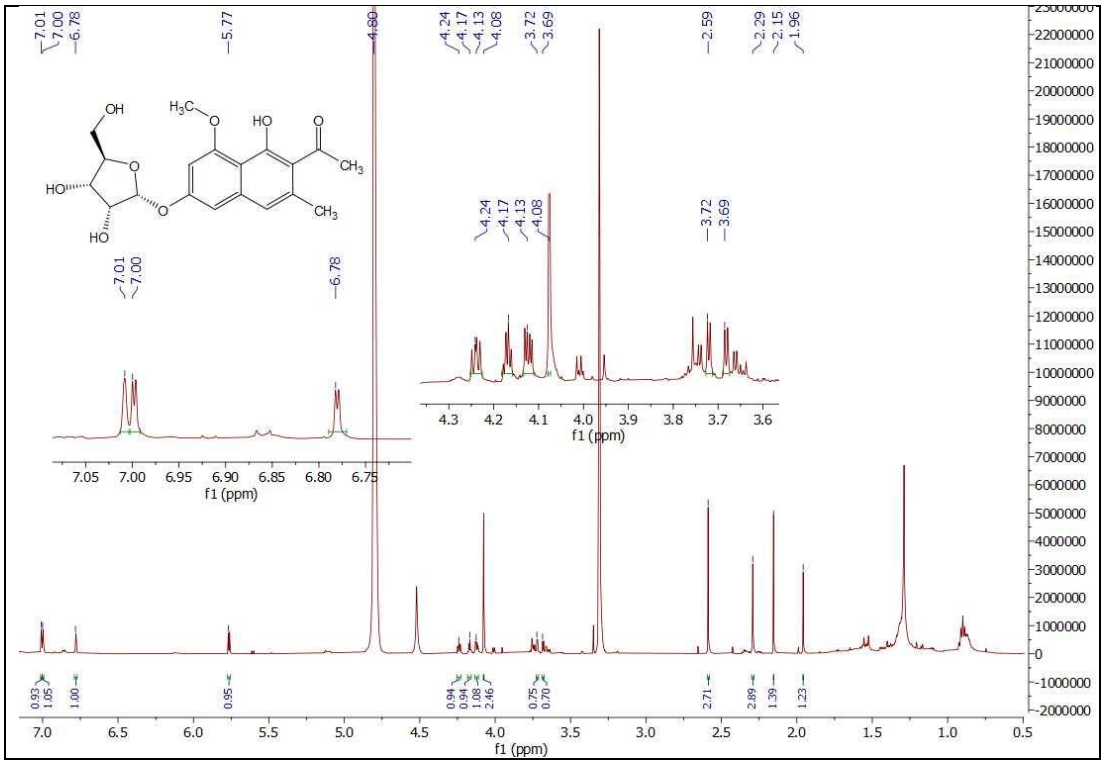

Appendix 61: ^{1}HNMR spectrum of (**53**) (MeOD-d_4)

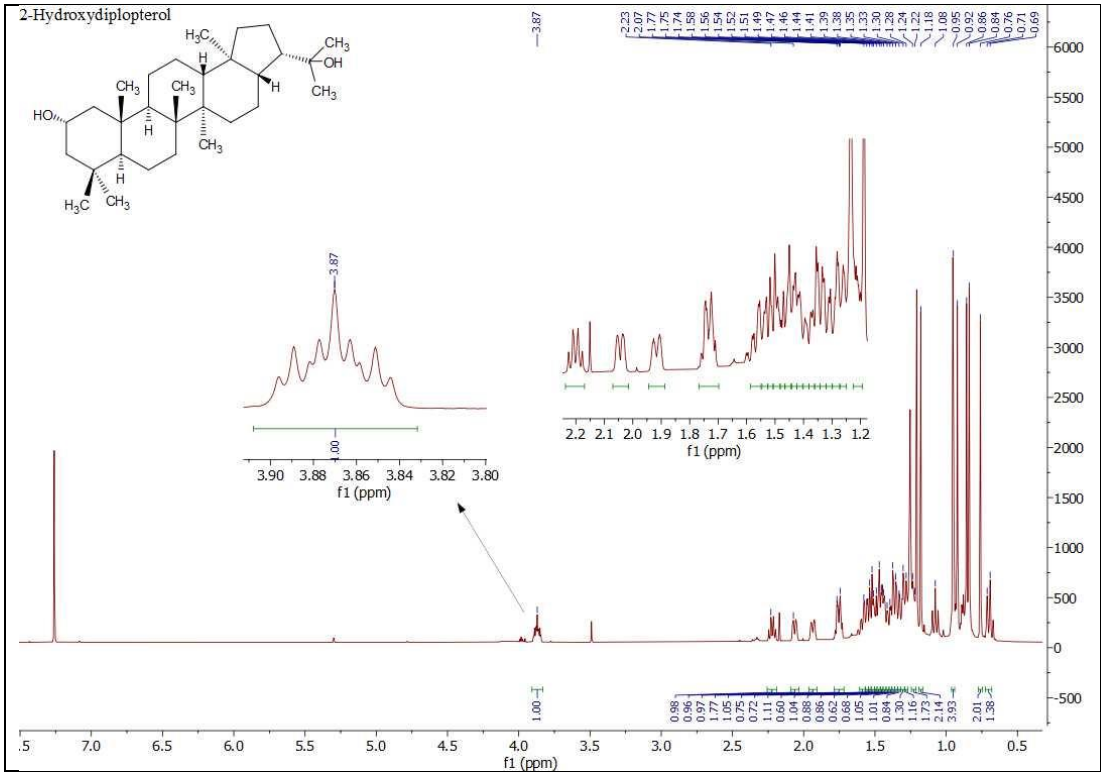

Appendix 62: ^{1}HNMR spectrum of 2-Hydroxydiplopterol (**54**) ($CDCl_3$)

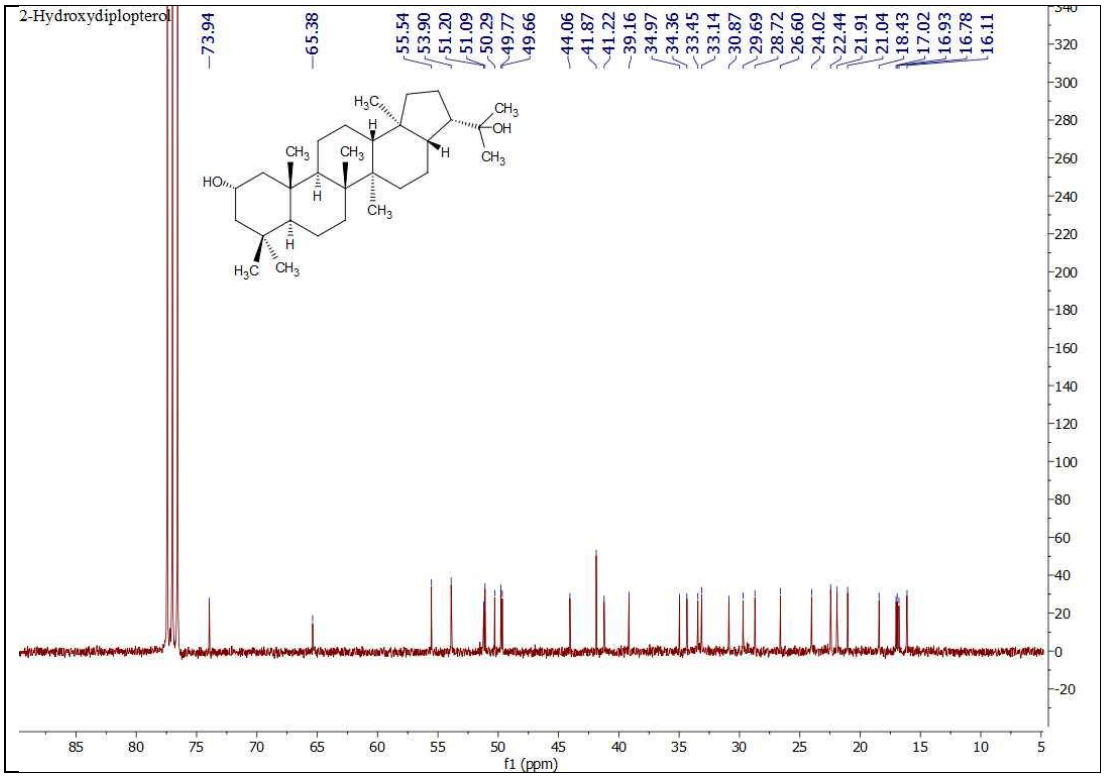

Appendix 63: ^{13}C NMR spectrum of 2-Hydroxydiplopterol (**54**) ($CDCl_3$)

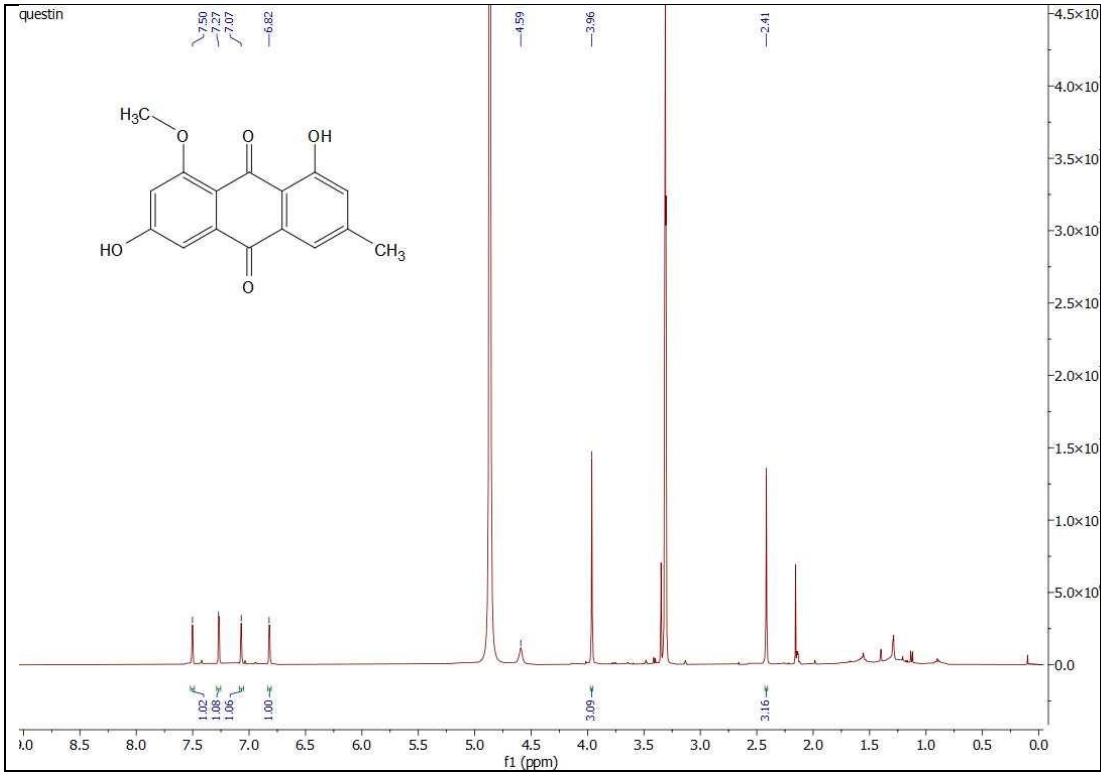

Appendix 64: $^{1}HNMR$ spectrum of Questin (**55**) (MeOD-d_4)

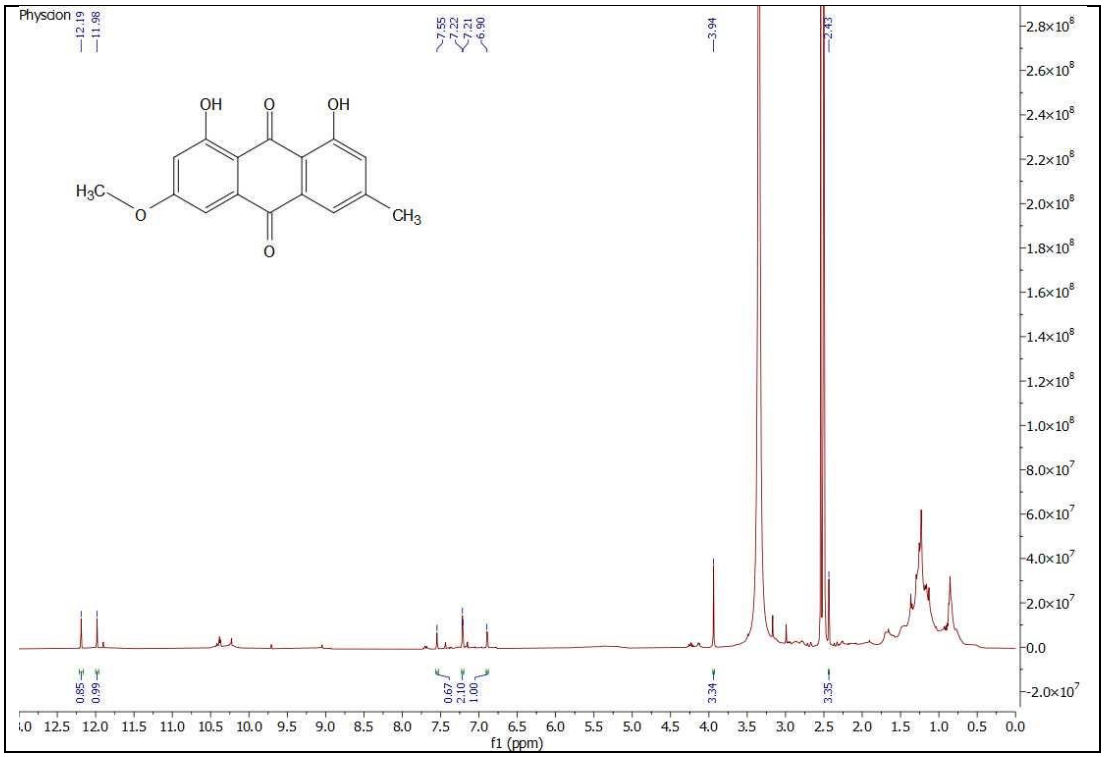

Appendix 65: ^{1}HNMR spectrum of Physcion (**56**) (DMSO-d_6)

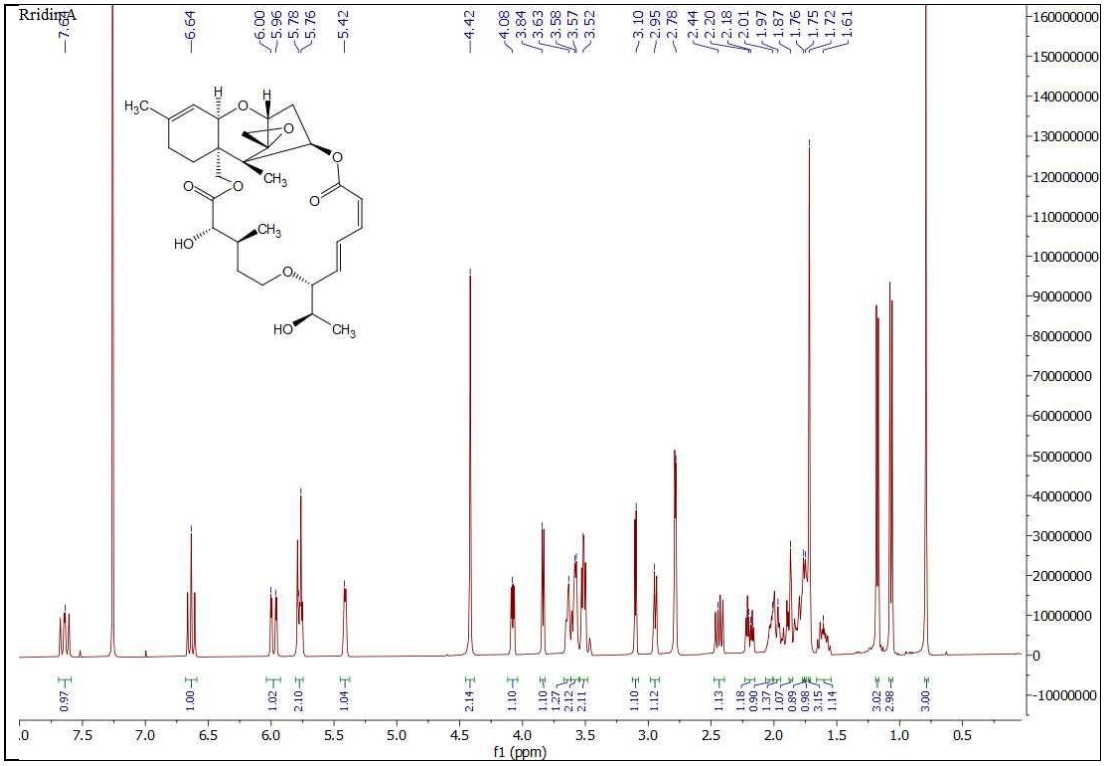

Appendix 66: ^{1}HNMR spectrum of Roridin A (**57**) ($CDCl_3$)

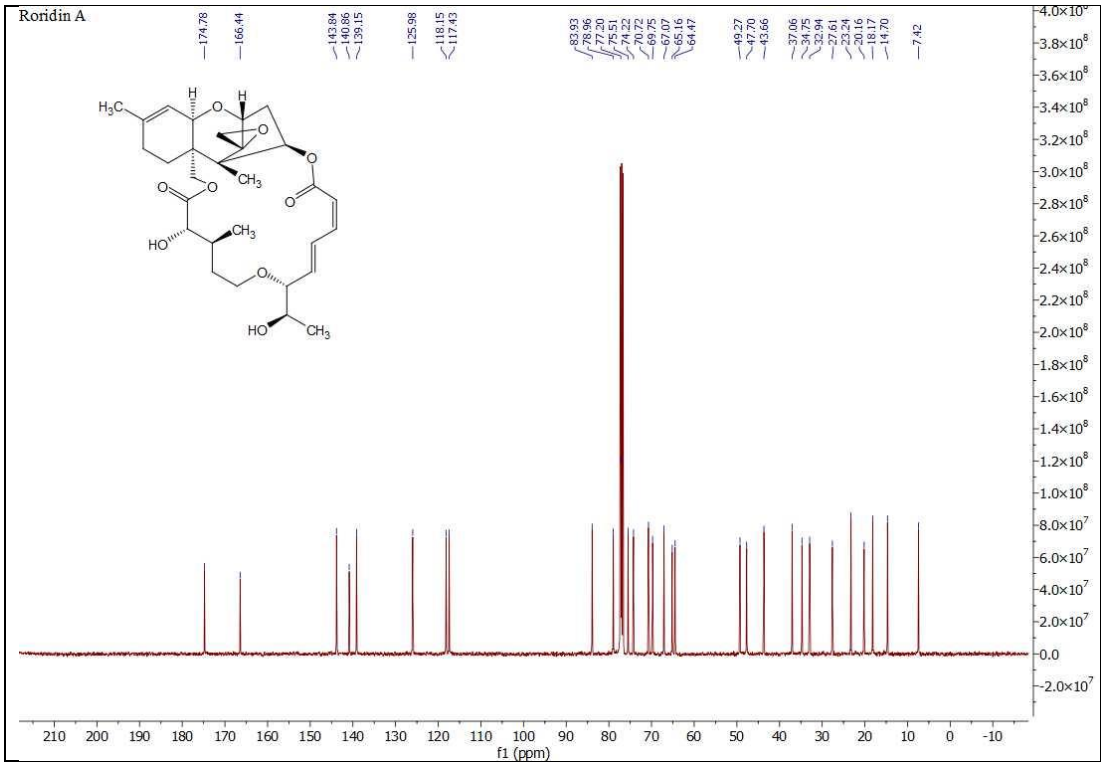

Appendix 67: ^{13}C NMR spectrum of Roridin A (**57**) ($CDCl_3$)

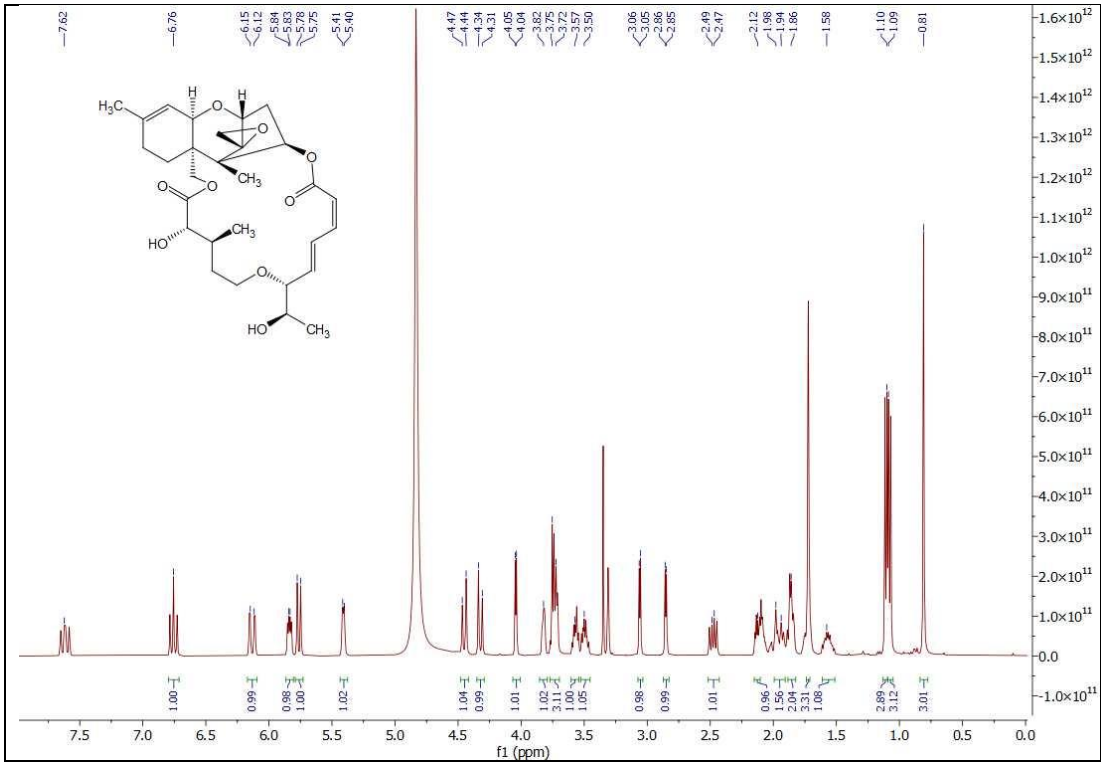

Appendix 68: $^{1}HNMR$ spectrum of Roridin A (**57**) (MeOD-d_4)

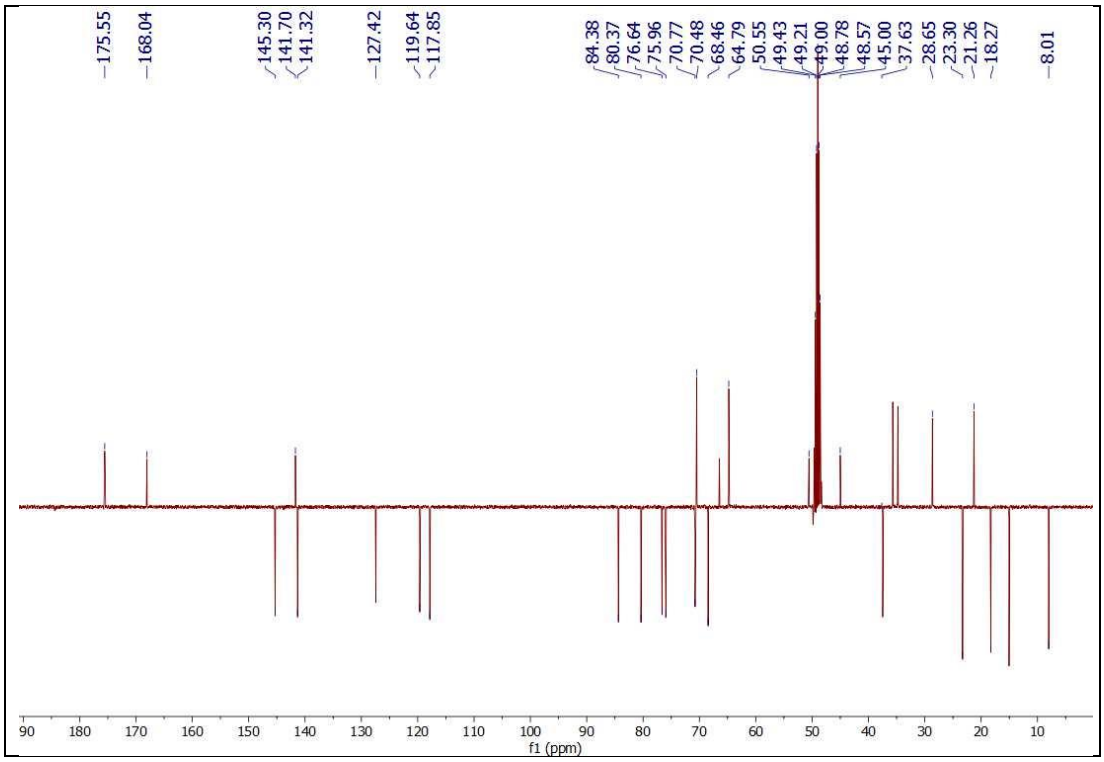

Appendix 69: CNMR DEPT-135 spectrum of Roridin A (**57**) (MeOD-d_4)

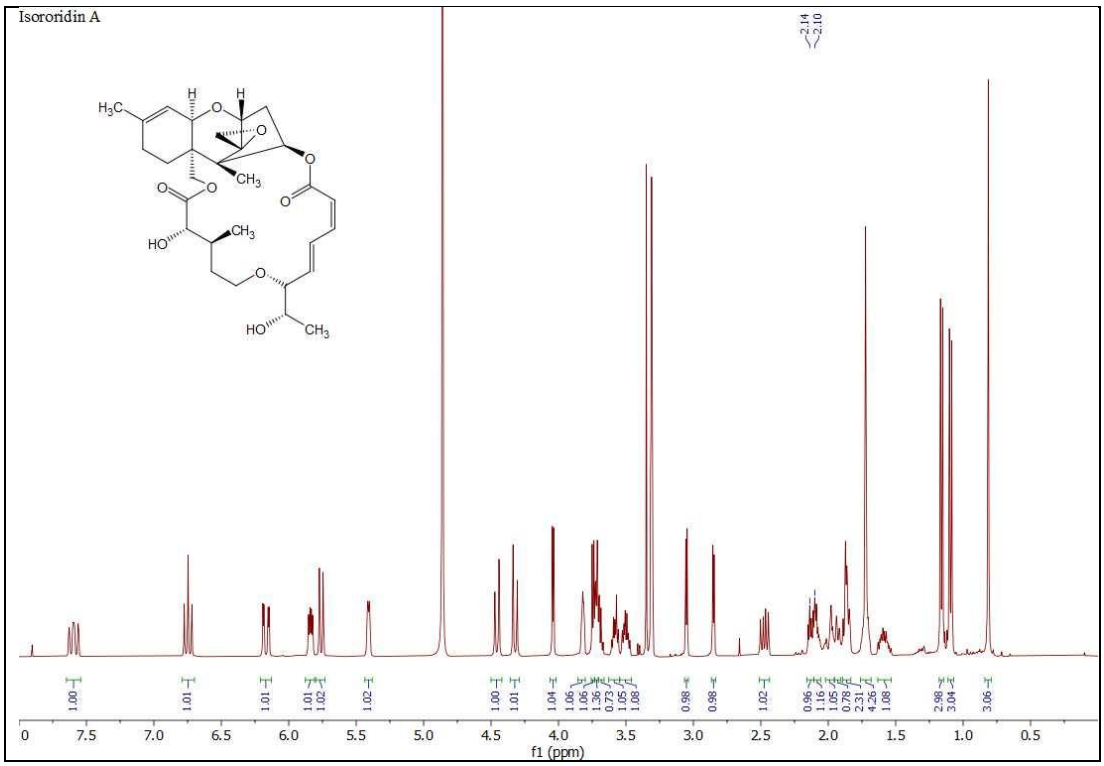

Appendix 70: ^{1}HNMR spectrum of Isororidin A (**58**) (MeOD-d_4)

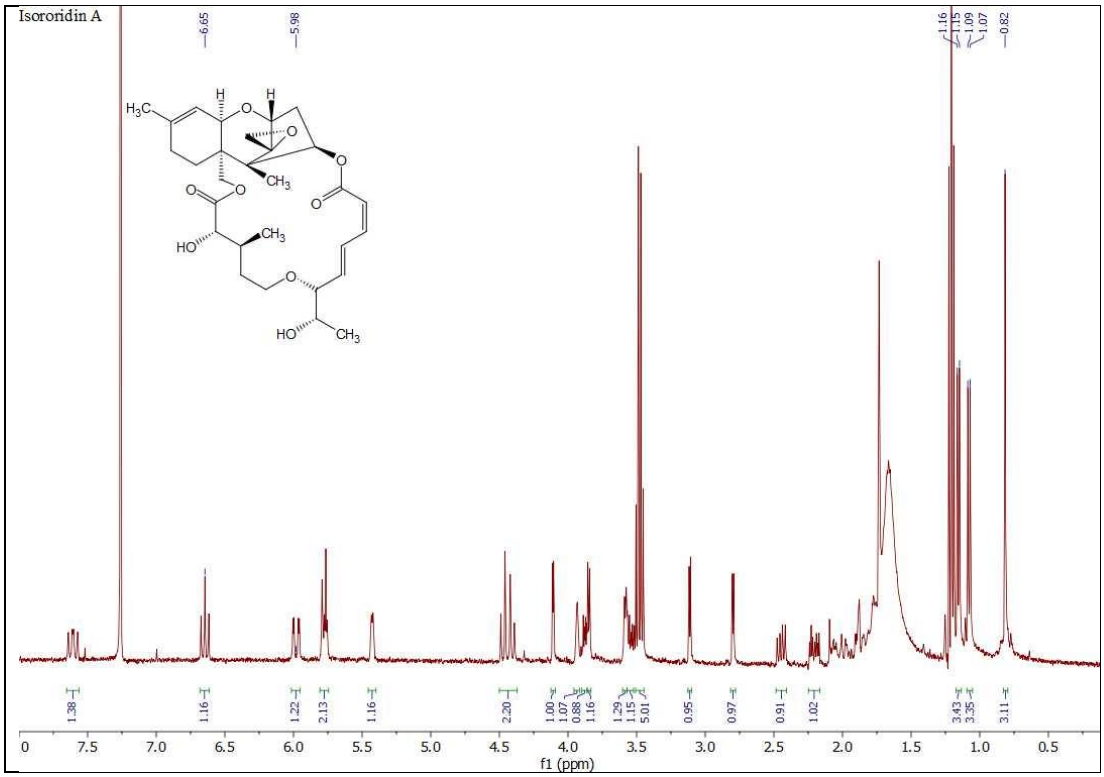

Appendix 71: ^{1}HNMR spectrum of Isororidin A (**58**) ($CDCl_3$)

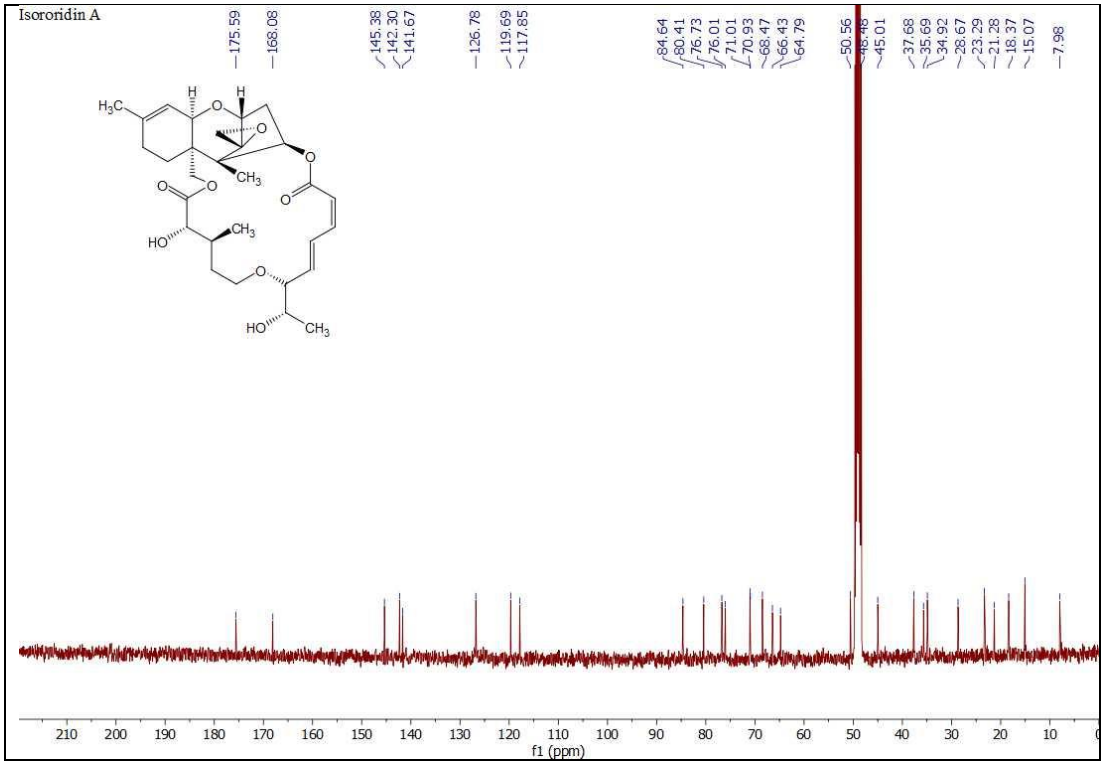

Appendix 72: ^{13}C NMR spectrum of Isororidin A (**58**) (MeOD-d_4)

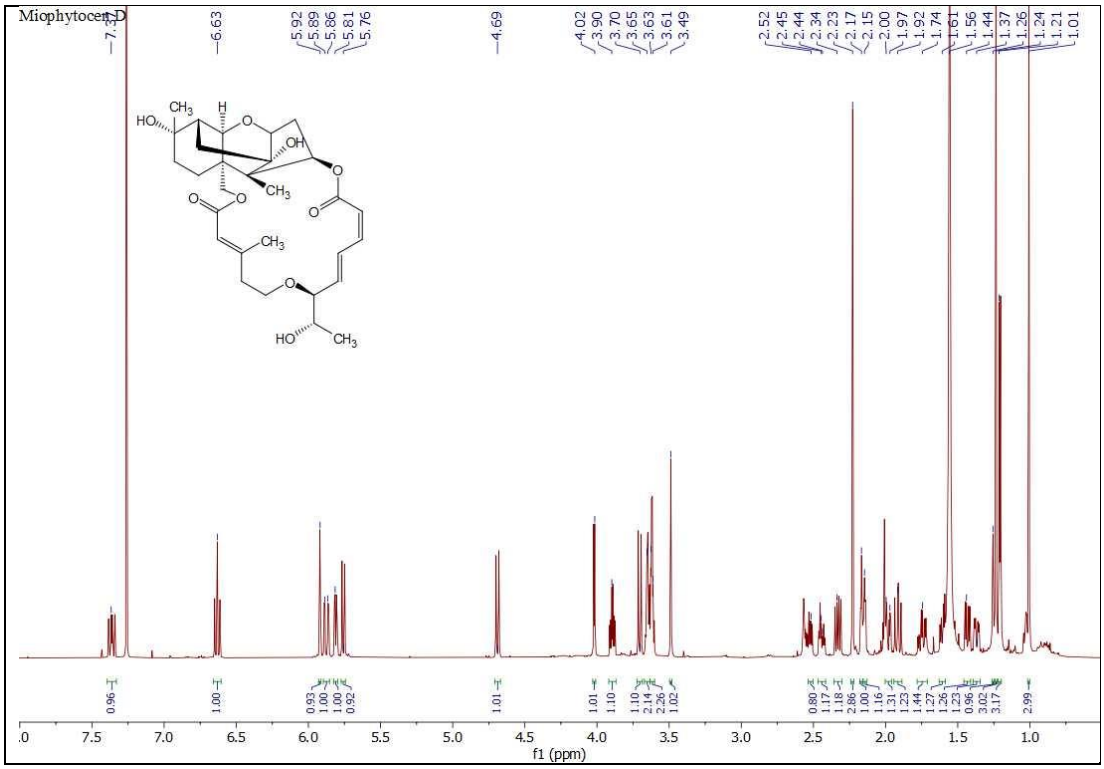

Appendix 73: ^{1}HNMR spectrum of Miophytocen D (**59**) ($CDCl_3$)

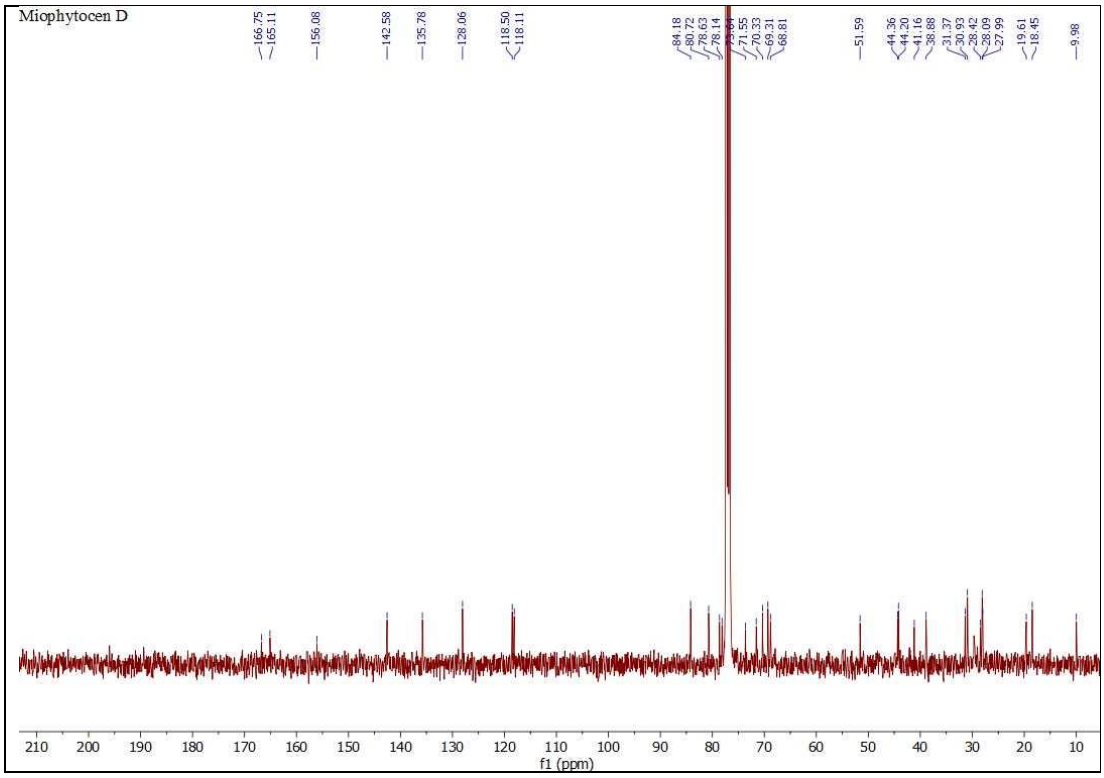

Appendix 74: ^{13}C NMR spectrum of Miophytocen D (**59**) ($CDCl_3$)

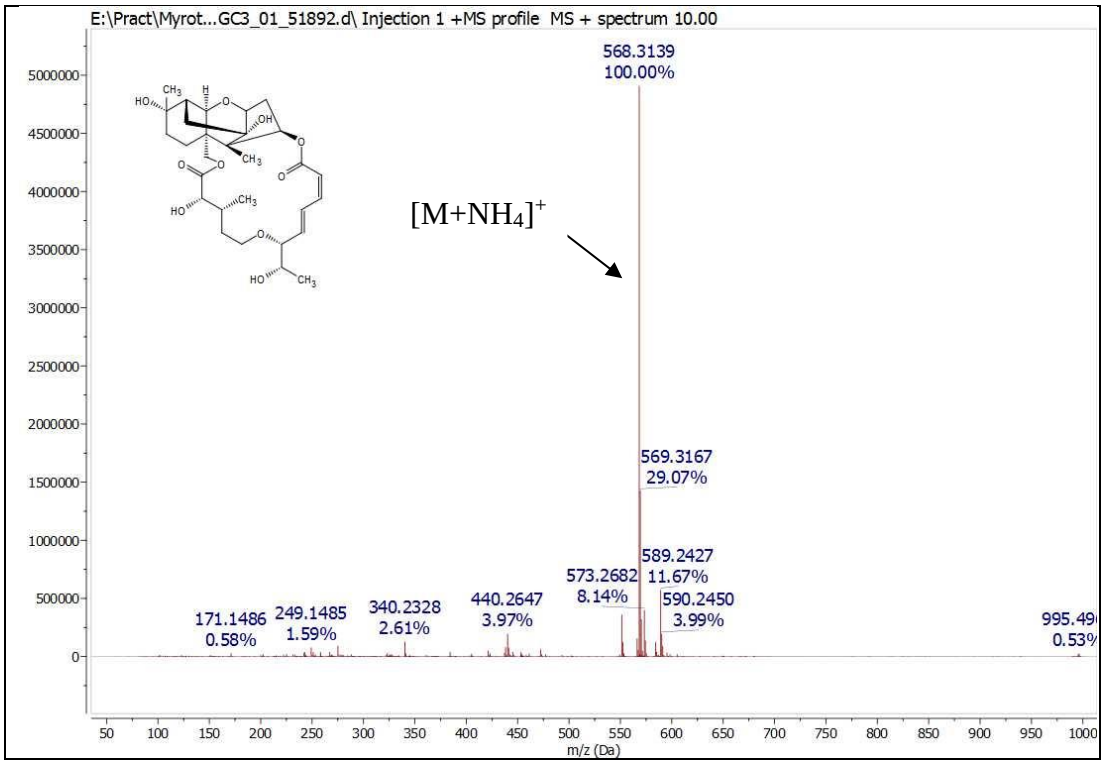

Appendix 75: HR(+)ESI-MS spectrum of Miophytocen E (**60**)

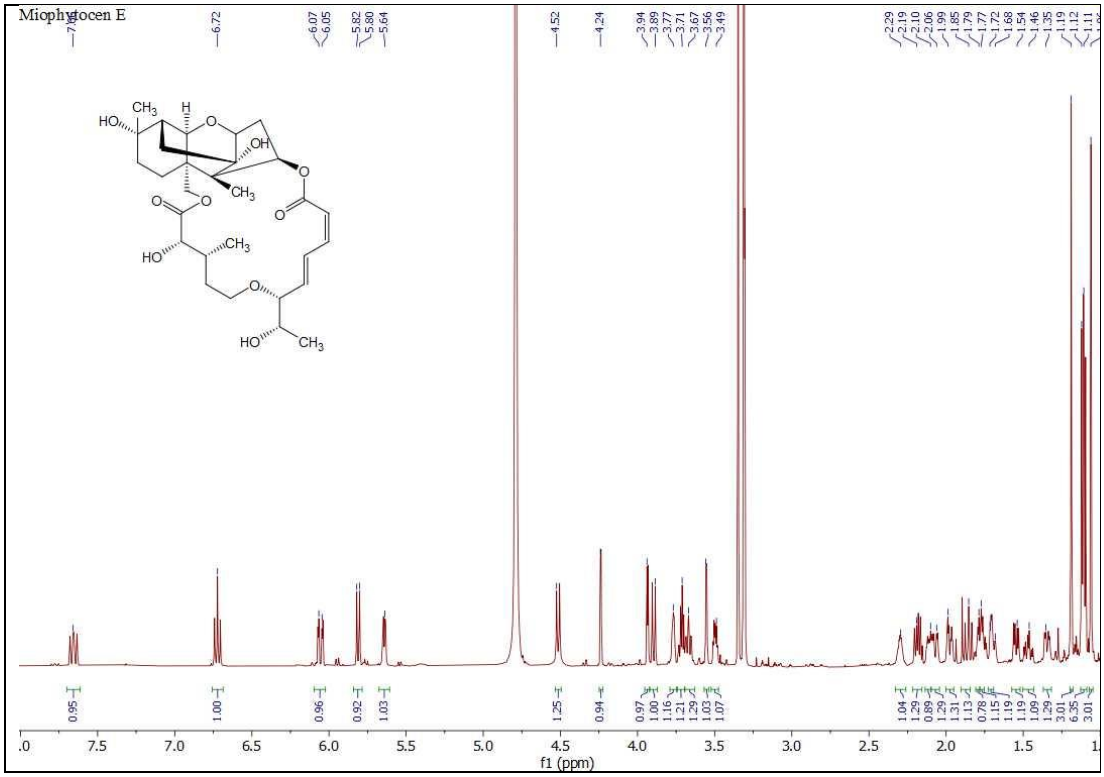

Appendix 76 : ^{1}HNMR spectrum of Miophytocen E (**60**) (MeOD-d_4)

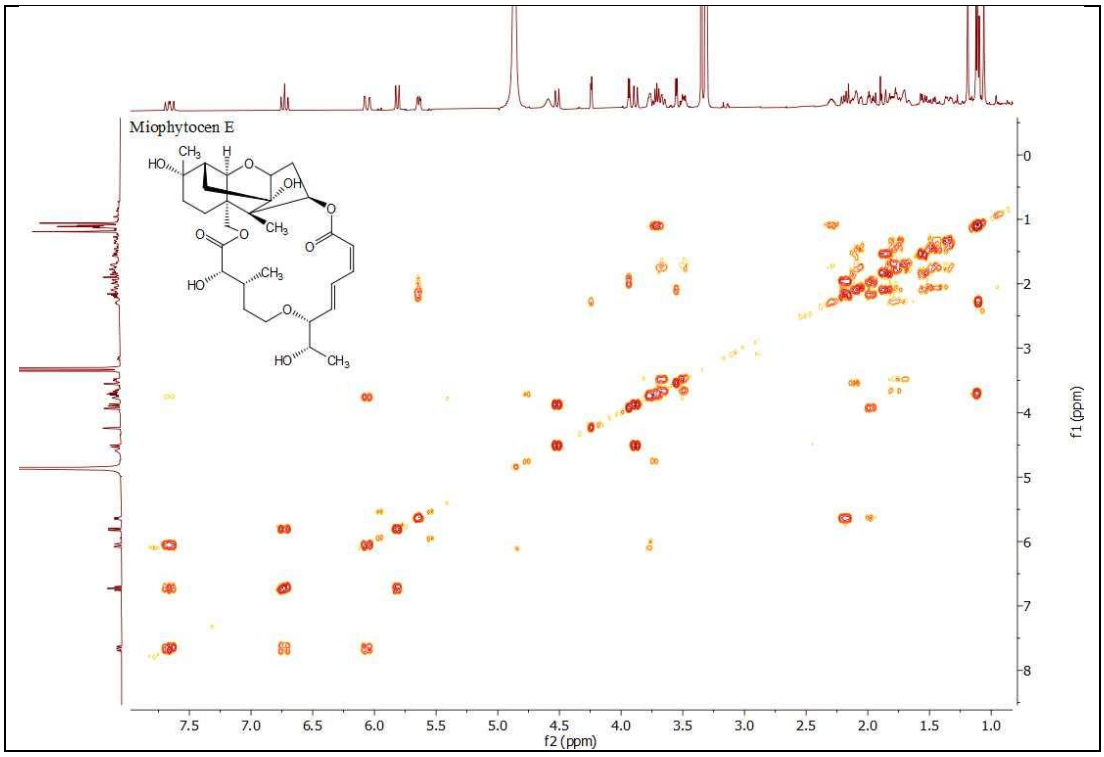

Appendix 77 : ^{1}H-^{1}H COSY spectrum of Miophytocen E (**60**) (MeOD-d_4)

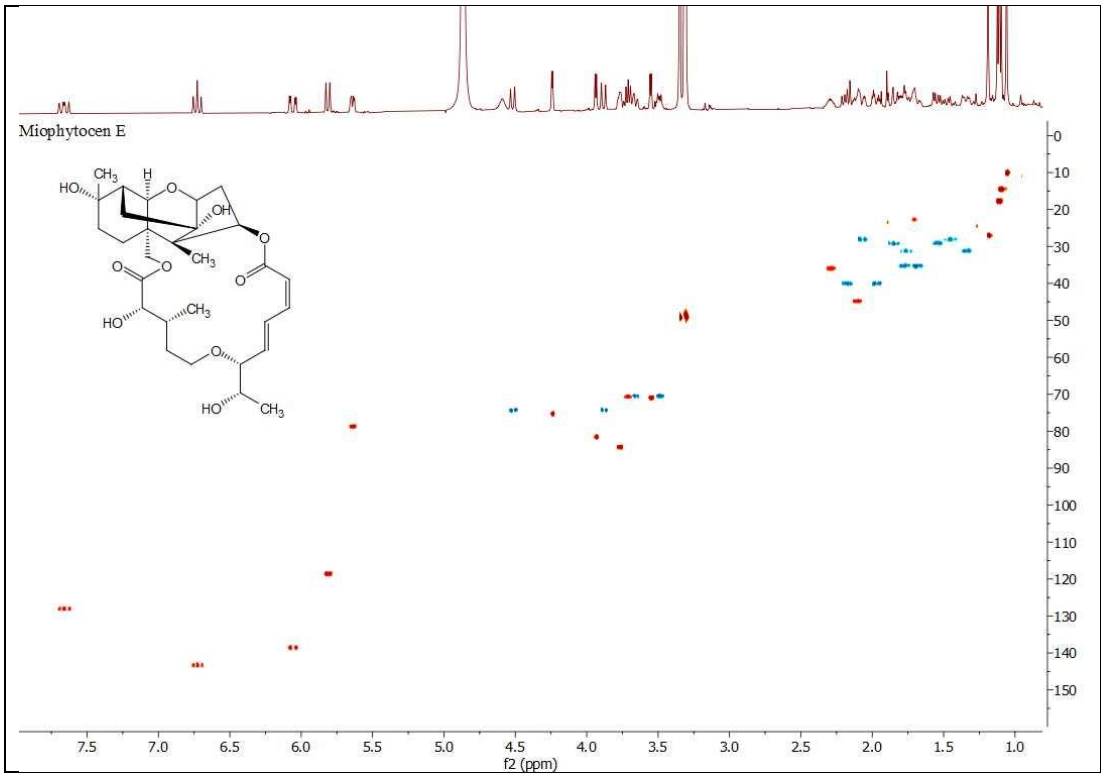

Appendix 78: HSQC spectrum of Miophytocen E (**60**) (MeOD-d_4)

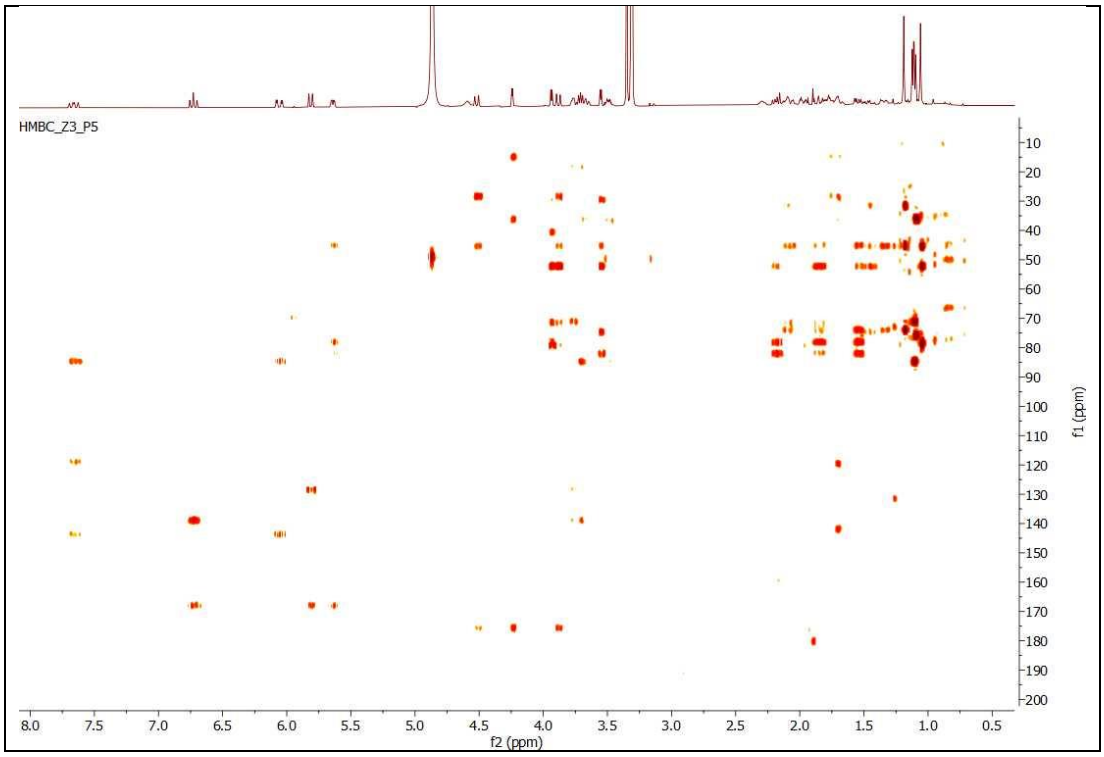

Appendix 79: HMBC spectrum of Miophytocen E (**60**) (MeOD-d_4)

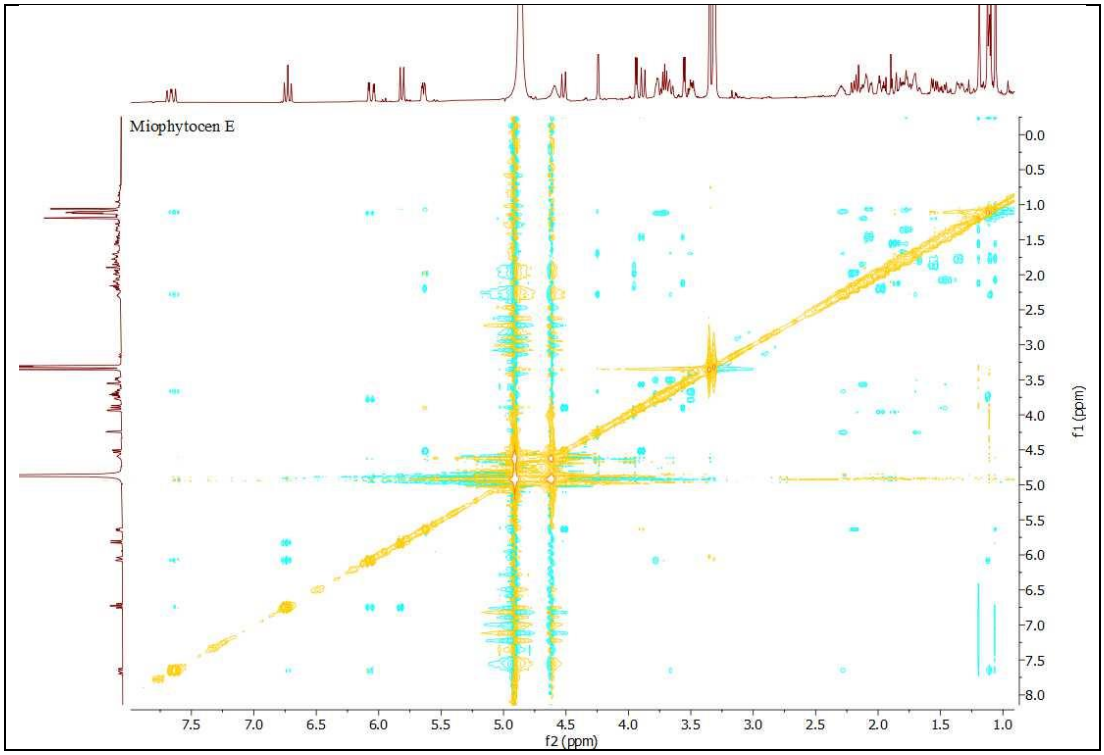

Appendix 80: NOESY spectrum of Miophytocen E (**60**) (MeOD-d_4)

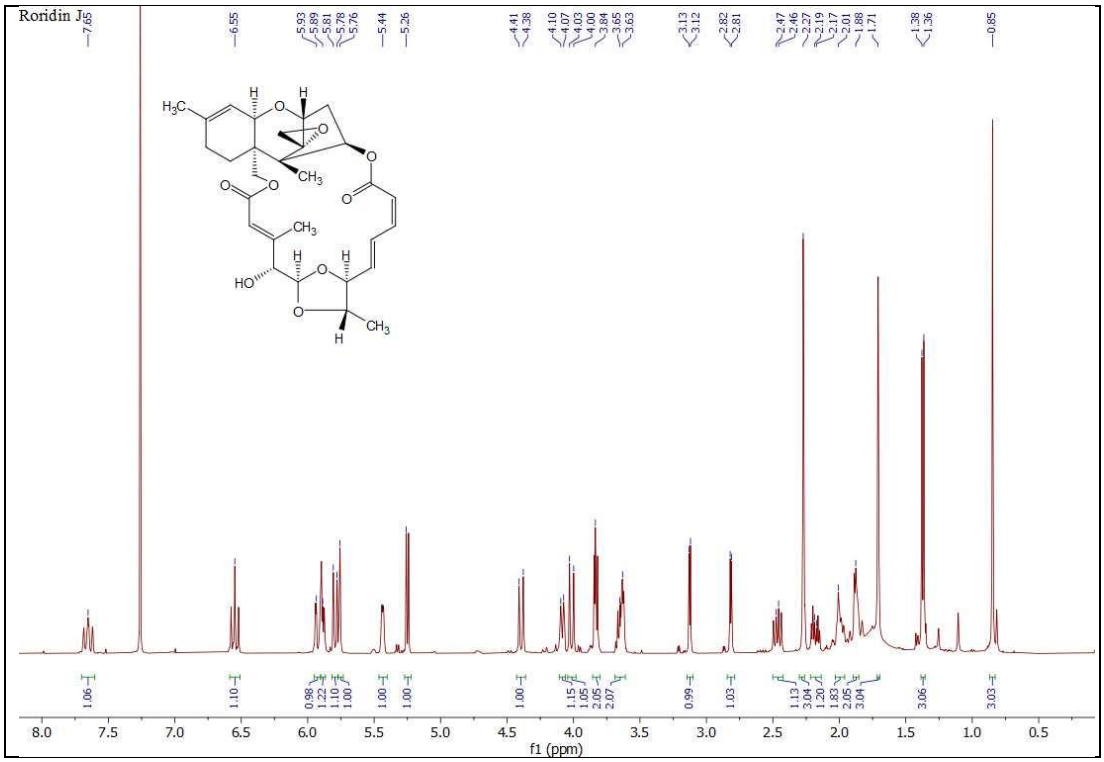

Appendix 81: ^{1}HNMR spectrum of Roridin J (**61**) ($CDCl_3$)

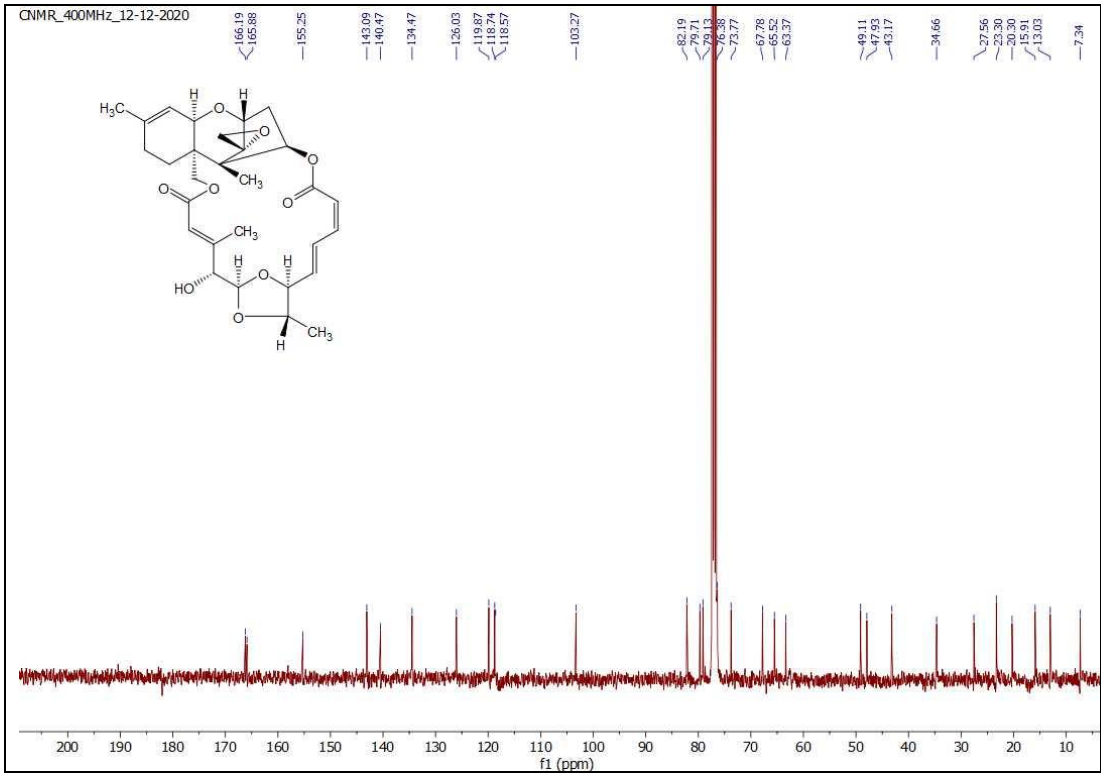

Appendix 82: ^{13}C NMR spectrum of Roridin J (**61**) ($CDCl_3$)

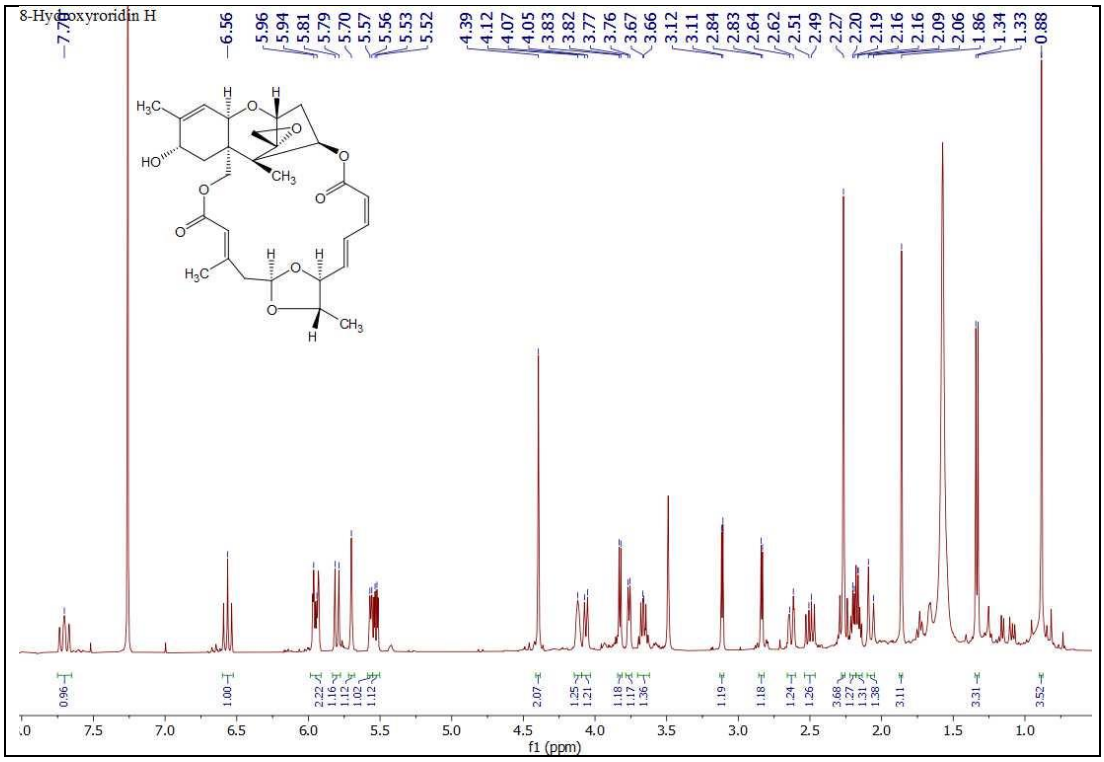

Appendix 83: ^{1}HNMR spectrum of 8-α-Hydroxyroridin H (**62**) ($CDCl_3$)

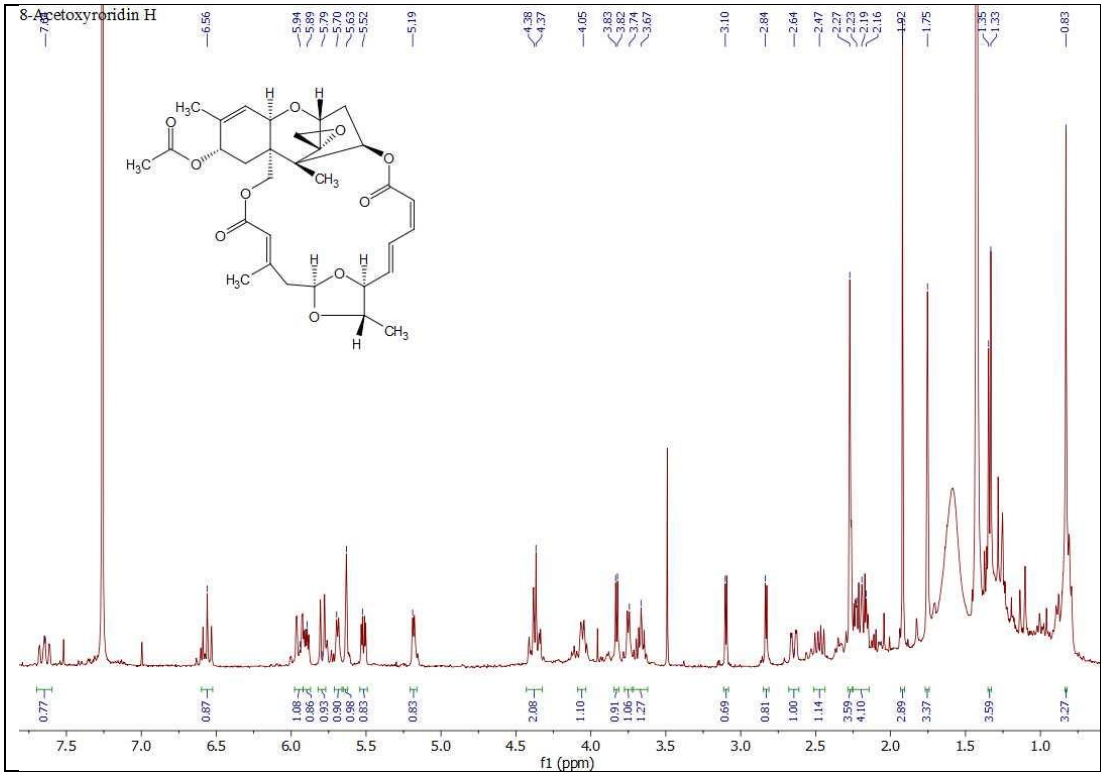

Appendix 84: ^{1}HNMR spectrum of 8-*α*-Acetoxyroridin H (**63**) ($CDCl_3$)

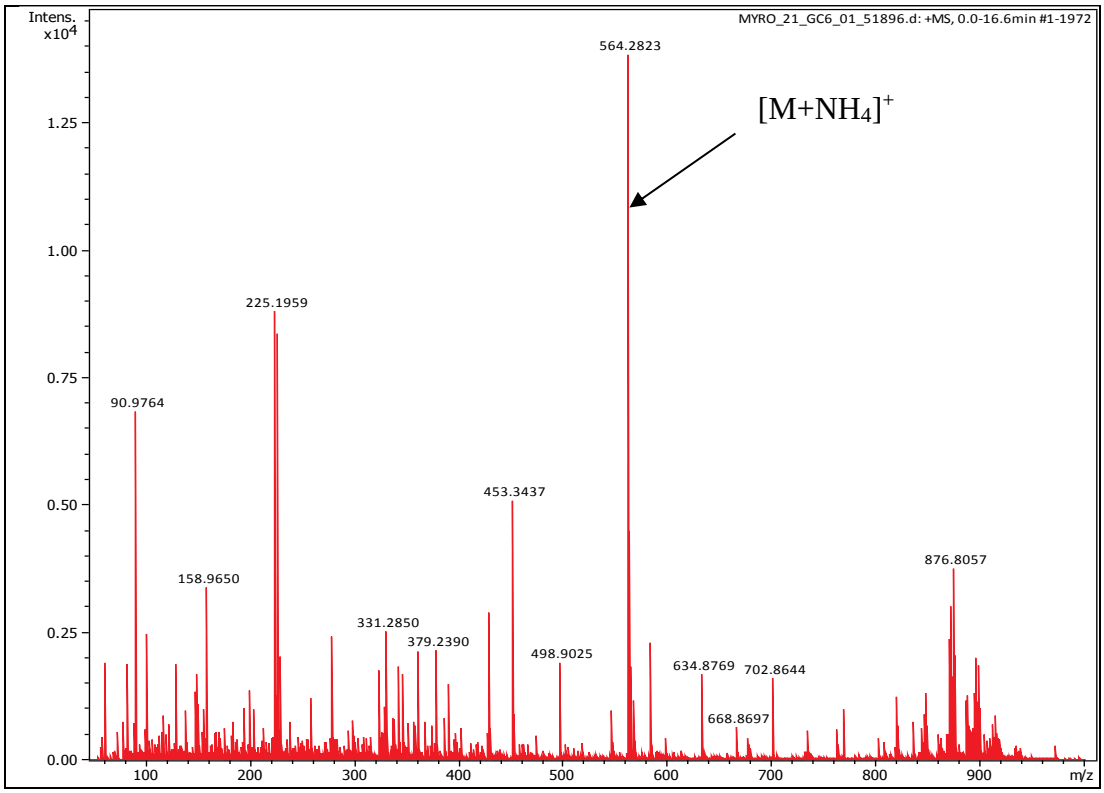

Appendix 85: HR-MS spectrum of Miophytocen F (**64**)

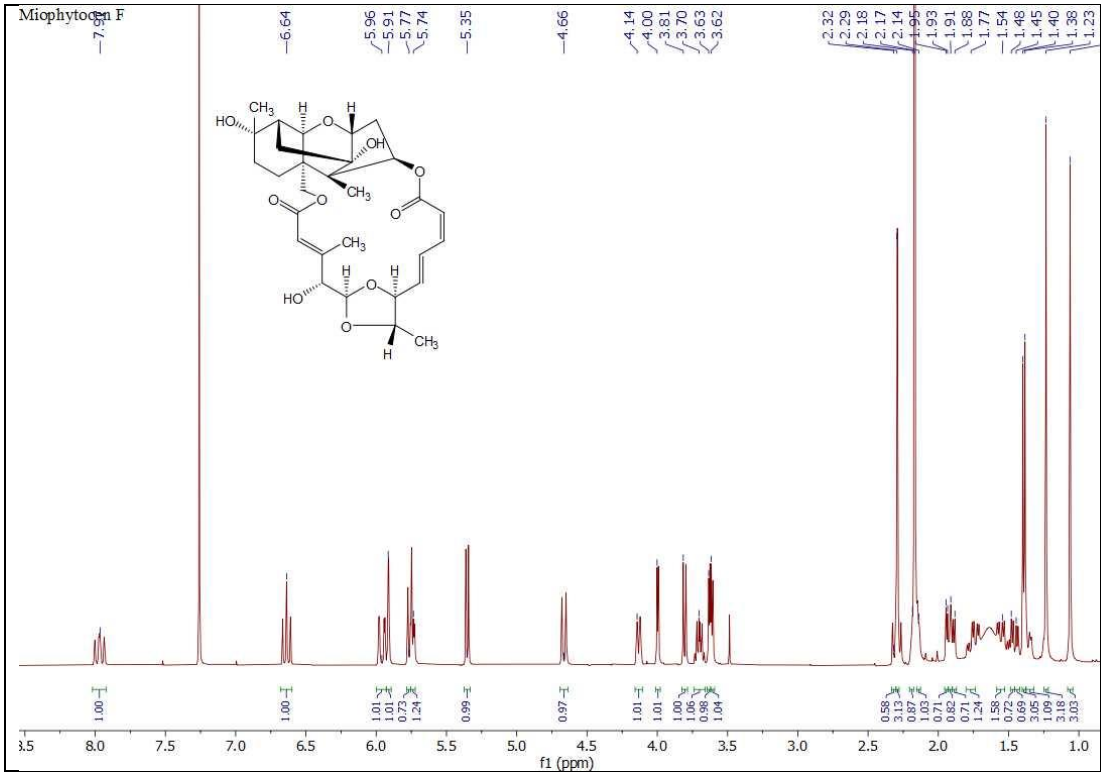

Appendix 86: ^{1}HNMR spectrum of Miophytocen F (**64**) ($CDCl_3$)

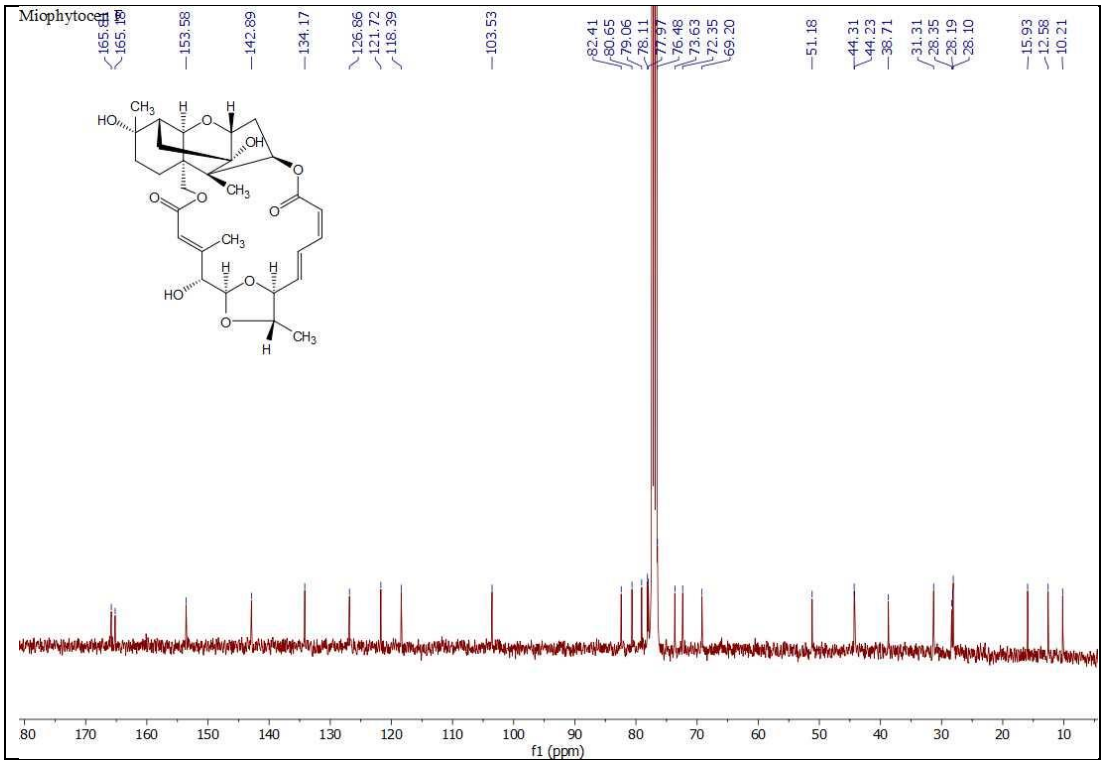

Appendix 87: ^{13}C NMR spectrum of Miophytocen F (**64**) ($CDCl_3$)

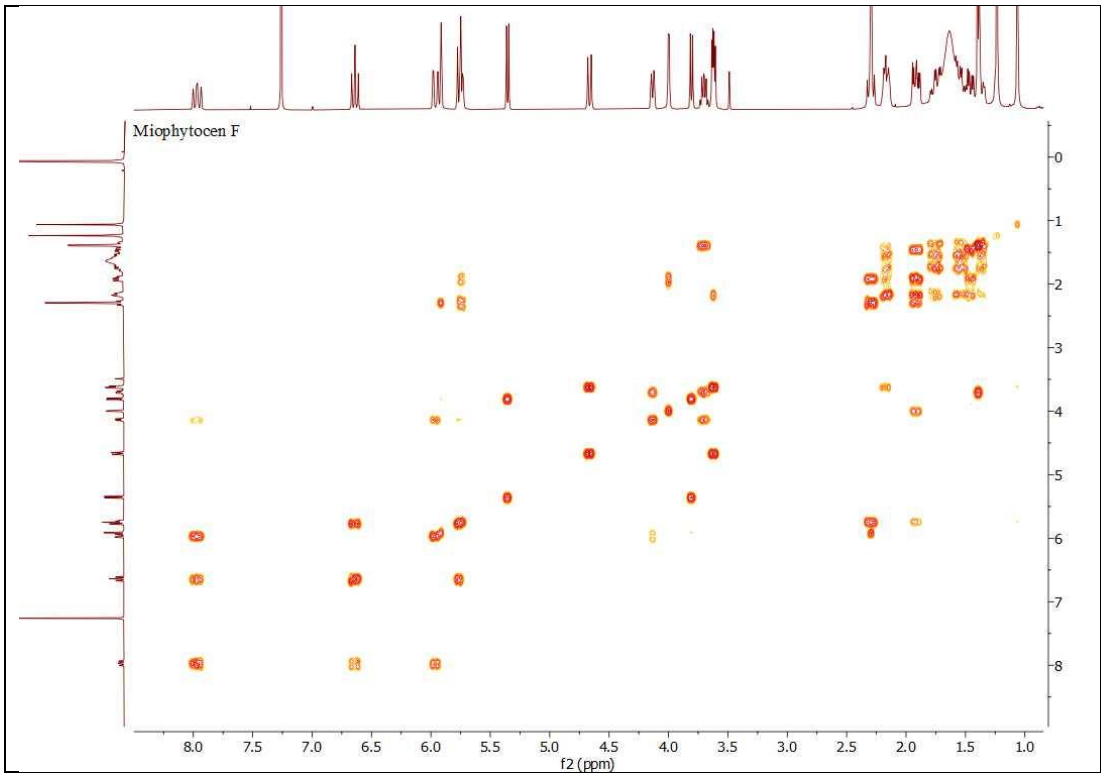

Appendix 88: ^{1}H-^{1}H COSY spectrum of Miophytocen F (**64**) ($CDCl_3$)

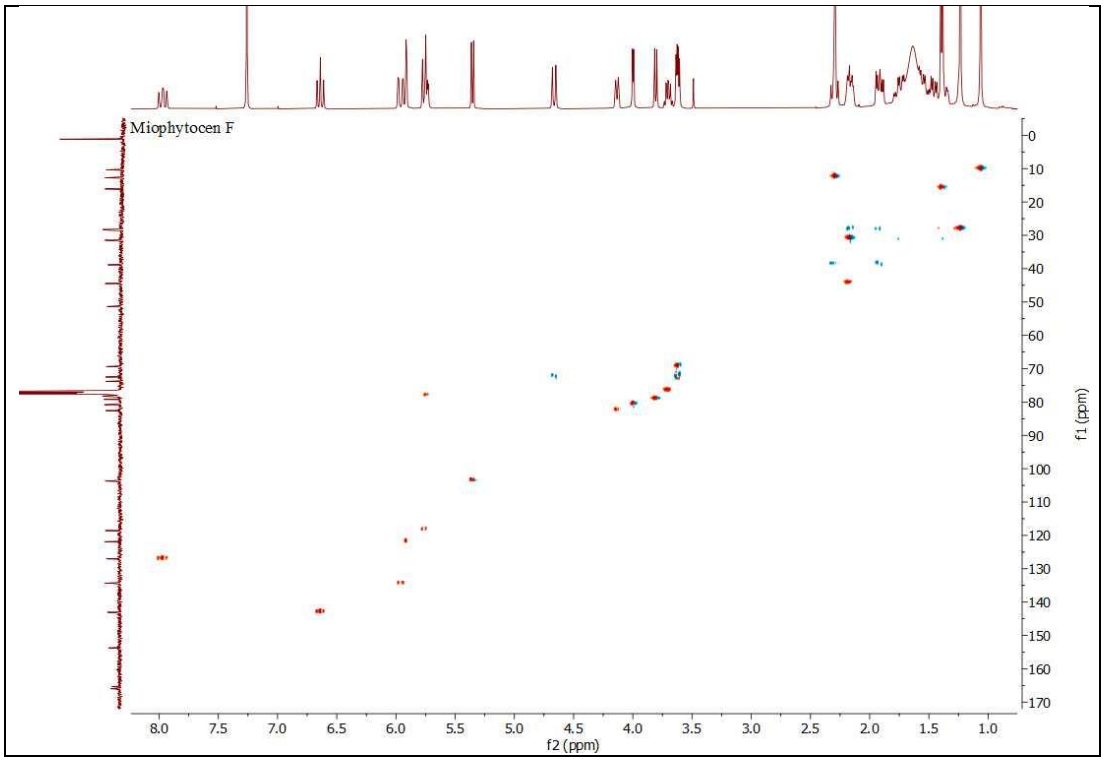

Appendix 89: HSQC spectrum of Miophytocen F (**64**) ($CDCl_3$)

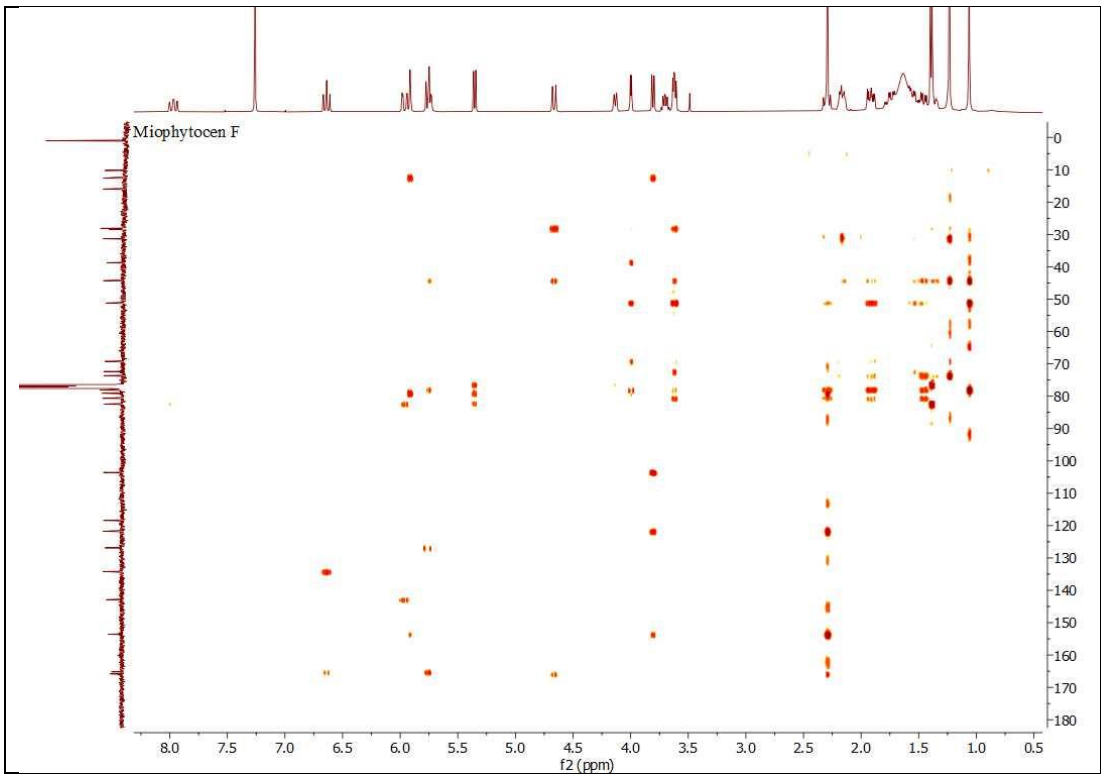

Appendix 90: HMBC spectrum of Miophytocen F (**64**) ($CDCl_3$)

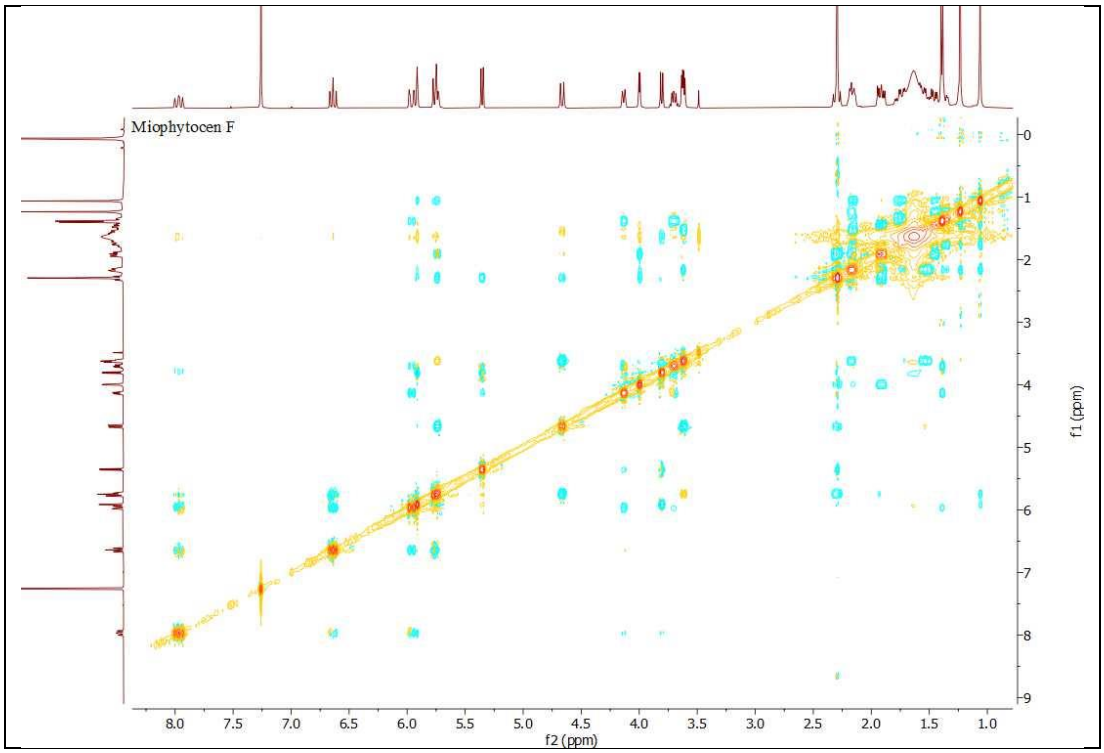

Appendix 91: NOESY spectrum of Miophytocen F (**64**) ($CDCl_3$)

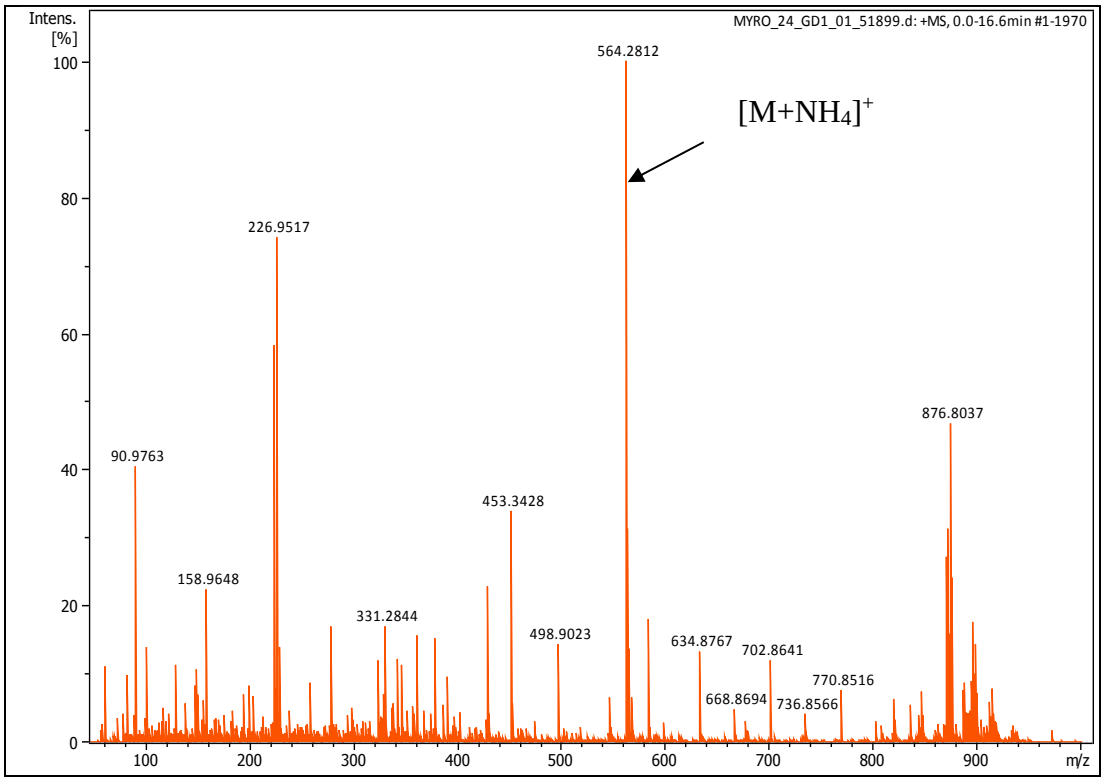

Appendix 92: Mass spectrum of Miophytocen G (**65**) ($M+NH_4$)

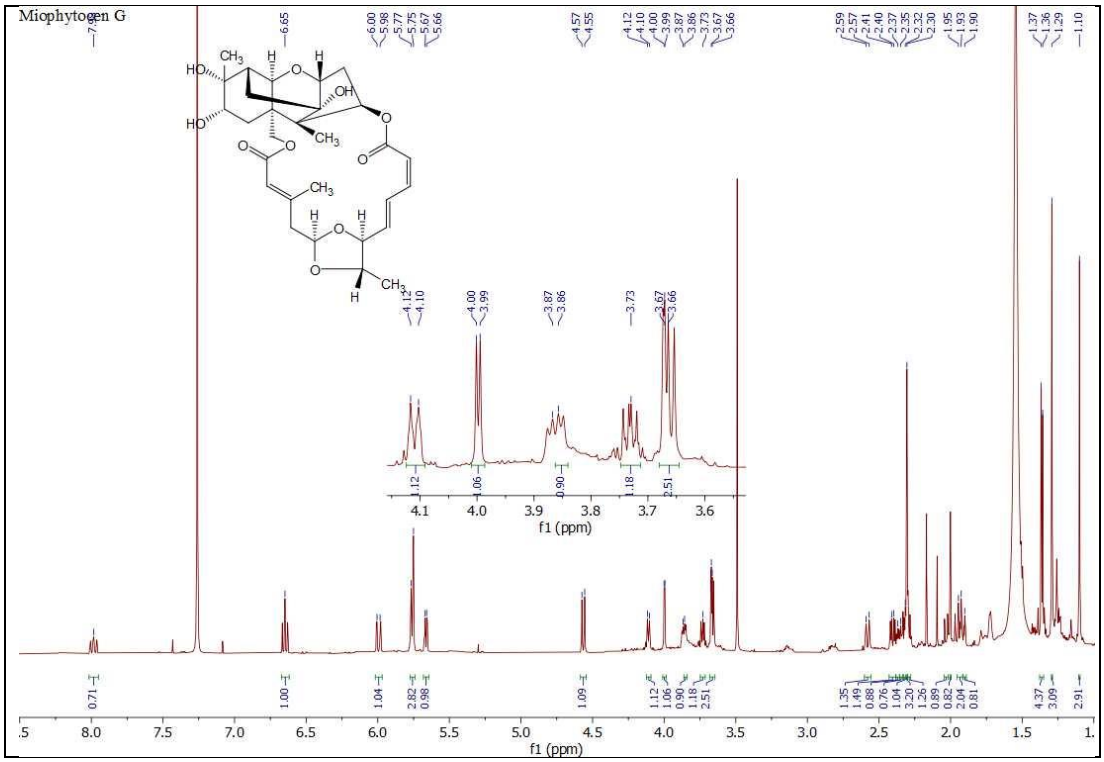

Appendix 93: ^{1}HNMR spectrum of Miophytocen G (**65**) ($CDCl_3$)

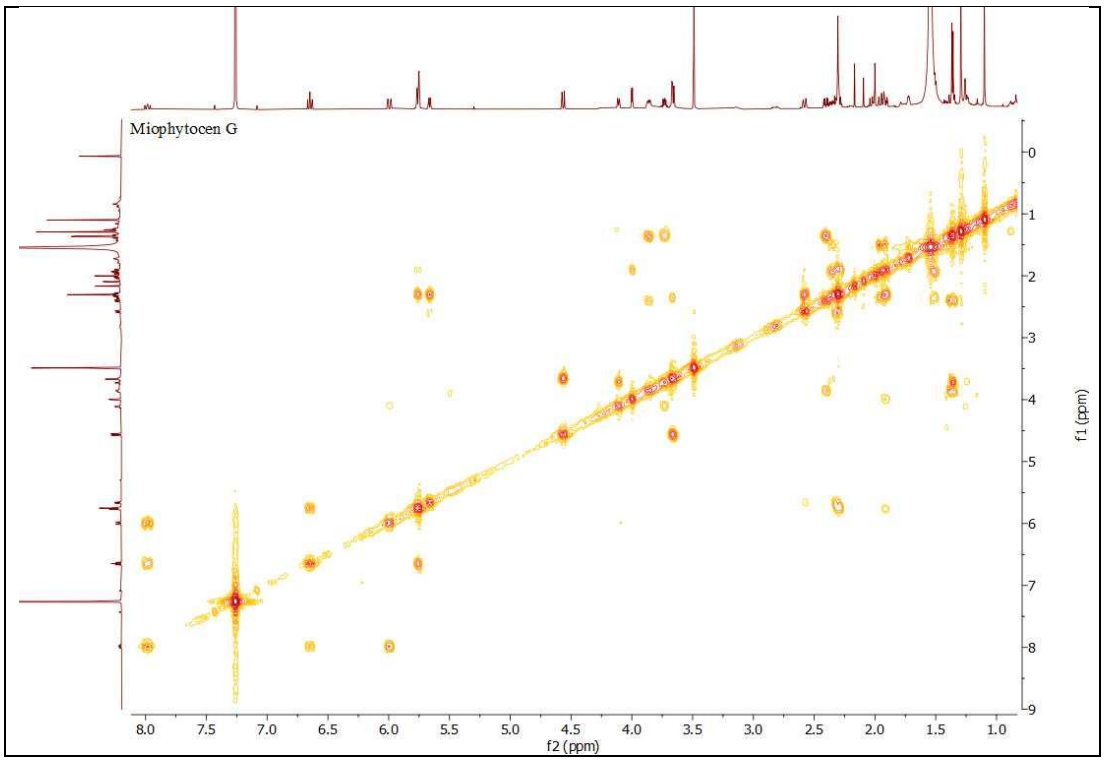

Appendix 94: ^{1}H-^{1}H COSY spectrum of Miophytocen G (**65**) ($CDCl_3$)

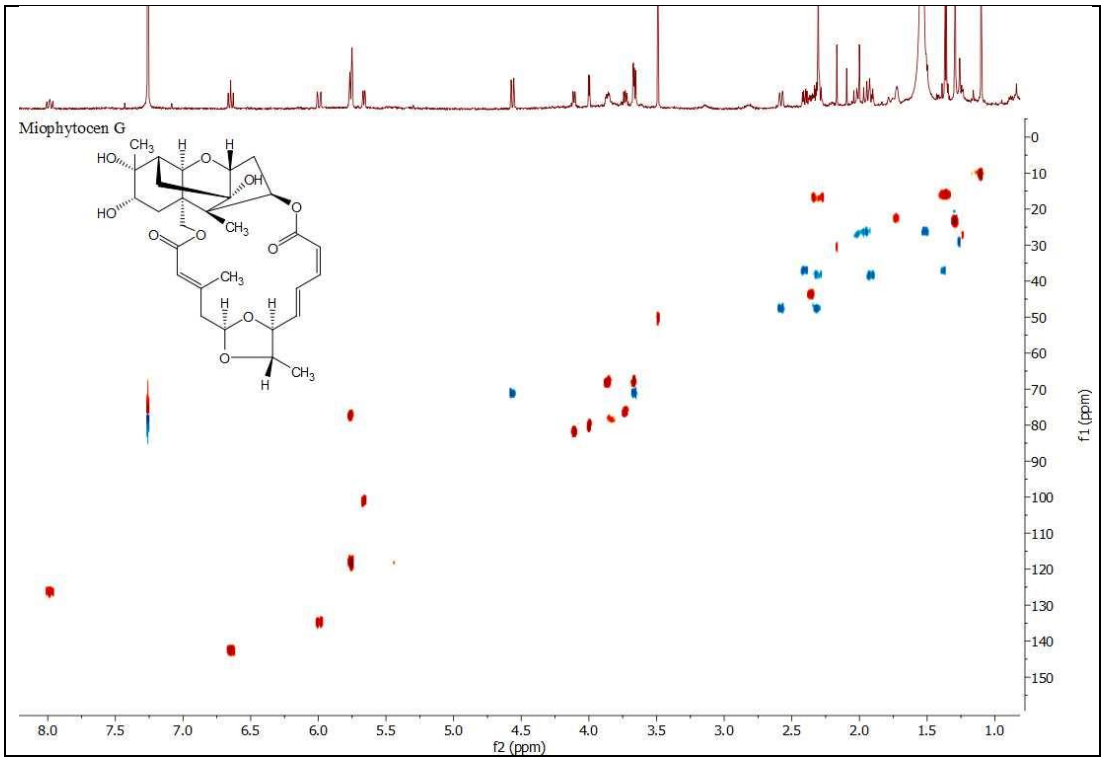

Appendix 95: HSQC spectrum of Miophytocen G (**65**) ($CDCl_3$)

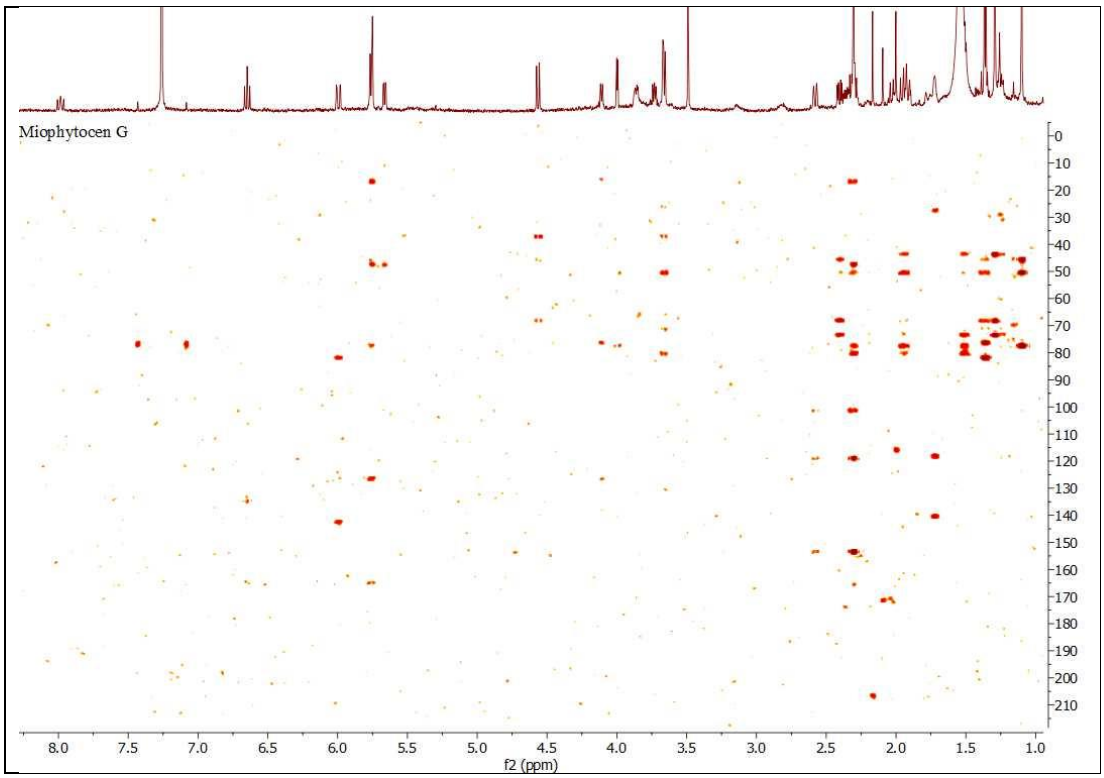

Appendix 96: HMBC spectrum of Miophytocen G (**65**) ($CDCl_3$)

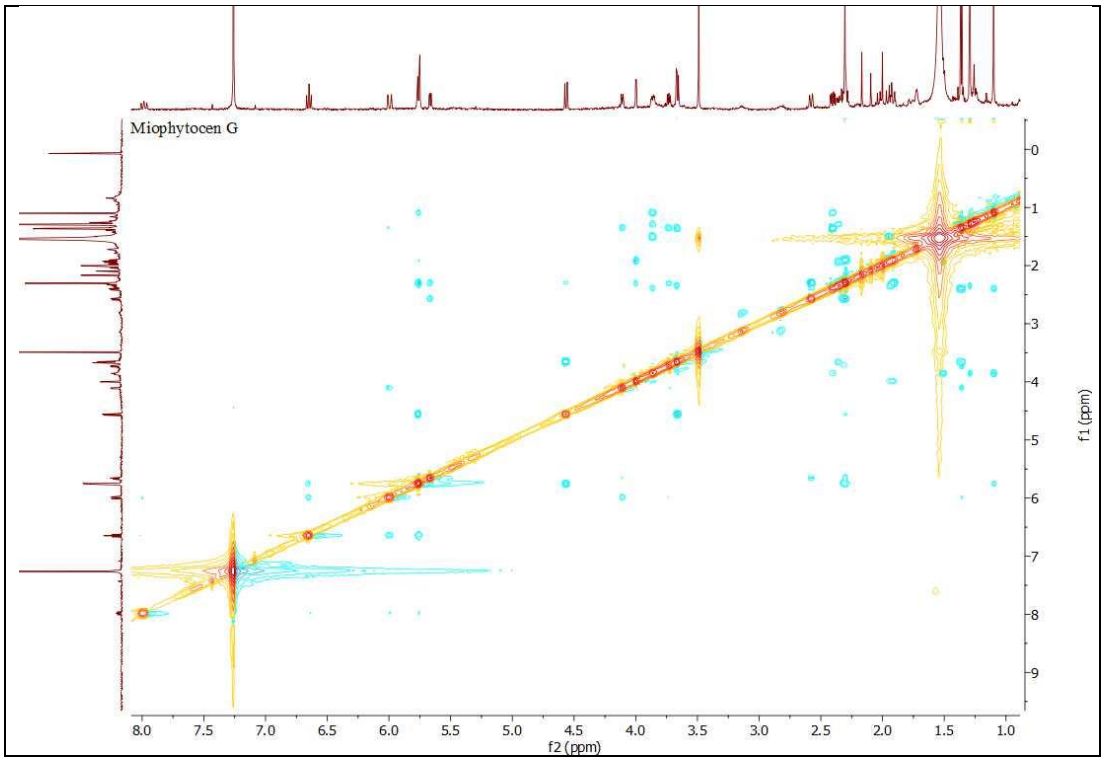

Appendix 97: NOESY spectrum of Miophytocen G (**65**) ($CDCl_3$)

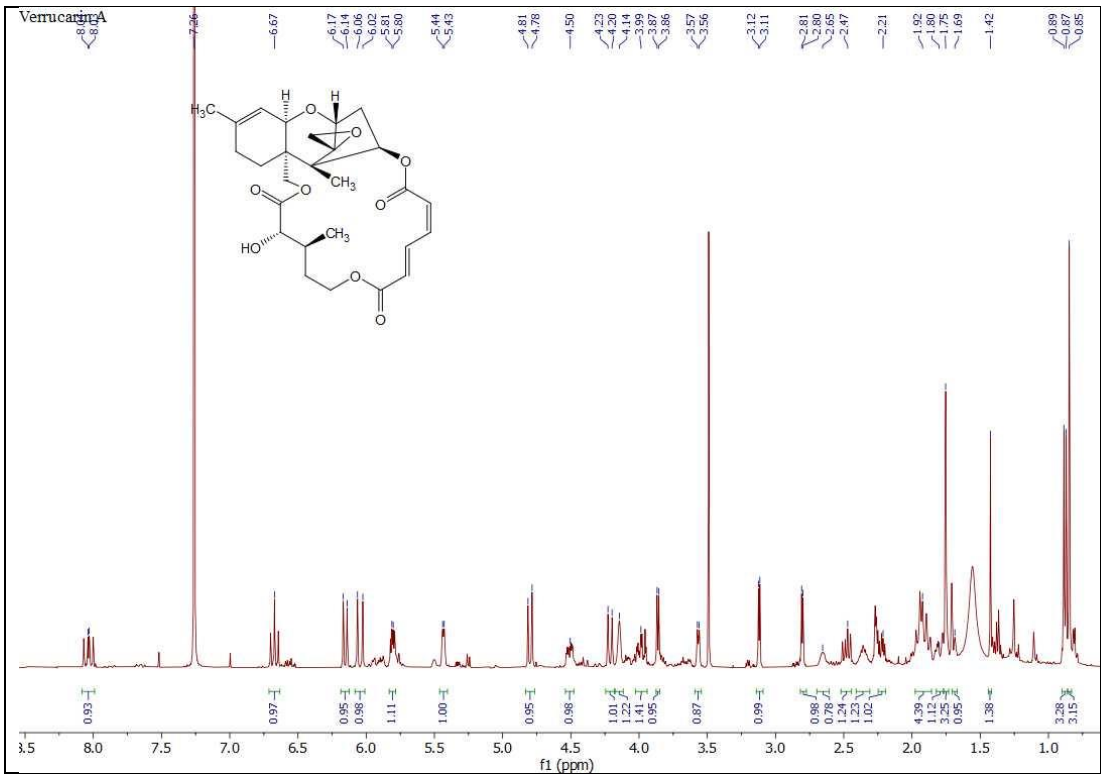

Appendix 98: ^{1}HNMR spectrum of Verrucarin A (**66**) ($CDCl_3$)

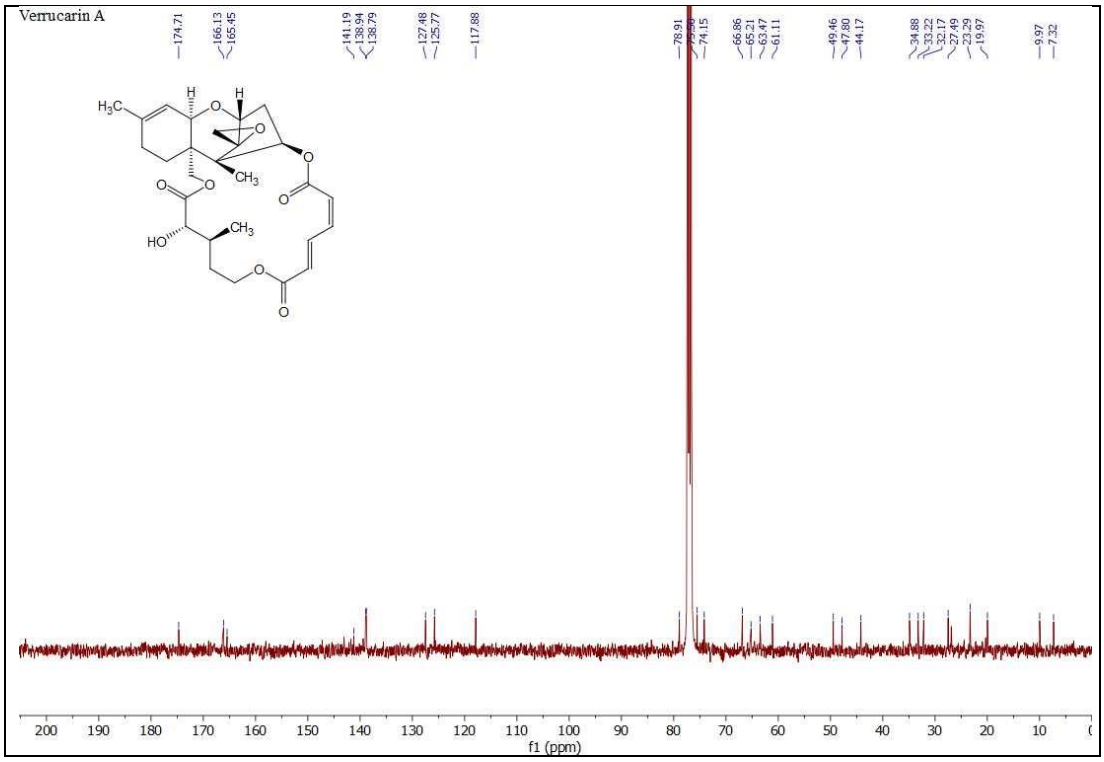

Appendix 99: ^{13}C NMR spectrum of Verrucarin A (**66**) ($CDCl_3$)

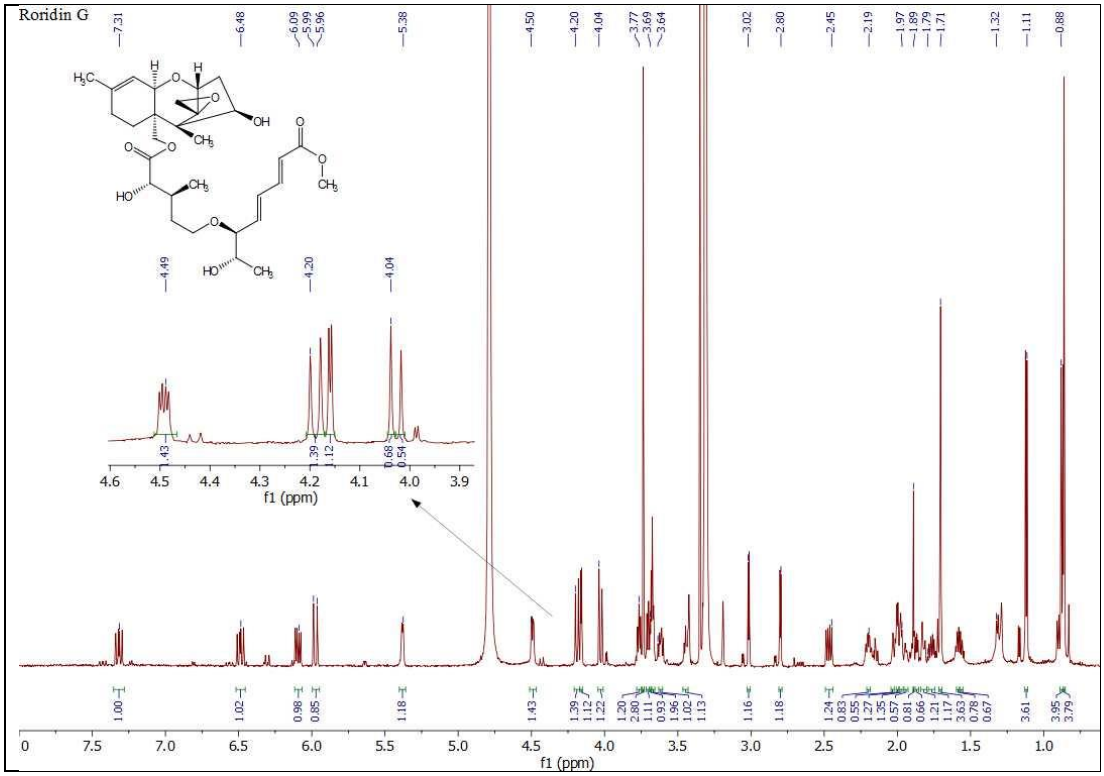

Appendix 100: $^{1}HNMR$ spectrum of Roridin G (**67**) (MeOD-d_4)

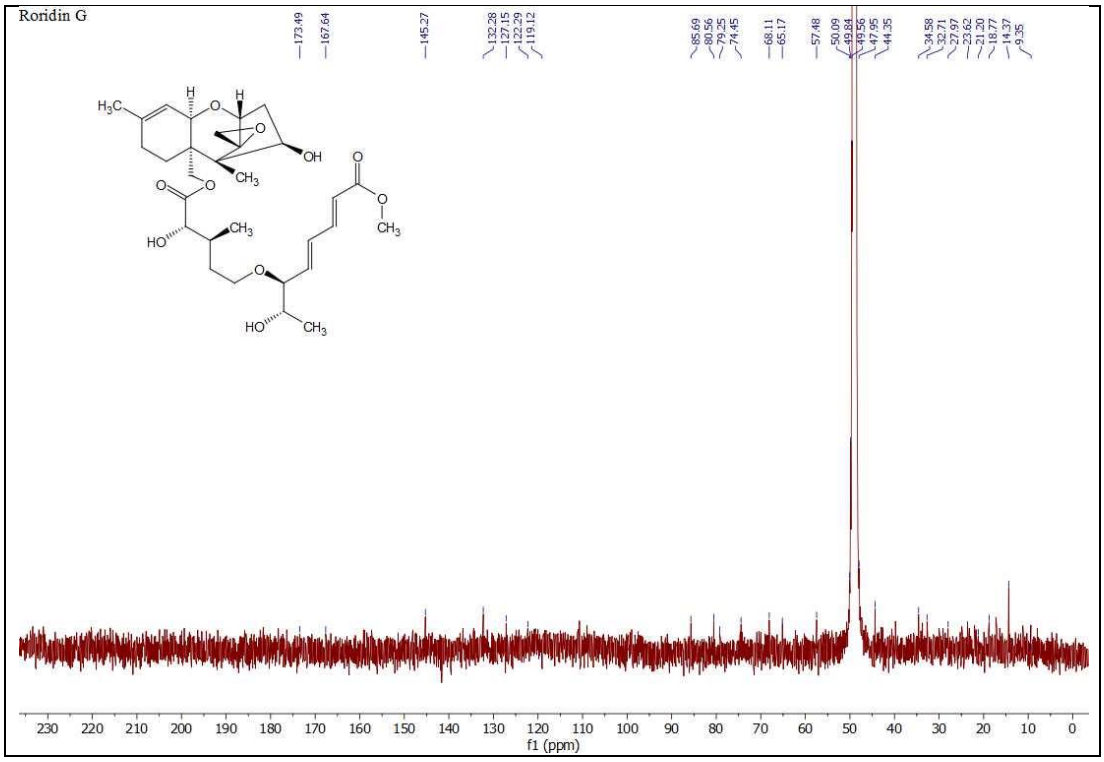

Appendix 101: ^{13}C NMR spectrum of Roridin G (**67**) (MeOD-d$_4$)

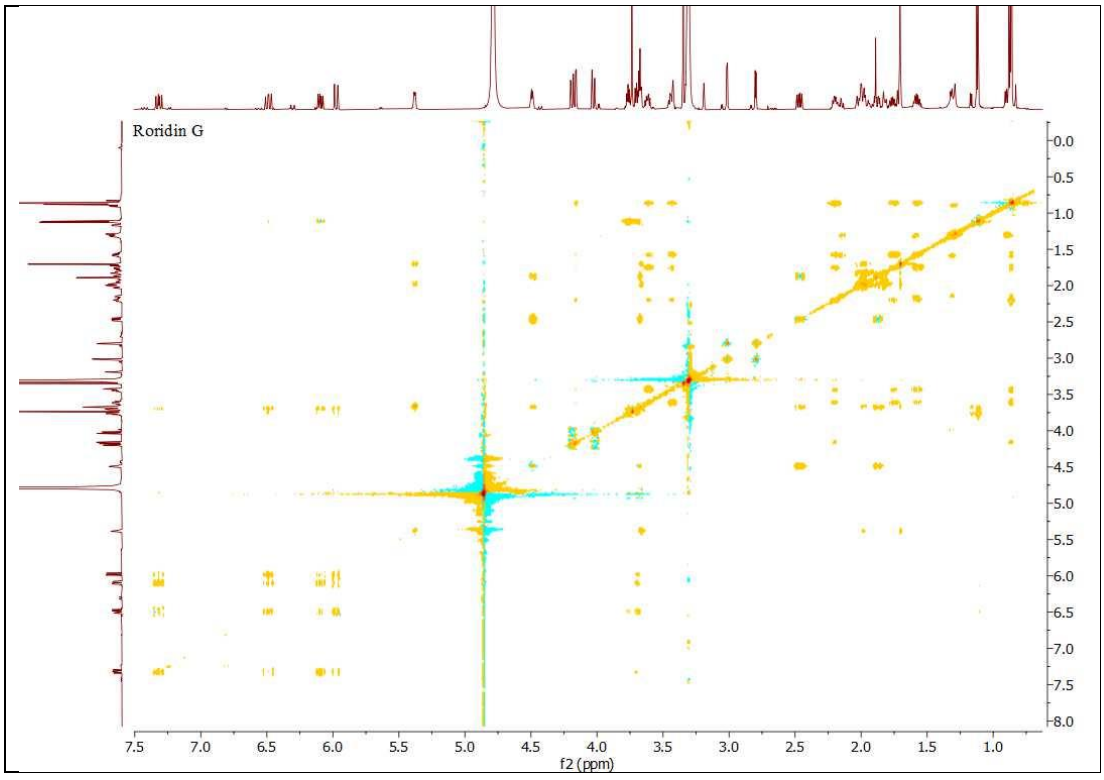

Appendix 102: TOCSY spectrum of Roridin G (**67**) (MeOD-d$_4$)

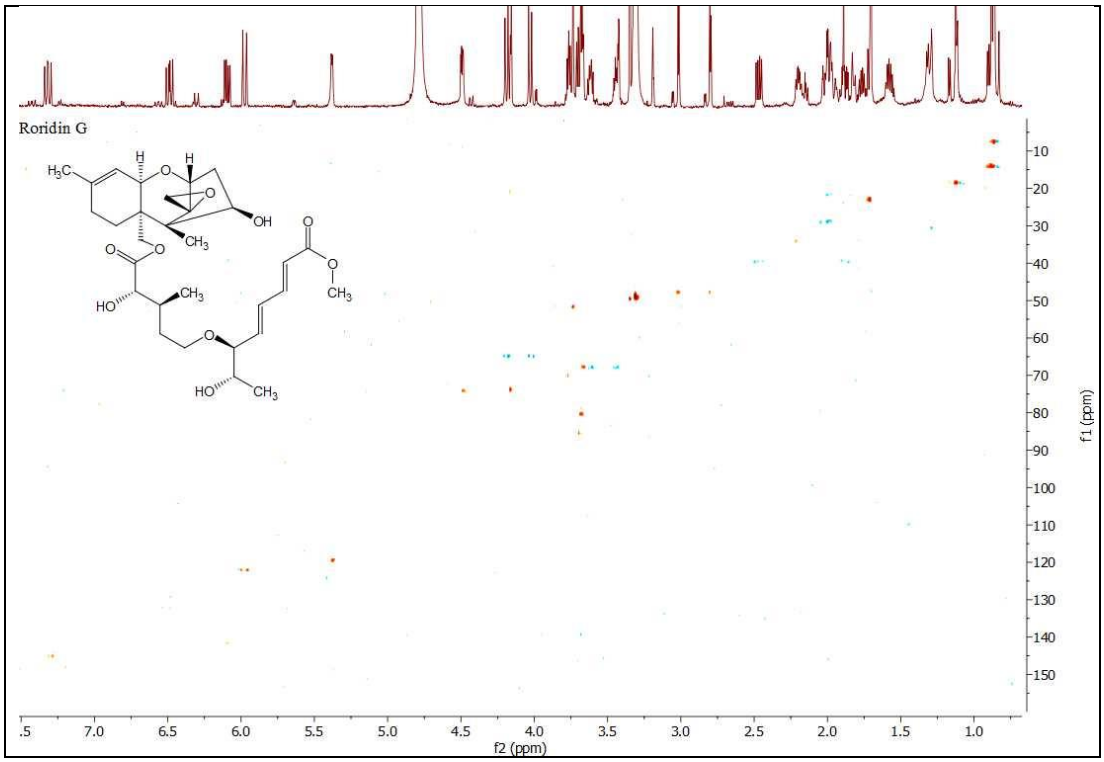

Appendix 103: HSQC spectrum of Roridin G (**67**) (MeOD-d_4)

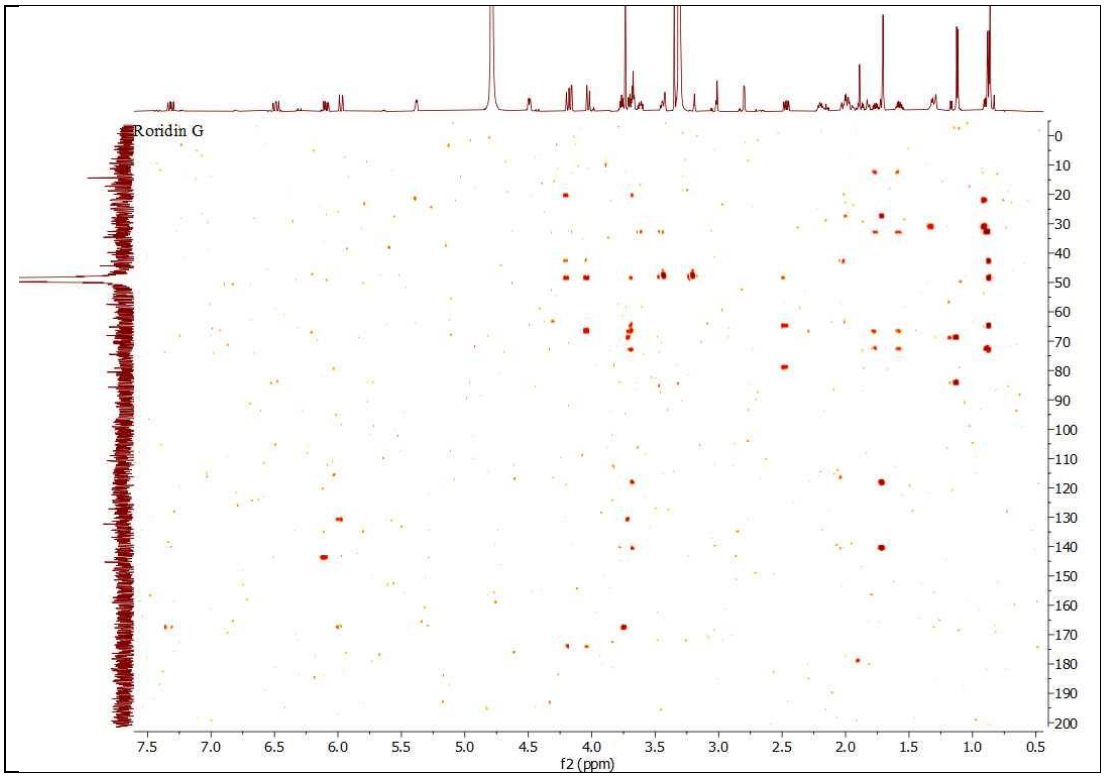

Appendix 104: HMBC spectrum of Roridin G (**67**) (MeOD-d_4)

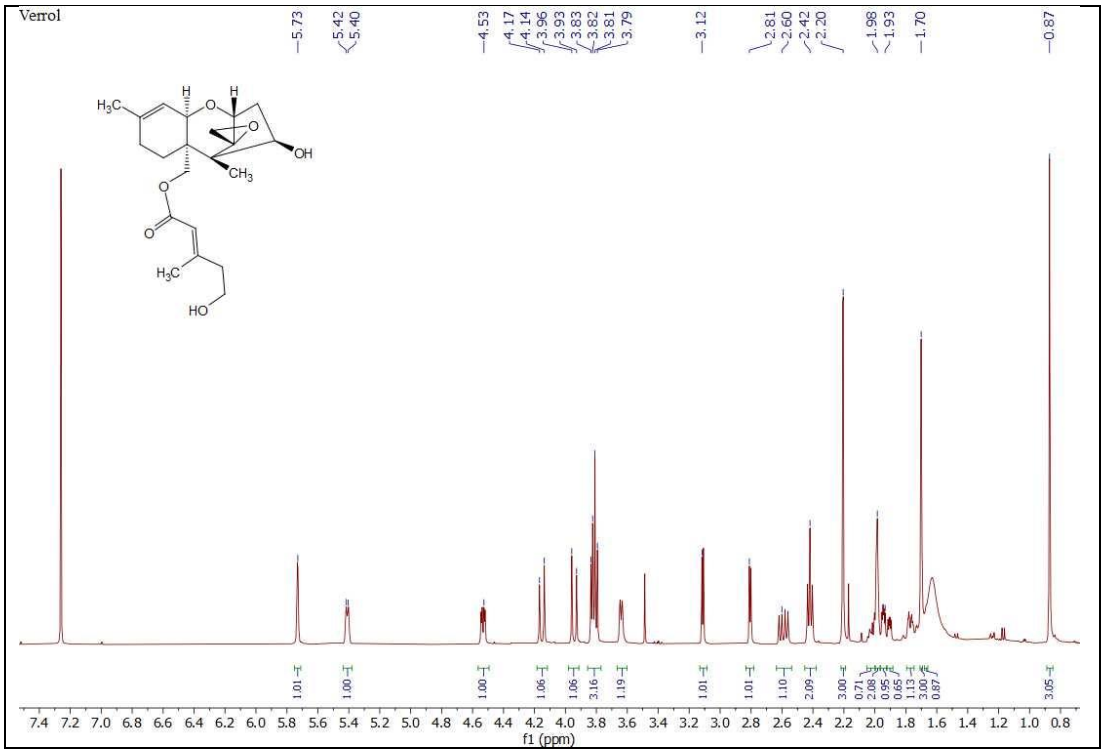

Appendix 105: ^{1}HNMR spectrum of Verrol (**68**) ($CDCl_3$)

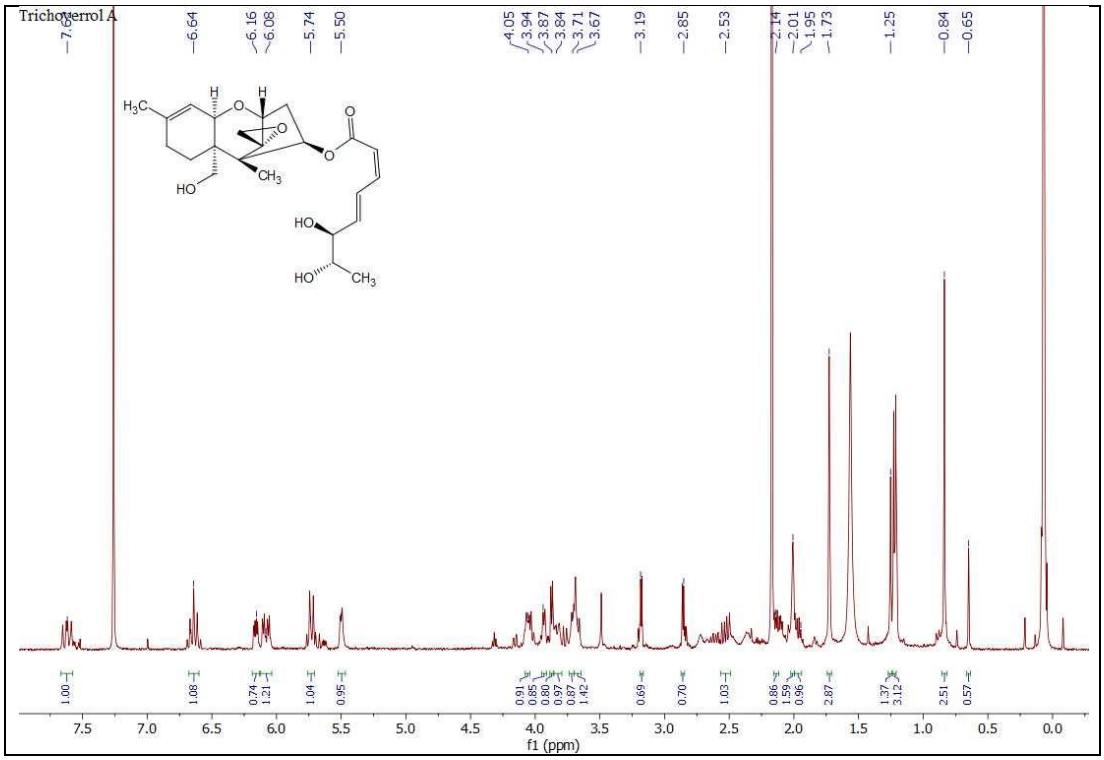

Appendix 106: ^{1}HNMR spectrum of Trichoverrol A (**69**) ($CDCl_3$)

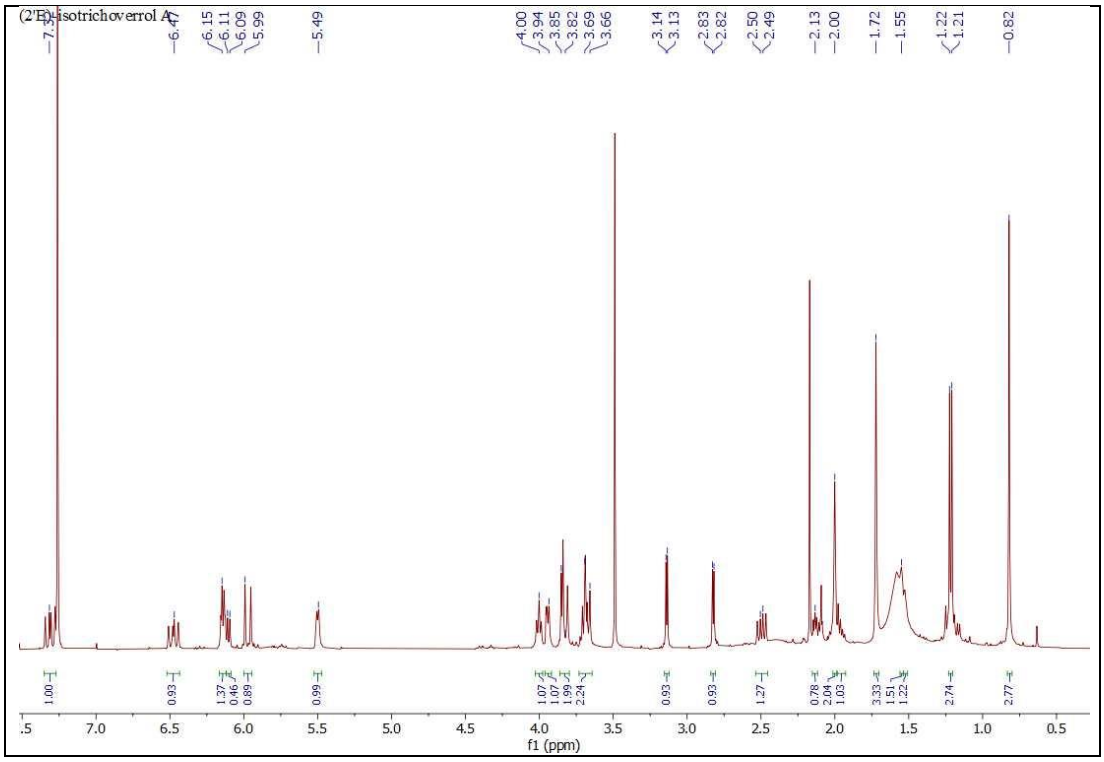

Appendix 107: ^{1}HNMR spectrum of 2'*E*-isotrichoverrol A (**70**) ($CDCl_3$)

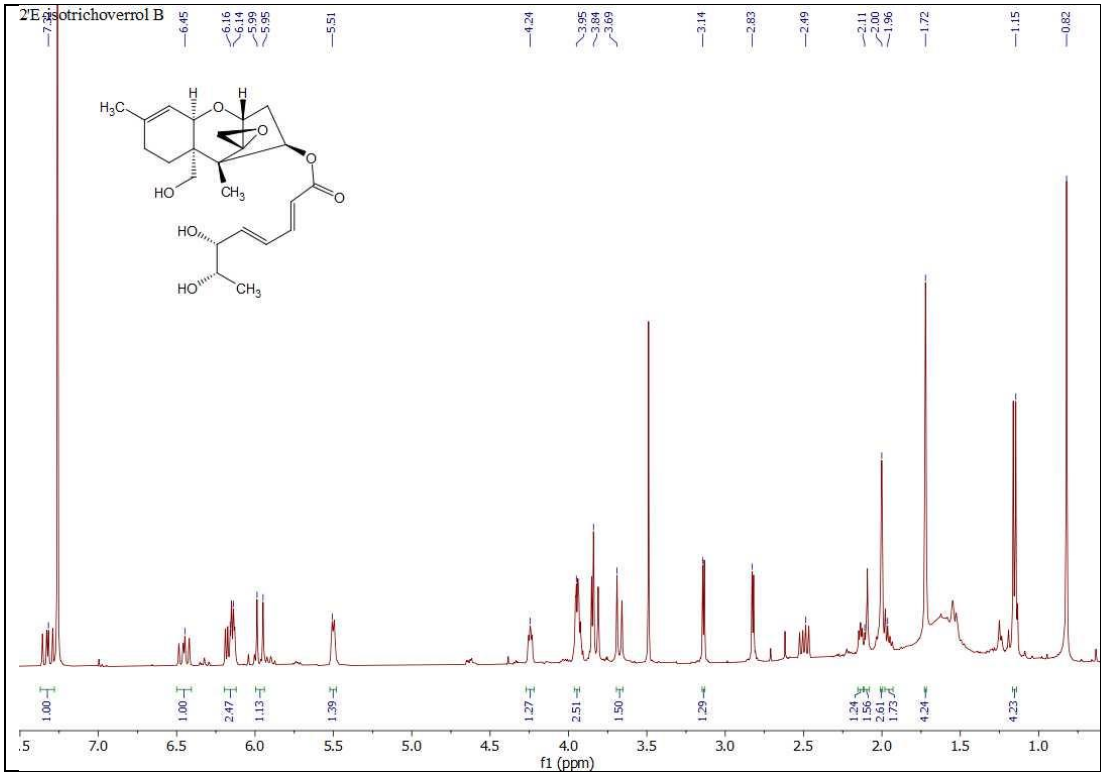

Appendix 108: ^{1}HNMR spectrum of 2'*E*-isotrichoverrol B (**71**) ($CDCl_3$)

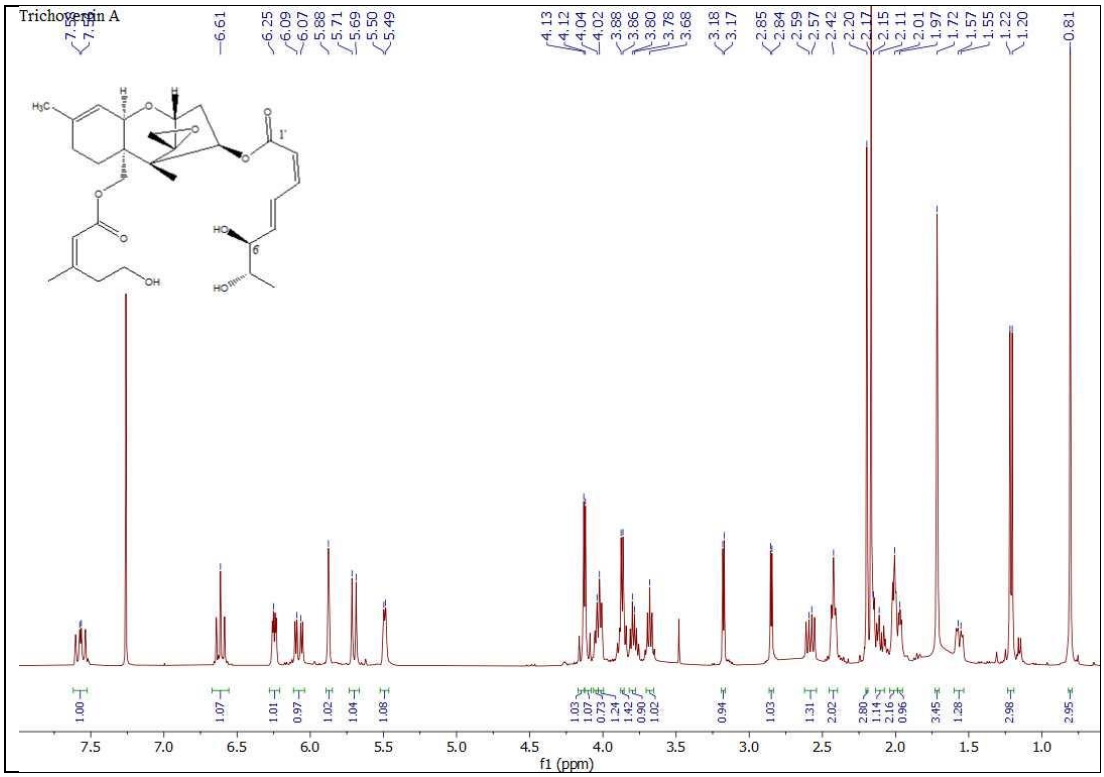

Appendix 109: ^{1}HNMR spectrum of Trichoverrin A (**72**) ($CDCl_3$)

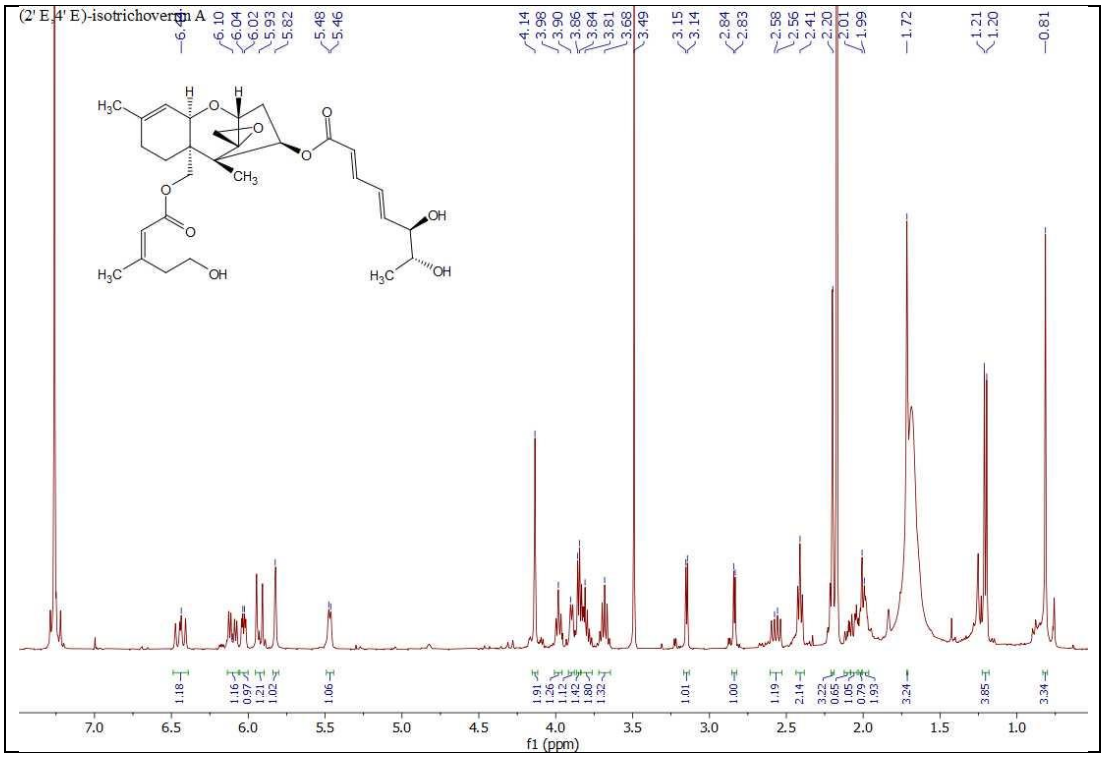

Appendix 110: ^{1}HNMR spectrum of (2' *E*,4' *E*)-isotrichoverrin A (**73**) ($CDCl_3$)

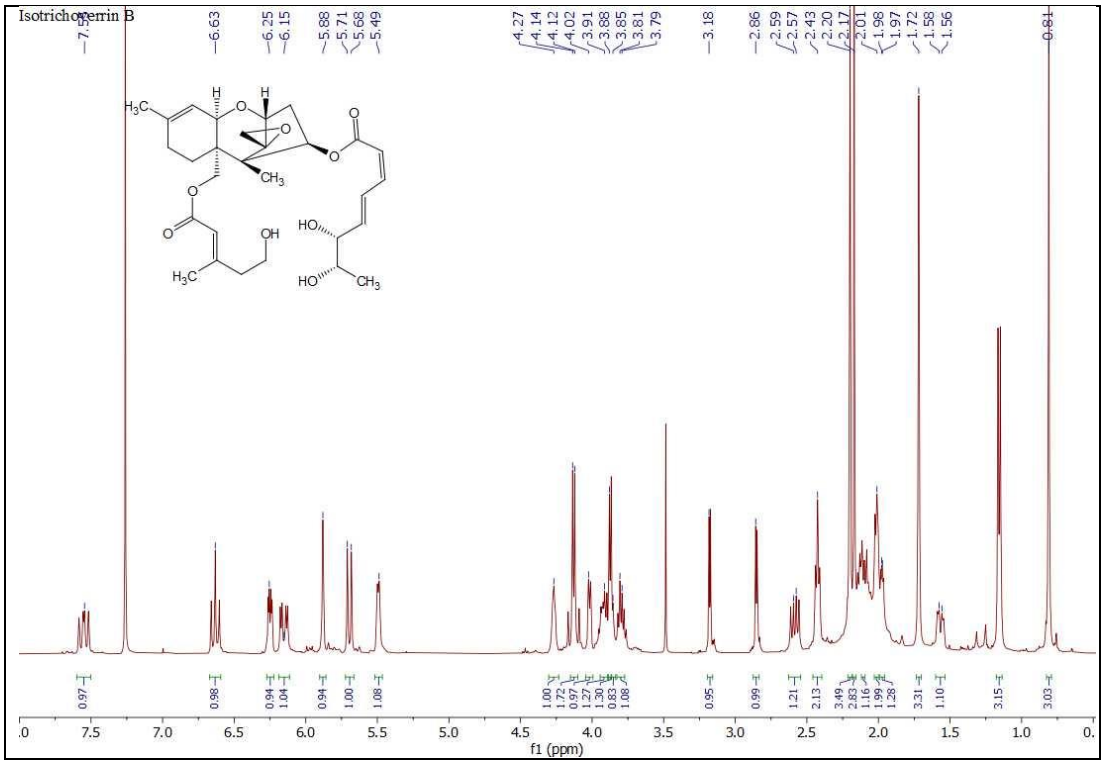

Appendix 111: ^{1}HNMR spectrum Isotrichoverrin B (**74**) ($CDCl_3$)

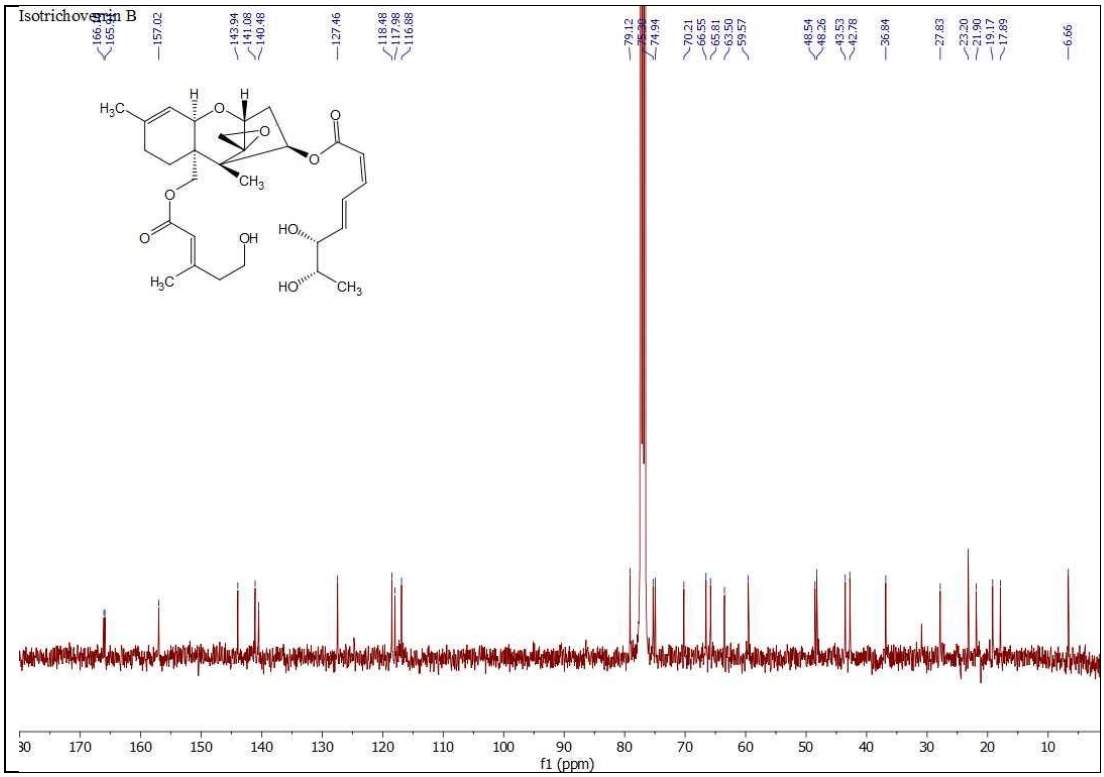

Appendix 112: ^{13}C NMR spectrum Isotrichoverrin B (**74**) ($CDCl_3$)

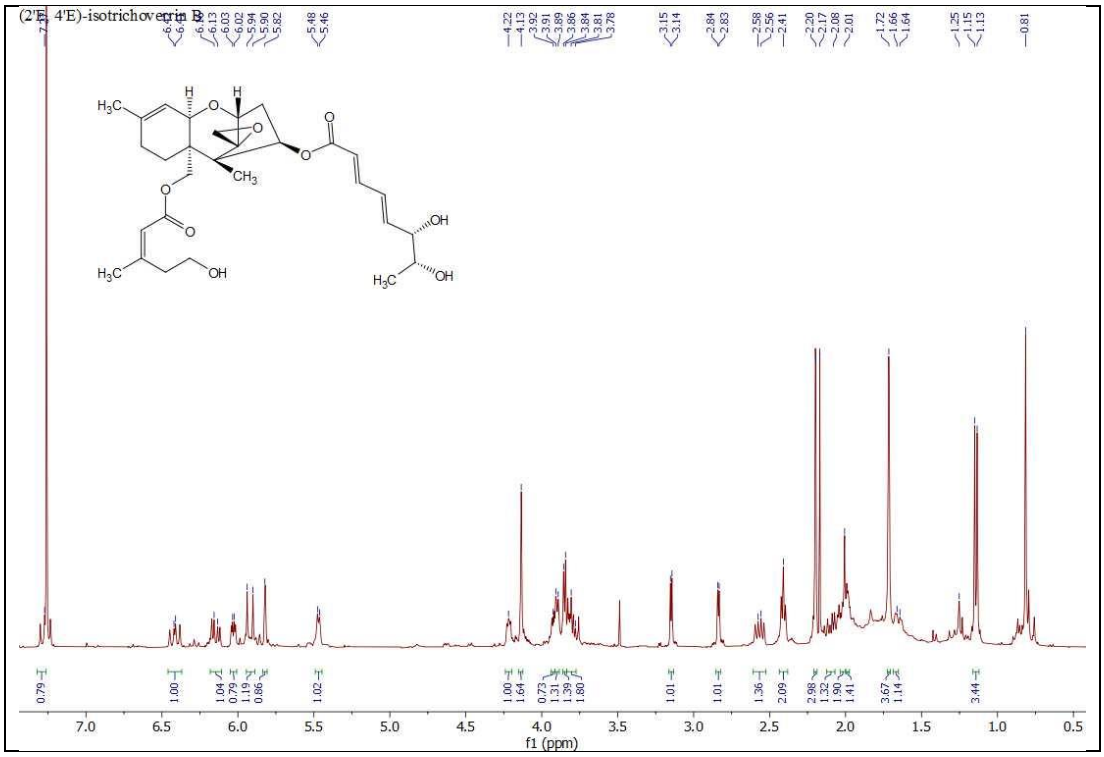

Appendix 113: ^{1}HNMR spectrum (2'*E*, 4'*E*)-isotrichoverrin B (**75**) ($CDCl_3$)

8. References

[1] M.S. Butler. The role of natural product in chemistry in drug discovery. *J. Nat. Prod*. **2004**, *67*, 2141-2153. DOI: 10.1021/np040106y

[2] N. Farnsworth, O. Akerele, A.S. Bingel, D.D. Soejarto and Z. Guo. Medicinal plants in therapy. *Bull. WHO*. **1985**, *63*, 965-981. PMID: 3879679

[3] D. Dias, S. Urban and U. Roessner. A Historical overview of natural products in drug discovery. *Metabolites*. **2012**, *2*, 303-336. DOI: 10.3390/metabo2020303

[4] J.K. Borchardt. The beginnings of drug therapy: Ancient mesopotamian medicine. *Drug News & Perspectives*. **2002**, *15*, 187-192. DOI: 10.1358/dnp.2002.15.3.840015

[5] G. Cragg and D.J. Newman. Biodiversity: A continuing source of novel drug leads. *Pure Appl. Chem*. **2005**, *77*, 7–24. DOI: 10.1351/pac200577010007

[6] G.M. Cragg and D.J. Newman. Natural products: a continuing source of novel drug leads. *Biochim Biophys Acta*. **2013**, *1830*, 3670-3695. DOI: 10.1016/j.bbagen.2013.02.008

[7] A. Fleming. On the Antibacterial Action of Cultures of a *Penicillium*, with Special Reference to their Use in the Isolation of *B. influenzæ*. *Br. J. Exp. Pathlol*. **1929**, *10*, 226-236. PMID: 11545337

[8] R. Bentley. Mycophenolic Acid: a one hundred year odyssey from antibiotic to immunosuppressant *Chem. Rev*. **2000**, *100*, 3801-3825. DOI: 10.1021/cr990097b

[9] D.J. Newman, G.M. Cragg and K.M. Snader. Natural products as sources of new drugs over the period 1981-2002. *J. Nat. Prod*. **2003**, *66*, 1022-1037. DOI: 10.1021/np030096l

[10] U. Gräfe, (**1999**). Secondary metabolites: from past to present. p. 117-123. In: *Drugs discovery from nature*. Grabley, S., Thiericke, R. (eds.). Springer-Verlag Berlin Heidelberg. DOI: 10.1007/978-3-642-60250-4_7

[11] S. Omura. Philosophy of new drug discovery. *Microbiol. Rev*. **1986**, *50*, 259-279. PMID: 3534537

[12] S. Sakuda, S. Tanaka, K. Mizuno, O. Sukcharoen, T. Nihira and Y. Yamada. Biosynthetic studies on virginiae butanolide A, a butyrolactone autoregulator

from Streptomyces. *J. Chem. Soc. Perkin Trans.* 1: **1993**, 2309-2315. DOI: 10.1039/P19930002309

[13] T. Beppu. Secondary metabolites as chemical signals for cellular differentiation. *Gene*. **1992**, *115*, 159-165. DOI: 10.1016/0378-1119(92)90554-3

[14] A. Zähner, H. Anke and T. Anke, (**1983**). Evolution and secondary pathways. pp 153-171. In: *secondary metabolism and differentiation in fungi*. J. W. Bennett, and A. Ciegler (eds.). Marcel Dekker, Inc., New York. Google Scholar

[15] J. Berdy. Bioactive Microbial Metabolites. *J. Antibiot*. **2005**, *58*, 1-26. DOI: 10.1038/ja.2005.1

[16] H. Laatsch. 1st Far-Eastern International Symposium on Life Sciences, Vladivostok, Sept. **2008**.

[17] D. L. Hawksworth. The magnitude of fungal diversity: the 1.5 million species estimate revisited. *Mycol. Res*. **2001**, *105*, 1422-1432. DOI: 10.1017/s0953756201004725

[18] J.M. Trappe and D.L. Luoma. In *The Fungal Community: Its Organization and Role in the Ecosystem*; 2nd ed.; G.C. Carroll, D.T. Wicklow; Marcel Dekker, Inc.: New York, **1992**; Vol. *9*, pp 17-27.

[19] I. Druzhinina and P.C. Kubicek. In The Mycota IV: *Environmental and Microbial Relationships IV*; 2nd ed.; Springer-Verlag: Berlin, **2007**; Vol. *IV*, pp 257-283.

[20] A. Ismaiel and J. Papenbrock. Mycotoxins: Producing Fungi and Mechanisms of Phytotoxicity. *Agriculture*. **2015**, *5*, 492-537. DOI: 10.3390/agriculture5030492

[21] J. Chapman, A.E. Ismail and C.Z. Dinu. Industrial Applications of Enzymes: Recent Advances Techniques and Outlooks. *Catalysts*. **2018**, *8*, 238. DOI: 10.3390/catal8060238

[22] L. Tedersoo S.S. Ramırez, U. Koljalg, M. Bahram, M. Doring, D. Schigel, T. May, M. Ryberg and K. Abarenkov. High-level classification of the Fungi and a tool for evolutionary ecological analyses. *Fungal Divers.* **2018**, *90*, 135–159. DOI: 10.1007/s13225-018-0401-0

[23] A.L. Gunatilaka. Natural products from plant-associated microorganisms: distribution, structural diversity, bioactivity, and implications of their occurrence *J. Nat. Prod*. **2006**, *69*, 509- 526. DOI: 10.1021/np058128n

[24] R.X. Tan and W.X. Zou. Endophytes: a rich source of functional metabolites. *Nat. Prod. Rep.* **2001**, *18*, 448-459. DOI: 10.1039/b100918o

[25] D. Wilson. Fungal endophytes: out of sight but should not be out of mind *Oikos* **1993**, *68*, 379 – 384. DOI: 10.2307/3544856

[26] S. Compant, B. Reiter, A. Sessitsch, J. Nowak, C. Clément and E. A. Barka. Endophytic Colonization of *Vitis vinifera L.* by Plant Growth-Promoting Bacterium *Burkholderia* sp. Strain PsJN. *Appl. Environ. Microbiol*. **2005**, *71*, 1685-1693. DOI: 10.1128/AEM.71.4.1685-1693.2005

[27] G. Strobel and B. Daisy. Bioprospecting for microbial endophytes and their natural products. *Mol. Biol. Rev.*. **2003**, *67*, 491 – 502. DOI: 10.1128/mmbr.67.4.491-502.2003

[28] J.K. Stone, C.W. Bacon and J.F. White. An overview of endophytic microbes: endophytism defined. In: C. W. Bacon and J. F. White (eds) Microbial endophytes. Dekker, New York, **2000**, p: 3- 30.

[29] M. Marler, D. Pedersen, O.T. Mitchell and R.M. Callaway. A polymerase chain reaction method for detecting dwarf mistletoe infection in Douglas-fir and western larch. *Can. J. Res.* **1999**, *29*, 1317-1321. DOI: 10.1139/x99-092

[30] I.C. Feller. Effects of nutrient enrichment on growth and herbivory of dwarf red mangrove (*Rhizophora mangle*). *Ecol Monogr*. **1995**, *65*, 477- 505. DOI: 10.2307/2963499

[31] A.F. Peters. Field and culture studies of *Streblonema Macrocystis* new species *Ectocarpales Phaeophyceae* from Chile, a sexual endophyte of giant kelp. *Phycologia*. **1991**, *30*, 365- 377. DOI: 10.2216/i0031-8884-30-4-365.1

[32] B. Schulz, C. Boyle, S. Draeger, A. Römmert and K. Krohn. Endophytic fungi: a source of novel biologically active secondary metabolites. *Mycol. Res.* **2002**, *106*, 996-1004. DOI: 10.1017/S0953756202006342

[33] N.B. Zimmerman and P. M. Vitousek. Fungal endophyte communities reflect environmental structuring across a Hawaiian landscape. *Proc. Natl. Acad. Sci*. USA. **2012**, *109*, 13022–13027. DOI: 10.1073/pnas.1209872109

[34] J. Bennett. Mycotoxins, mycotoxicoses, mycotoxicology and mycopathology. *Mycopathlogia*. **1987**, *100*, 3–5. DOI: 10.1007/BF00769561

[35] K. K Maggon,., S. K. Gupta, and T. A. Venkitasubramanian.. Biosynthesis of aflatoxins. *Bacteriol. Rev*. **1977**, *41*, 822–855. PMID: 23090

[36] R.J. Cole and R. H. Cox. Handbook of toxic fungal metabolites. *Academic Press, New York, N.Y.* **1981**. DOI: 10.1016/C2009-0-03073-6

[37] J. Forgacs and W.T. Carll. Mycotoxicoses. *Adv. Vet. Sci*. **1962**, *7*, 273-382.

[38] A. Graniti. The evolution of the toxic concept in plant pathology. In R. K. Wood, A. Ballio, and A. Graniti (ed.), Phytotoxins in plant diseases. *Academic Press, New York, N.Y.* **1972**, 1–18.

[39] J.W. Bennett and M. Klich. Mycotoxins. *Clin. Microbiol. Rev*. **2003**, *16*, 497-516. DOI: 10.1128/cmr.16.3.497-516.2003

[40] M.O. Moss, Mycotoxins. *Mycol. Res*. **1996**, *100*,513-523.

[41] R. A. Squire, Ranking animal carcinogens: a proposed regulatory approach. *Science*. **1981**, *214*, 877-880. DOI: 10.1126/science.7302565

[42] S.W. Peterson, Y. Ito, B. W. Horn and T. Goto. *Aspergillus bombycis*, a new aflatoxigenic species and genetic variation in its sibling species, *A. nomius*. *Mycologia*. **2001**, *93*, 689-703. DOI: 10.1080/00275514.2001.12063200

[43] M.A Klich, E.J. Mullaney, C.B. Daly, and J.W. Cary. Molecular and physiological aspects of aflatoxin and sterigmatocystin biosynthesis by *A. tamarii* and *A. ochraceoroseus*. *Appl. Microbiol. Biotechnol*. **2000**, *53*, 605-609. DOI: 10.1007/s002530051664

[44] T. Goto, D.T. Wicklow, and Y. Ito.. Aflatoxin and cyclopiazonic acid production by a sclerotium-producing *Aspergillus tamarii* strain. *Appl. Environ. Microbiol*. **1996**, *62*, 4036-4038. DOI: 10.1128/AEM.62.11.4036-4038.1996

[45] J.D. Groopman, T.W. Kensler, and C.P. Wild. Protective interventions to prevent aflatoxin-induced carcinogenesis in developing countries. *Ann. Rev. Pub. Health*. **2008**, *29*, 187-203.
DOI: 10.1146/annurev.publhealth.29.020907.090859

[46] P.F. Scholl and J.D. Groopman. Long-term stability of human aflatoxin B1 albumin adducts assessed by isotope dilution mass spectrometry and high performance liquid chromatography Fluorescence. *Cancer Epidemiol. Biomarkers Prev*. **2008**, *17*, 1436-1439.
DOI: 10.1158/1055-9965.EPI-07-2926.

[47] D.L. Eaton and J.D. Groopman (ed.). The toxicology of aflatoxins: human health, veterinary, and agricultural significance. *Academic Press*, San Diego, Calif. **1994**

[48] K.J. Van Der Merwe, P.S. Steyne, L.F. Fourie, D. B. Scott and J.J. Theron. Ochratoxin A, a toxic metabolite produced by *Aspergillus ochraceus* Wilh. *Nature*. **1965**, *5*, 1112-1113. DOI: 10.1038/2051112a0

[49] P. Bayman, J.L. Baker, M.A. Doster, T.J. Michailides and N.E. Mahoney. Ochratoxin production by the *Aspergillus ochraceus* group and *Aspergillus alliaceus*. *Appl.Env.Microbio.* **2002**, *68*, 2326-2329. DOI: 10.1128/AEM.68.5.2326-2329.2002

[50] S.E. Lee, B.S. Park, P. Bayman, J. L. Baker, W.S. Choi and B.C. Campbell. Suppression of ochratoxin biosynthesis bynaturally occurring alkaloids. *Food Addi .Contam.* **2007**, *24*, 391–397. DOI: 10.1080/02652030601053147

[51] P. Tryfinopoulou, L. Fengou and E.Z. Panagou. Influence of *Saccharomyces cerevisiae* and *Rhotodorula mucilaginosa* on the growth and ochratoxin A production of *Aspergillus carbonarius*. *LWT-Food Science and Technology*. **2019**, *105*, 66–78. DOI: 10.1016/j.lwt.2019.01.050

[52] T. Senthilkumar, D.S. Jayas, N.D.G. White, P.G. Fields and T. Grafenhan. Detection of fungal infection and Ochratoxin A contamination in stored wheat using near-infrared hyperspectral imaging. *J. Stored Prod. Rese*. **2016**, 65, 30-39. DOI: 10.1016/j.jspr.2015.11.004

[53] M.L. Abarca, M.R. Bragulat, G. Castellà and F.J. Cabañes. Ochratoxin A production by strains of *Aspergillus niger var. niger*. *Appl. Environ. Microbiol*. **1994**, *60*, 2650-2652. PMID: 8074536

[54] J.-T. Liu, W. Wu, M.-J. Cao, F. Yang and H.-W. Lin. Trienic α-pyrone and ochratoxin derivatives from a sponge-derived fungus *Aspergillus ochraceopetaliformis*. *Nat. Prod. Res*. **2018**, *32*, 1791–1797 DOI: 10.1080/14786419.2017.1402325

[55] L. Sánchez-Montero, J.J. Córdoba, B. Peromingo, M. Álvarez and F. Núñez. Effects of environmental conditions and substrate on growth and ochratoxin A production by *Penicillium verrucosum* and *Penicillium nordicum*: Relative risk

assessment of OTA in dry-cured meat products. *Food Res Int*. **2019**, *121*, 604-611. DOI: 10.1016/j.foodres.2018.12.025

[56] J.I. Pitt. Toxigenic fungi: which are important? *Medical Mycology*. **2000**, *38*, 17-22. PMID: 11204142

[57] L. Reddy and K. Bhoola. Ochratoxins-Food Contaminants: Impact on human health. *Toxins*. **2010**, *2*, 771-779. doi: 10.3390/toxins2040771

[58] C. Schlatter, J. Studer-Rohr and T. Rásonyi. Carcinogenicity and kinetic aspects of ochratoxin A. *Food Addit Contam*. **1996**, *13*, 43-44. PMID: 8972350

[59] Beardall, J. M., & Miller, J. D. Disease in humans with mycotoxins as possible causes. In J. D. Miller, & H. L. Trenholm (Eds.), Mycotoxins in grains: Compounds other than aflatoxin. USA: St. *Paul Eagen Press*. 1994, 487-539). DOI: 10.1590/S0036-46651994000500017

[60] R.R Marquardt and A.A Frohlich. A review of recent advances in nderstanding ochratoxicosis. *J Anim Sci*. **1992**, *70*, 3968-3988. DOI: 10.2527/1992.70123968x

[61] J.W. Bennett and R. Bentley. Pride and prejudice: the story of ergot. Perspect. *Biol. Med*. **1999**, *42*, 333–355. DOI: 10.1353/pbm.1999.0026

[62] P.C. Kruppa. Claviceps. *Biológico*. **2004**, *66*, 35-37. Google Scholar

[63] S.C. Bezuidenhout, W.C.A. Gelderblom, C.P. Gorst-Allman, R.M. Horak, W.F.O. Marasas, G. Spiteller, and R. Vleggaar. Structure elucidation of the fumonisins, mycotoxins from *Fusarium moniliforme*. *J. Chem. Soc. Chem. Commun*. **1988**, *1988*, 743-745. DOI: 10.1039/C39880000743

[64] J.P. Rheeder, W.F. Marasas, and H.F. Vismer.. Production of fumonisin analogs by *Fusarium* species. *Appl. Environ. Microbiol*. **2002**, *68*, 2102– 2105. DOI: 10.1128/AEM.68.5.2101-2105.2002

[65] D.T. Shah, D.D. Glover, and B. Larsen.. In situ mycotoxin production by *Candida albicans* in women with vaginitis. *Gynecol. Obstet. Investig*. **1995**, *39*, 67-69. DOI: 10.1159/000292381

[66] M.F. Dutton and A. Kinsey. Occurrence of mycotoxins in cereals and animal feedstuffs in Natal, South Africa 1994. *Mycopathologia*. **1995**, *131*, 31-36. DOI: 10.1007/BF01103901

[67] A. Srobárová and A. Pavlová. The pathogen localization and ZEN concentration in wheat infected by Fusarium graminearum in relation to nutrition. *Cereal Res. Commun.* **1997**, *25*, 449-450. Google Scholar

[68] E. Fadl-Allah, M. Stack, R. Goth and G. Bean. Production of fumonisins B1, B2 and B3 by *Fusarium proliferatum* isolated from rye grains. *Mycotoxin Res.* **1997**, *13*, 43-48. Google Scholar

[69] D. Pancaldi and I. Alberti. Le principali malattie su foglia e spiga del frumento. *L'Informat. Agar*. **2001**, *20*, 63-69. Google Scholar

[70] B.A. Blackwell, O.E. Edwards, A. Fruchier, J.W. ApSimon, and J.D. Miller.. NMR structural studies of fumonisin B1 and related compounds from *Fusarium moniliforme*. Fumonisins in food, *Adv Exp Med Biol*. **1996**, *392*, 75-91. Google Scholar

[71] R.D. Plattner, D. Weisleder, and S.M. Poling. Analytical determination of fumonisins and other metabolites produced by *Fusarium monili*forme and related species on corn. *Adv. Exp. Med. Biol*. **1996**, *392*, 57-64. Google Scholar

[72] A.C. Hetherington and H. Raistrick. Studies in the biochemistry of microorganisms. Part XIV. On the production and chemical constitution of a new yellow colouring matter, citrinin, produced from glucose by *Penicillium citrinum* Thom. *Phil. Trans. R. Soc*. London Ser. **1931**, *220*, 269-295. DOI: 10.1098/rstb.1931.0025

[73] L.L. Xu, F. Cao, S.-S. Tian and H.-J. Zhu. Alkaloids and Polyketides from the Soil Fungus *Aspergillus terreus* and Their Antibacterial Activities. *Chem. Nat. Comp.* **2017**, *53*, 1212–1215. DOI: 10.1007/s10600-017-2243-5

[74] M. Manabe. Fermented foods and mycotoxins. *Mycotoxins*. **2001**, *51*, 25–28. Google Schoolar

[75] W.W. Carlton and J. Tuite, P.J.V. Rodricks, C.W. Hesseltine, and M.A. Mehlman (ed.), Mycotoxins in human and animal health. Pathotox Publications., Inc., Park Forest South, Ill. *viridicatum* toxicology, *In.* **1977**, 525–555. Google Scholar

[76] D. Flajs and M. Peraica. Toxicological properties of citrinin. *Arh Hig Rada Toksikol*. **2009**, *60*, 457-464. DOI: 10.2478/10004-1254-60-2009-1992

[77] A. Ciegler, R.W. Detroy, and E.B. Lillejoj. Patulin, penicillic acid and other carcinogenic lactones, p. 409–434. In A. Ciegler, S. Kadis and S. J. Ajl (ed.), Microbial toxins: fungal toxins. *Academic Press*. New York, N.Y. **1971**, *VI*. Google Scholar

[78] A. Ciegler. Patulin. In J. V. Rodricks, C.W. Hesseltine, & M. A. Mehlman (Eds.), Mycotoxins in human and animal health. Park Forest South: Pathotox. **1977**, 609-624.

[79] C. Pinedo, S.A.I. Wright, I.G. Collado, R.J.M. Goss, R. Castoria, P. Hrelia, F. Maffei and R. Durán-Patrón. Isotopic labeling studies reveal the patulin detoxification pathway by the biocontrol yeast *Rhodotorula kratochvilovae*LS11. *J. Nat. Prod*. **2018**, *81*, 2692-2699. DOI: 10.1021/acs.jnatprod.8b00539

[80] A.C. Pier and J.L. Richard. Mycoses and mycotoxicoses of animals caused by Aspergilli. In J.W. Bennett, & M. A. Klich (Eds.), *Aspergillus: biology and industrial applications* Maryland: Butterworth-Heinemann. **1992**, 233-267. PMID: 1504600

[81] M.O. Moss and M.T. Long. Fate of patulin in the presence of yeast Saccharomyces cerevisiae. *Food Addit Contam*. **2002**, *19*, 387-399. DOI: 10.1080/02652030110091163

[82] H.S. Hussein and J.M. Brasel. Toxicity, metabolism, and impact of mycotoxins on humans and animals. *Toxicology*. **2001**, *167*, 101-134. DOI: 10.1016/S0300-483X(01)00471-1

[83] H. El-Nezami, N. Polychronaki, S. Salminen and H. Mykkanen. Binding rather than metabolism may explain the interaction of two food-grade *Lactobacillus* strains with zearalenone and its derative a-zearalenol. *Appl. Environ. Microbiol*. **2002**, 68, 3545-3549. DOI: 10.1128/AEM.68.7.3545-3549.2002

[84] W.H. Urry, H.L. Wehrmeister, E.B. Hodge, and P.H. Hidy. The structure of zearalenone. *Tetrahedron Lett*. **1966**, *27*, 3109–3114. DOI: 10.1016/S0040-4039(01)99923-X

[85] C.M. Placinta, J.P.F. D'Mello and A.M.C. MacDonald. A review of worldwide contamination of cereal grains and animal feed with *Fusarium mycotoxins*. *Anim. Feed Sci. Technol*. **1999**, *78*, 21-37. DOI: 10.1016/S0377-8401(98)00278-8

[86] T. Kuiper, P.M. Scott and H. Watanabe. Risk assessment of the mycotoxin zearalenone. *Regul. Toxicol. Pharmacol*. **1987**, *7*, 253-306. DOI: 10.1016/0273-2300(87)90037-7

[87] G.G Freeman and R.I. Morrison. The isolation and chemical properties of trichothecin, an antifungal substance from *Trichothecium roseum*. *Biochem. J*. **1949**, *44*, 1-5. DOI: 10.1042/bj0440001

[88] A.E. Desjardins, T.M. Hohn and S.P. McCormick. Trichothecene biosynthesis in *Fusarium* species: Chemistry, genetics, and significance. *Microbiol. Mol. Biol. Rev*. **1993**, *57*, 595-604. Google Scholar

[89] P.M. Scott. The natural occurrence of trichothecenes. *In* V. H. Beasley (ed.), Trichothecene mycotoxicosis: pathophysiologic effects. *CRC Press, Boca Raton, Fla*. **1989**, *I*, 1–26. Google Scholar.

[90] I. Rizzo, E. Varsavky, M. Haidukowski and H. Frade. Macrocyclic trichothecenes in *Baccharis coridifolia* plants and endophytes and *Baccharis artemisioides* plants. *Toxicon*. **1997**, *35*, 753-757. DOI: 10.1016/S0041-0101(96)00149-3

[91] N.J. Alexander, H.P. Robert and S.P. McCormick. "Genes, gene clusters, and biosynthesis of trichothecenes and fumonisins in *Fusarium*." *Toxin Rev*. **2009**, *28*, 198-215. DOI: 10.1080/15569540903092142

[92] J.F. Grovey. The trichothecenes and their biosynthesis. *Fortschr Chem Org Naturst*. **2007**, *88*, 63-130. Google Scholar

[93] M. Rychlik, H.U. Humpf, D. Marko, S. Danicke, A. Mally, F. Berthiller, H. Klaffke and N. Lorenz. Proposal of a comprehensive definition of modified and other forms of mycotoxins including "masked" mycotoxins. *Mycotoxin Res*. **2014** *30*, 197-205. DOI: 10.1007/s12550-014-0203-5

[94] D. Payros, I. Alssane-Krembi, A. Pierron, N. Loiseau, P. Pinton and I. Oswald. Toxicology of deoxynivalenol and its acetylated and modified forms. *Arch Toxicol*. **2016**, *90*, 2931-2957. DOI: 10.1007/s00204-016-1826-4

[95] F. Berthiller, C. Crews, C. Dalla'asta, S.D. Saeger, G. Haesaert, P. Karlovsky, I.P. Oswald, W. Seefelder, G. Speijers and J. Stroka. Masked mycotoxins: A review. *Mol. Nutr. Food Res*. **2013**, *57*, 165-186. DOI: 10.1002/mnfr.201100764

[96] A. Pierron, S. Mimoun, L.S Murate, N. Loiseau, Y. Lippi, A.P. Bracarense, G. Schatzmayr, J.-W. He, T. Zhou, W.D. Moll and I.P. Oswald. Microbial

biotransformation of DON: molecular basis for reduced toxicity. *Sci Rep*. **2016**, *6*, 29105. DOI: 10.1038/srep29105

[97] S.N. Wegulo. "Factors Influencing Deoxynivalenol Accumulation in Small Grain Cereals." *Toxins*. **2012**, *4*, 1157-1180. DOI: 10.3390/toxins4111157

[98] C.S. McLaughlin, M.H. Vaughn, J.M. Campbell, C.M. Wei and M.E. Staord. Inhibition of protein synthesis by trichothecenes. *In Mycotoxins in Human and Health*; Rodricks, J.V., Hesseltine, C.W., Mehlman, M.A., Eds.; Pathotox Publishers: Park Forest South, IL, USA, **1977**; pp. 263-275. Google Scholar

[99] N.G. de Loubresse, I. Prokhorova, W. Holtkamp, M.V. Rodnina, G. Yusupova and M. Yusupov. Structural basis for the inhibition of the eukaryotic ribosome. *Nature*. **2014**, *513*, 517–522. DOI: 10.1038/nature13737

[100] C. Arunachalam and F.M. Doohan. Trichothecene toxicity in eukaryotes: Cellular and molecular mechanisms in plants and animals. *Toxicol. Lett*. **2013**, *217*, 149–158. DOI: 10.1016/j.toxlet.2012.12.003

[101] Y. Ueno, M. Hosoya, Y. Morita, I. Ueno and T. Tatsuno. Inhibition of the protein synthesis in rabbit reticulocyte by nivalenol, a toxic principle isolated from *Fusarium nivale*-growing rice. *J. Biochem*. **1968**, *64*, 479-485. DOI: 10.1093/oxfordjournals.jbchem.a128919

[102] M. Maresca. From the gut to the brain: journey and pathophysiological effects of the food-associated trichothecene mycotoxin deoxynivalenol. *Toxins*. **2013**, *5*, 784-820. DOI : 10.3390/toxins5040784

[103] C. Terciolo, M. Maresca, P. Pinton and I.P. Oswald. Review article: Role of satiety hormones in anorexia induction by Trichothecene mycotoxins. *Food Chem. Toxicol*.. **2018**, *121*, 701-714. DOI: 10.1016/j.fct.2018.09.034

[104] E.O. Da Silva, A.P.F.L. Bracarense and I.P. Oswald. Mycotoxins and oxidative stress: where are we? *World Mycotoxin J*.. **2018** *11*, 113-134. DOI: 10.3920/WMJ2017.2267

[105] M.E. Stafford and C. S. McLaughlin. Trichodermin, a possible inhibitor of the termination process of protein synthesis. *J. Cell Physiol*. **1973**, *82*, 121–124. Doi: 10.1002/jcp.1040820114

[106] C.M. Wei and C.S. McLaughlin. Structure-function relationship in the 12, 13-epoxytrichothecenes novel inhibitors of protein synthesis. *Biochem. Biophys. Res. Commun*. **1974**, *57*, 838-844. DOI: 10.1016/0006-291X(74)90622-6

[107] C.J. Carter, M. Cannon and K.E. Smith. Inhibition of protein synthesis in reticulocyte lysates by trichodermin. *Biochem. J*. **1976**, *154*, 171-178. DOI: 10.1042/bj1540171

[108] Beasley, V. R. (ed.). Trichothecene mycotoxicosis: pathophysiologic effects. *CRC Press*, Boca Raton, Fla. **1989**, *I*.

[109] B.A. Rotter, D.B. Prelusky and J.J. Pestka. Toxicology of deoxynivalenol (vomitoxin). *J. Toxicol. Environ. Health*. **1996**, *48*, 1–34. DOI: 10.1080/009841096161447

[110] E. Mayer, B. Novak, A. Springler, H.E. Schwartz-Zimmermann, V. Nagl, N. Reisinger, S. Hessenberger and G.E. Schatzmayr. Effects of deoxynivalenol (DON) and its microbial biotransformation product deepoxy-deoxynivalenol (DOM-1) on a trout, pig, mouse, and human cell line. *Mycotoxin Res*. **2017**, *33*, 297–308. DOI : 10.1007/s12550-017-0289-7

[111] N.A. Foroud, R.A. Shank, D. Kiss, F. Eudes and P. Hazendonk. Solvent and water mediated structural variations in deoxynivalenol and their potential implications on the disruption of ribosomal function. *Front. Microbiol*. **2016**, *7*, 1239. DOI: 10.3389/fmicb.2016.01239

[112] R.A. Shank, N.A. Foroud, P. Hazendonk, F. Eudes and B.A. Blackwell. Current and future experimental strategies for structural analysis of trichothecene mycotoxins—A prospectus. *Toxins*. **2011**, *3*, 1518-1553. DOI: 10.3390/toxins3121518

[113] P. Chaudhary, R.A. Shank, T. Montina, J.T. Goettel, N.A. Foroud, P. Hazendonk and F. Eudes. Hydrogen-bonding interactions in T-2 toxin studied using solution and solid-state NMR. *Toxins*. **2011**, *3*, 1310-1331. DOI: 10.3390/toxins3101310

[114] G.S. Eriksen, H. Pettersson and T. Lundh. Comparative cytotoxicity of deoxynivalenol, nivalenol, their acetylated derivatives and de-epoxy metabolites. *Food Chem. Toxicol*. **2004**, *42*, 619-624. DOI: 10.1016/j.fct.2003.11.006

[115] E. Varga, G. Wiesenberger, C. Hametner, T.J. Ward, Y. Dong, D. Schöfbeck, S. McCormick, K. Broz, R. Stückler, R. Schuhmacher, R.; et al. New tricks of an old enemy: Isolates of Fusarium graminearum produce a type A trichothecene mycotoxin. *Environ. Microbiol*. **2015**, *17*, 2588-2600. Doi: 10.1111/1462-2920.12718

[116] B. Poppenberger, F. Berthiller, D. Lucyshyn, T. Sieberer, R. Schuhmacher, R. Krska, K. Kuchler, J. Gloss, C. Luschnig and G. Adam. Detoxification of the Fusarium mycotoxin deoxynivalenol by a UDP-glucosyltransferase from Arabidopsis thaliana. *J. Biol. Chem*. **2003**, *278*, 47905-47914. DOI: 10.1074/jbc.M307552200

[117] M. Kimura, I. Kaneko, M. Komiyama, A. Takatsuki, H. Koshino, K. Yoneyama and I. Yamaguchi. Trichothecene 3-O-acetyltransferase protects both the producing organism and transformed yeast from related mycotoxins. *J. Biol. Chem*. **1998**, *273*, 1654–1661. DOI: 10.1074/jbc.273.3.1654

[118] V. Betina. Structure-activity relationships among mycotoxins. *Chem.-Biol. Interactions*. **1989** *71*, 105-146. DOI: 10.1016/0009-2797(89)90030-6

[119] B.B. Jarvis, R.M. Eppley and E.P. Mazolla. Chemistry and bioproduction of macrocyclic trichothecenes. In: Ueno Y (ed) Trichothecenes chemical, biological and toxicological aspects. *Elsevier*, Amsterdam, **1983**, pp 20–38.

[120] A.E. Desjardins, S.P. McCormick and M. Appell. Structure-activity relationships of trichothecene toxins in an *Arabidopsis thaliana* leaf assay. *J Agric Food Chem*. **2007**, *55*, 6487-6492. DOI: 10.1021/jf0709193

[121] M. Appell and W. Bosma. Assessment of the electronic structure and properties of trichothecene toxins using density functional theory. *J Hazard Mater*. **2015**, *288*, 113-23. DOI: 10.1016/j.jhazmat.2015.01.051

[122] M.G. Malmierca, R.E. Cardoza, N. Alexander, S.P. McCormick, I.G. Collado, R. Hermosa, E. Monte and S. Gutiérrez. Relevance of trichothecenes in fungal physiology: Disruption of tri5 in *Trichoderma arundinaceum*. *Fungal Genet. Biol*. **2013**, *53*, 22-33. DOI: 10.1016/j.fgb.2013.02.001.

[123] J. Semeiks, D. Borek, Z. Otwinowski and N.V. Grishin. Comparative genome sequencing reveals chemotype-specific gene clusters in the toxigenic black mold *Stachybotrys*. *BMC Genom*. **2014**, *15*, 590. DOI: 10.1186/1471-2164-15-590 .

[124] D.W. Brown, R.B. Dyer, S.P. McCormick, D.F. Kendra and R.D. Plattner. Functional demarcation of the *Fusarium* core trichothecene gene cluster. *Fungal Genet. Biol*. **2004**, *41*, 454–462. DOI: 10.1016/j.fgb.2003.12.002

[125] D.W. Brown, R.H. Proctor R.B. Dyer and R.D. Plattner. Characterization of a Fusarium 2-gene cluster involved in trichothecene C-8 modification. *J. Agric. Food Chem*. **2003**, *51*, 7936–7944. DOI: 10.1021/jf030607+

[126] M. Kimura and I. Yamaguchi. The mystery of the trichothecene-3-O-acetyltransferase gene: *Tri101* evolved independently of other trichothecene biosynthetic genes in the gene cluster. *Pestic. Sci*. **1999**, *55*, 372-374. Google Scholar

[127] N.J. Alexander, S.P. McCormick, T.M. Larson and J.E. Jurgenson. Expression of *Tri15* in *Fusarium sporotrichioides*. *Curr. Genet*. **2004**, *45*, 157-162. Google Scholar

[128] R.S. Goswami and H.C. Kistler. "Heading for disaster: Fusarium graminearum on cereal crops. *Mol. Plant Patho.* **2004**, *5*, 515-525. DOI: 10.1111/j.1364-3703.2004.00252.x

[129] S.P. McCormick, N.J. Alexander and R.H. Proctor. Fusarium Tri4 encodes a multifunctional oxygenase required for trichothecene biosynthesis. *Can. J. Microbiol*. **2006**, *52*, 636-642. DOI: 10.1139/w06-011

[130] S.P. McCormick, A.M. Stanley, N.A. Stover and N.J. Alexander. "Trichothecenes: From Simple to Complex Mycotoxins." *Toxins*. **2011**, *3*, 802-814. DOI: 10.3390/toxins3070802.

[131] P.W. Brian and J.C. McGowan. Biologically active metabolic products of the mould *Metarrhizium glutinosum* S. Pope. *Nature*, **1946**, *157*, 334. Google Scholar

[132] P.W Brian, H.G. Hemming and E.G. Jefferys. Production of antibiotics by species of *Myrothecium*. *Mycologia*, **1948**, *40*, 363-368. DOI: 10.1080/00275514.1944.12017714

[133] J.F. Grove. Macrocyclic trichothecenes. *Nat. Prod. Rep*., **1993**, *10*, 429-448. Doi: 10.1039/NP9931000429

[134] M.P. de Carvalho, H. Weich and W.-R. Abraham. Macrocyclic Trichothecenes as Antifungal and Anticancer Compounds. *Curr. Med. Chem.*. **2016**, *23*, 23-35. DOI: 10.2174/0929867323666151117121521

[135] C.Tamm. The antibiotic complex of the verrucarins and roridins. *Fortschr. Chem. Org. Nat*. **1974**, *31*, 63-117. Google Scholar

[136] B.B. Jarvis and E.P. Mazzola. Macrocyclic and other novel trichothecenes – their structure, synthesis, and biological significance. *Acc. Chem. Res*. **1982**, *15*, 388-395. Google Scholar

[137] E. Härri, W. Loeffler, H.P. Sigg, H. Stiihelin, C. Stoll, C. Tamm and D. Wiesinger. Über die Verrucarine und Roridine, eine Gruppe von cytostatisch

hochwirksamen Antibiotica aus *Myrothecium*-Arten. *Helv. Chim. Acta*, **1962**, *4*, 839-853. DOI: 10.1002/hlca.19620450314

[138] Saikawa, Y.; Okamoto, H.; Inui, T.; Makabe, M.; Okuno, T.; Suda, T.; Hashimoto, K.; Nakata, M. Toxic principles of a poisonous mushroom *Podostroma cornu-damae*. *Tetrahedron*, **2001**, *57*, 8277-8281. DOI: 10.1016/S0040-4020(01)00824-9

[139] B.B. Jarvis, Y.-W. Lee, S.N. Comezoglu and C.S. Yatawara. Trichothecenes produced by *Stachybotrys atra* from Eastern Europe. *Appl. Environ. Microbiol*. **1986**, *51*, 915-918. DOI: 10.1128/AEM.51.5.915-918.1986

[140] S.-Y. Zhang, Z.-L. Li, L.-P. Guan, X. Wu, H.-Q. Pan, J. Bai and H.-M. Hua. Structure determination of two new trichothecenes from a halotolerant fungus *Myrothecium* sp. GS-17 by NMR spectroscopy. *Magn. Res. Chem*., **2012**, *50*, 632-636. DOI: 10.1002/mrc.3845

[141] R.M. Eppley, E.P. Mazzola, R.J. Highet and W. Bailey. Structure of satratoxin H, a metabolite of *Stachybotrys atra*. Application of proton and carbon-13 nuclear magnetic resonance. *J. Org. Chem*. **1977**, *42*, 240-243. DOI: 10.1021/jo00422a014

[142] N.-J. Yu, S.-X. Guo and H.-Y. Lu. Cytotoxic macrocyclic trichothecenes from the mycelia of *Calcarisporium arbuscular Preuss*. *J. Asian Nat. Prod. Res*. **2002**, *4*, 179-183. DOI: 10.1080/10286020290011387

[143] A.C. Whyte, J.B. Gloer, J.A. Scott and D. Malloch. Cercophorins A-C: novel antifungal and cytotoxic metabolites from the *coprophilous* fungus *Cercophora areolata*. *J. Nat. Prod*. **1996**, *59*, 765-769. DOI: 10.1021/np9603232

[144] M. Matsumoto, H. Minato, K. Tori and M. Ueyama. Structures of isororidin E, epoxyisororidin E, and epoxy- and diepoxyroridin H, new metabolites isolated from *Cylindrocarpon* species determined by carbon-13 and hydrogen-1 NMR spectroscopy. Revision of C-2′:C-3′ double bond configuration of the roridin group. *Tetrahedron Lett.* **1977**, *18*, 4093-4096. DOI: 10.1016/S0040-4039(01)83435-3

[145] K.P. Panozishvili and A.V. Borovkov. Roridin A from Dendrodochium toxicum. *Chem. Nat. Comp*., **1975**, *10*, 408. Google Scholar.

[146] D. Samples, D.W. Hill, C.H. Bridges and B.J. Camp. Isolation of a mycotoxin (roridin A) from *Phomopsis* spp. *Vet. Human Toxicol*. **1984**, *26*, 21-23. Google Scholar

[147] S.M. Kupchan, B.B. Jarvis, R.G. Dailey, W. Bright, R.F. Bryan and Y. Shizuri. Baccharin, a novel potent antileukemic trichothecene triepoxide from *Baccharis megapotamica*. *J. Am. Chem. Soc*., **1976**, *98*, 7092-7093. DOI: 10.1021/ja00438a066

[148] S.M. Kupchan, D.R. Streelman, B.B. Jarvis, R.G. Dailey and A.T. Sneden. Isolation of potent new antileukemic trichothecenes from *Baccharis megapotamica*. *J. Org. Chem*., **1977**, *42*, 4221-4225. DOI: 10.1021/jo00862a011

[149] B.B. Jarvis, S.N. Comezoglu, H.L. Ammon and C.K. Breedlove. New macrocyclic trichothecenes from *Baccharis megapotamica*. *J. Nat. Prod*., **1987**, *50*, 815-828. DOI: 10.1021/np50053a008

[150] B.B. Jarvis, S.N. Comezoglu, M.M. Rao, N.B. Pena, F.E. Boettner, T.M. Williams, G. Forsyth and B. Epling. Isolation of macrocyclic trichothecenes from a large-scale extract of *Baccharis megapotamica*. *J. Org. Chem*., **1987**, *52*, 45-56. Google Scholar

[151] J.J. Pestka and J.H. Forstell. Inhibition of human lymphocyte transformation by the macrocyclic trichothecenes roridin A and verrucarin A. *Toxicol. Lett*. **1988**, *41*, 215–222. DOI: 10.1016/0378-4274(88)90057-4

[152] E. Cunliffe, M. Cannon and J. Davies. Mechanism of inhibition of eukaryotic protein synthesis by trichothecene fungal toxins. *Proc Natl Acad Sci* U.S.A. **1974**, *71*, 30-34. DOI: 10.1073/pnas.71.1.30

[153] K. Palanivel, V. Kanimozhi, B.Kadalmani and M.A. Akbarsha. Verrucarin A, a protein synthesis inhibitor, induces growth inhibition and apoptosis in breast cancer cell lines MDA-MB-231 and T47D. *Biotechnol Lett*. **2013**, *35*, 1395-1403. DOI: 10.1007/s10529-013-1238-y

[154] V. Polizzi, B. Delmlle, A. Adams, A. Moretti, A. Susca, A. Picco, Y. Rosseel, R. Kindt, J.V. Bocxlaer, N.D. Kimpe, C.V. Peteghem and S.D. Saeger. JEM Spotlight: Fungi, mycotoxins and microbial volatile organic compounds in mouldy interiors from water-damaged buildings. *J Environ Monit*. **2009**, *11*, 1849-58. DOI: 10.1039/B906856B

[155] P. Kankkunen, E.Valimaki, J. Rinthahaka, J. Palomaki, T. Nyman, H. Alenius, H. Wolff and S. Matikainen. Trichothecene mycotoxins activate NLRP3 inflammasome through a P2X7 receptor and Src tyrosine kinase dependent pathway. *Hum Immunol*. **2014**, *75*, 134-40. DOI: 10.1016/j.humimm.2013.11.010

[156] C.J. Amuzie and J.J. Pestika. Suppression of insulin-like growth factor acid-labilesubunit expression--a novel mechanism for deoxynivalenol-induced growth retardation. *Toxicol Sci*. **2010**, *113*, 412-21. DOI: 10.1093/toxsci/kfp225

[157] Z. Islam, J. Shinozuka, J.R. Harkema J.J. Pestika. Purification and comparative neurotoxicity of the trichothecenes satratoxin G and roridin L2 from *Stachybotrys chartarum*. *J. Toxicol Environ Health A*. **2009**, *72*, 1242-51. DOI: 10.1080/15287390903129234

[158] T. Amagata, C. Rath, J.F. Rigot, N. Tarlov, K. Tenney, F.A. Valeriote and P. Crews. Structures and cytotoxic properties of trichoverroids and their macrolide analogues produced by saltwater culture of *Myrothecium verrucaria*. *J. Med. Chem.*, **2003**, *46*, 4342-4350. DOI: 10.1021/jm030090t

[159] C.C. Garcia, M.L. Rosso, M.D. Bertoni, M.S. Maier and E.B. Damonte. Evaluation of the antiviral activity against junin virus of macrocyclic trichothecenes produced by the hypocrealean epibiont of *Baccharis coridifolia*. *Planta Med.*, **2002**, *68*, 209-212. DOI: 10.1055/s-2002-23134

[160] G.A. Cordell and Y.G. Shin. Finding the needle in the haystack. The dereplication of natural product extracts. *Pure Appl. Chem.* **1999**, *71*, 1089-1094. Google Scholar

[161] H.P. Fiedler. Biosynthetic Capacities of Actinomycetes. 1 Screening for Secondary Metabolites by HPLC and UV-Visible Absorbance Spectral Libraries *Nat. Prod Lett.* **1993**, *2*, 119-128. DOI: 10.1080/10575639308043796

[162] J. Bukingham and S. Thompson, Dictionary of natural products and other information sources for natural products scientists, *Royal Society of Chemistry*, London, **1997**, 53-67.

[163] I. Dolamic, S. Knoppe, A. Dass and T. Bürg. First enantioseparation and circular dichroism spectra of Au38 clusters protected by achiral ligands *Natur Commun.* **2012**. DOI: 10.1038/ncomms1802

[164] R. Bara, I. Zerfass I, A.H. Aly, H. Goldbach-Gecke, V. Raghavan, P. Sass, A. Mandi, V. Wray, P.L. Polavarapu, A. Pretsch, W.H. Lin, T. Kurtan, A. Debbab, H. Broetz-Oesterhelt, P. Proksch. Atropisomeric dihydroanthra cenones as inhibitors of multi-resistant *Staphylococcus aureus*. *J Med Chem.*, **2013**, *56*: 3257-3272. DOI: 10.1021/jm301816a

[165] V. Kumar, A. Bharti, O. Gusain and G.S. Bisht. An improved method for isolation of genomic DNA from filamentous actinomycete. *J Sci Eng Tech Mgt.*, **2010**, *2*, 10-13. Google Scholar

[166] F. Ausubel, R. Brent, R. Kingston, D. Moore, J. Seidman, J. Smith, and K. Struhl. (**1998**) Current Protocols in Molecular Biology. Massachusetts General Hospital, Harvard Medical School. *Cambridge, MA.*

[167] M. Gardes, and T.D. Bruns. ITS primers with enhanced specificity for basidiomycetes-application to the identification of mycorrhizae and rusts. *Mol. Ecol.*, **1993**, *2*, 113-118. DOI: 10.1111/j.1365-294X.1993.tb00005.x

[168] W. Murayama, T. Kobayashi, Y. Kosuge, H. Yano, Y. Nunogaki and K. Nunogaki. A new centrifugal counter-current chromatograph and its application. *J. Chromatogr. A.*, **1982**, *239*, 643-649. DOI: 10.1016/S0021-9673(00)82022-1

[169] N. Amarouche, L. Boudesocque, C. Sayagh, M. Giraud, J. McGarrity, A. Butte, L. Marchal, A. Foucault and J.-H. Renault. Purification of a modified cyclosporine Aby co-current centrifugal partition chromatography: process developmentand intensification, *J. Chromatogr. A.*, **2013**, *1311*, 72–78 DOI: 10.1016/j.chroma.2013.08.053

[170] S. Adelmann, T. Baldhoff, B. Koepcke, G. Schembecker. Selection of operating parameters on the basis of hydrodynamics in centrifugal partition chromatography for the purification of nybomycin derivatives. *J. Chromatogr.A.*, **2013**, *1274*, 54-64. DOI: 10.1016/j.chroma.2012.11.031

[171] A.P. Foucault (Ed.), Centrifugal Partition Chromatography, Chromatographic Science Series, vol. 68, Marcel Dekker, New York, **1995**.

[172] N. Zga, Y. Papastamoulis, A. Toribio, T. Richard, J.C. Delaunay, P. Jeandet, J.H. Renault, J.P. Monti, J.M. Mérillon and P. Waffo-Téguo, Preparative purification of antiamyloidogenic stilbenoids from *Vitis vinifera* (Chardonnay) stems by centrifugal partition chromatography, *J. Chromatogr. B.* **2009**, *877*, 1000-1004. DOI: 10.1016/j.jchromb.2009.02.026

[173] J.-C. Delaunay, C. Castagnino, C. Chèze and J. Vercauteren. Preparative isolation of polyphenolic compounds from *Vitis vinifera* by centrifugal partition chromatography, *J. Chromatogr. A.* **2002**, *964*, 123-128. DOI: 10.1016/S0021-9673(02)00355-2

[174] A. Boonloed, G.L. Weber, K.M. Ramzy, V.R. Dias and V.T. Remcho. Centrifugal partition chromatography: A preparative tool for isolation and purification of xylindein from *Chlorociboria aeruginosa*. *J. Chromatogr. A.*, **2016**, *1478*, 19–25. DOI: 10.1016/j.chroma.2016.11.026

[175] I.A. Sutherland, S. Ignatova, P. Hewitson, L. Janaway, P. Wood, N. Edwards, G. Harris, H. Guzlek, D. Keay and K. Freebairn. *J. Chromatogr. A.*, **2011**, *1218*, 6114. DOI: 10.1016/j.chroma.2011.01.016

[176] L. Marchal, O. Intes, A. Foucault, J. Legrand, J.M. Nuzillard and J.-H. Renault. Rational improvement of centrifugal partition chromatographic settings for the production of 5-n-alkylresorcinols from wheat bran lipid extract: I. Flooding conditions—optimizing the injection step. *J. Chromatogr. A.*, **2003**, *1005*, 51. DOI: 10.1016/S0021-9673(03)00879-3

[177] A.P. Foucault and L. Chevolot. Counter-current chromatography: instrumentation, solvent selection and some recent applications to natural product purification. *J. Chromatogr. A.*, **1998**, *808*, 3-22. DOI: 10.1016/S0021-9673(98)00121-6

[178] E. Hopmann, A. Frey and M. Minceva. A priori selection of the mobile and stationary phase in centrifugal partition chromatography and counter-current chromatography. *J. Chromatogr. A.* 2012, 1238, 68-76. DOI: 10.1016/j.chroma.2012.03.035

[179] J.M. Menet, D. Thiebaut, Countercurrent Chromatography, Marcel Dekker, Eds. New York, (**1999**), vol. 82, Google Scholar

[180] M. Hamzaoui. Thesis: Methodological developments of Centrifugal Partition Extraction (CPE). Application to fractionation and purification of the natural substances derived from plants and white biotechnology. *(Institute of Molecular Chemistry Reims (UMR CNRS 7312), Groupe: "Isolation & Structures").* **2013**

[181] A.P. Foucault. Centrifugal partition chromatography Chromatographic ScienceSeries, vol. 68, Marcel Dekker, New York, 1995. Google Scholar

[182] F. Oka, H. Oka and Y. Ito. Systematic search for suitable two-phase solventsystems for high-speed counter-current chromatography. *J. Chromatogr. A.*, **1991**, *538*, 99-108. DOI: 10.1016/S0021-9673(01)91626-7

[183] A. Berthod. Countercurrent chromatography, the support-free liquid stationary phase Comprehensive Analytical Chemistry, vol. *38*, *Elsevier* Amsterdam, **2002**. Google Scholar

[184] P. Marfey. Determination of D-amino acids. II. Use of a bifunctional reagent, 1,5-difluoro-2,4-dinitrobenzene. *Carlsberg Res. Commun*., **1984**, *49*, 591−596. DOI: 10.1007/BF02908688

[185] C. Valgas, S.M.D. Souza, E.F. Smânia and A. Smânia. Screening methods to determine antibacterial activity of natural products. *Braz. J. Microbiol.*, **2007**, *38*, 369-380. DOI: 10.1590/S1517-83822007000200034

[186] S. Magaldi, S. Mata-Essayag, C.H. De Capriles, C. Perez, M. Colella, C. Olaizola and Y. Ontiveros, Y. Well diffusion for antifungal susceptibility testing. *Int. J. Infect. Dis.*, **2004**, *8*, 39-45. DOI: 10.1016/j.ijid.2003.03.002

[187] B. Schulz, C. Boyle, S. Draeger, A.K. Römmert, and K. Krohn. Endophytic fungi: a source of novel biologically active secondary metabolites. *Mycolo. Res.*. **2002** *106*, 996-1004. DOI: 10.1017/S0953756202006342

[188] M.A. Hasnat, M. Pervin and B.O. Lim. Acetylcholinesterase Inhibition and *in Vitro* and *in Vivo* Antioxidant Activities of *Ganoderma lucidum* Grown on Germinated Brown Rice. *Molecules*, **2013**, *18*, 6663-6678. DOI: 10.3390/molecules18066663

[189] N. Martins, S. Petropoulos and I.C. Ferreira. Chemical composition and bioactive compounds of garlic (*Allium sativum L*.) as affected by pre- and post-harvest conditions: A review *Food chem.*, **2016**, **211**, 41-50. DOI : 10.1016/j.foodchem.2016.05.029

[190] K.M. El-Gamal, A.M. El-Morsy, A.M. Saad, I.H. Eissa and M. Alswah. Synthesis, docking, QSAR, ADMET and antimicrobial evaluation of new quinoline-3-carbonitrile derivatives as potential DNA-gyrase inhibitors. *J. Mole. Struc.*, **2018**, *1166*, 15-33. DOI : 10.1016/j.molstruc.2018.04.010

[191] M. Hagras, M.A. El Deeb, H.S. Elzahabi, E.B. Elkaeed, A.B. Mehany and I.H. Eissa, *Journal of enzyme inhibition and medicinal chemistry*, 2021, **36**, 640-658.

[192] H.A. Mahdy, M.K. Ibrahim, A.M. Metwaly, A. Belal, A.B. Mehany, K.M. El-Gamal, A. El-Sharkawy and M.A. Elsohly. Design, synthesis, molecular

modeling, in vivo studies and anticancer evaluation of quinazolin. *Bioorg. Chem.*, **2020**, *94*, 103422. DOI: 10.1016/j.bioorg.2019.103422

[193] A.M. El-Naggar, I.H. Eissa, A. Belal and A.A. El-Sayed. Design, eco-friendly synthesis, molecular modeling and anticancer evaluation of thiazol-5(4H)-ones as potential tubulin polymerization inhibitors targeting the colchicine binding site *RSC Advances*, **2020**, *10*, 2791-2811. DOI: 10.1039/C9RA10094F

[194] A.W. Baur, W.M. Kirby, J.C. Sherris and M. Truck. Antibiotic susceptibility testing by a standardized single disk method. *Am J Clin. Pathol*., **1966**, *45*, 493 - 496. PMID: 5325707

[195] E. Caballero, C. Avendaño and J. Carlos Menéndez. Stereochemical issues related to the synthesis and reactivity of pyrazino[20,10-5,1]pyrrolo[2,3-b]indole-1,4-diones. *Tetrahedron: Asymm.* **1998**, *9*, 967–981. DOI: 10.1016/S0957-4166(98)00068-8

[196] X. Chen, L. Si, D. Liu, P. Proksch, L. Zhang, D. Zhou and W. Lin. Neoechinulin B and its analogues as potential entry inhibitors of influenza viruses, targeting viral hemagglutinin. *Eur. J. Med. Chem.*. **2015**, *93*, 182-195. DOI: 10.1016/j.ejmech.2015.02.006

[197] V. Wohlgemuth, F. Kindinger, X. Xie, B-G. Wang, and S-M. Li. Two Prenyltransferases Govern a Consecutive Prenylation Cascade in the Biosynthesis of Echinulin and Neoechinulin. *Org. Lett.*. **2017**, *19*, 5928−5931. DOI: 10.1021/acs.orglett.7b02926

[198] H. Fujimoto, T. Fujimaki, E. Okouyama and M. Yamazaki. Immunomodulatory conistituents from an ascomycete, *Microascus tardifaciens. Chem. Pharm. Bull*., **1999**, *47*, 1426-1432. DOI: 10.1248/cpb.47.1426

[199] C.M Maes, M. Potgiete and P.S. Steyn. N.m.r. assignments, conformation, and absolute configuration of ditryptophenaline and model dioxopiperazines. *J. Chem. Soc., Perkin Trans. 1*, **1986**, 861-866. DOI: 10.1039/P19860000861

[200] E. Bovio, L. Garzoli, A. Poli, A. Luganini, P.Villa, R. Musumeci, G.P. McCormack, C.E. Cocuzza, G. Gribaudo, M. Mehiri and G.C. Varese. Marine fungi from the sponge *Grantia compressa*: biodiversity, chemodiversity and biotechnological potential. *Mar. Drugs*. **2019**, *17*, 220. DOI: 10.3390/md17040220

[201] M. Chen, K.-L. Wang and C.-Y. Wang. Antifouling indole alkaloids of a marine-derived fungus *Eurotium* sp. *Chem. Nat. Compd*., **2018**, *54*, 207-209. Google Scholar

[202] A.J. Birch, G.E. Blance, S. David and H. Smith, 600. Studies in relation to biosynthesis. Part XXIV. Some remarks on the structure of echinulin. *J. Chem. Soc*., **1961**, 128-3131. DOI: 10.1039/JR9610003128

[203] G.J. Slack, E. Puniani, J.C. Frisvad, R.A. Samson and J.D. Miller. Secondary metabolites from Eurotium species, Aspergillus calidoustus and A. insuetus common in Canadian homes with a review of their chemistry and biological activities. *Mycological Res*., **2009**, *113*, 480-490. DOI: 10.1016/j.mycres.2008.12.002

[204] J. Gao, F. León, M.M. Radwan, O.R. Dale, A.S. Husni, S.P. Manly, S. Lupien, X. Wang, R.A. Hill, F.M. Dugan, H.G. Cutler and S.J. Cutler. Benzyl derivatives with in vitro binding affinity for human opioid and cannabinoid receptors from the fungus Eurotium repens. *J. Nat. Pro.*, **2011**, *74*, 1636-1639. DOI: 10.1021/np200147c

[205] J.H. Sohn, Y.-R. Lee, D.-S. Lee, Y.-C. Kim and H. Oh. PTP1B Inhibitory secondary metabolites from marine-derived fungal strains *Penicillium spp. and Eurotium sp*.. *J. Microbiol. Biotechnol*. **2013**, *23*, 1206-1211. DOI: 10.4014/jmb.1303.03078

[206] R. Wang, Q. Wan, Y. Zhang, F. Huang, K. Yu, D. Xu, Q. Wang and J. Sun. Emodin suppresses interleukin-1β induced mesangial cells proliferation and extracellular matrix production via inhibiting P38 MAPK. *Life Sci*., **2007**, *80*, 2481-2488. DOI: 10.1016/j.lfs.2007.04.010

[207] N.L. Zhou, T.-J. Zhu, S.-X. Cai, Q.-.Q Gu and D.-H. Li. Three new indole-containing diketopiperazine alkaloids from a deep-ocean sediment derived fungus Penicillium griseofulvum. *Helv. Chim. Acta*., **2010**, *93*, 1758-1763. DOI: 10.1002/hlca.200900443

[208] S.K. Talapatra, S.K. Mandal, A. Bhaumik, S. Mukhopadhyay, P. Kar, A. Patra and B. Talapatra. Echinulin, a novel cyclic dipeptide carrying a triprenylated indole moiety from an *Anacardiaceae*, a *Cucurbitaceae* and two *Orchidaceae* plants: detailed high resolution 2D-NMR and mass spectral studies. *J. Indian Chem. Soc*., **2001**, *78*, 773-778. DOI: 10.1002/chin.200309184

[209] H. Kamauchia, K. Kinoshitaa, T. Sugitab and K. Koyama. Conditional changes enhanced production of bioactive metabolites of marine derived fungus *Eurotium rubrum*. *Bioorg. Med. Chem. Lett*., **2016**, *26*, 4911-4914. DOI: 10.1016/j.bmcl.2016.09.017

[210] M.S.C. Pedras, K.C. Smith and J.L. Taylor. Production of 2,5 dioxopiperazie by a new isolate type of the blackleg fungus *Phoma lingam*. *Phytochem.*, **1998**, *49*, 1575-1577. DOI: 10.1016/S0031-9422(98)00271-4

[211] N.M. Gomes, T.D. Dethoup, N. Singburaudom, L. Gales, A.M.S. Silva, and A. Kijjoa. Eurocristatine, a new diketopiperazine dimer from the marine sponge-associated fungus *Eurotium cristatum*. *Phytochem. Lett*. **2012**, *5*, 717-720. DOI: 10.1016/j.phytol.2012.07.010

[212] C.P. Balado, H. Sun, C. Griesinger, A.R. de Lera, and A.N. Vμzquez. Residual dipolar coupling enhanced NMR spectroscopy and chiroptics: a powerful combination for the complete elucidation of symmetrical small molecules, *Chem.Eur.J*., **2011**, *17*, 11983-11986. Google Scholar

[213] Y. Li, K.L. Sun, Y. Wang, P. Fu, P.P. Liu, C. Wang, and W.M. Zhu. A cytotoxic pyrrolidinoindoline diketopiperazine dimer from the algal fungus *Eurotium herbariorum* HT-2. *Chin. Chem. Lett*., **2013**, *24*, 1049-1052. DOI: 10.1016/j.cclet.2013.07.028

[214] S.M. Li. Prenylated indole derivatives from fungi: structure diversity, biological activities, biosynthesis and chemoenzymatic synthesis. *Nat. Prod. Rep*., **2010**, *27*, 57-78. DOI: 10.1039/B909987P

[215] J. Kim, J.A. Ashenhurst and M. Movassaghi. Total synthesis of (+)-11,11'-dideoxyverticillin A. *Science*., **2009**, *324*, 238-241. DOI: 10.1126/science.1170777

[216] A. Dossena, R. Marchelli and A. Pochini. New Metabolites of *Aspergillus amstelodami* Related to the Biogenesis of Neoechinulin. *J. Chem. Soc., Chem. Commun*., **1974**, 771-772. DOI: 10.1039/C39740000771

[217] Y. Li, X. Li, S.-K. Kim, J.S. Kang, H.D. Choi, J.R. Rho and B.W. Son. Golmaenone, a new diketopiperazine alkaloid from the marine-derived fungus *Aspergillus sp*.. *Chem. Pharm. Bull.*, **2004**, *52*, 375-376. DOI: 10.1248/cpb.52.375

[218] M. Chen, K.-L. Wang and C.-Y. Wang. Antifouling Indole Alkaloids of a Marine-Derived Fungus *Eurotium* sp. *Chem. Nat Com*. **2018**, *54*, 207-209. Google Scholar

[219] K.S. Kim, X. Cui, D.-S. Lee, J.H. Sohn, J.H. Yim, Y.-C. Kim and H. Oh. Anti-inflammatory effect of neoechinulin A from the marine fungus *Eurotium sp*. SF-5989 through the suppression of NF-κB and p38 MAPK pathways in

lipopolysaccharide-stimulated RAW264.7 macrophages. *Molecules*., **2013**, *18*, 13245-13259. DOI: 10.3390/molecules181113245

[220] H. Nagasawa, A. Isogai, K. Ikeda, S. Sato, S. Murakoshi, A. Suzuki and S. Tamura. Isolation and structure elucidation of a new indole metabolite from *Aspergillus ruber*. *Agric. Biol Chem*., **1975**, *39*, 1901-1902. DOI: 10.1271/bbb1961.39.1901

[221] G.R. Pettit, F. Hogan, J.-P Xu, R. Tan, T. Nogawa, Z. Cichacz and R.K. Pettit. Antineoplastic agents. 536. New sources of naturally occurring cancer cell growth inhibitors from marine organisms, terrestrial plants, and microorganisms. *J. Nat. Prod*., **2008**, *71*, 438-444. DOI: 10.1021/np700738k

[222] S.-J. Yang, M.-C. Liu, N. Liang, H.-M. Xiang and S. Yang. Chemical constituents of *Cyrtomium fortumei* (J.) Smith. *Nat. Prod. Res*., **2013** *27*, 2066-2068. DOI: 10.1080/14786419.2013.824442

[223] W.-L. Wang, T.-J. Zhu, H.-W. Tao, Z.-Y. Lu, Y.-C. Fang, Q.-Q. Gu and W.-M. Zhu. Three Novel, Structurally Unique Spirocyclic Alkaloids from the Halotolerant B-17 Fungal Strain of *Aspergillus variecolor*. *Chem. Biodiversity*. **2007**, *4*, 2913-2919. DOI: 10.1002/cbdv.200790240

[224] W.M Zhong, J.F. Wang, X.F. Shi , X.Y. Wei, Y.C. Chen, Q. Zeng, Y. Xiang, X.Y. Chen, X.P. Tian, Z.H. Xiao, W.M. Zhang, F.Z. Wang and S. Zhang. Eurotiumins A-E, Five New Alkaloids from the Marine-Derived Fungus *Eurotium* sp. SCSIO F452. *Mar .Drugs*, **2018**, *16*, 136. DOI: 10.3390/md16040136

[225] R. Marchelli, A. Dossena, A. Pochini and E. Dradi. The structures of five new didehydropeptides related to neoechinulin, isolated from *Aspergillus amstelodami*. *J. Chem. Soc. Perkin Trans*., **1977**, *17*, 713-717. DOI: 10.1039/P19770000713

[226] K. Kuramochi, T. Aoki, A. Nakazaki, S. Kamisuki, M. Takeno, K. Ohnishi, K. Kimoto, N. Watanabe, T. Kamakura, T. Arai, F. Sugawara and S. Kobayashi. Synthesis of Neoechinulin A. *Synthesis*, **2008**, *23*, 3810–3818. DOI: 10.1055/s-0028-1083634

[227] A. Dossena, R. Marchelli and A. Pochini. Neoechinulin D, a new isoprenylated dehy-drotryptophyl metabolite from *Aspergillus amstelodami*. *Experientia*., **1975**, *31*, 1249. Google Scholar

[228] F.-Y. Du, X.-M. Li, C.-S. Li, Z. Shang and B.-G. Wang. Cristatumins A–D, new indole alkaloids from the marine-derived endophytic fungus *Eurotium cristatum* EN-220 . *Bioorg. Med. Chem. Lett*.. 2012, 22, 4650–4653. DOI: 10.1016/j.bmcl.2012.05.088

[229] D.-L. Li, X.-M. Li, T.-G. Li, H.-Y. Dang and B.-G. Wang. Dioxopiperazine Alkaloids Produced by the Marine Mangrove Derived Endophytic Fungus *Eurotium rubrum*. *Helv. Chim. Acta*., **2008**, *91*, 1888. DOI: 10.1002/hlca.200890202

[230] H. Gao, T. Zhu, D. Li, Q. Gu and W. Liu. Prenylated indole diketopiperazine alkaloids from a mangrove rhizosphere soil derived fungus *Aspergillus effuses* H1-1. *Arch. Pharm. Res*., **2013**, *36*, 952–956. DOI: 10.1007/s12272-013-0107-5

[231] H. Gao, W. Liu, T. Zhu, X. Mo, A. Mandi, T. Kurta´n, J. Li, J. Ai, Q. Gu, and D. Li. Diketopiperazine alkaloids from a mangrove rhizosphere soil derived fungus *Aspergillus effuses* H1–1. *Org. Biomol. Chem*., **2012**, *10*, 9501-9506. DOI: 10.1039/C2OB26757H

[232] M. Liu, S. Lin, M. Gan, M. Chen, L. Li, S. Wang, J. Zi, X. Fan, Y. Liu, Y. Si, Y. Yang, X. Chen, and J. Shi. Yaoshanenolides A and B: new spirolactones from the bark of *Machilus yaoshansis*. *Org. Lett*., **2012**, *14*, 1004-1007. DOI: 10.1021/ol300130s

[233] J. Du, M. Wang, R. Chen, and D. Yu. Two new bislabdane type diterpenoids and three new diterpenoids from the roots of *Cunninghamia lanceolata*. *Planta Med.*, **2001**, *67*, 542-547. DOI: 10.1055/s-2001-16491

[234] G. Gatti, R. Cardillo, C. Fuganti, and D. Ghiringhelli. Structure determination of two extractives from *Aspergillus amstelodami* by nuclear magnetic resonance spectroscopy. *J. Chem. Soc., Chem. Commun.*, **1976**, *12*, 435-436. DOI: 10.1039/C39760000435

[235] D.-L Li, X.-M. Li, T.-G. Li, H.-Y. Dang, and B.-G. Wang. Dioxopiperazine alkaloids produced by the marine mangrove derived endophytic fungus *Eurotium rubrum*. *Helv. Chim. Acta*., **2008**, *91*, 1888-1893. DOI: 10.1002/hlca.200890202

[236] S. Inoue, J. Murata, N. Takamatsu, H. Nagano, and Y. Kishi. Synthetic studies on echinulin and related natural products. V. Isolation, structure and synthesis

of echinulin-neoechinulin type alkaloids isolated from *Aspergillus amstelodami*. *Yakugaku Zasshi*., **1977**, *97*, 576-581.
DOI: 10.1248/yakushi1947.97.5_576

[237] O.F. Smetanina, A.N. Yurchenko, E.V. Girich, P.T.-H. Trinh, A.S. Antonov, S.A. Dyshlovoy, G. von Amsberg, N.Y. Kim, E.A. Chingizova, E.A. Pislyagin, E.S. Menchinskaya, E.A. Yurchenko, T.T. Thanh and S.S. Afiyatullov. Biologically Active Echinulin-Related Indolediketopiperazines from the Marine Sediment-Derived Fungus *Aspergillus niveoglaucus*. *Molecules*, **2020**, *25*, 1-11. DOI: 10.3390/molecules25010061

[238] C.A. Kuttruff, H. Zipse and D. Trauner. Concise Total Syntheses of Variecolortides A and B through an Unusual Hetero-Diels–Alder Reaction. *Angew. Chem., Int. Ed*., **2011**, *50*, 1402–1405. DOI: 10.1002/anie.201006154

[239] a) R.C. Beiera, B.P. Mundy and G.A. Strobel. Assignment of anomeric configuration and identification of carbohydrate residues by 13C NMR. 1. Galacto- and glucopyranosides and furanosides. *Can. J. Chem*., **1980**, *58*, 2800-2804. DOI: 10.1139/v80-448

b) C.K. Chu, F.M. El-kabbani and B.B Thompson. Determination of the Anomeric Configuration of C-Nucleosides by 1H and 13C NMR Spectroscopy. *Nucleosides & Nucleotides*, **1984**, *3*, 1-31.
DOI : 10.1080/07328318408079416

c) D.L. Kwok, R.A Outten, R. Huhn and G.D. Daves. 8-Ethyl-l-methoxybenzo[d]naphtho[l,2-b]pyran-6-C-Glycosides by Acid-Catalyzed Glycosylation. *J. Org. Chem*., **1988**, *53*, 5359-5361.
DOI: 10.1021/jo00257a032

d) T. Hosoya, E. Takashiro,T. Matsumoto and K. Suzuki. Total Synthesis of the Gilvocarcins. *J. Am. Chem. Soc*., **1994**, *116*, 1004-1015.
DOI:10.1021/ja00082a023

e) M.-H. Yang, Y.-S. Fang, L. Cai, Y. Li, J.-W. Dong, T.-P. Yin, C.-L. Huang, and Z.-T. Ding. A new flavone C-glycoside and a new bibenzyl from *Bulbophyllum retusiusculum*. *Nat. Prod. Res*., **2016**, *30*, 1617-1621.
DOI: 10.1080/14786419.2015.1126266

[240] V. Costantino, E. Fattorusso, C. Imperatore and A. Mangoni. Glycolipids from Sponges. 20. ^{3}J-Coupling Analysis for Stereochemical Assignments in Furanosides: Structure Elucidation of Vesparioside B, a Glycosphingolipid

from the Marine Sponge *Spheciospongia vesparia*. *J. Org. Chem.*, **2008**, *73*, 6158-6165. DOI: 10.1021/jo800837k

[241] R. Watanadilok, P. Sonchaeng, A. Kijjoa, A.M Damas, L. Gales, A.M.S. Silva and W. Herz. Tetillapyrone and Nortetillapyrone, Two Unusual Hydroxypyran-2-ones from the Marine Sponge *Tetilla japonica*. *J. Nat. Prod.*, **2001**, *64*, 1056-1058. DOI : 10.1021/np0100690

[242] D. Burns, W.F. Reynolds, G. Buchanan,.; P.B. Reese and R.G. Enriquez. Assignment of ^{1}H and ^{13}C spectra and investigation of hindered side-chain rotation in lupeol derivatives. *Magn. Res. Chem.*, **2000**, *38*, 488-493. DOI: 10.1002/1097-458X(200007)38:7<488::AID-MRC704>3.0.CO;2-G

[243] C. Mutai, D. Abatis, C. Vagias, D. Moreau, C. Roussakis and V. Rousis. Cytotoxic lupane-type triterpenoids from *Acacia mellifera*. *Phytochem.*, **2005**, *65*, 1159-1164. DOI: 10.1016/j.phytochem.2004.03.002

[244] **a**) C. Altona and M. Sundaralingam. Conformational analysis of the sugar ring in Nucleosides and Nucleotides. A New Description using the Concept of Pseudorotation. *J. Am. Chem. Soc.*, **1972**, *94*, 8205-8212. DOI: 10.1021/ja00778a043

b) E. Westhof and M.A. Sundaralingam. Method for the Analysis of Puckering Disorder in Five-Membered Rings: The Relative Mobilities of Furanose and Proline Rings and Their Effects on Polynucleotide and Polypeptide Backbone Flexibility. *J. Am. Chem. Soc.*, **1983**, *105*, 970-976. DOI: 10.1021/ja00342a054

[245] H-C. Hu, C.-Y. Li, Y.-H. Tsai, D.Y. Yang, Y.-C. Wu, T.-L. Hwang, S.-L. Chen, F. Fülöp, A. Hunyadi, C.-H. Yen, Y.-B. Cheng and F.-R. Chang. Secondary Metabolites and Bioactivities of *Aspergillus ochraceopetaliformis* isolated from *Anthurium brownii*. *ACS Omega.*, **2020**, *5*, 20991-20999. DOI: 10.1021/acsomega.0c02489

[246] M. Brakta, M. Roger, N. Farr, C. Brahim, G. Massiot, C. Lavaud, W.R. Anderson, D. Sinou and G.D. Daves. Assignment of Anomeric Configuration of C-Glycopyranosides and C-Glycofuranosides. A ^{1}H, ^{13}C and NOE Spectrometric Study. *J. Org. Chem.*, **1993**, *58*, 2992-2998. DOI: 10.1021/jo00063a015

[247] J.G. Napolitano, J.A. Gavin. C. Garcia, M. Norte, J.J. Fernandez and A.H. Daranas. On the Configuration of Five-Membered Rings: A Spin–Spin

Coupling Constant Approach. *Chem. Eur. J.* **2011**, *17*, 6338-6347. https://doi.org/10.1002/chem.201100412

[248] L.A. Donders, F.A.A.M. de Leeuw and C. Altona. Relationship Between Proton-Proton NMR Coupling Constants and Substituent Electronegativities IV. An Extended Karplus Equation Accounting for Interactions Between Substituents and its Application to Coupling Constant Data Calculated by the Extended Huckel Method. *Magn. Reson. Chem.* **1989**, *27*, 556-563. https://doi.org/10.1002/mrc.1260270608

[249] S.H. Sung, W.J. Jung and Y.G.C. Kim. A Novel flavonol lyxoside of *Orostachys japonicus* herb. *Nat. Prod. Lett.* **2002**, *16*, 29-32. https://doi.org/10.1080/1057563029001/4818

[250] S.I. Elshahawi, K.A. Shaaban, M.K. Kharel and J.S.A Thorson. A comprehensive review of glycosylated bacterial natural products. *Chem. Soc. Rev.* **2015**, 44, 7591-7697. https://doi.org/10.1039/C4CS00426D

[251] a) I.I Cubero and M.M. Martinez. Synthesis of 2-C-methyl-D-lyxose and 2-C-methyl-D-xylose. *Carboh. Res.* **1982**, *105*, 181-188. https://doi.org/10.1016/S0008-6215(00)84966-6

b) V. Popsavin, G. Sanja, B. Stojanovic, M. Popsavin, V. Pejanovic and D. Miljkovic. Conversion of D-xylose to protected D-lyxose derivatives and to D-lyxose, via the corresponding 1,2-anhydride. *Carboh. Res.* **1999**, *321*, 110-115. https://doi.org/10.1016/S0008-6215(99)00164-0

[252] A.S. Perlin, B. Casu and H.J. Koch. Configurational and conformational influences on the carbon-13 chemical shifts of some carbohydrates. *Can. J. Chem.* **1970**, 48, 2596-2606. https://doi.org/10.1139/v70-435

[253] M. Hricovíni, M. Gembicky, Z. Hricovíniov and J. Moncol, J. The crystal structure and solution behaviour of decyl- and dodecyl a-D-lyxopyranoside: X-ray, NMR, computational and Hirshfeld surface analysis. *J. Mol. Struct.* **2020**, 1202, 127348. https://doi.org/10.1016/j.molstruc.2019.127348

[254] F. Verberck and E.L Esmans. Conformational behaviour of some D-arabino, D-lyxo, D-xylofuranosyl pyridine C-nucleotides. *Spectrochim. Acta* **1995**, *51A*, 153-159. https://doi.org/10.1016/0584-8539(94)00224-Y

[255] S.H. Sung, W.J. Jung and Y.G. Kim. A Novel flavonol lyxoside of *Orostachys japonicus* herb. *Nat. Prod. Lett.*, **2002**, *16*, 29-32.
DOI: 10.1080/1057563029001/4818

[256] S.I. Elshahawi, K.A. Shaaban, M.K. Kharel and J.S. Thorson, J.S. A comprehensive review of glycosylated bacterial natural products. *Chem. Soc. Rev.*, **2015**, *44*, 7591-7697. DOI: 10.1039/c4cs00426d

[257] a) I.I. Cubero and M.M. Martinez. Synthesis of 2-C-methyl-D-lyxose and 2-C-methyl-D-xylose. *Carboh. Res.* **1982**, *105*, 181-188. DOI: 10.1016/S0008-6215(00)84966-6

b) V. Popsavin, G. Sanja, B. Stojanovic, M. Popsavin, V, Pejanovic and D. Miljkovic. Conversion of D-xylose to protected D-lyxose derivatives and to D-lyxose, via the corresponding 1,2-anhydride. *Carboh. Res.*, **1999**, *321*, 110-115. DOI: 10.1016/S0008-6215(99)00164-0

[258] A.S. Perlin, B. Casu and H.J. Koch. Configurational and conformational influences on the carbon-13 chemical shifts of some carbohydrates. *Can. J. Chem.*, **1970**, *48*, 2596-2606. DOI: 10.1139/v70-435

[259] M. Hricovíni, M. Gembicky, Z. Hricovíniov and J. Moncol. The crystal structure and solution behaviour of decyl- and dodecyl a-D-lyxopyranoside: X-ray, NMR, computational and Hirshfeld surface analysis. *J. Mol. Struct.*, **2020**, *1202*, 127348. DOI: 10.1016/j.molstruc.2019.127348

[260] F. Verberck and E.L. Esmans. Conformational behaviour of some D-arabino, D-lyxo, D-xylofuranosyl pyridine C-nucleotides. *Spectrochim. Acta.*, **1995**, *51A*, 153-159. DOI: 10.1016/0584-8539(94)00224-Y

[261] S. Anthony and B. Robert. [13C]–Enriched Tetrosesand Tetrofuranosides: An Evaluation of the Relationship between NMR Parameters and Furanosyl Ring Conformation. *J. Org. Chem.*, **1984**, *49*, 3292–3300. DOI: 10.1021/jo00192a009

[262] D. Zhao, F. Cao, X.-J. Guo, Y.-R. Zhang, Z. Kang, and H.-J. Zhu. Antibacterial indole alkaloids and anthraquinones from a sewage-derived fungus *Eurotium sp. Chem. Nat. Compd.*, **2018**, *54*, 399-401. Google Scholar

[263] D.L. Du, T. Zhu, H. Liu, Y. Fang, W. Zhu, and Q. Gu. Cytotoxic Polyketides from a Marine-derived Fungus *Aspergillus glaucus. J. Nat. Prod.*, **2008**, *71*, 1837-1842. DOI : 10.1021/np800303t

[264] F.-Y. Du X.-M. Li, J-Y. Song, C.-S. Li and B.-G. Wang. Anthraquinone Derivatives and an Orsellinic Acid Ester from the Marine Alga-Derived Endophytic Fungus *Eurotium cristatum* EN-220. *Helv. Chim. Acta.*, **2014**, *97*, 973-978. DOI: 10.1002/hlca.201300358

[265] T. Hoshino, S. Nakano, T. Kondo, T. Sato, and A. Miyoshi. Squalene–hopene cyclase: final deprotonation reaction, conformational analysis for the cyclization of (3*R*,*S*)-2,3- oxidosqualene and further evidence for the requirement of an isopropylidene moiety both for initiation of the polycyclization cascade and for the formation of the 5- membered E-ring. *Org. Biomol. Chem*., **2004**, *2*, 1456-1470. DOI: 10.1039/B401172D

[266] W.-L. Wang, P.-P. Liu, Y.-P. Zhang, J. Li, H.-W. Tao, Q.-Q. Gu1, and W.-M. Zhu. 2-Hydroxydiplopterol, A New Cytotoxic Pentacyclic Triterpenoid from the Halotolerant Fungus *Aspergillus variecolor* B-17. *Arch Pharm Res*., **2009**, *32*, 1211-1214. DOI: 10.1007/s12272-009-1904-8

[267] W.-Y. Liao, C.-N. Shen, L.-H. Lin, Y.-L. Yang, H.-Y. Han, J.-W. Chen, S.-C. Kuo, S.-H. Wu and C.-C Liaw. Asperjinone, A Nor-Neolignan, and Terrein, A Suppressor of ABCG2-expressing Breast Cancer Cells, from Thermophilic *Aspergillus terreus*. *J. Nat. Prod*., **2012**, *75*, 630−635. DOI: 10.1021/np200866z

[268] H. Zhang, Z. An and F. Zhou. Secondary Metabolites from Rhizopus sp., an Endophytic Fungus in *Astragalus membranaceus* and Preliminary Evaluation of Inhibition of Plant Pathogen Activity. *Chem. Nat. Compd*., **2020**, *56*, 366-369. DOI: 10.1007/s10600-020-03035-w

[269] S.K. Hyun, H. Lee, S.S. Kang, H.Y. Chung and J.S. Choi. Inhibitory activities of *Cassia tora* and its anthraquinone constituents on angiotensinconverting enzyme. *Phytother. Res*., **2009**, *23*, 178-184. DOI: 10.1002/ptr.2579

[270] S.-G. Choi, J. Kim, N.-D. Sung, K.-H. Son, H.-G. Cheon, K.-R. Kim and B.-M. Kwon. Anthraquinones, Cdc25B phosphatase inhibitors, isolated from the roots of *Polygonum multiflorum* Thunb. *Nat.Prod.Res*., **2007**, *21*, 487-493. DOI: 10.1080/14786410601012265

[271] R.S. Gonçalves, E.L. Silva, N. Hioka, C.V. Nakamura, M.L. Bruschi and W. Caetano. An optimized protocol for anthraquinones isolation from *Rhamnus frangula L*. *Nat. Prod. Res*. **2018**, *32*, 366-369. DOI: 10.1080/14786419.2017.1356836

[272] W.A. Abdel-Naime, A. Kimishima, A. Setiawan, J.R. Fahim, M.A. Fouad, M. S. Kamel and M. Arai. Mitochondrial Targeting in an Anti-austerity Approach involving Bioactive Metabolites Isolated from the Marine-Derived Fungus *Aspergillus sp*. *Mar.Drugs*. **2020**, *18*, 555, DOI: 10.3390/md18110555

[273] X. Li, X.-M Li, G.-M. Xu, C.-S. Li and B.-G. Wang. Antioxidant metabolites from marine alga-derived fungus *Aspergillus wentii* EN-48. *Phytochem. Lett*., **2014**, *7*, 120-123. DOI: 10.1016/j.phytol.2013.11.008

[274] P.M. Dewick (**2009**). The acetate pathway: fatty acids and polyketides. Medicinal Natural Products: A Biosynthetic Approach (ed. Dewick, P.M.), *Wiley*, ISBN 978-0-470-74168-9, 104-105. Google Scholar

[275] T.D. Bugg, D. Braddick, C.G. Dowson and D.I. Roper, Bacterial cell wall assembly: still an attractive antibacterial target. *Trends in biotech.*, **2011**, *29*, 167-173. DOI: 10.1016/j.tibtech.2010.12.006

[276] E. Henrich, Y. Ma, I. Engels, D. Münch, C. Otten, T. Schneider, B. Henrichfreise, H.-G. Sahl, V. Dötsch and F. Bernhard. Lipid Requirements for the Enzymatic Activity of MraY Translocases and in Vitro Reconstitution of the Lipid II Synthesis Pathway *J. Biol. Chem.*, **2016**, *291*, 2535-2546. DOI: 10.1074/jbc.M115.664292

[277] J.N. Sangshetti, S.S. Joshi, R.H. Patil, M.G. Moloney and D.B. Shinde. Mur Ligase Inhibitors as Anti-bacterials: A Comprehensive Review. *Current pharm. design*, **2017**, *23*, 3164-3196. DOI: 10.2174/1381612823666170214115048

[278] W. Breitenstein and C. Tamm. 13C-NMR.-Spectroacopy of the Trichothecane Derivatives Verrucarol, Verrucarins A and B and Roridins A, D and H. *Helv.Chem. Acta*., **1975**, *58*, 1172-1180. DOI: 10.1002/hlca.19750580419

[279] B.B. Jarvis, J.O. Midiwo, J.L. Flippen-Anderson, and E.P. Mazzola. Stereochemistry of the roridins. *J. Nat. Prod*., **1982**, *45*, 440-448. DOI: 10.1021/np50022a014

[280] T.A. Smitka, R.H. Bunge, R.J. Bloem, and J.C. French. Two new trichothecenes, PD 113,325 and PD 113,326. *J. Antibiot*., **1984**, *37*, 823-828. DOI: 10.7164/antibiotics.37.823

[281] S.R. Lee, S. Seok, R. Ryoo, S.U. Choi and K.H. Kim. Macrocyclic Trichothecene Mycotoxins from a Deadly Poisonous Mushroom, *Podostroma cornu-damae. J. Nat. Prod*., **2019**, *82*, 122-128. DOI: 10.1021/acs.jnatprod.8b00823

[282] G.G. Habermeh, L. Busam, P. Heyde, D. Mebs, C.H. Tokarnia, J. Döbereiner, and M. Sprau. *Toxicon*, **1985**, *23*, 731-745. DOI: 10.1016/0041-0101(85)90003-0

[283] L. Shen, R.H. Jiao, Y.H. Ye, X.T. Wang, C. Xu, Y.C. Song, H.L. Zhu, and R.X. Tan. *Chem. A- Eur. J.* **2006**, *12*, 5596-5602. DOI: 10.1002/chem.200600084

[284] R.M. Silverstein, F.X. Webster and D.J. Kiemle. Spectrometric Identification of Organic Compounds. Hoboken: John Wiley & Son Inc.; **2005**

[285] M. Matsumoto, A. Ito, A. Tonouchi, M. Okazaki and M. Hashimoto. Stereochemical correction and total structure of roridin J. *Tetrahedron*, **2017**, *73*, 5430-5435. DOI: 10.1016/j.tet.2017.07.048

[286] B.B. Jarvis, G.P. Stahly, G. Pavanasasivam, J.O. Midiwo, T. DeSilva, C.E. Holmlund, E.P. Mazzola and R.F. Geoghegan. Isolation and characterization of the trichoverroids and new roridins and verrucarins. *J. Org. Chem*., **1982**, *47*, 1117-1124. DOI: 10.1021/jo00345a044

[287] B.B. Jarvis, G.P. Stahly, G. Pavanasasivam, E.P. Mazzola. Antileukemic compounds derived from the chemical modification of macrocyclic trichothecenes. 1. Derivatives of verrucarin A. *J. Med. Chem*., **1980**, *23*, 1054. DOI: 10.1021/jm00183a018

[288] M.M. Wagenaar and J. Clardy. TwoNewRoridins Isolated from *Myrothecium sp. J. Antibiot*., **2001**, *54*, 517 – 520. DOI: 10.7164/antibiotics.54.517

[289] N.J. Yu, S.X. Guo and H.Y. Lu. Cytotoxic macrocyclic trichothecenes from the mycelia of *Calcarisporium arbuscula* Preuss *J. Asian Nat. Prod. Res*., **2002**, *4*, 179–183. DOI: 10.1080/10286020290011387

[290] G. Fragaki, I. Stefanaki, P. Dais and E. Mikros. Conformational properties of themacrocyclic trichothecenemycotoxin verrucarin A in solution. *Magn. Reson. Chem*., **2008**, *46*, 1102-1111. DOI: 10.1002/mrc.2298

[291] B.B. Jarvis, M. Vrudhula, and J. Midiwo. New Trichoverroids from *Myrothecium verrucaria*: Verrol and 12,13 Deoxytrichodermadiene. *J. Org. Chem*., **1983**, *48*, 2576-2578. DOI: 10.1021/jo00163a031

[292] B.B. Jarvis, S. Wang, and H.L. Ammon. Trichoverroid Stereoisomers. *J. Nat. Prod*., **1996**, *59*, 254-261. DOI: 10.1021/np960078m

[293] B.B. Jarvis, T. DeSilva, J.B. McAlpine, S.J. Swanson, and D.N. Whittern. New Trichoverroids from *Myrothecium Verrucaria* Isolated by High Speed Countercurrent Chromatography. *J. Nat Prod*., **1992**, *55*, 441-1446. DOI: 10.1021/np50088a009

[294] H.K. Abbas, B.B. Johnson, W.T. Shier, H. Tak, B.B. Jarvis and C.D. Boyette. Phytotoxicity and mammalian cytotoxicity of macrocyclic trichothecene mycotoxins from *Myrothecium verrucaria*, *Phytochem.*, **2002**, *59*, 309-313. DOI: 10.1016/S0031-9422(01)00464-2

[295] A. Andolfi, A. Boari, A. Evidente, and M. Vurro. Metabolites Inhibiting Germination of *Orobanche ramosa* Seeds Produced by *Myrothecium verrucaria* and *Fusarium compactum*. *J. Agric. Food Chem.*, **2005**, *53*, 1598-1603. DOI: 10.1021/jf048339i

[296] Z. Islam, J. Shinozuka, J.R. Harkema, and J.J. Pestka. Purification and comparative neurotoxicity of the trichothecenes satratoxin G and roridin L2 from *Stachybotrys chartarum*. *J. Toxicol. Environ. Health A.*, **2009**, *72*, 1242-1251. DOI: 10.1080/15287390903129234